GEOLINKS

INTERNATIONAL CONFERENCE

CONFERENCE PROCEEDINGS

BOOK 1

VOLUME 3

EXTENDED VERSION

AIR POLLUTION AND CLIMATE CHANGE

BIOTECHNOLOGIES

ENVIRONMENTAL GEOLOGY

SOIL SCIENCE

WATER RESOURCES

17-18 MAY 2021 | ONLINE EDITION

DISCLAIMER

This book contains papers which cover the sections: Air Pollution and Climate Change, Biotechnologies, Environmental Geology, Soil Science and Water Resources.

This book contains abstracts, keywords and full papers, which has gone under double blind peer review by the GEOLINKS Review Committee. Authors of the articles are responsible for the content and accuracy.

Opinions expressed might not necessary affect the position of GEOLINKS Committee Members and Scientific Council.

Information in the GEOLINKS 2021 Conference proceedings is subject to change without any prior notice. No parts of this book can by reproduced or transmitted in any form or by any mean without the written confirmation of the Scientific Council of GEOLINKS.

Published by SAIMA CONSULT LTD, Sofia, 1616, st. Beliya Kladenets, 15, fl. 3
Total print 50

ISSN 2603-5472
ISBN 978-619-7495-17-1
DOI 10.32008/GEOLINKS2021/B1/V3

GEOLINKS CONFERENCE
Secretariat Bureau
e-mail: contact@geolinks.info
URL: https://www.geolinks.info

ORGANIZERS AND SCIENTIFIC PARTNERS OF GEOLINKS INTERNATIONAL CONFERENCE

SLOVAK ACADEMY OF SCIENCES
CZECH ACADEMY OF SCIENCES
NATIONAL ACADEMY OF SCIENCES OF UKRAINE
BULGARIAN ACADEMY OF SCIENCES
POLISH ACADEMY OF SCIENCES
ACADEMY OF SCIENCES OF HUNGARY
SERBIAN ACADEMY OF SCIENCES
TURKISH ACADEMY OF SCIENCES
ACADEMY OF SCIENCES OF MOLDOVA
ISLAMIC WORLD ACADEMY OF SCIENCES
LATVIA ACADEMY OF SCIENCES

SCIENTIFIC COMMITEE OF GEOLINKS INTERNATIONAL CONFERENCE

DOC. ING. JOZEF MARTINKA, SLOVENIA
PROF. DSC. VOLODYMYR POHREBENNYK, UKRAINE AND POLAND
PROF. RADA JOAN, ROMANIA
ASSOC. PROF. VADIM ZHMUD, RUSSIA
PROF. NIKOLAOS SAMARAS, GREECE
PROF. MAYA DIMITROVA, BULGARIA
DR. AFSOON KAZEROUNI, USA
ASSOC. PROF. POENAR DANIEL PUIU, ROMANIA
PROF. VRACHNAKIS MICHAIL, GREECE
DR. ENG. VLAD MIHAI PĂSCULESCU, ROMANIA
ASSOC. PROF. DSC. GIUSEPPE SAPPA, ITALY
ASSOC. PROF. CARMEN-PENELOPI PAPADATU, ROMANIA
PROF. ANDON ANDONOV, BULGARIA
DR. DIMITRIS KALIAMPAKOS, GREECE
DOC. PAOLO BAZZOFFI, ITALY
DOC. FUAT TOPRAK, TURKEY
PHD ILDIKÓ-CSILLA TAKÁCS, ROMANIA
ASSOC. PROF. PHD ENG. IURES LIANA, ROMANIA
PROF. BAIBA RIVZA, LATVIA

CONTENT

Section AIR POLLUTION

Section BIOTECHNOLOGIES

Section ENVIRONMENTAL GEOLOGY

Section SOIL SCIENCE

Section WATER RESOURCES

Section

AIR POLLUTION AND CLIMATE CHANGE

Climate change and climatology
Emissions of heavy metals and gases affecting the Earth's climate
Air pollution, monitoring and preventing
Effects of air pollution
Air management
Ozone layer protection

OPTIONS FOR ASSESSING THE SUITABILITY OF URBAN ENVIRONMENTAL ACUPUNCTURE

Assoc. Prof. Barbara Vojvodíková, Ph.D. [1]
Assoc. Prof. Jiří Kupka, Ph.D.[2]
Ing. Adéla Brázdová[3]
Mgr. Radim Fojtík[4]
Ing. Mgr. Iva Tichá, Ph.D.[5]
[1] IURS – Institute for Sustainable Development of Settlements, Czech Republic
[1, 3, 4] Faculty of Civil engineering, VSB - Technical University of Ostrava, Czech Republic
[2] Faculty of Mining and Geology, VSB- Technical University of Ostrava, Czech Republic
[5] Faculty of Social studies, University of Ostrava, Czech Republic

ABSTRACT

To increase their resilience to climate change, cities are looking to apply elements of urban environmental acupuncture. The essence of such measures is many smaller sites that is functioning as mitigation measures. Many of these small places then create a large overall effect. The advantage of these small-scale measures is that they can be in densely populated areas The assessment tool described in this paper is designed for city representatives and is an aid to assess the suitability of applying a particular measure based on the parameters described. The evaluation itself then helps to decide whether the solution is suitable for a particular site or whether any of the parameters need to be adjusted to make it suitable, or whether it would be appropriate to change the proposed solution. The intention of the evaluation is not to assess the technical solution but relies primarily on the location, long-term (especially financial) sustainability and acceptance by the citizens of the city. The paper presents an example of the application of the evaluation to four sites in city Liptovský Mikuláš, describing the results and identifying parameters that can be improved to ensure the urban environmental acupuncture is accepted by citizens and thus future-proofed.

Keywords: *urban greenery, urban environmental acupuncture, sustainable city, urban climate resilience, adaptation strategy*

INTRODUCTION

Since their founding, cities have been undergoing several changes that are the result of a change in the needs of their inhabitants (fortification and de-fortification, industrialization and de-industrialization, etc.) [1]. These changes are reflected in the thickening of the urban core, the consolidation of surfaces and in the expansion of cities into suburbs, which is a significant trend of the last twenty years. Cities are facing many challenges in their pursuit of sustainable development. One of the main issues is a continuous increase in cities` population. By 2050, the urban population

is projected to account for 66 % (some sources say up to 70 %) of the population, and in cities in Africa and Asia it is projected to be as high as 80 % [2]. cities today face a challenge in the form of climate change [3]. Climate changes lead to a gradual temperature rise in cities which results in more intense heat islands [4]. Climate changes also increased risk of floods [5] which is mainly associated with pluvial floods [6], that cause local damage, often unrelated to overflowing persistent water body. An increase in urban density leads to a higher risk of heat islands formation as well as a higher risk of pluvial floods due to a reduction in green unpaved areas [7].

Proper management of green spaces in the city and their well-planned structure can has a positive impact on both the reduction of heat islands and the reduction of the consequences of pluvial floods [8]. Many cities have parks and green areas over 2 hectares in size in their urban structure. However, these green sites are typically quite far from each other, and their impact is not covering the whole city area [9]. In a high-density city structure, it is rarely possible to introduce new green areas of large size such as parks, it is ,therefore, necessary to seek other solutions [10]. The introduction of small green spots – "urban environmental acupuncture" (UEA) - represents such a solution. In adaptation strategies, we can find several requirements for the incorporation of green spots into the urban structure, but there are no guidelines how such application should be carried out.

- When implementing small green spots, it is necessary to address the following basic questions. Which localities are suitable for the application of urban green acupuncture?
- Which are suitable solutions?
- Which solutions are particularly suitable for a specific place?

The main motivation of the research was based on the following assumptions. Heavily urbanized environments with pressure for gradual thickening of buildings [11] use master plan that clearly defines and limits functional use of the areas. This makes it difficult to establish larger green areas that would serve as adaptation and mitigation measures within the adaptation strategy. However, smaller green spots can be placed on the plots without affecting the overall land use, which can follow the master plan. The proposed approach is part of the solution of the project SALUTE4CE. The objective of the research was to propose a procedure for evaluating potential sites, which would help city representatives in deciding on the location and the form of small green spots in the implementation of cities' adaptation strategies, master plans, strategic development plans or other documents. The end users of the procedure are cities' employees and representatives, to the needs and abilities of which the procedure is adopted and who had an opportunity to comment on its design in the professional discussions. The procedure also considers possible expectations of the public.

MATERIALS AND METHODS

The basic conditions that the evaluation system must have were defined as:

- Simplicity of the model.

- Fast application in relation to availability of the input data without lengthy and complex data gathering techniques.
- Reasonability of the proposed solutions.
- Genericity of the assessment allowing use of the procedure on a broad spectrum of various cities.

A potentially suitable place for application of small green spots “Potential Urban Environmental Acupuncture Spot” (PUEAS) would be:

- a place that is not maintained, is neglected or does not fulfil its function;
- a smaller site - ideally up to 0.2 ha but no more than 0.6 ha to allow for feasible implementation,
- a place that spoils image to its surroundings or even reduces property prices in vicinity.

Description of the determination method for assessment

The objective of the research was to propose assessment of the suitability of types of solutions. The assessment should fulfil these aims:

- The evaluation is based on the relationship between the locality and the type of UEA.
- The evaluation is applicable when comparing different types of UEA for one locality as well as when assessing multiple localities for one particular type of UEA.
- The analysis of selected localities aimed to identify the parameters of evaluation and subsequently evaluate these parameters.

The assessment is based on the following parameters:

- location of PUEGAS,
- difficulty of implementing the plan according to the policies of the official body (budget rules),
- requirements for future maintenance,
- involvement of local community and investor in an implementation of the UEA idea,
- future usability of implemented plan.

The location parameter is focused on the position in the urban structure. PUEAS are more important in central parts of cities where there typically is less greenery than in the outer parts. For such central location, environmental problems are expected to be more emphasized (for example heat distribution [12]) and at the same time, even the small-scale solution might have a significant effect on situation improvement.

The parameter of difficulty of implementing of the plan according to the powers of the official body (budget rules) evaluates the already assumed type of UEA. The preparation time factor is projected in the parameter. If the expected investments are in a volume requiring the approval of the entire assembly, the preparation time is much longer than if the approval of one person is sufficient.

The complexity of maintenance of the planned intervention is reflected in the expected additional costs. A higher level of maintenance poses problems for the future sustainability of the implemented UEA spot. If the maintenance complexity is high, it can pose a risk of being neglected in the future [13].

For optimal functionality and progress of the proposed measures within the UEA in the given locality, participation and involvement of the investor of the plan, but especially the public, which will be the end users of the expected benefits, is beneficial already in the first steps even in the selection of PUEAS [14]. Evaluation questions were compiled for this parameter, which were subsequently tested by the panel of experts. The level of participation and involvement is crucial, especially when comparing suitable sites for some particular type of UEA.

Direct involvement of citizens is of course related also to the perspective of the future use of the proposed UEA measure. The unrestricted public access option is preferred.

A point system was designed for selected parameters, which was subsequently tested at 16 localities that are already PUEAS. The testing was performed in collaboration with a panel of experts. The panel of experts consisted of the SALUTE4CE project team and representatives of cities and development organizations - the panel of experts totaled to 15 people.

The individual parameters were assigned a weight based on the conclusion of the panel of experts. Metfessel allocation was applied to determine the weight (using the criteria tree). The weight of individual parameters is given in Table 1.

Table 1. *Weight of individual parameters.*

Parameter	**Weight [%]**
location of PUEAS	25
difficulty of implementing the plan according to the policies of the official body (budget rules)	23
requirements for maintenance	23
involvement of local community and investor in an implementation of the UEA idea	15
usability of implemented plan	14

The total value is then determined by the weighted sum of the points for the responses (equation 1).

Total Value = Σ (Points for the response x Weight of the question) (1)

Table 2. *Description of the characteristics for the allocation of points for each parameter.*

Parameter	Parameter value	Points
PUEAS localization	Exposed locality in the core area of the city (compact construction area with a minimum share of greenery)	6
	Exposed locality outside the core area of the city (structurally not completely compact area, e.g. housing estate with a share of greenery)	5
	Unexposed location in the core area of the city (compact construction area with a minimum share of greenery)	4
	Unexposed locality outside the core area of the city (not completely compact area with a share of greenery)	3
	Scattered (loose) structure of the city with a predominant industrial zone	2
	Scattered (loose) settlement structure of the city with a higher proportion of greenery	1
Difficulty of implementing the plan (budget rules)	Low (in the competence of the mayor)	6
	Medium (in the competence of the city council)	4
	High (within the competence of the city assembly)	2
Requirements for maintenance	Zero maintenance - the project is "self-sufficient", no demands on staff or equipment -> no costs	6
	Low maintenance - the project is almost "self-sufficient", minimal demands on staff or equipment -> minimal costs	5
	Rather low maintenance - demands on trained staff, or. technique -> medium cost	4
	Medium maintenance - higher demands on trained personnel and equipment -> higher costs	3
	High maintenance - high demands on trained personnel and equipment -> high costs	2
	Very high maintenance - very high demands on trained personnel and equipment -> very high costs	1
Involvement of the local community and investor in the implementation of the UEA plan	The local community is interested (somehow) in improving, the investor is interested in improving conditions	6
	The local community is interested (somehow) in improving, the investor is not interested in improving conditions	3
	The local community is not interested, the investor is interested in improving conditions	3

	The local community is not interested, the investor is not interested in improving conditions	0
Usability of the implemented plan	General public - can actively use (garden)	6
	General public - can use passively (green wall on the block of flats)	4
	Limited public / closed society - can actively use (green roof)	2
	Limited public / closed society - can passively use (inaccessible atrium of a private building)	1

For research purposes, 40 sites have been selected. This set contained:

- 16 sites which were selected as "Potential urban environmental acupuncture spots" (PUEAS) by cities which already had plans for certain solution. These sites are further solved within SALUTE4CE project.
- 16 sites, which already represent small green spots – such as an existing community garden or an existing green wall. These sites have been selected by the project team as a reference for research.
- 8 sites, which have been identified by the project team as PUEAS, but they are not solved within SALUTE4CE project. They have been identified by applying defined selection criteria for PUEAS with special focus on abandoned and underused areas. These sites have been partially evaluated by the procedure

To determine the intervals of the total value (Table 3) so that the main goal of the whole research was met - the evaluation of a suitable solution for a specific PUEGAS. The main 32 localities were used to determine the intervals and 8 new localities were used for testing. Information was gathered using a spreadsheet. Information was collected from investors, representatives of the city as well as from public survey among citizens.

Based on the total value, the individual solutions were divided into four intervals (four categories) as shown in Table 3.

Table 3. *Application suitability categories proposed by UEA - distribution of the total calculated value into intervals*

Interval	Evaluation of the plan:	Category
<4,34; 6,00>	UEA type is suitable for the given locality	I.
<3,54; 4,2>	UEA type is conditionally suitable for the given locality	II.
<2,60; 3,40>	UEA type can be problematic for the given locality	III.
<0,94; 2,60)	UEA type is unsuitable for the given locality	IV.

RESULTS OF APPLICATION EVALUATION PROCEDURE

To demonstrate the application of the assessment procedure, four sites from the town of Liptovský Mikuláš were selected.

A - Part of the front facade of the House of Culture on Hollého Street) which represents the point application of the UGA. The House of Culture is located right in the heart of the city. The locality is characterized by high heat stress, lots of paved areas and the greenery is near. Solution - Green wall

B - Courtyard in the housing estate Podbreziny delimited by Hradišská, Jeffremovská and Senická streets, in the Podbreziny housing estate. The site is located on the outskirts of the city and in terms of attractiveness it is not an exposed place. The site is characterized by temperature stress in the summer months, low functionality of the green area. Solution - New greenery, workout playground.

C - Unused school garden of the primary school and kindergarten on Demänovská Street. The site is located on the outskirts of the city with a higher presence of greenery and in terms of attendance or attractiveness is not an exposed place. In addition, this unused area is located directly on the school premises, so access of the public will be limited. Solution - orchard, garden.

D - Peace Square, is located directly in the city centre, i.e., in the exposed part in the city centre, near the shopping centre. It is characterized by thermal stress, despite numerous and costly revitalizations in the past the square does not fulfil the function of the centre, has low functionality of green areas. Solution - green passage from climbing plants.

All four sites based on their attributes are PUEAS. The point evaluation of individual parameters is given, and the final classification is shown in Table 4.

Table 5. *Points of Parameters appropriate solution assigned to individual sites and*

Parameter	A	B	C	D
PUEGAS localization	6	5	1	6
Difficulty of implementing the plan (budget rules)	4	2	6	2
Requirements for maintenance of the future	3	5	4	3
Involvement of the local community and the investor in the implementation of the UGA plan	3	6	3	3
Usability of the implemented project	4	6	2	6
Total Value	4,12	4,60	3,28	3,94
Category	II.	II	III.	II.

CONCLUSION

From the examples given of the evaluation carried out, it can be documented that a decision on the suitability of any of the UEA solutions requires consideration of various parameters. It also gives the possibility to adjust some parameters. Applying the proposed evaluation procedure to the four sites, the following results were found. House of culture site. The green wall has been assessed as the UEA type is conditionally suitable for the given locality. There are two problem areas in the assessment. The first is the high maintenance costs, this parameter is quite difficult to work with. The occupant engagement parameter can be improved. In the recommendations for the town of Liptovský Mikuláš this information is key. The solution of the proposed for Courtyard in the housing estate was evaluated as UEA type is suitable for the given locality. For the locality- Unused school garden – result - UEA type can be problematic for the given locality. There are three key low-scoring parameters in the assessment. Location outside the central part of the town. Limited access to the school garden for the wider community. And associated public engagement. However, this locality is primarily educational in nature. The Peace Square site has been assessed as UEA type is conditionally suitable for the given locality. The issues here are problematic involvement in development plans, expensive maintenance, and little citizen involvement.

The assessment procedure developed is designed to assist in evaluating the suitability of the UEA for PUEAS. However, it is an auxiliary tool, and its purpose is to adjust the parameters if necessary, so that when the UAE is built, the city's efforts will be successful.

ACKNOWLEDGEMENTS

This research was funded by Interreg CENTRAL EUROPE Programme, grant number CE1472, SALUTE4CE - Integrated environmental management of Small Green Spots in FuncTional Urban Areas following the idea of acupuncture. This article got also administrative and technical support from IURS - Institute for Sustainable Development of Settlements.

REFERENCES

[1] Anas: A., Arnott, R., Small K. Urban Spatial Structures. Journal of economic Literature 1993, 36, pp.1426–1464.

[2]Montgomery, M.R.,The Urban Transformation of Developing World. Science 2008, 319, pp.761–764.

[3] Carter, J.G.; Cavan, G., Conelly, A., Guy, S., Handley, J., Kazmierczak, A. Climate change and the city: Building capacity for urban adaptation. Progress in Planning 2015, 95,pp. 1–66

[4] Yoon, E. J., Kim, B., Lee, D. K., Multiobjective planning model for urban greening based on optimalisation algorithms. Urban Forestry & Urban Greening 2019, 40, pp.183–194.

[5] Dragoni, W., Sukhija, B. Climate change and groundwater: a short review. Geological Society, Special Publications 2008, pp.288, 1–12.

[6] Werritty, A., Bassett, D., Geddes, A.; Hoolachan, A.; McMillan, M. Pluvial (rain-related) flooding in urban areas: the invisible hazard, 1st ed.; Joseph Rowntree Foundation: University of Dundee, United Kingdom, 2011, pp. 92.

[7] Gartland, L. Heat islands: understanding and mitigating heat in urban areas. Australian Planner 2012, 49, pp.363–364.

[8] Santamouris, M., Kolokotsa, D. Urban climate mitigation techniques, 1st ed.; Routledge: Abingdon, United Kingdom, 2016; pp. 208.

[9] Niedźwiecka-Filipiak, I., Rubaszek, J., Potyrała, J., The Method of Planning Green Infrastructure System with the Use of Landscape-Functional Units (Method LaFU) and its Implementation in the Wrocław Functional Area (Poland). Sustainability 2019, 11, pp. 394.

[10] Kabisch, N., Strohbach, M., Haase, D., Kronenberg, J., Urban green space availability in European cities. Ecological indicators 2016, 70, 586–596.

[11] Skovbro, A. Urban densification – a sustainable urban policy? The Sustainable City II 2002, 54, pp. 518–527.

[12] Sharma, R., Hooyeberghs, H., Lauwaet, D., De Ridder, K., Urban Heat Island and Future Climate Change—Implications for Delhi's Heat. Journal of Urban Health 2019, 96, pp.235–251.

[13] Ho, D.K.H., Greening the Urban Habitat: A Quantitative and Empirical Approach, 1st ed.; World Scientific Publishing Co. Pte. Ltd.: Singapore, 2020; pp. 220.

[14] Hurlbert, M., Gupta, J., The split ladder of participation: A diagnostic, strategic, and evaluation tool to assess when participation is necessary. Environmental science & policy 2015, 50, pp.100–113.

REDUCING GREENHOUSE GAS EMISSIONS BY IMPLEMENTING SUSTAINABLE INFRASTRUCTURE PROJECTS

Dr. Eng. Raluca Ioana Nicolae[1]
Drd. Ec. Petru Nicolae[2]
Ec. Ana-Maria Brăileanu[3]
[1, 2, 3] Geostud SRL, Romania

ABSTRACT

Climate change is an inevitable and urgent global challenge with long-term implications for the sustainable development of all countries. In order to respond to climate change, it is very important to identify new ways of reducing greenhouse gas emissions. The present paper emphasizes that the use of a greener and more efficient means of transport, such as a highway (in this case Buzău-Focșani) is more beneficial in terms of reducing greenhouse gas emissions than using old infrastructure. Through specific traffic data processing and dispersion modelling, it was shown that the polluting emissions will increase in the next years, in case of using the already existing road, while the use of a sustainable highway provides a downward trend for these emissions. The construction of the highway will have positive effects on air quality, will ensure a good traffic flow, but the benefits will be even greater when the replacing of the existing car fleet (Diesel vehicles) with hybrid and electric vehicles will take place.

Keywords: *GHG, emissions, highway, environment, mitigation*

INTRODUCTION

Global warming currently involves the main need of reducing greenhouse gas emissions in order to mitigate the anthropogenic influence on the climate system and allow ecosystems the opportunity to increase their resilience and adaptability capacity. Despite global efforts to reduce greenhouse gas emissions, the average temperature will continue to rise in the coming period, requiring urgent measures.

According to national estimates [1], GHG emissions increased in the transportation field by approx. 155%, compared to the emissions from 1989. This phenomenon can be attributed to the increase of mobility between 1990 and 2008, the urban expansion, the use of roads for passenger and freight transport and the intensification of air traffic.

In Romania, the effects of climate change are felt especially through changes of temperature, rainfall amounts and winds' frequency and intensity. According to Climate Change Scenarios [2], we are dealing with significant warming of about 2°C, since 1961, in almost the whole country, during the summer, with increasing rainfall and significant downward trend of the winds.

The present paper aims, through specific traffic data processing and dispersion modelling, to demonstrate the beneficial effect, in terms of greenhouse gas

emissions, of the development of a greater and greener type of infrastructure network, instead of the existing one.

In order to better highlight this aspect, the Buzău – Focșani highway was used as an example in this article. This highway is part of the TEN-T Core (Central) network, and it connects the south of the country with the NE region, the historical regions of Moldova and Bucovina, and also with Ukraine and the Republic of Moldova. As a strategic objective, it is intended to build a highway along the entire corridor.

METHODOLOGY

The route of Buzău - Focșani highway is located on the administrative territory of two counties, namely: Buzău (from km 0+000 to km 45+455) and Vrancea (from km 45+455 to km 82+440).

In order to determine the estimative quantities of pollutants emitted during the operation of the Buzau - Focșani highway compared to those emitted by the existing infrastructure (DN2 Urziceni - Buzău – Focșani), the Tier 1 methodology from the EMEP/EEA/2019 guidebook [3] was used.

For modelling the dispersion of air pollutants during the operation period, the BREEZE AERMOD/ISCTM program was used, a program based on the AERMOD mathematical dispersion model, developed and used by the United States Environmental Protection Agency.

Dispersion modelling involves several intermediate steps, such as preparing meteorological data, land surface data and information related to topography. The modellling takes into account the topographic and climatic characteristics for each location (sources of pollution) and can predict concentrations of pollutants from fixed sources, surface or volumes.

In order to calculate the emission quantities of vehicles during the operation phase, the following data were taken into account:

- average vehicle flow/year/ vehicle categories;

- average and total number of traveled km/year/vehicle categories;

The data obtained from the calculations were introduced in COPERT 5 and processed in the AERMOD program, in order to determine the concentrations and dispersion of pollutants from mobile emission sources. Pollutant dispersion calculus by vehicle type during operation is presented in Table 1, for the year 2050 [4].

The specific source of pollution during the operation period is represented by the road traffic on the new road artery. Using the specified calculation method, the concentrations of greenhouse gases (evaluated through CO_{2e}) were estimated.

To assess the impact on the environment from the perspective of pollutant emissions and climate change during operation, the methodology included in the Update of the Handbook on External Transport Costs - Final Report from 2014 [5]

was applied. In order to assess the impact on the environment, the following steps were taken:

- quantification of pollutant emissions (by using vehicle emission factors, vehicle types and traffic flow data);
- modelling the dispersion of pollutants around the source using complex atmospheric dispersion models.

Table 1. *Estimated amounts of CO emissions by vehicle type during operation*

Vehicle categories	Years					
	2025	**2030**	**2035**	**2040**	**2045**	**2050**
Buses - Highway	0.472	0.323	0.219	0.241	0.255	0.270
Buses - DN2 Urziceni - Buzău - Focşani	1.258	1.306	1.381	1.573	1.764	1.896
Heavy trucks - Highway	33.520	15.817	11.508	13.057	14.298	15.460
Heavy trucks - DN2 Urziceni - Buzău - Focşani	63.115	67.820	75.645	106.157	122.516	138.457
Light commercial vehicles - Highway	8.713	5.794	3.943	4.683	5.145	5.696
Light commercial vehicles - DN2 Urziceni - Buzău - Focşani	18.354	22.430	24.833	27.630	29.872	39.898
Light-duty vehicles - Highway	23.515	18.220	12.109	12.992	13.499	14.044
Light-duty vehicles - DN2 Urziceni - Buzău - Focşani	352.103	333.117	339.375	366.315	426.008	884.407
Total - Highway	**66.220**	**40.153**	**27.779**	**30.972**	**33.196**	**35.470**
Total - DN2 Urziceni - Buzău - Focşani	**434.831**	**424.673**	**441.234**	**501.675**	**580.160**	**1064.658**

RESULTS AND DISCUSSIONS

According to the presented data, the quantities of traffic emissions for the CO indicator, during the operation period, have an increasing trend for DN2 Urziceni - Buzău - Focșani (Baseline scenario) and a decreasing trend for the Buzău - Focşani Highway (Projection scenario).

Following the mathematical modelling of the pollutant dispersion based on the values of local background concentrations, the total quantities of emissions from mobile sources were obtained during the operating period for the baseline and projection scenario, presented in **Table 2**.

Table 2. *CO concentrations (mg/m^3) values obtained for a mediation period of 8 hours - for the years 2025, 2035 and 2050*

	DN2 Urziceni – Buzău - Focșani (Baseline scenario)			**Highway Buzău – Focșani (Projection scenario)**			**The limit values provided by Law no. 104/2011 (mg/m^3)**
	Traffic on DN2 Urziceni-Buzău-Focșani	Local background	**Total**	Traffic on Buzău – Focșani Highway	Local background	**Total**	
2025							
Route from Buzău county	0.00233	0.558	0.560	0.00024	0.558	0.558	10
Route from Vrancea county	0.00219	0.559752	0.562	0.00043	0.559752	0.560	10
2035							
Route from Buzău county	0.0023	0.558	0.560	0.0001	0.558	0.558	10
Route from Vrancea county	0.00216	0.559752	0.562	0.00018	0.559752	0.560	10
2050							
Route from Buzău county	0.00596	0.558	0.564	0.00013	0.558	0.558	10
Route from Vrancea county	0.00559	0.559752	0.565	0.00023	0.559752	0.560	10

The table above highlights the differences between the basic scenario, which involves maintaining the current situation of pollutant emissions by using the alternative route DN2 Urziceni - Buzău – Focșani, and the projection scenario, which involves reducing pollutant emissions by using the Buzău - Focșani highway. Thus, in the projection scenario, the concentration values are lower than the baseline scenario. The projection scenario has a higher efficiency, due to the maintenance of the concentrations during the operation period below the limit values and the target air quality values provided by Law no. 104/2011 (**Error! Reference source not found.**).

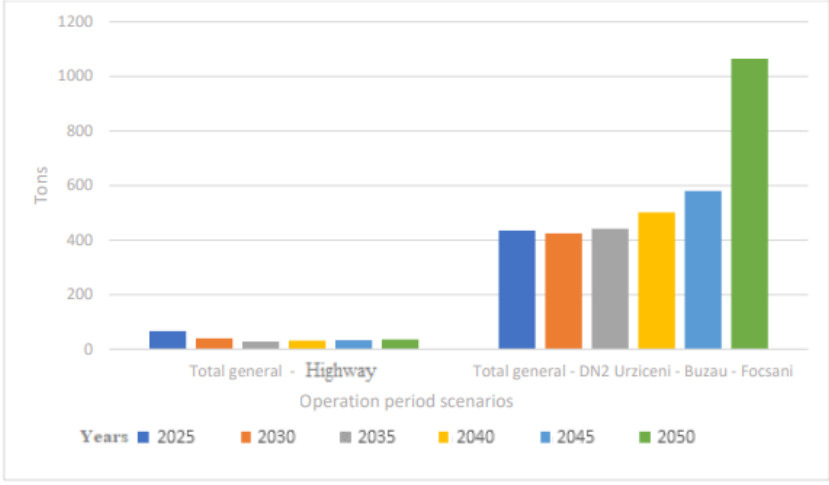

Fig. 1. *The evolution of the carbon monoxide quantities (CO) for the Buzău - Focşani highway and DN2 Urziceni - Buzău - Focşani for 2025 – 2050*

The construction of the highway will have positive effects on air quality, by reducing greenhouse gases, along national and county roads from which the highway will absorb traffic. This will lead to smoother traffic on these roads and to a reduction in greenhouse gas emissions into the atmosphere. In general, traffic on these roads is slow, with frequent braking and stopping. The construction of the highway will contribute to decongesting and improving traffic conditions.

Fig. 2 shows quantities of greenhouse gas (GHG) emissions expressed in tons of CO_{2e}, for mobile emission sources for the Buzău - Focșani highway, compared to the alternative route in the implementation area (DN2 Urziceni - Buzău - Focșani).

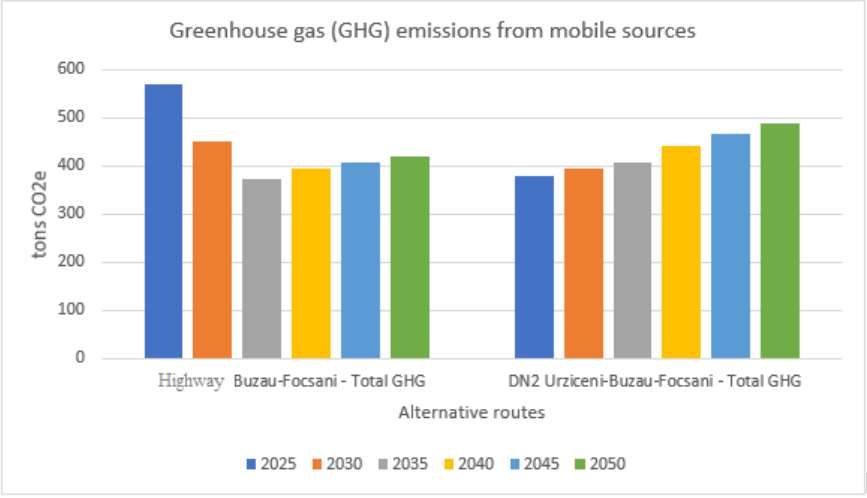

Fig. 2. *Comparative greenhouse gas emissions from mobile sources for the two alternative routes*

CONCLUSION

According to the presented data, the estimated quantities of greenhouse gas emissions from the burning of fossil fuels during the exploitation period, have an increasing trend for DN2 Urziceni - Buzău - Focșani and a stable trend for the Buzău - Focșani highway.

In case the highway project will not be implemented, the following conclusions can be drawn:

- following the regional industrial and touristic development, the route connecting the two municipalities (DN2) will be the subject of an increased number of vehicles transiting it; combined with traffic congestion, this will cause an increase in air pollutant emissions;
- the route connecting the two municipalities (DN2) will maintain its exposure to the risk caused by extreme weather and climatic conditions (accentuated by the absence of forest curtains), which can lead to traffic jams; these are associated with an increase in GHG emissions into the atmosphere.

In conclusion, the existing traffic on DN2 Urziceni - Buzău - Focșani, characterized by congestion and low speeds in the proximity of localities, in the long run, would cause an increase in emissions in the absence of the Buzău - Focșani highway.

The Buzău - Focșani highway will ensure a good traffic flow, the long-term trend being of gradual reduction of emissions. A significant reduction in the amount of emissions from traffic will also occur by replacing the existing car fleet (Diesel vehicles) with hybrid and electric vehicles.

REFERENCES

[1] Climate Change Service within the National Agency for Environmental Protection, National Inventory of Greenhouse Gas Emissions (GHG), 2012, available on the website www.ANPM.ro;

[2] Busuioc A., Caian M., Bojariu R., Boroneanț C., Cheval S., Baciu M., Dumitrescu A., Climate change scenarios in Romania, Romania, 2014, available on the website www.meteoromania.ro;

[3] European Environment Agency, EMEP/EEA air pollutant emission inventory guidebook, 2019, available on the website www.eea.europa.eu;

[4] Geostud SRL, Environmental impact report for „BUZĂU – FOCȘANI Highway", 2021

[5] Korzhenevych A., Dehnen N., Broecker J., Holtkamp M., Meier H., Gibson G., Varma A., Cox V., Update of the Handbook on External Transport Costs - Final Report, 2014, available on the website www.eea.europa.eu.

REDUCING THE ADVERSE EFFECTS OF THE OPERATION OF GAS FIRED MELTING FURNACES ON THE ENVIRONMENT

Assoc. Prof. Luboslav Straka, PhD.[1]
Assoc. Prof. RNDr. Tibor Krenicky, PhD.[2]
[1, 2] Technical University of Kosice, Faculty of Manufacturing Technologies, Presov, Slovakia

ABSTRACT

Due to the growing production on a global scale, the use of fossil fuels is also increasing. Therefore, the control of pollutant emissions produced in the industrial sphere has become a global concern. In general, an imperfect combustion process has a negative impact on the overall efficiency and economy of plant operation, but at the same time increases the share of total emissions in the environment. We also encounter this problem when operating gas fired melting furnaces. Therefore, the paper aimed to describe the results of experimental measurements of the number of emissions produced during the operation of a gas fired melting furnace, which in practice is mainly used for melting alloys. Experimental measurements were oriented to find the most suitable variant of the operating mode of the gas fired melting furnace with regard to minimizing the total amount of emissions produced.

Keywords: *combustion process, melting, emissions, melting furnace, efficiency*

INTRODUCTION

Melting furnaces use different energy sources. It is most often thermal energy produced by a combustion process or the transformation of an electric current. In the case of obtaining thermal energy by the combustion process, one of the common sources of this energy is natural gas. Natural gas can generally be characterized as a mixture of hydrocarbons, the vast majority of which is methane. The main products in its combustion are carbon dioxide (CO2) and water vapor. Although emissions of nitrogen oxides (NOx), sulfur dioxide (SO2) and other particles produced during the combustion of natural gas are several times lower compared to other fossil fuels, they are not negligible. In the case of the application of natural gas for the production of thermal energy, which is subsequently applied to the melting of metals in the melting furnace, the operating mode is decisive. Many current producers of products cast from various alloys try to maximize the performance of their melting furnaces to ensure the higher productivity of their production. In many cases, however, the performance, but especially the low efficiency of the melting furnace, is closely linked to the increased production of pollutants [1]. These negatively affect the environment. A certain solution to the negative impact of increased production of pollutants and their release into the air in much technological equipments is their reduction by means of separators and filters. However, in the case of gas fired melting furnaces, this is a problem [2].

Exhalates produced by melting metals in a gas fired melting furnace are very problematic to capture. Therefore, the paper aims to describe the results of experimental research aimed at eliminating the amount of pollutants produced during the operation of the gas fired melting furnace used mainly for melting alloys. The solution is based on the design of the most suitable variant of its operating mode in order to maximize the efficiency of the melting furnace and thus reduce the amount of emissions produced with increasing demands to increase the productivity of melting furnaces [4].

THEORETICAL ANALYSIS OF THE PROBLEM

Although many studies have shown that the proportion of pollutants produced in the combustion of natural gas is several times lower compared to other fossil fuels, this is not a completely negligible amount. This fact is also pointed out by several studies, during which it was found that the actual amount and concentration of pollutants produced during the combustion process is also significantly affected by the efficiency of the combustion process itself. In case the combustion process is insufficient, i. has low efficiency, emission values can increase several times. In addition, during the process of melting the alloys in the melting furnace, exhalants are also produced, which are produced by the melting alloy [5]. These emissions are practically impossible to prevent during the melting process of the alloy. Therefore, a certain solution is at least the reduction of pollution fumes produced during the combustion of natural gas. Several researchers working in the field are looking for ways to reduce these pollutants. They are trying to find ways to eliminate these pollutants released into the environment. However, in the case of melting furnaces, these methods are inefficient. Therefore, some researchers have focused more closely on eliminating emissions that occur in the process of melting alloys. This group of researchers tried to achieve lower emissions in the gas furnace, by increasing the proportion of oxygen [3]. The results of these experimental studies are described in detail in several works [6]. In this context, the results of other authors point to the negative fact that the application of oxygen in the gas fired melting furnace cools the molten alloy. This has the negative consequence of prolonging the melting process. With increasing time, there is an increase in the emissions produced, which in summary then means their total increase within one melting cycle [7]. Therefore, one of the suitable solutions for eliminating the production of pollutants in a gas melting furnace appears to be the optimization of its operating mode.

MATERIAL AND METHODS OF WORK

Experimental research was focused on finding ways to reduce emissions produced by the gas fired melting furnace during a one melting cycle [8]. One of the suitable solutions was considered to be the optimization of its operating regime in order to minimize pollutants while maintaining or, ideally, increasing its productivity. In the experiment, a gas fired melting furnace was used, the construction of which consists of steel profiles and sheets. The base is formed by a supporting frame, which is anchored in the base plate [9]. The melting furnace is

mounted on one side on two plain bearings and on the other side is mounted in a hydraulic cylinder [10]. The stroke of one end of the melting furnace during emptying is controlled by a hydraulic cylinder [11]. The following Fig. 1 shows the basic construction of the gas fired melting furnace.

An important structural part of the gas fired melting furnace used is the protective jacket. It consists of a lining with refractory bricks and ceramic insulation boards. The spaces of the outlet opening and the flue gas outlet as well as the movable door of the melting furnace are protected by refractory concrete. One of the most thermally stressed parts of the gas fired melting furnace is the burner area [12]. This construction part is protected by a special refractory material that can withstand temperatures up to 1600 °C. Heating of alloy in the used gas melting furnace is realized by means of two gas burners No. 1 and No. 2 with a maximum output of 2×700 kW. These are monobloc burners with programmable semi-automatic power control.

Fig. 1. *Container gas fired melting furnace*

Measuring device used in the experiment

Experimental measurement of the amount of pollutants produced during the melting of alloys in the gas fired melting furnace required the application of a special measuring device. These were measuring devices Testo 340, which is shown in the following Fig. 2.

Fig. 2. *Special emission measuring device Testo 340*

Using a special measuring device Testo 340, measurements of the content of pollutants produced by the gas fired melting furnace during the individual operating modes of melting the alloy were continuously performed. Total melting times were recorded during the individual operating modes, in which approximately the same amount of melt was applied in each case. Within the experiment, 5 different operating modes were applied. These were modes of operation of the gas melting furnace in which the mechanism of maximizing the melting power was applied, resp. a mechanism for minimizing the actual values of the emissions produced. The first operating mode "Maximum High Operation" was aimed at achieving the maximum output with both burners of the gas fired melting furnace. The second operating mode "Half High Operation" corresponded to maximizing the power of one of the burners of the gas fired melting furnace with partial support of the other burner. The third operating mode "Semi Operation" again corresponded to setting one of the burners of the gas fired melting furnace to full power, while the other burner was out of operation. The fourth operating mode "Low Operation" corresponded to the setting of the minimum output of both burners of the gas fired melting furnace. The last fifth operating mode "Very Low Operation" corresponded to setting one of the burners of the gas fired melting furnace to a minimum, while the other burner was out of operation

ANALYSIS OF THE OBTAINED DATA ON THE PRODUCED POLLUTANTS BY THE GAS FIRED MELTING FURNACE

Individual measurements of the content of pollutants produced during the operation of the gas fired melting furnace were performed with a special measuring device Testo 340. Measurements of the content of these emissions were performed in the individual operating modes No.1 - Maximum High Operation, No.2 - Half

High Operation, No.3 - Semi Operation, No.4 - Low Operation and No.5 - Very Low Operation. In addition to the content of pollutants, in the individual operating modes of the gas fired melting furnace, the operating times t_{op} required to achieve a ΔT of approximately 700 °C were also recorded. In the following Fig. 3, the results of the experimental measurement of the emissions produced by the gas melting fired furnace during the No.3 - Semi Operation mode can be observed.

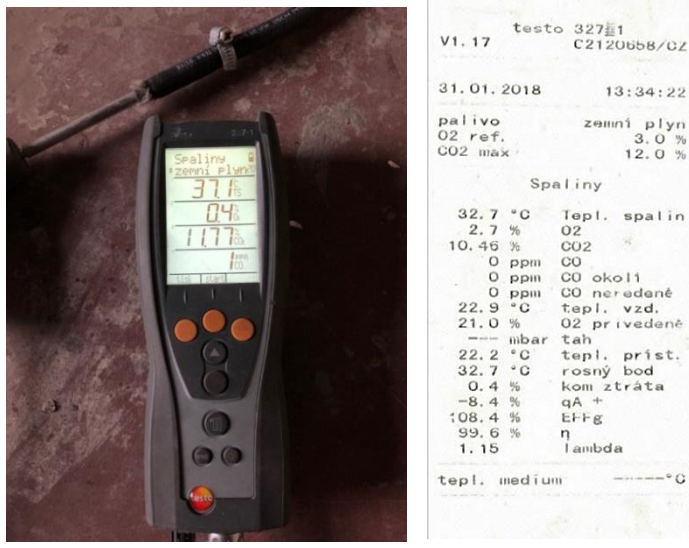

Fig. 3. *Recorded emissions of the gas fired melting furnace during the melting of alloy during operating mode No.3 -Semi Operation*

As part of the experimental measurements, we found that during the individual operating modes of the gas fired melting furnace, not only the content of actually produced pollutants changed, but also the total times required to reach the melting temperature T_m of alloy at about 720 °C. It was also found that despite the relatively low production of emissions in some operating modes of the gas fired melting furnace, the overall emission balance was higher than in the operating mode during which the currently increased emission values were achieved. This was due to extended operating time. In the following tab. 1 show the current values of the content of pollutants produced by the gas fired melting furnace in individual operating modes, as well as their total balance during one melting cycle.

Table 1. *Actual content of pollutants and their total balance during one melting cycle*

Monitored indicators		Operating mode of gas fired melting furnace				
		Maximum High Operation	*Half High Operation*	*Semi Operation*	*Low Operation*	*Very Low Operation*
Emissions	NOx (%)	0.0183	0.0187	0.0181	0.0199	0.0201
	CO (%)	0.0080	0.0083	0.0079	0.0093	0.0107
	CO_2 (%)	10.78	10.94	10.46	11.39	11.67
	TZL ($g.m^{-3}$)	0.0599	0.0674	0.0551	0.0774	0.0987
Operating time t_{op}	(hours)	10.0	11.5	13.0	13.5	14.0
Total balance	m_{pollut} (tons)	1.85	1.81	1.76	2.14	2.43
Environmental impact		**increased**	**increased**	**low**	**high**	**high**

From the Tab. 1, it can be observed that in the operating mode of the gas fired melting furnace No.1 - Maximum High Operation, the shortest operating time top at the level of 10 hours was achieved. On the contrary, the longest operating time was reached during the operating mode No.5 - Very Low Operation at the level of approximately 14 hours. From the point of view of the overall balance of pollutants produced during one melting cycle of the gas melting furnace, the operating mode No.3 - Semi Operation can be positively evaluated. In this mode of operation of the gas fired melting furnace, the lowest amount of emissions was produced at the level of approximately 1.77 tons. On the contrary, the worst overall balance of emissions produced during one operating cycle was recorded in operating mode No.5 - Very Low Operation.

From the point of view of the optimum operation of the melting furnace under consideration, it is appropriate to perform its optimization. The optimization was performed with a view to minimizing the total balance of emissions produced by the gas fired melting furnace during one melting cycle, as well as with a view to minimizing its total operating time. In the following Fig. 4, a graphical optimization of the operating mode of the gas fired melting furnace can be observed with respect to minimizing the total melting cycle time, as well as minimizing the total amount of emissions produced during one melting cycle.

The performed optimization proved that the most unsuitable variant of the operating mode of the gas fired melting furnace from the point of view of the production of pollutants is the operating mode No.3 - Semi Operation. In this operating mode, although one melting cycle lasts 13 hours, which is 3 hours longer compared to the shortest operating mode No.1 - Maximum High Operation. On the other hand, from the point of view of the production of pollutants during one melting cycle of the gas fired melting furnace, the lowest amount of pollutants is

produced m_{pollut} = 1.76 tons. Compared to the No.5 - Very Low Operation mode, which produces the highest amount of pollutants m_{pollut} = 2.43 tons, this represents a decrease of 0.67 tons. Therefore is the recommendation for the operation of this type of gas fired melting furnace is the application of the operating mode No.3 - Semi Operation, in which only one burner is in operation at full power.

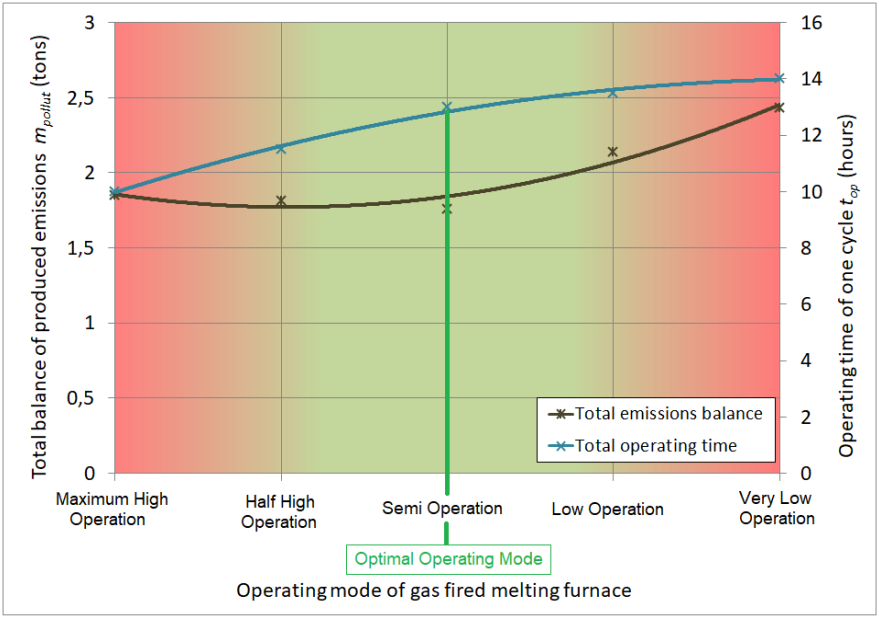

Fig. 4. *Graphical optimization of the operating mode of the gas fired melting furnace with regard to the minimization of the operating time t_{op} and the minimization of the total amount of m_{pollut} produced emissions*

CONCLUSION

It is generally known that the application of the gas fired melting furnace in practice produces a large number of contaminants [13]. The primary part of these pollutants is the combustion process, the secondary part of the pollutants released during the melting of a particular alloy. Even in the case of the use of the most modern technological equipment with active reduction of the production of pollutants, we cannot completely rule out the production of these harmful substances. At the same time, during the operation of gas fired melting furnaces, the production of pollutants is affected by the operating mode used. In practice, it is required that the melting times of the alloys be as short as possible. However, this has a negative impact on the overall balance of pollutants produced during one melting cycle. Therefore, in order to minimize the total amount of pollutants produced, it is necessary to select an operating mode of the gas fired melting furnace in which the operating time of one melting cycle is partially extended, but at the same time, the lowest overall balance of pollutants produced is achieved. In the case of the applied gas fired melting furnace, it was the No.3 - Semi Operation mode. In

this operating mode of the gas fired melting furnace, the lowest total emissions balance was produced at the level of 1.76 tons per one melting cycle.

ACKNOWLEDGEMENTS

The authors would like to thank the VEGA grant agency for supporting presented research work within the project VEGA 1/0205/19.

REFERENCES

[1] Banerjee S., Sanyal D., Sen S., Puri I.K., A methodology to control direct-fired furnaces, International Journal of Heat and Mass Transfer, vol. 47, pp. 5247-5256, 2004.

[2] Edward M.W., Donald L.S., Ken O., Evaluating aluminum melting furnace transient energy efficiency, Proceedings of Symposia held during TMS 2009, Annual Meeting and Exhibition, Warrendale TMS, pp. 43-51, 2009.

[3] Golchert B., Ridenour P., Walker W., Gu M., Selvarasu N.K., Zhou C., Effect of nitrogen and oxygen concentrations on Nox emissions in an aluminum furnace, Proc. ASME-IMECE, IMECE-15693, 2006.

[4] Li T.X., Hassan M., Kuwana K., Saito K., King P., Performance of secondary aluminum melting: Thermodynamic analysis and plant-site experiments, Energy, vol. 31, issue 12, pp. 1433-1443, 2006,

[5] Lazic L., Varga A., Kizek J., Analysis of combustion characteristic in an aluminum melting furnace, Metalurgija, vol. 44, issue 3, pp. 192-199, 2005.

[6] Nieckele A.O., Naccache M.F., Gomes M.S.P., Combustion performance of an aluminum melting furnace operating with natural gas and liquid fuel, Applied Thermal Engineering, vol. 31, pp. 841-851, 2011.

[7] Mukhopadhyay A., Puri I.K., Zelepouga S., Rue D.M., Numerical simulation of methane-air nozzle burners for aluminum remelt furnaces, Proc. ASME-IMECE, HTD-24234, 2001.

[8] Pandova I., Panda A., Valicek J., Harnicarova M., Kusnerova M., Palkova, Z., Use of sorption of copper cations by clinoptilolite for wastewater treatment, International Journal of Environmental Research and Public Health, Basel, vol. 15, issue 7, pp. 1-12, 2018.

[9] Straka L., Hasova S., The critical failure determination of the constructional parts of autonomous electroerosion equipment by applying Boolean logic, Academic Journal of Manufacturing Engineering, vol. 14, issue 2, pp. 80-86, 2016.

[10] Yan S. et al., Study on point bar residual oil distribution based on dense well pattern in Sazhong area, Journal of Mines, Metals and Fuels, vol. 65, issue 12, pp. 743-748, 2017.

[11] Zhang W., Wang, X., Simulation of the inventory cost for rotable spare with fleet size impact, Academic Journal of Manufacturing Engineering, vol. 15, issue 4, pp. 124-132, 2017.

[12] Majernik J., Gaspar S., Kmec J., Karkova M., Mascenik J., Possibility of Utilization of Gate Geometry to Modify the Mechanical and Structural Properties of Castings on the Al-Si Basis, Materials, vol. 13, no. 16, 3539, 2020.

[13] Gil S. et al., An Experimental Study on the Air Delivery and Gas Removal Method in a Model of Furnace for Ferroalloy Production, Metalurgija, vol. 53, Issue 4, pp. 447-450, 2014.

THE ENERGY OF SEA TIDES IN THE CONTEXT OF SOLVING CLIMATE PROBLEMS

Dr. Elena E. Shirkova [1]
Dr. Eduard I. Shirkov [2]
[1, 2] The Kamchatka Branch of Pacific Geographical Institute, Far Eastern Branch Russian Academy of Sciences, Russia

ABSTRACT

The article presents an overview of the technical, economic, and environmental arguments in favour of wider use of the gigantic energy potential of sea tides to solve the most important climate problem today – the reduction of anthropogenic pollution of the Earth's atmosphere with carbon dioxide.

The main idea of the considered solution is the replacement of carbon fuels for thermal power plants and transport with "green" hydrogen. The production of such hydrogen is carried out by electrolysis using the energy of carbon–free renewable sources.

Tidal hydroelectric power plants are the cheapest, largest and most economically safe electricity supplier for the production of green hydrogen today. Until now, this direction of the energy sector has not become widespread due to the high capital intensity, as well as due to the geographic remoteness of the places where tidal energy is concentrated from large centres of electricity consumption.

The explosive growth in global hydrogen demand in recent years alleviates the problem of very expensive transport and large losses in long distance transmission of electricity. Hydrogen can be transported without loss and relatively cheaply by pipelines and sea tankers over unlimited distances.

The use of the energy of the highest tides and flow in the Pacific Ocean for the production of "green" hydrogen is proposed in the revived project of construction of the world's largest Penzhinsk Tidal Hydroelectric Power Plant (the Sea of Okhotsk' north–east, Russia).

Keywords: *tidal energy in hydrocarbon energy, reducing greenhouse gas emissions, capturing and storing atmospheric carbon dioxide, the world's largest tidal power plant*

INTRODUCTION

The existing international agreements and mechanisms for reducing CO_2 emissions into the atmosphere and the ocean have not yet yielded the expected results, and the growing level of carbon dioxide concentration in the atmosphere and hydrosphere of the Earth is steadily approaching the point of no return. In such conditions, the world community is left with no other alternatives, except for toughening agreements and mechanisms for reducing emissions, as well as forcing

the transition of the world economy from predominantly carbon to hydrogen energy.

The climate summit in Glasgow, scheduled for this fall (2021), is intended to try to solve the first direction of solving climate problems. Further development of the use of carbon–free renewable energy sources (RES) can contribute to solving the second direction of these problems. The still underutilized energy potential of oceanic tides is the core matter of this review.

DISCUSSIONS

More than half a century (since 1961) experience of operating the first tidal hydroelectric power plant (TPP) on the estuary of the Rance River (in Brittany, France) has shown that such plants are one of the most environmentally friendly and cheapest in operation carbon–free energy suppliers. At the same time, the construction of such stations is very costly, and their generation of electricity, with a high monthly and annual stability, is not constant within a day.

Russia has accumulated a significant (albeit, mainly experimental) experience in reducing capital costs in the construction of TPPs due to the production of floating modules of their dams at the factory and in the future – towing these modules already with the equipment installed in them to the places of TPP construction [1].

Orthogonal hydraulic units, highly efficient and cheaper than those currently used in world practice, have been developed and tested in experimental operation. According to the developers of these technologies, this makes it possible to reduce the capital cost of the TPP to 1 thousand US dollars per 1 kW of installed capacity [2] at an actual cost of 2.5 thousand dollars per 1 kW, which was formed during the construction of the largest today the South Korean Sihwa Lake Tidal Power Station (2011). This is a significant opportunity to overcome the most important of the above–mentioned economic barriers in the expansion of TPP construction.

Most recently, the British tidal turbine manufacturer SIMEC Atlantis Energy unveiled its latest development, the 2 MW AR2000 system, which will become the largest tidal turbine with a service life of 25 years, which is another new technological breakthrough in tidal power [3].

The second major economic drawback of the discussed energy generation technology – the intraday unevenness of energy production at tidal power plants – can be compensated by the cooperation of TPPs with other types of generation (solar, wind, nuclear, and even traditional thermal) in territorial power systems.

However, the most effective ways of leveling the intraday unevenness of electricity generation at TPPs today should be considered:

Firstly, the use of their cheap energy for large–scale production of such ecologically perfect fuel for thermal power plants that have not yet exhausted their resource and vehicles with internal combustion engines.

And, secondly, for the capture of excess carbon from the air and sea water, its liquefaction and subsequent burial in deep oceanic trenches. That is a direct solution to one of the most pressing climatic problems – the transfer of some part of excess atmospheric and hydrospheric carbon from its short biosphere cycle (– atmosphere and hydrosphere – biosphere) into a long – geospheric (geological) cycle for many thousands of years. That means, practically forever.

Finally, another important, but now an indirect effect of large–scale production of liquefied hydrogen at TPP can be considered a multidimensional synergistic stimulation of commercial demand for the development of advanced technologies for the production, storage and transportation of this new (possibly exchange-traded) commodity with an inexhaustible raw material base, for a new carbon-free energy and other sectors of the economy of the future, for the formation of wider front in solving climate problems.

According to experts [1], it is possible to construct a TPP with a total capacity of up to 787 GW with an electric power generation of up to 2037 TWh per year in areas favourable for the construction of TPPs on the world's seashore. Including in Russia about 250 TW.

At the same time, only about a dozen TPPs with a total installed capacity of up to 500 MW are still operating in the world. The most powerful of them – Sihwa Lake Tidal Power Plant (254 MW), was commissioned in the Republic of Korea in 2011. Its capacity is only slightly higher than the capacity of the first industrial TPP at the estuary of the Rance River – 240 MW (Brittany, France, 1961) [2].

Two more TPPs with a capacity of 1500 and 800–1300 MW are currently under construction [4]. Thus, the actual use of the available natural potential of cheap and environmentally friendly tidal energy in the world is still very insignificant, despite the long mastered and constantly improving technologies for its production.

Such a seemingly illogical situation for a market economy can be explained by at least three factors:

Such a seemingly illogical situation for a market economy can be explained by at least three factors:

- significantly higher unit capital costs than in the construction of other types of power plants;
- the relative rarity and considerable remoteness of the targets favourable for the construction of TPPs from the existing centres of large–scale electricity consumption. This circumstance additionally increases the total capital costs when using the energy of the tides for the construction of powerful and long power transmission lines from the TPP to consumers;
- as well as the above–mentioned feature of the energy of tides – its intraday irregularity, which implies the need for daily compensation for failures in the generation of electricity from TPPs and, therefore, the need for them to work in tandem with a power plant of another type of corresponding capacity, or to connect to fairly large territorial power systems.

These and some other problems that have hindered the fuller use of the huge potential of tides in the world energy sector until now are being solved today, on the one hand, by the gradual reduction of the capital cost of building a power plant, mentioned above, and on the other hand, by the explosive growth of the world economy's demand for such a universal, environmentally impeccable and urgent energy fuel as hydrogen, which is necessary to solve the escalating climate problems.

According to [5], the annual global production of hydrogen in 2017–2019 was 55–65 million tons, which were consumed mainly in the chemical and oil refining industries. Energy consumption of hydrogen has so far been predominantly experimental in nature.

According to the European Roadmap for the Development of the Hydrogen Economy [6], in 2005 the total energy demand in the EU was about 14,000 TWh, of which 325 TWh (8 million tons) was hydrogen [6].

In the near future, this map considers two scenarios, according to which the supply of hydrogen to the EU market by 2050 should be from 12 to 18 and from 16 to 55 million tons [6].

Other countries of the world are also rapidly build up plans their plans for the production of hydrogen, although quantitatively the forecasts of the annual volume of the hydrogen market by countries sharply differ: from 500–2000 TWh to 2050 [7]. According to other more optimistic estimates, the world's hydrogen production by 2050 could grow to one billion tons per year [8]. At the same time, it is noted that today there is no answer to the question of the availability of energy resources for such a sharp increase in hydrogen production, especially if we bear in mind the "green" hydrogen – hydrogen obtained by electrolysis of water with the help of energy, which excludes the emission of carbon during its production.

It should be noted that the authors of [8] in the latter case express fair doubts. Indeed, modern capacities and structure of electricity generation even in Russia, where the share of electricity generation at thermal power plants in 2020 was already less than 60 % [9] (which is not the worst indicator in the world energy sector). But for the production of "green" hydrogen in Russia, there are still no sufficient reserves of capacity at power plants with carbonree electricity generation technology: hydroelectric power plants, nuclear power plants, wind power plants and solar power plants.

However, a resource that is overlooked in this article [8], is tidal energy potential. It is a major source of carbon-free energy generation for the production of precisely "green" hydrogen, adequate to the economic and environmental requirements.

On the entire Pacific coast of the Earth, this potential has the highest parameters in the Penzhinsk Guba of the Shelikhov Bay (northeastern part of the Sea of Okhotsk) between the territories of the Kamchatka and the Magadan Region of Russia.

The largest tides in the Pacific Ocean occur here – from 9 to 13 meters. Due to an area of the Penzhinsk Bay of about 21 thousand square kilometers, up to 500 cubic kilometers of water moves through its "gate" every day. Here, back in the seventies of the last century in the USSR, it was planned to build the most forceful power plant in the world – the Penzhinsk TPP. Its design capacity during construction in various sections (North or South – see figure 1) was from 21 to 87 GW. Possible annual power generation was expected from 72 up to 200 billion kWh [10].

Fig. 1. *Map diagram of the placement of the Northern and Southern gates of the projected Penzhinsk Tidal Power Plant [11].*

For various reasons, but, first of all, due to the lack of sufficiently large consumers of electricity in the nearby territories, as well as due to the unacceptably high cost of its transportation over long distances, the implementation of this ambitious project was constantly postponed. Only with the emergence of a high market demand for "green" hydrogen, which can be transported without losses through pipelines or tankers, this project got a chance to be implemented.

According to TASS report dated July 13, 2021, «H_2 Clean Energy» company, together with the Kamchatka Territory Development Corporation, has begun to develop an updated project for the construction of the world's largest Penzhinsk Tidal Power Plant in the Sea of Okhotsk. Its capacity is initially supposed to be used primarily for the production of "green" hydrogen [12].

The same company envisages the construction of a hydrogen production plant in Magadan with the aim of exporting it to the countries of the Asia–Pacific region and, together with RUSNANO, they plan to create a hydrogen hub in the Murmansk region, as well as redesign the Mamakan Hydroelectric Power Station in the Irkutsk region for hydrogen production. Thus, Russia has made a serious claim for significant participation in the efforts of the world community to implement the

transition of world energy to a carbon–free foundation, and hence in the practical solution of global climate problems.

Of course, the use of even the entire energy potential of the ebb and flow of the Ocean will not fully provide this transition, which is absolutely necessary for mankind. But in the longer term, improving solar energy technologies will be able to finally close the problem of anthropogenic pollution of the planet's atmosphere with carbon dioxide.

Large tidal power plants similar to the Penzhinsk TPP, working mainly for the production of "green" hydrogen, should help to win the time necessary for such a revolutionary technical solution to the problem.

The authors consider the message of this article in attracting the attention of international organizations designed to solve the problems of negative climate change, as well as the world business community to support this ambitious project in every possible way.

CONCLUSION

In the natural capital of the world economy there is a significant, but so far underutilized energy resource – the tidal energy of the Ocean generated by the gravitational interaction of the Earth, the Moon and the Sun.

Significant in time world experience of using tidal power plants (TPP) has shown their high technical reliability, economic efficiency and environmental safety.

The only technological disadvantage of the PES is the intraday irregularity of electricity generation. In modern conditions, this natural disadvantage of TPPs may not have a negative significance when using the relatively cheap electricity they generate to obtain "green" hydrogen – ecologically perfect fuel for thermal power plants and transport with internal combustion engines. A fuel that can contribute to a fairly rapid (albeit technically difficult) transition of the world economy from predominantly carbon-based energy to a carbon-free one.

Right this transition, together with the energy support of the technical possibility of the excess carbon direct capture from the environment with a purpose of its future disposal, they represent practically the only real prospect for a significant breakthrough in solving the aggravating climate crisis caused by an increase in the concentration of carbon dioxide in the atmosphere and hydrosphere of the Earth.

The implementation of this energy transition can, to a certain extent, could be facilitated by the construction of the world's largest Penzhinsk TPP in the Sea of Okhotsk (Russia), which plans to produce the "green" hydrogen as a core feature of project’s concept. A joint decision to develop a new project for this TPP was made by “H_2 Clean Energy” and JSC “Kamchatka Territory Development Corporation”.

REFERENCES

[1] Bernshtein L.B., Silakov V.N., Gelfer .L., Kuznetsov .N., Monosov M.L., Monosov L.M., Nekrasov A.V., Platov V.I., Suponitsky L.I., Tonkoyan G.A., Usachev I.N. & Erlikhman B.L. (1987). Tidal power plants. Moscow: Energoatomizdat. (in Russ.).

[2] Popel O.S. & Fortov V.E. (2015). Renewable energy in the modern world. Tidal power plants. Moscow: Publishing House of MEI. (in Russ.). Retrieved from https://ozlib.com/838656/tehnika/prilivnye_elektrostantsii (in Russ.).

[3] GIS–PROFI (2021). The world's most powerful tidal turbine of 2 MW. Electronic technical library "GIS–PROFI". Retrieved from https://gisprofi.com/gd/documents/britantsy–prezentovali–krupnejshuyu–v–mire–prilivnuyu–turbinu–na–2–mvt.html (in Russ.).

[4] Electricity and environmental protection. Energy functioning in the modern world (2011). Buryachok T.A., Butso Z.Yu., Varlamov G.B., Dubovskiy S.V. & Zhovtyanskiy V.A. Retrieved from http://energetika.in.ua/ru/books/book–5 (in Russ.).

[5] Mitrova T., Mel'nikov Yu. & Chugunov D. (2019). Hydrogen Economy as a Way to Low–Carbon Development. The Energy Centre of Moscow School of Management Skolkovo.

[6] Hydrogen Roadmap Europe. Report. A sustainable pathway for the european energy transition (2019). Retrieved from https://www.hydrogeneurope.eu/sites/default/files/Annual_Report_2019_Hydrogen_Europe_final.pdfhttps://www.fch.europa.eu/sites/default/files/Hydrogen%20Roadmap%20Europe_Report.pdf. DOI:10.2843/341510.

[7] RBK (2021). Hydrogen Energy in Russia and Europe: Market Prospects for $ 700 Billion. Retrieved from https://trends.rbc.ru/trends/green/5ef46e379a7947a89c25170d. (in Russ.).

[8] Degtyarev K. S., Berezkin M. Yu. (2021). On the problems of the hydrogen economy / Journal of Environmental Earth and Energy Study (JEEES) №1. 14–23. DOI: 10.5281/zenodo.4662942. (in Russ.).

[9] SO UPS (2021). Information review "Unified Energy System of Russia: interim results" (operational data). January 2021. Retrieved from https://www.so–ups.ru/fileadmin/files/company/reports/ups–review/2021/ups_review_0121.pdf.

[10] Burmistrova S. (2021). In Kamchatka, the Soviet project on hydrogen for $ 200 billion is being revived. Retrieved from https://www.rbc.ru/business/12/07/2021/60ec4ab99a7947fca921f1eb?from=from_main_4&fbclid=IwAR1u7Rtc9ZAuxjrrLB70x_klVlxzEE48if9AcviAjjnDNjQoHMLskx8YTes (in Russ.).

[11] Usachev I.N. The energy of sea tides in Kamchatka (Penzhinsk TPP Project) (2006). Development of renewable energy sources in Russia: opportunities and practice (evidence from Kamchatka region) (pp. 33–37). Collection. Moscow: «Greenpeace Council», Russian Branch (in Russ.)

[12] TASS (2021). In Kamchatka, they began to develop a project for a tidal power plant in the Sea of Okhotsk. Retrieved from https://tass.ru/ekonomika/11889389 (in Russ.)

THE IMPACT OF THE INDOOR ENVIRONMENTAL QUALITY ON STUDENTS' PERFORMANCE

Lect. Eng. PhD. Rus Tania[1]
Assoc. Prof. Eng. PhD. Beu Dorin[2]
Lect. Eng. PhD. Ciugudeanu Calin[3]
[1, 2, 3] Technical University of Cluj-Napoca, Faculty of Building Services Engineering, Romania

ABSTRACT

The indoor environment quality is a key factor in people's lives, which directly affects their comfort, performance, health and well-being. The main factors that contribute to the indoor environmental quality are thermal comfort, air and lighting quality and acoustics.

This study aims to extend the current knowledge on the impact of IEQ on students' performance. Field measurements on environmental factors were performed in two similar classrooms, with the same number of students engaged in a written examination. Compliance of the indoor environmental parameters with the current standards regulations was performed. Students' performance was quantified by their exam grades. The results of the field measurements show that, in both classrooms, the acoustics and air quality do not fulfil the standard regulations, especially in the case of carbon dioxide concentration which exceeds a lot the threshold limit of 1000 ppm. The outcomes of the study also reveal that in the classroom where the concentration of carbon dioxide is higher, the students scored lower grades, therefore we can conclude that indoor environmental quality has an impact on students' performance.

Keywords: *indoor environmental quality, thermal comfort, air quality, lighting, acoustic*

INTRODUCTION

In recent years, researchers are focused on Indoor Environment Quality (IEQ) evaluation and improvement, since more than 90% of the time people carry out their various activities indoors [1]. Ensuring a high level of IEQ is an essential factor in obtaining healthy environments in buildings. The indoor environmental quality is defined as the interaction between various environmental factors such as thermal comfort, air and lighting quality and acoustic [2], [3].

Thermal comfort is defined as "that condition of mind that expresses satisfaction with the thermal environment" [4]. The most popular way to assess thermal comfort is through the heat-balance approach, which is defined by two indices, the Predicted Mean Vote (PMV) and the Predicted Percentage of Dissatisfied (PPD). PMV index is established from the interaction of four physical environmental parameters (indoor temperature, mean radiant temperature, relative humidity and air velocity) and two personal variables (metabolic rate and clothing

insulation). PPD index is defined as the percentage of occupants that could experience local discomfort.

Indoor Air Quality (IAQ), another important environmental factor, is directly associated with the concentration of pollutants and ventilation rates inside buildings and has a high impact on IEQ [5]. A poor IAQ can reduce occupants' productivity and cause health problems [6]. The main factor affecting IAQ is the high concentration of carbon dioxide (CO_2).

A poor lighting quality can cause discomfort, therefore visual comfort is another critical factor affecting indoor environmental quality. In the standard EN 12464-1 [7] are presented the illuminance values that are required to be maintained for a high visual comfort. The study of Heschong [8] regarding the relationship between daylight and human performance, showed the importance of good daylighting, large windows and the possibility of windows openings, on the faster educational progress.

The last factor considered to be crucial and contributes to a high level of indoor environmental quality, especially in offices and schools, is the acoustic comfort. Researchers proved that a poor room acoustic, with excessive noise, reduces peoples' concentration and productivity. In standard EN15251 [9] are presented the acceptable values for the relative loudness of the human ear and of the A-weighted sound pressure levels (dB(A)).

Even though the first steps were made in raising awareness about the importance and influence of the IEQ on the quality of life, many steps must be made to achieve healthy environments. However, in the last couple of years there is an increasing trend in the request for IEQ high quality solutions especially in hospitals, offices and schools to ensure healthy environments and occupants' wellbeing.

Educational establishments such as schools or universities are complex buildings designed to meet the requirements of both teachers and students. An increased level of IEQ is a crucial factor in the intellectual acquisition and proper development of young people. Previous studies reported the IEQ influence on occupants' health, productivity, satisfaction and wellbeing [10-12].

To have a better knowledge on the IEQ impact over the performance of students engaged in different activities, it is necessary to widen the research in this field. Therefore, the purpose of this study is to investigate the effects of indoor environment quality on students' outcomes of a written examination. A case study of two similar classrooms where students took a written examination is presented. Firstly, through this study is assessed the compliance with the regulations of standards [4,5,7,9] and then is investigated if the indoor environmental quality has an impact on students' performance quantified by exam's grades.

METHODS AND MATERIALS

The investigation of IEQ was conducted during winter in one of the educational establishments of the Technical University of Cluj-Napoca, namely the Faculty of Building Services Engineering. The measurements were carried out in a period

when the city was affected by fog and the outdoor temperature during the day had a minimum 0˚C value of and a maximum one of +4˚C.

The early ’70s built building, located close to the city centre of Cluj-Napoca, undergone a significant retrofit between 2005 and 2008. The educational establishment is naturally ventilated through windows openings and infiltrations through the building's elements, and is heated during cold seasons with a centralized heating system. The thermal plant prepares and delivers thermal agents to fan coil units mounted on the exterior walls, under the windows made from PVC frames and double glazing. The area of one window is 5 m^2 which facilitates the access of an important amount of natural light. The artificial light inside the building is provided by louvre luminaires with fluorescent lamps. In many classrooms there are vertical blinds, to reduce glare from sun.

The field study of IEQ was conducted in two similar classrooms, where students took a written examination. The classrooms have three exterior walls, have the same orientation and are situated on the same side of the building, one at the ground floor (classroom A) and the other at the third floor (classroom B). The differences between the classrooms are their area, classroom A has 125 m^2 while classroom B has 78 m^2, and the number of windows. The layouts of the classrooms are presented in Figure 1.

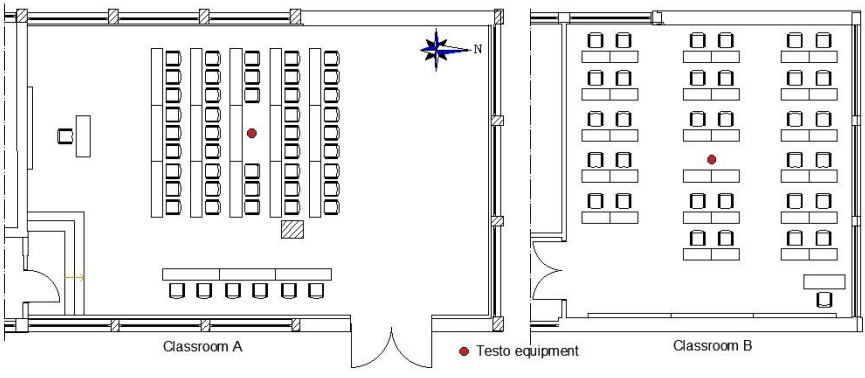

Fig. 1. *Floor plan of the classrooms with the position of the measurement instruments.*

At the research participated a total of 54 people, 27 in each classroom, all students in the first year of the Bachelor studies. Students’ written examination was at the same discipline, with same grade of difficulty and was timetabled between 10:00 and 11:30 AM.

The indoor environmental parameters such as air temperature, mean radiant temperature, relative humidity, air velocity, carbon dioxide concentration, illuminance and sound level were recorder with various instruments. The specification of the apparatus are detailed in Table 1.

***Table 1**. Technical specifications of the instruments used.*

Instrument	Recorded parameter	Range	Accuracy
Testo 480 – indoor air quality probe	Air temperature	0 ÷ 50˚C	±0.5 ˚C
	Relative humidity	0 ÷ 100% RH	±1.8% RH
	Air velocity	0 ÷ 5 m/s	±0.03 m/s
	CO2 concentration	0 ÷ 5000 ppm	±75 ppm
Testo 480 – globe probe	Mean radiant temperature	0 ÷ 120˚C	-40 to+1000˚C
GL SPECTIS 1.0+ Flicker spectrophotometer	Illuminance Color temperature Color rendering	0 ÷ 99999 Lux	±3 Lux
Testo 815 – sound level meter	Sound level	32 ÷ 130 dB	±1.0 dB

After the analysis of standards recommendations [4], [5], [7], [9] regarding the placement of the measuring devices, the position of the instruments inside the classrooms was cautious selected (see fig.1). The measuring devices were placed approximately in the middle of the occupied area at height of 1.1 m. In the case of artificial lighting, the measurement grid was selected according to point 4.4 from [7] at a height of 0.8 m. To prevent local influences of the measuring devices, a distance of at least 1 meter was kept away from any possible source (students, walls, windows). Environmental parameters were recorded every 5 minutes.

RESULTS AND DISCUSSIONS

Our field study comprises short-term objective measurements to understand how various factors of the indoor environment can affect students' performance. The followed factors are air temperature (˚C), mean radiant temperature (˚C), relative humidity (%RH), air velocity (m/s), CO_2 concentration (ppm), illuminance (lux) and sound level (dBA).

Indoor thermal environment

The indoor thermal environment can have a meaningful impact on students' performance and well-being and represents an important part of indoor environmental comfort.

For the determination of the physical conditions of the thermal environment in terms of students' acceptability and comfort, the PMV equation presented in ASHRAE Standard 55 [4] was employed. The equation is a function of four environmental parameters (air temperature, mean air temperature, air velocity and relative humidity) and two personal variables (metabolic rate and clothing insulation). Based on the observation method and according to standard's recommendations, the metabolic rate for typical tasks was considered 1 met, while the clothing insulation for typical ensembles totalized a value of 0.92 clo. Further, the PPD equation that predicts the percentage of students who feel dissatisfied with the environment was employed.

The minimum, maximum and mean values of the recorded indoor thermal environment, PMV and PPD are presented in Table 2.

Table 2. *Recorded values of the indoor thermal environment.*

Variables	Classroom A			Classroom B		
	Minimum	Maximum	Mean	Minimum	Maximum	Mean
Air temperature [˚C]	23	24.1	23.9	22.6	28.1	26.2
Radiant temperature [˚C]	22.8	24.3	24	22.7	28.2	26.3
Relative humidity %RH]	27.2	34.1	31.7	34.3	47.8	40.4
Air velocity [m/s]	0.11	0.12	0.11	0.12	0.13	0.12
PMV [-]	-0.38	-0.03	-0.11	-0.49	1.21	0.6
PPD [%]	5	7.9	5.25	5	35.8	12.6

The PMV-PPD method is widely used by the research community to assess the thermal environmental acceptability for healthy adults. Compliance with the ASHRAE 55 Standard in terms of acceptability and comfort is achieved if -0.5<PMV<+0.5 and PPD<10%.

The mean resulting values of the PMV and PPD are presented along with a graphical representation of their intersection and are shown in Figure 2 for classroom A, respectively Figure 3 for classroom B.

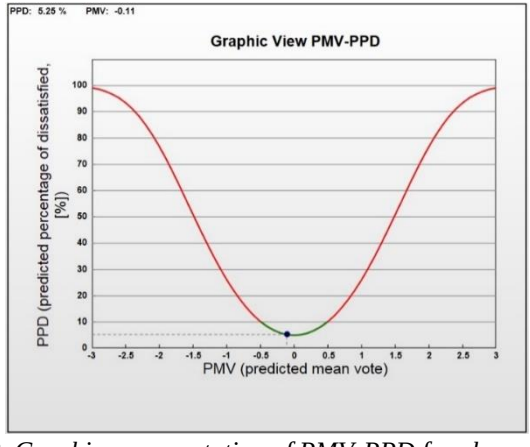

Fig. 2. *Graphic representation of PMV-PPD for classroom A.*

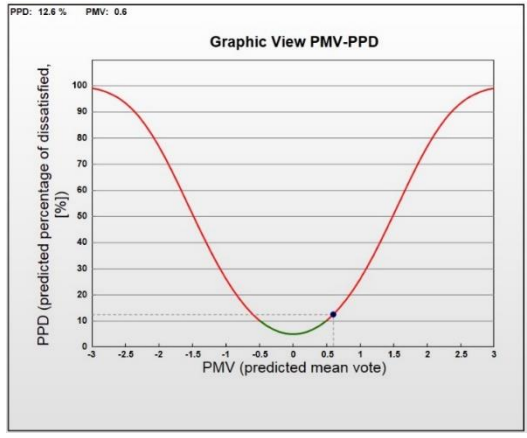

Fig. 3. *Graphic representation of PMV-PPD for classroom B.*

From the above figures it can be observed that the thermal environment acceptability and comfort in classroom A meets the standard recommendations, while in classroom B the upper limit (+0.5 for PMV and 10% for PPD) is a little bit exceeded.

Air quality

The indoor air quality is usually expressed in terms of ventilation required for reduction of air pollutants and CO_2 concentration. The carbon dioxide concentration is mostly affected by occupants' body mass, density and the relationship between it and IAQ has been for a long time researched [13]. In ASHRAE Standard 62.1 [5] are specified the minimum rates of ventilation and the acceptable values for CO_2 concentration for a good indoor air quality. In Figure 4 is shown the evolution of CO_2 concentration in both classrooms.

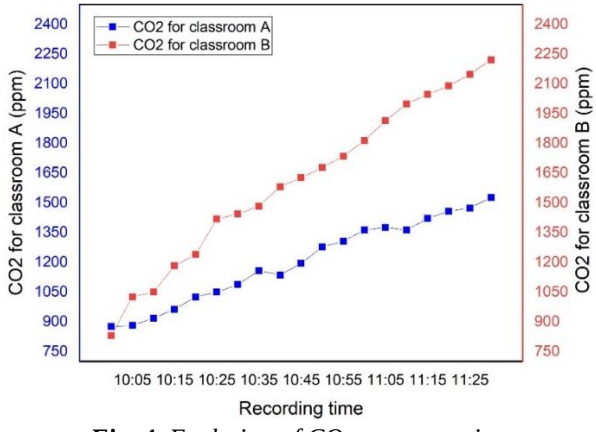

Fig. 4. *Evolution of CO_2 concentration*

The measured CO_2 concentration exceeds in both classrooms the threshold limit (1000 ppm) of the standard [5]. Therefore, the air quality inside both

classrooms fails to meet acceptability and can create discomfort, health problems and difficulties in concentration.

One of the reasons for such high values of CO_2 concentration is related to the low ventilation rate. The building is naturally ventilated, thus ventilation is made through window openings and infiltration, but given the fact that measurements occurred during winter and the outside temperature was low (approximately 1.5˚C), the windows weren't opened during the recording timetable. Another cause for such a high concentration of CO_2 is due to the outside fog that affected the city at the measuring time. Cluj-Napoca is a large and crowded city with many factories around it and plenty of cars, so when the fog settles down the outdoor air quality is poor. When the experiments occurred, the outside concentration of CO_2, at 9:50 A.M., was 725 ppm. From Figure 4 it can be observed that in classroom B the concentration of CO_2 is higher and increases more rapidly and that is due to occupants' density. In classroom A the ration between area and one student is 4.62 (m^2/student) while in classroom B is 2.88 (m^2/student).

Lighting quality

Previous researches have emphasized the significance of real-life experiments and acquiring quantitative information due to observable differences between actual operating environments.

During the building's retrofit process, previous bare battens luminaires with two T12 fluorescent lamps of 40W with magnetic ballast, were replaced with louvre luminaires with two T8 fluorescent lamps of 36W - 765, again with magnetic ballast.

The requirements for artificial lighting (illuminance Em, uniformity U0 and color rendering Ra, according to [7] are presented in Table 3 alongside with the recorded values during students' examination. Even though the exams started at 10:00 A.M. and the classrooms benefited of natural light, the artificial lighting was on because the in-site measurements occurred during winter and outside was fog.

Table 3. *Types of activity in educational buildings and lighting parameter.*

Room type	Em [lux]	U0	Ra	Specific Requirements
EN 12464.1 recommendations				
Classrooms	500	0.6	80	Lighting should be controllable
Recorded values				
Classroom A	585.4	0.61	82.1	Lighting is not controllable
Classroom B	510.2	0.64	82.3	

As it can be seen from the above table, the classrooms fulfil the norms requirements. The differences between values are due to the numbers of windows, classroom A having many more compared with classroom B.

Acoustic environment

To analyze the classrooms' indoor acoustic environment the recording of the sound pressure level was every 25 minutes, after the exam started when all the students started to resolve the problems, in the middle of the timeframe and before the time for examination ended. In Table 4 are presented the EN 15251 [9] recommended criteria for the sound level and the results obtained during the measurements.

Table 4. *Recorded values of the indoor thermal environment.*

Zone	EN 15251 recommendations dB(A)	Mean sound level dB(A)
Classroom A	30 ÷ 40	51.5
Classroom B	30 ÷ 40	50.2

The mean sound level in both classrooms was a little above the threshold limits of 40 dB(A), which shows high level of sound pressure, therefore, can induce discomfort for students. The high recorded values of the sound pressure level are due to the outside noise, due to building's placement to the proximity of an intense circulated boulevard.

Impact of IEQ on students' performance

Average grades have been widely used and accepted in almost all schools and universities to measure performance. In our study, we also use the results of the written examination to quantify students' performance.

In both classrooms, students' written examination occurred in the same day and timeframe, at the same discipline, while they were overseen by teachers from other disciplines. The subjects received by students to be solve were the same. The exam papers were then corrected by the teacher in charge with the discipline. The evaluation scale of the grades is from 1 to 10, students pass the exam if they score at least 5. The results of the exams are presented in a comparative graph presented in Figure 5. The grades obtained by students from classroom A had an average on 6.88 respectively 6.07 from classroom B.

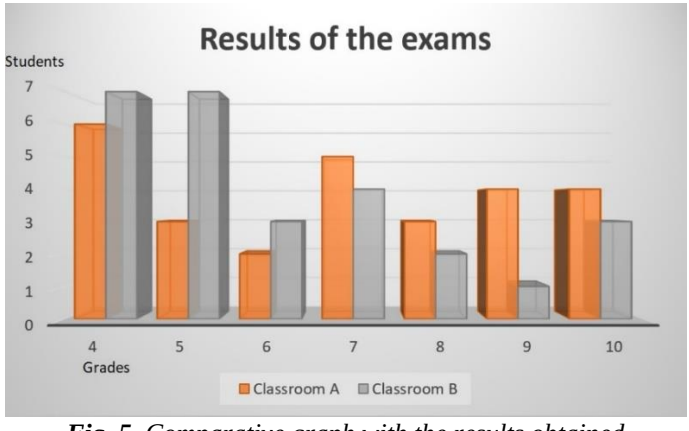

Fig. 5. *Comparative graph with the results obtained*

From the comparative graph, it is observed that students from classroom B received lower grades and the promotability rate is a little bit reduced compared with the students from the other classroom, although at the partial exam undergone in the middle of the semester the results were similar. The explanations of these results could be many starting from students' preparation for the exam, subjects' difficulty, to stress factor and lack of concentration.

By analyzing the results obtained from the recorded values of environmental parameters, the lighting quality in both classrooms meets the requirements of standards [7]. Therefore, one can't relate the low grades and differences in the exam results to this factor. The sound level in both classrooms was above the upper limit of the standard recommendations [9]. The values recorded didn't excessively pass the acoustic threshold limit, so one can state that a small discomfort in terms of noise was present. Regarding occupants' thermal comfort in classroom A the thermal environment is slightly cool respectively slightly warm in classroom B. According to standard recommendations [4], only classroom A meets the requirements of a comfortable and acceptable indoor thermal environment. Previous studies [11,14] have highlighted that a slightly cool environment supports occupants to concentrate to their tasks, whereas a slightly warm environment creates thermal discomfort and focusing issues. In terms of air quality, the measurements revealed that in both classrooms the threshold limit of 1000 ppm [5] was overpassed. Previous studies highlighted that poor air quality, with high levels of CO_2 have direct impact on occupants' concentration, performance, health and well-being [11,13]. Therefore, we can state that a decisive influence on students' performance had the air quality and high concentration of CO_2, especially in classroom B where the results of the exam were lower, and the concentration of CO_2 reached alarming values.

CONCLUSIONS

The indoor environment plays a significant role in people's lives, which directly affects humans` work, quality of life, well-being, environment, energy status and economy.

In this study, the IEQ of two similar classrooms is assessed through measurements of various environmental factors (thermal comfort, air quality, lighting quality and acoustics). The results reveal that classroom A fails to meet the requirements of the standard for air quality and acoustics, whereas classroom B for thermal comfort, air quality and acoustics.

The impact of the indoor environmental quality on students' performance is highlighted especially in classroom B, where students scored lower grades compared to the students from the other classroom, influenced by the high concentrations of CO_2.

The limitations of this study are due to the short-term measurements and the reduced number of students involved. Larger samples of students and long-term measurements are required to fully understand which of the four factors have a strong influence on the impact of IEQ on occupants' performance.

REFERENCES

[1] United States Environmental Protection Agency. Report on Environment: Indoor Air, 2011.

[2] Sarbu I., Sebarchievici C., Aspects of indoor environmental quality assessment in buildings, Energy and Buildings, vol. 60, pp 410–419, 2013.

[3] Heinzerling D., Schiavon S., Webster T., Arens E., Indoor environmental quality assessment models: A literature review and a proposed weighting and classification scheme. Building and environment, vol. 70, pp 210-222, 2013.

[4] ASHRAE, ANSI/ASHRAE 55, Thermal Environmental Conditions for Human Occupancy, Atlanta, USA, 2013.

[5] ANSI/ASHRAE Standard: 62.1, Ventilation for Acceptable Indoor Air Quality, 2010. American Society of Heating, Refrigerating and Air-Conditioning Engineers, Atlanta, USA, 2010.

[6] Sundell J., Levin H., Nazaroff W.W., Cain W.S., Fisk W.J., Grimsrud D. T., Weschler C.J., Ventilation rates and health: multidisciplinary review of the scientific literature. Indoor air, vol. 21 issue 3, pp 191-204, 2011.

[7] CEN, EN 12464-1 - Light and Lighting- Lighting of Workplaces- Part 1: Indoor Workplaces, Belgium, 2011.

[8] Heschong L., Daylighting in Schools: An Investigation into the Relationship between Daylighting and Human Performance. Detailed Report HMG-R-9803, 1999.

[9] CEN, EN-15251: Indoor Environmental Input Parameters for Design and Assessment of Energy Performance of Buildings Addressing Indoor Air Quality, Thermal Environment, Lighting and Acoustics, Belgium, 2007.

[10] Arif M., Katafygiotou M., Mazroei A., Kaushik A., Elsarrag E., Impact of indoor environmental quality on occupant well-being and comfort: A review of the literature. International Journal of Sustainable Built Environment, vol 5(1), pp 1-11, 2016.

[11] Vilcekova S., Meciarova L., Burdova E.K., Katunska J., Kosicanova D., Doroudiani, S., Indoor environmental quality of classrooms and occupants' comfort in a special education school in Slovak Republic. Building and Environment, vol. 120, pp 29-40, 2017.

[12] Wong L.T., Mui K.W., Tsang T.W., An open acceptance model for indoor environmental quality (IEQ). Building and Environment, vol. 142, pp 371-378, 2018.

[13] Kapalo P., Domnita F., Bacotiu C., Podolak M., The influence of occupants’ body mass on carbon dioxide mass flow rate inside a university classroom–case study. International journal of environmental health research, vol. 28(4), pp 432-447, 2018.

[14] Jowkar M., de Dear R., Brusey J., Influence of long-term thermal history on thermal comfort and preference. Energy and Buildings, vol. 210, 109685, 2020.

Section

BIOTECHNOLOGIES

Biotechnology in healthcare
Plants and animal biotechnology
Bioinformatics, biochemistry and biosafety
Bioprocessing of food, food technologies
Biological control of pests
Genetic engineering and molecular diagnostic
Bio-energy production and environmental bioremediation
Biosafety, systems biology and bioethics

COMPREHENSIVE BIOTECHNOLOGICAL APPROACH TO PROCESSING OF PEA FLOUR FOR FOOD AND FODDER PURPOSES

Ph.D. Student Denis Kulikov[1]
Ph.D. Ruzaliya Ulanova[2]
Prof. Dr. Valentina Kolpakova[3]
[1, 3] All-Russian Research Institute for Starch Products – Branch of V.M. Gorbatov Federal Research Center for Food Systems of Russian Academy of Sciences, Russia
[2] S.N. Vinogradsky Institute of Microbiology, Federal Research Center "Fundamental Foundations of Biotechnology", of Russian Academy of Sciences, Moscow, Russia

ABSTRACT

Investigations were carried out to optimize the growth parameters of the symbiosis of cultures of the yeast *Saccharomyces cerevisiae* 121 and the fungus *Geotrichum candidum* 977 on whey waters formed from pea flour as a secondary product in the production of protein concentrates after precipitation of proteins at the isoelectric point. The whey remaining after protein precipitation is bioconverted at optimal parameters of crop growth (pH of the medium, amount of inoculum, temperature) with the formation of microbial plant concentrate (MPC) for feed purposes. Serum cultures assimilated stachyose, glucose, maltose, arabinose, and other pentoses. The mass fraction of protein in the concentrate was 57.90-61.68 % of DS. The composition of MPC obtained from biomass is balanced in essential amino acids with a speed of 107-226 %. The fatty acid composition is represented by 97 % fatty acids and 3 % - esters, aldehydes, ketones with the properties of fragrances, photo stabilizers, odor fixers, preservatives and other compounds. The ratio of the sum of saturated and unsaturated acids is 1:3, the content of cis-isomers is 91.1 %, trans-isomers are 5.1 %, omega-6 fatty acids are 19.73 %. The quality and safety indicators indicated that it is promising for use in the diet of animals.

Keywords: *pea flour, processing, serum, bioconversion, microbial-plant concentrate, amino acid composition, fatty acid composition*

INTRODUCTION

Modern trends in the development of food production indicate that in the coming years, the deficit of protein in human and animal nutrition will not decrease, and the need for new high-quality (dietary) protein sources will increase. The number of hungry people in the world is growing, at the moment it has reached a third of the entire population of the Earth, part of the population is experiencing a deficiency of complete protein [1]. One of the ways to eliminate the deficit is to obtain protein preparations from plant materials. In this case, secondary products of processing raw materials into proteins or starch can be involved in the scheme of processing by the bioconversion method. The biomass of microorganisms can be

used as part of the diets of farm animals to increase their productivity and for human nutrition as new sources of proteins. Known bioconversion products from various types of by-product sources of the food industry and agriculture. Since ancient times, legumes have been used in the diet of people, including those who, for one reason or another, do not eat meat [2], [3]. Of particular interest is one of the traditional leguminous crops for European countries, including Russia, - peas, the use of which makes it possible to create technologies for protein concentrates, flour, isolates and by-products [4]. Information on the processing of secondary products formed from leguminous crops is still limited, despite the interest in this area. Thus, on the basis of a by-product formed during the extraction of pea protein, using filamentous fungi, a food mycoprotein concentrate was synthesized to "replace" meat. Studies were carried out with strains of fungi: *Aspergillus oryzae*, *Fusarium venenatum*, *Monascus purpureus*, *Rhizopus oryzae* fermentation at 35 ± 2 °C for 48 hours. The protein content in the mushroom biomass reached 43.13-59.74 %. It has been shown that the introduction of this process into production will provide about 680 kg of mushroom biomass with 38 % of additional protein for each 1 ton of by-product [5]. We have also proved the possibility of bioconversion of the secondary product (extract) of processing triticale grain into starch together with pea flour, and obtaining a feed concentrate with a mass fraction in% on DS: protein 55.8−75.1, carbohydrates - 18.9−32.83, fat 3.56−13.56, ash 2.05–8.27 [6]. Cultures of microorganisms actively developing on the substrate were selected, and a symbiotic starter culture from the fungus was compiled from them. *Geotrichum candidum* 977 and yeast *Saccharomyces cerevisiae* 121, providing the growth of biomass in a carbohydrate, nitrogen-containing medium. The serum formed after the isolation of concentrated proteins from the composition with pea flour was benign for culture media of microbiological synthesis with fungus and yeast. We also obtained preliminary positive results with this composition of microorganisms using serum formed during the isolation of proteins from chickpea [7] and pea [8] grains according to the scheme using enzyme preparations without optimization of parameters.

The aim of this work was to improve the process of bioconversion of grain whey, formed as a secondary product of the processing of flour from pea grain into protein concentrate, by the symbiosis of the yeast *S. cerevisiae* and the fungus *G. candidum* 977, by optimizing the growth parameters of microorganisms with the subsequent characterization of the feed microbial-plant concentrate.

MATERIALS AND METHODS

The objects used were pea whey made from flour obtained from Yamal grain with 11.6 % moisture and mass fraction, % of DS: protein (Nx6.25) - 25.7; ash - 2.67; fat - 1.46; starch - 51.50; carbohydrates - 18.76. Enzyme preparations from Novozymes A/S (Denmark) were used to isolate protein concentrates and the secondary product of grain whey from flour: Shearzym 500 L, Viscoferm L, Fungamyl 800 L, AMG 300 L 2500, and Distizym Protacid from Erbslon. The yeast *Saccharomyces cerevisiae* 121 from the collection of the Institute of Microbiology named after S.N. Vinogradskiy and a new strain of the fungus *Geotrichum*

candidum 977, the phylogenetic position of which was determined jointly with the State Research Institute of Genetics (Russia) [9].

The amount of protein in the solution was determined by the Lowry method, nitrogenous substances in flour and in MPC - by the Kjeldahl method (GOST 10846-91); moisture - GOST 13586.5-93; ash - GOST 10847-2019; fat - GOST 29033-91, carbohydrates - by the difference between 100 % and the sum of the remaining components. The amino acid composition of MPC was determined on an L-8800 chromatograph (Hitachi, Japan) in the standard mode of analysis of protein hydrolysates with a sulfonated styrene-divinylbenzene copolymer and a stepwise gradient of Na-citrate buffer solution with increasing pH and molarity (GOST 32195-2013). When calculating the rate of essential amino acids, we used the FAO / WHO standard protein scale (2011) [10]. The carbohydrate composition of serum and extracts was investigated on a Shimadzu GCMS 2010 gas chromatograph (Japan), the fatty acid composition of MPC lipids - on a chromatograph with a Simadzu GCMS-QP 2010 Ultra mass detector at 120°C, an injector - 200°C; interface – 205°C, detector – 200 °C on an SLB-IL82 column (30 m, 0.20 mkm, d = 0.25 mm) with a carrier helium at a flow rate of 35.6 cm / s, flow division 1:10. The gradient mode varied from 120°C to 260°C at a rate of 5 °C/min for 2 minutes. Lipids were isolated according to the Folch method, evaporated on a rotary evaporator, dissolved in chloroform, hydrochloric acid methanol (Supelco Methanolic-HCl 0.5 N) was added, sealed in a vial and heated at 90 °C for 1 h. Museum cultures from wort agar were subcultured into a test tube with serum remaining after protein isolation, and cultured for 24 h. Then the culture was subcultured into 300 cm^3 flasks with 50 cm^3 nutrient medium, grown on a shaker at a rotation speed of 150 min^{-1} and a temperature of 27±1°C for 48 hours. Serum with pH 6.0 - 6.5 was used to prepare nutrient media. The serum was sterilized at a pressure of 0.1 MPa, cooled, a suspension of cultures was introduced into the substrate and grown at different temperatures for 24 - 48 h with stirring on a rocking chair at a rate of 150 min-1. The suspension was inactivated at 95 ± 5°C for 10 - 15 min and cooled for 10 - 15 min at a temperature of 22 ± 2°C. The biomass was separated from the culture liquid by centrifugation at 4000 min – 1 for 10 min. The biomass (KMPK-1) and the biomass with the culture liquid (KMPK-2) were dried on a Hochvacuum HVDTG-50 lyophilizer (Germany) in a vacuum at -80 °C.

The experimental data were processed in the TableCurve 2D 5.1, TableCurve 3D 4.0, Mathematica 10.3, and Statistica 10 programs. The confidence interval of the arithmetic means was calculated according to the significance level p = 0.05.

RESULTS AND DISCUSSION

The extraction of proteins from the pea suspension was carried out by a biotechnological method using hydrolytic enzyme preparations (EPs) of various actions (cellulases, xylanases, amylases, proteases) in stages. The scheme and parameters of protein extraction for each stage are presented in [8]. The hydromodule 1:15 was used, the EP concentration was 1.5 %/g of protein, the fermentation time was 4 hours, the reaction temperature was 55 ± 1°C, and the stirring speed was 200 min^{-1}. After precipitation of the protein at the isoelectric point and centrifugation of the suspension, serum was formed, which was subjected to

bioconversion to synthesize feed protein preparations. The mass fraction of dry substances (DM) in pea whey averaged 3.5±0.5 %, nitrogenous substances (Nx6.25) - 28.35 ± 0.8 %, true proteins - 11.06±0.23 %, in% of DS. Table 1 shows that in the process of protein extraction from flour with amylases, cytases and hemicellulases, the amount of high molecular weight carbohydrates in the dissolved part after the 2nd stage decreased by 2 %, tri-, tetra-disaccharides - almost 2 times, and the amount of glucose, on the contrary, - increased by 36 %, fructose, galactose, xylose - 3 times.

Table 1. *The content of carbohydrates by stages of protein extraction,% of the total content in flour*

Product	HMWC*	Stachyose Raffinose	Sucrose, maltose	Glucose	Fructose, galactose, xylose	Arabinose
Extract Stage 1	23.43	23.93	0+31.81	10.11	8.40	2.31
Extract Stage 2	21.12	11.95	6.70+12.33	20.48	24.79	2.64
Extract Stage 1	14.77	20.27	8.99+ 10.91	13.89	28.39	2.78
Serum	32.01	26.38	0+14.98	9.66	12.06	4.90

Note: HMWC – High molecular weight compounds*

At the third stage of extraction, under the influence of proteases, the share of HMWC decreased by 37 %, disaccharides - by 38 %, but the amount of monosaccharides (fructose galactose, xylose) increased 3.4 times. Thus, the nutrient medium for the synthesis of substances by microorganisms has been enriched with assimilable low molecular weight carbohydrates.

To determine the optimal conditions for increasing the productivity of the yeast *S. cerevisiae* and the fungus *G. candidum* 977, we studied the effect of the substrate pH, temperature, and the amount of inoculum on biomass synthesis for 3 days. For this, the matrix of the experiment was compiled (Table 2), the results of which were processed in the Statistica 12.5 program.

Table 2. *Matrix for planning the experiment of growth of cultures on serum*

No.	pH	Temperature, °C	Seed amount, %	Mass fraction of biomass, g/dm^3
1	5	20	3	0.611
2	5	25	2	0.816
3	5	30	1	0.757
4	5	35	4	0.570
5	6	20	4	0.776
6	6	25	3	0.774
7	6	30	2	0.711
8	6	35	1	0.573
9	7	20	1	0.791
10	7	25	4	0.811
11	7	30	3	0.708
12	7	35	2	0.413
13	8	20	2	0.616
14	8	25	1	0.751
15	8	30	4	0.553
16	8	35	3	0.313

Table 3 shows the values of the regression coefficients and the level of significance p. The equation for the dependence of the mass fraction of biomass md, g/dm^3 on influencing factors was as follows:

$$md = -2.94 + 0.544 \cdot pH - 0.0356 \cdot pH^2 + 0.181 \cdot t - 0.003 \cdot t^2$$
$$-0.147 \cdot cm + 0.0276 \cdot cm^2 - 0.00447 \cdot pH \cdot t$$

All coefficients of the equation are significant ($p \leq 0.05$) (Table 3). An adequate description of the data was indicated by the results of the experiment, the data of the calculation by the equation, their absolute error (Table 4) and the correlation graph $R = 0.9644$ (Figure 1).

Table 3. *Regression coefficients and significance level p*

Factor	Regr. Coefficients; Var.:md; R-sqr=,9644; Adj: 93325 (Spreadsheet1) 3 factors, 1 Blocks, 16 Runs; MS Residual=,0014517 DV: md					
	Regression Coeff.	Std.Err.	T (8)	p	-95, % Cnf.Limt	+95, % Cnf.Limt
Mean/Interc.	-2,93662	0,593210	-4,95040	0,001120	-4,30457	-1,56868
(1) pH(L)	0,54434	0,133016	4,09228	0,003475	0,23760	0,85107
pH(Q)	-0,03563	0,009525	-3,74006	0,005705	-0,05759	-0,01366
(2)t(L)	0,18057	0,023871	7,56456	0,000065	0,12553	0,23562
t(Q)	-0,00304	0,000381	-7,99191	0,000044	-0,00392	-0,00217
(3)cm(L)	-0,14700	0,054163	-2,71404	0,026492	-0,27190	-0,02210
cm(Q)	0,02756	0,010471	2,63238	0,030067	0,00342	0,05171
1L by 2L	-0,00447	0,001739	-2,57322	0,032962	-0,00849	-0,00046

Table 4. *Experimental (1), calculated (2) data and absolute error*

No.	1	2	Absolute error	No.	1	2	Absolute error
1	0.611	0.647450	-0.036450	9	0.791	0.775625	0.015375
2	0.816	0.762500	0.053500	10	0.811	0.809175	0.001825
3	0.757	0.780425	-0.023425	11	11	0.708	0.672100
4	0.570	0.554225	0.015775	12	12	0.413	0.437900
5	0.776	0.756350	0.019650	13	0.616	0.631775	-0.015775
6	0.774	0.793900	-0.019900	14	0.751	0.734825	0.016175
7	0.711	0.734325	-0.023325	15	0.553	0.593750	-0.040750
8	0.573	0.577625	-0.004625	16	0.313	0.282050	0.030950

The equation made it possible to determine the dependence of the mass fraction of biomass *md* on the influencing factors and to determine their values for its maximum yield. Figure 2 shows, as an example, the regularity of the change in biomass from the pH value and the temperature of the environment C^0 with the amount of seed $cm = 2\%$.

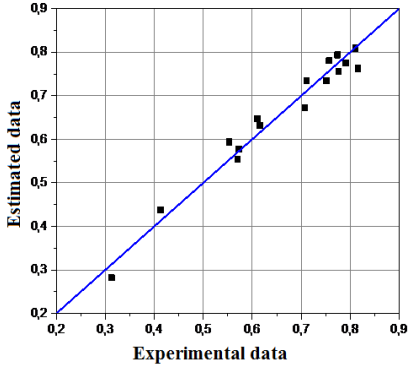

Fig. 1*. Correlation graph*

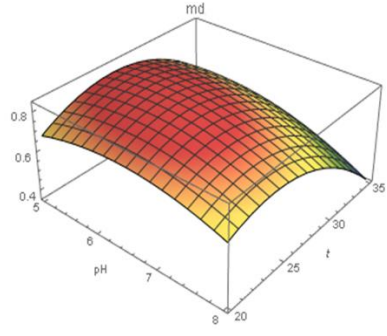

Fig. 2. *Dependence of the mass fraction of biomass on pH and temperature*

From the equation in the Mathematica 12.1 program, the values of the factors for the maximum biomass yield (0.88 g/dm3) are determined: pH of the medium - 6.03, *C*=25.7°, seed quantity *cm*=4%. At lower pH values (4.5-5.0) or higher (7.5-8.0), the growth of microorganisms slowed down. Cultivation of symbiosis of cultures had a positive effect on the accumulation of biomass and protein; for the symbiosis of cultures, the amount of protein in the biomass was 61.68% of DS (Table 5), while from biomass with the culture liquid - 57.90%.

Table 5. *Chemical composition of MPC from biomass on serum*

Moisture, %	Mass fraction, % of DS			
	Protein (Nx6.25)	Ash	Lipids	Carbohydrates
6.81±0.4	61.68±0.47	8.60±0.03	8.31±0.36	21.41±0.55

In the process of synthesis, stachyose, maltose, arabinose were completely absorbed from serum, more than half - glucose and almost all other pentoses (Table 6). The assimilation of stachyose by these yeasts corresponded to the literature data. On the other hand, in the MPC, the number of HMWC has doubled, the nature of which has to be deciphered.

Table 6. *Carbohydrate composition of pea serum (1) and MPC (2),% of the total*

Product	HMWC	Stachyose	Raffinose	Sucrose, maltose	Glucose	Fructose, galactose, xylose	Arabinose
1	32.01	26.38	0	0+14.98	9.66	12.06	4.90
2	68.83	0	26.21	0	3.87	1.09	0

The amino acid composition of MPC from biomass and from biomass with culture liquid is mostly represented by glutamic, aspartic acids, glycine, alanine, lysine (Figure 3).

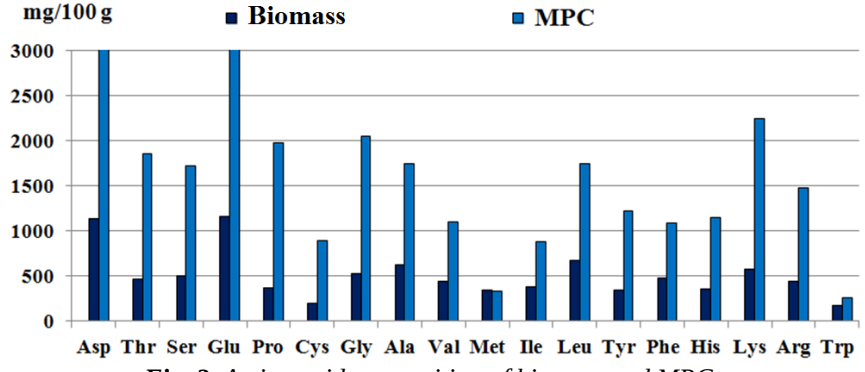

Fig. 3. *Amino acid composition of biomass and MPC*

The amino acid rate of biomass of cultures for all essential acids was 107-226%, for MPC with a culture liquid it was high for histidine, lysine, threonine, sulfur-containing amino acids (81-128%), and for valine, leucine, isoleucine it was not higher 48%. The fatty acid composition (FAC) of MPC is represented by 30 components, among which 97 % are fatty acids that are part of animal fats, vegetable oils, marine organisms, 3 % are esters, aldehydes, ketones with the properties of aromatizing essential oils, metabolites of the human body, photo stabilizer, odor fixatives, preservatives and other compounds. The ratio of the sum of saturated (23.51 %) and unsaturated fatty acids (71.67 %) is 1:3, the content of cis isomers is 91.1 %, trans isomers - 5.1 %, omega-6 fatty acids (linoleic) -

19,73 %. MPC did not have a negative effect on the vital parameters of experimental rats [11], which indicated its safety and prospects for use.

CONCLUSION

The optimization of the process of biotransformation of the chemical composition of the secondary product of pea flour processing into food protein concentrate (serum) into a microbial-plant concentrate by a symbiosis of cultures of the fungus *G. candidum* 977 and yeast *S. cerevisiae* 121 has been carried out. adequately describing the dependence of the crop biomass yield on technological parameters: pH of the medium, temperature and amount of seed. The microbial-plant concentrate from the biomass of cultures with a protein mass fraction of 57.90 and 61.68 % of DS was biologically valuable (the rate of essential amino acids was 107-226 %), had a high biological efficiency of lipids: out of 30 types of fatty acids, 97 % were acids included in composition of animal fats, vegetable oils and marine organisms. The ratio of saturated (23.51 %) and unsaturated fatty acids (71.67 %) was 1:3, the content of trans isomers was 5.1%, and omega-6 fatty acids (linoleic) were 19.73 %. The use of the concentrate is promising for animal diets.

REFERENCES

[1] World Health Organization, Food and Agriculture Organization of the United Nations. Driving commitment for nutrition within the UN Decade of Action on Nutrition // WHO/NMH/NHD/17.11, FAO/CA1340EN/1/09.18., 2018. 12 p.

[2] Söderberg J. Functional properties of legume proteins compared to egg proteins and their potential as egg replacers in vegan food // Swedish University of Agricultural Sciences, Uppsala, Sweden Publication, 2013. 37 p.

[3] Singhal A., Karaca A.C., Tyler R., Nickerson M. Pulse Proteins: from processing to structure-function relationships // Grain Legumes, 2016. DOI: 10.5772/64020

[4] Pruter T. Alternative crops for a traditional potato starch producer *69th Starch Convention in Detmold, Germany,* 2018. 35 p.

[5] Pedro F., Souza Filho, Ramkumar B. Nair, Dan Andersson, Patrik R. Lennartsson, Mohammad J. Taherzadeh. Vegan-mycoprotein concentrate from pea-processing industry byproduct using edible filamentous fungi // Fungal Biology and Biotechnology, 2018. No. 5. P. 5-8.

[6] Kolpakova V.V., Ulanova R.V., Kulikov D.S. and al. Grain composites with complementary amino acid composition for food and feed purposes, Food Engineering and Technology, 2019. Vol. 2 (49). P. 301-311. DOI: 10.21603/2074-9414-2019-2-301-311 [In Russian]

[7] Kulikov D., Kolpakova V., Slozhenkina M., Ulanova R., Chumikina L. Biotechnological process for producing protein products from chickpeas with a high biological value // 20th International Scientific Multidisciplinary Conference on Earth and Planetary Sciences SGEM 2020 Conference Period: 18-24 August,

2020 Albena, Bulgaria. Vol. 20, Bk. 6.1, P. 175-182. doi: 10.5593/sgem2020/6.1/s25.023

[8] Kulikov D.S., Kolpakova V.V., Ulanova R.V, Chumikina L.V., Bessonov V.V. Biological processing of pea grain to obtain food and feed protein concentrates // Biotechnology, 2020. Vol. 36. No 4. P. 49-58. DOI: 10.21519/0234-2758-2020-36-4-49-58 [In Russian]

[9] Kolpakova V.V., Ulanova R.V., Kulikov D.S. Modification of secondary products of processing triticale into starch with a new strain of the fungus *Geotrichium candidum* // E3s Web of Conference, 2020. Vol. 224, Article number: 04033. TPACEE-2020 10.1051/e3sconf/202022404033

[10] Dietary protein quality evaluation in human nutrition: Report of an FAO Expert Consultation. Rome: FAO, 2013. 66 p.

[11] Kolpakova V., Kulikov D., Ulanova R., Lukin N., Gaivoronskaya I. Bioconversion of cereal serum – a secondary product for producing protein concentrates from pea and chickpeas. GEOLINKS International Conference on geosciences. Conference proceedings. 23-25 March, 2020, Imperial Hotel, Plovdiv, Bulgaria, Book 1. Vol. 2. P. 59-67.

CONSIDERATIONS ON SARS-COV-2 DIAGNOSIS IN THE LABORATORY OF UNIVERSITY EMERGENCY CLINICAL HOSPITAL OF CONSTANTA

Assoc. Prof. Dr. Ramona Stoicescu[1]
M.D. Razvan-Alexandru Stoicescu[2]
Ph.D. Student Codrin Gheorghe[3]
Lecturer Dr. Adina Honcea[4]
Lecturer Dr. Iulian Bratu[5]
Assoc. Prof. Dr. Verginica Schroder[6]
[1, 4, 5, 6] Ovidius University of Constanța, Faculty of Pharmacy, Constanta, Romania
[3] Ovidius University of Constanta, Faculty of Medicine, Constanta, Romania
[1] Emergency Clinical County Hospital, Constanta, Romania
[2] Emergency Clinical Hospital, Bucharest, Romania

ABSTRACT

Coronaviruses are members of the Coronaviridae family. They are enveloped, non-segmented, positive-sense, single-stranded RNA viruses. Their genome size is about 30 kilobases (kb) which consist, at the 5' end, of non-structural open reading frames (ORFs: ORF1a, ORF 1b) which code for 16 non structural proteins, and at the 3' end the genes which code for four structural proteins including membrane (M), envelope (E), spike (S), and nucleocapsid (N) proteins. Due to the rapid spread of COVID-19, a reliable detection method is needed for patient diagnosis especially in the early stages of the disease. WHO has recommended nucleic acid amplification tests such as real-time reverse transcription-polymerase chain reaction (RT-PCR). The assay detects three SARS-CoV-2 RNA targets: the envelope (E) gene, the nucleocapsid (N) gene and a region of the open reading frame (ORF1) of the RNA-dependent RNA polymerase (RdRp) gene from SARS-CoV-2 virus isolate Wuhan-Hu-1. Our study was made in the first 3 months of the year 2021 using the real-time RT PCR results obtained in the Cellular Biology ward of the University Emergency Clinical Hospital. In our lab we are testing the inpatients from the hospital wards (Neurology, Pediatrics, Surgery, Internal medicine, ICU, Cardiology, etc.); we are also testing the outpatients from Dialysis and Oncology, 2 days prior to their therapy; we also test the health care personnel. The number of tests we performed was: in January 1456, with 399 positive results (27.4%), 33 deaths; in February 1273 tests, 221 positive (17.36%), 16 deaths; in March 1471 tests, 373 positive (25.36%), 37 deceased.

Keywords: *SARS-CoV-2, real-time-RT PCR, envelope, nucleocapsid, RdRp genes*

INTRODUCTION

Coronaviruses are a group of enveloped viruses which can cause diseases in birds and mammals, including humans [1].

Seven coronaviruses have been identified so far which can cause mild to lethal respiratory tract infections in humans [1].

HCoV-229E, HCoV-OC43, HCoV-NL63, and HCoV-HKU1 are the 4 low risk members of *Coronaviridae* family. They generally produce mild upper respiratory tract infections representing up to 30% of cases of common colds in adults. In immunocompromised patients, in infants or elderly people these Corononaviruses can also produce lower respiratory tract infections.

Coronaviruses which are more dangerous and can cause severe infections are SARS-CoV or SARS-CoV1 (Severe acute respiratory syndrome coronavirus), MERS-CoV (Middle East Respiratory Syndrome coronavirus) and SARS-CoV-2 also known as 2019-nCoV [2].

Coronaviruses are enveloped, non-segmented, positive-sense, single-stranded RNA viruses. Their genome consists of non-structural open reading frames (ORFs) and four structural proteins including membrane (M), envelope (E), spike (S), and nucleocapsid (N) proteins [3].

Their name derives from corona appearance, given by club-like spikes that project from their surface [1].

MATERIALS AND METHODS

Diagnostic tests have been considered as the main alternative for the control of coronavirus disease (COVID-19) as a correct diagnosis allows correct decisions.

The tests can be organized into two main categories: virological diagnosis recommended for the initial detection of the virus, and serological tests, recommended for assessing the disease progression.

Virological diagnosis comprises 3 categories of laboratory detection methods for human coronaviruses: RNA amplification-based detection methods (including RT-PCR, real-time RT-PCR and isothermal amplification-based methods/ nucleic acid-based tests), viral RNA biosensors and whole virus or viral proteins detection assays [1].

The polymerase chain reaction (PCR) technique can synthesize a large number of a specific DNA sequence. It is a three-step cycle that consists of denaturation, annealing and extension [4].

The reverse transcription PCR (RT-PCR) technique was developed for specific RNA detection. The target RNA is converted to cDNA by the reverse transcriptase enzyme. The obtained cDNA is amplified by PCR [4].

Real-time RT-PCR or quantitative RT-PCR (qRT-PCR) is a technique in which amplification and detection steps have been combined together to decrease the detection time and increase the sensitivity and specificity of the method [5].

Serologic tests detect the immune response of the infected patients. Specific IgM starts to develop after 7 days and becomes detectable around 10 days after the infection onset. Specific IgG productions start around 10-14 days after infection and are detectable around day 21 and are maintained for a high level for a longer period of time [6].

A reliable detection method is needed for patient diagnosis especially in the early stages of the disease.WHO has recommended nucleic acid amplification tests (NAAT), such as reverse transcription-polymerase chain reaction (RT-PCR) [7]

In our Cellular Biology Laboratory at the University Emergency Clinical Hospital Constanta, we use real-time RT PCR for SARS-CoV-2 diagnosis. The specimens are represented by oro/nasopharyngeal swabs.

Detection of infection by SARS-CoV-2 relies on the efficient detection of the viral genome using RT PCR.

The assay detects three SARS-CoV-2 RNA targets: the envelope (E) gene, the nucleocapsid (N) gene and a region of the open reading frame (ORF1) of the RNA dependent RNA polymerase (RdRp) gene from SARS-CoV-2 virus isolate Wuhan-Hu-1.

First step is represented by RNA extraction from samples. RNA extraction is a key pre-analytical step in RT-PCR, achieved using commercial kits.

Our laboratory is equipped with 3 extractors: RBC Bioscience using MAGCore automated nucleic acid extraction kit, 1-16 samples per run; Bioneer EXI PREP 16DX using Exi Prep viral RNA kit, 8-16 samples per run, as a multiple of 8; Bioneer EP 48 DX-BXA 057 using Exi prep 48 Viral RNA kit, 8-48 samples per run as a multiple of 8.

Once RNA is extracted the eluates are amplified. The target RNA is converted to cDNA by the reverse transcriptase enzyme. The obtained cDNA is amplified by PCR.

Our lab is equipped with 2 amplifiers: Bioneer Exicycler 96 using Accupower SARS-CoV-2 using Multiplex Real-time RT PCR amplification kit, and Biorad CFX 96 Real-time System using Primer Design/ Gensig amplification kit.

Amplification takes place in a thermal cycler. Each PCR cycle theoretically doubles the amount of targeted sequence in the reaction. Each cycle of PCR includes steps for template denaturation (94°C), primer annealing (40–60°C) and primer extension (70–74°C).

To apply PCR to the study of RNA, the RNA sample must first be converted to cDNA to provide the necessary DNA template for the thermostable polymerase. This process is called reverse transcription (RT), hence the name RT-PCR.

Reverse transcriptases (RTs) are RNA-directed DNA polymerases. RTs catalyzes the synthesis of a DNA copy (cDNA) of the target RNA molecules using a reverse transcription primer, dNTPs (deoxyribonucleotide triphosphate), and Mg^{2+} or Mn^{2+} as a cofactor [8].

RESULTS AND DISCUSSIONS

Our study was made in the first 3 months of year the 2021 using the real-time RT PCR. The laboratory is testing the inpatients from the hospital wards (Neurology, Pediatrics, Surgery, Internal medicine, ICU, Cardiology, etc); the outpatients from Dialysis and Oncology, 2 days prior to their therapy; the hospital employees (health care personnel, front desk medical clerks, administrative and technical staff, hospital housekeepers).

The number of tested patients were:

In January 1456, with 399 positive results (27.4%)

In February 1273 tests, 221 positive (17.36%)

In March 1471 tests, 373 positive (25.36%).

According to hospital statistics the number of deceased patients in University Clinical Emergency Hospital Constanta due to Covid 19 infections were: 33 deceased patients in January, 16 deceased patients in February, 37 deceased patients in March.

The distribution of positive cases with relation to the month and the hospital wards (for inpatients, outpatients) and hospital staff workplace can be seen in table 1.

Table 1. *Positive cases*

	January	January	February	February	March	March
Ward	Health care personnel	Patients	Health care personnel	Patients	Health care personnel	Patients
Emergency ward	2	241	2	165	2	239
Hemodialysis	0	4	0	1	1	7
Oncology	1	3	0	2	0	7
Internal medicine 1	2	1	0	5	2	17
Internal medicine 2	2	14	0	0	1	12
Nephrology	0	7	0	6	0	3
Neurology	0	8	0	1	0	6
Gastroenterology	1	2	0	3	3	8
ICU	2	11	0	6	0	15
Cardiology	2	12	0	0	0	7
Orthopedics	3	4	2	0	2	0

Op theater orthopedics	1	0	0	0	1	0
Cardiovascular surgery	4	3	0	1	4	5
Surgery ward 2	1	0	0	0	0	0
Surgery ward 1	1	10	1	6	2	4
Urology	0	0	1	2	0	0
New born	1	0	0	1	0	0
Ob/ gynecology ward 2	0	0	0	1	1	0
Ob/gynecology ward 1	0	1	1	1	0	0
Neurosurgery ward	2	5	2	1	2	2
Ophthalmology	0	0	0	0	0	1
Otorhinolaryngology (ORL)	1	2	0	0	0	0
Pediatrics	0	15	0	1	0	4
Pediatric surgery	1	0	0	0	1	1
Psychiatry	6	4	0	0	0	2
Osteoarticular tuberculosis (OATB) ward	0	2	0	0	0	1
Palliative care	0	1	0	0	0	2
Physical and Rehabilitation Medicine Sanatorium	0	1	1	2	1	1
Dermatology	0	3	0	0	0	0
Pneumoftisiology	1	2	0	2	0	1
Physical and Rehabilitation Medicine	4	1	1	0	0	0
Pathology	1	0	0	0	0	0
Functional exploration dep.	0	0	0	0	1	0
Radiotherapy	0	0	0	1	0	0
Ambulatory	0	0	2	0	0	0
Hospital Technical staff	2	0	0	0	0	0
Hospital administration	0	0	0	0	1	0
Medical front desk clerk	1	0	0	0	0	0
Center for mental health	0	0	0	0	1	0
Hospital housekeeper staff	0	0	0	0	2	0
TOTAL	**42**	**357**	**13**	**208**	**28**	**345**

During 3 months there were tested and confirmed positive a number of 993 patients and 83 health care personnel and other professional workers in the hospital.

CONCLUSION

The University Emergency Clinical Hospital is following WHO recommendation of using nucleic acid amplification tests (NAAT)/ reverse

transcription-polymerase chain reaction (RT-PCR) for diagnosing SARS-Co-V-2 infection (gold standard)

The Hospital's Cellular Biology Laboratory performs real-time RT PCR for inpatients, outpatients from Haemodialysis and Oncology and medical and auxiliary staff.

During 3 months were performed 4200 RT-PCR tests with 993 positive tests for patients and 83 positive tests for hospital employees.

The positivity rate for all tested persons was 27.4% in January, 17.36% in February and 25.36% in March.

The highest positivity rate was for patients from the Emergency ward, representing 60.4% in January, 74.66% in February, 64.07% in March out of all performed tests.

The highest number of positive cases among health care personnel in January was in Psychiatry ward 6 cases, Cardiovascular surgery 4 cases, Physical and Rehabilitation Medicine 4 cases, Orthopedics 3 cases; in February: Emergency ward 2 cases, Orthopedics 2 cases; in March: 4 cases in Cardiovascular surgery, 3 cases Gastroenterology, 2 cases in the Emergency ward, 2 cases in Surgery ward number 2.

The number of infected health care workers was small compared with the number of infected patients due to strict infection control measures (protection equipment, hand hygiene, disinfection) and vaccination campaign which started in December 2020.

REFERENCES

[1] Ehsan Shabani, Sayeh Dowlatshahi, and Mohammad J. Abdekhodaie, Laboratory detection methods for the human coronaviruses https://www.ncbi.nlm.nih.gov/pmc/articles/PMC7520381/

[2] Ding X. Liu, Jia Q. Liang, and To S. Fung, Human Coronavirus-229E, -OC43, -NL63, and -HKU1 (*Coronaviridae*), Encyclopedia of Virology. 2021 : 428–440.,Published online 2021 Mar 1. doi: 10.1016/B978-0-12-809633-8.21501-X, PMCID: PMC7204879

[3] Chen Y, Liu Q, Guo D. Emerging coronaviruses: genome structure, replication, and pathogenesis. *J Med Virol.* 2020;92:418–423. doi: 10.1002/jmv.25681. [PMC free article] [PubMed] [CrossRef] [Google Scholar]

[4] Wei Zhang,Rong-Hui Du, Bei Li, Xiao-Shuang Zheng, Xing-Lou Yang, Ben Hu, Yan-Yi Wang, Geng-Fu Xiao, Bing Yan, Zheng-Li Shi,and Peng Zhou, Molecular and serological investigation of 2019-nCoV infected patients: implication of multiple shedding routes Emerg Microbes Infect. 2020; 9(1): 386–389. Published online 2020 Feb 17. doi: 10.1080/22221751.2020.1729071

[5] Alireza Tahamtan and Abdollah Ardebili. Expert Rev Mol Diagn. Real-time RT-PCR in COVID-19 detection, Published online 2020 Apr 22. doi: 10.1080/14737159.2020.1757437

[6] Hongyan Hou, Ting Wang, Bo Zhang, Ying Luo, Lie Mao, Feng Wang, Shiji Wuand Ziyong Sun Detection of IgM and IgG antibodies in patients with coronavirus disease 2019, Clin Trans Immunology. 2020; 9(5): e1136. Published online 2020 May 6. doi: 10.1002/cti2.1136PMCID: PMC7202656, PMID: 32382418

[7] World Health Organization (2020) Laboratory testing for 2019 novel coronavirus (2019-nCoV) in suspected human cases

[8] https://www.promega.ro/resources/guides/nucleic-acid-analysis/pcr-amplification/

DETERMINATION OF POLYPHENOLIC COMPOUNDS OF *LYSIMACHIA NUMMULARIA* L.

Suciu Felicia[1]
Roșca Adrian Cosmin[2]
Lupu Carmen[3]
Popescu Antoanela[4]
Badea Victoria[5]
[1, 2, 3, 4] Faculty of Pharmacy, Ovidius University of Constanța, Romania
[5] Faculty of Dentistry, Ovidius University of Constanța, Romania

ABSTRACT

The history of medicinal plants is associated with the evolution of civilization.

In all regions of the world, the history of nations shows that these plants have always occupied an important place in medicine, in cosmetic products, and culinary preparations.

The paper aims to determine the total polyphenols in different parts of the species *Lysimachia nummularia* L.

In our study, we focused on the extraction of polyphenolic compounds in different solvents.

The solvents used in the extraction were: 40% ethanol, concentrated methanol, in water.

The total polyphenol content was determined by spectrophotometric methods, a method from the European Pharmacopoeia 10.0, with minor modifications.

The total polyphenol content of different extracts varied depending on the extraction process.

Different parts of the plant and different solvents were used in the determinations carried out to establish the optimal extraction method for the organs of *Lysimachia nummularia* L.

Keywords: *Lysimachia, polyphenolic compounds, active principle, spectrophotometry, extracts*

INTRODUCTION

Polyphenols are a large family of naturally occurring organic compounds characterized by multiples of phenol units, they include flavonoids, tannins, anthocyanins, proanthocyanins, stilbenoids, some of which have been used historically as dyes and for tanning garments [1], [2]. Polyphenolic compounds are abundant in many plants and structurally diverse, they are the most important active principles with antioxidant action [3].

From the specialized literature it is known the presence of phenolic compounds in the species *Lysimachia nummularia* L. [4].

Thus, in various studies, appreciable amounts of active principles was determined in all plant organs as follows: polyphenolic compounds, 1.77-3.00 (g / 100g expressed in pyrogallol), flavonosides 0.36-1.77 (g / 100g, expressed in hyperosides), tannins 0.97 -1.95 (g / 100g), hydroxycinnamic acids 0.63-1.25 (g / 100g, expressed as rosmarinic acid) [5].

The highest amount of polyphenols was found for *Lysimachia vulgaris* L. (76.122±0.35 mg/g) and also the content of flavonoids (26.42±1.3mg/g) [6].

Different hungarian samples of *Lysimachia nummularia* L. and *Lysimachia vulgaris* harvested in early and late flowering stage showed the highest total polyphenolic content of these two species (34.2±0.15mg/g and 30.0±0.12mg/g respectively) [7].

Lysimachia nummularia L. is a species of the *Primulaceae* family, known for its antioxidant properties correlated with the content in polyphenolic compounds [8].

MATERIALS AND METHODS

Lysimachia nummularia L., were collected in July 2020, from the edge of Lake Tău-Brazi in the Roșia Montană area.

The determination of total polyphenols was made on plant products obtained from the species *Lysimachia nummularia* L.: *Lysimachiae radix, Lysimachiae herba* and *Lysimachiae flores*.

The vegetable products were obtained from the species *Lysimachia nummularia* L. after drying and sorting and then crushing them.

Solutions to be analyzed: The vegetable products (three samples) were refluxed for 30 minutes with 150 mL of solvent, the quantities listed in Table I. For the vegetal product *Lysimachiae flores*, smaller amounts of vegetal product were used due to the fact that the flowers were collected in smaller quantities.

Table 1. *Working protocol*

Sample	Vegetal products	Solvent	The amount of vegetal product (g)	The amount of vegetal product (g)	The amount of vegetal product (g)
1.	*Lysimachiae herba*	Ethanol 40% (v/v)	1,0233	1,0021	1,0452
2.	*Lysimachiae herba*	Ethanol 96º	1,0494	1,0693	0,9965
3.	*Lysimachiae herba*	Water	1,0534	1,0237	1,0005
4.	*Lysimachiae radix*	Ethanol 40% (v/v)	1,1097	1,0025	1,0597
5.	*Lysimachiae radix*	Ethanol 96º	1,0390	1,0889	1,0875
6.	*Lysimachiae radix*	Water	1,2066	1,0058	1,1052
7.	*Lysimachiae flores*	Ethanol 40% (v/v)	0,2052	0,2144	0,2311
8.	*Lysimachiae flores*	Ethanol 96º	0,200	0,210	0,2245
9.	*Lysimachiae flores*	Water	0,2349 dried vegetal product	0,2233 dried vegetal product	0,2147 dried vegetal product

The spectrophotometric method was used in this study for the development of the analytical procedure for assessing TPC (total polyphenolic content) by Folin-Ciocâlteu method. The used method is based on the general procedure recommended by the European Pharmacopoeia (European Pharmacopoeia 2020) [9] for the determination of total tannins with slight modifications.

The solutions were filtered through a filter material in 250 mL volumetric flasks. The solutions were made up to the mark by washing the vegetable products with the solvent used (solution A).

In 25 mL volumetric flasks were added 5 mL of solution A (all solutions), filtered through filter paper, and made up to the mark with water (solution B).

Exceptions were samples 7, 8 and 9 which were not diluted, further used in this form.

We put 2 mL of solution B (for samples 1-6), and 2 mL of solution A (for samples 7-9) were added to 25 mL flasks, over which 1 mL of Folin-Ciocâlteu reagent, 10 mL, was added water and Na_2CO_3 290g / L at 25 mL. After the stage, a blue coloration has formed. The samples were left to stand for 30 minutes and the

absorbances at the wavelength λ = 760 nm were read, using water as the compensation liquid.

The spectrophotometric determination was performed on a Jasco V650 spectrophotometer.

Pyrogallol standard. In a 100 mL volumetric flask 50 mg of pyrogallol were brought and dissolved in 50 mL of water. It was then filled to the brim with water (stock solution). In a 100 mL volumetric flask, dilute 5 mL of the pyrogalol stock solution with water and makeup to the mark with the same solvent (dilute pyrogallol solution). In a 25 mL volumetric flask, 2 mL of the dilute pyrogallol solution was added to which was added 1 mL of Folin-Ciocâlteu reagent, 10 mL of water and 292 g / L Na_2CO_3 at 25 mL. A blue coloration has formed. It was left to stand for 30 minutes and the absorbance (A2) was read at the wavelength λ = 760 nm using water as the compensating liquid.

Pyrogallol was purchased from Sigma-Aldrich and Folin-Ciocalteau reagent from Merck (Darmstadt, Germany).

***Table. 2**. Determination of total polyphenols. Working protocol*

Sample	**Solution**	**Folin Ciocâlteu reagent**	**Water**	**Sodium carbonate 290g/L**	**Absorbance** λ = 760 nm
1.1	2 mL sol. B	1 mL	10 mL	la 25 mL	0,4350
1.2	2 mL sol. B	1 mL	10 mL	la 25 mL	0,4145
1.3	2 mL sol. B	1 mL	10 mL	la 25 mL	0,4449
2.1	2 mL sol. B	1 mL	10 mL	la 25 mL	0,2001
2.2	2 mL sol. B	1 mL	10 mL	la 25 mL	0,2563
2.3	2 mL sol. B	1 mL	10 mL	la 25 mL	0,2214
3.1	2 mL sol. B	1 mL	10 mL	la 25 mL	0,4221
3.2	2 mL sol. B	1 mL	10 mL	la 25 mL	0,4220
3.3	2 mL sol. B	1 mL	10 mL	la 25 mL	0,4140
4.1	2 mL sol. B	1 mL	10 mL	la 25 mL	0,2158
4.2	2 mL sol. B	1 mL	10 mL	la 25 mL	0,2225
4.3	2 mL sol. B	1 mL	10 mL	la 25 mL	0,2405
5.1	2 mL sol. B	1 mL	10 mL	la 25 mL	0,1951
5.2	2 mL sol. B	1 mL	10 mL	la 25 mL	0,2007
5.3	2 mL sol. B	1 mL	10 mL	la 25 mL	0,1998
6.1	2 mL sol. B	1 mL	10 mL	la 25 mL	0,4562
6.2	2 mL sol. B	1 mL	10 mL	la 25 mL	0,4443

6.3	2 mL sol. B	1 mL	10 mL	la 25 mL	0,4621
7.1	2 mL sol. A	1 mL	10 mL	la 25 mL	0,4143
7.2	2 mL sol. A	1 mL	10 mL	la 25 mL	0,4122
7.3	2 mL sol. A	1 mL	10 mL	la 25 mL	0,4206
8.1	2 mL sol. A	1 mL	10 mL	la 25 mL	0,2021
8.2	2 mL sol. A	1 mL	10 mL	la 25 mL	0,2022
8.3	2 mL sol. A	1 mL	10 mL	la 25 mL	0,2051
9.1	2 mL sol. A	1 mL	10 mL	la 25 mL	0,4091
9.2	2 mL sol. A	1 mL	10 mL	la 25 mL	0,4086
9.3	2 mL sol. A	1 mL	10 mL	la 25 mL	0,4177
Standard - Pyrogallol	2 mL sol. diluted pyrogalol	1 mL	10 mL	la 25 mL	0,3905

The percentage content of total polyphenols for samples 1-6 was calculated according to the following formula:

$$\% \text{ total polyphenols} = \frac{62{,}5 \times A1 \times m2}{A2 \times m1}$$

A modified formula is used to determine the polyphenols in samples 7-9, as one of the dilutions has not been made:

$$\% \text{ total polyphenols} = \frac{12{,}5 \times A1 \times m2}{A2 \times m1}$$

m_1 = mass of the sample taken in work, in grams

m_2 = pyrogallol mass, in grams (0.05 g)

A_1= absorbance of the sample

A_1= absorbance of the standard

Statistical evaluation was performed with using GraphPad Prism 9 software (GraphPad, USA).

RESULTS AND DISCUSSIONS

The amount of polyphenols obtained is shown in the table below:

Table 3. *Determination of total polyphenols*

Sample	Total polyphenols g% dried vegetable grodus	Mean	Standard deviation
1.1	3,7195	3,6877	0,0594
1.2	3,6192		
1.3	3,7245		
2.1	1,6684	1,9032	0,2173
2.2	2,0973		
2.3	1,9440		
3.1	3,5061	3,5779	0,0626
3.2	3,6070		
3.3	3,6206		
4.1	1,7027	1,8778	0,1531
4.2	1,9433		
4.3	1,9872		
5.1	1,6442	1,6222	0,0192
5.2	1,6138		
5.3	1,6087		
6.1	3,3105	3,6131	0,2817
6.2	3,8678		
6.3	3,6610		
7.1	3,4932	3,3228	0,1722
7.2	3,3264		
7.3	3,1489		
8.1	1,7483	1,6650	0,0838
8.2	1,6659		
8.3	1,5807		
9.1	2,7874	2,9433	0,1637
9.2	2,9287		
9.3	3,1138		

All samples were performed in triplicate and the mean value was reported.

The amount of polyphenols varied significantly depending on the extraction solvent and the plant product.

The highest amount of polyphenols was determined in *Lysimachiae herba*, in the order of 40% alcohol> water> ethanol. In *Lysimachiae radix* the smallest amount of polyphenolic compounds was obtained as follows: water%> alcohol 40%> ethanol. In *Lysimachiae flores* an average amount of polyphenolic compounds was obtained in the following order: alcohol 40%> water> ethanol.

From the results we can deduce that alcohol 40% is the best extractive solvent for all vegetal products of the species except the root, but the amount of polyphenols in alcohol % is large enough to choose the solvent, alcohol 40, for the extraction of total polyphenols.

The amount of total polyphenols falls in the range, 1.5-3%, mentioned in the literature [5], [6], [7].

Results represent the average of three replicates, from three independent determinations. Results are presented as mean ± standard deviation (SD) and were statistically analysed using GraphPad Prism 9 software (GraphPad, USA), by means of two-way ANOVA followed by Tukey's multiple comparisons test. Differences between the groups were considered statistically significant at $p < 0.05$.

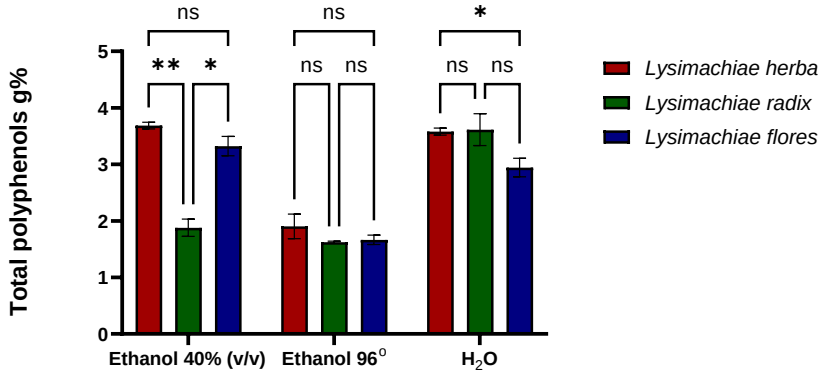

Fig. 1. *Multiple comparison of total polyphenols content of Lysimachia nummularia L.*

Values were expressed as Mean ± SD ($n = 3$). Significance is indicated by *$p < 0.05$, **$p < 0.01$, ***$p < 0.001$, ns: $p > 0.05$ (Fig.1).

CONCLUSION

Polyphenolic compounds were determined in all organs of the plant *Lyzimachia nummularia* L. (*Primulaceae*).

The largest amount of polyphenolic compounds was determined in the aerial part of the species *Lyzimachia nummularia* L.

The amount of polyphenolic compounds determined in alcohol 40 % led us to say that this solvent is the best extraction solvent of the three solvents tested.

Thus, in order to obtain an extract from all the organs of the species Lyzimachia nummularia L. to be standardized in polyphenolic compounds, we can further use ethanol 40 % as extraction solvent.

The large amount of polyphenolic compounds determined in ethanol 40 %, leads us to believe that the extract we will obtain will have very good antioxidant

properties, and which could be used in the therapy of many diseases, which require a high consumption of antioxidants.

REFERENCES

[1] Seeram, N. P., Berry fruits for cancer prevention: current status and future prospects. Journal of Agricultural and Food Chemistry, 56(3), 2008, 630-635.

[2] Zengin, A. C. A., Crudu, M., Maier, S. S., Deselnicu, V., Luminita, A. L. B. U., Gulumser, G., ... & Mutlu, M. M,. Eco-leather: Chromium-free Leather Production Using Titanium, Oligomeric Melamine-Formaldehyde Resin, and Resorcinol Tanning Agentsand the Properties of the Resulting Leathers. Ekoloji, 21(82), 2012, 17-25.

[3] Csepregi, R., Temesfői, V., Das, S., Alberti, Á., Tóth, C. A., Herczeg, R., ... & Kőszegi, T., Cytotoxic, antimicrobial, antioxidant properties and effects on cell migration of phenolic compounds of selected Transylvanian medicinal plants. Antioxidants, 9(2), 2020, 166.

[4] Munin, A., & Edwards-Lévy, F., Encapsulation of natural polyphenolic compounds; a review. Pharmaceutics, 3(4), 2020, 793-829.

[5] Tóth, A., Riethmüller, E., Alberti, Á., Végh, K., & Kéry, Á., Comparative phytochemical screening of phenoloids in Lysimachia species. Extraction, 2, 2020, 0-10.

[6] Hanganu, D., Olah, N. K., Mocan, A., Vlase, L., Benedec, D., Raita, O., & Toma, C. C., Comparative polyphenolic content and antioxidant activities of two Romanian Lysimachia species. studies, 2016, 15, 16.

[7] Toth, A., Toth, G., & Kery, A., Polyphenol composition and antioxidant capacity of three Lysimachia species. Natural product communications, 9(10), 1934578X1400901017, 2014.

[8] Włodarczyk, M., Pasikowski, P., Osiewała, K., Frankiewicz, A., Dryś, A., & Gleńsk, M., In search of high-yielding and single-compound-yielding plants: new sources of pharmaceutically important saponins from the Primulaceae family. Biomolecules, 10(3), 2020, 376.

[9] ***European Directorate for the Quality of Medicines, Oak bark in European Pharmacopoeia, In European Pharmacopoeia 10.0; EDQM, Strasburg, France, 2021; p. 1557.

DETERMINATION OF THE OPTIMAL CONCENTRATIONS OF PECTIN AND CALCIUM CHLORIDE FOR THE SYNTHESIS OF CHITOSAN-PECTIN MICROPARTICLES

Prof. Dr. Alla A. Krasnoshtanova[1]
Anastasiya D. Bezyeva[2]
[1, 2] D. Mendeleev University of Chemical Technology of Russia, Moscow, Russia

ABSTRACT

The oral route of drug inclusion is the most convenient for the patient. In addition to ease of use, this method of drug inclusion has such advantages as non-invasiveness of inclusion, absence of complications during injection; comparative safety for the organism due to the passage of the active substance and auxiliary compounds through the gastrointestinal tract; the possibility of introducing larger doses of the drug at one time. However, despite the obvious advantages, the oral route of inclusion has a number of significant disadvantages that significantly limit its use for a number of drugs. Among them are: relatively slow therapeutic action of the drug with this route of inclusion; the aggressive effect of a number of drugs (for example, antibiotics) on the gastrointestinal tract; low bioavailability of a number of substances (especially high molecular weight hydrophilic compounds), caused by poor permeability of the intestinal epithelium for hydrophilic and large molecules, as well as enzymatic and chemical degradation of the active substance in the gastrointestinal tract.

There are various approaches used in the development of oral drug delivery systems. In particular, for the targeted delivery of drugs, it is proposed to use nano- and microcapsules with mucoadhesive properties. Among the polymers used for the synthesis of these microparticles, it is preferable to use pH-dependent, gelable biopolymers that change their structure depending on the acidity of the environment. Microcapsules obtained from compounds with the above properties are capable of protecting the active substance (or from the active substance) in the stomach environment and ensuring its release in the intestine. These properties are possessed by such polysaccharides as alginate, pectin, carrageenan, xylan, etc. The listed biopolymers are non-toxic, biocompatible, and biodegradable, which makes microparticles containing these polysaccharides promising as oral drug delivery systems. To impart mucoadhesive properties to nanoparticles, complexes of the listed polymers with chitosan are used.

In this research, pectin, a polysaccharide formed mainly by residues of galacturonic acid, was used as a structural polymer. The concentrations of substances in the initial solutions were selected that were optimal for the synthesis of microcapsules. The main parameters for evaluating the resulting microparticles were the size of the capsules (less than 1 μm for oral inclusion), the zeta-potential,

showing the tendency of the microparticles to stick together, and the completeness of the binding of the microparticles to chitosan.

It was found that the optimal solutions for the synthesis of microparticles are: 15.7 ml of a solution of pectin 0.093% by weight, 3.3 ml of a solution of chitosan 0.07% by weight and 1.0 ml of a solution of $CaCl_2$ 20 mM. The diameter of the microparticles obtained by this method was 700-800 nm, and the value of their zetta-potential, equal to - (34 ± 3) mV, does not cross the particle adhesion threshold. It was also found that the synthesis of microparticles at these concentrations of calcium chloride provides the most complete binding of chitosan to their surface, which increases the mucoadhesive properties of microparticles.

Keywords: *pectin, chitosan, microparticles, sorption capacity*

INTRODUCTION

The oral route of inclusion of drugs is the most convenient in therapy due to the ease of use for the patient, atraumatic introduction into the body and the possibility of taking large doses of the drug [1]. However, this method of drug inclusion also has a number of disadvantages that limit its use. Among them, one can single out low bioavailability for a number of active substances, the effect of aggressive drugs on the gastrointestinal tract (in particular, this item refers to various kinds of antibiotics) [1], the destruction of biological substances of a protein nature under the action of enzymes of the gastrointestinal tract and its aggressive environment [1], [2], low permeability of the intestinal mucosa for high molecular weight compounds [2] and a relatively slow therapeutic effect of the drug with this route of inclusion [1]. Modern advances in biotechnology have led to the possibility of industrial production of protein-based drugs and their widespread use in therapeutic practice [3]. These trends make the search for and development of new oral drug delivery systems a promising topical direction for almost two decades.

There are various approaches used in the development of oral drug delivery systems. In particular, for targeted delivery of drugs, it is proposed to use nano- and microcapsules with mucoadhesive properties [2], [3]. Among the polymers used for the synthesis of these microparticles, it is preferable to use pH-dependent, gelable biopolymers that change their structure depending on the acidity of the environment. Microcapsules obtained from compounds with the above properties are able to protect the active substance (or from the active substance) in the stomach environment and ensure its release in the intestine [3]. These properties are possessed by such polysaccharides as alginate, pectin, carrageenan, xylan, etc. [4]. The listed biopolymers are non-toxic, biocompatible, and biodegradable, which makes microparticles containing these polysaccharides promising as oral drug delivery systems [4]. To impart mucoadhesive properties to nanoparticles, complexes of the listed polymers with chitosan are used [4]. Chitosan is a biodegradable non-toxic polysaccharide consisting of randomly linked β- (1-4) D-glucosamine units and N-acetyl-D-glucosamines (with a predominance of residues of the first monomer in the composition). This biopolymer is capable of forming stable polyelectrolyte complexes with the aforementioned polysaccharides and, due to its mucoadhesive properties, is able to increase the residence time and the amount

of the active substance at the site of adsorption, creating a concentration gradient leading to the rapid absorption of protein molecules through the intestinal mucosa [3].

In this research, pectin, a polysaccharide formed mainly by residues of galacturonic acid, was used as a structural polymer. The scheme of the formation of a polyelectrolyte complex of chitosan-pectin microparticles is shown in Fig. 1-2

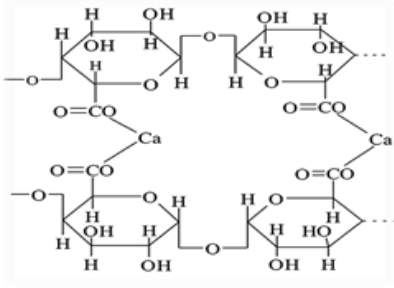

Fig. 1. *Scheme of the formation of calcium bridges between pectin molecules through carboxyl groups*

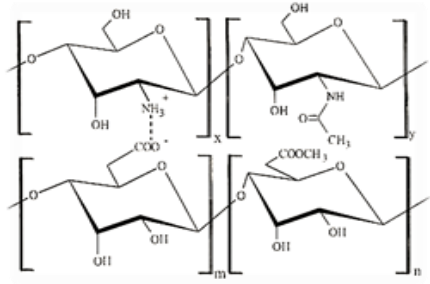

Fig. 2. *Scheme of the formation of the polyelectrolyte complex of chitosan with pectin*

The aim of this work is to determine the optimal ratio of the concentrations of the initial solutions of pectin, chitosan, and calcium chloride for the synthesis of chitosan-pectin microparticles that are effective when therapeutic molecules are included in them.

MATERIALS AND METHODS

The objects of this investigation were: low molecular weight chitosan (200 kDa) with a degree of diacetylation of 85%, manufactured by Sigma-Aldrich; apple pectin with a molecular weight of 12 kDa and a degree of metaxylation of 66% produced by Cargill (France); lyophilizate of doxorubicin hydrochloride for the preparation of a solution for intravascular and intravesical administration, produced by the pharmaceutical company "Teva".

To synthesize chitosan-pectin microparticles, 7.5 ml of a 22 mM calcium chloride solution was added to 117.5 ml of a 0.094% (mass) pectin solution (pH 4.3) dropwise at a rate of 0.125 ml/min using a peristaltic pump with constant stirring on a magnetic stirrer (stirring speed 800 rpm). At the end of the addition of the chitosan solution to stabilize the microparticles, the prepared suspension of microparticles was stirred on a magnetic stirrer for 30 minutes at a speed of 800 rpm. The separation of microparticles from the solution was carried out by centrifugation at a speed of 10,000 rpm for 30 minutes. To obtain microparticles loaded with a substance (in this investigation doxorubicin was used as an active compound), it was added to the initial pectin solution.

The size and zetta potential of the obtained microparticles were determined using a JEOL 1610LV scanning electron microscope with an SSD X-Max Inca

Energy energy dispersive spectrometer for electron probe microanalysis (JEOL, Japan; Oxford Instruments, Great Britain).

The completeness of the incorporation of chitosan into polyelectrolyte complexes was determined by the method of IR spectroscopy of the supernatant carried out on an IR Fourier spectrometer with an ATR attachment and additional equipment Nicolet 380 (Thermo Fisher Scientific Inc., USA) [5].

The capacity of chitosan-pectin microparticles for doxorubicin was determined by measuring the residual amount of doxorubicin in the supernatant obtained after centrifugation of the suspension. The concentration of doxorubicin was established by determining the optical density of the sample at a wavelength of 475 nm [6].

RESULTS AND DISCUSSION

The main criteria by which the primary assessment of the obtained chitosan-pectin microparticles was carried out were their size (the permitted size of the preparation for oral administration is up to 1000 microns) [7], the zetta-potential, which characterizes their tendency to sticking together (sticking threshold | 27-29 | mV), as well as the completeness of binding of chitosan to microparticles.

At the first stage, it was necessary to determine the optimal concentration of the initial solution of the structure-forming polysaccharide (pectin) for the synthesis of microparticles. For this purpose, a series of chitosan-pectin microcapsules were prepared by varying the initial concentration of the pectin solution at constant concentration values of solutions of calcium chloride (18 mM) and chitosan (0.07% by weight).

The size of the obtained microparticles and their zeta-potential were measured. The measurement results are presented in Table 1.

Table 1. *Characteristics of chitosan-pectin microparticles synthesized using solutions of pectin with various concentrations at constant concentrations of solutions of chitosan (0.07% by weight) and calcium chloride (18 mM)*

Pectin concentration,% mass	Microparticle diameter, nm	Zetta potential of microparticles, mV
0.042	500-600	-(33±2)
0.085	500-600	-(39±3)
0.093	600-700	-(32±2)
0.102	800-900	-(29±1)
0.111	1000-1100	-(22±1)

From the presented data, it can be seen that the maximum permissible sizes for oral administration of microparticles are reached at a concentration of a pectin solution of 0.102% by weight, however, these microparticles have a zetta potential close to the sticking threshold. Proceeding from this, the optimal concentration of the solution at which the synthesized polysaccharide microparticles have the

maximum allowable size and do not have a tendency to stick together was taken equal to 0.093%.

The next step was to determine the optimal concentration of the binder solution (calcium chloride) for the synthesis of microparticles. For this purpose, samples of chitosan-pectin microcapsules were prepared by varying the initial concentration of calcium chloride solution at constant concentration values of solutions of pectin (0.093 wt%) and chitosan (0.07 wt%). The size and zetta potential of the synthesized microparticles were measured. The measurement results are presented in Table 2.

The presented data show that an increase in the concentration of the initial solution of calcium chloride leads to an increase in the zetta potential of chitosan-pectin microparticles, that is, their tendency to stick together decreases. All synthesized microparticles have an acceptable range of zetta-potential values. The maximum size of microparticles is reached at solution concentrations of 20 and 22 mM. An increase in the concentration of the binder leads to a decrease in their size. It can be assumed that this is due to the fact that only a small part of chitosan was able to bind to a complex with microparticles.

Table 2. *Characteristics of chitosan-pectin microparticles synthesized using solutions of calcium chloride with various concentrations at constant concentrations of solutions of pectin (0.093% by weight) and chitosan (0.07% by weight)*

Concentration of $CaCl_2$, mM	Diameter of microparticles, nm	Zetta-potential of microparticles, mV
18	600-700	-(32±2)
20	700-800	-(34±3)
22	700-800	-(35±3)
24	500-600	-(36±3)
26	500-600	-(37±3)

The completeness of the inclusion of chitosan in the polyelectrolyte complex has already been mentioned as one of the key criteria for evaluating the synthesized microparticles. To determine it, the IR spectra of the supernatant liquid obtained after the separation of microparticles were recorded.

As a control, the IR spectrum of a solution containing: 25 ml of a 0.07% chitosan solution, 117.5 ml of a CH_3COOH solution (pH 4.3) and 7.5 ml of water was taken. The results are shown in Fig. 1-3.

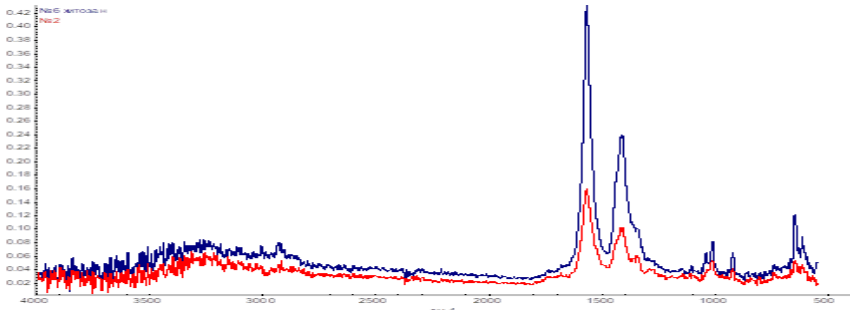

Fig. 1. *Spectrum of the supernatant liquid obtained after the separation of microparticles, in comparison with the chitosan solution with the initial concentration; concentration of solutions for synthesis: pectin 0.093% by weight, chitosan 0.07% by weight, $CaCl_2$ 20 mM*

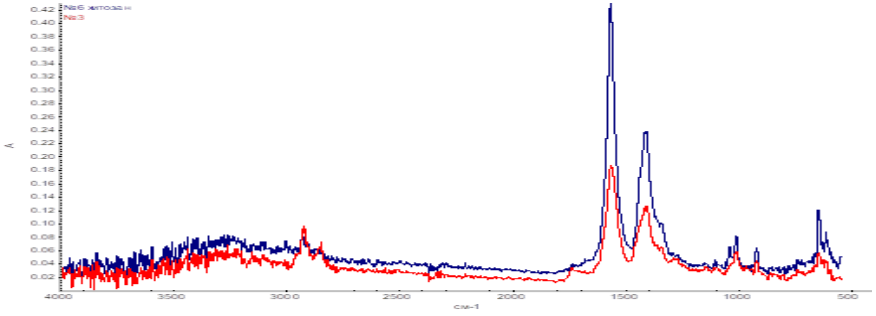

Fig. 2. *Spectrum of the supernatant liquid obtained after the separation of microparticles in comparison with the chitosan solution with the initial concentration; concentration of solutions for synthesis: concentration of solutions for synthesis: pectin 0.093% by weight, chitosan 0.07% by weight, $CaCl_2$ 22 mM*

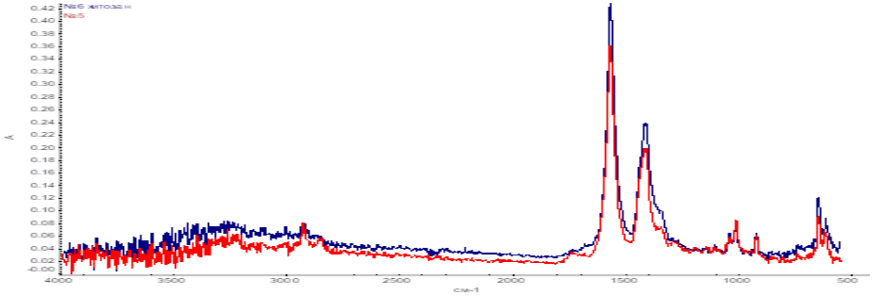

Fig. 3. *Spectrum of the supernatant liquid obtained after the separation of microparticles in comparison with the chitosan solution with the initial concentration; concentration of solutions for synthesis: pectin 0.093% by weight, chitosan 0.07% by weight, $CaCl_2$ 26 mM*

From the data obtained, it can be seen that the most complete binding of chitosan to microparticles is provided at a concentration of the initial calcium chloride solution of 20 mM. The spectrum taken from the supernatant obtained after the separation of microparticles synthesized using a 26 mM calcium chloride solution shows that chitosan, in fact, did not bind to microparticles and almost all remained in the supernatant.

Thus, according to the above criteria, the following initial solutions are optimal conditions for the synthesis of microparticles: 117.5 ml of a 0.093% mass pectin solution, 25 ml of a 0.07% mass chitosan solution and 7.5 ml of a 20 mM calcium chloride solution.

The next stage of the work is to determine the effectiveness of using these microparticles for the inclusion of therapeutic substances in them using doxorubicin as an example. First of all, their capacity for this connection was assessed.

To determine the capacity of microcapsules for doxorubicin when preparing a suspension of microcapsules, the studied antibiotic was added to the pectin solution, varying its concentration in the range of 0.021 - 0.13 mg/ml.

The concentration of the antibiotic not included in the microparticles in the supernatant was monitored by measuring the optical density at 475 nm. Separately, the background was measured - the supernatant obtained after the deposition of unloaded microparticles. The results on the capacity of microparticles for doxorubicin and the degree of its sorption are shown in Fig. 4-5.

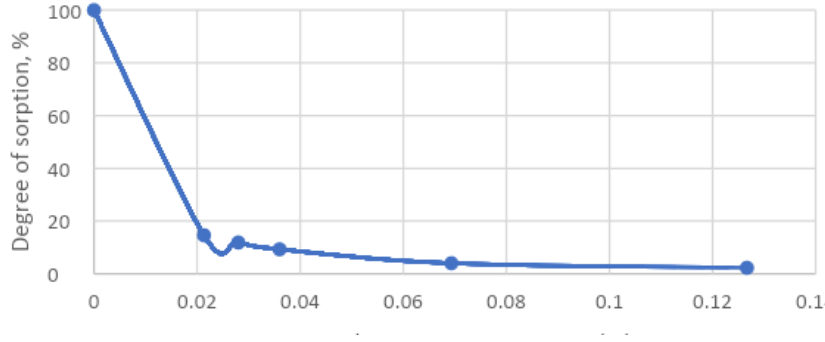

Fig. 4. *Dependence of the degree of sorption of doxorubicin into chitosan-pectin microparticles (synthesized using a 20 mM $CaCl_2$ solution) on its concentration in suspension*

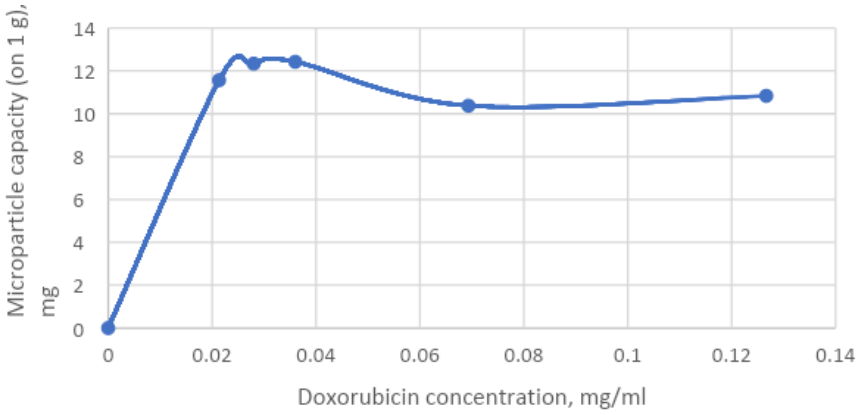

Fig. 5. *Dependence of the amount of doxorubicin included in chitosan-pectin microparticles (synthesized using a 20 mM $CaCl_2$ solution) on its concentration in suspension*

The graphs show that microparticles synthesized using a 20 mM calcium chloride solution have a low capacity for doxorubicin (12.34 mg doxorubicin / g microparticles) and a low degree of sorption of this antibiotic. Therefore, they are ineffective for the inclusion of low molecular weight therapeutic drugs.

For comparison, the capacity of chitosan-pectin microparticles synthesized using a 0.093 wt% pectin solution, a 0.07 wt% chitosan solution and a 22 mM calcium chloride solution was determined. The concentration of doxorubicin in the initial pectin solution was varied in the range of 0.0133 - 0.133 mg/ml. The results on the capacity of microparticles and the degree of sorption of doxorubicin in them are shown in Fig. 6-7.

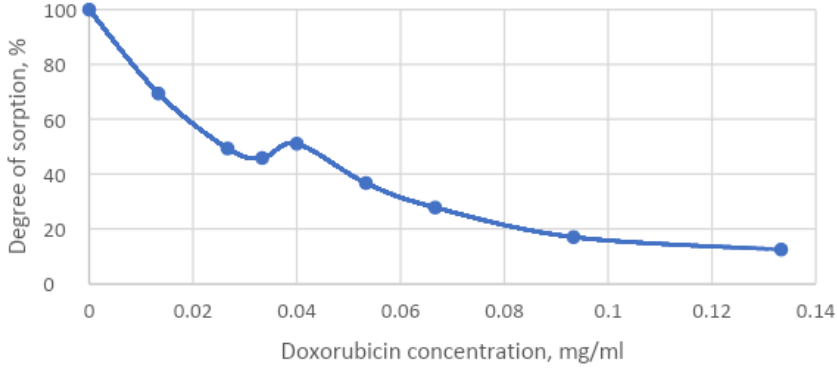

Fig. 6. *Dependence of the degree of sorption of doxorubicin into chitosan-pectin microparticles (synthesized using a 20 mM $CaCl_2$ solution) on its concentration in suspension*

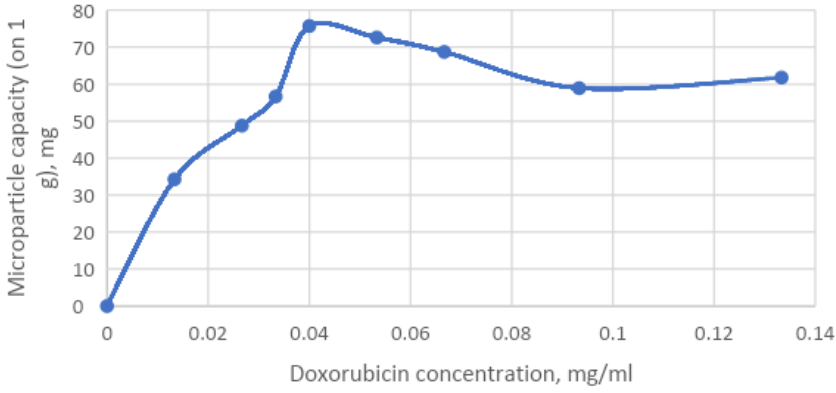

Fig. 7. *Dependence of the amount of doxorubicin included in chitosan-pectin microparticles (synthesized using a 20 mM $CaCl_2$ solution) on its concentration in suspension*

From the obtained dependences it can be seen that these microparticles, in comparison with the previous ones, are able to absorb a larger amount of doxorubicin (the maximum degree of sorption reached 69.4%) and have a higher capacity than the previous ones by 6.4 times (the degree of sorption reaches 77.28 mg of doxorubicin / g microparticles).

These results confirm the feasibility of using these chitosan-pectin microparticles for the inclusion of low-molecular-weight therapeutic drugs. In this regard, the following initial solutions are optimal conditions for the synthesis of microparticles: 117.5 ml of a 0.093% mass pectin solution, 25 ml of a 0.07% mass chitosan solution and 7.5 ml of a 22 mM calcium chloride solution.

CONCLUSION

Received chitosan-pectin microparticles, the diameter of which was 700-800 nm. The zetta potential of the microparticles was - (35 ± 3) mV, which indicates the absence of adhesion tendencies in microparticles. The spectrum of the supernatant obtained after the separation of microparticles confirms the inclusion of most of the chitosan in the polyelectrolyte complex.

The optimal ratio of the concentrations of structural components in the initial solutions for the synthesis of microparticles was selected: pectin solution - 0.093% by weight; chitosan solution - 0.07% by weight; CaCl2 solution - 22 mM. It was found that the initially established criteria for evaluating the optimal conditions for the synthesis of microparticles do not guarantee their effectiveness and high capacity for therapeutic drugs.

The optimal concentration of doxorubicin in the suspension (0.04 mg/ml), at which the maximum incorporation of this antibiotic into chitosan-pectin microparticles is achieved (degree of sorption is 52.11%), has been determined. Based on the data that the concentration of microparticles in the suspension is 6

mg/ml, and their dry weight is 4.5%, the doxorubicin capacity of microparticles is 77.28 mg/g of dry microparticles.

REFERENCES

[1] Kravchenko I.A. Methods for introducing drugs into the body, M .: Astroprint, 82 pp., 2009.

[2] Michael Goldberg, Challenges for the oral delivery of macromolecules/ Michael Goldberg, Isabel Gomez-Orellana// Nature Publishing Group – 2003. – Vol. 2. – p. 289 – 295

[3] Kyeongsoon Park, Ick Chan Kwon, Kinam Park. Oral protein delivery: Current status and future prospect, Reactive & Functional Polymers. Vol.71. PP. 280-287, 2011.

[4] E.A. Kirzhanova, M.A. Pechenkin, N.B. Demina, N.G. Balabushevich Micro- and nanoparticles from alginate and chitosan for transmucosal protein delivery, Bulletin of Moscow University. Ser. 2. Chemistry – vol.57/ 2. PP. 103 – 111, 2016.

[5] Vasiliev AV, Grinenko EV, Shchukin AO Infrared spectroscopy of organic and natural compounds. SPb .: SPbSWTA, P.29, 2007.

[6] Knyazev R.A., Trifonova N.V., Polyakov L.M. Transport form of anticancer drugs doxorubicin and melphalan based on apolipoprotein A-I of blood plasma, Journal "Modern problems of science and education". vol. 6, PP. 2016

[7] Russian Federation. Ministry of Health care. On the approval of the rules for the manufacture and dispensing of medicinal products for medical use by pharmacy organizations, individual entrepreneurs who have a license for pharmaceutical activities N 751н dated October 26, 2015.

HPV GENOTYPES COINFECTIONS AND HEALTH RISK - PRELIMINARY STUDY OF THE EAST ROMANIAN POPULATION

Ph.D. Student Codrin Gheorghe[1]
Assoc. Prof. Dr. Schröder Verginica[2]
Assoc. Prof. Dr. Stoicescu Ramona[3]
Lecturer Dr. Honcea Adina[4]
Assoc. Prof. Dr. Dumitru Irina[5]
[1, 5] Ovidius University of Constanta, Faculty of Medicine, Constanta, Romania
[3, 4] Ovidius University of Constanta, Faculty of Pharmacy, Constanta, Romania
[5] Clinical Infectious Diseases Hospital, Constanta, Romania

ABSTRACT

The study aims to identify the degree of infection and co-infection with HPV strains in people of different ages, to assess the risk associated with lack of immunization of the Romanian population. In this study we are looking at the prevalence and relationship of the different types of HPV strains present in the 37 cases with suspected HPV infection that were analyzed, in the period 2018-2019, within the Prodiagnostic analysis laboratory, in Constanța, Romania. Of the total number of people analyzed for the case study, 45.94% (17 out of 37) tested positive for HPV infection. The analysis of the frequency of strains by risk categories shows that the highest percentage was 48% in the case of high-risk strains, followed by the percentage of frequency of strains with unknown risk (44%) and that of low-risk strains (8 %); The analysis by age indicates the maximum infection rate recorded belonging to the age group between 23 and 34 years. The association between strains and the 50% frequency indicates an important aspect of the infection as well as important data for diagnosis and treatment and involves more rigorous monitoring of patients with such associations, the risk increases with the associations.

Keywords: *HPV, co-infections, strains, screening, lesions*

INTRODUCTION

HPV are double-stranded DNA viruses that infect the stratified epithelium of the skin and mucous membranes. There have been identified approximately 200 strains with potential for induction of transformations. HPV serotypes are differentiated between one another by the genetic sequence of the external L1 protein capsid. Of these, 15 are classified as having high oncogenic risk (16,18, 31, 33, 35, 39, 45, 51, 52, 56, 58, 68, 73 and 82), 3 with probable oncogenic risk (26, 53 and 66) and 12 with low oncogenic risk (6,11, 40, 42, 43, 44, 54, 61, 70, 72, 81, CP6108) [1].

The infection appears to begin with the virus entering through a site of epithelial disruption (microlesion) that allows viral access to the basal epithelial layer. HPV-16 penetration occurs through clathrin-facilitated endocytosis, although other types of HPV may have other mechanisms of cell penetration [2].

Cervical HPV infection with oncogenic risk causes cervical morphological lesions, from normal (normal cytology) to various stages of preneoplastic lesions (CIN 1, CIN 2, CIN 3 / CIS) and invasive cervical cancer. Cervical infection is established by determining HPV DNA in cervical cells by various methods.

Clinically, the most important manifestation of HPV infection in the cervix is considered to be cervical intraepithelial neoplasia (CIN). CIN are cellular lesions with unstable genetic bases, presenting a risk of evolution in extensive cervical cancer, of 30-40%. These untreated lesions, CIN 2 or CIN 3, can cause cervical cancer in a few years or even decades later. The average period of natural evolution to invasive neoplasm is about a few years (12 years) [3].

Certain HPV serotypes more frequently induce oncogenesis, which includes them in the high-risk oncogenic HR-HPV strains, namely serotypes 16, 18 and 45.

These data suggest that in laboratory evaluation, high-risk oncogenic HPV DNA genotyping is a necessary test in suspected lesions and is an important indicator of the risk of developing high-grade or more advanced squamous intraepithelial lesions [4].

Immunohistochemical, cytogenetic and molecular studies [7] have shown that low-risk HPV types do not integrate into the host cell genome, while high-risk types are integrated into the nucleus of epithelial cells in the cervix.

Following integration, the protein product of HPV-16 and 18, proteins E7 and E6 respectively, inactivate the tumor suppressor genes, p53 and the RB-1 gene, allowing uncontrolled cell proliferation. It was possible to document morphological abnormalities in cervical lesions, observing a good correlation with underlying cellular events, by using techniques such as proliferation of cellular antigen (PCNA), expression of p16, p53 and nucleolus organizer region (NOR)[3].

HPV is a necessary cause of cervical cancer, but it is not a sufficient cause. Other cofactors are needed for progression from cervical HPV infection to cancer. Tobacco smoking, high parity, long-term hormonal contraceptive use and HIV co-infection have been identified as established cofactors. Co-infection with *Chlamydia trachomatis* and *Herpes simplex* virus type-2, immunosuppression and certain dietary deficiencies are other likely cofactors [4]. Genetic and immunological host factors and viral factors other than type, such as type variants, viral load, and viral integration, are likely important, but have not been clearly identified [4], [5], [9], [11].

The study aims to identify the degree of infection and co-infection with HPV strains in people of different ages, to assess the risk associated with lack of immunization of the Romanian population.

MATERIALS AND METHODS

37 cases with suspected HPV infestation were analyzed, in the period 2018-2019, within the Prodiagnostic analysis laboratory, in Constanța, Romania. People were between 23 and 64 years old. The endocervical epithelium was taken and analyzed by HPV DNA detection and genotyping in the specialized laboratory of Matei Basarab Medical Center, Bucharest. The following HPV types were tested:

1. With increased oncogenic risk 14 HR-HPV strains: 16, 18, 31, 33, 35, 39, 45, 51, 52, 56, 58, 59, 66, 68;
2. With low oncogenic risk 3 LR-HPV strains: 6, 11, 42;
3. Other types of HPV: 26.40, 53, 54, 55, 61, 62, 64, 67, 69, 70, 71, 72, 73, 81, 82, 83, 84, IS 39, CP6108.

The results were statistically analyzed and interpreted [12], [13].

RESULTS AND DISCUSSION

Human papillomavirus (HPV) infection is strongly implicated in the etiology of cervical cancer. High-risk HPV types, most commonly types 16 and 18 and less often types 31, 33, 52 and 58 are present in 70-100% of cervical cancer cases. HPV types 6 and 11 are most commonly found in warts, and mixed HPV types can be found in dysplasia [6].

The analysis of the presence of HPV strains shows that there are 25 different strains, belonging to three categories, taking into account the risk:

1. high-risk HPV strains (61, 52, 31, 56, 66, 16, 51, 39, 58, 18, 35, 59)
2. low-risk strains (6, 42)
3. other strains (81,54, 62, 67, Cp6108, 70, 71, 55, 69, 53, 84).

Of the total number of people analyzed for the case study, 45.94% (17 out of 37) tested positive for HPV infection.

As can be seen in Table 1, most cases indicate that there are several associated strains (co-infection) and with different degrees of risk. It should be noted that 6 of the 17 positive cases analyzed (35.29 %) show the association between 2, 3 or 4 high-risk strains. Another 6 cases show co-infection between high-risk strains and other lesser-known strains (Table1).

Table 1. *Frequency of HPV strains in the group of participants (n = 17) positive and aspects regarding co-infection and frequency of strains (LR = low-risk, HR = high risk)*

Crt. no.	Strain type	Frequency (%)	Co-infections
	HPV81	23.52	81, 61, 52, 62
	HPV61 (HR)	17.64	61, 81, 54, 31, 16, 18, 71, 62, 39, 42, 84, CP6108
	HPV 52 (HR)	29.41	52, 54, 62, 31, 62, 35, 59, 55, 69, 35
	HPV54	11.76	54, 31, 16, 18, 71
	HPV31 (HR)	17.64	31, 56, 66, 16, 18, 71, 62,35,59,55,69
	HPV56 (HR)	5.88	56, 66
	HPV66 (HR)	5.88	0
	HPV62	29.41	62, 67, 16, 70, 35, 59, 55, 69, CP6108
	HPV CP6108	11.76	CP6108, 62, 67, 61, 39, 42, 84
	HPV67	5.88	67, CP6109
	HPV16 (HR)	17. 64	16, 70, 39, 58, 18, 71,
	HPV70	5.88	70, 16, 62
	HPV 51 (HR)	5.88	0
	HPV 39 (HR)	11.76	39, 16, 58, 61, 62, CP6109, 42, 84, CP6109
	HPV 58 (HR)	5.88	58, 16, 39
	HPV 6 (LR)	5.88	0
	HPV 18 (HR)	5.88	18, 71, 16, 31, 54, 61
	HPV 71	5.88	71, 18, 16, 31, 54, 61
	HPV 35 (HR)	11.76	35, 52, 31, 62, 59, 55, 69
	HPV 55	5.88	55, 35, 52, 31, 62, 59, 69
	HPV 59 (HR)	5.88	59, 55, 35, 52, 31, 62, 69
	HPV 69	5.88	69, 55, 35, 52, 31, 62, 59
	HPV 53	5.88	0
	HPV 42 (LR)	5.88	42, 61,81, 54, 31, 16, 18, 71, 62, 39, 84, CP6109
	HPV 84	5.88	84, 61,81, 54, 31, 16, 18, 71, 62, 39, 42, CP6109

As can be seen in the analysis, 21 of the 25 strains (84%) are co-infected, in some cases more than 2 strains being present in the same person (Table 1). These aspects are important for diagnosis and treatment and involve more rigorous monitoring of patients with such associations.

The analysis of the frequency of strains by risk categories highlights the fact that the highest percentage was 48% in the case of high-risk strains, followed by the percentage of frequency of strains with unknown risk (44%) and that of low-risk strains (8 %), Figure 1.

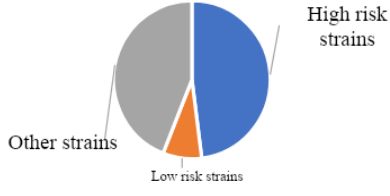

Fig. 1. *Frequency (%) of HPV strains by risk categories, identified in the case of the analyzed group*

Of the total number of strains analyzed, 12 are very high risk (HR-HPV). These strains are found with a frequency between 10- 40%. The most common are HPV52, HPV61, HPV31 and HPV16 from these having 25% frequency (HPV61, HPV31, HPV16) and 41% HPV52, Figure 2.

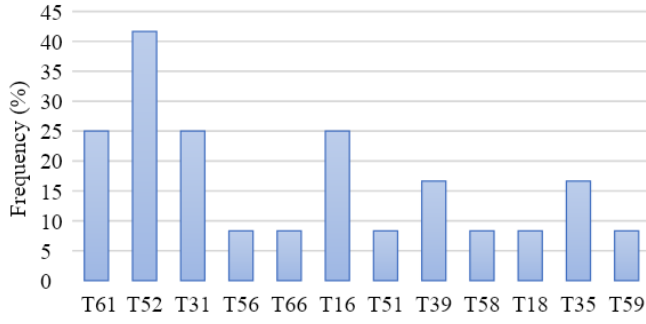

Fig. 2. *Frequency of high-risk HR-HPV strains*

Worldwide, it is generally considered that the most frequently encountered serotypes in patients with CIN 3 or more advanced lesions are HPV 16 and 18. Recent studies have shown large differences in the variation of the serotype 18 prevalence of advanced neoplastic lesions [6], [11].

From the category of strains with unknown or low risk (LR-HPV), only 4 strains (T81, T54, T62, TCP6109) are noted as having a frequency of over 10% (Figure 3).

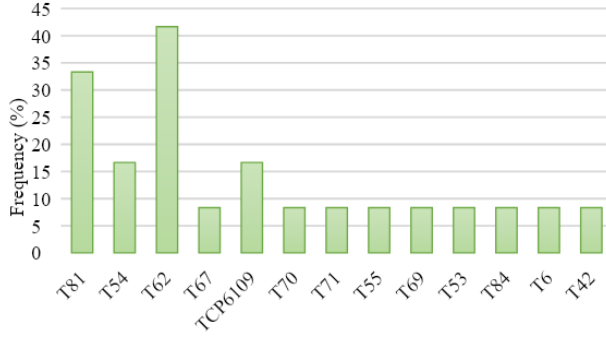

Fig. 3. *Frequency of low-risk (LR-HPV) or unknown risk HPV strains*

The analyzed batch was divided into three classes of age (Fig. 4), a percentage of 25%, the maximum recorded belonging to the group between 23 and 34 years. This result can be associated with conceptual differences in the relationship between partners and education.

There are no known data on the socioeconomic level of people screened or any other factors that would promote the risk of contamination: immunosuppression, smoking, inadequate use of contraceptive methods, infections, sexual behavior, gene polymorphism's [9], [10], [11], [14].

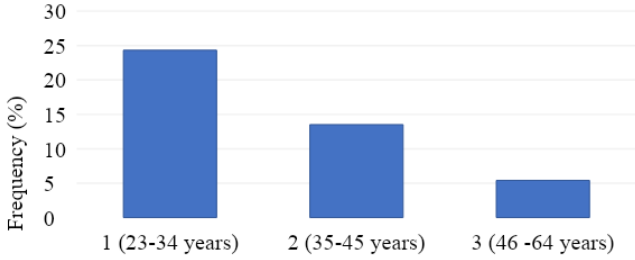

Fig. 4. *Frequency of comparative HPV-positive samples by age classes*

In a similar study from the north Romanian population, prevalence results showed out of the total tested samples, about 37.3% from samples were positive for HPV/DNA. From them 23.3% were single HPV type infections and 14% tested positive for multiple HPV types [6].

The Global strategy towards eliminating cervical cancer as a public health problem adopted by the WHA in 2020, recommends a comprehensive approach to cervical cancer prevention and control. The recommended set of actions should be multidisciplinary[15], including components ranging from community education, social mobilization, vaccination, screening, treatment and palliative care across the life course [9].

Cervical cancer screening involves testing for pre-cancer and cancer, more and more testing for HPV infection is performed. Testing is done among women who have no symptoms and may feel perfectly healthy. When screening detects an HPV infection or pre-cancerous lesions, these can easily be treated, and cancer can be avoided. Screening can also detect cancer at an early stage and treatment has a high potential for cure. Screening has to be linked to the treatment and management of positive screening tests. Screening without proper management in place is not ethical.

The World Health Assembly adopted the global strategy to accelerate the elimination of cervical cancer as a public health problem and its associated goals and targets for the period 2020–2030 [8], [9].

Romania is struggling with a high rate of cervical cancer. The National Screening Program for the early detection of cervical cancer targets a segment of the extended population (about 6 million women). To date, about 700,000 women have benefited from free Babeș Papanicolaou testing services (coverage rate 12%). It is estimated that 49% of all possible cases of cervical cancer have been prevented by population screening.

It is considered that in Romania the information about the risk of cervical cancer is no longer sufficient, and methods of awareness of cervical cancer causes and prevention can reduce risk by 80%, if there is a mass proportion gain [9].

CONCLUSION

Of the total number of people analyzed for the case study, 45% (17 out of 37) tested positive for HPV infection.

Frequency analysis of strains by risk categories reveals that the largest percentage was recorded in the strains with high risk (48%), followed by the frequency of strains with unknown risk (44%) and that of strains with low risk (8 %).

The analysis by age class indicates the maximum of recorded strains belonging to the age group between 23 and 34 years. This result can be associated with conceptual differences in the relationship between partners and education.

In our study the most common high-risk serotypes were HPV61, HPV31, HPV52, and HPV16. These strains are found with a frequency between 10 - 40%. The most common are HPV52, HPV61, HPV31 and HPV16 having the values of frequency at 25% (HPV61, HPV31, HPV16) and 41% respectively (HPV52).

The association between strains and the 45% frequency indicates an important aspect of the infection as well as important data for diagnosis and treatment and involves a more rigorous monitoring of patients with such associations, the risk increases with the associations.

REFERENCES

[1] Sabet F., Mosavat A., Ahmadi Ghezeldasht S., Basharkhah S., Shamsian S.A.A, Abbasnia S., Shamsian K., Rezaee S.A., Prevalence, genotypes and phylogenetic analysis of human papillomaviruses (HPV) in northeast Iran. International Journal of Infectious Diseases, 103:480-488, 2021.

[2] Moody C.A., Laimins L.A., Human papillomavirus oncoproteins: pathways to transformation. Nat. Rev. Cancer, 550-560, 2010.

[3] Fernandes J.V., DE Medeiros Fernandes T.A., DE Azevedo J.C., Cobucci R.N., DE Carvalho M.G., Andrade V.S., DE Araújo J.M., Link between chronic inflammation and human papillomavirus-induced carcinogenesis (Review). Oncol. Lett. (3):1015-1026, 2015.

[4] Bruni L., Albero G., Serrano B., Mena M., Gómez D., Muñoz J., Bosch FX., de Sanjosé S., ICO/IARC, Information Centre on HPV and Cancer (HPV Information Centre). Human Papillomavirus and Related Diseases in the World. Report 17, pp 243-244, 2019.

[5] Burd E.M., Human papillomavirus and cervical cancer. Clin. Microbiol. Rev., pp 1-17, 2003.

[6] Ursu RG, Onofriescu M, Nemescu D, Iancu LS., HPV prevalence and type distribution in women with or without cervical lesions in the Northeast region of Romania, Virol J., 2011, 8:558;

[7] Verissimo, J.F., Araújo De Medeiros A.T. F., Veríssimo De Azevedo J.C., Cobucci R.N.O., Freire De M. G., Andrade V.S. and Araújo J.M.G., Link between

chronic inflammation and human papillomavirus induced carcinogenesis (Review), Oncology Letters, 9: 1015-1026, 2015.

[8] https://www.who.int/en/news-room/fact-sheets/detail/human-papillomavirus-(hpv)-and-cervical-cancer;

[9] Bruni L., Albero G., Serrano B., Mena M., Gómez D., Muñoz J., Bosch F.X., de Sanjosé S. ICO/IARC, Information Centre on HPV and Cancer (HPV Information Centre). Human Papillomavirus and Related Diseases in the World. Summary Report 17 June 2019, www.hpvcentre.net.

[10] Georgescu M., Ginghina O., Raita S., Tapaloaga D., Ilie L., Negrei C., Popa D. E, Varlas V., Multescu R., Rosca A.C., Mirica R., Georgescu D., Natural alternative remedies in the background of updated recommendations for the prophylactic and therapeutic approach of *Clostridium difficile* infections, Farmacia, 66, pp 563-572, 2018.

[11] Stefanescu C., Calistru P., Voinea C., Gherlan G., Prevalence and distribution of high-risk genotypes of HPV in women with cervical intraepithelial neoplasia (CIN), in CDT "Victor Babes", Revista Romana de Boli Infectioase, XV, 4, 2012.

[12] E. C. Lupu, S. Lupu, A. Petcu, EB lifetime distributions as alternative to the EP lifetime distributions, Annals of "Ovidius" University from Constanţa, Mathematics Series, 22, (3), pp.115-125, 2014.

[13] A. Leahu, E. C. Lupu, Statistical simulation and prediction in software reliability. Annals of "Ovidius" University from Constanţa, Mathematics Series, 16, 1, pp 81-90, 2008.

[14] Torres-Poveda K., Burguete-García A.I., Bahena-Román M., Méndez-Martínez R., Zurita-Díaz M.A., López-Estrada G., Delgado-Romero K., Peralta-Zaragoza O., Bermúdez-Morales V.H., Cantú D., García-Carrancá A., Madrid-Marina V., Risk allelic load in Th2 and Th3 cytokines genes as biomarker of susceptibility to HPV-16 positive cervical cancer: a case control study. BMC Cancer, 24, 16:330, 2016.

[15] Erdem H, Puca E, Ruch Y, Santos L, Ghanem-Zoubi N, et al. Portraying infective endocarditis: results of multinational ID-IRI study, Eur J Clin Microbiol Infect Dis. 38(9):1753-1763, 2019.

LABORATORY METHODS AND PREVALENCE OF SARS-COV-2 INFECTIONS IN THE 2ND SEMESTER OF 2021 IN THE EMERGENCY CLINICAL COUNTY HOSPITAL OF CONSTANTA

Assoc. Prof. Dr Stoicescu Ramona[1,3]
M.D. Stoicescu Razvan-Alexandru[2]
PhD Student Gheorghe Codrin[3]
Assoc. Prof. Dr. Schroder Verginica[4]
[1, 4] Ovidius University of Constanța, Faculty of Pharmacy, Constanța, Romania
[3] Ovidius University of Constanța, Faculty of Medicine, Constanța, Romania
[1] Emergency Clinical County Hospital Constanța, Romania
[2] Emergency Clinical Hospital Bucharest, Romania

ABSTRACT

Diagnosing infections with SARS-CoV-2 is still of great interest due to the health and economic impact of COVID pandemic. The 4th wave of the COVID-19 pandemic is expected and is considered to be stronger and faster due to the dominance of Delta variant which is highly contagious [1].

SARS-CoV-2 also known as 2019-nCoV is one of the three coronaviruses (together with SARS-CoV or SARS-CoV1/Severe acute respiratory syndrome coronavirus), MERS-CoV /Middle East Respiratory Syndrome coronavirus) which can cause severe respiratory tract infections in humans [2].

Early diagnosis in COVID 19 infection is the key for preventing infection transmission in collectivity and proper medical care for the ill patients.

Gold standard for diagnosing SARS-Co-V-2 infection according to WHO recommendation is using nucleic acid amplification tests (NAAT)/ reverse transcription polymerase chain reaction (RT-PCR).

The search is on to develop reliable but less expensive and faster diagnostic tests that detect antigens specific for SARS-CoV-2 infection. Antigen-detection diagnostic tests are designed to directly detect SARSCoV-2 proteins produced by replicating virus in respiratory secretions so-called rapid diagnostic tests, or RDTs.

The diagnostic development landscape is dynamic, with nearly a hundred companies developing or manufacturing rapid tests for SARS-CoV-2 antigen detection [3].

In the last 3 months our hospital introduced the antigen test or Rapid diagnostic tests (RDT) which detects the presence of viral proteins (antigens) expressed by the COVID-19 virus in a sample from the respiratory tract of a person. All RDT were confirmed next day with a RT-PCR.

The number of positive cases detected during 3 months in our laboratory was 425. There were 326 positive tests in April, 106 positive tests in May and 7 positive tests in June. Compared with the number of positive tests in the 1st semester of 2021, the positive tests have significantly declined.

Keywords: *SARS-CoV-2, real time-RT PCR, Antigen, Rapid diagnostic tests*

INTRODUCTION

Diagnostic tests have been considered of paramount importance for the control of coronavirus disease (COVID-19). Diagnostic is even more important as the 4th wave of COVID 19 pandemic is expected.

Coronaviruses are enveloped, non-segmented, positive-sense, single-stranded RNA viruses.

SARS-CoV-2 possess 16 non-structural proteins (such as RNA dependent RNA polimerase RdRp) encoded by ORFs: ORF1a, ORF 1b and structural proteins (encoded within the 3′ end of the viral genome) including membrane (M), envelope (E), spike (S), and nucleocapsid (N) proteins [4].

The S glycoprotein is a class I fusion protein and directs attachment to the host receptor. It is formed by functional subunits, S1 and S2. Subunit S1 is formed by N terminal domain (NTD) and Receptor Binding Domain (RBD).

Subunit S2 contains fusion peptide (FP), heptad repeat 1 (HR1), central helix (CH), connector domain (CD), heptad repeat 2 (HR2), transmembrane domain (TM), cytoplasmic tail (CT). The SARS-CoV Spike fusion protein subunit S2 plays an important role in viral entry by initiating fusion of the viral and cellular membranes [5]

MATERIALS AND METHODS

Diagnostic tests for COVID-19 can be organized in virological diagnosis, recommended for virus detection, and serological tests, recommended for assessing the disease progression/development of immune response.

Virological diagnoses used in our laboratory were RNA amplification-based detection methods/ real-time RT-PCR, and viral proteins detection assays/ Rapid Diagnostic tests (RDT).

RT- PCR is an in vitro diagnostic real-time reverse transcription-PCR assay intended for the qualitative detection of nucleic acid from SARS-CoV-2 in nasopharyngeal/oropharyngeal swabs, anterior/mid-turbinate nasal swabs, nasopharyngeal washes/aspirates or nasal aspirates, and bronchoalveolar lavage specimens from individuals suspected of COVID-19 by their healthcare provider. [6]

The assay detects three SARS-CoV-2 RNA targets: the envelope (E) gene, the nucleocapsid (N) gene and a region of the open reading frame (ORF1) of the RNA dependent RNA polymerase (RdRp) gene from SARS-CoV-2 virus isolate Wuhan-Hu-1.

First step is represented by RNA extraction from samples. Once RNA is extracted the eluates are amplified. The target RNA is converted to cDNA by the reverse transcriptase enzyme. The obtained cDNA is amplified by PCR. Amplification takes place in a thermal cycler. Each cycle of PCR includes steps for template denaturation (94°C), primer annealing (40–60°C) and primer extension (70–74°C). [7]

WHO recommends using nucleic acid amplification tests (NAAT)/ reverse transcription polymerase chain reaction (RT-PCR) for diagnosing SARS-Co-V-2 infection as a gold standard.

RT-PCR testing is limited to certified Clinical Laboratory/Molecular Biology laboratories which require trained personnel, specific chemical supplies and expensive instruments. This can limit the number of tests that can be done.

Therefore alternatives were used for a rapid result mainly in symptomatic patients which were admitted in different hospital wards.

Antigen rapid Diagnostic Tests (Ag-RDTs) detect antigens from clinical specimens using a simple-to-use immunochromatographic (lateral flow) test format.

RDTs are typically a nitrocellulose strip enclosed in a plastic cassette with a sample well. When the infected patient's sample is combined with the test buffer and added to the sample well of the test strip, target antigens in the mixture bind to labelled antibodies and migrate together; they are subsequently captured by an antibody bound to the test line, triggering a detectable colour change. Depending on the test (and the antibody labels used), the colour change can be read by the operator with or without the aid of a reader instrument [8]. RDTs for COVID-19 can produce results in around 10−30 minutes versus the many hours required for most NAATs [8].

SARS-CoV-2 Ag-RDTs are authorized for use under emergency conditions and have not undergone comprehensive and stringent regulatory review.

The RDTs used in the Emergency County Hospital of Constanta were Rapid SARS-CoV-2 Antigen test card from Xiamen Boson and SD Biosensor COVID-19 Ag Test.

WHO recommends that a small set of samples from SARS-CoV-2 NAAT-confirmed positive and negative samples may be tested in parallel to assess whether the new kit meets performance requirements. In our lab we re-tested all Ag-RTD with RT-PCR with a very good correlation.

RESULTS AND DISCUSSIONS

Our study was made in the 2nd trimester of year 2021 using the real time RT PCR and Ag- RTD. The laboratory is testing the inpatients from the hospital wards and the hospital employees.

During first 3 months of 2021 (January, February, March) were tested with RT-PCR and confirmed positive a number of 993 patients and 83 health care personnel and other professional workers in hospital.

In the 2nd semester of 2021 (April, May, June), the total number of positive tests has significantly decreased. There were 425 positive tests for patients and 14 positive tests for hospital staff. Tests were made using RT-PCR and Ag-RDTs confirmed with RT-PCR.

The distribution of positive cases in the 2nd trimester of 2021 with relation to the month and the hospital wards (for inpatients, outpatients) and hospital staff workplace is presented in the next tabel.

Month	**April**	**April**	**May**	**May**	**June**	**June**
Ward	Health care personnel	Patients	Health care personnel	Patients	Health care personnel	Patients
Emergency ward	0	249	0	59	0	3
Hemodialysis	0	3	0	0	0	0
Oncology	0	8	0	2	0	0
Internal medicine 1	0	6	0	5	0	1
Internal medicine 2	0	3	0	1	0	1
Nephrology	0	0	0	1	0	0
Neurology	1	4	1	6	0	0
Gastroenterology	0	1	0	1	0	0
ICU	0	3	0	2	0	0
Cardiology	2	16	1	11	0	2
Orthopedics	1	1	0	0	0	0
Op theater orthopedics	0	0	0	0	0	0
Cardiovascular surgery	0	1	0	1	0	0
Surgery ward 2	0	1	0	0	0	0
Surgery ward 1	0	1	0	1	0	0
Urology	0	2	0	0	0	0
Ob/ gynecology ward 2	3	0	0	0	0	0
Ob/gynecology ward 1	0	0	0	0	0	0
Neurosurgery ward	0	0	0	8	0	0
Otorhinolaryngology	0	1	0	0	0	0
Pediatrics	0	11	0	4	0	0
Pediatric surgery	0	0	0	0	0	0

Psychiatry	0	2	0	0	0	0
Osteo-articular tuberculosis	0	0	0	0	0	0
Palliative care	0	0	0	0	0	0
Physical Rehabilitation	0	2	0	0	0	0
Dermatology	0	0	0	0	0	0
Pneumo-phthisiology	0	0	0	0	0	0
Radiotherapy	0	0	0	1	0	0
Forensic medicine	0	0	1	0	0	0
Hospital Technical staff	0		0		0	
Hospital administration	0		0		0	
Medical front desk clerk	0		0		0	
Hospital housekeeper staff	4		0		0	
TOTAL	**11**	**315**	**3**	**103**	**0**	**7**

CONCLUSIONS

The Cellular Biology laboratory of the University Emergency Clinical Hospital is testing for SARS-CoV-2 infections using RT-PCR technique. Due to emergency needs during night shifts, patients are tested in the emergency ward using Antigen RDTs. All tested patients using rapid antigen tests are retested the next day with RT-PCR.

During 2nd trimester of 2021 were performed 2998 RT-PCR tests (1375 in April, 988 in May, 635 in June) were with 425 positive results (326 positive tests in April, 106 positive tests in May and 7 positive tests in June). The positivity rate was 23.70% in April, 10.72% in May, 1.10% in June.

There was a strong decline in the prevalence of SARS-CoV-2 infection.

The highest positivity rate was for the patients from the Emergency ward.

There were few cases among health care personnel due to prophylactic measures such as equipment and vaccination and also by natural immunization after infection. There is no routine screening for antibody seroprevalence among healthcare workers.

RT-PCR detects active SARS-CoV-2 infection and has high sensitivity and specificity but are expensive, requires laboratory infrastructure and skilled personnel, with a turnaround time of hours or days.

Ag RDT detects active SARS-CoV-2 infection, easy to perform, quick results enabling rapid implementation of infection control measures, less expensive than RT-PCR, but with variable sensitivity and specificity. Lower sensitivity means the

negative predictive value is lower than for RT-PCR. Confirmatory RT-PCR of Ag-RDT positive is required in low prevalence settings and for Ag-RDT negative in high prevalence settings. Negative Ag-RDT cannot be used to remove a contact from quarantine [9].

REFERENCES

[1] Vaugan Adam, Delta to dominate world, New Sci. 2021 Jul 3; 250(3341): 9. Published online 2021 Jul 2. doi: 10.1016/S0262-4079(21)01121-0, PMCID: PMC8253579, PMID: 34248243,

[2] Ding X. Liu, Jia Q. Liang, and To S. Fung, Human Coronavirus-229E, -OC43, -NL63, and -HKU1 (Coronaviridae), Encyclopedia of Virology. 2021 : 428–440.,Published online 2021 Mar 1. doi: 10.1016/B978-0-12-809633-8.21501-X, PMCID: PMC7204879

[3] https://apps.who.int/iris/bitstream/handle/10665/334253/WHO-2019-nCoV-Antigen_Detection-2020.1-eng.pdf

[4] Chen Y, Liu Q, Guo D. Emerging coronaviruses: genome structure, replication, and pathogenesis. J Med Virol. 2020;92:418–423. doi: 10.1002/jmv.25681.

[5] Zhe Yan, Kathryn V. Holmes, and Robert S. Hodges Expression and Characterization of Recombinant S2 Subunit of SARS-coronavirus S Fusion Protein https://www.ncbi.nlm.nih.gov/pmc/articles/PMC7123102/

[6] Nidhi Verma, Dhaval Patel, and Alok Pandya, Emerging diagnostic tools for detection of COVID-19 and perspective, https://www.ncbi.nlm.nih.gov/pmc/articles/PMC7683280/

[7] https://www.promega.ro/resources/guides/nucleic-acid-analysis/pcr-amplification/

[8] Antigen-detection in the diagnosis of SARS-CoV-2 infection using rapid immunoassays. Interim guidance. 11 September 2020. Geneva: World Health Organization; 2020. (https://www.who.int/publications/i/item/antigen-detection-in-the-diagnosis-of-sars-cov-2infection-using-rapid-immunoassays, accessed 18 November 2020).

[9] https://www.who.int/publications/i/item/diagnostic-testing-for-sars-cov-2

MATHEMATICAL MODELS FOR THE SYNTHESIS OF PLANT-BASED COMPOSITIONS WITH IMPROVED AMINO ACID COMPOSITION

Ph.D. Student Irina Gaivoronskaya[1]
Prof. Dr. Valentina Kolpakova[2]
[1, 2] All-Russian Research Institute for Starch Products – Branch of V.M. Gorbatov Federal Research Center for Food Systems of Russian Academy of Sciences, Kraskovo, Russia

ABSTRACT

The aim of the work was to optimize the process of obtaining multicomponent protein compositions with high biological value and higher functional properties than the original vegetable protein products. Was realized studies to obtain biocomposites on the base of pea protein-oat protein and pea protein-rice protein. Developed composites were enriched with all limited amino acids. For each of the essential amino acids, the amino acid score was 100% and higher. Protein products used in these compositions are not in major allergen list, which allows to use these compositions in allergen-free products and specialized nutrition. To determine biosynthesis parameters for compositions from pea protein and various protein concentrates with the use of transglutaminase enzyme, was studied effect of concentration and exposition time on the amount of amino nitrogen released during the reaction. Decreasing of amino nitrogen in the medium indicated the occurrence of a protein synthesis reaction with the formation of new covalent bonds. Were determined optimal parameters of reaction: the hydromodule, the exposure time, the concentration of EP of the preparation, were obtained mathematical models. Studies on the functional properties of composites, the physicochemical properties of the proteins that make up their composition, and structural features will make it possible to determine the uses in the manufacture of food products based on their ability to bind fat, water, form foam, gels, and etc.

Keywords: *plant-based preparations, transglutaminase, protein compositions, amino acid score, biological value*

INTRODUCTION

The increase in the population of the planet allows experts today to predict the progressive shortage of protein foods. The shortage of protein on the planet is estimated at 10-25 million tons per year. Approximately half of the world's population suffers from a lack of protein. The lack of food protein is not only an economic, but also a social problem of the modern world [1]. With the help of biotechnological processes with the usage of microorganisms have not yet had any success in obtaining new alternative sources of this mandatory and valuable component of food. This dramatically increases the role of natural proteins, enhances the importance of high-tech technological processes in their production and use in the form of new forms. Plant-based diet containing a complete protein in

the required amount might be created on the base of usage of protein preparations obtained from protein-containing sources with different chemical composition and biological value. Most of the cereals are deficient in lysine, one of the most important from the essential amino acids in human nutrition, while legumes contain this amino acid in sufficient quantity. On the other hand, cereal proteins can supplement legume proteins with the deficient amino acid methionine [2]. Along with soy proteins, with appropriate functional properties, pea, rice and oat proteins also can be successfully used for enrichment and enhancing of the biological value of food products [3]. With the usage of enzyme preparation transglutaminase for the biosynthesis of composite protein products with increased biological value from a technological point of view, it may be important to vary the content of free amino groups in the used plant preparations. Adding proteins with a high content of free amino groups, in particular lysine, to proteins with a low amount of them will increase the reactivity of the latter [4] and form modules with a given composition and functional properties.

The aim of this work is an optimization of parameters of biosynthesis multi-protein compositions, created on the base of pea protein with the selection of their composition on the basis of the quantitative content of amino acids in them, and above all, essential, so that the human body received full proteins, and this protein product could be more widely used in the manufacture of food products.

MATERIALS AND METHODS

The main materials used were samples of pea (Roquette, France), rice (Beneo, Belgium) and oat (Tate & Lyle, Sweden),. The chemical composition of protein concentrates is shown in Table 1. The enzyme preparation used was the enzyme preparation (EP) of the 'classical' transglutaminase (TG) (Novozymes, Denmark).

Table 1. *The chemical composition of protein products*

Protein product	Humidity, %	Protein, %	Fat, %	Insoluble fibers, %	Carbohydrates, %
Pea	10,0	84,0	5,0	1,0	0
Rice	12,0	79,0	5,0	3,2	6,0
Oat	6,0	56,0	3,0	2,0	18,0

Conclusion about the reaction, with the transglutaminase enzyme, between proteins with different chemical nature was based on the amount of released amine nitrogen. Amine nitrogen was determined by formol titration. To do this, 50 cm^3 of distilled water was added to 10 g of the fermented DWG mixture with protein concentrates taken at certain ratios, then the mixture was dispersed for 4-5 minutes at 500 min^{-1}. The mixture was centrifuged at 5500 min^{-1} for 20 minutes. The supernatant was decanted, 5 cm^3 from it was transferred into a glass beaker, mixed with 20 cm^3 of distilled water after has been measured the pH. The pH meter electrodes were loaded into the test suspension. Neutralization of free carboxyl groups was performed with 0.05 N NaOH solution. Alkali was added while stirring, following the readings of the potentiometer. When the pH of the solution reached 7, was added 0.5 cm^3 of the formula mixture with phenolphthalein 50 cm^3 of 40% formalin + 2 cm^3 of 1% alcohol solution of phenolphthalein). The mixture was

titrated with 0.05N NaOH solution to pH 9.1-9.5, which corresponded to the bright red staining of the sample. All reagents were chemically pure.

Amine nitrogen (in mg /%) (N) was calculated by the formula: N = A * 0.7 * 100 / V, where: A -is the amount of cm^3 of 0.05N NaOH, followed by titration; V- is the amount of solution for titration; 0.7- is the amount of nitrogen in g, corresponding to 1 cm^3 of 0.05 N NaOH solution.

For the preparation of two-component fermented compositions, weighed protein products at their specific ratios were mixed on a stirrer at a speed of 500 min^{-1}. Samples of transglutaminase EP were placed in a microbiological test tube with a cap, was added 3,6 cm^3 of phosphate buffer solution with predetermined pH, mixed vigorously, and was added 1 g of a mixture of protein products. The tubes were placed in a thermostat, shaken at 170 min^{-1} and a temperature of 50 °C.

For the preparation of two-component fermented compositions, weighed protein products at their specific ratios were mixed on a stirrer at a speed of 500 min^{-1}. Samples of transglutaminase EP were placed in a microbiological test tube with a cap, was added 10.5 cm^3 of distilled water, in accordance with a given hydromodule, mixed vigorously, and was added 1 g of a mixture of protein products. The tubes were placed in a thermostat, shaken at 170 min^{-1} and a temperature of 50°C, and the proteins were reacted at different flow times and concentrations.

RESULTS AND DISCUSSION

With the help of the program developed by us on the basis of the Monte Carlo calculation method, were compiled protein compositions with an improved amino acid profile. In time of calculating was used amino acid composition data of protein products for the proposed mixtures, data for the reference protein based on the recommendations of the FAO WHO (2011) [5]. For pea and oat concentrates, the optimum ratio of proteins in the composition was 1: 1 (table 2), for pea and rice concentrates - 1: 0.6 (table 2). These ratios provided the optimal amino acid fastness and were economically feasible.

Table 2. *An amino acid score of proteins from compositions of the protein concentrates,%*

Indicators	Protein compositions			Protein concentrate	
	PEA	OAT	RICE	PEC/OC	PEC/RC
Mass fraction of proteins, %	84.0	56,3	79.5	70.2	81.8
Amino acids	Score, %				
Valine	125	65	137	132	157
Leucine	134	62	124	135	158
Isoleucine	156	62	113	149	170
Threonine	152	56	176	142	196
Lysine	148	33	147	117	141
Methionine + cysteine	151	103	136	181	177
Phenylalanine + tyrosine	47	82	147	101	105

Note: PEC – pea concentrate; OC – oat concentrate; RC-rice concentrate

The data showed that rice concentrate had the highest amino acid scores, oat protein had the lowest values, pea concentrate contained insufficient amounts of sulfur-containing amino acids, which does not contradict the literature data. Amino acid composition of protein compositions with pea concentrate, in comparison with individual samples, was significantly improved due to rice and oat concentrates. This increase is especially valuable in all two-component composites for lysine, threonine, phenylalanine and rytosine, sulfur-containing amino acids, the deficiency of which is noted in most grain crops [6]. The most balanced in terms of amino acids was the PEC/RC composite composition, the most unbalanced (in sulfur-containing amino acids) - the PEC/OC composition composite.

To optimize the parameters of the biosynthesis of compositions from protein concentrates using TG was studied the effect of concentration of EP, exposure time and hydromodule on the amount of amino nitrogen released during the reaction with the enzyme.

Considering that in transglutaminase reactions, the transfer of amino groups - NH_2 between molecules occurs with the formation of new covalent bonds, the amount of amino nitrogen in the studied systems decreased, therefore, by the number of unreacted amino groups, it was possible to judge the course of the synthesis process between different types of proteins.

To obtain results on the influence of various factors on the content of amino nitrogen for the composition of pea protein-oat protein, methods of mathematical planning of the experiment were used, with pH = 6.8–7.0 (const), temperature = 50 ° C (const). The exposure time (X3) was changed in the range of 5 ÷ 20 min, the hydronic module (X1) - in the range of 1: 5 to 1: 8, the concentration of EP (X2) - from 0.0015 to 0.003 U / g protein (table 3).

Table 3. *The effect of the concentration of EP, the exposure time and hydromodule on the amount of amine nitrogen in the process of synthesis of the composition of the pea concentrate-oat concentrate*

№	Concentration of EP, U/g for DS	Exposure time, min	Hydromodule	Amine nitrogen, mg%
1	0,0015	5	1:5	7,98
2	0,0015	10	1:6	7,28
3	0,0015	15	1:7	6,16
4	0,0015	20	1:8	7,98
5	0,002	5	1:6	9,38
6	0,002	10	1:7	7,56
7	0,002	15	1:8	6,86
8	0,002	20	1:5	8,4
9	0,0025	5	1:7	6,44
10	0,0025	10	1:8	7,84
11	0,0025	15	1:5	7,14
12	0,0025	20	1:6	8,4
13	0,003	5	1:8	7,7
14	0,003	10	1:5	7,42
15	0,003	15	1:6	7,7
16	0,003	20	1:7	7,7

According to the experiment data, using the TableCurve 3D program, were constructed response surfaces for amino nitrogen (Fig. 2). Data processing in programs Matematika and Table Curve 3D

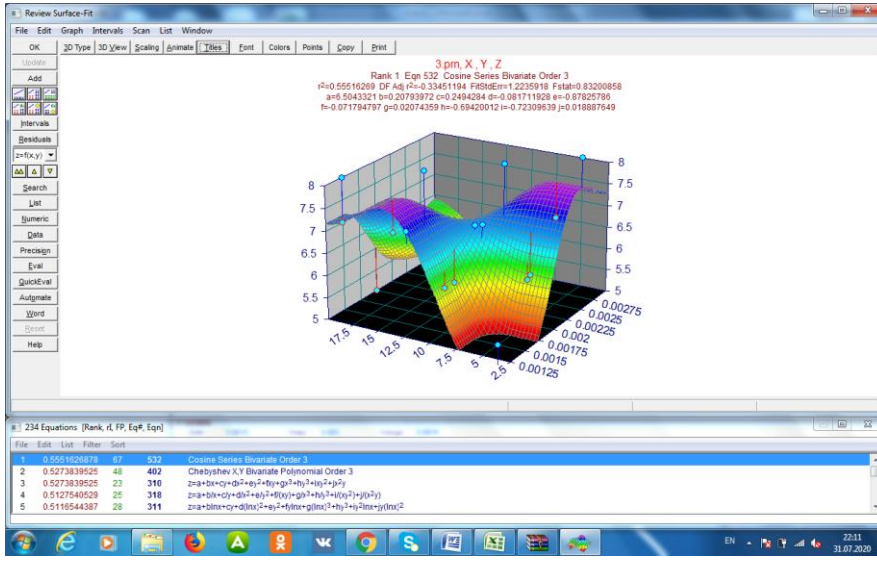

$$Y = 7.4865 + 149X_1 + 0.0335X_2\text{-}0.1145X_3$$

where x –concentration of EP, g/g of protein; y-time of exposition, min; z- back hydromodule

Fig. 2. *The dependence of the amount of amine nitrogen on the reaction parameters for the composition of pea concentrate-oat concentrate*

To obtain the results on the influence of various factors on the content of amino nitrogen for the composition of pea protein concentrate-rice protein, were used methods of mathematical planning of the experiment. Taking into account the data obtained during the protein concentrate-rice protein experiment, the most effective reaction parameters were selected: pH - 6.8–7.0 (const), temperature 50°C (const). The exposure time (X3) was changed in the range of 5 ÷ 20 min, the hydromodule (X1) - in the range of 1: 5 to 1: 8, the concentration of OP (X2) - from 0.0015 to 0.003 U / g protein (table 4).

Table 4. *The effect of the concentration of EP, the exposure time and hydromodule on the amount of amine nitrogen in the process of synthesis of the composition of the pea concentrate-rice concentrate*

№	Concentration of EP, U/g for DS	Exposure time, min	Hydromodule	Amine nitrogen, mg%
1	0,0015	5	1:5	7,28
2	0,0015	10	1:6	7,14
3	0,0015	15	1:7	7,14
4	0,0015	20	1:8	6,72
5	0,002	5	1:6	7,28
6	0,002	10	1:7	7,28
7	0,002	15	1:8	7,14
8	0,002	20	1:5	7,84
9	0,0025	5	1:7	7
10	0,0025	10	1:8	7,42
11	0,0025	15	1:5	7,98
12	0,0025	20	1:6	7,98
13	0,003	5	1:8	7,28
14	0,003	10	1:5	8,4
15	0,003	15	1:6	8,26
16	0,003	20	1:7	7,84

According to the experiment data, using the TableCurve 3D program, were constructed response surfaces for amino nitrogen (Fig. 3). Data processing in programs Matematika and Table Curve 3D

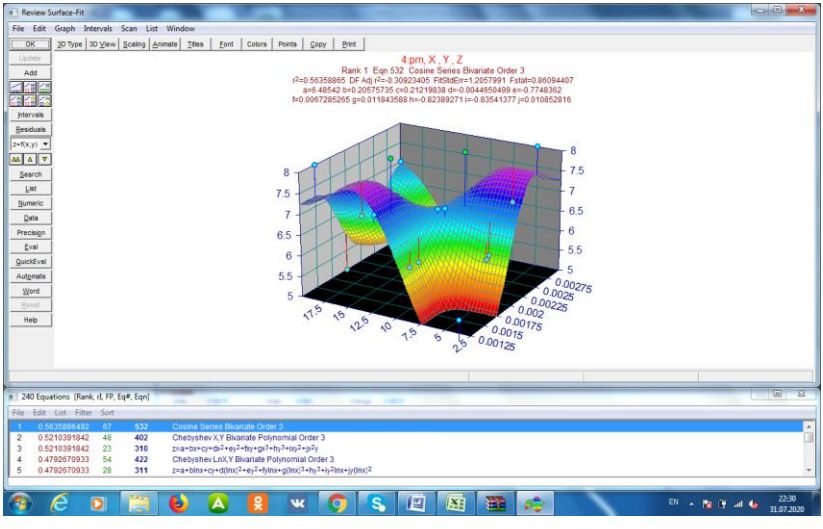

$$Y = 7.5775 + 567X_1 + 0.0245X_2\text{-}0.2555X_3$$

where x –concentration of EP, g/g of protein; y-time of exposition, min; z- back hydromodule

Fig. 3. *The dependence of the amount of amine nitrogen on the reaction parameters for the composition of the pea concentrate-rice concentrate*

For the composition of pea concentrate-oat concentrate, the patterns of change in the amount of amine nitrogen in the course of the reaction were similar to the patterns characteristic of the composition of pea concentrate-rice concentrate. The minimum amount of amino nitrogen after reaction with TG in the composition of pea concentrate-oat concentrate was observed in the reaction medium at a concentration of 0.0015 g / g of protein, exposure time of 15 minutes and a water ratio of 1: 7. The minimum amount of amino nitrogen after reaction with TG in the composition of pea concentrate-rice concentrate was observed in the reaction medium at a concentration of 0.0015 g / g of protein, exposure time of 20 minutes and a water ratio of 1: 8.

CONCLUSION

Due to its unique properties, TG is widely used in the meat and dairy industry for the aggregation of protein molecules in the production of restructured products from raw materials of various qualities [7], [8], [9]. The enzyme is safe, produced by inexpensive sources of biosynthesis, which makes its use wide. Significantly less TG is used in the manufacture of baked goods (bread, biscuits) [4], [10], [11] and isolated studies are known to produce compositions from vegetable proteins [12].

With the help of a program developed on the basis of the Monte-Carlo calculation method, were compiled protein concentrate compositions with improved amino acid composition. Taking into account the mass fraction of protein and the amino acid composition of the concentrates, their ratios and amino acid levels are determined for protein-protein composites obtained from various types of plant materials (peas, rice, oats). Composites are enriched with lysine, threonine, sulfur-containing amino acids in relation to cereals and leguminous crops. Using biotechnological reactions with the participation of the enzyme class transferase (transglutaminase) obtained biocomposites composition: pea concentrate-oat concentrate, pea concentrate-rice concentrate. Experimentally using the method of formol titration according to the amount of amino nitrogen remaining in the reaction medium, the reaction parameters were determined: the duration of its flow and the concentration of the enzyme preparation.

For the composition of pea concentrate-oat concentrate, the minimum amount of amino nitrogen after reaction with TG in a two-component product was observed in the reaction medium at a concentration of 0.0015 g / g of protein, exposure time 20 minutes and a water ratio of 1: 7; for the composition of pea concentrate-rice concentrate, the minimum amount of amino nitrogen was released in reaction with TG at a concentration of 0.0015 g / g of protein, exposure time of 20 minutes and a water ratio of 1: 8. These data indicated a high intensity of the reaction of the synthesis of new forms of proteins. Compositions of concentrates with potato protein did not contain deficient essential amino acids, soon approached the reference protein as much as possible, or it was higher. Further studies will show what functional and technological properties created protein composites will possess and in which food products they can be used.

REFERENCES

[1] Donchenko L.V. Technology of functional food products: textbook for high schools. — 2nd edition. — Moscow: Jurait, 2018. — pp.101-102

[2] Iqbal A, Khalil IA, Ateeq N and Khan MS, Nutritional quality of important food legumes. Food Chem, 97:331-335 (2006)

[3] Tömösközi S, Lásztity R, Haraszi R and Baticz O, Isolation and study of the functional properties of pea proteins. Nahrung/Food 45:399-401 (2001).

[4] Marco C, Rosell CM. Breadmaking performance of protein enriched, gluten-free breads. Eur Food Res Technol. 2008;227:1205–1213. doi: 10.1007/s00217-008-0838-6.

[5] Dietary protein quantity evaluation in human nutrition: Report of an FAO Expert Consultation.-Rome: FAO,2013-66pp.

[6] Koehler P., Wieser H. Chemistry of Cereal Grains. In: M. Gobbetti and M. Gunzle (eds.). Handbook on Sourdough Biotechnology, 11. 2013. Chapter 2, Springer Science+Business Media New York . DOI 10.1007/978-1-4614-5425-0_2

[7] Kuraishi C., Sakamoto J., Yamazaki K., Susa Y., Kuhara C., Soeda T. Production of restructured meat using microbial transglutaminase without salt or cooking. J. Food Sci. 1997. V. 62. pp. 488–490. doi: 10.1111/j.1365-2621.1997.tb04412.x

[8] Ozer B., Kirmaci H.A., Oztekin S., Hayaloglu A., Atamer M. Incorporation of microbial transglutaminase into non-fat yogurt production. Int. Dairy J. 2007. V. 17. pp. 199–207. doi: 10.1016/j.idairyj.2006.02.007

[9] Lorenzen P.C., Neve H., Mautner A., Schlimme E. Effect of enzymatic cross-linking of milk proteins on functional properties of set-style yoghurt. Int. J. Dairy Technol. 2002. V. 55. pp. 152–157. doi: 10.1046/j.1471-0307.2002.00065.x

[10] Lorenzen P.C., Neve H., Mautner A., Schlimme E. Effect of enzymatic cross-linking of milk proteins on functional properties of set-style yoghurt. Int. J. Dairy Technol. 2002. V. 55. pp. 152–157. doi: 10.1046/j.1471-0307.2002.00065.x

[11] Kuraishi C., Yamazaki K., Susa Y. Transglutaminase: its utilization in the food industry. Food Rev. Int. 2001. V. 17. pp. 221–246. doi: 10.1081/FRI-100001258

[12] Kolpakova V.V., Gaivoronskaya I.S., Gulakova V.A., Sardzhveladze A.S., Composition on the basis of plant-based proteins with the use of transgutaminase // International Multidisciplinary Scientific GeoConference SGEM (Bulgaria, Albena, 2018) – pp.119-126

METHODS FOR QUANTIFICATION OF THE MAIN CANNABINOIDS IN CBD OIL

Assoc. Prof. Ph.D. Student Nicoleta Mirela Blebea[1]
Prof. Simona Negreș Ph.D.[2]
[1] Pharmacology and Clinic Pharmacy Department, Faculty of Pharmacy, Ovidius University, Constanta, Romania
[1, 2] Pharmacology and Clinic Pharmacy Department, Faculty of Pharmacy, Carol Davila UMF, Bucharest, Romania

ABSTRACT

Cannabidiol (CBD) is an alkaloid present in *Cannabis sativa*, together with tetrahydrocannabinol (THC) and more than 120 other substances belonging to a group of compounds named cannabinoids. Due to the continuous increased usage of CBD oils, it became necessary to be developed efficient methods for the identification of its compounds and especially for the characterization of the cannabinoids from the commercial specimens. Cannabinoids may be detected by many and different analytical methods, including immunoassays (EMIT®, Elisa, fluorescent polarization, radioimmunotest), techniques of flat chromatography: classic thin layer chromatography (TLC), optimum performance laminar chromatography (OPLC) and multiple development automatization (AMD), gas chromatography-mass spectrometry (GC-MS), high-performance liquid chromatography-mass spectrometry (HPLC-MS). Ultraviolet signal (UV) is used for the quantification of major cannabinoids and the mass spectrometer is used for the quantification of minor cannabinoids. The purpose of this study was to compare the performances of TLC, Ultra High-Performance Liquid chromatography with Photodiode Array Detection (UHPLC with PDA) and LC-MS/ MS technique for the qualitative and quantitative determination of cannabinoids in 3 commercial oils with CBD. Having in view that CBD may be found in many forms of oils, on the legal market of the internet, we believe that the development of a method for the qualitative and quantitative determination may be an interesting subject for the pharmaceutical professional persons.

Keywords: *CBD oils, cannabinoids, analytical, THC, quantification.*

INTRODUCTION

The Cannabis family includes *Cannabis sativa* and *Cannabis indica* species. *Cannabis sativa* contains over 500 unique compounds, including over 120 natural cannabinoids. There were reported many therapeutical properties attributed to their pharmacological characteristics, which leads to a significant interest in their use in nutraceuticals and other consumption products [1]. The *Cannabis* plant was used from the oldest times for producing hemp fibers (for clothes, rope and paper), seeds that may be used as food for animals and also as a medicinal plant. CBD is one of the main alkaloids from the composition of cannabis plants together with other identified alkaloids [2]. The two major neuroactive compounds from the cannabis

plants are: the main psychoactive alkaloid, tetrahydrocannabinol (THC) and non-psychoactive alkaloid CBD [3].

Taking into account the present legislation, there are small differences regarding the quantities of THC admitted in the hemp products, the concentrations varying between 0,05 and 0,6% [4]. In the plant, the cannabinoids are mostly present under the form of acids, which are decompounded by decarboxylation. CBD is widely used although its benefic effects are reported especially based on the casuistical observations [5],[6]. In some countries, the products with CBD are legal, while in other countries they are forbidden, thus aggravating the confusion. At present, CBD is used as an active ingredient in the following products: Epidiolex® - oral solution (contains only CBD), approved in 2018 by Food and Drug Administration (FDA) as a medical product used for the treatment of seizures associated with Dravet and Lennox-Gastaut syndromes and Sativex® - oral-mucosal spray (contains both CBD and THC, in the percentage of 1:1) [7], [8], [9]. More clinical studies are in progress for the potential treatment of neurological and behavioral disorders. As CBD has a complex mechanism of action, there is a high potential of its use in the treatment of different pathologies [4].

The quantification of cannabinoids is essential for the proper labeling of cannabis products, for quality control, as well as for establishing the legality regarding the content of THC. The oils with CBD contain potentially useful nontoxic phyto cannabinoid substances. Together with the increase of the interest of the patients for the oils with CBD, there are indicated more researches for a better understanding of their therapeutic potential and of the safety profile [1], [10], [11], [14].

The present paper describes a series of analytical methods used for the separation of cannabinoids necessary for the analysis of the oils with CBD from the market. Using chromatographic methods we can determine the original composition of cannabinoids in oils by direct analysis [11]. CBD oil is traded for being used by children (for Dravet syndrome, ADHD, autism) [12], old persons (Alzheimer disease, dementia, Parkinson disease, cardiovascular diseases, inflammatory diseases) [13], patients that suffer from complications (cancer, multiple sclerosis, chronic pain, diabetic complications, arthritis, epilepsy) [11] and even for pets (anxiety, appetite, sleep, osteoarthritis) [15]. From this reason, the qualitative and quantitative certification is necessary through a selective, simple and fast method. The oil-rich in CBD became more and more popular and it is administrated under the form of sublingual drops, gelatinous capsules or as unguent local ointment [11]. At present, the market is in the progress of developing towards more sophisticated products, including oral capsules, liposomal products, skin lotions and chewing gums that contain CBD [6], [7].

MATERIALS AND METHODS

TLC

With the help of this technique and of the kit from alpha-CAT ® the main ingredients from cannabis may be visualized due to a reaction of a specific coloration, which represents the cannabinoids present in the oils with CBD or from

the cannabis product. Up to 4 specimens may be tested for each chromatographical plate.

TLC is the first method used for the chemical analysis of cannabis. It has the advantage of parallel analyses, although it has limits in resolution and sensitivity. The advantages are the reduced costs, the simple preparation of the specimens and the nondestructive method. Moreover, it allows the use of a wide range of chemical reactive substances for detection.

I used 3 modalities of oils traded on the internet, which I named as follows for easier identification: specimen 174 – product declared with a content of 1350 mg/100 ml total concentration of cannabinoids, specimen 175 - product declared with a content of 2, 5% CBD, specimen 181 - product declared with a content of 8% CBD, 4mg/drop.

Whether our specimen has a decreased or increased rate of cannabinoids, we can calculate a factor of multiplication for testing of the rate of THC is decreased or increased in the oils with CBD analyzed. We apply this simple rule based on the weight of the specimen: Factor of multiplication = (100 mg x 2µl) / weight of the specimens (mg) X extraction fluid (µl).

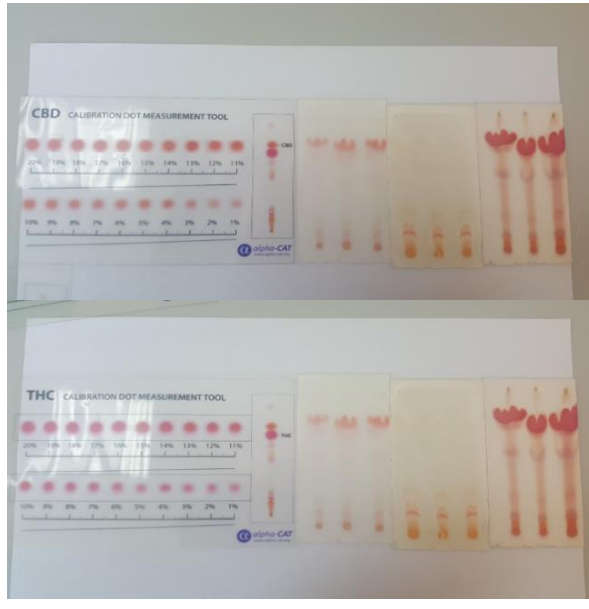

Fig.1. *Comparing with the area cu rigla graphical ruler of cannabinoids alpha-CAT® for CBD and THC, specimens 174, 175, 181.*

At present, TLC is a cheap method for the analysis of cannabinoids approved by the Office of the United Nations for Drugs and Crimes for the routine control of the content of cannabinoids. For the applications that require a high sensitivity for instance in pharmacology, it is not an indicated method.

UHPLC-PDA

Through UHPLC technique with PDA detection it was followed the separation and quantitative determination of CBD present in 3 oils. The chromatographical separation was made using a PerkinElmer Brownlee Analytical C18 column (50mm × 4,6mm id, 5µm) or the equivalent, using the evaluation in gradient with 0,1% acid formic in water as mobile phase A and 0,1% acid formic in acetonitrile as mobile phase B. For quantification, the length of detection wave was set at 210 nm.

The method was established and optimized in the following chromatographical conditions: debit-1mL/min, temperature of the column -30°C, injecting volume-5µL, mobile phases - formic acid and formic acid with acetonitrile(V/V).

Solvents, standards and specimens: Solution of cannabidiol, 1,0 mg/ml SLBM6755V; Standard Analytic Standard Sigma Aldrich; Methanol absolute, for HPLC, LiChrosolv®; Acetonitrile, for HPLC, LiChrosolv®; Formic Acid for LC / MS, Fischer Chemical®; 2-propanol, for HPLC, LiChrosolv®; 3 variants of hemp oils from Romania and Netherlands.

Table 1. *Exact Quantification of CBD for the 3 oil specimens*

Sample Name	Avg. Amount	Units	Avg. Plates (Foley-Dorsey)	Avg. Tailing Factor	Avg. Resolution	Avg. Area
Stand CBD 20 ppm	0.0000	µg/mL	11,217	1.407	2.27	2,203,748.7
CBD 174 D100	35.2245	µg/mL	7,385	1.083	1.25	2,803,382.6
CBD 175 D100	48.3351	µg/mL	N/A	0.000	1.09	3,319,760.2
CBD 181 D4500	27.3011	µg/mL	6,110	0.995	0.00	2,491,310.3

The optimized method is a simple, fast, selective, sensitive and useful method for the verification of the stability of CBD in the pharmaceutical forms, may be useful for quality control of the medicine products, both under the form of active substance and pharmaceutical formulations. The perspective of the study consists in applying this method on different pharmaceutical forms but also on different types of specimens (biological, soil, water, etc.)

LC-MS

I researched a technique of qualitative and quantitative analysis of CBD and CBG from three commercial hemp oils with the help of a UHPLC device with MS detector. The fluid chromatography system PerkinElmer® Flexar UHPLC connected to a LC/MS PerkinElmer® 5500 QTRAP model detector allows the analysis of different compounds at low concentrations (e.g. pesticides, contaminant, mycotoxin, dopant substances, drugs). The technique combines the separation power of UHPLC and the MS capacity of obtaining information about the mass and structure of the analytes. The mass spectrometer separates ions in gas phase based on m/z (load/mass). The chromatographical separation was performed using a

Perkin Elmer Brownlee Analytic DB AQ C18 (1,9 µm 100x2,1 mm) column or an equivalent with elution in gradient, debit 400 µL/min, temperature of the column 40°C, injecting volume 5µL.

The method developed detected the corresponding drops for the two compounds CBD and CBG. The calibration curve was outlined in the interval 10 - 100 ng / mL. The detection limit at the level of 3, 12 ng / mL was validated. The preparation of the specimens eliminates the use of chloroform, which was used regularly in the analysis of cannabinoids, decreasing the costs of materials, using more ecological solvents and improving the safety of the laboratory.

Table 2. *Exact quantification of CBD for the specimen of hemp oil*

Product statement	**CBD content mg/mL**
CBD oil 13.5 mg/mL	3.194
Ozonated hemp oil with 2.5% CBD and terpene oil	2.250
CBD oil 4 mg/drop	123.525

In the research literature it is widely reported that CBD coelutions with a CBG related cannabinoid but their molecular weights are different [1], [10]. For this reason, the analytic result UHPLC-PDA was confirmed with a MS complementary technique. This analytical method may be used for different applications, for instance for the quantitative and qualitative control of the CBD oil by a selective, simple and fast method.

The content of CBD of the commercial specimens analyzed in this study is not clearly specified by the manufacturer. The analysis of the three specimens of hemp oil revealed the real concentration of CBD from the specimens, highlighting the necessity of this type of analytical method.

CONCLUSION

The hemp oil from *Cannabis sativa* L. is a natural source rich in important nutritive substances, not only polyunsaturated fat acids and proteins, but also terpenes and cannabinoids, which contribute to the therapeutical benefits of the oil with CBD. Therefore, it is important to exist an analytical method for the determination and quantification of cannabinoids for establishing the exact concentration from the commercial specimens, an interesting subject for the professionals from the pharmaceutical domain.

HPLC-PDA is widely applied in the quantification of cannabinoids, as the approach is a facile one, robust and cheap. Nevertheless, LC-MS / MS is the most versatile among the methods, both regarding the dynamic range, and related to the offer of a real image of the content of CBD of the oils analyzed. The most frequently are used columns with reverse phase (mainly C18 variant or biphenyl) with a solvent of methanol-water containing 0,1% formic acid. The analytical benefits of the triple-quadrupole LC-MS / MS system are sensitivity, selectivity and

identification of the mass. As for the analysis of terpenes, UHPLC-PDA is not able to detect most of the terpenes, the connection to MS being compulsory. Flavonoids may be very well analyzed with all the detection methods connected to LC.

Based on the information presented in this study, ideal quantification method of cannabinoids is LC-MS / MS for the cannabinoids using the PerkinElmer system, especially in clinical research. This analytical method may be used for different applications, quantitative and qualitative control of CBD oil by a selective, simple and fast method.

The perspective of the study is to apply these methods to the different pharmaceutical forms, but also to other types of specimens (biological, soil, water, etc.). It is also an interesting alternative for the routine analyses in the criminalistic sciences. The analytical methods easily characterize and quantify CBD in the oils available from the commercial sources for offering a robust instrument for the determination of the potency, safety and quality, with usages both in human medicine and in the veterinary one.

ACKNOWLEDGEMENTS

We would like to thank the Scient Research Center for Instrumental Analysis, Tâncăbești, 1 Petre Ispirescu Street, 077167, Tâncăbești, Ilfov, Romania for the equipment provided.

REFERENCES

[1] Turner S.E., Williams C.M., Iversen L., Whalley B.J., Molecular Pharmacology of Phyto cannabinoids, Progress in the Chemistry of Organic Natural Products, Switzerland, 2017, vol.103, pp.61-101;

[2] Lafaye G., Karila L., Blecha L., Benyamina, Cannabis, cannabinoids, and health, Dialogues in clinical neuroscience, France, 2017, vol. 19/issue 3, pp.309–316;

[3] Ibarra-Lecue I., Mollinedo-Gajate I., Meana J.J., Callado L.F., Diez-Alarcia R., Uriguen L., Chronic cannabis promotes pro-hallucinogenic signaling of 5-HT2A receptors through Akt/mTOR pathway, Neuropsychopharmacology , U.S., 2018, vol.43, pp.2028–2035;

[4] Vlad R.A., Hancu G., Ciurba A., Antonoaea P., Rédai E. M., Todoran N., Muntean D. L., Cannabidiol-therapeutic and legal aspects. Die Pharmazie-An International Journal of Pharmaceutical Sciences, Germany, vol.75 /issue 10, pp.463-469, 2020.

[5] Elliott J., DeJean D., Clifford T., Coyle D., Potter B.K., Skidmore B., Alexander C., Repetski A.E., Shukla V., McCoy B., Wells G.A., Cannabis-based products for pediatric epilepsy: A systematic review, Epilepsy., U.K., 2019, vol.60/ issue 1, pp. 6-19;

[6] Lattanzi S., Brigo F., Trinka E., Zaccara G., Cagnetti C., Del Giovane C., Silvestrini M., Efficacy and Safety of Cannabidiol in Epilepsy: A Systematic Review and Meta-Analysis, Drugs, U.S., 2018, vol.78/issue 19, pp. 1791-1804;

[7] Giacoppo S., Bramanti P., Mazzon E., Sativex in the management of multiple sclerosis-related spasticity: An overview of the last decade of clinical evaluation, Multiple Sclerosis and Related Disorders, U.K., 2017, vol.17, pp. 22–31;

[8] Bartner L.R., McGrath S., Rao S., Hyatt L.K., Wittenburg L.A. ,Pharmacokinetics of cannabidiol administered by 3 delivery methods at 2 different dosages to healthy dogs, Canadian journal of veterinary research, Canada, vol.82/issue3, pp.178–183, 2018.

[9] Sekar K., Pack A., Epidiolex as adjunct therapy for treatment of refractory epilepsy: a comprehensive review with a focus on adverse effects, F 1000 Research, U.K., 2019, vol.8 pp.1–8;

[10] Berman P., Futoran K., Lewitus G.M., Mukha D., Benami M., Shlomi T., Meiri D., A new ESI-LC/MS approach for comprehensive metabolic profiling of Phyto cannabinoids in Cannabis, Scientific reports, U.K., 2018, vol.8/ issue 1, p.14280;

[11] Blebea N.M., Costache T., Negreș S., The qualitative and quantitative analysis of CBD in hemp oils by UHPLC with PDA and applications. Scientific Papers: Series D, Animal Science, The International Session of Scientific Communications of the Faculty of Animal Science, Romania, vol. 62/issue 1, pp.138-142, 2019.

[12] Devinsky O., Patel A.D., Cross J.H., Villanueva V., Wirrell E.C., Privitera M., Greenwood S.M., Roberts C., Checketts D., VanLandingham K.E., Zuberi S.M., Effect of Cannabidiol on Drop Seizures in the Lennox-Gastaut Syndrome, The New England journal of medicine, U.K., vol.378/issue 20, pp.1888-1897, 2018.

[13] Chagas M.H., Zuardi A.W., Tumas V., Pena-Pereira M.A., Sobreira E.T., Bergamaschi M.M., dos Santos A.C., Teixeira A.L., Hallak J.E., Crippa J.A., Effects of cannabidiol in the treatment of patients with Parkinson's disease: an exploratory double-blind trial, Journal of psychopharmacology, U.K., vol.28/issue11, pp.1088-1098, 2014.

[14] Hazekamp A., The trouble with CBD oil, Medical cannabis and cannabinoids, Switzerland, vol.1/issue 1, pp.65-72, 2018.

[15] Gamble L.J., Boesch J.M., Frye C.W., Schwark W.S., Mann S., Wolfe L., Brown H., Berthelsen E.S., Wakshlag J.J., Pharmacokinetics, Safety, and Clinical Efficacy of Cannabidiol Treatment in Osteoarthritic Dogs, Frontiers in veterinary science, U.K., 2018, vol.5 p.165;

OBTAINING NUCLEIC ACID PREPARATIONS AND THEIR HYDROLYSATES FROM BIOMASS OF METHANE-OXIDIZING BACTERIA

Prof. Dr. Alla A. Krasnoshtanova[1]
Elisaveta K. Borovkova[2]
[1, 2] D. Mendeleev University of Chemical Technology of Russia, Moscow, Russia

ABSTRACT

Due to the unfavourable environmental, social and economic situation, the need for the treatment of oncological diseases and diseases associated with impaired activity of the immune system is increasing. A lot of these drugs are made on the basis of nucleic acid components, the industrial production of which is practically non-existent in Russia. Therefore, a task of current interest is to develop the basis of the technology for obtaining components of nucleic acids, which can be widely used in medicine as immunomodulatory, wound-healing, antiviral, and diagnostic medicine, as well as for cancer treatment.

Most of the described in literature methods of isolating nucleic acid components from plant, animal and microbial raw materials are based on the use of toxic and expensive organic solvents, that's why it is impossible to apply these methods outside of laboratory conditions. The most promising source of raw materials for nucleic acids is the biomass of microorganisms (yeast and bacteria) from biomass, since the use of such source makes it possible to quickly obtain a large enough amount of biomass, and, consequently, a larger amount of nucleic acids. This allows obtaining DNA in addition to RNA. RNA and DNA substances can be used to obtain nucleosides and nitrogenous bases, which are also widely used in medicine.

The purpose of these studies was to select the conditions for the extraction of RNA and DNA from the biomass of methane-oxidizing bacteria in one technological cycle, as well as to compare the efficiency of alkaline and acid hydrolysis of microbial RNA and DNA. The need for a two-stage extraction of nucleic acids from the biomass of methane-oxidizing bacteria in order to separately extract RNA and DNA was Substantiated. It was ascertained that at the first stage of extraction at a temperature of 90 ° C, pH 9.0 for 90 min, at least 85% of RNA is extracted. After the separation of the extract by centrifugation, the partially denuclearized biomass must be re-processed under the same conditions in order to extract DNA by at least 83%. The modes of concentration of RNA and DNA solutions by ultrafiltration were selected. It was found that in order to achieve effective deposition of nucleic acids at the isoelectric point, the concentration of the RNA solution must be carried out on the UPM-10 membrane at the concentration degree of 7, and the DNA solution on the UPM-100 membrane at the concentration degree 6. The dynamics of decomposition of nucleic-protein complexes in the medium of monoammonium phosphate was investigated. It was shown that the

transition of NA into solution by at least 80% is achieved at a monoammonium phosphate concentration of 1.7 M, a temperature of 55 ° C for 90 min. The use of 5-fold washing of oligonucleotide substances with acidified water (pH 2.0) to remove excess mineral impurities was substantiated. A comparative assessment of acid and alkaline hydrolysis of RNA and DNA was carried out in order to obtain derivatives of nucleic acids.

Keywords: *methane-oxidizing bacteria, RNA, DNA, acid hydrolysis, alkaline hydrolysis*

INTRODUCTION

Due to the unfavourable environmental, social and economic situation, the need for the treatment of oncological diseases and diseases associated with impaired activity of the immune system is increasing. A lot of these drugs are made on the basis of nucleic acid components. DNA and RNA preparations of various origins, as well as their derivatives are promising therapeutic and immunomodulatory agents and can be used in food, cosmetic and other industries [1], [2].

In the cell nucleic acids are in a complex with proteins and lipoproteins. Therefore, the complexity of the isolation of nucleic acids lies in separating them from the above impurities, as well as their high degree of destruction under the influence of external factors. In this regard, the choice of reagents for DNA isolation, which inhibit or inactivate cellular nucleases, but leave the native structure of nucleic acids intact, is of great importance [3], [4].

A common method for the isolation of nucleic acids is the destruction of cells of microorganisms and animal tissues. In laboratory conditions, cell disintegration is carried out using liquid nitrogen or mechanical grinding with silicon oxide (or aluminum oxide). This step can be realized directly in a lysis buffer containing nucleases and proteases [5].

After lysis, there are two possible approaches to purifying the target DNA. The first involves processing a DNA solution by extraction with an organic solvent (phenol, chloroform), followed by precipitation of DNA with alcohols and dissolution in water and Tris-EDTA buffer. According to the second approach, differential sorption of DNA is carried out on a solid support (most often, silica gel), after which the sorbent is washed with organic solvents, and then the DNA is washed off with water or Tris-EDTA buffer.

Each of these approaches has advantages and disadvantages. In the first case, it is possible to obtain high molecular weight DNA (more than 15000 nucleotide pairs), however, significant DNA losses are possible, and the resulting preparations contain a significant amount of impurities. In the second case, it is possible to obtain highly purified preparations, however, the isolated DNA turns out to be of low molecular weight.

Known methods for producing RNA from yeast allow the isolation of low-polymer RNA, for example [6], which is used in medicine in the treatment of a wide range of diseases: from viral infections to memory disorders [7].

Work [8] describes a method for obtaining high-polymer RNA from yeast by suspending it in an aqueous 0.3-1.2 M solution of 2-ethylhexanoic acid containing 0.1-0.5 M NaCl at 92-98°C. The disadvantage of this method is the use of a synthetic, expensive and highly toxic lytic agent - 2-ethylhexanoic acid, which requires deep purification of the final product, as a result of which this method is not economical and practically not scalable.

In the article [9], an attempt was made to replace 2-ethylhexanoic acid with a large-tonnage food reagent, which significantly reduces the cost of the process since it makes it practically waste-free and easily scalable.

In the research [10] it is proposed to incubate biological material with pre-treated 3.5-7% solution of hydrofluoric acid for 2-6 hours with finely dispersed meshed glass in a buffer solution containing chaotropic agent, which makes it possible to reduce process duration, increase RNA yield and ensure isolation of both low-molecular and high-molecular RNA fractions.

In a number of works it is proposed to isolate RNA from the blood by sorption on ion-exchange resins in quaternary ammonium form [11], cationite in H^+-form [12], from cells of microorganisms, plant and animal tissues by treatment with acid reagents, sorption on cationite in combination with treatment with proteases, desorption of nucleic acids with ionites with buffer solutions [13].

Most of the described in literature methods of isolating nucleic acid components from plant, animal and microbial raw materials are based on the use of toxic and expensive organic solvents, that's why it is impossible to apply these methods outside of laboratory conditions.

The most promising source of raw materials for nucleic acids is the biomass of microorganisms (yeast and bacteria) from biomass, since the use of such source makes it possible to quickly obtain a large enough amount of biomass, and, consequently, a larger amount of nucleic acids. This allows obtaining DNA in addition to RNA. RNA and DNA substances can be used to obtain nucleosides and nitrogenous bases, which are also widely used in medicine.

The purpose of these studies was to select the conditions for the isolation of RNA and DNA from the biomass of methane-oxidizing bacteria in one technological cycle, as well as to compare the effectiveness of alkaline and acidic hydrolysis of microbial RNA and DNA.

MATERIALS AND METHODS

The object of the study was condensed biomass of methanoacidating bacteria Methylococcus capsulatus, containing 20% dry substances, 10% nucleic acids (including 13.5% DNA), 65% raw protein. The determination of total nitrogen was carried out by the Kjeldahl micrometode. The phosphate ion concentration was determined by the Fiske-Subarrow method. The concentration of nucleic components was determined by Spirin and the concentration of DNA by Dische.

The process of concentrating nucleic acids solutions was carried out on a laboratory ultrafiltration apparatus with a volume of 1000 ml, using membranes of the UPM type (polysulfonamide membranes).

In the analysis of the nucleic acids hydrolysates, the high molecular weight fraction was separated by precipitation with 50% trichloroacetic acid. The low molecular weight fraction was analyzed by the Spirin method.

RESULTS AND DISCUSSION

Several methods of extracting nucleic components from the biomass of bacteria are known from the literature, but they are often multistage [3] and involve the use of organic solvents, for example, phenol and chloroform.

The most promising is the use of an aqueous alkali solution as an extractant. In these studies, it was proposed to extract nucleic acids from a 20% suspension of biomass of Methylococcus capsulatus bacteria at a pH of 9 and a temperature of 90 ° C. Extraction was carried out for 4 hours. At certain time intervals, suspension samples were taken, biomass was separated by centrifugation at 6000 rpm, and the concentration of total nucleic components in extracts was determined by the Spirin method, DNA by the Dishe method. On the basis of the obtained data, the degree of extraction of total nucleic acids and DNA was determined. The obtained results are shown in Fig. 1, from which it follows that the extraction time providing the extraction of total nucleic acids by not less than 94% should not exceed 180 minutes (3 hours). It should be noted that primarily RNA having a lower molecular weight is extracted from microbial cells, and DNA extraction begins only in the 90th minute of the process.

Thus, it was found that in order to achieve at least 94% recovery of nucleic acids in the form of protein-nucleic complexes, extraction should be carried out at a temperature of 90°C, pH 9.0, extraction time - 3 hours. At the same time, the degree of DNA extraction is 97.6%, and RNA is 94.1%.

According to previous studies, these concentrations of nucleic acids do not allow their effective precipitation at the isoelectric point, therefore, the preliminary concentration of the obtained extract by ultrafiltration is required. To separate the mixture of DNA-protein and RNA-protein complexes, the effectiveness of the ultrafiltration method was evaluated using membranes with cutoff molecular weights of 100 and 10 kDa.

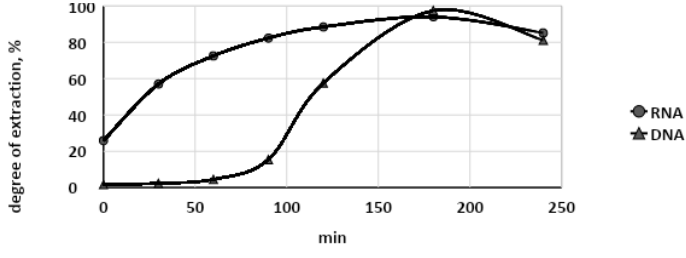

Fig. 1. *Dynamics of extraction of total nucleic acids and DNA from biomass of methanoxic bacteria Methylococcus capsulatus*

Initially, the nucleic extract was concentrated on the membrane UPM-100 to concentrate the DNA-protein complex and reduce the viscosity of the resulting filtrate. To evaluate the effectiveness of the ultrafiltration process, differential and integral selectivity and specific productivity were determined. Figure 2 shows the dependence of the specific productivity of the UPM-100 membrane on the concentration of nucleic acids in the concentrate.

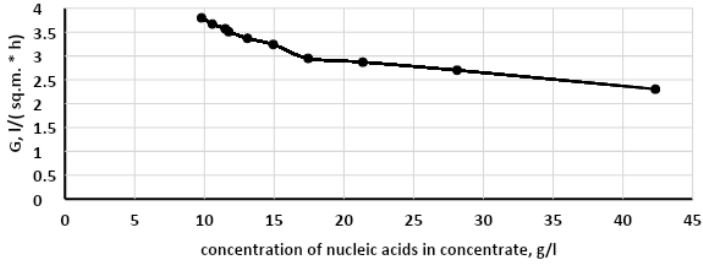

Fig. 2. *Dependence of specific productivity of UPM-100 membrane on the concentration of nucleic acids in concentrate*

From the above data, it follows that a decrease in specific productivity of 1.5 times is observed only at a concentration of total nucleic acids above 30 g/l, which is quite sufficient for subsequent effective precipitation of nucleic acids.

Figure 3 shows the differential selectivity relationships of membrane UPM-100 for nucleic components (2) and for DNA (1). From the data obtained, it can be seen that the values of selectivity for nucleic acids and DNA are close to each other, that is, there is no enrichment of the DNA concentrate. Therefore, a single-step extraction is not feasible, and a 2-step extraction option was studied in the next stage of the studies.

Sequential extraction of nucleic acids from the biomass of methane-oxidizing bacteria was carried out as follows. At the first stage carried out extraction of RNA at a temperature of 90 wasps within 90 min. On the expiration of the specified time biomass was separated centrifugation at 6000 rpm within 30 min. The received extract was directed to an ultraconcentration stage on UPM-10 membrane. The partially denucleinized biomass was suspended in distilled water to obtain a 10% suspension. DNA extraction was carried out at 90 ° C, pH 9.0 for 90 minutes, taking suspension samples at predetermined intervals at which the DNA concentration was determined by Dishe's method. The dynamics of DNA extraction are shown in Figure 4.

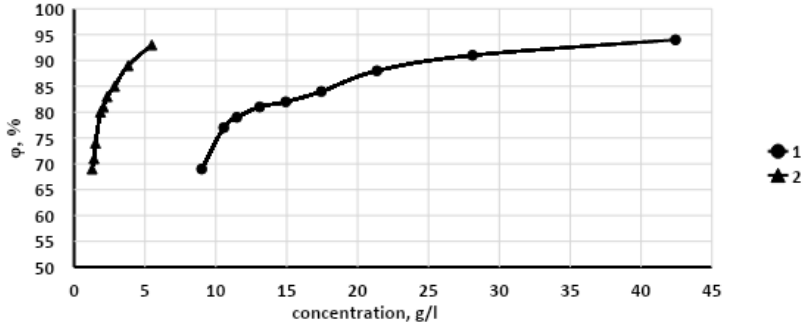

Fig. 3. *Dependence of differential selectivity of the membrane UPM-100 on DNA (1) and nucleic acids (2) on the concentration of nucleic acids and DNA in the concentrate.*

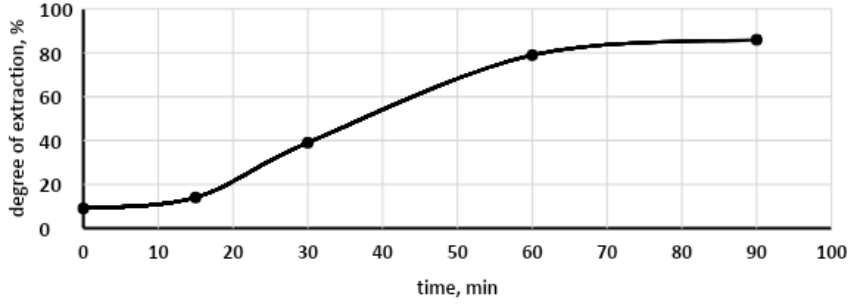

Fig. 4. *Dynamics of DNA extraction from biomass of methane-oxidizing bacteria in 2-stage extraction*

It follows from the figure that in 90 minutes of extraction, a DNA extraction rate of at least 85% is achieved. A further increase in extraction time is not advisable, as this leads to DNA destruction.

Thus, an RNA-containing extract (RNA concentration 8.0 g/l) and a DNA-containing extract (DNA concentration 1.4 g/l) were obtained. The extracts obtained were further concentrated by ultrafiltration on membranes UPM-10 and UPM-100, respectively.

The concentration of the RNA-containing extract was carried out on the membrane of the UPM-10, and the DNA-containing extract on the membrane of the UPM-100.

Similar to the ultra concentration studies described above, specific performance, integral and differential selectivity were determined for the concentration process in both cases. Figures 5 and 6 show the dependencies of specific performance and differential selectivity on the concentration of nucleic acids in the concentrate. From the presented data, it can be seen that a significant decrease in the performance of the ultrafiltration plant is observed at an RNA

concentration in the concentrate of more than 23 g/l, which allows concentrating the RNA-containing extract by at least 6 times. The RNA integral selectivity is not less than 72%.

These data indicate that the DNA concentration process is characterized by high differential selectivity (above 86%), as well as a decrease in the performance of the ultrafiltration device by no more than 1.5 times, which allows concentrating the DNA extract by no less than 6 times.

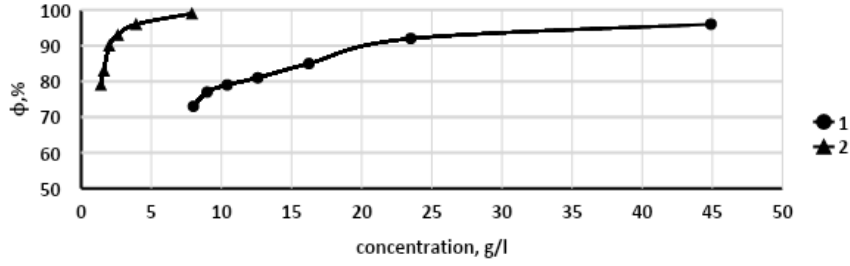

Fig. 5. *Dependence of differential selectivity of membrane UPM-100 on the concentration of DNA (1) and membrane UPM-10 on the concentration of RNA (2) in concentrate*

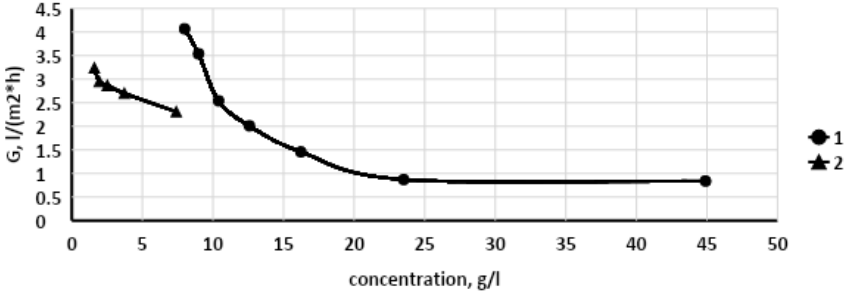

Fig. 6. *Dependence of specific productivity of membrane UPM-100 on the concentration of DNA (1) and membrane UPM-10 on the concentration of RNA (2) in concentrate*

As a result of the ultra-concentration step, an RNA-containing concentrate and a DNA-containing concentrate were obtained, from which the RNA-protein and DNA-protein complexes were precipitated at an isoelectric point.

To this end, the resulting concentrates were cooled to 4-6 ° C, after which the pH of these solutions was set to 1.8-2.0 using a concentrated hydrochloric acid solution. The precipitated DNA-protein and RNA-protein complexes were separated by centrifugation at 6000 rpm for 15 minutes. From the obtained data, the degree of precipitation of nucleoproteins was calculated, the values of which were: for the DNA-protein complex - 80%; for the RNA-protein complex - 83%.

To decompose the protein-nucleic complex, a solution of diammonium phosphate was used, which interacts with the protein of the intracellular protein-nucleic complex and allows the release of nucleic acids in free form. In this case, the protein-phosphate complex precipitates, and nucleic acids pass into solution. The process was carried out at a temperature of 60 ° C, concentration of mmonium phosphate 2.0 mol/l, pH of medium 6.0-6.5. Samples of the suspension were collected periodically, the precipitate was separated by centrifugation at 6000 rpm, and the concentration of RNA in the supernatant was determined by Spirin and DNA by Dishe's method. From the obtained data, the proportion of dissolved nucleic acids from their content in the initial protein-nucleic complexes was determined (Figure 7).

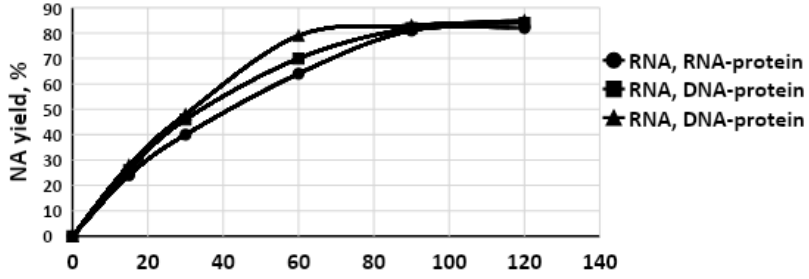

Fig. 7. *Dynamics of nucleic acid dissolution in monoammonium phosphate solution*

From Figure 7 it follows that for both protein-nucleic complexes in 90 minutes, nucleic acid yield to the solution at the level of 80-85% is achieved. Therefore, the optimal processing time of the protein nucleic complexes was assumed to be 90 minutes.

Further, the precipitate of the protein-phosphate complex was separated by filtration, and RNA and DNA were precipitated from the obtained solutions in the same manner as described above. To purify the RNA and DNA precipitates from phosphate ions, they were washed with water acidified to pH 2.0, treated with 96% ethyl alcohol solution and dried at 50 ° C. The RNA preparation contained at least 85% of the main substance, and the DNA preparation contained at least 76%.

As previously noted, RNA and DNA preparations are generally the starting materials for the production of nucleosides and nitrogenous bases. Acid and alkaline hydrolysis are used for their production. Therefore, at the next stage of work, the effectiveness of these hydrolysis methods was compared. from which it follows that both in the case of RNA and DNA, alcaline hydrolysis proceeds with a higher yield under milder conditions.

Table 2. *Effectiveness of acid and alkaline hydrolysis of RNA and DNA preparations*

Preparation	Hydrolysis conditions			Hydrolysis products yield, %
	Temperature, °C	Hydrolyzing agent	Concentration of hydrolyzing agent, %	
RNA	90	Sodium hydroxide	10	14,4
RNA	115	Sodium hydroxide	10	20,6
RNA	90	Sodium hydroxide	20	20,6
RNA	115	Sodium hydroxide	20	13,4
RNA	90	Hydrochloric acid	36	9,5
RNA	115	Hydrochloric acid	36	11,6
DNA	90	Sodium hydroxide	10	27,8
DNA	115	Sodium hydroxide	10	28,0
DNA	90	Sodium hydroxide	20	27,3
DNA	115	Sodium hydroxide	20	25,4
DNA	90	Hydrochloric acid	36	27,9
DNA	115	Hydrochloric acid	36	25,2

CONCLUSION

The need for two-step extraction of nucleic acids from the biomass of methane-oxidizing bacteria in order to separately extract RNA and DNA is justified. It was found that at the first stage of extraction at a temperature of 90°C, pH 9.0 during 90 minutes, at least 85% RNA is recovered. When partially denucleinized biomass is reprocessed under the same conditions, DNA is extracted by at least 83%.

It has been found that in order to achieve efficient precipitation of nucleic acids at an isoelectric point, concentration of the RNA solution must be carried out on the membrane UPM-10 at a concentration degree of 7, and the DNA solution on the membrane UPM-100 at a concentration degree of 6.

A study of the degradation dynamics of protein-nucleic complexes in the medium of monoammonium phosphate showed that the transition of nucleic acids into a solution of at least 80% is achieved at a concentration of monoammonium phosphate of 1.7 M, a temperature of 55°C for 90 minutes.

It has been established that the hydrolysis of both RNA and DNA is expediently carried out using sodium hedroxide with a concentration of 10% at a temperature of 120° C.

REFERENCES

[1] Vanyushkin B. F. A spontaneous journalist's gaze at the world of DNA (nucleotide composition, sequences, methylation), Biochemistry, vol. 72./issue 12. PP. 1583-1593, 2007.

[2] Lee Y.K., Kim H.W., Liu C.L., Lee H.K. A simple method for DNA extraction from marine bacteria that produce extracellular materials, Journal of Microbiological Methods. vol. 52/issue 2. P. 245-250. 2003.

[3] In Woo Lee, Han Oh Park. Method for obtaining DNA from fish spermatogonium. Patent US 6759532. 2002.

[4] Tsyrenov V. Zh., Gomboeva S. V., Zakharova M. A. Obtaining low molecular weight DNA from fish milk of the Baikal region, Irkutsk State University Bulletin. Series: Biology. Ecology. vol. 10. PP.3-10. 2014.

[5] Laktionov P.P., Tamkovich S.N., Simonov P.A., Rykova E.Yu., Vlasov V.V. Method for isolating DNA from microorganisms. RU Patent No 2232768.2004.

[6] Yamkovaya TV, Kuzovkova EV, Zheleznova Yu. P., Zagrebel'nyi SN, Panin LE, Yamkova VI A method for obtaining high-polymer RNA from yeast. RF patent No 2392329.2010.

[7] Yamkovaya TV, Vansovskaya IV, Zagrebelny SN, Panin LE, Yamkovaya VI Method of obtaining high-polymer RNA from waste brewer's yeast. RU patent No 2435862.2011.

[8] Laktionov P.P., Tamkovich S.N., Simonov P.A., Rykova E.Yu. Nucleic acid isolation method. RU patent No 2232810.2004.

[9] Sakurai, Toshinari, Hitachinakashi, Kuno, Norihito, Chiyodaku, Uchida, Kenko Chiyodaku, Yokobayashi, Toshiaki. RNA extraction method, RNA extraction reagent, and method for analyzing biological materials. Japan patent EP 1 529 841. 2005.

[10] Yamkovaya TV, Zagrebelny SN, Panin LE, Yamkovaya VI. A method of obtaining a protein-free biologically active preparation of high-polymer RNA from dry baker's yeast Saccharomyces cerevisiae, RU Patent No. 2510854.2014.

[11] Kyoko Kojima, Hino, Satoshi Ozawa, Musashino. Method for isolating and purifying nucleic acids. Patent US No 2002/0192667. 2002.

[12] Khripko Yu. I., Smirnov PN, Bateneva NV Method of isolation of nucleic acids. RU patent No 2584346.2015.

[13] Gabriele Christoffel. Method of isolating purified RNA, Patent US N9487550. 2016.

PHARMACOGNOSTIC ANALYSIS AND ANALYSIS OF THE PHENOLIC COMPOUNDS OF THE AERIAL PARTS OF THE SPECIES *CERASTIUM BULGARICUM* UECHTR. SIN. *CERASTIUM GRACILE* DUFOUR.

Popescu Antoanela[1]
Suciu Felicia[2]
Lupu Carmen[3]
Stoicescu Iuliana[4]
Roșca Adrian Cosmin[5]
[1, 2, 3, 4, 5] Faculty of Pharmacy, Ovidius University of Constanta, Romania

ABSTRACT

The main objective of the paper was the pharmacognostic analysis of the microscopic and chemical species of the aerial part of the species *Cerastium bulgaricum* Uechtr. sin. *Cerastium gracile* Dufour, to establish the chemical composition and especially to identify active principles that scientifically substantiate the traditional use of the plant product.

The microscopic analyses of the vegetative organs (stem and leaf) the species *Cerastium bulgaricum* Uechtr led to the conclusion that its histo-anatomical structure is specific to *Caryophyllaceae*.

Following the global chemical analysis, active principles known in the literature for the antioxidant potential were identified. Following the preliminary quantitative determinations (drying loss, determination of soluble substances) results comparable to those in the literature on the content of volatile substances and soluble substances were obtained.

The separation, identification and quantification of poliphenols compounds were made through high performance of liquid chromatography (HPLC), standardized method according to USP30-NF25 Monograph.

Keywords: *Cerastium bulgaricum Uechtr, Cerastium gracile Dufour, Caryophyllaceae, phenol compound, HPLC*

INTRODUCTION

The aim of our study was the determination of microscopic characteristics, chemical composition, volatil oil and poliphenols compounds, of the aerial part of *Cerastium bulgaricum* Uechtr from România.

The species of the genus *Cerastium* (keras = horn, about its bent horn-shaped fruit) are herbaceous, annual or perennial, fragile, with heights between 5 and 60 cm, distributed in Romania in dry or wet places, on sandy or salty soils, on rocks and screes, close to walls or roadsides, from plain to the alpine zone [1], [2], [3].

No data regarding the therapeutic uses of the species of the genus *Cerastium* were encountered in the specialized medical literature, but in certain areas of the Apuseni Mountains the locals use some species of this genus empirically, as a decoction to stop the hemorrhage of various etiologies and as alcoholic extract to treat rheumatism [1].

Anne Catherine Emmerich (a Roman Catholic Augustinian Canoness Regular of Windesheim, mystic), using herbs for epilepsy. "She prayed many times to be told of a cure for them, and at last was able to describe a certain little flower known to her which she had seen St. Luke pick and use to cure epilepsy" [4].

MATERIALS AND METHOD

Cerastium bulgaricum Uechtr were collected from Celic Dere monastery, Tulcea in northern Dobrogea, Iunie 2019.

For the preliminary pharmacognostic determinations, the pharmacognostic analysis was used as a working tool (microscopic examination, qualitative chemical analysis, determination of drying loss).

The qualitative chemical analysis is based on the successful extraction of the plant product used, with solvents of different polarities and the identification by reactions characteristic of each group of active principles.

The reagents used in identifying the active principles are reagents for analysis from various domestic and imported companies.

Determination of drying loss is a preliminary quantitative pharmacognostic method that represents the degree of humidity of plant products, which must be within certain limits, to ensure the preservation of plant products.

The working method involves the following technique.

The weighing vials with the vegetable products previously brought to a constant mass, together with the sample taken, are kept in the oven at 105^0 C for 3-4 hours, unless otherwise provided, cooled in a desiccator and weighed. Continue drying for 1 hour, followed by cooling in the desiccator and weighing until the samples reach a constant mass. A KERN ABJ analytical balance was used to weigh the samples.

The volatile oil content of the vegetal products was detarminated with Clevenger method.

The separation, identification and quantification of poliphenols compounds were made through high performance of liquid chromatography (HPLC), standardized method according to USP30-NF25 Monograph [5].

- *Apparatus*: HPLC Agilent 1200, with quaternary pump, DAD, thermostat, degassing system, autosampler.
- *Performance conditions*: chromatographic column type C18, 250 mm × 4.6 mm; 5 µm (Zorbax XDB or equivalent); mobile phase: solution A - 0.1% phosphoric acid, solution B - acetonitrile, eluted in the

gradient (Table I); temperature: 35ºC; flow rate: 1.5 mL/min; detection: UV 310 nm; injection volume: 20 µl; analysis time: 22 minutes.

Table 1. *Work gradient of HPLC analysis*

Time, min.	**Solution A, mL %**	**Solution B, mL %**
0-13	90	10
13	7	22
13	78	22
14	60	40
17	60	40
17,5	90	10
22	90	10

The test sample is a methanolic extract obtained from the aerial part of the species *Cerastium bulgaricum* Uechtr and was prepared as follows: 10 g of vegetable product were extracted with 100 mL of 70% methanol. The extracted solution obtained was filtered and the 100 mL volumetric flask was filled with 70% methanol.

The obtained extractive solution was filtered and made up to the bottom with a 100 mL volumetric flask with 70% methanol.

Reference substances (solutions in 70% methanol): Standard (methanolic solutions 70%) used were: E – resveratrol = 37 mg/mL, Z – resveratrol = 0,22 mg/mL.(Z – resveratrol was obtained from E – resveratrol exposed 12 hours at 254 nm, UV), caffeic acid = 0,36 mg/mL, chlorogenic acid = 0,37 mg/mL, cinnamic acid = 0,58 mg/mL, vanillin = 0,42 mg/mL, gallic acid = 0,39 mg/mL, ferulic acid = 0,48 mg/mL, 3-methylgallic acid = 0,34 mg/mL, ellagic acid = 0,43 mg/mL, p-coumaric acid = 0,51 mg/mL (Table II, Figure 1).

Table 2. *The Retention time of standards (*standard deviation for six injections)*

Nr. Crt.	**Compound**	**Retention time** ± SD
1.	*E* - resveratrol	14,467 ± 0,017
2.	*Z* – resveratrol	15,751 ± 0,058
3.	Caffeic acid	4,598 ± 0,036
4.	Chlorogenic acid	3,501 ± 0,015
5.	Cinnamic acid	15,867 ± 0,007
6.	Vanilin	6,919 ± 0,051
7.	Gallic acid	0,990 ± 0,025
8.	Ferulic acid	8,565± 0,058
9.	Ellagic acid	15,303± 0,027
10.	p-Coumaric acid	7,187± 0,019
11.	3-Methylgallic acid	2,606± 0,008

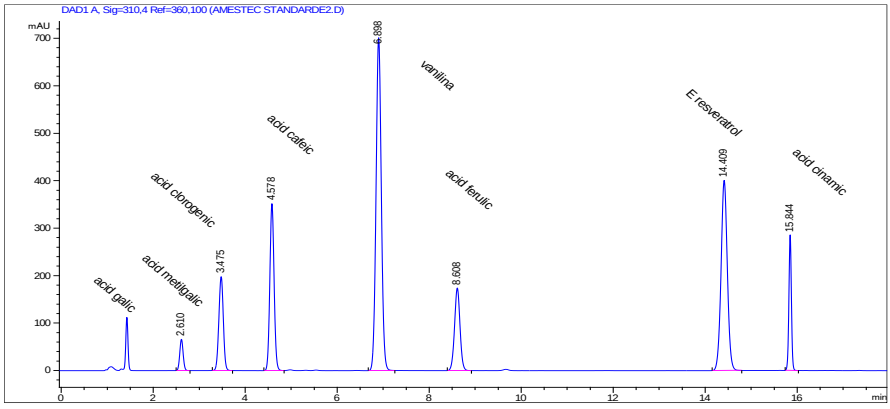

Fig. 1. *HPLC chromatogram of standards*

Statistical analysis

Statistical analyses were performed by analysis of variance (ANOVA soft SPSS 10). Data were presented as mean ± standard deviation (SD).

RESULTS AND DISCUSSIONS

The analysis of the transversal sections through the vegetative organs (stem and leaf) (Figure 2, Figure 3) the species *Cerastium bulgaricum* Uechtr led to the conclusion that its histo-anatomical structure is specific to *Caryophyllaceae* [6], [7], [8].

The microscopic analyses of the powder showed the presence of upper and lower epidermis of leaf, fragments of leaf lamina, the vessels of the stem, tectorial and secretory hairs and dyacitic stomata (figure 4).

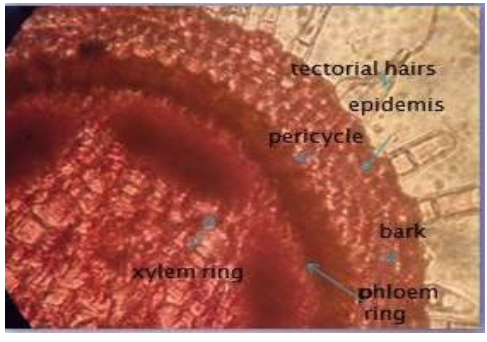

Fig. 2. *Transversal section through the stem10 x*

Fig. 3. *Transversal leaf section through the leaf 40 x*

Fig. 4. *The microscopic analyses of the powder 10 x*

The vegetal product contains 2,0412% - 2,4202 g% water soluble substances.

The volatile oil content of the vegetal product determined by the Clevenger method was 0,08% mL.

The qualitative chemical analysis showed the presence of sterols, flavonoids and coumarins aglycons (in etheric solutions), flavonoids, coumarins, tannins, monosaccharides and other reducing compounds.

Using HPLC, we have determinated chlorogenic acid, caffeic acid, gallic acid, ellagic acid, cinnamic acid and p coumaric acid (figures 5, 6, 7), table III.

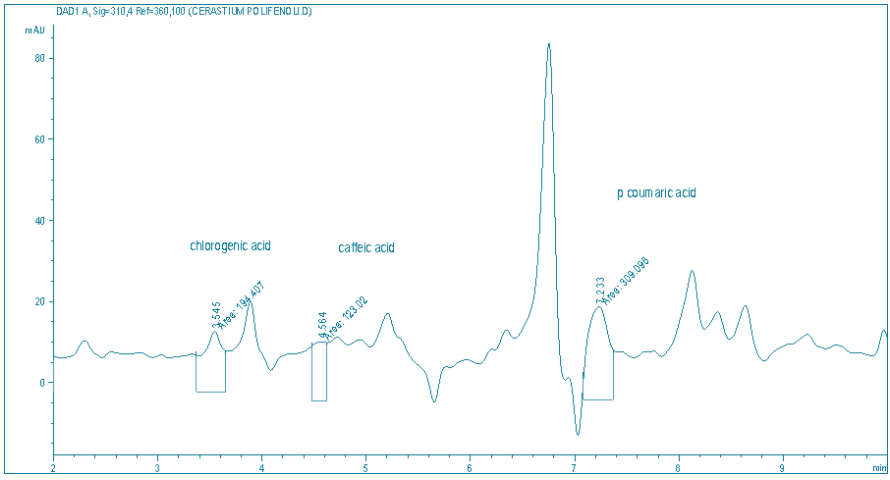

Fig. 5. *HPLC chromatogram*

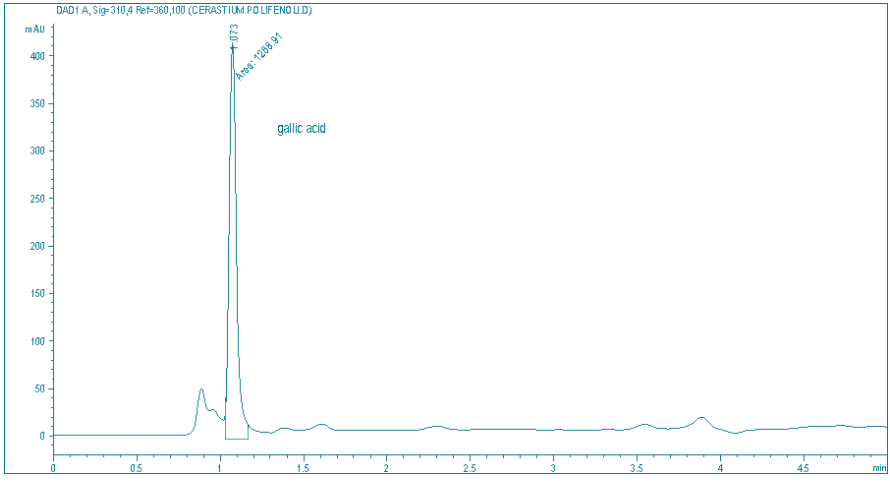

Fig. 6. *HPLC chromatogram*

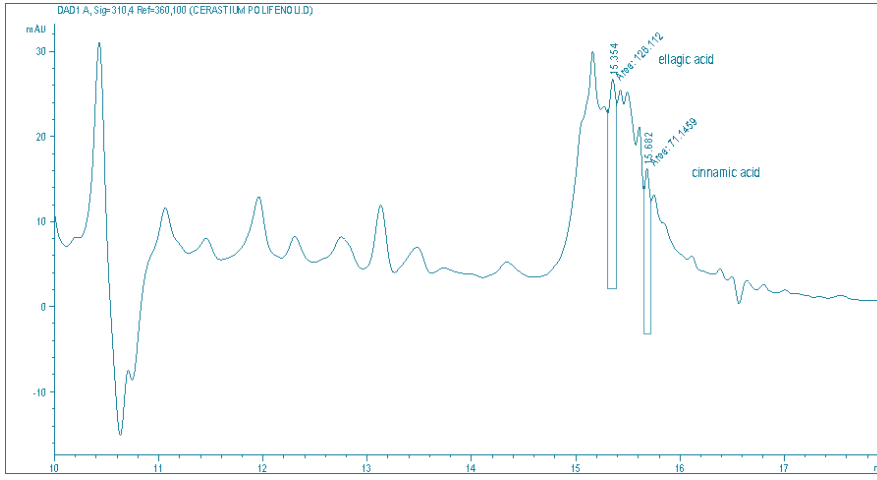

Fig. 7. *HPLC chromatogram*

Table 3. *Polyphenolic compounds determined by HPLC analysis*

Sample	Acid clorogenic mg%	acid cafeic mg%	Acid galic mg%	Acid elagic mg%	Acid cinamic mg%	Acid p cumaric mg%
Cerastium bulgaricum herba	4,086	10,986	1176,676	597,683	36,962	25,110

The presence of the free gallic acid is remarked. Verifying it with the general chemical analysis results we are sure that the intensity of the reaction for the identification of the tannins is given by its presence.

Science literature point out antiviral effects of phenol compounds (caffeic and gallic acids), antibacterial effect (caffeic, chlorogenic and gallic acids), antimycotic effect (caffeic and gallic acids), low level lipids effect (chlorogenic acid) [8].

CONCLUSIONS

The microscopic analyses of the species *Cerastium bulgaricum* Uechtr led to the conclusion that its histo-anatomical structure is specific to *Caryophyllaceae*.

The qualitative chemical analysis, as well as the determination of the volatile oil identified and detected active principles used in phytotherapy.

Cerastium bulgaricum herba contain phenolcarboxilic acids (chlorogenic, caffeic, p coumaric, ellagic, cinnamic and gallic). We measured some of them: chlorogenic acid (4,086 mg %), caffeic acid (10,986 mg %), ellagic acid (597,683 mg %) cinnamic acid (36,962 mg %) p coumaric acid (25,110 mg %) and gallic acid (1176,676 mg %).

All the detected compounds are recognised for antioxidant and anti-infective properties [8].

Cerastium bulgaricum Uechtr can be a future candidate for obtaining selective herbal extracts, rich in phenolic compounds with antioxidant activity [8].

The results obtained from HPLC analysis of polyphenolic compounds extracted from from the aerial part of the species in the study justify research orientation towards the assessment of antioxidant capacity.

REFERENCES

[1] Arcuş, M., Lilios, G., Doroftei, E., & Doicescu, D., THE HISTO-ANATOMOCAL ANALYSIS OF THE SPECIES CERASTIUM TOMENTOSUM L.(CARYOPHYLLACEAE). Annals of the Romanian Society for Cell Biology, 2012, 17,1.

[2] Dubois, M. A., Zoll, A., Bouillant, M. L., & Delaveau, P., Di-C-Glycosylflavones du Cerastium arvense ssp. arvense nouvelles pour les Caryophyllaceae. Planta medica, 46(09), 1982, 56-57.

[3] Couladis, M., & Tzakou, O., Volatile constituents of Cerastium candidissimum Corr. from Greece. Journal of Essential Oil Research, 12(6), 2000, 691-692.

[4] Emmerich A. C., The Life of The Blessed Virgin Mary, Translated by Sir Michael Palairet apud http://www.ecatholic2000.com/anne/lom.shtml.

[5] *** NF 25, United States Pharmacopeia and the National Formulary (USP 30/NF 25). Rockville (MD): The United States Pharmacopeial Convention, Inc.; 2007.p. 914.30/NF 25). Rockville (MD): The United States Pharmacopeial Convention, Inc.; 2007, 914.

[6] Dimitrov, D., & Vutov, V., BIODIVERSITY OF PLANTS AND NATURAL HABITATS IN THE VICINITIES OF ARAPYA BAY, ROPOTAMO NATURAL RESERVE, ALEPU BEACH, SINEMORETS AND SILISTAR CAPE (BULGARIAN SOUTHERN BLACK SEA COAST). Trakia Journal of Sciences, 17(4), 2019, 359.

[7] Adler, J. H., & Salt, T. A., Phytosterol structure and composition in the chemosystematics of the caryophyllales. In The Metabolism, Structure, and Function of Plant Lipids, Springer, Boston, MA, 1987, 119-121.

[8] Im LEE, J., KIM, Y. A., Chang-Suk, K. O. N. G., Jinhyeok, L. E. E., Haejin, K. I. M., & Youngwan, S. E. O., Inhibitory Effects of Crude Extract of the Arctic Terrestrial Plant Cerastium sp. on Growth of Human Cancer Cells, 한국생물공학회 학술대회, 2009, 154-154.

PRELIMINARY STUDIES RELATED TO MICROSCOPY AND THE SEDEM EXPERT SYSTEM PROFILE ON FREEZED-DRIED EXTRACT OF *LYTHRI HERBA*

Assist. Researcher Valeriu Iancu[1]
Assoc. Prof. Dr. Laura Adriana Bucur[2]
Assoc. Prof. Dr. Verginica Schröder[3]
Dr. Eng. Manuela Rossemary Apetroaei[4]
PhD Student Irina Mihaela Iancu[5]
[1,2,3,5] Ovidius University of Constanța, Faculty of Pharmacy, 6 Căpitan Al. Șerbănescu Street, Constanța, Romania
[4] Mircea cel Bătrân Naval Academy, Faculty of Navigation and Naval Management, Constanța, Romania

ABSTRACT

The floral tips of the plant species Lythrum salicaria L. represent a rich source of total polyphenols, among which with the largest share we mention tannins, and this is why this plant material has a standardized monograph in the European Pharmacopoeia 10.0th edition.

According to the literature accessed so far, the plant material has antioxidant, anti-inflammatory, hemostatic, antibacterial and antifungal properties, along with modulatory action on carbohydrate metabolism.

Powder microscopic examination is an important step in establishing the identity of the plant species used, highlighting elements specific to the aerial part such as spiral vessels of the stem, fragments of the spongy mesophyll with calcium oxalate clusters cells and anomocytic stomata.

The application of the SeDeM method on dried plant extracts represents an innovative trend in pharmaceutical technology and contributes to the collection of data in a structured and standardized form.

In this paper, the functions and applications of the SeDeM expert system are illustrated upon the freeze-dried extract of Lythri herba for the purpose of easier identification and standardization. Future applications may include obtaining chewable gums or tablets by direct compression.

Keywords: *Lythri herba, microscopic examination, SeDeM expert system, direct compression*

INTRODUCTION

Lythrum salicaria L. is a plant known in traditional medicine due to its astringent and hemostatic properties in gastrointestinal diseases such as diarrhea and dysentery. This plant species proved its effectiveness during the First World

War and was successfully used as an infusion in the treatment of soldiers with dysentery [1].

The composition rich in total polyphenols and especially in ellagic tannins of the *Lythri herba* plant material highlights the importance of this species extracts in phytotherapy [1], [2], [3].

The first important step in establishing the identity of the *Lythri herba* plant material is the microscopic examination in powder, being known as a standard technique in determining plant species [4].

The SeDeM Expert Diagram System is a galenic pre-formulation system, which evaluates the suitability of excipients and active pharmaceutical ingredients (API's) for direct compression (DC) into tablets as well as predicting possible formulations to obtain acceptable direct compressible tablets. Until now, the SeDeM expert system has become one of the most successful preformulation methods, since it gathers almost all the frequently used physical parameters to fully characterize the properties of pharmaceutical powders.

Practical applications of SeDeM includes determination of the suitability of an API to be subjected to direct compression technology, determine the amount of excipient required for the compression of an API that is not apt for direct compression, practical application of the mathematical equation to calculate the amount of excipient required for a deficient API to be subjected to direct compression technology, quality control of batches of a single API or excipient used for direct compression, to differentiate the excipient in the same chemical family, to differentiate excipients of the same functional type, to develop orally disintegrating tablets by direct compression using SeDeM-ODT experimental program [5].

Also, the SeDeM expert system contributes to the manufacturing classification system (MCS) and Quality by Design Development. Consequently, this innovative tool is consistent with the current requirements of regulatory health authorities such as the FDA and ICH.

MATERIAL AND METHOD

The materials used in this study were the freeze-dried aqueous extract of *Lythri herba*, the powdered aerial parts of the dried *Lythrum salicaria* L. plants harvested in August 2019 from Năvodari area, Dobrogea, Romania, Novex-Holland microscope, Canon 710 digital camera. Freeze-drying method of aqueous extract of *Lythri herba* plant material increase the stability in time of the aqueous extract and facilitates subsequent retesting [3].

SeDeM expert system is based upon ICH guidelines and is comprised of 12 parameters divided into six factors, covering all the characteristics related to flow, compressibility and disintegration behavior of powder. Based on physical characteristics and functionality of the ingredients, these parameters are grouped and described as follows [6]:

A. Dimension factor

Parameters included in this factor affect the size of the tablet and its ability to pile up. Measurements of these parameters also include particle volume, inter-particle void volume and internal pore volume. Parameters included in this group are:

1) Bulk density (Da)
2) Tapped density (Dc)

B. Compressibility factor

The factor comprised of the parameters related to compressibility of powder and includes the following:

3) Inter-particle porosity (Ie)
4) Carr index (IC%)
5) Cohesion index (Icd)

C. Flow ability / powder flow factor

This factor governs flow ability of the powder during compression and includes the following:

6) Hausner ratio (IH)
7) Angle of repose (α)
8) Flowability (t")

D. Lubricity / stability factor

Lubricity during compression and stability of the compressed tablets are affected by the parameters included in this factor. These are the following:

9) Loss on drying (%HR)
10) Hygroscopicity (%H)

E. Lubricity / dosage factor

Parameters included in this factor affect the lubricity and dosage of the tablet and comprised of the following:

11) Percentage of particles measuring < 50 μ (%Pf)
12) Homogeneity index (Iθ)

Acceptable limit values for each parameter of SeDeM expert system

Certain limit values are set for each parameter included in SeDeM expert system on the basis of experimental results and values described in the Handbook of Pharmaceutical Excipients [7].

Graphical presentation of results from SeDeM expert system

Results of SeDeM expert system are graphically presented as SeDeM diagram built on the basis of basic parameters. Values obtained from the experimental determination or calculations of various parameters are converted to *r* values by applying specific factors, representing radii of the diagram. The diagram is formed by connecting radius values with linear segment, having 0 as a minimum value, 10 as maximum value, and 5 as minimum acceptable value. [6]

Table 1. *Parameters and methods included in the expert system SeDeM*

Incidence factor	Parameter (Symbol)	Methods	Unit	Equation	Limit value (v)	Radius (r)
Dimension	Bulk density (Da)	Sect. 2.9.15 Eur.Ph.	g/ml	$Da = \mathbf{P/Va}$	0-1	10v
	Tapped density (Dc)	Sect. 2.9.15 Eur.Ph.	g/ml	$Dc = \mathbf{P/Vc}$	0-1	10v
Compressibility	Interparticle porosity (Ie)	Non-compendial / computed	-	$Ie = \frac{\mathbf{Dc-Da}}{\mathbf{Dc}} \times Da$	0-1.2	10v/1.2
	Carr index (IC)	Non-compendial / computed	%	$IC = \frac{\mathbf{Dc-Da}}{\mathbf{Dc}} \times 100$	0-50%	v/5
	Cohesion index (Icd)	Non-compendial	N	Experimental	0-200	v/20
Flowability / Powder flow	Hausner ratio (IH)	Sect. 2.9.36 Eur. Ph	-	$IH = \mathbf{Dc/Da}$	3-1	(30-10v)/2
	Angle of repose (α)	Sect. 2.9.36 Eur. Ph	-	$\alpha = \mathbf{\tan^{-1} H/r}$	50-0	10-(v/5)
	Flowability (t″)	Sect. 2.9.36 Eur. Ph.	s	Experimental	20-0	10-(v/2)
Lubricity / Stability	Loss on drying (%HR)	Gen. meth. 2.9.32 Eur.Ph.	%	Experimental	10-0	10-v
	Hygroscopicity (%H)	Gen. meth. 5.11 Eur Ph.	%	Experimental	20-0	10-(v/2)
Lubricity / Dosage	Particles < 50µ (%Pf)	Gen. meth. 2.9.12 Eur. Ph.	%	Experimental	50-0	10-(v/5)
	Homogenity index (Iθ)	Gen. meth. 2.9.12 Eur. Ph.	-	$I\theta = \frac{\mathbf{Fm}}{\mathbf{100+\Delta Fmn}}$	0-2 x 10^{-2}	500v

RESULTS AND DISCUSSIONS

Powdered aerial parts of dried Lythri herba and freeze-dried aqueous extract of Lythri herba

Aerial parts of *Lythrum salicaria* L. (*Lythri herba*) were collected in August 2019 from Năvodari area, Constanța city, Romania and one specimen has been

deposited in the "exicata" collection of the Pharmacognosy discipline within the Faculty of Pharmacy, Ovidius University in Constanța, Romania.

The freeze-dried aqueous extract of *Lythri herba* was obtained by the concentration method with rotavapor and lyophilization of the aqueous extract from the floral tips of *Lythrum salicaria* L. (Fig. 1D).This obtaining method The dried floral tips from the *Lythrum salicaria* L. (Fig. 1A-1B) species was milled obtaining a brown-yellow powder (Fig. 1C).

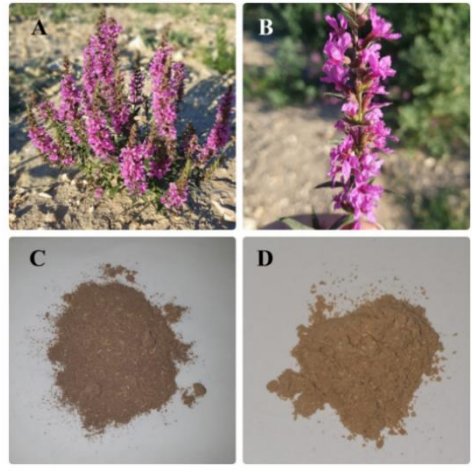

Fig. 1. *A. Lythrum salicaria L. species, B. Lythri herba plant material, C. Powdered aerial parts of Lythri herba, D. Freeze-dried aqueous extract of Lythri herba*

Microscopic characterization of the Lythri herba powder

The *Lythri herba* plant material has the following characteristic elements derived from stems consisting of spiral and ringed small-caliber stem vessels (Fig. 2a), accompanied by fiber bundles (Fig. 2b) and unicellular or multicellular covering trichomes (Fig. 2c).

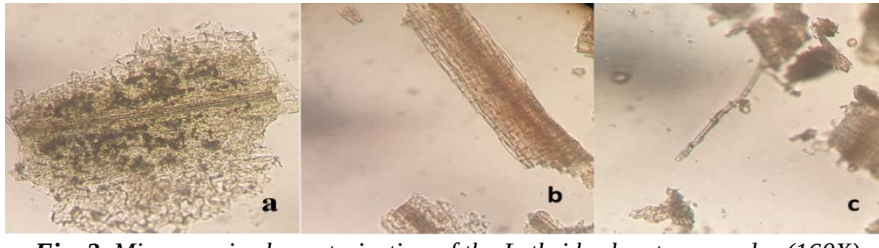

Fig. 2. *Microscopic characterization of the Lythri herba stem powder (160X)*

In the powder of the plant material *Lythri herba* we noticed the following leaf characteristic elements such as small spiral vessels (Fig. 3a), unicellular or bicellular covering trichomes (Fig. 3b), anomocytic stomata (Fig. 3c) and spherical cells, thin-walled and with calcium oxalate crystals (Fig. 3d).

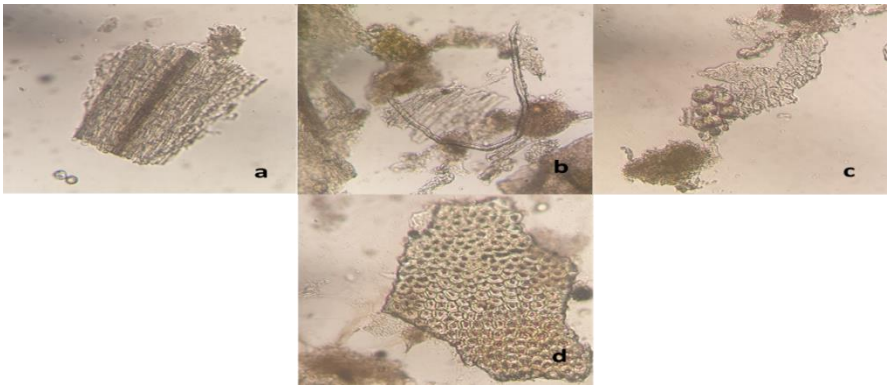

Fig. 3. *Microscopic characterization of the Lythri herba leaf powder (160X)*

Microscopic elements characteristic of the flower were noticed in the powder of the plant material *Lythri herba* such as petal epidermal cells with sinuous walls and granular cuticles (Fig. 4a), unicel-lular or bicellular trichomes covering the calyx of the flower (Fig. 4b) and numerous spherical pollen grains, with three germinating pores and thin exine (Fig. 4c).

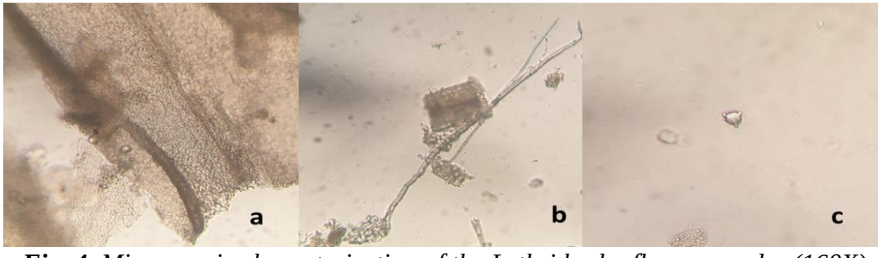

Fig. 4. *Microscopic characterization of the Lythri herba flower powder (160X)*

The initial experiments followed the analysis of the micrometric properties of the plant material in order to specify the flow and compression capacity. Determining the density of a powder is an important feature in the analysis of micrometric properties, as it is considered to be an indicator of powder processing by tasing and compacting. The higher the density of the powder, the greater its ease of forming tablets. The two micrometric parameters (IC and IH) are also important characteristics in the design, formulation and maintenance of the quality of any pharmaceutical product and research [5, 8]. Superior quality of the drug ensures its increased bioavailability in the body, an expected effect and limited side effects reported by pharmacovigilance studies [9].

By analysing the results obtained (Table 2) it can be observed that the values of the micrometric parameters for the dry extract fall into the category of low-flow powders, according to Carr [10, 11]. The low density of the powder, before and after tasing (Da = 0.15, Dc = 0.23) the advanced degree of finesse, the intermolecular links (Ie = 0.05) explain the adhering properties of the material, the poor flow and the difficulty of future direct compression.

Table 2. *Results from the SeDeM Expert Diagram System of the freeze-dried aqueous extract of Lythri herba plant material*

Parameter	Da (g/ml)	Dc (g/ml)	Ie	IC (%)	IH	α (º)	t" (s)
Results	0.15	0.23	0.05	34.5	1.53	-	-
Radius *(r)*	1.5	2.3	0.42	6.9	7.35	0	0
Incidence factor (mean value)	Dimension		Compressibility		Flowability/ powder flow		
	1.9		-		2.45		

The experiments for the angle of repose and the flow time did not returned any results because the powder analysed did not flow through the funnel. This negative aspect is attributed to the low density, electrostatic character, adhesion to the walls of the flow paths and underlines the poor flow of plant material.

The mean values for incidence factors dimension (1.9) and flowability (2.45) are lower than the acceptable value of 5, which concludes that the physical properties of the powder (particle geometry, surface texture, cohesion forces) negatively influence the flow of plant material.

Judicious analysis of compression capacity requires future experiments for the cohesion index, hygroscopic character, selection of directly compressible excipients.

In order to achieve the complete profile obtained by applying the SeDeM expert system, we aim to continue the experiments related to compression, dosage and stability. Moreover, by obtaining the SeDeM diagram, the profile of the dry extract, with its advantageous properties but also deficient ones, can be seen more clearly.

For future studies, directly compressible excipients may be selected in order to compensate the deficiencies of the API and theoretically provides the final mixture the characteristics to be compressed. In this way, the information provided by the SeDeM system allows the formulator to start working with excipients that have a high probability to provide suitable formulations, thus reducing the lead time of formulation.

CONCLUSION

The microscopic characterization in powder helped to determine the identity of the species *Lythrum salicaria* L. from Romania, because all the elements highlighted in this study corresponded to the data from the monograph *Lythri herba* of the European Pharmacopoeia 10th edition.

Application of the SeDeM expert system contributes to the realization of a complete pharmaco-technical profile for the plant material powder that includes: dimensional properties, compression capacity, reology, stability and dosing. The application of galenic correction formulas and the visual interpretation of the results facilitates the selection of the appropriate excipients for compression and reduction of the time of formulation.

Moreover, the SeDeM expert system contributes to the collection of data in a structured and standardized form, facilitating the exchange of knowledge between researchers. In this respect the iTCM database contains 73 botanical extracts alongside 91 pharmaceutical excipients in solid-state.

REFERENCES

[1] Piwowarski, J. P.; Granica, S.; Kiss, A. K. Lythrum salicaria L. Underestimated medicinal plant from European traditional medicine. A review. *Journal of ethnopharmacology*, 2015, 170: 226-250

[2] Pârvu C., 2005, ,,Enciclopedia plantelor - plante din flora României", vol. V, Ed. Tehnică, București, pag 221-223

[3] Iancu, I. M., Bucur, L. A., Schroder, V., Mireșan, H., Mihai, S., Iancu, V., & Badea, V. (2021). Phytochemical evaluation and cytotoxicity assay of lythri herba extracts. *Farmacia*, 69, 51-58.

[4] European Pharmacopoeia 10th Edition'', EQM, Council of Europe, Strasbourg, 2020.

[5] Khan, Amjad, et al. "SeDeM-ODT Expert System: A Solution to Challenges in Characterization of Pharmaceutical Powders and Powdered Material." *Advanced Functional Materials*. IntechOpen, 2020.

[6] Shahi, S. R., & Tadwee, I. (2017). SeDeM in Preformulation of Solid Oral Dosage Form: A Review. *Advances in Applied and Pharnaceutical Sciences Journal*, 1(1), 11-17.

[7] Sheskey P. "Handbook of Pharmaceutical Excipients", Ed. Pharmaceutical Press, 2020, ISBN 0857113755

[8] Chiriță, C., Ștefănescu, E., Zbârcea, C. E., Mireșan, H., Negreș, S., Nuță, D. C., & Marineci, C. D. (2019). Experimental pharmacological research regarding the antidepressant effect of associating doxepin and selegiline in normal mice. *Journal of Mind and Medical Sciences*, 6(2), 261-270.

[9] Ștefănescu, E., Pleșu, M., Scutari, C., Junghină, A., & Mireșan, H. (2015). Metoclopramide neurological side effects screening; a pharmacovigilence study in Romanian community pharmacies. *Journal of Mind and Medical Sciences*, 2(1), 55-66.

[10] Iancu, V., Roncea, F., Cazacincu, R. G., Lupu, C. E., Miresan, H., Dănăilă, C. N., & Lupuleasa, D. (2016). Response surface methodology for optimization of diclofenac sodium orodispersible tablets (ODTs). *Farmacia*, *64*, 210-6.

[11] Freeman, R., 2000, "The flowability of powders-an empirical approach", *Int. Conf. Powder & Bulk Solids Handl.*, IMechE HQ, London.

PRODUCTION OF ANTIBODIES FROM POULTRY YOLK (IgY) AND INVESTIGATION OF THEIR IMMUNOCHEMICAL PROPERTIES

Prof. Dr. Alla A. Krasnoshtanova[1]
Alesya N. Yudina[2]
[1, 2] D. Mendeleev University of Chemical Technology of Russia, Moscow, Russia

ABSTRACT

A particularly important aspect of immunology is to develop non-invasive methods of obtaining antibodies which could be a great alternative to traditional ones that based on the harmful procedure of isolation of immunoglobulins from animal blood sera. That's why the extraction of antibodies from poultry egg yolks (IgY) is the most promising. Due to the fact of variation of IgY structural features that determine the definite immunochemical properties, yolk antibodies in comparison with mammalian immunoglobulins (IgG) does not interact with rheumatoid factor (Rf), contribute to the activation of the complement system, bind to the Fc-receptor (FcR), and also has weak cross-reactivity, which confirms the possibility of their widespread use in medicine and food. Also the presence of phylogenetic distance between chickens and mammalians guarantees immune response against conservative mammalian protein molecules which is highly important for the creation of new generation test systems.

The aim of this work is to develop a selective method of producing high-purity immunoglobulin Y preparations from the yolk of chicken eggs.

There were adopted selective conditions of isolation of IgY under spontaneous thawing procedure at the room temperature of firstly frozen yolk solution in a sodium-phosphate buffer mixed with water (pH 5.0) in a ratio of 1:6, which leads to receiving a water-soluble fraction further precipitated with the sodium chloride at a concentration of 10% of the solution mass and subsequently concentrated using ultrafiltration with membrane UAM-10, that allows achieving the content of IgY not less than 95% per dry substance in immunoglobulin fraction. It is possible to produce a protein fraction with a protein content of at least 9 g/l.

The purity of the immunoglobulin fraction was verified using polyacrylamide gel electrophoresis. The presence of a light chain in the IgY solution was proved to be a low-molecular compound using the method of gel-filtration-chromatography. The immunological activity of IgY was studied with respect to bovine serum albumin (BSA) as an antigen. The enzymatic resistance of IgY against proteolytic enzymes was tested in area of the gastrointestinal tract.

Keywords: *egg yolk, IgY, immune response, gastrointestinal enzymes, ultrafiltration*

INTRODUCTION

At present time, the development of a new generation of pharmaceuticals based on antibodies' compounds is accelerating. The possibility of their passive administration and the achievement of a rapid therapeutic effect are the main advantages of such drugs.

Egg yolk is a rich source of immunoglobulins(Ig). The total content of gaining Ig is over 100 mg per chicken egg [1], [2]. Most of the yolk immunoglobulins belong to IgY class. Other classes such as IgA and IgM are also antibody components of the yolk but in smaller quantities.

IgY is a systemic immunoglobulin with a molecular weight of approximately 170 kDa. It consists of two heavy (H) and two light (L) chains connected by disulfide bonds and forming a monomeric link (H2L2). The molecular weights of the heavy and light chains are 71 kDa and 26 kDa, respectively [1], [3].

It is known that the variable part of the H-chain encodes a region of the DNA molecule that has variable (V), connective (J), and diversity (D) segments. The rearrangement of these segments doesn't lead to the phenomenon of gene hyperconversion, because of the absence of any development of IgY immunogenetic diversity during the process.

IgY is currently being considered as a promising substitution for mammalian immunoglobulins (IgG). The greatest interest is focused on the variation of IgY structural features which determine the characteristic immunochemical properties. Due to the absence of the hinge region of IgG, chicken antibodies (IgY) are less exposed to proteolytic degradation and fragmentation. There's a limited flexibility zone based on proline and glycine amino acid residues instead of the flexibility zone of the hinge region in IgY [4]. Moreover, IgY does not interact with the Fc-receptor, which is responsible for the implementation of numerous effector functions; they are not able to activate the human complement cascades. Also IgY do not have cross-reactivity and does not bind to the rheumatoid factor (Rf-factor) [5].

Purified yolk antibodies (IgY) are able to conserve their activity for six months at room temperature. In addition, affine-purified and biotinylated IgY retains high activity after five years of storage at 4°C [6].

The technology of production of IgY from the egg yolk requires a specific treatment that provides the isolation of immunoglobulins from the lipophilic matrix of the yolk. This is achievable by a two-step purification procedure of IgY from the yolks. The first stage is the separation of the water- soluble fraction (WF) containing IgY from lipids and lipoproteins. The second stage is based on the segregation of IgY out of the water-soluble protein fraction [7]. To remove the lipophilic components of the yolk, the crude extract of immunoglobulins is precipitated under the action of various reagents (polyethylene glycol, dextran sulfate, alginate, caprylic acid, organic solvents). After that the lipid aggregates could be removed by centrifugation, filtration, diluting of the yolk solution or even by freezing-thawing procedure of the diluted yolk solution. In the second stage, the pure IgY fraction should be prepared from the crude aqueous extract of immunoglobulin. Yolk antibodies are firstly salted out and then purified by chromatography

(exclusive, ion exchange, thiophilic, affinity chromatography). In some cases it's necessary to carry out repeated precipitation of immunoglobulins. Depending on the using purification method the degree of purity and the total yield of the final immunoglobulin preparation are in rang of 85-98% and 1,0-9,8 mg/ml, respectively [7]. These methods for the isolation of IgY are promising for their implementation in technologies for the development of medicines, food additives, functional nutrition, as well as the creation of modern test systems for the early diagnosis and prevention of many diseases, which will reduce the usage of non-invasive therapies on animals aimed to obtain mammalian antibodies (IgG) [8], [9]. That's why the creation of high-quality medicines is required to carry out high degree purification, which guarantees the exact composition of the immunoglobulin fraction.

The aim of this work is directed to the development of a method for obtaining high-purity immunoglobulin Y preparations from the poultry yolk.

MATERIALS AND METHODS

Poultry eggs of Public Joint Stock Company «Snezhka» plant production were used as the object of the study. The eggs have next characteristics: humidity is about 74%; the fat content of the yolk is 32.6%; the content of phospholipids in egg yolk is 29.6%; the crude protein contents in egg protein fraction and in the yolk are 10.6% and 16.6%, respectively.

Determination of crude protein content was performed by the Kjeldahl method, the concentration of protein content in the solution was measured using the biuret method. The determination of the molecular weight of the protein and the degree of its purification was evaluated by gel-filtration-chromatography and polyacrylamide gel electrophoresis in denaturing conditions.

The process of concentration of IgY solutions was performed using ultrafiltration with UAM-type membranes (ultrafiltration acetate cellulose membranes) with molecular weights cut-off of 100 and 10 kDa.

The immunological activity of IgY was investigated using the method of precipitation antibodies with antigen. Bovine serum albumin (BSA) was chosen as an antigen. BSA was prepared in aqueous solution of distilled water with a concentration of 1 mg/ml. The turbidity of the solution after adding equal aliquots of antibodies and antigen preparations was checked against the control sample at a wavelength of 440 nm in cuvettes with a light-absorbing layer thickness of 10 mm.

The enzymatic resistance of IgY against proteolytic enzymes of the gastrointestinal tract was studied using the parallel profile technique.

To build the parallel profile of the gastrointestinal tract area, aliquots of IgY solution and definite enzyme solution were added to preliminarily prepared sodium-phosphate buffer salt (PBS) solutions and hydrochloric acid (HCl) solution with required value of pH the way shown on Figure 1.

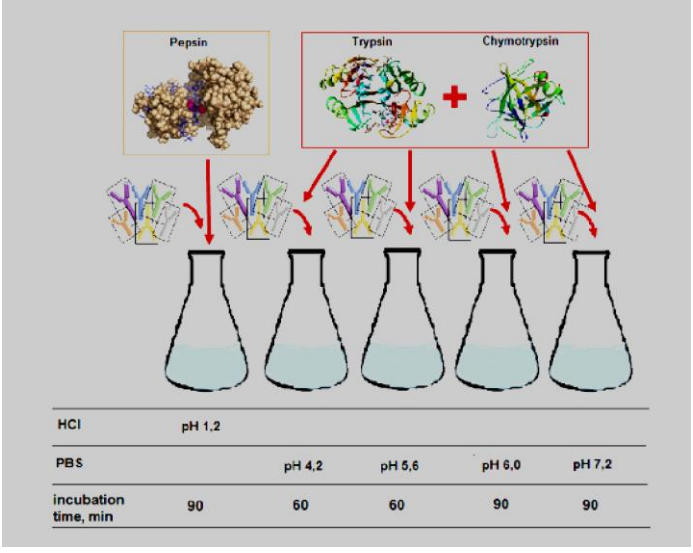

Fig. 1. *Parallel profile of gastrointestinal tract area.*

Consequently, prepared solutions were incubated at 37-40^{0}C being periodically stirred during 60 or 90 minutes depending on gastrointestinal tract section. The dynamics of IgY destruction were constructed by taking samples every 15 minutes from the solutions. All of the above pH values correspond to the acidity values of the human small intestine.

Pepsin was transformed in solution with concentration of 0.1 mass %. According to the literature data average activity of trypsin and chymotrypsin in the human gastrointestinal tract is 15 U/l [10].

Activities of enzymes were defined using the modified Anson method. Degree of IgY destruction was mesuared using the modified Lowry method.

RESULTS AND DISCUSSION

During the previously conducted methods of isolation of IgY, based on precipitation process to segregate proteins and residual fats from the native and ethanol-treated yolk. However, these methods did not allow to obtain a final product with a protein content of more than 54%.

At the next stage of work, after separating the eggs into white and yolk, the yolk was transferred to filter paper for thorough removal of the protein trace. The yolk-shell was additionally decanted.

Then the yolk mass was mixed with an equivalent volume of sodium-phosphate buffer salt (PBS) solution with a pH of 7.4 using a magnetic stirrer to achieve homogeneity. Aliquots were taken from the prepared solution for subsequent dilutions in tap water adjusted to pH 5.0 using 0.2 N HCl in 6 and 8 times [7]. The mixtures were frozen at temperature of -20^{0}C, and then subjected to spontaneous thawing through a paper filter at room temperature. A transparent protein solution,

called a water-soluble fraction (WF), was obtained after filtration. The protein content in obtained filtrates, depending on the initial dilution of the yolk mass, are shown in Table 1.

Table 1. *Effect of the dilution multiplicity on the protein content in the filtrates*

№	Dilution multiplicity	Protein content in the filtrates, g/l
1	6	7.2
2	8	6.1

Based on the small difference between the obtained concentrations in both dilutions, it was not possible to determine the unambiguous dilution multiplicity of the yolk suspension. Therefore, further fractionation of the proteins contained in the WF was carried out by means of specific precipitation with sodium chloride salts added to filtrate solutions in concentrations equal to 5 and 10 mass %. The freshly prepared fractions were kept for a day at 4℃ to induce complexation processes. Filtration through a folded filter was chosen as the primary purification of the target product against ballast proteins and dissolved salts. The protein content of the obtained filtrates was determined using the biuret method. The experimental results are shown in Table 2.

Table 2. *Effect of the degree of dilution of the yolk mass and the content of sodium chloride on the protein yield*

№	Dilution multiplicity	Content of NaCl, mass %	Protein content , g/l
1	6	5	8.1
		10	9.7
2	8	5	10.3
		10	10.1

Based on the results obtained, it can be concluded that the highest concentration of protein is observed in the filtrate at a dilution ratio of 8 and at a concentration of sodium chloride of 5 mass %.

After that the high-molecular fraction containing immunoglobulin Y was washed from residual salts and ballast proteins using ultrafiltration (UF) on the UAM – 100 membrane. The calculated values of the protein content in solutions after UF and the integral selectivity for protein are presented in Table 3. Consequently, the best dilution of the yolk mass at which the highest value of the index φ is observed, corresponds to 6, and the concentration of the added reagent (NaCl) is 10 mass %.

Table 3. *Effect of dilution multiplicity of the yolk mass and the concentration of sodium chloride on the efficiency of ultrafiltration*

№	Dilution multiplicity	Concentration of NaCl, mass %	Protein content after cocentration, g/l	Integral selectivity φ, %
1	6	5	3.58	56
		10	3.26	66
2	8	5	4.49	56
		10	3.82	62

The dilution multiplicity equal to 8 was unsuccessful due to the presence of a strong opalescent effect in the water-soluble fraction, which indicates an incompleted separation of protein and lipid fractions.

According to the literature data, purified yolk antibodies (IgY) are able to maintain their activity for 6 months at room temperature. In addition, affine-purified and biotinylated IgY retains high activity after five years of storage at 4°C [10].

In order to confirm the efficiency of the method for isolating IgY developed at the previous stage of the study, it was advisable to evaluate the fractional composition of the obtained fraction using polyacrylamide gel electrophoresis in denaturing conditions.

During the analysis, the bands corresponding to the molecular weights of the H - and L-chains of IgY were identified. The electrophoresis data is shown on Figure 2.

Electrophoresis data show that the two bands correspond to the molecular weights of the light (28 kDa) and heavy (63 kDa) chains of IgY, which coincides with the literature information [11].

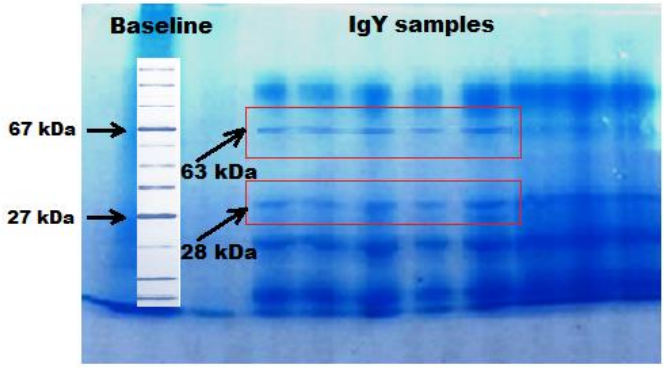

Fig. 2. *Electrophoresis data of IgY*

Since the gel contains several lower bands corresponding to impurity proteins with molecular weights of about 15 kDa, as well as fractions of proteins with molecular weights in the range of 1-100 kDa, it was concluded that the obtained immunoglobulin fraction is not sufficiently pure.

UAM-10 membrane with a lower molecular weight cut-off was tested to purify the target product from low molecular weight fragments by ultrafiltration.

After ultra-concentration, the target product was washed against mineral salts using diafiltration mode. The results of the determination of the best diafiltration multiplicity are shown in Table 4.

The experimental data show that after third diafiltration a solution with a protein content of 12.18 g/l was obtained, which indicates an increase of total protein content in 4.5 times. Based on the content of a dry substance in sample, the

resulting immunoglobulin preparation contained at least 95 mass % of the main substance.

During diafiltration the losses of the target protein is minimal, while the salt concentration in the immunoglobulin concentrate is reduced by 16 times, which allows to recommend the method of ultra-concentration and subsequent diafiltration to obtain purified immunoglobulin Y fraction.

Table 4. *Effect of the diafiltration multiplicity on the physico-chemical parameters of diafiltrates and a protein concentrate*

Diafiltration multiplicity	Residue content of NaCl in protein concentrate, g/l	Integral selectivity φ, %	Dry substance content of diafiltrate, %	Protein content in concentrate (in respect to dry substance content of diafiltrate), %
1	5.0	99.8	5.6	70.4
2	2.5	98.8	2.4	82.5
3	1.3	95.3	1.6	89.9
4	0.6	95.8	0.8	95.0

The solution obtained as a result of washing using diafiltration mode on the UAM-10 membrane with protein content of at least 98% of dry weight and with protein concentration of 16.2 g/l was tested using the gel chromatography method for the presence of low-molecular components.

Since the weight of the light chain of immunoglobulins is 26, 000 Da the G-50 sefadex was chosen as the carrier for the separation proteins and peptides, which molecular weights are in the range of 1, 500 – 30, 000 Da.

The result of the protein distribution for fractions is shown on Figure 2.

Based on collected data it follows that the light chain of immunoglobulin is present in the immunoglobulin solution as the only low-molecular compound. According to the calibration graph, its molecular weight is approximately 26 kDa, which corresponds to the literature information.

Consequently, the presence of a light chain and the absence of protein compounds with a lower molecular weight in the IgY solution was proved to be a low-molecular compound using the method of gel-chromatography, which also indicated the effectiveness of chosen purification method by diafiltration.

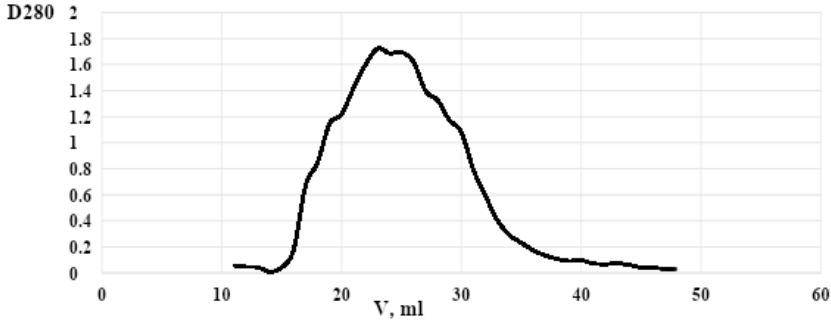

Fig. 3. *Data of gel-chromatography of light chain (L) of IgY*

IgY was proved to be immunologically active by adding bovine serum albumin (BSA) as an antigen. Results of turbidity demonstrated an intensive interaction of precipitants, which confirms the immunochemical properties of the IgY antibodies.

The final experiment was conducted to examine the process of destruction of IgY under the enzymatic conditions of the gastrointestinal tract area. Portions of enzyme preparations with adopted activity values were added into buffer solutions with IgY as previously described on Figure 1 to build the parallel profile of the gastrointestinal tract area. The collected results are shown on Figure 4.

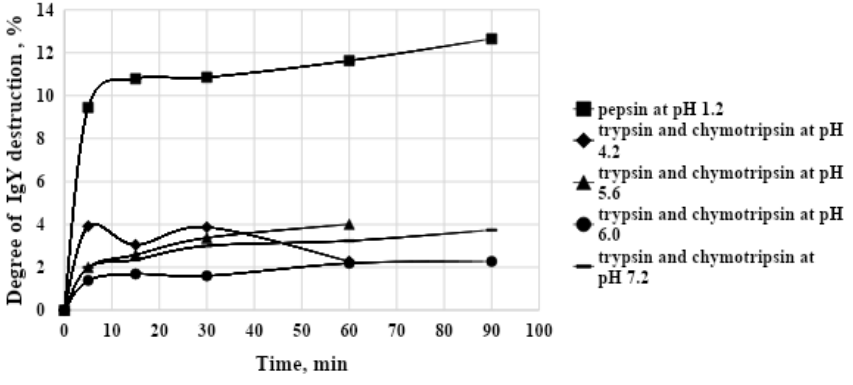

Fig. 4. *Degree of IgY destruction under the enzymatic conditions of the gastrointestinal tract area*

The data of the graph demonstrate brightly expressed degradation of IgY under the influence of pepsin at pH 1.2 and stability of IgY molecule under the influence of trypsin and chymotrypsin, which corresponds to literature [10].

CONCLUSION

A method for selective isolation of immunoglobulin Y from egg yolk was developed, based on the technology of freezing and spontaneous thawing under conditions that do not cause strong opalescent effect. It is possible to obtain a protein fraction with a protein content at least 9 g/l by diluting the yolk suspension

solution in 6 times and adding sodium chloride as a precipitating agent in amount of 10 mass %.

IgY was purified from low-molecular impurities using diafiltration mode on the UAM-10 membrane, which ensures the protein content at least 98% of dry substance in the preparation.

The purity of the immunoglobulin fraction of the yolk was electrophoretically tested. The presence of a light chain (L) in IgY solution was proved to be a low-molecular compound using method of gel-chromatography.

The immunochemical properties were tested using precipitation with BSA as an antigen.

The construction of a parallel profile of the gastrointestinal tract area proved the destruction of IgY under the influence of pepsin at pH 1.2 and enzymatic resistance of IgY under the influence of trypsin and chymotrypsin at different pH values correspond to the acidity values of the human small intestine.

REFERENCES

[1] Kaplin V.S., Kaplina O.N. IgY technologies in medicine. Avian yolk antibodies in immunotherapy, International Reviews: Clinical Practice and Health. PP. 59-75. 2016.

[2] Kaplin V.S., Kaplina O.N. IgY technologies. Avian yolk antibodies, Biotechnology, vol.33/issue 2. PP. 29-40. 2013.

[3] Wei Nie, Chao Zhao, Xiaoxiao Guo et. al. Preparation and identification of chicken egg yolk immunoglobulins against human enterovirus 71 for diagnosis of hand-foot-and-mouth disease, Analytical Biochemistry. vol. 573. PP. 44–50. 2019.

[4] E.P.V. Pereira, M.F. van Tilburg, E.O.P.T. Florean, M.I.F. Guedes. Egg yolk antibodies (IgY) and their applications in human and veterinary health: A review. International Immunopharmacology. vol 79. PP. 293-303 2019.

[5] Warr, G.W., Magor, K.E. and Higgins, D.A. (1995). IgY: clues to the origins of modern antibodies, Immunol. Today. vol. 16, PP. 392–398. 1995.

[6] Efremova M.S. Isolation of immunoglobulin Y from blood serum of hens and egg yolk. Mat. conf. "State and prospects for the development of veterinary science in Russia" Veterinary medicine and feeding. vol. 4. PP.34-35. 2013.

[7] P. Hodek, P. Trefil, J. Simunek et. Al. Optimized Protocol of Chicken Antibody (IgY) Purification Providing Electrophoretically Homogenous Preparations, J. Electrochem. Sci. vol.8. P. 113 – 124. 2013.

[8] Yudina A.N., Krasnoshtanova A.A. Selection of the optimal scheme for the isolation of immunoglobulins from the yolk of poultry eggs. "Biochemical Physics", Moscow, PP. 247-250. 2019.

[9] Yudina A.N. A.A. Krasnoshtanova Methods for the isolation of immunoglobulins from the yolk of poultry eggs. Congress materials "Advances in chemistry and chemical technology", D. Mendeleev University of Chemical Technology of Russian. Moscow, vol. 33, PP. 49-50. 2019.

[10] E.P.V. Pereira, M.F. van Tilburg, E.O.P.T. Florean et. al. Egg yolk antibodies (IgY) and their applications in human and veterinary health: a review, International Immunopharmacology. vol. 73. PP. 293-303. 2019.

[11] Hartmann C., Wilhelmson M. The hen's egg yolk: a source of biologically active substances, World's Poultry Sci. J. vol. 57/issue 1. PP. 14–28. 2001.

QUALITY ASSURANCE IN PHARMACEUTICAL OPERATIONS

Assist. Prof. Ph.D. Student Blebea Nicoleta Mirela[1]
[1] Faculty of Pharmacy, Ovidius University of Constanta, Constanta, Romania
[1] Faculty of Pharmacy, University of Medicine and Pharmacy Carol Davila, Bucharest, Romania

ABSTRACT

The specialized literature does not confer a consensual definition of the quality in the pharmaceutical procedures. Nevertheless, most definitions imply the satisfaction of eth customers' needs. The customers of the pharmaceutical procedures are the patients and also the professional persons from the domain of health that prescribe, issue and administrate medicines. The pharmacist is a professional person who is in direct contact with the patient, being the first professional person to whom the patients address when the affection is a mild one and they need counselling regarding the medication or diagnostic. The more complex the medication of the patient is, the more probable the side effects shall be. The morbidity and mortality may be consequences at the error of medication. The appearance of some medicines increases directly proportional to the errors of prescribing the medication. The quality in using the medication implies the choice of the medicine, the optimization of the compliance of the patient with the treatment, avoiding side effects, assuring the therapeutical objectives. The possibilities of appearing the errors being numerous, it is easy to understand why the assurance and improvement of the quality of the pharmaceutical procedures are important aspects for pharmacists and patients. The present paper has as purpose the qualitative improvement of the pharmaceutical procedures by the help of the pharmacist, thus the pharmacy becoming a supplier of pharmaceutical care of the best quality.

Keywords: *quality assurance, patient care, pharmaceutical operations, pharmacist*

INTRODUCTION

At the world level, there is the concern for building a new health system adapted to the 21st century. In this regard, the system that assures quality care in pharmacotherapy and assessment of the quality of using the medication represents a guarantee efficient and safe pharmacotherapy for the patient and society. The assurance of quality in pharmaceutical care represents more and more solicited and important concerns for the profession of pharmacist [5].

Quality may seem an ambiguous term, as we can recognize quality when we see it, but the definition of quality is most of the time subjective. In Webster´s Dictionary quality is defined as a level of excellence [11]. This definition helps at analyzing the definitions of the specific quality from the domain of health and supports the idea according to which quality represents continuous excellence.

From the definition given by the Office of Technology Assessment we can assert that in the process of medical care, quality may be measured and used for the care offered to the patients. Although the patients are not always the best arbitrators of the quality of the pharmaceutical care, as they may not know what they want, may not have clear ideas about what they need. Therefore, the pharmacist has the duty to offer services of qualitative care to the patient [1].

Pharmaceutical services

The pharmacies take an integral part from the system of health care. The pharmacists are authorized professional persons for assuring pharmaceutical care in health and they develop their activity in conformity with the legislation and regulations in force, as well as the strict and professional rules [12]. This is the vision of the international organizations: World Health Organization (OMS) and the European Commission [15].

The pharmaceutical services represent the assembly of all actions performed by the pharmacist, necessary for warranting the pharmaceutical care of the population. Their purpose is to ensure the best answer to the needs and health problems of the population entirely and of the patient individually. The pharmaceutical services are part of the health system and have as a purpose the improvement of the health condition and increase of life quality of the population [6], [8], [9], [13], [14].

If we focus on the **European Union**, a report of the **Pharmaceutical Group of European Union (PGEU)** classifies the pharmaceutical services according to the frequency of their supply in the member states. Thus, they consider the **release of medicines based on medical prescription as an essential service** performed by the pharmacist, met in all the member states, in some countries being remunerated as a service, in other countries the benefit being related only to the markup (as it is the case of Romania). In the category of the pharmaceutical services frequently supplied, we find the **measuring of the different clinical parameters (**glycemia, body weight, blood pressure, cholesterol), **collecting the expired or not used medicines from the population, programs for giving up smoking, programs for managing different chronic** diseases (diabetes, arterial hypertension, asthma), as well as the night service (on-call). Among the services that begin to take shape in certain states, mainly in countries with developed economy, are found anti-**flu vaccination**, phone or online counseling, as well as the counselling and **monitoring of the patient to the initiation of a new treatment [6], [8], [9], [14].**

The pharmacist is the professional from the domain of health, easily to be approached, who is in direct contact with the patient, being the first professional to whom the patients address when the affection is a mild one and they need counselling related to the medication or diagnostic [1].

Pharmaceutical care

Pharmaceutical care consists of the responsible provision of the therapy with medicine for obtaining some clear results that improve or maintain the quality of the patient's life. Pharmaceutical care is a term with international recognition, defined as being the practice in which the pharmacist assumes his responsibility for

the needs of the patient regarding the medicine and is considered responsible for the satisfaction of these needs [1].

Therefore more and more, the task of the pharmacist is to ensure that the treatment with a medicine of a patient is properly indicated, is the most efficient available, the most suitable possible and the most convenient for the patient. By assuming this direct responsibility for the health needs of the patient, the pharmacists may bring a significant contribution to the result of the therapy with medicines and the quality of the patients 'life [2], [6], [8], [9], [14].

Methods of assuring the quality

In the domain of pharmacy, the raw materials or the structure for qualitative care are numerous and different: the number of pharmacists on a shift, the area of confidentiality, the quality of the pharmacists, the total area of the pharmacy, the bibliographical materials about medicines and access to on-line information, the stock of medicines and the counselling areas.

As the pharmacists are responsible for all the stages of using the medicines, the processes within the pharmacy may refer to any of these stages: prescribing, release, administration and monitoring. Among the indicators of the processes there are found the compliance with the clinical norms, the percentage of the prescriptions evaluated from the point of view of fairness and the percentage of the patients counseled.

The results represent the stimulant of the management of the therapy with medicines, which determine the pharmacists to assume a role in educating the patients and the management of the chronic diseases. Among these activities, they succeed to improve the pharmaceutical care of the patients through: (1) Increase of the control of the patients on their medical affections [3], [7] and (2) Decrease of using the resources from the budget of the system of health insurances [7]; (3) Improvement of the knowledge of the patients regarding the diseases and their medication [2], [11]; (4) Increase of adopting and maintaining the non-pharmaceutical regime [11]; (5) Increase of satisfaction of patients regarding the care they benefit from [4], [7]; (6) Saving the money of the patients [4], [7]; (7) Improvement of the quality of the patients' life [2], [11].

The capacity of the pharmacists to identify, settle and prevent the problems related to medication, as well as assuming the responsibility in the domain of chronic diseases make the object of many papers, their results representing the final purpose of the therapy and they may be analyzed through more methods [1], [2], [4], [10].

One of the methods, the model "Extension for Community Healthcare Outcomes ECHO®", suggests three types of results of the medical care: economical, clinical and humanistic. The project ECHO® is an approach of managing the disease that has as purpose the increase of the knowledge of the suppliers and standardization of the best practices for screening, care and treatment of a disease. ECHO® is based on a basic principle of learning related on cases, in which the clinicians and the suppliers of pharmaceutical care attend a teleconference meeting hosted by a central team for presenting individual cases, in

order to consult a multidisciplinary team of specialists and for studying the cases. The discussion related on the case are interactive, exploiting the ideas of a multidisciplinary team. The sessions of ECHO® offer the possibility of building a dynamic community of trainees.

The economic results include direct costs and consequences, both medical and nonmedical, and indirect costs and consequences as well as nonmaterial costs. Such an approach is necessary for helping at the optimization of the increasing costs associated with chronic diseases and diseases that may be prevented with the help of pharmaceutical care [5].

The clinical results are medical events that occur after the disease or the treatment. The criteria of the clinical results include morbidity and mortality, the incidence rates or the spread of the symptoms. These criteria represent a direct measure of the quality, but are difficult to assess in the pharmacy. For the evaluation of the results, in pharmacy can be used specific indicators or markers, for instance glycosylate hemoglobin (HbA1C), blood pressure (HTA)-indicator of the probability of a stroke.

The studies emphasize the effect of the advanced pharmaceutical care on the adherence of the diabetic patients to treatment and the efficiency of the therapeutical results related to medicines that improve eventually the quality of the patient's life. More and more important part of the activity of the pharmacist becomes the provision of information related to the modality of using the medicines by each patient, as every person is different, with different particularities, unique affections and needs of medical care [1].

The methods of human evaluation are the methods for the evaluation of the impact of the disease and its treatment on the quality of life based on the health condition of the patient, preferences and satisfaction of the patient and application of the pharmacotherapeutic decisions.

The quality of life was defined as the evaluation of the functional effects of the disease and of the therapy prescribed, as they are perceived by the patient. These effects are physical, emotional and social effects on the patient [5].

The human results are the consequences of the disease or treatment on the functionality of the patient in society or on the actual and future quality of life. These consequences may be classified as positive and negative. An example of a positive result is that the expected effect from a medicine to be manifested accordingly, this being a modality of measuring the efficiency of using the respective medicine. A negative result is the occurrence of a side effect or negative after having used a medicine. The pharmacoeconomic evaluation must include the possibilities of measuring both types of results. The evaluation of the positive results only may mislead with regard to the costs, by excluding the costs caused by the negative results [5].

The human results include criteria of the human aspects, such as the satisfaction of the patients and the quality of life. A survey related to the satisfaction of the patients regarding the services of pharmaceutical care may be useful for the evaluation of the results in case of the patients that benefit from these services. Most

of the surveys include either specific measures for a disease, or general measures for maintaining the health condition. In exchange, an evaluation of the quality of life may be useful for establishing the impact of the therapy with medicine on the patient in general.

Building an economic model may help the pharmacist anticipate the impact that the decisions of using the medicine have on the patient and on the health system and rush the process of reevaluation regarding the management of formulating decisions regarding the policy of using the medicines, while new medicines enter the market and replace the old ones. The most recent application of the pharmacoeconomic principles and methods is for justifying the value of different services of pharmaceutical care [5].

Standardization is considered one of the most powerful instruments for improving quality. When a person does the same thing every time, the chances to make errors decrease significantly. In the pharmacy, standardization is the easiest method, the most widespread and the most efficient for improving quality. In fact, the transition to standardization stimulated the critical ways that are focused not only to prevent errors, but also to optimize the results, the reduction of the costs and obtaining the satisfaction according to the American Pharmacists Association. These supportive systems may be used for alerting the pharmacist regarding the possible problems**.**

Another mechanism that may help the pharmacists is the use of protocols and verification lists, which diminish the confusion according to the Agency for Healthcare Research and Quality. The protocols usually prevent issuing a prescription until it is approved by a final verification by the pharmacist. The policies and protocols diminish the confusion.

The improvement of the access to information leads to the improvement of quality. The studies reveal the fact that the pharmacists take decisions for using the medicines more correctly, if they have access to complex and complete information about the patients, as well as the treatment profile, allergies, comorbidities [13].

CONCLUSION

If we apply the ideas mentioned above in the pharmaceutical practice, we may state that the qualitative improvements shall produce the clinical results wanted, such as an increased quality of life, as well as a greater satisfaction of the patients. In the end this will make the pharmacy create the image of a supplier of pharmaceutical care of the best quality.

The processes for improving the quality were used for monitoring the errors of medication and for avoiding the errors of prescribing.

In general, the techniques for improving the quality were used in an institutional frame, but they become more and more frequent in eth pharmacies that offer services of assisted care.

Quality represents the essential component of the competent and professional pharmaceutical practice. Many of the changes for improving the quality are simple,

may be fast implemented but they have a massive impact on the quality of the patients' care.

Quality in the domain of the pharmaceutical care reached a position of maximum visibility and the pharmacist is recognized as the key – actor in this process. Therefore, the pharmacists shall be required more and more to be involved in assuring the quality of all the segments within the system of using the medicines.

REFERENCES

[1] Blebea N.M., Stefănescu E., Zbârcea C.E., Mușat O., Chiriță C., Negreș S., The Evaluation of the Consumption of Dietary Supplements at Diabetic Patients, Proceedings of The Romanian National Congress of Pharmacy – 17th Edition, 21st Century Pharmacy – Between Intelligent Specialization and Social Responsibility , FilodirittoEditore – Proceedings, Romania, pp. 29-34, 2018.

[2] Blebea N.M., Negreș S., The Impact of Pharmaceutical Care on Patients with Chronic Hypertension, Proceedings of the Inaugural Edition of the Virtual Congress with International Participation Nutrition, Diet Therapy & Food Safety in the Context of the COVID-19, NutriTerra, Romania, pp.206-209,2 020.

[3] Clifford R.M., Davis W.A., Batty K.T. et al., Effect of a pharmaceutical care program on vascular risk factors in type 2 diabetes: The Fremantle diabetes study, Diabetes Care, U.S., vol.28/ issue 4, pp.771-776, 2005.

[4] Cranor C.W., Bunting B.A. Christensen D.B., 2003, The Asheville Project: Long –term clinical and economic outcomes oh community pharmacy diabetes care program, Journal of American Pharmacists Association, U.S., vol..43/issue 2, pp.173-184, 2003.

[5] Cristea A.N., Clinical Pharmacy, Romania, vol.2, pp.46-56, pp.509-537, 2017.

[6] European Community Pharmacy Services & Activities, PGEU Database 2015-2016, Pharmaceutical Group of the European Union, Belgium, November 2017.

[7] Garrett D.G., Bluml B.M., Patient self-management program for diabetes: first-year clinical, humanistic, and economic outcomes, J Am Pharm Assoc , U.S., 2005; vol. 45 pp.130–137, 2005.

[8] International Pharmaceutical Federation, Pharmacy: A Global Overview, Workforce, medicines distribution, practice, regulation and remuneration, The Netherlands, 2017.

[9] International Pharmaceutical Federation, Sustainability of Pharmacy Services. Advancing Global Health, The Netherlands, 2015.

[10] Mangiapane S., Schulz M., Community pharmacy-based pharmaceutical care for asthma patients, Annals of Pharmacotherapy, Germany, no39, pp.1817-1822, 2005.

[11] Merriam-Webster , Merriam-Webster's collegiate dictionary, Springfield, Massachusetts, U.S., 2003.

[12] Romanian Parliament, Law No.226/2008 of the pharmacy, Pharmacy law. Romania, 2008 .

[13] Warholak-Juarez T., Rupp M.T., Salazar T.A., Effect of patient information on the quality of pharmacists` drug use review decisions, Journal of the American Pharmacists Association, U.S., vol. 40/issue 4, pp.500-508, 2000.

[14] Wiedenmayer K., Summers S. R., Mackie C.A., Gous A.G.S., Everard M., Tromp D., World Health Organization and International Pharmaceutical Federation, Developing pharmacy practice A focus on patient care, Handbook, Switzerland, Edition 2006.

[15] World Health Organization, Transforming and scaling up health professionals'education and training, Switzerland, 2013.

RESEARCH OF THE INFLUENCE OF THE MODE PARAMETERS OF THE WATER-VACUUM EXTRACTION PROCESS ON THE YIELD OF BIOLOGICALLY ACTIVE SUBSTANCES INONOTUS OBLIQUUS

Prof. Ruslan R. Safin[1]
Assoc. Prof. Shamil R. Mukhametzyanov[2]
Assoc. Prof. Albina V. Safina[3]
Assoc. Prof. Nour R. Galyavetdinov[4]
Assis. Valeriy V. Gubernatorov[5]
[1, 2, 3, 4, 5] Kazan National Research Technological University, Russia

ABSTRACT

Inonotus obliquus or chaga birch mushroom has a fairly wide range of applications in the cosmetic, food and pharmaceutical industries due to the wide range of biologically active substances it contains. The analysis of foreign and domestic studies testifies to the ongoing research in the field of extraction of valuable components from chaga, however, issues of intensification of processes and the development of new methods of extraction remain topical. One of these methods is the water-vacuum extraction of chaga, which consists in alternating the stages of the process at atmospheric and reduced pressure. The aim of the study is to determine the optimal time parameters of the individual stages of the water-vacuum extraction of chaga to optimize the operating parameters of the process. The object of the study was chaga collected in forest plantations in central Russia in the spring season, and crushed to particles ranging in size from 0.1 to 1.2 mm. The experiments were carried out on a laboratory version of a vacuum extraction unit, which allows for the classical infusion and extraction of chaga at various variations in the pressure of the medium. Studies have shown that preliminary evacuation of dry raw materials and the introduction of a rarefied medium into the process of water extraction of chaga makes it possible to intensify the extraction process and has a positive effect on the yield and activity of extractive substances. It has been established that the preliminary evacuation of crushed chaga makes it possible to increase the efficiency of subsequent extraction and to increase the yield of valuable components by 15-18%. The optimal time for this stage was 5 minutes. The effective duration of the infusion step at atmospheric pressure was 30 minutes, and the subsequent evacuation is expediently carried out for 10 minutes. Based on the results of the presented work, the optimal scheme for carrying out the process of water-vacuum extraction of chaga was determined.

Keywords: *chaga birch mushroom, water extraction, vegetable raw materials, rarefied medium, extractive substances.*

INTRODUCTION

The significant content of biologically active substances and antiseptics in natural plant raw materials causes an increased interest in their use in medical preparations. This direction is especially important for modern medicine, when in matters of protection against infections, preference is given to environmentally friendly methods of strengthening immunity and herbal medicines.

One of the raw materials of this origin is the chaga birch mushroom, which has established itself as a storehouse of biologically active substances necessary for the human body. Chaga is successfully used in the pharmaceutical industry as an enhancer of the action of other drugs, as well as as an independent remedy for treating diseases of the gastrointestinal tract and cardiovascular system. Chaga is famous for its fairly high content of antioxidants, thanks to which it can be used as a prophylactic anticancer agent [1], [2]. The acids present in chaga have a therapeutic effect on the human body and normalize metabolism. The chromogenic complex contained in chaga slows down the development of cancer cells in the initial stages and relieves pain in the subsequent stages of the development of the disease. Chaga is also successfully used as food additives due to its high content of fiber, resins, polysaccharides and acids, which help to maintain the immune system and improve appetite [3]. The content of sterols in chaga helps to lower blood cholesterol and reduce the risk of cardiovascular disease. The tannins present in it can fold protein in the blood and contribute to the formation of a protective film on the mucous surfaces of organs. The use of decoctions based on chaga allows you to stimulate the work of brain tissues by improving the functioning of neurons. In general, we can say that chaga is a good carrier of a complex of therapeutically active substances, with the correct extraction of which it is possible to obtain sufficiently effective components for the production of medicines, as well as food additives that stimulate human immunity.

A fairly large number of works have been devoted to the study of chaga, the particular interest of which is caused by various compounds of chaga passing into its aqueous extraction. For example, in a study by A.A. Shivrina, E.V. Lovyagin and E.G. Platonov [4], a chemical analysis of chaga and a concentrate based on it was carried out, which showed that the investigated mushroom has a fairly good pharmaceutical potential.

In the work of V.F. Korsun and K.A. Treskunov [5] analyzed raw chaga, which found that chaga also contains lectins belonging to the class of complex glycoproteins, the content of which contains magnesium and calcium ions. The study found that the content of these substances allows drugs based on chaga to exhibit a hypoglycemic effect, to reduce the blood sugar content of diabetic patients, due to the ability to reversibly bind carbons.

Liuping Fan and others [6] in their work found that the chaga birch mushroom contains a water-soluble polysaccharide (ISP2a), which not only showed antitumor activity, but could also significantly increase the body's immunity. The studies also found that the ISP2a polysaccharide allowed an increase in lymphocyte counts and an increase in TNF-a content.

Despite all the above advantages of this raw material, there is a problem of extracting biologically active substances from raw chaga. Studies [7,8] have shown that it is the extraction methods that directly determine the future concentration, quantitative yield, and therapeutic activity of the extracted substances. Today, most of the pharmaceutical enterprises of the Russian Federation extract the necessary components from chaga by the method of water extraction, which is characterized by the simplicity and low cost of the hardware design of the process [9, 10]. It is also generally accepted that with water extraction there is a greater preservation and extraction of biologically active substances relative to other methods. Currently, there are various options for the extraction of plant raw materials with water, but they all have their obvious disadvantages, such as the duration of the process and the relatively low yield of extractives.

Studies have shown that the introduction of a rarefied medium into the process of water extraction of chaga allows for a deeper impregnation with the extractant by washing it out of the pores, and the alternation of the stages of the process at atmospheric and reduced pressure has a positive effect on the yield and activity of extractives [11], [12], [13].

The purpose of this work is to study the process of water-vacuum extraction of chaga and determine the optimal time parameters of individual stages of extraction in relation to the process of preliminary evacuation, the optimal time for infusion of the extract at atmospheric pressure and subsequent extraction with a decrease in the pressure of the medium.

METHODS AND MATERIALS

Chaga collected from forest plantations in central Russia (the Republic of Mari El) in the spring season was used as a test material. The choice of the place and time of collection was determined by studies [14], [15], in which the unambiguous dependence of the influence of these factors on the concentration of therapeutically active substances in chaga, and, consequently, on the value of the extracts obtained, was proved.

Raw chaga was crushed using a drum crusher and separated into fractions using a set of sieves. In experimental studies, chaga particles were used, the size of which varied in the range of 0.1-1.2 mm. Distilled water (hydromodule 1:10) was used as an extractant.

The studies were carried out on a specially designed laboratory setup that allows both classical aqueous extraction by infusion and extraction using a rarefied medium at various pressure parameters (Figure 1). The method of water-vacuum extraction consists in alternating the stages of extracting target components at atmospheric pressure and during the process of evacuation.

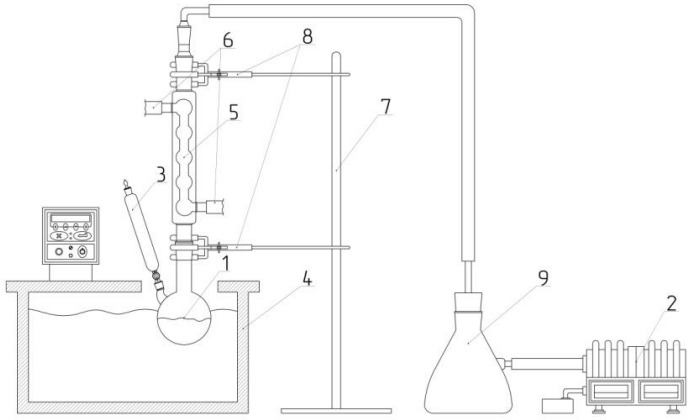

Fig. 1. *Laboratory version of the vacuum extraction unit: 1) thick-walled flask with a spout; 2) vacuum pump; 3) a volumetric flask with a tap; 4) liquid thermostat; 5) refrigerator; 6) refrigerator taps; 7) tripod; 8) presser feet; 9) Bunsen flask.*

The presented vacuum extraction plant operates as follows: crushed raw chaga is loaded into a flask with thick glass 1, which is subjected to a pre-evacuation process by turning on a vacuum pump 2 (pre-evacuation stage). Next, the chaga is poured with an extractant through a volumetric flask with a tap 3. The pressure is brought to atmospheric and infusion occurs (extraction stage at atmospheric pressure). The thermostat 4 is used to maintain a constant extraction temperature. The duration of the holding stage is set by the experiment plan. Next, the stage of evacuation begins. The refrigerator 5 installed at the top of the flask 1, in which the refrigerant circulates through the outlets 6, helps to minimize the loss of the extract during infusion and to exclude the ingress of liquid in the process of lowering the pressure of the medium. The presented structure is held by a tripod 7 and fastened with the presser feet 8. To completely exclude the ingress of liquid into the vacuum pump, a Bunsen flask 9 is used, through which the entire installation is directly connected to the vacuum pump 2.

According to the research plan of the process of water-vacuum extraction, as a result of experiments, the duration of such stages was determined as (Figure 2):

- stage of preliminary evacuation of raw chaga;
- stage of infusion at atmospheric pressure;
- the stage of extraction during evacuation.

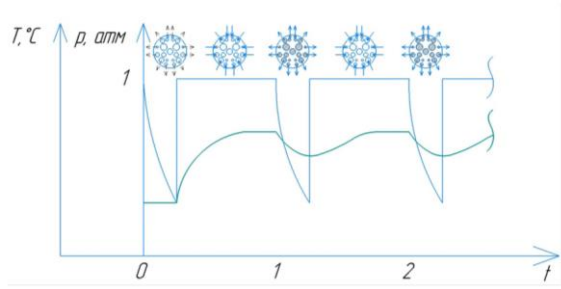

Fig. 2. *Scheme of the process of water-vacuum extraction*

RESULTS

The experiment to determine the pre-evacuation time was carried out while maintaining a constant extraction temperature and infusion time of the extract for 60 minutes. Crushed raw chaga was immersed in a flask and subjected to a preliminary evacuation process for 5, 10, 15, and 20 minutes at a medium pressure of 0.1 atm. Then the extractant preheated to 60 ° C was added to the raw material and the infusion process was carried out. The resulting extract was dried for 12 hours at a temperature of 70 ° C to obtain a dry residue. The dry residue was determined by the gravimetric method.

The results of the yield of extractive substances depending on different values of the time of preliminary evacuation of raw chaga are shown in Figure 3.

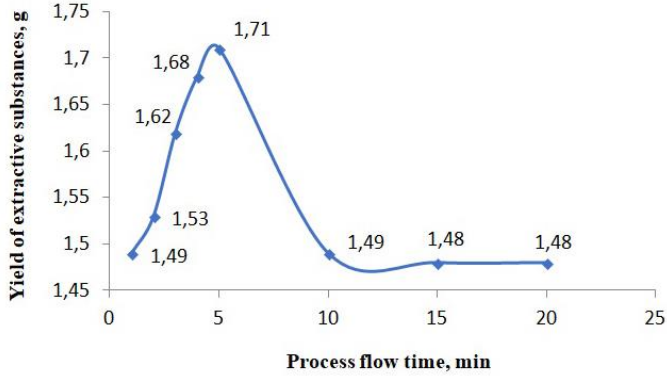

Fig.3. *Graph of the influence of the pre-evacuation time on the yield of extractives*

Based on the data obtained, it was found that the most optimal time for the pre-evacuation process is 5 minutes, since at this time parameter the highest concentration of biologically active substances was observed relative to other time values.

The experiment to determine the duration of the infusion stage at atmospheric pressure was carried out as follows. Raw chaga was subjected to a preliminary evacuation process for 5 minutes, then the extract was infused for 15, 30, 45 and 60

minutes at a constant temperature of 60 ° C. The weight of the obtained extract (dry residue) was determined as described above. The results of the experiment are shown in Figure 4.

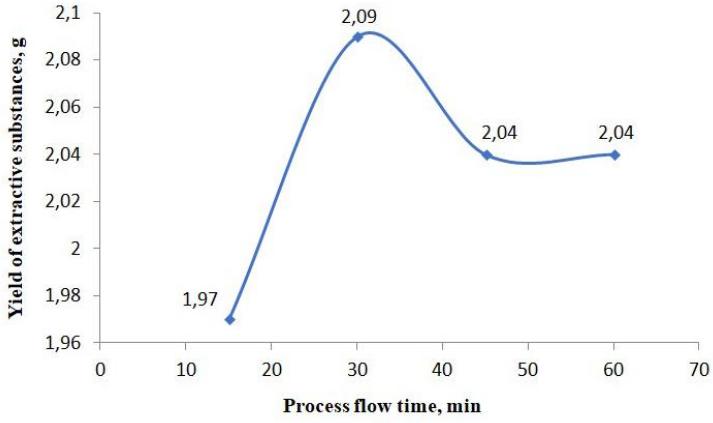

Fig. 4. *Graph of the influence of the duration of the infusion stage at atmospheric pressure on the yield of extractives*

As can be seen from the graph, the highest yield of extractives is observed when infused for 30 minutes. A further increase in the extraction time leads to a decrease in the yield of the target components by 3.5%.

The experiment to determine the optimal extraction time with a decrease in the pressure of the medium (the stage of evacuation) was carried out in two ways: without preliminary evacuation of raw chaga and with the inclusion of this stage in the experiment. The experiments were carried out with the same aforementioned parameters.

The results of the experiments carried out to determine the duration of the vacuuming stage for various methods of preparing dry raw materials are shown in Figure 5.

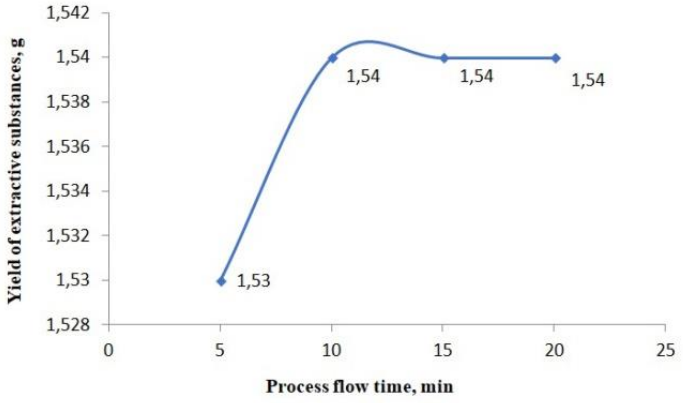

a)

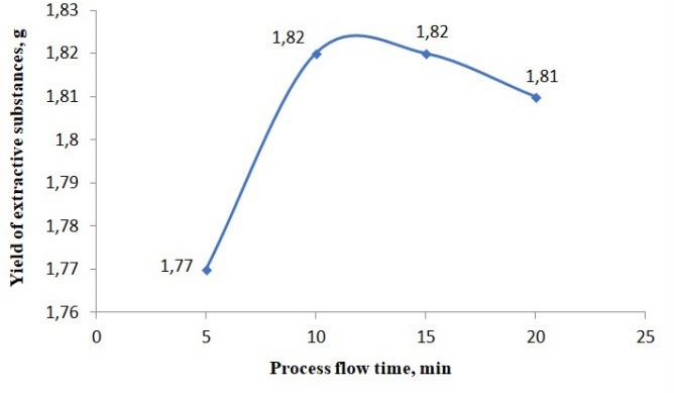

b)

Fig.5. *Influence of the duration of the evacuation stage on the yield of extractive substances: a) without a preliminary evacuation stage; b) with preliminary evacuation*

In the first case, without preliminary degassing, chaga was infused with a heated extractant for 30 minutes at atmospheric pressure, then the extraction process was carried out with a decrease in pressure (vacuum stage). The time of the evacuation stage was varied in the range of 5, 10, 15, and 20 minutes at a medium pressure of 0.1 atm.

In the second case, the raw chaga was subjected to a preliminary evacuation process for 5 minutes. Further, the process proceeded according to the scheme described above, while maintaining the parameters of the experiment. The yield of extractives was determined by the gravimetric method based on the dry residue.

From the presented graphs it can be seen that in both cases the maximum yield of the target components is achieved with a vacuum duration of 10 minutes. Further continuation of the depressurization stage does not affect the extraction efficiency. The inclusion of the stage of preliminary degassing of dry chaga intensifies the

subsequent extraction process, which is expressed in an increase in the yield of extractive substances by 15-18% with an equal duration of this stage.

CONCLUSION

Today, the topical direction of industry and scientific research is the use of natural plant materials in the production of medicines and cosmetics, as well as food additives. Chaga birch mushroom is in high demand among the listed fields of activity because it contains a huge amount of biological substances useful for the human body. The analysis of the applied methods and methods for the extraction of biologically active substances confirms the relevance of studies devoted to the intensification of extraction processes and the development of new methods for the extraction of valuable components from the chaga birch mushroom. Based on this, a method of water-vacuum extraction of chaga was developed, which consists in alternating the modes of the pressure of the medium in the apparatus, corresponding to different stages of heat and mass transfer processes.

Studies have shown that preliminary evacuation of dry raw materials and the introduction of a rarefied medium into the process of water extraction of chaga makes it possible to intensify the process and has a positive effect on the yield and activity of extractive substances. To work out the operating parameters and the practical implementation of this method, experimental studies were carried out to determine the duration of each stage of the water-vacuum extraction process relative to the maximum yield of extractive substances. Experimentally, the following optimal time parameters of individual stages have been determined with respect to the maximum yield of extractive substances. The duration of the stage of preliminary evacuation of dry raw materials is 5 minutes. Infusion at atmospheric pressure is optimal for 30 minutes, and subsequent evacuation - for 10 minutes. It is proved that the introduction of the stage of preliminary evacuation of dry material makes it possible to intensify the subsequent extraction process and to increase the yield of extractive substances by 16-18%. Based on the results of the presented work, the optimal scheme for carrying out the process of water-vacuum extraction of chaga was determined, which consists in the following. Crushed raw chaga with a particle size of 0.1 to 1.2 mm must be subjected to a preliminary evacuation process for 5 minutes at a pressure of 0.1 atm. Next, pour the extractant preheated to 60 ° C and infuse at atmospheric pressure while maintaining this temperature for 30 minutes. After that, lower the atmospheric pressure to 0.1 atm within 10 minutes. The resulting extract must be separated from the meal and dried.

These parameters ensure the efficiency of the extraction process and contribute to the production of extracts with high therapeutic properties.

REFERENCES

[1] Gubernatorov V. V., Khasanshin R. R., Safin R. R. The use of chaga in medicine and biomedical technologies / In the collection: Youth and the XXI century-2017. materials of the VII International Youth Scientific Conference: in 4 volumes. 2017. pp. 296-298.

[2] Shashkina M. Ja., P. N. Shashkin, A. V. Sergeev., Chemical and medico biological properties of chaga (Inonotus obliquus) / Pharmaceutical Chemistry Journal, Russia, vol. 40/ issue 10, pp. 37-44, 2006.

[3] Parfenov A, Vyshtakalyuk A, Sysoeva M, Sysoeva E, Latipova A, Gumarova L and Zobov V 2019 Hepatoprotective effect of inonotus obliquus melanins: in vitro and in vivo studies BioNanoScience 9:2 528-38.

[4] Shivrina A. N., Lovyagina E. V., Platonova E. G. On the chemical composition of chaga / Chaga and its therapeutic use in stage IV cancer. L., 1959. pp. 55-62.

[5] Korsun V. F., Krasnopolskaya L. M., Korsun E. V., Avkhukova M. A. Antitumor properties of mushrooms. - M.: Practical medicine, 2012. - 210 p.

[6] Liuping Fan, Shaodong Ding, Lianzhong Ai, Kequan Deng(2012) A water-soluble polysac-charide from chaga mushroom had potential as a natural antitumor agent with immunomodulatory activity. // CarbohydrPolym. 2012 Oct 1 ;90(2):870-4. Epub 2012 Jun 17. PMID: 22840014

[7] Safin R.R., Mukhametzyanov S.R., Gubernatorov V.V. Water vacuum-oscillating extraction of chaga / В сборнике: IOP Conference Series: Materials Science and Engineering. International Scientific-Practical Conference on Quality Management and Reliability of Technical Systems 2019. 2019. С. 012086.

[8] Liya Liang, Zesheng Zhang and Hao Wang 2009 Antioxidant activities of extracts and subfractions from Inonotus Obliquus International Journal of Food Sciences and Nutrition 60:2 175-84

[9] Safin R. G., Gubernatorov V. V., Safina A.V., Khuzeev M. V. Review of modern research in the field of extraction of biologically active substances from the birch fungus chaga for pharmaceutical and food industries / Woodworking industry. 2019. No. 3. pp. 93-103.

[10] Mazurkiewicz W 2006 Analysis of aqueous extract of Inonotus obliquus Acta Poloniae Pharmaceutica 63:6 497-501

[11] Safina A.V., Gubernatorov V. V., Garaev R. R., Razumov E. Yu. Intensification of the process of water extraction of chaga by periodically lowering the pressure of the medium / Woodworking industry. 2017. No. 2. pp. 50-53.

[12] Sung Hak Lee. Antitumor activity of water extract of a mushroom, Inonotus obliquus, against HT-29 human colon cancer cells / Sung Hak Lee, Hee Sun Hwang, Jong Won Yun // Phytotherapy research. P.-1784-1789.

[13] Razumov E.Y., Safin R.R., Sysoeva M.A., Khabibrakhmanova V.R., Gubernatorov V.V. Intensification of water extraction process of chaga by means of recurrent pressure reduction of the media / В сборнике: 18th International Multidisciplinary Scientific GeoConference SGEM 2018. Conference proceedings. 2018. С. 835-842.

[14] Safin R, Razumov E, Khasanshin R, Gubernatorov V and Saerova K 2018 Effect of growth conditions on qualitative characteristics of chaga mushroom Int.

Multidisciplinary Sci. GeoConf. Surveying Geology and Mining Ecology Management (SGEM 18th.) 781-88

[15] Razumov E. Yu., Safin R. R., Serova K. V., Gubernatorov V. V., Gubernatorova A. E. The influence of growing conditions on the quality indicators of chaga / Woodworking industry. 2018. No. 2. pp. 51-57.

RESEARCH ON THE BOTANICAL AND PHARMACOGNOSTIC PARTICULARITIES OF THE INDIGENOUS SPECIES *LYSIMACHIA NUMMULARIA* L.

Suciu Felicia[1]
Arcuș Mariana[2]
Roșca Adrian Cosmin[3]
Bucur Laura[4]
Popescu Antoanela[5]
Badea Victoria[6]
[1, 2, 3, 4, 5] Faculty of Pharmacy, Ovidius University of Constanta, Romania
[6] Faculty of Dentistry, Ovidius University of Constanta, Romania

ABSTRACT

Preliminary pharmacochemical research on *Lysimachia nummularia* L. was performed by dint of pharmacognostic analysis (macroscopic examination, global chemical analysis, preliminary quantitative determinations).The article includes the analysis of the macroscopic characters of the vegetative organs (root, stem and leaf), as well as of the reproductive organs (flower, fruit, seed) belonging to the spontaneous native species *Lysimachia nummularia* L.

Morphological features were described and discussed. The identification of these aspects was done with the naked eye, but also with the help of a hand magnifier and a binocular magnifier. The results revealed that the external appearance of the plant justifies the species belonging to the genus *Lysimachia*, family *Primulaceae*. They are found in the glabrous and creeping appearance of the plant, opposite, almost round leaves, solitary, yellow flowers, axillary with vigorous pedicels, perianth pentamer, actinomorphic, dialisepal and dialipetal, globular capsule fruit. The semi-hydrophilic nature is found in the presence of adventitious roots that develop both from the rhizome and at the nodes of the stem. The preliminary quantitative determinations performed were loss by drying as well as soluble substances of the species *Lysimachia nummularia* L. Following the global chemical analysis, active principles known in the literature for the antioxidant potential were identified. Following the preliminary quantitative determinations (drying loss, determination of soluble substances) results comparable to those in the literature on the content of volatile substances and soluble substances were obtained.

Keywords: *Lysimachia, macroscopic, pharmacognostic analysis, active principle*

INTRODUCTION

The paper aims at a broader study both botanical - morphological and histoanatomical, but especially pharmacognostic and phytochemical of the species *Lysimachia nummularia* L. (Fam. *Primulaceae*). The idea of this study started from

the fact that in the literature, the plant has proven, following scientific research, to be beneficial in various diseases, due to the presence of some active principles with phytotherapeutic potential in the structure of its tissues.

Thus, in traditional medicine, it is used internally to treat ulcers, diarrhea, dysentery and tuberculosis, and externally to heal wounds and skin ulcers [1].

In cultured medicine, studies have shown the presence of polyphenolic compounds, flavonoids, anthocyanosides, tannins [2], [3], [4], [5], [7], [8], due to which the plant would have a significant antioxidant potential, as well as a triterpene saponoside - nummulariozide [9], [10], isolated from the underground parts, showing cytotoxic (antitumor) activity important in five human cancer cell lines [6], [12], [13], [14], to which are added the antibacterial, antirheumatic and analgesic effects.

In this article we tried a preliminary study aimed at knowing the macroscopic characteristics of both vegetative (root, stem, leaf) and reproductive (flower, fruit, seed) organs belonging to the native spontaneous species *Lysimachia nummularia* L and preliminary pharmacognostic determinations (chemical analysis qualitative, preliminary quantitative analysis).

MATERIALS AND METHODS

The working material was represented by the plant *Lysimachia nummularia* L., harvested on July 19, 2020, on the edge of Lake Tău-Brazi in the Roșia Montană area (Fig. 1). Here, the plant in full anthesis, develops on considerable surfaces, forming well-defined associations and dominates the area due to its plagiotropic feature (Fig. 2). The collected specimens were herbivored and determined in the Pharmaceutical Botany Laboratory within the Faculty of Pharmacy, using for this purpose the flora determinants from the laboratory equipment [15]. Several herbaceous specimens are in the custody of the Pharmaceutical Botany Laboratory.

For the preliminary pharmacognostic determinations, the pharmacognostic analysis was used as a working tool (macroscopic examination, qualitative chemical analysis, determination of drying loss, determination of soluble substances).

To establish the macroscopic characters, the species was analyzed with a hand magnifier and a binocular magnifier.

The pharmacognostic analysis consists of two groups of methods: quantitative methods and qualitative methods.

Qualitative methods lead to the determination of the identity of a plant product and include the Examination, macroscopic, microscopic and chemical (microchemical and qualitative chemical).

Quantitative methods aim to determine the purity and quality of a plant product.

For the pharmacognostic analysis were used the vegetal products obtained from the species *Lysimachia nummularia* L.: *Lysimachiae* radix, *Lysimachiae* herba and *Lysimachiae* flores.

The vegetable products were obtained from the species *Lysimachia nummularia* L. after drying and sorting.

The qualitative chemical analysis is based on the successive extraction of the plant product used, with solvents of different polarities and the identification by reactions characteristic of each group of active principles. The reagents used in identifying the active principles are reagents for analysis from various domestic and imported companies.

Determination of drying loss is a preliminary quantitative pharmacognostic method that represents the degree of humidity of plant products, which must be within certain limits, so as to ensure the preservation of plant products.

The working method involves the following technique.

The weighing vials with the vegetable products previously brought to a constant mass, together with the sample taken, are kept in the oven at 105^{0}C for 3-4 hours, unless otherwise provided, cooled in a desiccator and weighed. Continue drying for 1 hour, followed by cooling in the desiccator and weighing until the samples reach a constant mass. A KERN ABJ analytical balance was used to weigh the samples.

Determination of soluble substances is the amount of substances that are soluble in a given solvent, per 100 grams of dried vegetable product. This preliminary quantitative determination has indicative value as regards the amount of active principles soluble in a given solvent.

Taking into account the solubility of the active principles known in the literature, as well as the extraction possibilities, we used in this determination three solvents, namely: ethanol 40% (v / v), ethanol 96% (v / v) and water. Thus, the determination of soluble substances was performed for each plant product (*Lysimachiae* radix, *Lysimachiae* herba and *Lysimachiae* flores) in the three solvents mentioned above.

The following working technique was used to determine the soluble substances:

2.5 g of vegetable product, sprayed according to the provisions of the respective monograph, are weighed on the analytical balance and brought into a vial with a ground-in stopper; add 100 g of the solvent provided, shake vigorously several times, leave to soak for 23 hours, shake again for 1 hour and filter, removing the first portions of the filtrate. 10 g of the filtrate are evaporated to dryness on a water bath in a pre-calibrated weighing ampoule. The weighing vial with residue is dried in the oven; at 105^{0} C, for 3-4 hours, cool in the desiccator and weigh.

RESULTS AND DISCUSSIONS

Lysimachia nummularia L., is a herbaceous, perennial plant (Figure 1, Figure 2), spread through meadows and bushes, in forests, streams, wet depressions, through water holes, meadows and on the waterfront, in the plains and hilly regions from all over the country.

Fig.1. *Association with Lysimachia nummularia L.*

Fig. 2. *General appearance of the species Lysimachia nummularia L.*

From a macroscopic point of view, underground, it presents a rhizome with nodes and internodes, with thin adventitious roots starting from the nodes (Figure 3). The stem is sudden, 10-50 cm long, glabrous, simple or weakly branched, in four edges, at nodes with bundles of adventitious roots (Figure 4).

Fig. 3. *Lysimachia nummularia L. – roots with nodes and internodes*

Fig. 4*. Lysimachia nummularia L.- simple glabrous stems*

The leaves are opposite, round or elliptical, obtuse, with entire edges, very shortly petiolated, with red glandular points (Figure 5).

The solitary hermaphroditic flowers, arranged in the axils of the leaves (Figure 5), have floral pedicels the length of the leaves, sometimes even longer. The floral coating is a perianth made of calyx and corolla.

Fig. 5. *Lysimachia nummularia L. - Opposite round elliptical leave*

Fig. 6. *Lysimachia nummularia L. Solitary flowers in the leaf axils*

The actinomorphic calyx consists of five free sepals, 7 mm long, with cordiform lacinas, separated to the base (dialisepal) (Figure 6, 7).

Fig. 7. *Lysimachia nummularia L. - calyx with cordiform lacinae*

Fig. 8. *Lysimachia nummularia L. - calyx with cordiform lacinas - dialisepal pentamerous corolla*

The corolla is intensely yellow, with a glandular reddish dotted interior, about 15 mm wide, twice as wide as the calyx, divided almost to the base into obovate, obtuse lacrines with full edges. It is pentamerous, actinomorphic, dialisepal (Figure 8).

The androecium consists of five stamens (Figure 9), two to three times shorter than the corolla, with hairy glandular filaments at the base. Stamen length style. The fruit is a capsule only rarely developed, globular, 4-5mm long, shorter than the calyx, whitish yellow, with small red secretory sacs. Blackish seeds, in 3 edges, warty, 1-1.5 mm long.

Fig. 9. *Lysimachia nummularia L. - Androecium of 5 stamens*

Following the general chemical analysis performed, the following types of active principles were identified as follows:

In the roots of *Lysimachia nummularia* L. were identified: volatile oil, sterols (triterpenes), flavonic aglycones, carotenoids, coumarins, tannins (gallic tannins, catechin tannins), flavonosides, coumarins heterozidates, heterozides o, triterpenes, (ortho dihydroxy phenols) ODP, poliosis, polyuronides, saponosides.

The following classes of active principles have been identified in the plant product *Lysimachiae* herba: volatile oil, sterols (triterpenes), flavonic aglycones, carotenoids, fatty acids, coumarins, tannins (Galician tannins, catechin tannins), flavonoids, heterosidium coumarins, heterosides, ODP, reducing compounds, oases, polyoses, polyuronides, saponosides.

Following qualitative chemical analysis, the flowers of *Lysimachia nummularia* L. contain: volatile oil, sterols (triterpenes), flavonic aglycones, carotenoids, fatty acids, coumarins, tannins (gallic tannins, catechin tannins), flavonoids, heteropidate coumarins, ODP, reducing compounds, oases, polyoses, polyuronides.

Comparing the results obtained by us with those mentioned in the literature we found the following:

- the presence of flavonosides is also mentioned in the literature in all parts of the plant *Lysimachia nummularia* L. Thus, throughout the plant were identified rifolin, isoquercitrin, myricitrin, mearnsitrin, syringetin 3-galactoside, kaempferol 3-O-rhamnosyl (1 → 2) galactus, quercetin 3-O-neohesperidioside, rutin, kaempferol 3-O-(2,6-dirhamnosylgalactoside) and quercetin 3-O- (2,6-dirhamnosylgalactoside) [5];
- species of the genus *Lysimachia* contain kaempferol, quercetin and myricetin in: L. vulgaris, L. *nummularia*, L. *punctata*, L. *christinae*, L. *ciliata* and L. *clethroides*, respectively, which demonstrates the presence of flavonic aglycones identified by us [7];

- polyphenolic compounds were also determined in species of the genus Lysimachia sp, *Lysimachia nummularia* L., *Lysimachia vulgaris* L. and *Lysimachia punctata* L [6].
- Thus, the identification of the constituents from the groups of active principles highlighted in the researched plant product will be possible also through the correlation between metabolism and phylogeny.

The loss results for the plant products *Lysimachiae* radix, *Lysimachia*e herba and *Lysimachiae* flores are summarized in the table below:

Table 1. *Results of preliminary determinations*

Nº	**Vegetable product**	**Loss on drying Quantity (g% ± SD)**
1.	*Lysimachiae radix*	8,6043 ±0,5125
2.	*Lysimachiae herba*	8,54086±0,1070
3.	*Lysimachiae flores*	7,4941±0,5408

The values of the loss by drying show that the vegetal product taken in work falls within the limits allowed by FR X and Ph. E. 10.0 (3 - 13%) in terms of the content of volatile substances at 100^{0}C, to ensure their good shelf life. Regarding the content of soluble substances in different solvents, it is observed that most substances are soluble in 40% ethanol.

Table 2. *Results of preliminary determinations - soluble substances*

Crt. no.	**Vegetable product**	**Determination of soluble substances in different solvents**	**Soluble substances (g% ± SD) Dried vegetable product**
1.	*Lysimachiae radix*	Ethanol soluble substances 40%	54,1038±0,4055
		Ethanol soluble substances 96 %	23,5023±0,7913
		Water soluble substances	41,3076±0,6882
2.	*Lysimachiae herba*	Ethanol soluble substances 40%	62,9067±1,1140
		Ethanol soluble substances 96 %	27,6922±0,4269
		Water soluble substances	54,5582±0,3369
3.	*Lysimachiae flores*	Ethanol soluble substances 40%	81,4685±1,3784
		Ethanol soluble substances 96 %	53,6120±0,9132
		Water soluble substances	66,6908±1,2166

CONCLUSION

The analysis of the macroscopic characters of the studied species confirms that the plant is *Lysimachia nummularia* L. from the *Primulaceae* family, because these characteristics are in accordance with the description of the species in the literature, respectively in the flora determinants in Romania. Among these characters are the plagiotropic feature, the glabrous appearance of the vegetative organs, the opposite position of the almost round leaves, the solitary, axillary yellow flowers.

The presence of several groups of active principles in all organs of the species *Lysimachia nummularia* L. leads us to the conclusion that the species is of interest and can be researched for therapeutic recovery purposes.

The product does not contain cardiotonic alkaloids and heterosides (toxic compounds) or anthracenosides (laxative compounds). The values of drying loss show that the vegetable products used correspond to their preservability.

As the largest amount of substances are soluble in 40% ethanol, it determines us in the following research to take extracts obtained in 40% ethanol.

REFERENCES

[1] Pârvu C., Enciclopedia plantelor, vol. I, Tehnică, București, 2003, 67.

[2] Neli K. O., Studiul extractelor vegetale – mai mult decât analize fitochimice, Universitatea de Vest „Vasile Goldiș" Arad, Iulie 2018.

[3] Tóth A., Riethmüller E., Alberti Á., Végh K., Kéry Á., Comparative phytochemical screening of phenoloids in *Lysimachia species*, European Chemical Bulletin, Vol. 1, nr. 1-2, 2012.

[4] Toth A., Toth G., Kerya A., Polyphenol Composition and Antioxidant Capacity of Three *Lysimachia Species*, Natural Product Communications, Vol. 9 (10) 2014, 1473-1478.

[5] Toth, A., Riethmuller, E., Vegh, K., Alberti, A., Beni, S., & Kery, A.. Contribution of individual flavonoids in *Lysimachia species* to the antioxidant capacity based on HPLC-DPPH assay. Natural product research, 32(17), 2018, 2058-2061.

[6] Luczak S., Swiatek L., Daniewski M, Phenolic acid in herbs *Lysimachia nummularia* L. and L. vulgaris., Acta Polonie Pharmaceutica, 1989.

[7] Yasukawa K., Ogawa H., & Takido M., Two flavonol glycosides from *Lysimachia nummularia*, Phytochemistry, 29(5), 1990, 1707-1708.

[8] Podolak I., Kokzurkiewicz P., Michalik M., Galanty A., A new cytotoxic triterpene saponin from *Lysimachia nummularia* L., Cercetarea carbohidraílor, Volume 375, 28 iunie 2013, 16-20.

[9] Podolak I., Koczurkiewicz P., Galanty A., Michalik M., Cytotoxic triterpene saponins from the underground parts of six *Lysimachia* L. species., Biochem. Syst. Ecol. 2013; 47, 116–120.

[10] Hanganu D., Kinga O. N., Mocan A., Vlase L., Benedec D., Raita O., Toma C. C., Conținut polifenolic comparativ și activități antioxidante ale două specii de lizimachie românești, Revista de Chimie –București, 2016.

[11] Yildirim A. B., Guner B., Karakas F. P., Turker A. U., Evaluation of antibacterial, antitumor, antioxidant activities and phenolic constituents of field-grown and in vitro-grown *Lysimachia vulgaris* L., Afr. J. Tradit. Complement Altern. Med 14(2), 2017, 177–187.

[12] Csepregi R., T. Viktória, Das S., Ágnes Alberti, Proprietăți și efecte citotoxice, antimicrobiene, antioxidante asupra migrației celulare a compușilor fenolici ai plantelor medicinale transilvane selectate, Antioxidanți, 2020, 9, 166.

[13] *** Flora României, 1952-1976, vol. VII, Acad. R.P.R.-R.S.R., 42-46.

[14] Ciocârlan V., Flora ilustrată a României. Pteridophyta et Spermatophyta, Ceres, București, 2009, 1067.

[15] ***Farmacopeea Română, editia a X-a, Medicala, Bucuresti, 2021.

RESULTS OF SOME ROMANIAN TOMATO AND EGGPLANT CULTIVARS GRAFTED ONTO INTERSPECIFIC (GENUS *LYCOPERSICON*) ROOTSTOCK

Mădălina Doltu[1]
Dorin Sora[2]
Vlad Bunea[3]
[1, 2] Research and Development Institute for Processing and Marketing of Horticultural Products – Horting, Bucharest, Romania
[3]Technical University of Civil Engineering of Bucharest, Romania

ABSTRACT

This experience aims at identifying an optimal rootstock for Romanian tomato and eggplant cultivars and the influence on plant yield and growth. These vegetables (tomato and eggplant) are very important crops worldwide and in Romania. Tomato and eggplant plants are very sensitive to climatic fluctuations and can affect fruit yield. Grafting on species from the *Solanaceae* family is a practice that increases productivity, fruit quality, resistance to diseases and pests, abiotic factors. The work was conducted at the Horting Research Institute, Romania. The biological material used was different tomato and eggplant; two scions, Siriana F1 (tomato), Luiza variety (eggplant) and a rootstock, Emperador F1 (tomato). The Emperador rootstock and others are very used in worldwide for ecological and conventional cultures. By comparing the tomato and the eggplant yield of the researched grafted and non-grafted variants it has been shown that grafted cultivars have had very good values, being higher with 19.78% and 29.13% than at non-grafted plants. Following the studies undertaken in the research greenhouse period 2019-2020, a rootstock from genus *Lycopersicum* (Emperador) was tested and some results are in this scientific paper.

Keywords: *grafted vegetables, quality, Solanaceae, yield*

INTRODUCTION

Grafting technology can be employed by farmers that cannot afford soil steaming and pesticides. Today grafting is also being employed to enhance crop response to a variety of abiotic stresses, and improve plant growth, yield and fruit quality.

A study was conducted on the graft compatibility between the eggplant rootstocks and the hybrid tomato cultivars grown in Tanzania [8]. In addition to this, because of the environmental concerns posed by chemical pesticides, proactive cultural practices are often recommended, including crop rotation, solarization, resistant cultivars and the grafting onto resistant rootstocks [6]. There is a need for environmentally sound and economically feasible alternatives [1].

The plants that were grafted onto tomato rootstocks and showed significantly greater vegetative growth, leading to taller, more robust plants than those grafted on eggplant rootstocks, as well as in relation to the non-grafted control [7].

Grafting is a valuable tool for managing problems of tomato soil-borne pathogens and pests, but often generates unpredictable effects on crop yield and product quality. To observing these rootstocks-induced changes, experimental designs including many rootstock-scion combinations are required [5].

Some resistant solanaceous rootstocks are used worldwide (wild species and commercial hybrids as Emperador F1 and other).

This research regarding the identification of an optimal rootstock for tomato and eggplant crops from Romania is important to highlight yield of some scion-rootstock genotypic combinations.

The researches in tomato and eggplant grafting are study field of some horticulture researchers from the Horting Institute, Romania since 2002.

MATERIALS AND METHODS

Biological materials

The work was carried out in a Research and Development Laboratory from the Horting Institute, Bucharest, Romania.

The biological material used was different tomato and eggplant; two scions, Siriana F1 (tomato), Luiza variety (eggplant) and a rootstock, Emperador F1 (tomato).

Siriana F1 (*Solanum lycopersicum* L.) are tomatoes from the Research and Development Station for Vegetable Growing, Buzău, Romania. These tomatoes are tested in grafted and ungrafted cultures in some greenhouses at the Horting Institute. Siriana F1 has a great vigor, spherical and red fruit, 150 g/fruit and 4-5 seminal lodges/fruit. This tomato hybrid is early (110-115 days), indeterminate plant and well adapted to greenhouses and field conditions.

Luiza (*Solanum melongena* L.) is a semi-early eggplant variety created in the Research and Development Institute for Vegetable and Floriculture Vidra, Romania. It is a variety with pear-oblong fruit, dark purple color and a fruit with 200-300 g. Luiza is an eggplant variety recommended for cultivation in greenhouse and field.

Emperador F1 (*Lycopersicon esculentum* x *L. hirsutum*) is a commercial rootstock created in the Rijk Zwaan Company, Netherlands. It is vigorous and very resistant to the attack of the *Fusarium* sp., *Verticillium* sp. and *Tomato Mosaic Virus*. It is recommended for greenhouse and field.

Experience design

This experience has been implemented in 30 plants (3 replications of 10 plants per every variant). The work scheme was: V1 – grafted Siriana tomatoes (20.000 plants/ha);

V2 – non-grafted Siriana tomatoes (27.000 plants/ha); V3 – grafted Luiza eggplants (18.000 plants/ha); V4 – non-grafted Luiza eggplants (24.000 plants/ha).

Biometrical determinations

Biometric determinations were carried out on the tomato and the eggplant fruits (yield per hectare). For total carbohydrate analysis were used using ten fruits/variants and the Bertrand method recommended by some researchers [3], extracting the carbohydrates from the product with the help of water, purifying the plant extract and dosing reducing sugars in the purified extract.

Statistical analysis

The Duncan test has been used to determine some differces between the total tomato and eggplant yield per hectare.

RESULTS AND DISCUSSIONS

Yield

The Emperador rootstock was influence on fruit yield (Table 1).

Table 1. *Fruit yield (tomatoes and eggplants)*

Variant	Species	Yield (t/ha)	Difference	
			t/ha	%
V1 – grafted Siriana	tomato	55.1^{b}	9.1	119.78
V2 – non-grafted Siriana	”	46^{a}	-	100
V3 – grafted Luiza	eggplant	49.2^{b}	11.1	129.13
V4 – non-grafted Luiza	”	38.1^{a}	-	100

Note: after the Duncan’ *s test; p <0,05*

The *Lycopersicon* rootstock (Emperador) has had a positive influence on yield of Siriana tomato and Luiza eggplant cultivars grown in a plastic house from Romania.

In Table 1, there are differences up to 19.78% at Romanian Siriana tomato and 29.13% at Romanian Luiza eggplant compared to the same non-grafted plants.

Some researchers [4], reported a positive effect and at others *L. esculentum* x *L. hirsutum* rootstocks (Beaufort). Other researchers reported a positive effect on yield of some grafted tomato fruits [9] and some grafted eggplant fruits [2], compared to non-grafted plants.

Quality

The Emperador rootstock was influence on carbohydrates content (Table 2).

Table 2. *Total carbohydrates in tomato and eggplant fruits*

Variant	Species	Total carbohydrates (%)	Difference (+/-)
V1 – grafted Siriana	tomato	3.06^{NS}	0.05
V2 – non-grafted Siriana	”	3.01	-
V3 – grafted Luiza	eggplant	2.42^{NS}	0.08
V4 – non-grafted Luiza	”	2.41	-

Note: after the Duncan' s test; p <0,05; NS: no significance

The *Lycopersicon* rootstock (Emperador) has had a positive influence on carbohydrates content of Siriana tomato and Luiza eggplant cultivars grown in a plastic house from Romania, but no significance. In Table 2, there are differences up to 0.05% at Romanian Siriana tomato and 0.08% at Romanian Luiza eggplant compared to the same non-grafted plants.

Some researchers [9] reported a significant positive effect of grafting on the sugar content.

CONCLUSION

The Emperador rootstock is used for tomato and eggplant cultures because it is growing fruit yield (differences up to 19.78% at Romanian Siriana tomato and 29.13% at Romanian Luiza eggplant) and it did not influence the quality by carbohydrate content.

The *Lycopersicon* rootstocks (Emperador and others) are used in Romania for ecological and conventional cultures.

Graft research on different rootstocks is recommended to determine compatibility in culture. And other researchers [8] recommend that further studies are required to determine rootstocks that are vigorous enough to carry scions of hybrid tomato cultivars to improve graft success and plant growth

By comparing the yield of the studied grafted and non-grafted plants it has been shown that grafted tomato and eggplant variants have had the best values, higher than at non-grafted plants.

The use of grafted tomato and eggplant plants, the scion x rootstock combinations researched in this paper, can be cultivated in the vegetable cultures from the south-east of Romania.

ACKNOWLEDGEMENTS

This work was supported by founding source Project ADER 7.3.5, financed by Agriculture and Rural Development Ministry.

REFERENCES

[1] Ajwa H., Klose S., Nelson S., Minuto A., Gullino, M., Lamberti F., Lopez A., Jose M., Alternatives to Methyl bromide in Strawberry Production in the United

States of America and the Mediterranean Region, Phytopathologia Mediterranea, vol. 42, pp 220-244, 2003;

[2] Bletsos, F., Thanassoulopoulos, C.C., Roupakias, D.G. (2003). Effect of grafting on growth, yield, and Verticillium wilt of eggplant. HotScience 183, 186-186.

[3] Hoza G., Doltu M., Becherescu A.D., Apahidean A.I., Dinu M., Bogoescu M. Response of Different Grafted Eggplants in Protected Culture, Jurnal Notulae Botanicae Horti Agrobotanici Cluj-Napoca (Not Bot Horti Agrobo), vol. 45(2), pP 473–480, 2017;

[4] Maršić N.K., Osvald J. The influence of grafting on yield of two tomato cultivars (Lycopersicon esculentum Mill.) grown in a plastic house, Acta agriculturae slovenica, vol. 83(2), pp 243-249, 2004;

[5] Mauro R.P., Agnello M., Onofri A., Leonardi C., Giuffrida F., Scion and Rootstock Differently Influence Growth, Yield and Quality Characteristics of Cherry Tomato, Plants Basel. Vol. 9(12), pp 1725-1746, 2020;

[6] Na Liu, Baoli Zhou, Xin Zhao, Bo Lu, Yixiu Li, Jing Hao. Grafting Eggplant onto Tomato Rootstock to Suppress Verticillium dahliae Infection, The Effect of Root Exudates, vol. 44(7), pp 2058-2062, 2009;

[7] Passam H.C., Stylianou M., Kotsiras A. Performance of Eggplant Grafted on Tomato and Eggplant Rootstocks, Europ. J. Hort. Sci., vol. 70(3), pp 130–134, 2005;

[8] Shipepe B.T., Msogoya T.J. Graft Compatibility Between Eggplant Rootstocks and Hybrid Tomato (Solanum lycopersicum Mill.) Cultivars, Tanzania Journal of Agricultural Sciences, vol. 17(2), pp 31-38, 2018;

[9] Turhan, A., Ozmen N., Serbeci M.S., Seniz V. Effects of grafting on different rootstocks on tomato fruit yield and quality, Horti. Sci. (Prague), vol. 38(4), pp 142-149, 2011.

SARS-COV-2 CORONAVIRUS: NOMENCLATURE, CLASSIFICATION, STRUCTURE, HISTORY, SYMPTOMS EPIDEMIOLOGY, PATHOGENESIS, ETIOLOGY, DIAGNOSES, TREATMENT, AND PREVENTION

Hanan Al-Khalaifah[1]
Mohammad Al-Otaibi[2]
Abdulaziz Al-Ateeqi[3]
[1, 2, 3] Kuwait Institute for Scientific Research, Environment and Life Sciences Research Center, Kuwait

ABSTRACT

With the onset of the coronavirus pandemic in December 2019 in China, and the alarming rate at which it has spread across the world has unleashed not only fear, but has taken a toll on social, economic, health, and governing capabilities of the various countries infected with the virus. The pandemic is affecting all aspects of life, including industries such as the animal production industry all over the world. This includes plant, livestock and poultry production. Food security is accordingly impacted, as these industries are vital elements that are contributing to securing food to populations worldwide. In this review, light is shed on the origin of coronaviruses with special emphasis on COVID-19. It also includes introduction of symptoms, epidemiology and pathogenesis, etiology, and prevention. As the disease progresses, scientists are working around the clock in the hope of an effective vaccine, and they managed to introduce some to the worldwide populations. The world faces challenges on a day-to-day basis until most people are vaccinated.

Keywords: *coronaviruses, COVID-19, epidemiology, vaccine*

INTRODUCTION

The COVID-19 pandemic has affected people worldwide and is the fifth pandemic after the Spanish flu of 1918. It originated in Wuhan, China, and has now escalated to more than 200 countries and has infected individuals of almost all ages. The onset of the disease progresses with milder symptoms such as fever, upper respiratory tract symptoms, shortness of breath, and diarrhea and some individuals are asymptomatic. In those patients with severe infection, pneumonia, multiple organ failure, and death have been reported. The pandemic has now claimed the lives of millions and has gained the attention of public health researchers worldwide [1], [2], [3].

The world has previously also suffered epidemics due to coronaviruses in the form of severe acute respiratory syndrome (SARS)-CoV which emerged in Guangdong province of China and again, in September 2012, the Middle East respiratory syndrome (MERS)-CoV. These viruses have a natural and zoonotic

origin which can be reflected in the SARS-CoV-2. The Covid-19 pandemic has not only disrupted physical health but has also negatively impacted mental health, economy, and social framework and large healthcare systems of the world .Government authorities of the world are putting their heads together to determine the safety and precautionary measures. Scientists are continually and tirelessly researching probable diagnostics and vaccines to curb the spread of this pandemic which has proven to be more than a challenge. Currently, there exist only therapeutic and preventive ways to deal with the outbreak [4].

Nomenclature and classification

Coronaviruses belong to the largest group of RNA viruses and are enclosed with positive-strand genomes of 26-32 kb in length. They are abbreviated as "CoVs" due to their crown-like appearance when scanned under an electron microscope [5]. They are classified under the Nidovirales order and include other families such as Coronaviridae, Arteriviridae, Mesoniviridae, and Roniviridae. The Coronaviridae family is again subdivided into Coronavirinae and the Torovirinae [6]. Based on the genetic differences and serological cross-reactivity, the Orthocoronavirinae subfamily is further divided into Alphacoronavirus, Betacoronavirus, Gammacoronavirus, and Deltacoronavirus [7]. The Betacoronavirus group was earlier divided into four lineages: A, B, C, and D. Although recently these have been reclassified and renamed as Embecovirus, Sarbecovirus, Merbecovirus, and Nobecovirus. A fifth subgenus, Hibecovirus, has also been added [6].

The alpha-CoVs consists of human and animal viruses, the beta-CoVs, consists of murine and human viruses, the gamma-CoVs consists of viruses from cetaceans and birds and delta-CoVs consists of viruses from pigs and birds [8]. CoVs have traversed the species barriers and have become transmissible to humans. To date, seven human CoVs (HCoVs) have been identified from which two, HCoV-229E and HCoV-NL63 are α-CoVs and the rest β-CoVs which include HCoV-OC43, HCoV-HKU1, severe acute respiratory syndrome coronavirus (SARS-CoV), Middle East respiratory syndrome coronavirus (MERS-CoV) and SARS-CoV-2. These HCoVs have originated from bats, mice, or domestic animals [5].

Structure of coronaviruses

The coronaviruses have a diameter of about 120 nm along with club-shaped protein spikes protruding from the surface, appearing like a solar corona. They possess four principal structural proteins which are; spike (S; 1160–1400 amino acids), membrane (M; 250 amino acids), envelope (E; 74–109 amino acids), and nucleocapsid (N; 500 amino acids) proteins, all of which are encoded within the 3′ end of the viral genome [6]. The S glycoprotein (~150 kDa) is a class I fusion protein and directs attachment to the host receptor. This S protein is cleaved by a host cell protease into distinct subunit, S1, and S2. The former constitutes the major receptor-binding domain of the S protein whereas the latter makes up the stalk of the spike molecule. The M protein is present in abundance, it is small (~25–30 kDa) and gives shape to the virion. The E protein (~8–12 kDa) is present in minute quantities in the virion and the N protein is unique due to its presence in the nucleocapsid [9].

A brief history of discovery of human coronaviruses (HCoVs)

One of the first strains to be isolated from infected individuals with respiratory problems in 1966 was HCoV-229E. The symptoms observed in infected patients were common cold, headache, sneezing, malaise, sore throat, fever, and cough. The following year, HCoV-OC43 strain was isolated from organ cultures. The infections caused by these strains were closely similar to those caused by HCoV-229E. These two strains are actively transmitted during winters. The incubation time of these viruses is on average less than a week and an illness period of two weeks. Studies on human volunteers showed that healthy and fit persons infected with the HCoV-229E strain showed mild flu-like symptoms and a few patients showed acute respiratory tract infection. Phylogenetic evidence has indicated that these strains have originated from bats or rodents [5].

The severe acute respiratory syndrome or more commonly known as SARS was the third HCoV to be discovered and the first to be well-documented. It is otherwise called atypical pneumonia. It was first traced back to Guangdong Province of China in November 2002. The World Health Organization (WHO) reported 8096 infections and 774 casualties in just a span of one year in more than 30 countries. There was a 50% mortality rate observed in the elderly subjects. This virus is believed to have originated from the SARS-CoV found in wild feline animals such as the palm civet in the markets of China and was transmitted to humans by contact when handling these creatures. However, it was later observed that palm civets from the wild or farms were negative for SARS-CoV which could be an indicator that they only served as intermediate hosts and the natural animal host was Chinese horseshoe bats [5]. It is transmitted in humans through cough droplets or mucosae which contain infected fomites. The virus originated in China and then spread to other parts of the world via interpersonal transmission from hospitals, medical institutions, homes, workplaces, and public transport [10]. The symptoms for SARS-CoV were muscular pain, headache, fever, weakness, and chills, followed by dyspnoea, cough, and respiratory discomfort as of late symptoms. On a cellular level, alveolar damage, epithelial cell proliferation, and an increase in macrophages were observed in infected individuals. About 20-30 % of patients needed intensive care and ventilation. The HCoVNL63 strain was more widespread among young children, the elderly, and those with respiratory sicknesses. The underlying symptoms observed were coryza, conjunctivitis, fever, and bronchiolitis. Its rate of incidence was high during early summer, spring, and winter. Another strain, HCoV-KKU1 was linked with acute asthmatic exacerbation in the elderly [5].

The MERS coronavirus (MERS-CoV) was initially isolated in Jeddah, Saudi Arabia from an infected person in September 2012 who was suffering from acute pneumonia and renal failure. The WHO reported 288 deaths, with a mortality rate of 34.5% between September 2012 till July 2014. The virus was contracted by a man returning from Saudi Arabia to South Korea and led to the outbreak of the disease with deaths numbering 36 and a mortality rate of 19.4%. The spread of the MERS-CoV infection is believed to be zoonotic as genomic analysis showed that the virus originated from a bat, which was then transmitted to dromedary camels, the intermediate hosts for transmission to humans [10].

The COVID-19 coronavirus- A pandemic

A brief background

The last twenty years have seen the emergence of several viral diseases as mentioned previously like the SARS-CoV, H1N1, and the MERS-CoV. We now know that these respiratory diseases caused by CoVs can cross species barriers and cause severe illnesses in humans [4].

The COVID-19 pandemic has taken the world by storm since its emergence in December 2019. It originated from Huanan Seafood Market in Wuhan City, Hubei province of China, one of the most densely populated cities with a population crossing 11 million. The wet market traded not only fish but various live animals such as poultry, bats, marmots, and snakes [11]. Hospitals started receiving patients showing severe pneumonia-like symptoms of unknown origin. Surveillance systems installed post the SARS epidemic were again set in motion and throat swab samples collected from infected individuals were tested and on December 31st, 2019, China through the WHO declared the outbreak of the virus. The virus was confirmed to be a CoV. It was found to have a similarity of more than 95% with the bat coronavirus and more than 70% with the SARS-CoV. Samples obtained from the seafood market confirmed the presence of the virus indicating its origin from that place. Cases of infected persons skyrocketed and several cases were reported even though they did not have any exposure to the market. The first fatality was reported on 11th January 2020. The epidemic became explosive during the Chinese New Year when reports of cases started emerging from people returning from Wuhan. Hubei province was soon placed under lockdown and extended to other cities as well. The infection was transmissible from those individuals who did not show any sign of sickness (asymptomatic) and also before the initiation of symptoms [12].

The upsurge of the COVID-19 pandemic which started in China was officially declared by WHO as a state of Public Health Emergency of International Concern (PHEIC) on 30th January 2020. They stated that the spread of the virus could be slowed down employing timely detection, isolation, quick and speedy treatment, and rapid and efficient system to trace contacts [12]. By this time, the virus had already extended to 18 countries and four countries reported cases that spread from human contact. The virus was previously termed 2019-nCoV, the ICTV termed it as the SARS-CoV-2 virus due to its similarity with SARS-CoVs that caused the SARs outbreak. The Director-General of WHO, Dr. Tedros Adhanom Ghebreyesus stated on February 11, 2020, that the disease would be termed ‘COVID-19”, which is the acronym of "coronavirus disease 2019". The situation spiraled out of control on the 11th of March when the number of cases out of China increased 13 times, the countries with infected individuals had tripled with 118,000 cases in 114 countries and more than 400 deaths. This is when the WHO declared the COVID-19 situation as a pandemic [4], [13].

Symptoms of COVID-19

The symptoms of the infection start appearing post-incubation interval of an average of 5.2 days. The onset of the symptoms until death (if happens) ranges from 6-41 days. This duration is conditioned based on the age and overall immune system of the patient. It is lower in older patients, greater than 60 years in comparison with younger individuals and people with underlying diseases (i.e., hypertension, chronic obstructive pulmonary disease, diabetes, cardiovascular disease). The familiar symptoms at the start of the disease are fever in some people, cough, fatigue, and varies with sputum production, headache, hemoptysis, diarrhea, dyspnoea, and lymphopenia [14]. The clinical features range from asymptomatic to acute respiratory distress syndrome (ARDS) and multiorgan failure [12]. The uniqueness of COVID-19 as compared to previous beta-CoVs is that it affected lower airways which resulted in rhinorrhoea, sneezing, and sore throat [14].

Epidemiology and pathogenesis

As per the report of the WHO COVID-19 dashboard, currently, there are 108,918 new cases, 7,127,753 confirmed cases and 407,159 deaths globally as of 10:47 am CEST June 2020. The data for case comparison of confirmed cases in the WHO regions is as follows: Americas- 3,415,174; Europe- 2,303,361; Eastern Mediterranean- 677,338; South-East Asia- 392,674; Western Pacific- 193,178 and Africa- 145,287. Infection is spread through numerous ways but most commonly from sizable droplets when coughing and sneezing from symptomatic and asymptomatic people, by touching contaminated surfaces and then touching the facial area. The virus may be found in the stools and contaminated water sources. It can remain viable on surfaces for several hours or days [12]. The duration for which the virus can last on several surfaces is plastic- 2-3 days, stainless steel- 2-3 days, cardboard- 1 day, copper- 4 hours. Aerosol transmission of the virus occurs in case of prolonged exposure in closed spaces. People who are either pre- or asymptomatic can be responsible for at least 80% transmission. In intensive care units (ICUs) contamination is dangerously higher than general wards and is known to be present on floors, computers, trash can, sickbed rails, and up to 4 meters from patients. These CoVs can be immobilized by the use of lipid solvents and fumigants like ether (5%), ethanol, and disinfection with chlorine, peroxyacetic acid, and chloroform. Data collected from primary investigations in Wuhan conducted by China CDCs showed that the doubles weekly and basic reproduction number (R0 - R naught) is 2.2 [4].

Human-to-human transmission initially occurred in Wuhan within families, and also among relatives and friends who came in contact with infected persons. It was reported that 31.3% of patients were those who visited Wuhan and 72.3% of patients who came in contact with people from Wuhan. The rate of transmission among medical personnel took place at 3.8% COVID-19 patients [15].

Etiology of COVID-19

The SARS-CoV-2 originates from the betaCoV genus, it is round or elliptic with a diameter of about 60-140 nm. The genome isolated from a patient from Wuhan showed that the virus had an 89% nucleotide which identifies with bat

SARS-like- CoVZXC21 and 82% with human SARS-CoV which is why it is given the name SARS-CoV-2. It contains 29891 nucleotides encoding 9860 amino acids [4].

Diagnosis of COVID-19

Diagnosis is carried out by molecular testing on samples such as throat swabs, nasopharyngeal swab, sputum, endotracheal aspirates, and bronchoalveolar lavage. Some laboratory investigations are non-specific. The white blood cell count is generally less. A possibility of lymphopenia; a lymphocyte count of less than 1000 is normally indicative of chronic disease. The platelet count is either within range or low. The C-reactive protein (CRP) and erythrocyte sedimentation rate (ESR) are slightly higher but procalcitonin levels are normal. A high procalcitonin level can indicate bacterial co-infection. The ALT/AST, prothrombin time, creatinine, D-dimer, CPK, and LDH may rise and high levels are associated with severe disease [12]. An X-ray of the chest area shows bilateral multifocal alveolar opacities, in advanced infection but is normal in early stages. Chest computed tomography (CT) is used for COVID-19 pneumonia in initial stages [4].

Treatment of COVID-19

To date, there is no antiviral treatment or vaccine available against COVID-19. Presently treatments that exist mainly rely on symptomatic and respiratory parameters. The detection and treatment of pneumonia caused by COVID-19 as issued by the National Health Commission of China recommend oxygen therapy and extracorporeal membrane oxygenation (ECMO) to patients with refractory hypoxemia. Several antiviral drugs and systemic corticosteroid treatments including oseltamivir, peramivir, zanamivir, ganciclovir, acyclovir, and ribavirin, as well as methylprednisolone, are not recommended. Based on previous experiences with dealing with the SARS-CoV and MERS-CoV, several drugs have been used for treating COVID-19. The US has reported that its first case of the virus was successfully treated using the drug Remdesivir. Chloroquine which is used to treat malaria in combination with Remdesivir had proven to be effective [15]. The use of non-invasive (NIV) and invasive mechanical ventilation (IMV) is required during times of respiratory failure caused due to resistance to oxygen therapy [4]. Besides all of the aforementioned, the first step that should be taken in isolation to prevent transmission of the virus to any other person. Mild symptoms can be controlled at home and through proper hydration and nutrient-rich diet [12].

Prevention of COVID-19

As there is no confirmed treatment for this disease, prevention is of utmost importance. For mild symptoms, isolation at home is recommended with proper ventilation and sufficient sunlight [12]. The WHO along with other organizations recommend the following [4]:

- Keep away from persons having acute respiratory infections
- Washing of hands for a minimum of twenty seconds, particularly after contact with infected individuals or environment

- Using sanitizer and avoiding contact with face or mouth after touching contaminated surfaces
- Avoid exposure to domestic or wild animals
- Persons with any respiratory symptoms should avoid crowds, wear a mask, follow proper etiquettes of covering their mouth when coughing or sneezing with disposable tissues or clothes

Healthcare workers face the biggest threat in COVID-19 transmission. They should take the utmost care by following all necessary protocols, starting with wearing a surgical mask or N95 masks and protective gear and goggles if they need to be near a patient and following the recommended hygiene practice of handwashing after a duration of 15 minutes or so. They should also be checked regularly for the onset of the symptoms. Patients can only be discharged if they have no fever for three days and two consecutive negative molecular tests of a one-day sampling interval. Lockdowns have been incorporated in all affected countries, people were asked to stay away from crowded places and limit travel. Although the use of masks for healthy people is not recommended by WHO as it has not been shown to protect against the disease but in China, the government has enforced wearing masks [12].

The COVID-19 outbreak has disrupted the economic, medical, and public health of the majority of the world. Health care workers are being overworked, frustrated, and exhausted besides facing high risks of infection [15]. The scenario brought about by the COVID-19 pandemic is constantly changing and is reflective of the mortality rates, research, and the never-ending search for a potential vaccine. The world will be able to normalize only as time progresses and every country is free of COVID-19.

CONCLUSION

Through the numerous literature sources and documents released since the outbreak of this pandemic in December 2019 in China, this paper offers a structured point of view of the CoVs, in terms of classification, history, and detailed review of the COVID-19 disease. Such publications introduce the newcomer to the public that should be aware of the current pandemic. With each day passing, the virus brings out a new angle of public and global health. It has wreaked havoc in the world with so many questions still unanswered and what seems to be a never-ending search for a vaccine making and development. The medical personnel has been facing the ever-challenging side of this virus along with governments to contain and provide all necessary resources to sustain human life and minimize losses. The public worldwide should be trained on practices to reduce infection and face the virus. All people with all ages and sectors should cooperate to face the pandemic and save their lives.

ACKNOWLEDGMENT

The author expresses her gratitude to the Kuwait Institute for Scientific Research (KISR) and Kuwait Foundation for the Advancement of Sciences (KFAS) for their constant technical and financial support.

REFERENCES

[1] Park M, Cook AR, Lim JT, Sun Y, Dickens BL. A systematic review of COVID-19 epidemiology based on current evidence. Journal of Clinical Medicine. 2020;9(4):967.

[2] Al-Khalaifah H, Al-Nasser A, Abdulmalek N, Al-Mansour H, Ahmed A, Ragheb GJFiVS. Impact of SARS-Con-V2 on the Poultry Industry in Kuwait: A Case Study. 2020;7:656.

[3] Al-Khalaifah H. Modulatory Effect of Dietary Polyunsaturated Fatty Acids on Immunity, Represented by Phagocytic Activity. Frontiers in Veterinary Science. 2020;7:672.

[4] Cascella M, Rajnik M, Cuomo A, Dulebohn SC, Di Napoli R. Features, evaluation and treatment coronavirus (COVID-19). Statpearls [internet]: StatPearls Publishing; 2020.

[5] Ye Z-W, Yuan S, Yuen K-S, Fung S-Y, Chan C-P, Jin D-Y. Zoonotic origins of human coronaviruses. International journal of biological sciences. 2020;16(10):1686.

[6] Li X, Luk HK, Lau SK, Woo PC. Human Coronaviruses: General Features. Reference Module in Biomedical Sciences. 2019.

[7] de Wit JS, Cook JK. Avian coronaviruses. Taylor & Francis; 2020.

[8] Burrell CJ, Howard CR, Murphy FA. Fenner and White's Medical Virology: Academic Press; 2016.

[9] Fehr AR, Perlman S. Coronaviruses: an overview of their replication and pathogenesis. Coronaviruses: Springer; 2015. p. 1-23.

[10] Fong I. Emerging animal coronaviruses: First SARS and now MERS. Emerging Zoonoses: Springer; 2017. p. 63-80.

[11] Sohrabi C, Alsafi Z, O'Neill N, Khan M, Kerwan A, Al-Jabir A, et al. World Health Organization declares global emergency: A review of the 2019 novel coronavirus (COVID-19). International Journal of Surgery. 2020.

[12] Singhal T. A review of coronavirus disease-2019 (COVID-19). The Indian Journal of Pediatrics. 2020:1-6.

[13] Al-Khalaifah HS, Khalil AA, Amer SA, Shalaby SI, Badr HA, Farag MFM, et al. Effects of Dietary Doum Palm Fruit Powder on Growth, Antioxidant Capacity, Immune Response, and Disease Resistance of African Catfish, Clarias gariepinus (B.). 2020;10(8):1407.

[14] Rothan HA, Byrareddy SN. The epidemiology and pathogenesis of coronavirus disease (COVID-19) outbreak. Journal of autoimmunity. 2020:102433.

[15] Guo Y-R, Cao Q-D, Hong Z-S, Tan Y-Y, Chen S-D, Jin H-J, et al. The origin, transmission and clinical therapies on coronavirus disease 2019 (COVID-19) outbreak–an update on the status. Military Medical Research. 2020;7(1):1-10.

SENSORY CHARACTERISTICS OF TABLE EGGS AS AFFECTED BY FORTIFICATION OF LAYING FEED RATIONS WITH DIFFERENT FAT SOURCES

Hanan Al-Khalaifah[1]
Afaf Al-Nasser[2]
Tahani Al-Surrayai[3]
[1, 2, 3] Kuwait Institute for Scientific Research, Environment and Life Sciences Research Center, Kuwait

ABSTRACT

The major objective of this research paper was to investigate the effect of enrichment with different oil sources on the egg quality traits in laying hens. A total of 300 one-day-old pullets were used. There were seven dietary treatments of 10 % diet of the following: soybean oil (SO), sunflower oil (SFO), canola oil (CO), flaxseed oil (FLO), fish oil (FO), a mix of fish oil and soya oil (SO+FO), and DHA algal biomass oil. Each treatment contained six replicates with seven birds each. Random samples of 10 eggs per treatment were used; making 70. The organoleptic parameters included tests on smell, taste, color, and texture. The results revealed that there were no significant differences between the eggs from hens fed the different dietary treatments in terms of the organoleptic parameters used. Flaxseed oil, Fish oil and a mixture of Soy oil +Fish oil can be efficiently used to enrich poultry eggs with n-3 PUFA. However, FLO and flaxseeds can be safely used to avoid the fishy smell of poultry products, if present upon reheating.

Keywords: *egg, flaxseed, fish oil, algal biomass, organoleptic*

INTRODUCTION

Dietary supplementation with high-fat sources such as oils serves several critical functions in the body. These include providing a source of metabolic energy, acting as critical components of cell membranes and acting as precursors for eicosanoids production [1, 2]. Examples of oils that were recently used in poultry feed include algal, echium, fish, algal biomass DHA and linseed oils. Some research studies have reported that oils have positive benefits in layers production performance, in addition to their ability to modulate egg lipid composition [3-5].

Table eggs have been fortified with these beneficial fatty acids, especially the n-3 PUFA that have great benefit for the general health status, in addition to their ability to modulate the fatty acid profile of the tissues [6-9].

On the other hand, using fat oils in poultry feed rations may be claimed to reduce the antioxidation indices in the Table eggs and in the hen's body. This may result in to reduced egg quality in terms of smell and texture. This is mainly due to the production of free oxygen radicals as a result of lipid oxidation [8, 10-12].

Accordingly, the current research study was conducted to investigate the effect of using various sources of fat oils in laying feed rations on the sensory characteristics of the produced Table eggs.

MATERIALS AND METHODS

Sensory evaluation was conducted with hardboiled eggs. The eggs were collected and kept at 5ºC for 2 d to facilitate peeling. They were boiled for 15 min and kept in water at around 35ºC to keep them warm until they were served for sensory evaluation [13]. Untrained panelists were asked to evaluate warm hard-boiled eggs after cutting them in halves. Apple juice was offered as a carrier. Each panelist was presented with seven peeled eggs individually placed in plastic plates corresponding to treatments 1 to 7. Each egg was randomly placed and labeled using one-digit randomized numbers representing the seven treatments.

The surveys presented to panelists included brief instructions and a short definition of the study attributes. The attributes tested and the definitions provided to panelists were aroma, yolk color, albumen color, texture, and taste. Panelists were asked to score these definitions carefully and away from any previous experience with boiled eggs. Panels were carried out in a room at 24ºC, separate from the cooking area and under normal light to avoid visual differences in yolk and albumin color. The taste panels were scheduled from 11:00 am to 2:00 pm.

RESULTS AND DISCUSSION

The quality evaluation of the eggs from hens fed the different supplemental oils is shown in Table 1. For further illustration, the results are shown in the form of figures. As shown in the figures, the majority of the panelist answers indicated that the smell, color, taste, and texture of the produced eggs were acceptable and that, there were no significant differences between the eggs from hens fed the different dietary treatments.

Table 1. *Quality Evaluation of the Eggs from Hens Fed the Different Supplemental Oils*

Treatments / Measurements	**SO**	**SFO**	**FLO**	**FO**	**CO**	**FO+SO**	**Notes**
Smell							
Regular	21	21	16	20	19	20	
Irregular	1	1	6	2	3	2	
Yolk color							
Pale	5	14	8	16	13	16	
Yellow	13	8	12	6	8	5	
Orange	4	0	2	0	1	1	
Albumen Color							
Regular	20	22	19	20	20	22	
Irregular	2	0	3	2	2	0	
Taste							
Bad	0	0	4	4	0	0	
Normal	3	5	5	7	3	3	
Good	12	14	10	6	11	10	
Very Good	7	3	3	5	8	9	
Texture							
Regular	21	21	19	19	19	21	
Irregular	1	1	3	3	3	1	

SO= Soya oil, SFO= Sunflower oil, FLO= Flaxseed oil, FO= Fish oil, CO= Canola oil, SO+FO= Soya oil + Fish oil

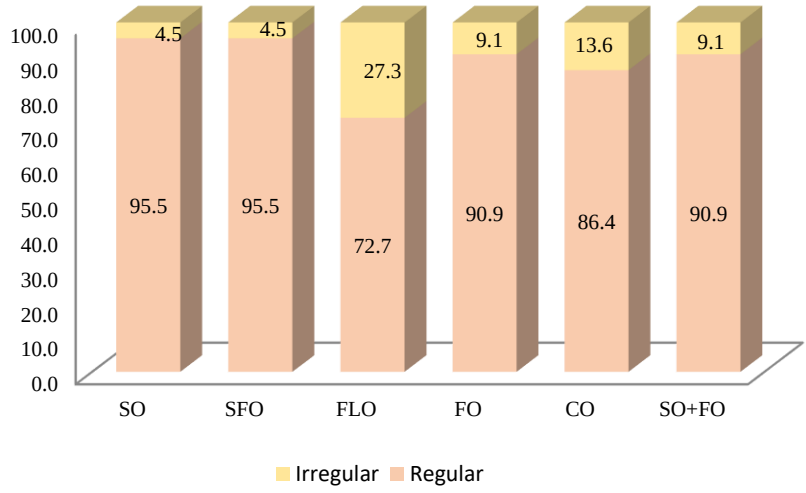

SO= Soya oil, SFO= Sunflower oil, FLO= Flaxseed oil, FO= Fish oil, CO= Canola oil, SO+FO= Soya oil + Fish oil

Fig. 1. *Smell Evaluation of the Eggs from Hens fed Different Supplemental Oils.*

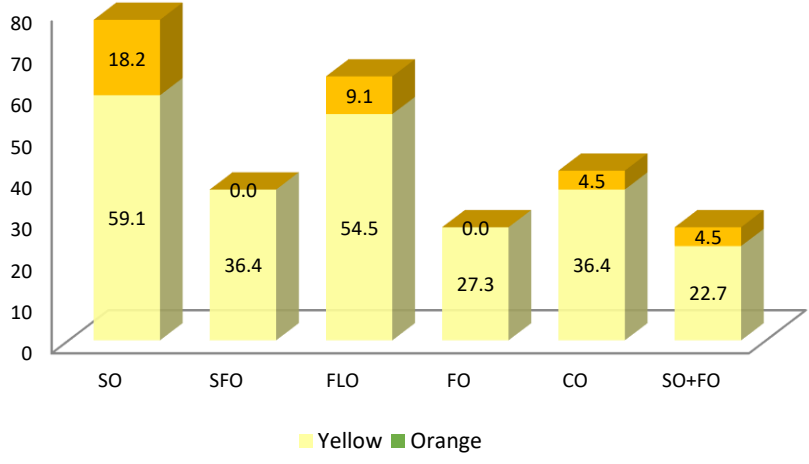

SO= Soya oil, SFO= Sunflower oil, FLO= Flaxseed oil, FO= Fish oil, CO= Canola oil, SO+FO= Soya oil + Fish oil

Fig. 2.*Yolk Colour Evaluation of the Eggs from Hens fed Different Supplemental Oils.*

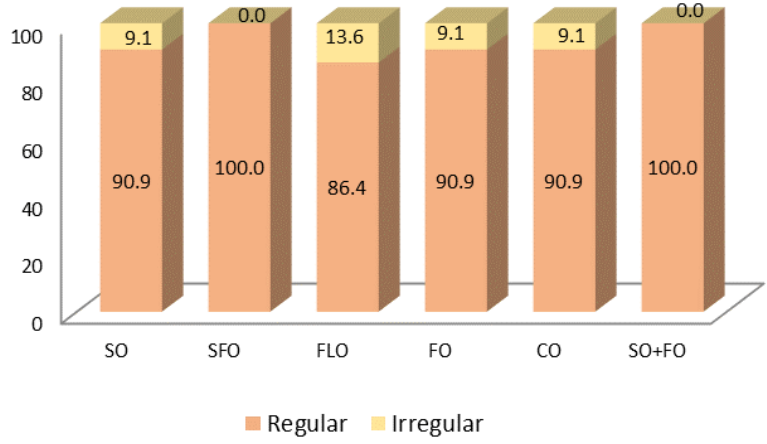

SO= Soya oil, SFO= Sunflower oil, FLO= Flaxseed oil, FO= Fish oil, CO= Canola oil, SO+FO= Soya oil + Fish oil

Fig. 3. *Albumin Colour Evaluation of the Eggs from Hens fed Different Supplemental Oils.*

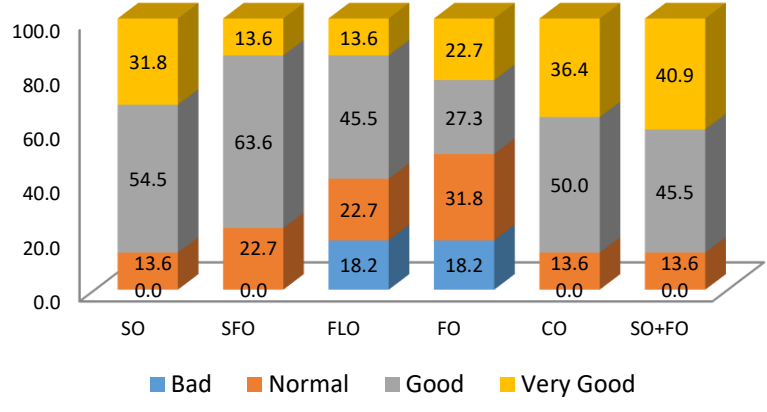

SO= Soya oil, SFO= Sunflower oil, FLO= Flaxseed oil, FO= Fish oil, CO= Canola oil, SO+FO= Soya oil + Fish oil

Fig. 4. *General Taste Evaluation of the Eggs from Hens fed Different Supplemental Oils.*

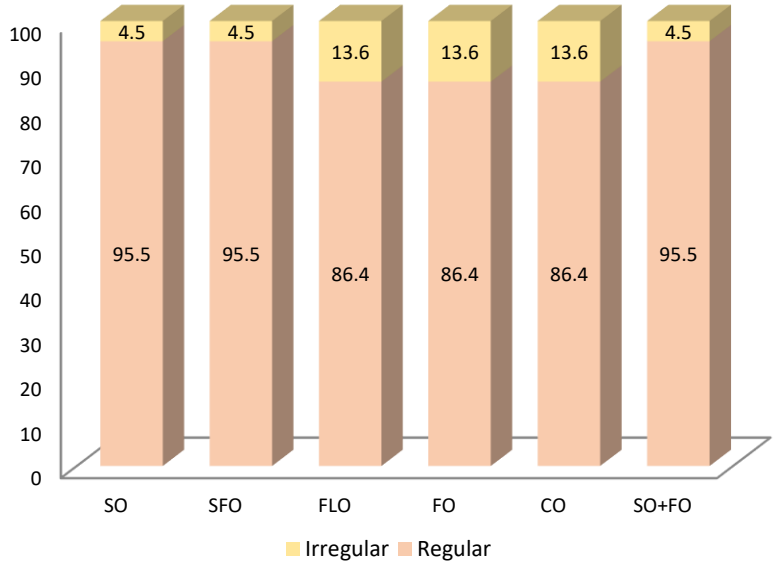

SO= Soya oil, SFO= Sunflower oil, FLO= Flaxseed oil, FO= Fish oil, CO= Canola oil, SO+FO= Soya oil + Fish oil

***Fig. 5**. Texture Evaluation of the Eggs from Hens fed Different Supplemental Oils.*

CONCLUSION

Flaxseed oil, fish oil and a mixture of Soy oil +Fish oil can be efficiently used to enrich poultry eggs with n-3 PUFA. However, fish oil may induce a fishy smell over reheating, if used in the feed in a percentage that exceeds the recommended level (i.e. 10% of diet in the current experiment). On the other hand, plant sources of n-3 fatty acids such as flaxseed oil and flaxseeds can be safely used to avoid the fishy smell of fish oil in poultry products, if present upon reheating.

ACKNOWLEDGMENT

The author expresses her gratitude to the Kuwait Institute for Scientific Research (KISR) and Kuwait Foundation for the Advancement of Sciences (KFAS) for their constant technical and financial support.

REFERENCES

[1] Wealleans A, Jansen M, Di Benedetto Mjbps. The Addition Of Lysolecithin To Broiler Diets Improves Growth Performance Across Fat Levels And Sources: A Meta-Analysis Of 33 Trials. 2020;61(1):51-6.

[2] Al-Khalifa H, Givens D, Rymer C, Yaqoob P. Effect Of N-3 Fatty Acids On Immune Function In Broiler Chickens. Poultry Science. 2012;91(1):74-88.

[3] Attia Y, Al-Khalaifah H, El-Hamid A, Al-Harthi M, El-Shafey A. Effect Of Different Levels Of Multienzymes On Immune Response, Blood Hematology And Biochemistry, Antioxidants Status And Organs Histology Of Broiler Chicks Fed Standard And Low-Density Diets. Frontiers In Veterinary Science. 2020;6:510.

[4] Al-Khalaifah Hs, Badawi Me, Abd El-Aziz Rm, Ali Ma, Omar Ae. Effect Of Egyptian Leek Leaf Extract Supplementation On Productive And Economic Performance Of Broilers. Frontiers In Veterinary Science. 2020;7.

[5] Al-Nasser A, Al-Khalaifah H, Khalil F, Al-Mansour H. Poultry Industry In The Gulf Cooperation Council With Emphasis On Kuwait. World's Poultry Science Journal. 2020;76(3):577-89.

[6] Al-Khalaifah H, Al-Nasser A, Givens D, Rymer C, Yaqoob P. Comparison Of Different Dietary Sources Of N-3 Polyunsaturated Fatty Acids On Immune Response In Broiler Chickens. Heliyon. 2020;6(1):E03326.

[7] Calder Pc, Waitzberg Dl, Klek S, Martindale Rgjjop, Nutrition E. Lipids In Parenteral Nutrition: Biological Aspects. 2020;44:S21-S7.

[8] Omar Ae, Al-Khalaifah Hs, Mohamed Wa, Gharib Hs, Osman A, Al-Gabri Na, Et Al. Effects Of Phenolic-Rich Onion (Allium Cepa L.) Extract On The Growth Performance, Behavior, Intestinal Histology, Amino Acid Digestibility, Antioxidant Activity, And The Immune Status Of Broiler Chickens. Frontiers In Veterinary Science. 2020;7:728.

[9] Ibrahim D, Al-Khalaifah Hs, Abdelfattah-Hassan A, Eldoumani H, Khater Si, Arisha Ah, Et Al. Promising Role Of Growth Hormone-Boosting Peptide In Regulating The Expression Of Muscle-Specific Genes And Related Micrornas In Broiler Chickens. Animals. 2021;11(7):1906.

[10] Attia Y, Al-Khalaifah H, Ibrahim M, Abd Al-Hamid A, Al-Harthi M, El-Naggar A. Blood Hematological And Biochemical Constituents, Antioxidant Enzymes, Immunity And Lymphoid Organs Of Broiler Chicks Supplemented With Propolis, Bee Pollen And Mannan Oligosaccharides Continuously Or Intermittently. Poultry Science. 2017;96(12):4182-92.

[11] Attia Y, Al-Khalaifah H, Abd El-Hamid H, Al-Harthi M, El-Shafey A. Growth Performance, Digestibility, Intestinal Morphology, Carcass Traits And Meat Quality Of Broilers Fed Marginal Nutrients Deficiency-Diet Supplemented With Different Levels Of Active Yeast. Livestock Science. 2020;233:103945.

[12] Al-Nasser A, Al-Khlaifa H, Al-Bahouh M, Khalil F, Boareki M, Ragheb G. Challenges Facing Poultry Production In Kuwait. World's Poultry Science Journal. 2015;71(02):339-48.

[13] Caston L, Squires E, Leeson S. Hen Performance, Egg Quality, And The Sensory Evaluation Of Eggs From Scwl Hens Fed Dietary Flax. Canadian Journal Of Animal Science. 1994;74(2):347-53.

STUDIES OF MUCOADHEZIVE MATRIXES BASED ON CHITOSAN AND *LYTHRUM SALICARIA* L. PLANT EXTRACT

Ph. D. Student Irina Mihaela Iancu[1]
Assoc. Prof. Dr. Laura Adriana Bucur[2]
Assoc. Prof. Dr. Verginica Schröder[3]
Dr. Eng. Manuela Rossemary Apetroaei[4]
Assist. Dr. Valeriu Iancu[5]
Prof. Dr. Victoria Badea[6]
[1, 6] Ovidius University of Constanta, Faculty of Dental Medicine, Department of Microbiology, Constanta, Romania
[2, 3, 5] Ovidius University of Constanta, Faculty of Pharmacy, Constanta, Romania
[4] Mircea cel Batran Naval Academy, Faculty of Navigation and Naval Management, Constanta, Romania

ABSTRACT

The *Lythrum salicaria* L. plant, from the *Lythraceae* family, has multiple beneficial effects on the human body, through pharmacological properties imprinted by its secondary metabolites, namely tannins.

Chitosan-based biomedical materials are of increasing interest precisely due to the uniqueness of their properties, namely biocompatibility, nontoxicity, biodegradability, antimicrobial and antioxidant nature. The combination of chitosan with the plant extract aimed at obtaining new matrices, with clearly superior characteristics, compared to each material (chitosan and plant extract). This could be due to the presence of amino groups in the structure of chitosan, known to be active at a pH slightly acidic and which could be chemically bound to the phenolic groups of tannic acids (the predominant components of the plant extract).

The study aimed to obtain for the first-time mixtures of different concentrations of aqueous solutions of *Lythri herba* plant extract with standard chitosan 1 % in lactic acid (1 %) solution, which allowed achieving compatible and stable membranes. Microscopic evaluation of the membranes were made, following the uniformity of the surfaces, the homogeneity, the distribution of chitosan relative to the extract, and their stability in PBS saline buffer. The behavior of these membranes gives us a perspective on their use in dentistry and pharmaceuticals.

In addition, the current paper has shown the existence of chitosan in the composition of the obtained membranes and their ability to maintain constant hydration and flexibility over a certain period.

Keywords: *chitosan, Lythri herba, membranes, epifluorescence microscopy*

INTRODUCTION

Lythrum salicaria L. is a well-known medicinal plant since ancient times, used for conditions such as diarrhea and dysentery. Its name comes from the Greek word *lithron*, which means coagulated blood and probably refers to its hemostatic properties or the color of its flower and *salicaria* due to the shape of the leaves similar to that of willow species (Salix sp.) [1].

Lythrum salicaria L. is a rich source of polyphenols, including ellagitannins, flavonoids, flavan-3-oils, phenolic acids, and anthocyanosides [1], which adds value to the extracts of this plant species for medical applications.

At present, the scientific interest in the development of biodegradable films through elementary and easy methods has increased. Natural polymers, such as chitin, chitosan, cellulose, or gelatin have become an acceptable choice; due to the different advantages they have [2]. Chitosan is the most used biopolymer in medical fields due to its non-toxic, biodegradable, biocompatible, antimicrobial, antioxidant nature [3], as well as for its abundant availability and its low-cost [4].

Recent studies evaluate chitosan-based membranes in which plant extracts, or their secondary metabolites have been incorporated [5], precisely due to the increased ability of chitosan to form membranes [6] and its mucoadhesive property [7]. The ease of processing into gels, nanoparticles, microparticles, membranes, nanofibers, and even in the form of sponges is another advantage of chitosan [8].

Given the properties of the biopolymer and the reactivity of its amino groups, membranes made for the first time from weakly acidic solutions of standard chitosan (lactic acid 1%) in which were incorporated the aqueous extract with various concentrations of *Lythri herba*, are to be evaluated in terms of surface characteristics, stability, and hydration.

MATERIALS AND METHODS

The materials used in this study were dry *Lythri herba* extract, obtained by the concentration method with rotavapor and lyophilization of the aqueous extract from the floral tips of *Lythrum salicaria* L. (harvested in August 2019, from Năvodari area, Dobrogea, Romania), and standard chitosan powder (from Sigma Aldrich) with medium molar mass (300-400 kDa) and deacetylation degree (DDA) between 75% - 85%.

Obtaining membranes with 1% standard chitosan concentration in diluted lactic acid solutions and aqueous Lythri herba extract

The mixture obtained from 1% standard chitosan (CS) in 1% lactic acid solution was poured on a Teflon support and placed in the oven at a temperature of 50 °C, for 3 hours. The standard chitosan membrane (1 %) obtained has a yellowish, uniform appearance and was chosen as a reference in this study. Similarly, by slightly mixing the acidic chitosan solutions with aqueous plant extract (v / v = 1: 1), standard chitosan membranes (1%) were obtained mixed with *Lythri herba* extract, of different concentrations (0.5 g/L, 1 g/L, and 2 g/L) and their colors were ranged from light brownish to the dark brown.

Microscopic evaluation of new membranes obtained

In order to perform this evaluation, fragments of a few mm from each membrane were sectioned, making preparations, which were subsequently observed with the Optika Microscopes Italy epifluorescence microscope, Series B-350, model B-353LD2 at magnitude X200, used in the field of fluorescence B (ex 450-480 nm.).

The percentage hydration (%) determination of new membranes

The hydration properties of the membranes were measured by evaluating their hydration degree using the improved method of Al-Dhubiab *et all*, (2016) [9]. The surfaces of 1 cm^2 with initial weight (m_i) were cut from membranes, immersed into a small volume of saline PBS phosphate-buffered and kept in an incubator at 37 °C temperature for 10, 20, and 30 minutes. After each time interval, the small pieces of membranes were removed from the solution, dried slightly, and weighed again (m_f). The percentage of membrane hydration was determined using the equation of Nair *et all*, (2013) [10]:

$$\text{Hydration (\%)} = \frac{m_f - m_i}{m_f} \cdot 100, \text{ where:}$$

m_i = initial mass of the membrane, m_f = final mass of the membrane after being kept in the buffer solution.

RESULTS AND DISCUSSIONS

Obtaining membranes with 1% standard chitosan concentration in diluted lactic acid solutions and aqueous Lythri herba extract

The obtained membranes are mixtures of diluted acidic solutions with standard chitosan (1%) and aqueous *Lythri herba* extracts of different concentrations (0.5 g/L, 1 g/L and 2 g/L). Known for its many benefits, including regeneration [11], the plant offers potential in terms of developing products with mucoadhesive applications and gives protective, antibacterial and healing action in case of lesions of the oral mucosa.

Solubilized chitosan in the diluted lactic acid solutions (through the amino groups from its structure) has combined with extract components and the membranes obtained have a uniform appearance, slightly brownish color, due to the presence of tannins from the extract composition (Figure 1).

Suitable for the working protocol, the membranes obtained are according to Figure 1.

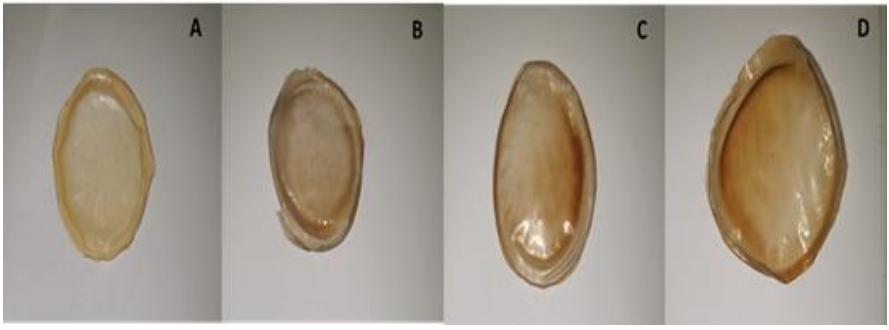

Fig. 1. *1 % standard chitosan membranes (CS) in lactic acid and aqueous Lythri herba extract.* ***A****. 1 % CS membrane in lactic acid,* ***B.*** *1 % CS membrane in lactic acid with 0.5 g/L Lythri herba,* ***C.*** *1 % CS membrane in lactic acid with 1 g/L Lythri herba,* ***D.*** *1 % CS membrane in lactic acid with 2 g/L Lythri herba*

Microscopic evaluation of new membranes obtained

The microscopic analysis confirms the presence of chitosan in membranes, due to its ability to emit autofluorescence at the wavelengths specified above, stating that for this analysis no specific dyes are used. Furthermore, the epifluorescence microscopy clearly highlights the details of the multilamellar arrangement in parallel layers and the oblique arrangement of filaments specific to chitosan structures (Figure 2). In addition, the microstructure of these membranes has numerous porosities and the colored components of *Lythri herba* are visibly included in the membranes.

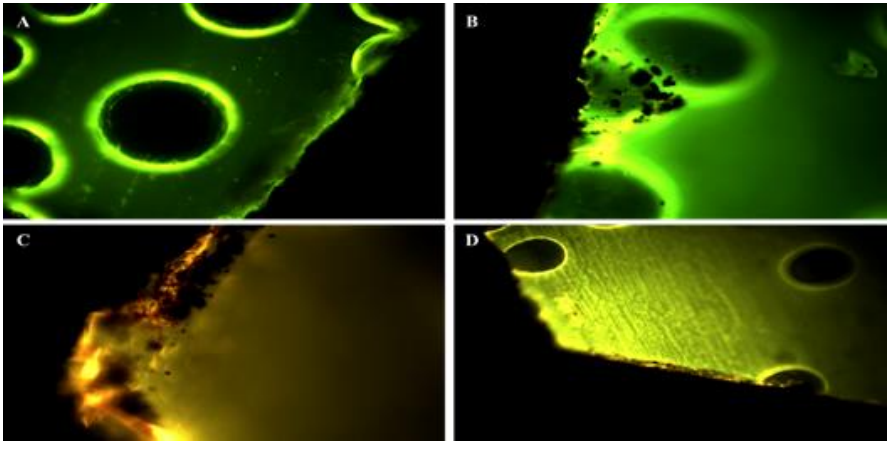

Fig. 2. *Chitosan membranes in 1 % lactic acid solution under the epifluorescence microscope (x200),* ***A*** *–CS (1 %) membrane,* ***B*** *–CS (1 %) membrane with Lythri herba extract (0.5 g/L),* ***C*** *– CS (1 %) membrane with Lythri herba extract (1 g/L),* ***D*** *–CS (1 %) membrane with Lythri herba extract (2 g/L)*

The percentage hydration (%) determination of new membranes

In mucoadhesive applications, knowing the hydration degree for membranes is especially useful, as it could be an important preliminary aspect for other tests, such as biocompatibility. Our study highlights the structural stability and the possibility to establish a contact time between chitosan-extract mixtures and mucoadhesive surfaces.

Following exposure of the membranes in PBS buffer, an increase in their hydration was observed in the first 10 minutes after exposure, followed by stagnation in terms of weight in the following time intervals (Figure 3) compared to CS (1 %) membrane, chosen as a reference sample.

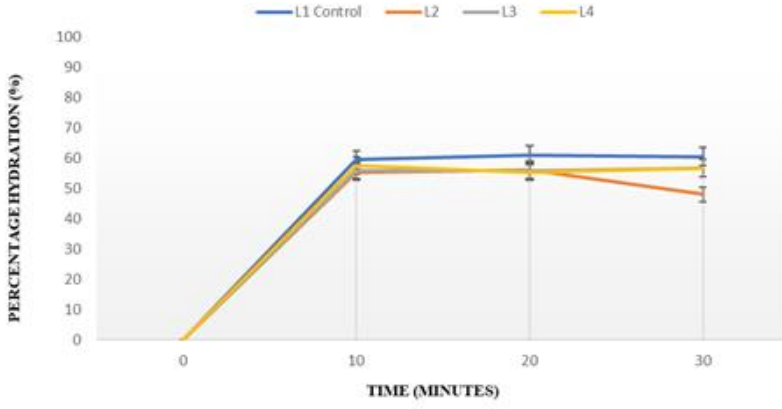

Fig. 3. *Degree of hydration of CS (1 %) membranes in lactic acid solution tested as a function of time (minutes) (± SD).* ***L1*** *(CS in 1 % lactic acid),* ***L2*** *(a mixture of CS 1 % in lactic acid + Lythri herba extract 0.5 g / L),* ***L3*** *(mixture of CS 1 % in lactic acid + Lythri herba extract 1 g/L),* ***L4*** *(mixture of CS 1 % in lactic acid + Lythri herba extract 2 g/L)*

At the time interval of 10 minutes, the membranes in lactic acid solution (1 %) appeared to be stable, without deformations, and showing a tendency to roll. The colors of the tested membranes, during hydration, did not have any noticeable change, which denotes the stability of the bonds (of chemical nature) between chitosan and the components of the analyzed extract.

At the time interval of 20 minutes all tested membranes in diluted lactic acid solution (1 %) exhibit stability, without deformations, but visibly they are much more flexible. Membrane L1, the reference sample (standard chitosan in 1 % lactic acid) is softer and more flexible than membranes with aqueous *Lythri herba* extracts (L2, L3, L4) incorporated. Compared to the membranes that remained in the alkaline buffer PBS for 10 minutes, it is no longer observed the same tendency of rolling of the edges; except for this observation of the L4 membrane is making (Figure 4).

At the hydration time interval of 30 minutes, the membranes in 1% lactic acid solution are visibly softer, without deformations, and no longer show the same

tendency to roll as the membranes after the time interval of 10 minutes, except for this observation making the L3 membrane, whose edges have rolled more.

Low mechanical resistance in water of standard chitosan (1 %) membranes were common points of the various studies performed [12], [13], a statement also proven in the current paper on the L1 membrane of standard chitosan (1 %) in 1 % lactic acid solutions.

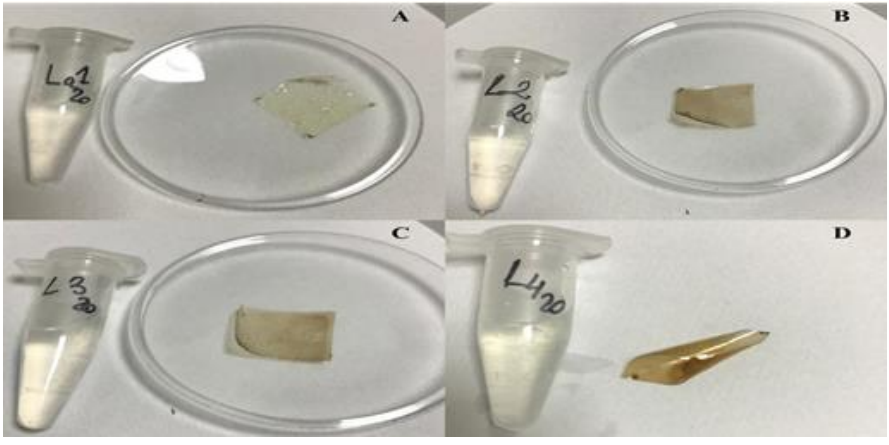

Fig. 4. *CS membranes in 1% lactic acid tested.* ***A*** *- L1 (CS in 1 % lactic acid),* ***B*** *- L2 (mixture of CS 1 % in lactic acid + Lythri herba extract 0.5 g/L),* ***C*** *- L3 (mixture of CS 1 % in lactic acid + Lythri herba extract 1 g/L),* ***D*** *- L4 (mixture of 1 % CS in lactic acid + Lythri herba extract 2 g/L)*

This study presents strong stability and flexibility of the membranes made from the mixture of chitosan with *Lythri herba* extract. The results obtained confirm the hypothesis of the study to create from chitosan a favourable matrix for the compounds of the analyzed plant, to promote obtaining a resistant, and flexible system, but also with therapeutic potential induced by the components of Lythri herba extract.

The correlation between extract concentration and hydration stability of membranes reveals an interaction with chitosan, which is even higher as the extract quantity increases. This information is supported by data from the literature according to which chitosan interacts, through its amino groups, with some groups of polyphenols contained in plant extracts [14].

Our studies on the cytotoxic activity of the extract [15] showed low toxicity of *Lythri herba* solutions, which further strengthens the potential support that the extract could induce.

As a result, our study focused to obtain stable chitosan-extract membranes with promising applications for the therapy of mucosal surfaces or those interacting with aqueous solutions.

CONCLUSION

To the best of our knowledge, this is the first time when membranes with potential in therapeutic applications are obtained by mixing in a compatible and stable ratio of solutions of standard chitosan (1%) in lactic acid (1%) with the aqueous solutions of *Lythri herba* plant extract.

Epifluorescence microscopy confirmed the presence of fluorescent chitosan in membranes and clearly showed its multilamellar, oblique, and superficial layer arrangement.

The membranes obtained for the first time showed constant hydration over time and had a flexible, elastic, and deformation-free behavior, these features are necessary for mucoadhesive biomaterials, to their use in the medical and pharmaceutical field.

Following the analyses carried-out, our study showed the therapeutic potential of *Lythrum salicaria* L., which could be improved by combining with chitosan, at appropriate concentrations in the form of membranes (mucoadhesive films), in order to increase the number of pharmaceutical or biomedical applications.

REFERENCES

[1] Piwowarski, J. P.; Granica, S.; Kiss, A. K. Lythrum salicaria L. Underestimated medicinal plant from European traditional medicine. A review. *Journal of ethnopharmacology*, 2015, 170: 226-250.

[2] Sakthiguru, N., & Sithique, M. A. (2020). Fabrication of bioinspired chitosan/gelatin/allantoin biocomposite film for wound dressing application. *International journal of biological macromolecules*, 152, 873-883.

[3] İlk, S., Ramanauskaitė, A., Bilican, B. K., Mulerčikas, P., Çam, D., Onses, M. S., ... & Zang, L. S. (2020). Usage of natural chitosan membrane obtained from insect corneal lenses as a drug carrier and its potential for point of care tests. *Materials Science and Engineering*: C, 110897.

[4] Hu, Q., & Luo, Y. (2016). Polyphenol-chitosan conjugates: Synthesis, characterization, and applications. *Carbohydrate polymers*, 151, 624-639.

[5] Kaya, M., Khadem, S., Cakmak, Y. S., Mujtaba, M., Ilk, S., Akyuz, L., ... & Deligöz, E. (2018). Antioxidative and antimicrobial edible chitosan films blended with stem, leaf and seed extracts of Pistacia terebinthus for active food packaging. *RSC advances*, 8(8), 3941-3950.

[6] Bajić, M., Ročnik, T., Oberlintner, A., Scognamiglio, F., Novak, U., & Likozar, B. (2019). Natural plant extracts as active components in chitosan-based films: A comparative study. *Food Packaging and Shelf Life*, 21, 100365.

[7] Khutoryanskiy, V. V. Advances in mucoadhesion and mucoadhesive polymers. *Macromolecular bioscience*, 2011, 11.6: 748-764.

[8] Ahmed, S., & Ikram, S. (2016). Chitosan based scaffolds and their applications in wound healing. *Achievements in the life sciences*, 10(1), 27-37.

[9] Al-Dhubiab, B. E., Nair, A. B., Kumria, R., Attimarad, M., & Harsha, S. (2016). Development and evaluation of buccal films impregnated with selegiline-loaded nanospheres. *Drug Delivery*, 23(7), 2154-2162.

[10] Nair, A. B., Kumria, R., Harsha, S., Attimarad, M., Al-Dhubiab, B. E., & Alhaider, I. A. (2013). In vitro techniques to evaluate buccal films. *Journal of Controlled Release*, 166(1), 10-21.

[11] Jouravel, G., Guénin, S., Bernard, F. X., Elfakir, C., Bernard, P., & Himbert, F., New biological activities of *Lythrum salicaria* L.: Effects on keratinocytes, reconstructed epidermis and reconstructed skins, Applications in dermo-cosmetic sciences. *Cosmetics*, 2017, 4(4), p. 52

[12] De Masi, A., Tonazzini, I., Masciullo, C., Mezzena, R., Chiellini, F., Puppi, D., & Cecchini, M. (2019). Chitosan films for regenerative medicine: fabrication methods and mechanical characterization of nanostructured chitosan films. *Biophysical Reviews*, 1-9.

[13] Hps, A. K., Saurabh, C. K., Adnan, A. S., Fazita, M. N., Syakir, M. I., Davoudpour, Y., ... & Dungani, R. (2016). A review on chitosan-cellulose blends and nanocellulose reinforced chitosan biocomposites: Properties and their applications. *Carbohydrate polymers*, 150, 216-226.

[14] Jing, Y., Diao, Y., & Yu, X. (2019). Free radical-mediated conjugation of chitosan with tannic acid: Characterization and antioxidant capacity. *Reactive and Functional Polymers*, 135, 16-22

[15] Iancu, I., M., Bucur, L., A., Schroder, V., Mireșan, H., Mihai, S., Iancu, V., Badea, V., Phytochemical evaluation and cytotoxicity assay of Lythri herba extracts, *Farmacia*, 2021, 69(1), 51-58

STUDIES ON THE MORPHO-ANATOMICAL PARTICULARITIES OF *LYSIMACHIA NUMMULARIA* L.

Suciu Felicia[1]
Arcuș Mariana[2]
Roșca Adrian Cosmin[3]
Bucur Laura[4]
Popescu Antoanela[5]
Badea Victoria[6]
[1, 2, 3, 4, 5] Faculty of Pharmacy, Ovidius University of Constanta, Romania
[6] Faculty of Dentistry, Ovidius University of Constanta, Romania

ABSTRACT

The objective of the study was the histo-anatomical analysis of the root, stem and leaf belonging to the species *Lysimachia nummularia* L. from the *Primulaceae* family.

The plant is native to Europe, but has been introduced to North America, where it is considered an invasive species in some areas. It aggressively spreads in favourable conditions, such as low wet ground or near ponds. It is moderately difficult to remove by hand pulling. Any tiny piece left behind will regrow. The research results led to the following assessments: root with primary structure and beginning of secondary structure, the presence of calcium oxalate druze in the bark, endoderm and primary type conducting bundles. The results of the study also demonstrated the existence of the stem with four prominent ribs, a meatic-type bark with small secretory channels and a central cylinder with a secondary structure. Another element studied from a histo-anatomical point of view; leaf with dorsi-ventral bifacial structure, with heterogeneous asymmetrical structure, collateral free-woody bundle, without periectors. From the morpho-anatomical data described, it can be concluded that the species *Lysimachia nummularia* L. belongs to the family *Primulaceae* and is related to other species of the genus *Lysimachia.*

Keywords: *Lysimachia, Primulaceae, microscopy, vegetative organs.*

INTRODUCTION

Lysimachia nummularia L. (*Primulaceae*) (Figure 1), is a herbaceous, perennial, chamefite plant, widespread in our country, in wetlands, in meadows and on the waterfront, through bushes and meadows, ditches and micro-depressions in mountain, hill and plain regions. Globally it is found in Europe, the Caucasus, introduced in Japan and North America.

According to the classification system proposed by Cronquist [2], Takhtajan [3] and Zimmerman [4], accepted by Ehrendorfer [5, 6] and adopted and supplemented by I. Pop et al., *Lysimachia nummularia* L. [7], has the following systematic classification [8]: *Magnoliophyta*, Class *Magnoliatae*, Subclass

Dilleniidae, Order *Primulales*, Family *Primulaceae*, Genus *Lysimachia*, Species *nummularia* L.

Known since antiquity, the plant was discovered by Lysimachus (in Pliny the Elder), and its name is also found in Dioscorides as Lysimacheios, indicating a species of the genus *Lysimachia*, probably given in honor of the Thracian king, Lysimachus. The green parts of the plant contain hemolytic saponosides, tannins, flavonosides, phenolic acids, polyuronides, which is why it has medicinal uses both internally and externally [9].

Popularly known as yolk or straight, *Lysimachia nummularia* L, has a sudden, glabrous stem, round opposite leaves and solitary, yellow axillary flowers [10].

In the present study, we aimed to identify and describe the anatomical structure of vegetative organs in order to identify the peculiarities of *Lysimachia nummularia* L, necessary to differentiate the peculiarities of the plant species from other species of the genus *Lysimachia*.

MATERIAL AND METHOD

The fresh plant was harvested on July 19, 2020, from the edge of Lake Tău-Brazi in the Roșia Montană area of Alba County (Figure 2), where the yolk forms large associations (Figure 1). In order to research from a histo-anatomical point of view, the material represented by the vegetative organs (root, stem and leaves) was subjected to several stages of work. Fixation and preservation of the fresh material was performed in 70% ethyl alcohol. The sectioning was done manually, with the help of the hand microtome and the botanical razor, using as support the elderflower marrow.

The obtained sections were subjected to the bleaching process (with sodium hypochlorite) for 20-35 minutes, after which they were washed with acetic water and distilled water [11], [12]. The sections were then stained with iodine green and ruthenium red (staining used in plant histo-anatomical studies) as follows: The sections were first stained with iodine green (1 minute), washed with 90% ethyl alcohol, and then stained with ruthenium red (1 minute) and finally washed with distilled water [13], [14].

The colored sections were mounted in drops of glycerol gelatin, between the slide and the slide, thus making permanent preparations. After the preparations thus obtained, color photographs were taken with the OPTIKA photon microscope, with Canon A540 digital camera. Scale for photographs = 100 μm.

Fig. 1. *Plant association with straight*

Fig. 2. *Lysimachia nummularia L.*

RESULTS AND DISCUSSIONS

Cross section through the root

The following characters are distinguished:

- the contour of the section is circular, slightly wavy (Figure 3);
- the structure is primary with the beginning of secondary structure, due to the presence of a multilayered suber formed of cells with thin walls (Figure 4);

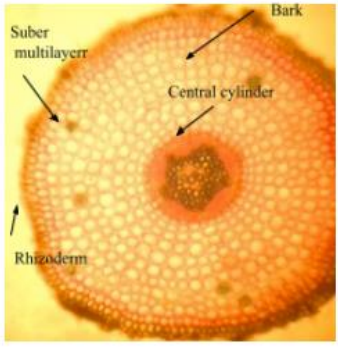

Fig. 3. *Cross section through the root of Lysimachia nummularia L. (6x)*

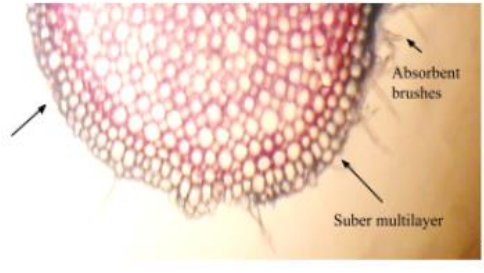

Fig. 4. *Cross section through the root of Lysimachia nummularia L. (10x) -detail*

On the outside there is a rhizoderm, formed by a single layer of cells with external walls slightly thicker than the others, covered by a cuticle that forms a characteristic relief; some cells turned into single-cell absorbent hairs. The primary bark is very thick, comprising 8-10 layers of round oval cells, with thin cellulosic walls and intercellular spaces; it is differentiated into exoderm, cortical parenchyma

and endoderm; the cells are larger in the middle of the bark and smaller outwards and inwards (Figure 4).

The exoderm, well highlighted, is unistratified, with large cells, slightly elongated radially, with moderately thickened and suberified walls.

The cortical parenchyma is compact and moderately cholenchymatized to the exoderm, but for the most part it has cells of circular contour, with thin walls, leaving small intercellular spaces between them, forming a true meatic parenchyma; cells with calcium oxalate dredges are observed in some places:

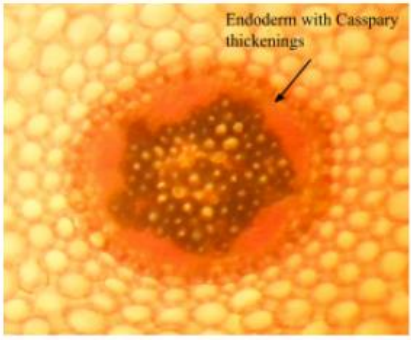

Fig. 5. *Cross section through the root of Lysimachia nummularia L. Endoderm with Casspary thickenings (100x)*

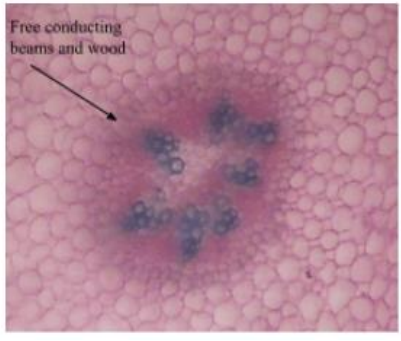

Fig. 6. *Cross-section through the root of Lysimachia nummularia L. Free-conducting beams and wood (100x)*

The last layer of the bark is a primary type endoderm, with the cells elongated tangentially and arranged in an orderly manner, alternating with those of the pericycle; shows obvious lenticular thickenings (Casspary thickenings) (Figure 5);

The central cylinder, located deep, starts with a unilayered pericycle, on which 5-7 wooden beams rest, alternating with as many free beams included in the fundamental parenchyma of the central cylinder (Figure 6); the liber consists of Liberian vessels (sieved tubes), attachment cells and Liberian parenchyma; the wooden fascicles are formed by wooden vessels of meta and protoxylem and very few wooden parenchyma cells; the metaxillem vessels go to the center of the root, occupying part of the spinal cord; the marrow, interrupted by a group of metaxillem vessels, consists of medullary parenchyma of the meatic type.

Stem cross section

The cross section through the stem has the following characters:

The contour of the cross section is elliptical-oval, with four visibly prominent ribs at the ends (Figure 7); on the outside there is a single-layered epidermis, formed by isodiametric cells, with domed external walls; they have a round-square shape, are uniformly thickened all around and covered by a thin ribbed cuticle; from place to place there are stomata formed by cells slightly smaller than the cells of the epidermis (Figure 8);

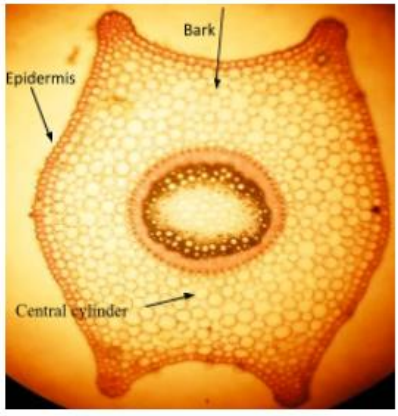

Fig. 7. *Cross section through the stem of the species Lysimachia nummularia L. (100x)*

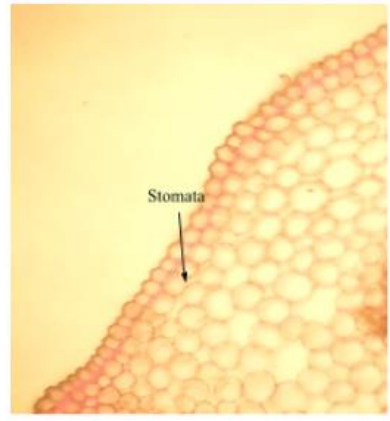

Fig. 8. *Cross section through the stem of the species Lysimachia nummularia L. Detail from the epidermis (100x)*

The bark is parenchymal-cellulose of meatic type, with rounded cells, bigger and bigger inwards; from place to place it has wide air spaces between cells and small secretory canals; the hypodermic layer, slightly cholenchymatized consists of cells smaller than the rest of the bark; near the ribs the thickening process is more pronounced than in the rest of the hypodermis;

The innermost layer of the bark is a primary type endoderm, with its thickening of the Casspary visible and made up of cells of different sizes; the central cylinder consists of conductive tissues of secondary origin, arranged in an annular and represented by an outer ring of free secondary and an inner ring of secondary wood, which arose from the activity of the bill of exchange; it does not start with a special type of danger; the free ring is slightly thinner than the wooden one; the wooden ring has discontinuities, in which thicker areas, consisting of several vessels, alternate with thinner portions, consisting of fewer vessels and of smaller caliber.

The secondary free ring consists of sieved tubes, attachment cells and Liberian parenchyma cells.

The wooden ring consists of protoxilem vessels, towards the outside and metaxilem vessels, towards the centre of the cord; the vessels are arranged in series, in order and are surrounded by cellulosic woody parenchyma; the medullary rays are narrow, relatively unobvious.

The marrow is thick, parenchymal-cellulosic, meatic type, consisting of two types of cells: very large, in the centre of the spinal cord and very small at its periphery, some cells at the periphery of the spinal cord are oxaliferous (Figure 8).

Leaf cross section

The leaf cross section has the following characters:

- in cross section, the median rib is prominently visible at the abaxial face of the tongue, and at the adaxial face there is a slightly deepened groove (Figure 9);
- at the level of the nerve there is a single hypodermic layer of colenchyma, a fundamental parenchyma formed by large isodiametric cells with thin parts and large intercellular spaces, and in the centre, a large, free-wood beam with primary structure, next to which appears a beam of very small dimensions (Figure 10);
- the conducting beam is surrounded by a unilayered parenchyma sheath, formed by uniformly arranged cells; it consists of a free cord, towards the lower epidermis and a wooden cord, towards the upper epidermis; under the free cord is a sclerenchyma sheath;

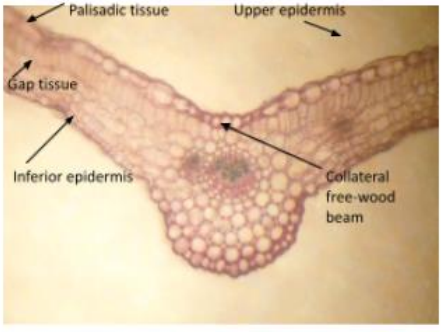

Fig. 9. *Cross section through the leaf of the species Lysimachia nummularia L. (100 x)*

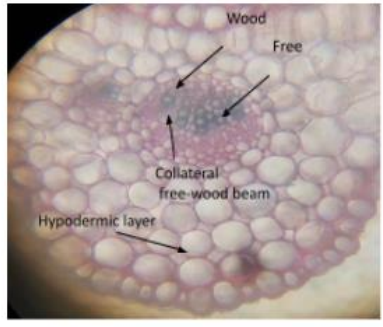

Fig. 10. *Cross section through the leaf of the species Lysimachia nummularia L. Detail of the median rib (100x)*

- the release cord has sieved tubes, attachment cells and Liberian parenchyma;
- the wooden cord consists of radial rows of proto- and metaxillem vessels, separated by cellulosic woody parenchyma (Figure 8);
- the upper epidermis consists of a single layer of very large, vesicular cells, of different sizes, with the outer wall thicker than the others and covered by a very thin cuticle; from place to place there are stomata, less than in the lower epidermis; tector brushes are missing (Figure 10);
- the lower epidermis, formed by a single layer of cells, has larger cells at the level of the median nerve, but of different sizes, and at the level of the tongue, much smaller cells; all are interrupted by stomata.

- the mesophile has 5-6 layers of cells and consists of a unistratified palisade on the upper face (the cells being 3-4 times higher than wide) and a lacunar multilayered parenchyma on the lower face;
- the limb has a dorsoventral bifacial structure.

CONCLUSION

The analysis of the cross sections through the vegetative organs of the species *Lysimachia nummularia* L. showed that the analyzed species has a structure characteristic of the group to which it belongs, respectively of the *Primroses*. Thus, the root has a primary structure with a little developed central cylinder, the 6-7 wooden bundles, alternating with the free ones.

The endoderm has lenticular thickenings (Casspary punctuation); the primary endoderm shows obvious Casspary scores.

The bark is of the meatic type with large intercellular spaces and cells with calcium oxalate dredges.

The stem has the contour of the elliptical-oval cross section, at the ends with four visibly prominent ribs. The leaf has epidermis covered by an obvious cuticle, asymmetric heterogeneous mesophilic, is devoid of periectors and has a dorsiventral bifacial structure with unistratified palisade tissue.

The conducting beam is of the collateral type, consisting of a free cord, towards the lower epidermis and a wooden cord, towards the upper epidermis; under the free cord there is a sclerenchymal sheath.

REFERENCES

[1] Săvulescu T. et al., Flora R.P.R., vol. VII, Acad. R.P.R., 1960, 42-46.

[2] Cronquist A., The evolution and classification of flowering plants, Botanical Garden, New York, 1988.

[3] Takhtajan A.L., Diversity and classification of flowering plants, Koeltz, Konigstein, 1996.

[4] Zimmermann W., Die phylogenie der Pflanzend, G. Thieme Verlag, Stuttart, 1959.

[5] Ehrendorfer F., Closing remarks: systematics and evolution of Centrospermous families, Plant Syst. And Evol., Volume 126, 1971, 99-105.

[6] Ehrendorfer F., Samenpflanzen, Strasburger, s Lehrbuch der Botanik, 32, Aufl. Stuttgart, New York, 1983.

[7] Pop I., Hodișan I., Mititelu D., Lungu L., Cristurean I., Mihai Gh., Systematic Botany, Didactics and Pedagogy, Bucharest, 1983, p. 419.

[8] Ștefan N., Ivănescu Lăcrămioara, Elements of morphology and vegetal taxonomy, Univ. Al. I. Cuza, Iași, 2002, p. 345.

[9] Pârvu C., Enciclopedia plantelor, volume II, Tehnică, București, 2003, 77.

[10] Ciocârlan V., The illustrated flora of Romania. Pteridophyta et Spermatophyta, 3rd ed., Ceres, Bucharest, 2009, 1067.

[11] Sîrbu I., Ștefan N., Oprea A., Vascular plants from Romania, illustrated field determiner, Victor B, Bucharest, p. 554.

[12] Andrei M., Paraschivoiu R. M., Botanical Microtechnics, Niculescu, Bucharest, 2003.

[13] Șerbănescu-Jitariu G., Andrei M., Mitroiu-Rădulescu Natalia, Petria Elena. Practicum of plant biology, Ceres Publishing House, Bucharest, 1983.

[14] Toma C., Gostin I., Vegetal H., Junimea Publishing House, Iași, 2000.

TESTING THE BIOLOGICAL ACTIVITY OF *LYTHRI HERBA* EXTRACT FOR APPLICATIONS IN MEDICAL BIOTECHNOLOGIES

Ph. D. Student Irina Mihaela Iancu[1]
Assoc. Prof. Dr. Laura Adriana Bucur[2]
Assoc. Prof. Dr. Verginica Schröder[3]
Dr. Eng. Manuela Rossemary Apetroaei[4]
Assoc. Prof. Dr. Horațiu Mireșan[5]
Prof. Dr. Victoria Badea[6]
[1, 6] Ovidius University of Constanta, Faculty of Dental Medicine, Department of Microbiology, Constanta, Romania
[2, 3, 5] Ovidius University of Constanta, Faculty of Pharmacy, Constanta, Romania
[4] Mircea cel Batran Naval Academy, Faculty of Navigation and Naval Management, Constanta, Romania

ABSTRACT

Nowadays we are witnessing an increased interest in phytotherapy and implicitly for herbal products that have lower side effects. One medicinal plant whose popularity has decreased significantly in recent years is *Lythrum salicaria* L., loosestrife, known in Romanian traditional medicine for its beneficial effects against gastrointestinal diseases.

The aim of this study is to evaluate the biological activity of three different extracts (aqueous, alcoholic, acetonic) from the flower tips of *Lythrum salicaria* L. using the BSLA (Brine Shrimp Lethality Assay) test and the antimicrobial activity of the extracts on two reference bacterial strains which are important for the medical field (*Staphylococcus aureus* and *Escherichia coli*) through the diffusimetric method.

We demonstrated the fact that the *Lythri herba* plant product extracts (aqueous, alcoholic, and acetonic) lack acute toxicity, as well as the moderate antibacterial effect on the *Gram-positive* reference strain, *Staphylococcus aureus*, thus highlighting the possibility of using the plant in biomedical applications.

Keywords: *Lythri herba, antibacterial activity, Artemia salina.*

INTRODUCTION

Medicinal plants are rich sources of biologically active compounds, are easy to procure, and are inexpensive. For these reasons, they continue to have a growing interest in the research and development of new antibacterial and antifungal products, for which no resistance has developed.

Basically, the chemicals produced by plants are divided into two categories, primary and secondary metabolites. Primary metabolites are involved in the

synthesis of the basic elements of the plant, while secondary metabolites are involved in the defense mechanism of the plant against various microbial infections. Important secondary metabolites in medicine include flavonoids, alkaloids, terpenes, tannins, and phenolic compounds. Unlimited opportunities for drug discovery have been offered by plant extracts, whether they are pure compounds or standardized extracts, due to their chemical diversity [1].

Lythrum salicaria L. (*Lythraceae* family) is a plant species known in traditional European medicine for its healing effects against dysentery, diarrhea, intestinal inflammation, hematuria, leukorrhea, epistaxis, dysmenorrhea, lupus, eczema, anemia, urogenital inflammation, hemorrhoids, diseases of the gastrointestinal tract, colitis and stomatitis [2].

Studies on the bioactivity of extracts from the *Lythrum salicaria* L. plant began in the nineteenth century and highlighted pharmacological effects such as antidiarrheal, anti-inflammatory, antioxidant, antimicrobial, hemostatic, metabolic, antihypertensive, and hypoglycemic effects [3].

The antimicrobial activity of *Lythrum salicaria* L. plant extracts was investigated against pathogenic species such as *Candida albicans*, *Micrococcus luteus*, *Bacillus subtilis*, *Escherichia coli*, *Pseudomonas aeruginosa*, *Staphylococcus aureus*, *Staphylococcus epidermis*, *Proteus mirabilis* [4].

Cytotoxicity studies are the first useful step in determining the potential toxicity of a test substance, including plant extracts or biologically active compounds isolated from plants. Minimal or no toxicity is essential for the successful development of pharmaceutical or cosmetic preparation and, in this regard, cell toxicity studies to play crucial roles [5].

The low cytotoxic activity of extracts (aqueous and hydro-ethanolic) from the *Lythrum salicaria* L. (*Lythri herba*) plant, highlighted by the BSLA (Brine Shrimp Lethality Assay) test in previous studies, allowed important assessments of the possibility of using the extract in biomedical applications [6].

Starting from these data, the current paper aimed to evaluate the biological effects induced by extracts (aqueous, ethanolic, and acetonic) from the floral tips of the *Lythrum salicaria* L plant species.

The study was performed on the "*in vivo*" model BSLA (Brine Shrimp Lethality Assay) to indicate cytologically induced manifestations, as well as on two bacterial strains of medical importance (*Staphylococcus aureus* and *Escherichia coli*) [7] for the preliminary evaluation of antimicrobial activity and modern perspectives [8].

MATERIALS AND METHODS

Obtaining plant extracts

The floral tops of the Lythrum salicaria L. plant, harvested in July 2020 from the Năvodari area, Constanța, Romania, were cleaned and then dried at room temperature, in the shade. The plant material was then extracted with different

solvents (water, 96% ethyl alcohol, and pure acetone) by refluxing for two hours and then filtered through filter paper. After filtration, the aqueous extractive solution was concentrated by rotavapor and lyophilized, and the alcoholic and acetonic extractive solutions were left in porcelain capsules to evaporate under a niche. The dry extracts obtained were stored in sealed glass vials in the desiccator until the next evaluations could take place.

Evaluating the cytotoxicity of the plant extracts by BSLA test

The larvae were obtained by incubating cysts of *Artemia* sp. (Hobby, Grafschaft, Germany), in artificial salt water (35 ppm), with aeration and continuous lighting. The larvae from stage I naupliar, obtained after hatching, in the first 24 hours, were introduced in the test vessels. Between 15 - 20 specimens of stage, I larvae were transferred to each well of the test microplates and evaluated under a stereomicroscope (Optika B-350, Italy) every 24h.

Concentrations of 50, 100, 200, 250, 300 µl / mL of each extract were analyzed in a total volume of 1 mL. Larvae introduced into saline without extract were evaluated as negative control samples.

The plant extracts (alcoholic and acetonic) were solubilized in 0.1 % dimethylsulfoxide solvent (DMSO), achieving a ratio of 1:20 (v:v). The *Artemia salina* L. larvae were not fed throughout the test period (48 hours), thus avoiding interaction between test solutions and their food. The larvae were assessed for motility, survival, or mortality within 24 hours of testing. Statistical analysis was performed with StatPlus Mac Pro, version v6, Analyst Soft Inc statistical analysis program for MacOS.

Microscopic observations were made on living organisms, the preparations being analyzed directly, the larvae being transparent.

Antimicrobial evaluation of plant extracts, using the diffusimetric method

Two reference bacterial strains were chosen, namely *Staphyloccocus aureus*, a *Gram-positive*, aerobic, unencapsulated coke, also called "superbacteria", because it no longer responds to the action of many antibiotics, and *Escherichia coli*, a *Gram-negative* bacterium from the enterobacteria group. Further information on microbial strains is provided in **Table 1**.

Table 1. *Microbial species, reference source, cultivation medium and assay medium*

Microbial species	Reference source	Cultivation medium	Assay medium
Staphylococcus aureus	ATCC* 29213	Columbia + 5 % sheep blood**	Mueller-Hinton***
Escherichia coli	ATCC* 25922	Columbia + 5 % sheep blood**	Mueller-Hinton***

Note:*ATCC - American Type Culture Collection,
** Columbia + 5 % sheep blood – Lot 64379472,
*** Mueller-Hinton – Lot 64372104.

The antimicrobial activity was determined by the diffusion method in a culture medium seeded with the reference strains we mentioned in the table above.

On the Petri dishes, each bacterial strain used was seeded in the Mueller-Hinton medium, then the plate was divided into four equal parts in which sterile filter paper rounds impregnated with constant volumes (10 µl) were applied with sterile tweezers from each test solution (negative control solvent DMSO 10%, aqueous extract, ethanolic and acetonic solubilized in DMSO 10%). The plates were then thermostated at 37°C for 24 hours. Following this, each diameter of the inhibition area around the filter paper impregnated in the test substance was recorded. The expression was performed using the grades "sensitive" (S), "intermediate" (I), and "resistant" (R) to the action of the extracts tested by *Lythri herba*.

RESULTS AND DISCUSSIONS

Obtaining plant extracts

Lythri herba plant product extracts (aqueous, alcoholic, acetonic) were obtained according to the following image (**Figure 1**) and their phytochemical composition was synthesized in **Table 2** depending on the nature of the solvent according to the literature.

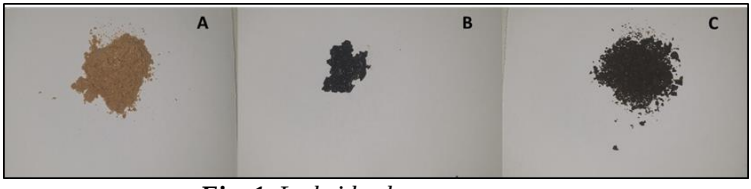

Fig. 1. *Lythri herba extracts*
A *– Aqueous extract,* ***B*** *– Alcoholic extract,* ***C*** *– Acetonic extract.*

Table 2 – Phytochemical profile of the Lythri herba extracts

Lythri herba extracts	Contents	References
Aqueous	• total polyphenols (16.39 %) • tannins (10.53 %) • anthocyanins (0.3598 %)	[6]
Alcoholic	• total polyphenols (8.3-27.3 %) • tannins (6.6-21.9 %)	[4]
Acetonic	• total polyphenols (278 ± 3.04 mg gallic acid equivalents/g extract) • flavonoids (4.38 ± 0.13 mg rutin equivalents/g extract) • hydroxycinnamic acids (69.6 ± 0.81 mg caffeic acid equivalents/g extract) • condensed tannins (not detected)	[9]

Evaluating the cytotoxicity of the plant extracts by BSLA test

The plant is known to have a complex composition. It is appreciated due to its polyphenols, tannins, flavonoids, phenolic acids, etc. content [3].

At the same time, more and more studies reveal different pharmacological effects given both the solvent used in the extraction and the model ("*in vivo*" or "*in vitro*") used for evaluation [10].

The effects observed during the experiment show differences which correlate with the level of concentrations (**Figure 1**), for both extracts. Important and quantified manifestations were those related to the motility of the tested organisms, respectively the reduction of swimming and the appearance of jerky, spasmogenic movements. The changes were identified after 20 hours of exposure and persisted in the same percentage until the end of the experiment (24 hours).

Sublethal manifestations of larvae were recorded during the observations. The lack of acute toxicity is explained by the low toxicity of the *Lythri herba* extract, but also by the dilutions obtained in DMSO.

The alcoholic extract (ALCLy) analyzed induced percentage increases of quantified effects (jerky movements), but below the 50% mark, at concentrations between 50 µl / mL and 250 µl / mL. However, the decreases of these manifestations at the maximum tested concentration of 300 µl / mL are surprising. The explanations can be given by the high level of carbohydrates and proteins [10] which, possibly, blurred the discomfort created to the larvae by other phytochemicals.

The jerky motility can be compared to muscle spasms, the larvae have cells similar to myocytes with which they ensure swimming movements. In the literature, the spasmogenic effects of the extract have been mentioned and studied. Thus, the "*in vivo*" studies of Bencsik, T., from 2014 correlated the contractions of the smooth intestinal muscles with the level of caffeic acid or catechin in the extract. It has also been observed that alcoholic extract of *Lythri herba* induces acetylcholinesterase (ACE) inhibition [10]. ACE inhibition may also be possible in these tested organisms, which would explain the altered movements of the larvae.

The enzyme acetylcholinesterase (ACE), is present in these organisms since the embryonic period and has a significant increase in the early stages of larval development [11].

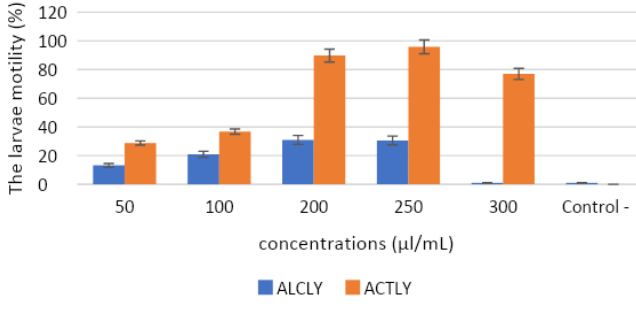

Fig. 1. *The larvae abnormal motility evaluated (%), after 24 h exposure (ALCLy- alcoholic extract of Lythri herba, ACTLy – acetonic extract of Lythri herba)*

The acetone extract is less known in terms of its biological effect. Observations show an increase in abnormal manifestations of motility (**Figure 1**), in a significant proportion (76-95%). The effects are recorded at high concentrations (200, 250, 300 µl / mL) (**Figure 1)**, compared to larvae exposed to 50 and 100 µl / mL, as well as to control samples, without extract.

Statistical analysis indicates a linear stimulus-effect correlation for organisms exposed to concentrations between 50-250 µl / mL of alcoholic extract - ALCLy (Fig. 2 A), ($p < 0.001$) and at concentrations between 50-300 µl / mL of acetonic extract -ACTLy (Fig. 2 B), and the prediction has statistical significance [12], [13].

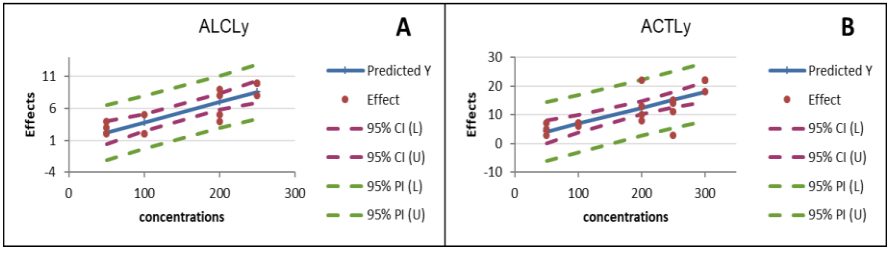

Fig. 2. *Representation of the tested larvae response* ***A*** *- in the alcoholic extract (ALCLy) by linear regression (CI - 95% Confidence Interval, PI -95% Prediction Interval, p - value = 0.00037),* ***B*** *- in the acetonic extract (ACTLy) by linear regression (CI - 95% Confidence Interval, PI - 95% Prediction Interval, p-value = 0.00016*

In addition to the response related to the change in larval motility, observations on cytomorphology were made. The analysis was relevant by observing general changes in the larval body as well as inhibiting organogenesis and appendicular buds, respectively (**Figure 4, A-F**).

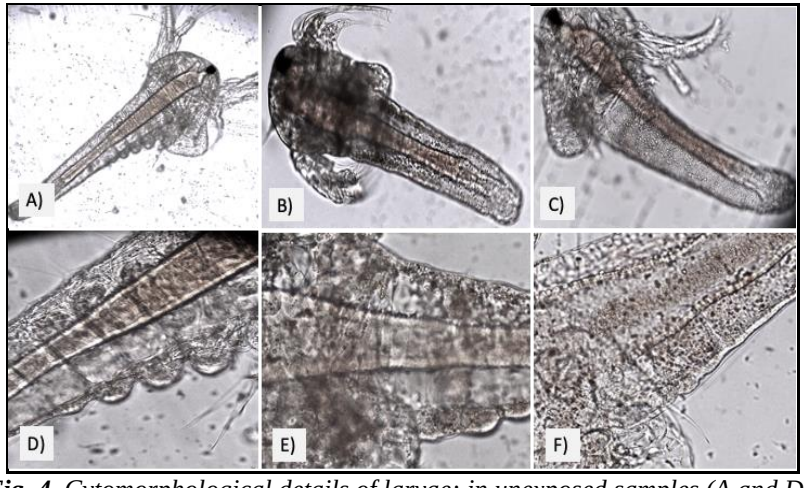

Fig. 4. *Cytomorphological details of larvae: in unexposed samples (A and D), exposed in ALCLy (B, E), and acetone (C, F); magnification x100 (A); x200 (B, C); x400 (D, E, F)*

Antimicrobial evaluation of plant extracts, using the diffusimetric method

The results obtained from the evaluation of the antibacterial action of the *Lythri herba* aqueous, ethanolic, and acetonic extracts are summarized in **Table 3**.

Table 3. *Diameters of inhibition areas (mm) of Lythri herba extracts and control on bacterial cultures (mean ± SD)*

Microbial species	ATCC	DMSO (mm)	Aqueous extract (mm)	Ethanolic extract (mm)	Acetonic extract (mm)
Staphylococcus aureus (G+)	29213	0	R (9.66 ± 1.52)	R (9.66 ± 2.08)	S (17.66 ± 1.52)
Escherichia coli (G-)	25922	0	R (< 5 mm)	R (< 5 mm)	R (< 5 mm)

Note: 10 % DMSO solvent has no inhibitory effect, R – resistant, S – sensitive.

As can be seen in **Table 3**, all three *Lythri herba* extracts do not generate areas of inhibition for the *Gram-negative* species studied, namely *Escherichia coli*. In the case of the *Gram-positive* species (*Staphylococcus aureus*) only the acetonic extract has the largest inhibitory zone, unlike the much smaller inhibitory diameters and resistant mutants of the aqueous and ethanolic extracts. The 10 % DMSO solvent used to solubilize the extracts obtained did not show an inhibitory effect.

These observations are also supported by the following conclusive images (**Figure 5**).

In the review of Piwowarski J. (2015) it was observed that the inhibition area for *Escherichia coli* of various *Lythri herba* extracts is between 0 - 15 mm, and for *Staphylococcus aureus* it is between 0 - 30 mm. The differences between the values of the areas of inhibition on these bacterial strains are due to the extraction methods and the various solvents used on the *Lythrum salicaria* L. plant [3].

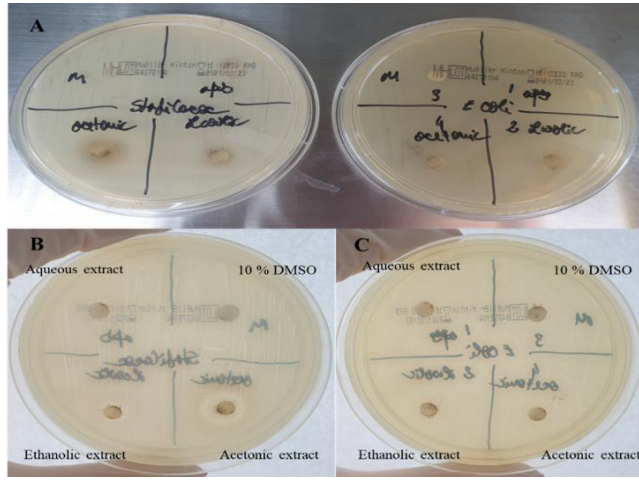

Fig. 5. *Lythri herba extracts (aqueous, ethanolic, and acetonic) effects on Staphylococcus aureus and Escherichia coli (**A**), Staphyloccocus aureus (**B**), Escherichia coli (**C**)*

The values obtained in this paper are similar to the results of the 2021 study by Turker A. U. et all. [2] in which *Staphyloccocus aureus* was shown to be sensitive

to the action of aqueous and alcoholic *Lythri herba* extracts, and the representative of *Gram-negative* bacteria, namely *Escherichia coli*, to demonstrate total resistance to both extracts (aqueous and alcoholic) solubilized in DMSO.

CONCLUSION

Evaluating the biological activity of *Lythri herba* extracts (aqueous, alcoholic, and acetonic), using BSLA, highlighted their lack of acute toxicity thus allowing the use of extracts in future biomedical applications.

The biological changes identified "*in vivo*" induced by the action of the compounds contained in the extract on the *Artemia salina* L. larvae are associated with behavioral changes, such as jerky movements, and cellular changes such as the inhibition of appendicular primordia growth areas. Both ALCLy and ACTLy extracts induced a gradual increase in larval discomfort, correlated with the level of concentration of the extract to which the organisms were exposed.

The *Lythrum salicaria* L. plant showed, through its extracts (aqueous, alcoholic, and acetonic), antibacterial activity on the *Gram-positive* reference bacterium, *Staphylococcus aureus* (ATCC 29213) and total resistance to the *Gram-negative* reference bacterium, *Escherichia coli* (ATCC 25922). These results are similar to those in the literature; the differences between the areas of inhibition can be explained by the diversity of extraction methods, the nature of the solvents used, and the structural specificity of the cell walls of *Gram-positive* and *Gram-negative* bacteria.

REFERENCES

[1] Tahir, L., & Nazir, R. Dental Caries, Etiology, and Remedy through Natural Resources. *Dental Caries-Diagnosis, Prevention and Management*, Zühre Akarslan, IntechOpen, 2018, DOI: https://doi. org/10.5772/intechopen, 75937, 19.

[2] Turker, A. U., Yildirim, A. B., Tas, I., Ozkan, E., & Turker, H. chemical profile, antibacterial and antioxidant potentials. *Biotechnol Lett*, 2021, 26(2), 2499-2510.

[3] Piwowarski, J. P., Granica, S., & Kiss, A. K.. Lythrum salicaria L.—Underestimated medicinal plant from European traditional medicine. A review. *Journal of ethnopharmacology*, 2015, 170, 226-250.

[4] Al-Snafi A., E., Chemical constituents and pharmacological effects of Lythrum salicaria- A review, *IOSR Journal of Pharmacy*, 2019, 9.6, pp. 51-59.

[5] Mcgaw, L. J., Elgorashi, E. E., & Eloff, J. N. (2014). Cytotoxicity of African medicinal plants against normal animal and human cells. *In Toxicological survey of African medicinal plants*, 2014, pp. 181-233, Elsevier.

[6] Iancu, I., M., Bucur, L., A., Schroder, V., Mireșan, H., Mihai, S., Iancu, V., Badea, V., Phytochemical evaluation and cytotoxicity assay of *Lythri herba* extracts, *Farmacia*, 2021, 69(1), 51-58.

[7] Erdem H, Puca E, Ruch Y, Santos L, Ghanem-Zoubi N, et al. Portraying infective endocarditis: results of multinational ID-IRI study. Eur J Clin Microbiol Infect Dis. 2019 Sep;38(9):1753-1763. doi: 10.1007/s10096-019-03607-x. Epub 2019 Jun 11. PMID: 31187307.

[8] Octav Ginghina, George Traian Alexandru Burcea- Dragomiroiu, Bianca Galateanu, Ariana Hudita, Silvia Dragomir, Doina Draganescu, Andra Balanescu, Cosmin Adrian Rosca, Carmen Giuglea, Daniela Elena Popa, Anca Pantea-Stoian, Carolina Negrei- Long –term safety of biosimilar medicinal products-key for administration? Revista Farmacia, 2019, Vol. 67, 1, 18-26.

[9] Lopes, A., Rodrigues, M. J., Pereira, C., Oliveira, M., Barreira, L., Varela, J., ... & Custodio, L.. Natural products from extreme marine environments: Searching for potential industrial uses within extremophile plants. *Industrial Crops and Products*, 2016, 94, 299-307.

[10] Bencsik, T. Comparative histological, phytochemical, microbiological, and pharmacological characterization of some Lythrum salicaria L. Populations, 2014, unv. Diss. University of Pécs.

[11] Raineri, M.; Falugi, C. Acetylcholinesterase activity in embryonic and larval development of Artemia salina Leach (Crustacea Phyllopoda). *Journal of Experimental Zoology*, 1983, 227.2: 229-246, https://doi.org/10.1002/jez.1402270207

[12] Lupu, E., C., Lupu, S., Petcu, A., *EB lifetime distributions as alternative to the EP lifetime distributions*, Analele Univ. Ovidius Constanţa, Seria Matematică, Vol. 22(3), 2014, ISSN 1224-1784, p.115-125 (I.F. 0.333, I.S. 0.088).

[13] Leahu, A., Lupu, E., C., Statistical simulation and prediction in software reliability. Analele Univ. Ovidius Constanţa, Seria Matematică, vol. XVI (1), 2008, ISSN 1224-1784, p 81-90.

THE DIFFERENT SCREENING METHODS FOR THE CERVICAL LESION DIAGNOSTIC AND THE ECONOMIC AND SOCIAL IMPLICATIONS OF SCREENING AMONG FEMALE POPULATION

Ph.D. Student Codrin Gheorghe[1]
Assoc. Prof. Dr. Schröder Verginica[2]
Assoc. Prof. Dr. Stoicescu Ramona[3]
Assoc. Prof. Dr. Dumitru Irina[4]
[1, 4] Ovidius University of Constanta, Faculty of Medicine, Constanta, Romania
[2, 3] Ovidius University of Constanta, Faculty of Pharmacy, Constanta, Romania
[3, 4] Clinical Infectious Diseases Hospital, Constanta, Romania

ABSTRACT

The study aims to compare different screening methods that are currently being used to confirm a cervical intraepithelial lesion (CIN) underlying the inherent advantages of the varied examination procedures. In this study we are looking at the quality contrast of the different paraclinical examinations relative to the cost, invasiveness and cultural acceptance of such procedures. Every year, more than 100,000 women in EU countries are diagnosed with cervix uteri cancers (CCU). This type of cancer can be prevented if precancerous cells are detected and treated. HPV is found in over 90% of cervix uteri cancers. In Europe, more than half of the countries have implemented screening programs for cervical cancer, and most European countries now have national HPV vaccination programs, however target populations vary depending on the epidemiological evidence and the budgetary level of each countries health system.

In this study we evaluated and compared the current and modern techniques used for cervix cellular diagnostics. Also, this study helps improve the understanding on the economic and social implications of screening among female population and the impact it has on healthcare system relieving. Romania recorded an incidence of 22.6 cases of cervix uteri cancers / 100.000 women (age standardized rate), and a mortality of 9.6 / 100.000, ranking second highest in the EU zone.

Keywords: *screening, cervical cancer, HPV, spectroscopy, Raman*

INTRODUCTION

Cervical cancer is among the most preventable cancers. Pre-cancerous lesions can easily be detected through screening before they become cancerous. When screening detects pre-cancerous lesions, these can be treated and thus the cancer can be avoided.

Human papillomavirus (HPV) is the essential driver of cervical malignant growth. More than 3/4 of sexually active women get it in the span of their lives. The prevalence of HPV increases with severity of the lesion. There are over 200 types of HPV with potential for induction of cellular transformations, but two of these strains, HPV-16 and 18, the two vaccine-preventable types contribute to over 70% of all cervical cancer cases, between 41%-67% of high-grade cervical lesions and 16-32% of low-grade cervical lesions. After HPV-16/18, the six most common HPV types are the same in all world regions, namely 31, 33, 35, 45, 52 and 58; these account for an additional 20% of cervical cancers worldwide. The HPV vaccine is almost 100% effective in preventing the persistent HPV infections that cause cervical cancer [1], [2].

Since the introduction of the Papanicolau's smear and cervical cancer screening, there have been other attempts to update and develop new screenings methods as minimally invasive as possible that would bring benefits to different economic regions of the world.

BURDEN OF HPV RELATED DISEASE

About 604,127 new cervical cancer cases are diagnosed annually globally (estimates for 2020) ranking in 3rd place as the most common cancer site in females. It is established that well-organised cervical screening programs or widespread good quality cytology can reduce cervical cancer incidence and mortality [3].

Screening methodologies contrast between nations. Some countries have population-based programs where in each round of screening women in the target population are individually identified and invited to attend screening. This type of program can be implemented nationwide or only in specific regions of the country [2].

As the European Guidelines recommend, a program with an organized population-based nature may substantially improve the accessibility and equity of screening access while simultaneously improving effectiveness and cost-effectiveness. The vital elements to be determined inside such a program are the target age, screening spans, and screening algorithm. The latter alludes to the essential screening test and the ensuing administration of results at each progression of the algorithm [4].

SCREENING OF CERVICAL TISSUE

Conventionally cervical cancers are diagnosed by visual inspection with acetic acid (VIA), HPV testing, polar probe, Pap smear (PAP) and colposcopy. However, these methods are not providing high sensitivity and specificity; furthermore, the diagnostic potential is highly subjective as it depends on the skills and experience of the persons who were analyzing the samples (Figure 1). Although biopsy and resulting histopathology are considered as the gold standard strategy for cancer diagnosis, it is an intrusive technique and has numerous impediments particularly for mass screening of patients with multiple suspicious lesions. In this context, extensive studies are under progress in the development of real-time, non-invasive and cost-effective molecular diagnostic modality using various techniques [5].

Present studies are centered around concurrent multispectral analysis which provides higher sensitive and accurate diagnosis.

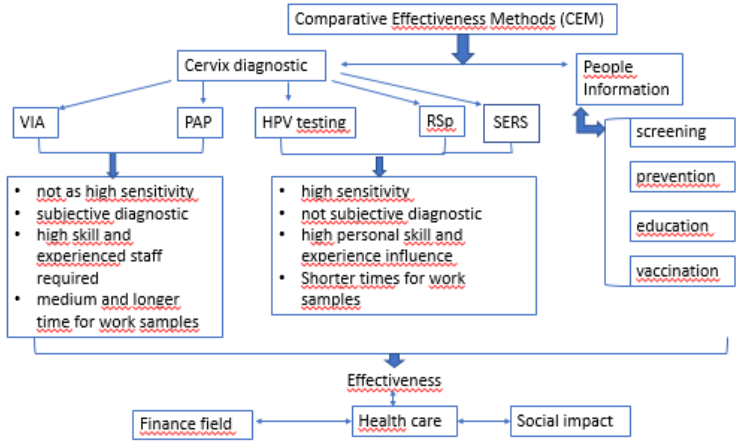

Fig. 1. *Comparative effectiveness methods (CEM) system for cervix diagnostic*

Diffuse Reflectance Spectroscopy

Steady-state reflectance spectroscopy (RSp) is a technique where light after multiple scattering in the tissue is collected and studied for qualitative and quantitative information. A study of reflectance spectroscopy involving 324 sites of 164 precancerous patients carried out by Mirabal et al. has found the discrimination ability between squamous normal and high-grade squamous intraepithelial lesions with sensitivity and specificity of **72**% and **83**% respectively. In spite of the fact that DRS has many advantages, even the slightest error like probe-to-tissue pressure can alter the accuracy of the spectra [6].

Surface-Enhanced Raman Spectroscopy (SERS)

Since the Raman effect is a weak phenomenon, researchers around the globe have tried to enhance the weak effect. One such novel technique is enhancing the Raman signals by nanoparticles known as SERS. The aid of multivariate statistical analysis is inevitable to glean meaningful inferences from the enormous data set obtained from these spectroscopic studies [6].

Spectro-cytology by label-free surface-enhanced Raman fingerprints and chemometrics

Varsha Karunakaran et al. explored a spectroscopic modality in which different spectral fingerprints were obtained by utilizing label-free ultrasensitive surface-enhanced Raman scattering (SERS) technique on exfoliated cell samples of the cervix. Three different approaches i.e. single-cell, cell-pellet and extracted DNA from oncology clinic as confirmed by Pap test and HPV PCR were employed. Gold nanoparticles as the SERS substrate favoured the increment of Raman intensity exhibited signature identity for Amide III/Nucleobases and carotenoid/glycogen

respectively for establishing the empirical discrimination. Moreover, all the spectral invention was subjected to chemometrics including Support Vector Machine (SVM) which furnished an average diagnostic accuracy of **94**%, **74**% and **92**% of the three grades (LSIL, HSIL, Cervical Cancer) [7].

Cervical cancer has been well studied by conventional Raman spectroscopy in the past several years for differentiating normal and abnormal subjects using blood serum, cells, tissues, in vivo etc. When contrasted with the regular Raman spectroscopy, SERS is a ultrasensitive strategy requiring less acquisition time, better signal-to-noise ratio, increased fold intensity, specificity and Raman cross section. Employing SERS in exfoliated cell samples for cervical cancer detection will provide direct understanding into the cause of abnormalities offering some unmistakable advantages over different procedures like less time preparing the samples and minimal influence of water bands [7], [8].

Raman spectroscopic detection of high-grade cervical cytology

In a study done by Jing Wang et al., 210 ten tissue sections from 210 patients (Among them, 60 were diagnosed as cervicitis, 30 as CIN I, 30 as CIN II, 30 as CIN III, 30 as cervical squamous cell carcinoma, and 30 were diagnosed as cervical adenocarcinoma by pathological diagnosis) which yielded 157 spectra of CIN I tissue, 138 of CIN II tissue, 155 of CIN III tissue, 166 of cervical squamous cell carcinoma tissue, and 201 of cervical adenocarcinoma tissue, totaling 1110 spectra [8]. The spectra was analyzed and interpreted then using the SVM algorithm to build an efficient diagnosis model to classify the six tissues.

The main Raman characteristic peaks of the cervical tissues were summarized, and the differences of biochemical components of the 6 types of cervical tissues were analyzed. After rehashed tests, the characterization impact was improved. The accuracy of the cervical tissues was **85.7**% which indicated that Raman spectroscopy combined with support vector machine could be used to successfully classify the different types of samples [7], [8].

Rapid screening using Raman spectroscopy based on GA-SVM

In a study conducted by Chen Chen et al., 196 HPV negative secretion samples and 58 HPV positive samples were analyzed using Raman spectroscopy and multivariate statistical analysis.

By using algorithms for noise reduction, the background of the Raman spectras were normalized and the processed spectras were used to build a model for analysis (The airPLS-PLS-GA-SVM hybrid model process) which further improved the accuracy and quality of the data extracted.

Because this technology has the advantages of being fast, noninvasive, and low cost, it has broad application prospects. The accuracy of using airPLS-PLS-GA-SVM to diagnose cervical diseases was up to **98.6**%, which indicates the great potential of using Raman spectroscopy to screen cervical diseases and prevent cervical cancer in the future [8].

SOCIAL AND ECONOMIC CONCERNS

In low and middle-income countries (LMICs), where cervical cancer burden is highest, screening coverage is much lower. In these settings, low Pap screening accessibility (due to limited resources, infrastructure, and trained personnel) and poor sensitivity of the existing low-cost cervical cancer screening option, visual inspection with acetic acid (VIA), are boundaries to effective screening [9].

Primary HPV screening has advantages over Pap that can benefit both high and low-income settings. HPV testing has higher sensitivity than Pap to detect cervical pre-cancers, allowing broadened screening intervals, and HPV testing requires less training for sample collection. Figure 1

Some studies proposed HPV tests using self-collected samples which were shown to have comparable sensitivity to clinician-collected samples for detecting cervical intraepithelial neoplasia grade 2 or higher (CIN2+), making HPV self-sampling (HPV-SS) a feasible screening option. Women of different ages, ethnicities, and nationalities reported HPV-SS to be highly acceptable [9].

Cervical cancer remains a significant public health problem in Romania. It ranks third in the country after breast and colorectal cancer. Unfortunately, the first attempt of campaign vaccination in Romania proved short to deliver.

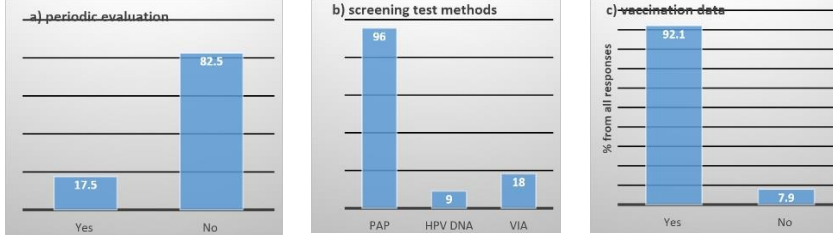

Fig. 2. *HPV information - responses of a survey conducted online a) periodic evaluations of cervix lesions, b) methods used for screening, c) vaccination data for 21-30 ages groups*

In a survey conducted online, 116 of 126 (92.1%) participants responded that they did not get any HPV vaccines (Figure 2) even though most of them talked about it with their medical practitioners. Furthermore, our survey found that 82.5% of the participants did not get any form of cervical examination (Figure 2). The highest rate of respondents was in the age group of 21-30 (75 of 126 or 59.5%).

DISCUSSION

The lack of cost-effectiveness studies outside of Western Europe, especially in LMICs, that include data on real-world implementation scenarios, represents an important gap in the literature. Future cost-effectiveness studies within screening programs should model the impact of new triage strategies, the development of HPV-SS outreach materials, and increasing HPV vaccination rates [9].

The research community is in pursuit of molecular fingerprinting which differentiates samples between different biological conditions with emphasis on

real-time, minimal invasiveness and high-thorough analysis. One such analysis is that of the SERS combined with multivariate statistical analysis which proves to be a high specificity, low-cost analysis which could be employed in all types of economical regions.

Furthermore there is also the need of educating the population about the dangers of HPV. Comparative studies have shown that vaccination and regular screening against HPV even though imply national programs which require some additional spending, on the long run surpass the cost of treating the possible cervical cancer patients.

REFERENCES

[1] Sabet F., Mosavat A., Ahmadi Ghezeldasht S., Basharkhah S., Shamsian S.A.A, Abbasnia S., Shamsian K., Rezaee S.A., Prevalence, genotypes and phylogenetic analysis of human papillomaviruses (HPV) in northeast Iran. International Journal of Infectious Diseases, 103:480-488, 2021.

[2] Bruni L., Albero G., Serrano B., Mena M., Gómez D., Muñoz J., Bosch F.X., de Sanjosé S. ICO/IARC, Information Centre on HPV and Cancer (HPV Information Centre). Human Papillomavirus and Related Diseases in the World. Summary Report 17 June 2019, www.hpvcentre.net

[3] International Agency for Research on Cancer, WHO, https://gco.iarc.fr/

[4] Chrysostomou, A.C.; Stylianou, D.C.; Constantinidou, A.; Kostrikis, L.G. Cervical Cancer Screening Programs in Europe: The Transition Towards HPV Vaccination and Population-Based HPV Testing. *Viruses* **2018**, *10*(12):729, 2018.

[5] Pappu Raja, Prakasarao Aruna, Dornadula Koteeswaran, Singaravelu Ganesan, Characterization of blood plasma of normal and cervical cancer patients using NIR Raman spectroscopy, Vibrational Spectroscopy, Volume 102, 2019.

[6] Daniel A., Savarimuthu W.P. (2019) Current Advances in Optical Screening for Cervical Cancer. In: Farghaly S. (eds) Uterine Cervical Cancer. Springer, 2019.

[7] Varsha Karunakaran, Valliamma N. Saritha, Manu M. Joseph, Jyothi B Nair, Giridharan Saranya, Kozhiparambil G. Raghu, Kunjuraman Sujathan, Krishnannair S. Kumar, Kaustabh K. Maiti, Diagnostic spectro-cytology revealing differential recognition of cervical cancer lesions by label-free surface-enhanced Raman fingerprints and chemometrics, Nanomedicine: Nanotechnology, Biology and Medicine, Volume 29, 2020.

[8] Wang, J., Zheng, CX., Ma, CL. *et al.* Raman spectroscopic study of cervical precancerous lesions and cervical cancer. *Lasers Med Sci*, 2021.

[9] Colin Malone, Ruanne V. Barnabas, Diana S.M. Buist, Jasmin A. Tiro, Rachel L. Winer, Cost-effectiveness studies of HPV self-sampling: A systematic review, Preventive Medicine, Volume 132, 2020.

THE USE OF OIL-CAKE (SUNFLOWER) IN THE DEPOLLUTION OF PETROLEUM INFESTED WATER

Assoc. Prof. Dr. Timur Chis[1]
Drd. Ing. Stefan Petrache[2]
Dr. Ing. Olga Sapunaru[3]
[1] Ph.D. Department, Oil and Gas University, Ploiesti, Romania
[2]Oil and Gas University, Ploiesti, Romania
[3]Ovidius University of Constanta, Romania

ABSTRACT

Oil pollution of surface and groundwater is an undesirable phenomenon but it is possible to happen. The pollutant can appear as a result of leaks from the transport pipelines, the damage of the oil extraction and processing installations, and the distribution states of the petroleum products.

In the vast majority of interventions to combat pollution, polymeric sorbents are used which are spread over the pollutant and then washed with warm water.

This technology does not completely clean the pollutants, and the polymeric sorbents are difficult to remove.

Oil-cake (sunflower) is a grated residue after oil extraction and contains the amino acid lysine and high content of fiber and methionine. At a quantity of 100 kg of sunflower seeds, a processor obtains a quantity of 35 kg of residual mass consisting of a sunflower meal.

This product can be used as a sorbent for petroleum products, being then used to produce green energy.

The physical properties of two sorbent substances (sunflower oil and peat) are presented.

Also, their adsorption capacities for four pollutants specific to the oil industry (gasoline, diesel, paraffin oil and sulfur oil) are analyzed, as well as the adsorption kinetics.

The adsorption equations of the pollutants are also described.

Keywords: *Oil-cake (sunflower),sorbent, oil products, water, pollution*

INTRODUCTION

Oil pollution of surface waters can be removed by:

- crowding (dispersion) of the film to favour its spread under the action of natural factors, with the help of dispersants.
- chemical neutralization of toxic hydrocarbon products, by "binding" them in various less active combinations.

- adsorption of hydrocarbons on the surface of special materials, easier to control and recover.
- oil film burning (not indicated).
- biodegradation of the oil film with the help of microorganisms.

The use of biodegradable adsorbents on the surface of the water, in extreme cases, must be accompanied by their immediate recovery and removal from the environment. These adsorbents are 100% biodegradable are oleophilic, but only partially hydrophobic.

These adsorbents can adsorb an amount of pollutant 3 to 15 times larger than their mass, but some of them have the disadvantage that they also absorb an amount of water which causes them to sink faster and greatly prevents their collection.

Failure to recover from water causes the maintenance of oil pollution in the polluted area or, worse, causes the occurrence of secondary pollution, in the same place or in different places, much more harmful and dangerous than the initial pollution.

The aggregates of 100% natural biodegradable adsorbent product.

biodegradable adsorbents can form agglomerations of petroleum product and adsorbent, which are heavier than water density and transfer to its bottom [1].

The phenomenon is much more complex, the agglomerates of adsorbent / petroleum product deposited on the bottom of the water basin enter the degradation process only after a time of 90 - 120 days and are not completely realized after 120 days [2].

The reality is that the 100% natural biodegradable adsorbent product degrades first and long before the oil product, the degradation of the last component (oil product) being less intense.

After degradation of the 100% natural biodegradable adsorbent, the amount of petroleum product left undegraded on the bottom of the water basin slowly rises to the surface of the water. Most of the organic materials can only be used on land and are not recommended to be used on water to eliminate oil spills.

The grated residue (oil-cake) after oil extraction contains the amino acid lysine and high content of fiber and methionine.

At a quantity of 100 kg of sunflower seeds, a processor obtains a quantity of 35 kg of residual mass consisting of sunflower meal.

40 kg of oil are produced from 100 kg of sunflower seeds and 25 kg are oily residues.

This product can be used as a sorbent for petroleum products, being then used for energy production in power plants (its use as fuel).

PREVIOUS STUDIES

The recovery of crude oil, petroleum products, mineral oils (Table 1) and their waste accidentally discharged into surface waters, when they are in the form of very thin films, is achieved in the final phase by using sorbents [3], [4], [5].

Adsorbents are those solids or liquids that have the property of absorbing vapors or dissolved substances.

Ad / absorbents (sorbents) are divided into three main categories of materials :

- natural organics: peat (peat moss), sawdust, cut hammers, straw, carbon-based products;
- natural inorganics: clay, perlite, vermiculite, glass wool, sand or volcanic ash (Table 2 and 3);
- synthetic: polyurethane, polyethylene, polypropylene, etc.

Of these three categories of sorbents, only natural organic materials are biodegradable, while natural and synthetic inorganic materials are non-biodegradable adsorbent materials.

Biodegradation refers strictly to the decomposition of sorbents after the recovery of petroleum products from the polluted area. The largest amounts of adsorbents used in Romania on the water were and are 100% natural organic adsorbent materials, biodegradable, floating on the surface of the water. In over 90% of cases, imported peat sorbents. More 10 % of sorbents are synthetic [6].

PRESENT STUDY

In order to ensure adequate scientific support, in conducting the study, research methods and means were used, both general and specific, namely:

- The method of analysis and synthesis - consisted in consulting bibliographic sources to obtain general data;
- Observation method - was used for laboratory research in order to make observations, measurements;
- Comparative method - was used to evaluate the absorption capacity of the 2 natural adsorbents analyzed;

Tests were performed with sorbents such as peat and sunflower oil.

Also used were 4 pollutants specific to the oil industry (the most persistent pollutants in accidental pollution with petroleum products), namely Romanian Oil, Russian Export Blend Crude Oil, Diesel and gasoline (Table 1).

Table 1. *Properties of polluants using in analysis*

Polluants	Diesel	Gasoline	Romanian Oil	Russian Oil
Density, kg/dm^3 at 20°C,	0.823	0.736	0.838	0.8615
Viscosity, cst,	2.45 at 40°C	18.41 at °C	21.21 at °C	20,58 at °C
Freezing point, °C	-23	-20	+8	-8

Table 2. *Density of sorbents using in analysis*

Polluants	peat	sunflower oil
kg/dm^3 at 20°C	0.157	0.228

Table 3. *Properties of sunflower oil*

Properties	Value
Ca, %	0,3
P, %	0.98
Gross fat, %	1,34
Crude cellulose, %	16
Lysine, %	1,25
Methionine, %	1,34
Crude protein , %	33

To determine the properties of sorbents we using regulation developed by ASTM (American Society for Testing and Materials named Standard Test Methods for Sorbent Performance of Adsorbents (F716-09 and ASTM F726 – 12).

The first experiment was performed between the petroleum products and the sorbents used:

a) Addition of sorbents to used petroleum products to 20ºC temperature,

b) Measurement of absorption capacity at 15 minutes and 24 hours to 20ºC temperature.

In Figure 1,2,3 is presented the mixtures of diesel, oil and sorbents.

Sorption capacity testing

The quality of the sorbents is to retain the hydrocarbons. The experiment consisted in observing the encapsulation capacity of the oil and determine the amount of liquid absorbed by the amount of sorbent (g petroleum product / g sorbent) (figure 4).

Capillary ascent testing

This test highlights the phenomenon of absorption by capillary action, a phenomenon that takes place the removal of petroleum products from the affected environment.

The sorbents act through both the absorption and the adsorption mechanism.

The absorbents act as sponges and collect the product by the action of capillarity or suction. They allow the liquid to enter the space of the pores of the material from which they are made, while the adsorbents attract the liquid on their surface but do not allow their penetration into the material. In some cases, sorbent materials can use both principles to recover the oil product.

We tested the kinetics of the capillary rise of different liquids in the pores of sorbents.

The REBCO type crude oil, diesel and petrol (75 ml) were introduced in a column (1.5 cm diameter and 12 mm length), filled with natural peat sorbents and sunflower stew (up to 4 cm).

The volume of oil absorbed by the sorbent was monitored.

The results obtained are represented in Figure 5,6 and Table 4 and 5.

Fig. 1. *Diesel in contact with sunflower*

Fig. 2. *Romanian Oil in contact with sunflower*

***Fig. 3**. Romanian Oil in contact with peat*

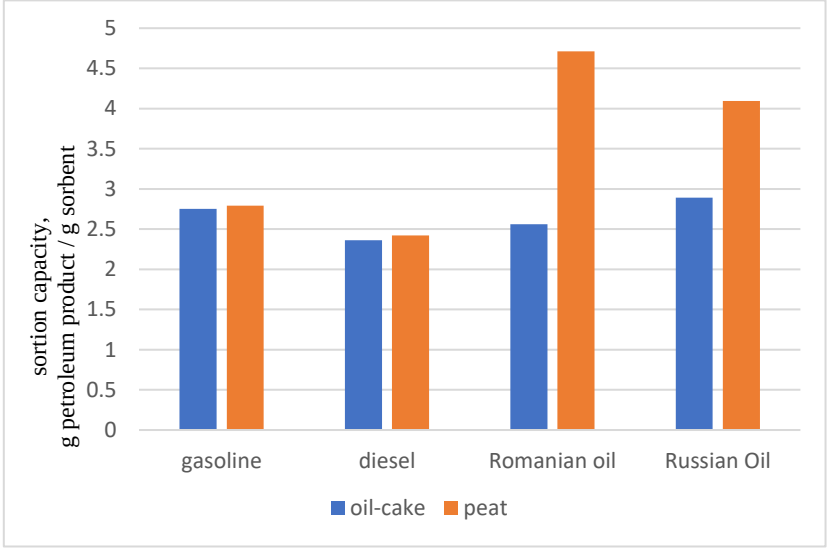

***Fig. 4**. Sortion capacity of oil-cake and peat*

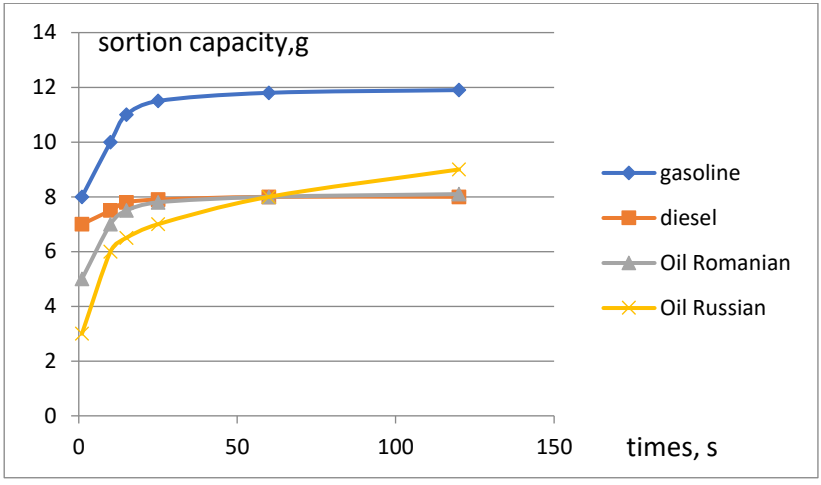

Fig. 5. *Kinetics of fluid retention in peat pores*

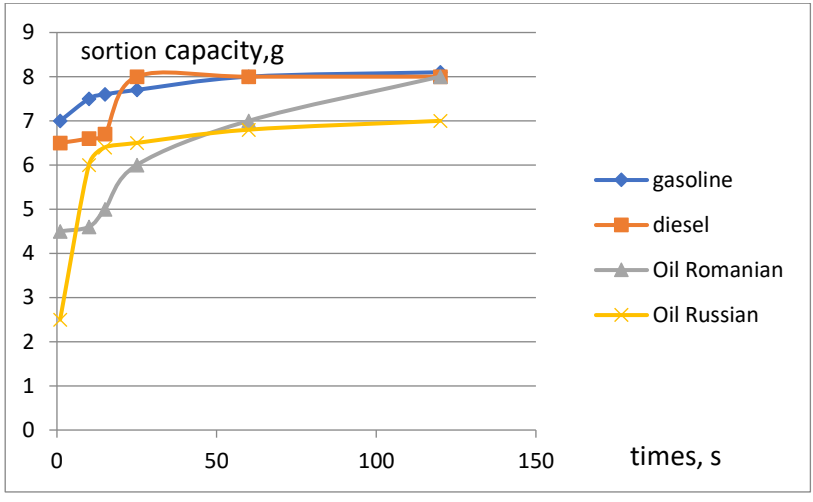

Fig. 6*. Kinetics of fluid retention in oil-cake*

Table 4*. Equation of kinetics retention in peat pores*

Poluants	Equation y is sortion capacity x is times to sortion	R^2
Gasoline	y = 0.8663ln(x) + 8.2295	0,9324
Russian oil	y = 1.235ln(x) + 3.0613	0.9982
Romanian oil	y = 0.6698ln(x) + 5.3232	0.9193
Diesel	y= 0.2247ln(x) + 7.0593	0.9219

***Table 5**. Equation of kinetics retention in oil cake*

Poluants	Equation y is sortion capacity x is times to sortion	R^2
Gasoline	y = 0.2354ln(x) + 6.9787	0.9925
Russian oil	y = 0.7424ln(x) + 3.7329	0.7593
Romanian oil	y = 0.7424ln(x) + 3.7329	0.7593
Diesel	y = 0.7424ln(x) + 3.7329	0.7593

CONCLUSION

In the article, we presented the effects of oil pollution on two natural sorbents (easy to find in nature). The first sorbent (peat) is widely used in the oil-polluted environment recovery industry. The second adsorbent is proposed by us for use, having important adsorption capacities and being a residual product.

At this time, the sunflower meal is burned in ovens, having a low caloric capacity.

By using it as an adsorbent you can increase the caloric capacity and especially by refining you can recover the oil product.

Based on the studies carried out in the previous chapters of the paper, the following conclusions were obtained:

- the peat retains the oil production in the first 20 seconds, followed by a period of filling the pores,
- sunflower meal is useful for retaining heavy products (high density),
- the output capacity is 2.5-4 times greater than the weight of the sorbent,
- sunflower meal is a good and useful sorbent, is then used for the production of electricity or heat.

In this paper we wrote the logarithmic equation of determination is sortion capacity function by times to sortion.

REFERENCES

[1] W.B. Jiao, Y.Q. Zhang, K. Yu, J.R. Zhou, H.L. Cao, J. Lü. Porous Graphitic Biomass Carbons as Sustainable Adsorption and Controlled Release Carriers for Atrazine Fixation (2019). ACS Sustainable Chemistry & Engineering, 7 (24) , 20180-20189. https://doi.org/10.1021/acssuschemeng.9b06269

[2] A.G.Ciufu, T.Chis, T.Dobre (2015). Adsorption of crude oil using biosorbents in accidental oil spills, Bulletin of Romanian Chemical Engineering Society. 2, 2, 2015.46-51

[3] T.Schneckenburger, S.Thiele-Bruhn, Sorption of PAHs and PAH derivatives in peat soil is affected by prehydration status: the role of SOM and

sorbate properties (2020). J Soils Sediments 20, 3644–3655. https://doi.org/10.1007/s11368-020-02695-z

[4] Al-Degs, Y.S., El-Barghouthi, M.I., El-Sheikh, A.H., and Walker, G.M. (2008), Effect of solution pH, ionic strength, and temperature on adsorption behavior of reactive dyes on activated carbon, Dyes Pigm., 77 (1), 16–23

[5] T.R Annunciado, T.H.D. Sydenstricker and S.C.Amico (2005).Experimental investigation of various vegetable fibers as sorbent materials for oil spills, Marine Pollution Bulletin, 50, 1340–1346

[6] E. González-Pradas, M. Villafranca-Sánchez, M. Fernández-Pérez, M. Socías-Viciana, M.D. Ureña-Amate (1998), Sorption and leaching of diuron on natural and peat-amended calcareous soil from Spain, Water Research, Volume 32, Issue 9, 1998, Pages 2814-2820,ISSN 0043-1354, https://doi.org/10.1016/S0043-1354(98)00021-9

Section

ENVIRONMENTAL GEOLOGY

Economic and environmental objectives
Economic instruments in environmental policy
Cost-benefit analysis
Environmental expenditure of enterprises
Eco-innovations for sustainable development
Environmental evaluation and decision-making

ASSESSMENT OF ENVIRONMENTAL CHANGES DURING MINING OF FELDSPAR DEPOSITS IN UKRAINE

Dr. Geol.-Mineral. Sci., Dr. Geogr. Sci., Dr. Eng. Sci., Prof. Georgii Rudko[1]
Assoc. Prof. Ph.D. Mariia Kurylo[2]
Ph.D. Student Maksym Ozerko[3]
[1] State Commission of Ukraine on Mineral Resources, Kyiv, Ukraine
[2, 3] National Taras Shevchenko University of Kyiv, Kyiv, Ukraine

ABSTRACT

Possible negative impacts on the environment during mining of feldspar deposits with open-pit and underground mine are defined. The main changes have been identified, which are as follows: air pollution, soil destructions, change of relief, a local decrease in groundwater level, pollution by sewage and waste.

Destructions of the soil cover are fixed under the dumps of the quarry and in the path of the movement of quarry equipment. Through the development of a pit and dumps, the primary relief acquires significant changes and the action of forces caused primarily by gravity is activated, aimed at smoothing out negative and positive relief forms.

An increase in the height difference from the dump ridge to the bottom of the quarry and the formation of a significant, pronounced depression of the relief redirects the surface runoff, increases its speed, and reduces infiltration into the soil. Mining development caused drainage of groundwater due to its release to the surface and evaporation.

Air pollution has a bigger scale than other components of negative impacts. The main impact of mining activities is due to emissions of pollutants into the atmosphere as a result of blowing dust from the surface of dumps and emissions from quarry transport and their deposition on the soil and storage of industrial waste. The main pollutants are inorganic dust with content of SiO_2 - 65-82% and Al_2O_3 - 11-21%.

Separately, the article discusses the impact on the environment during multi-components deposits` exploitation, where feldspar concentrates are produced as by-products. Several deposits in Ukraine belong to the group: Bakhtyn (fluorite ores), Nosachivske (titanium-ilmenite ores), Perzhanske deposits of rare metals, Mazurivske (tantalum and niobium ores). Most of them are planned to be mined underground, which saves more land resources in comparison with open workings. The placement of mine shafts and industrial sites for their maintenance requires an area of about 30 hectares. All of them have a complex ore processing with the separation of several concentrates, which necessitates the use of flotation and other reagents. The development of such deposits involves the organization of tailings and circulating water supply of the processing plant.

Keywords: *feldspar deposits, environmental changes, mining, assessment*

INTRODUCTION

The relevance of assessing the impact of feldspar mining on the environment is associated with an increase in the scale of production. In Ukraine, dozens of deposits are mined for use in the construction and production of ceramics. Globally feldspar consumption has been gradually increasing in ceramics, glass industry for solar panels, housing, and building construction.

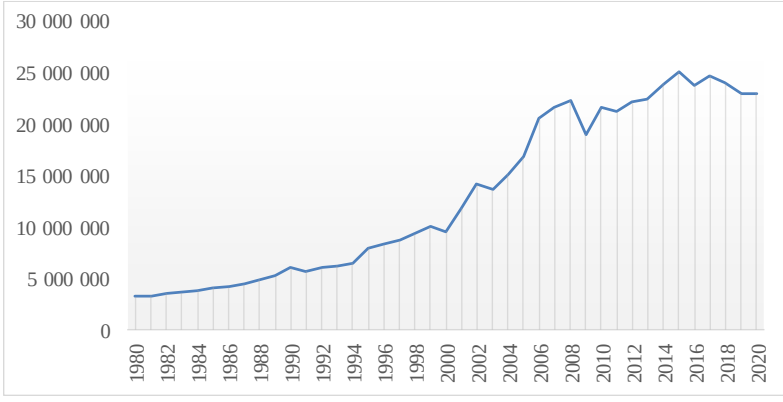

Fig. 1. *Feldspar global production dynamics in metric tons (according to statistical data usgs.gov [6])*

The total production of feldspar raw materials in Ukraine amounted to 634.63 thousand tonnes in 2019.

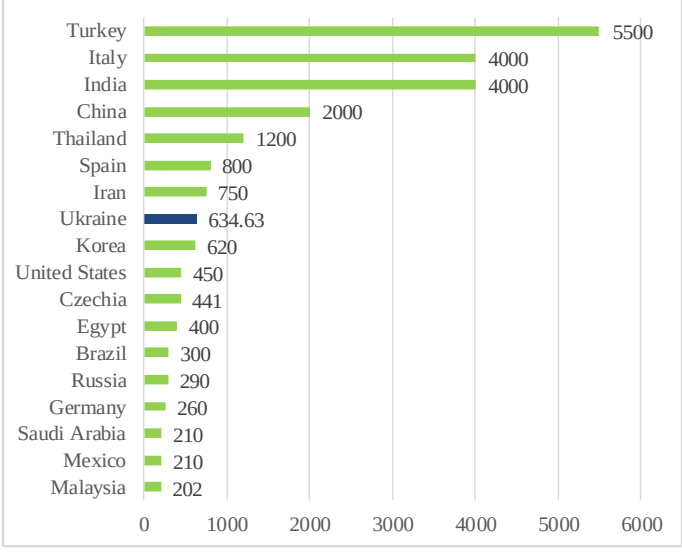

Fig. 2. *Feldspar production in 2019 by country (according to statistical data usgs.gov [6], and statistical data for Ukraine - State Information Geological Fund of Ukraine [1])*

Environmental impact assessment is mandatory in Ukraine for mining enterprises [7] and for feldspar, deposits have their peculiarities. The main source of feldspar raw materials in Ukraine is multi-component deposits. These objects belong to different genetic and mining types, which determine the impact on the environment that occurs during development. The following diagram illustrates the features of mining methods and the processing of feldspar raw materials by the type of deposits (figure 3).

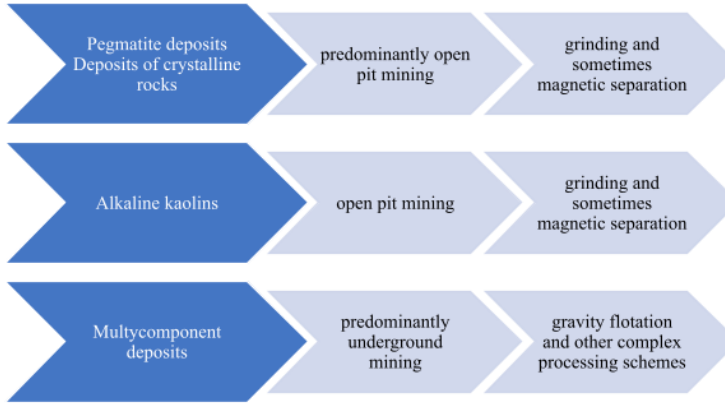

Fig. 3. *Features of mining methods and processing of feldspar raw materials by the type of deposits*

Possible negative impacts on the environment during *open-pit mining* of feldspar deposits are as follows: air pollution, soil destructions, change of relief, a local decrease in groundwater level, pollution by sewage, and waste. The area of disturbed land and the volume of waste with the open method depends on the size of the reserves and the stripping ratio. As a rule, this ratio is less than 1, which has a positive effect on the profitability of mining. The soil is less than 10% of the total overburden volume and the enterprises store it separately for further reclamation. As a rule, the production capacity of mining enterprises ranges from 50 to 200 thousand tons per year, which provides at least 20 years of operation.

Destructions of the soil cover are fixed under the dumps of the quarry and in the path of the movement of quarry equipment. Through the development of a pit and dumps, the primary relief acquires significant changes and the action of forces caused primarily by gravity is activated, aimed at smoothing out negative and positive relief forms.

The main impact of mining activities is due to emissions of pollutants into the atmosphere as a result of blowing dust from the surface of dumps and emissions from quarry transport and their deposition on the soil and storage of industrial waste. The main pollutants are inorganic dust with a content of SiO_2 - 65-82% and Al_2O_3 - 11-21% [5].

An increase in the height difference from the dump ridge to the bottom of the quarry and the formation of a significant, pronounced depression of the relief

redirects the surface runoff, increases its speed, and reduces infiltration into the soil. Mining development caused drainage of groundwater due to its release to the surface and evaporation.

Air pollution has a bigger scale than other components of negative impacts. During the mining operation, a significant amount of gaseous substances of spent fuel and other technological substances, as well as suspended particles of the quarry rock, are emitted into the air.

The influence of mining activity on the disturbance of landscapes and biocenosis should be studied separately. These factors depend on the availability of those items on the territory and the scale of land alienation.

Deposits of crystalline rocks often require preliminary disintegration using drilling and blasting operations. In such cases, the stability of the geological environment and its assimilation potential must be assessed. The boundaries of the development of the deposits in the plan ensure compliance with the 500-meter sanitary protection zones.

Other features of the impact on the environment are multi-components deposits, where feldspar concentrates are produced as by-products. Several deposits in Ukraine belong to the group: Bakhtyn (fluorite ores), Nosachivske (titanium-ilmenite ores), Perzhanske deposits of rare metals, Mazurivske (tantalum and niobium ores).

Most of them are planned to be mined underground, which saves more land resources in comparison with open workings. The placement of mine shafts and industrial sites for their maintenance requires an area of about 30 hectares. All of them have a complex ore processing with the separation of several concentrates, which necessitates the use of flotation and other reagents. The development of such deposits involves the organization of tailings and circulating water supply of the processing plant.

The impact on the atmosphere is different from open-pits since dust pollution from mining is less due to production volumes and is concentrated in underground buildings. Processing can be a source of air pollution and pollutants depend on the composition of enrichment reagents.

For the Nosachivske, Bakhtyn, and Perzhanske deposits listed above, it is planned the mining system with backfilling. Considering the underground mining, overburden rocks in a large volume will not be, and those crystalline rocks that will be raised to the surface will be used in the construction of a mining and processing complex. For these deposits, it`s proposed to organize the recycling water supply system of the processing plant. A decrease in the level of groundwater in the adjacent territories is possible [3], [4].

In terms of land resources, it is planned to withdraw land and change their intended purpose for the placement and operation of main, auxiliary, and auxiliary buildings and structures associated with the use of subsoil for mining. Contamination of the soil with oil products from faulty equipment is assumed;

violation of the soil cover during the surface construction of the mining and processing complex.

The planned activities are considered to have a minor and tolerable impact on flora and fauna. Sources of increased noise from mining operations may cause minor impacts on habitats, breeding conditions, and animal migration routes. As a result of the implementation of the planned activities, an insignificant permissible impact on the spatial, species, population diversity of flora objects is possible.

Individual design solutions are directed to the processing and use of production waste. On the example of the Mazurivske deposit, the production of feldspar concentrate is associated with processing stored waste. It allows us to free up large areas of tailings and eliminate the source of potential environmental hazards given the existing connection of tailings with the river Kalchyk basin. However, a base of feldspar raw materials can be created for the ceramic industry quite quickly and without significant investment. Such production will become a testing ground for the preparation of the complex development of the Mazurivske deposit [2].

Generalized objects of influence on the environment for the named types of deposits are shown in Table 1.

Table 1. *Main objects of influence on the environment for feldspar deposit un Ukraine*

Type of deposit	List of feldspar deposit un Ukraine	The main objects of influence on the environment
Pegmatite deposits	Bilchakivske, Ustia village, Hruzlivetske, Lozuvatske, Volodymyrivske, Balka Velykoho Taboru	Open-pit, drilling and blasting operations, crushing plant, overburden dumps
Deposits of crystalline rocks	trachytes of the Verbova site, microgranodiorites of the Dubrynetske deposit	
Alkaline kaolins	Prosianivske, Pershozvanivske, Biliayivske, Katerynivske	Open-pit, crushing, and grinding plant, overburden dumps, processing plant for dry, wet, and electromagnetic separation, tailings
Multicomponent deposits	Bakhtyn (fluorite ores), Nosachivske (titanium-ilmenite ores), Perzhanske deposits of rare metals, Mazurivske (tantalum and niobium ores)	underground mine, processing plant (gravitation, flotation, and electromagnetic separation), tailings

CONCLUSION

Objects of negative impact for different types of deposits are highlighted:

1. for pegmatite deposits and deposits of crystalline rocks it is open-pit, drilling and blasting operations, crushing plant, overburden dumps;

2. for kaoline deposits it is (except for the above) processing plant for dry, wet, and electromagnetic separation, tailings;
3. for multicomponent deposits - underground mine, processing plant, tailings.

Possible negative impacts on the environment during open-pit mining of feldspar deposits are air pollution, soil destructions, change of relief, a local decrease in groundwater level, pollution by sewage, and waste. For underground mines, important changes are disturbances in the rockmass and its stability, changes in the regime and composition of surface and ground waters. For all facilities where there are processing plants, the development and condition of tailing dumps and the possibility of processing waste are critical.

Important and effective measures for improving facilities are the reduction of disturbed mining areas and their early reclamation, backfilling during underground mining, the maximum extraction, and processing of all useful components of minerals, which reduces the amount of production waste.

REFERENCES

[1] Balance of mineral reserves of Ukraine. Issue 72. Feldspar raw materials. Kyiv, State Research and Production Enterprise "State Information Geological Fund of Ukraine", 2018. *(in Ukrainian)*

[2] Cherniyenko N.M. Complex use of ores of the Mazurivske deposit, Pryazovia region, http://ea.donntu.org:8080/jspui/bitstream/123456789/7226/1/215-222.pdf *(in Ukrainian)*

[3] Conclusion on environmental impact assessment of mining Nosachivske deposit// http://eia.menr.gov.ua/uploads/documents/2522/reports/ 9846711dd23548eb3c49153d17086c5f.pdf *(in Ukrainian)*

[4] Conclusion on environmental impact assessment of extraction and processing of the Perzhanske deposit//http://eia.menr.gov.ua/uploads/documents/3271/reports /420b60111f02a021002d13c0d8614294.pdf *(in Ukrainian)*

[5] Conclusion on environmental impact assessment of the development of the Pyatyrichanka site of the Dubrivka alkaline kaolin deposit//http://eia.menr.gov.ua/uploads/documents/6682/reports/q5utEyl1tK.pdf *(in Ukrainian)*

[6] Feldspar Statistics and Information. National Minerals Information Center. USGS// https://www.usgs.gov/centers/nmic/feldspar-statistics-and-information

[7] On environmental impact assessment. Law of Ukraine. Vedomosti Verkhovnoi Rady (VVR), 2017, № 29, p.315. *(in Ukrainian)*

LONG-PERIOD SURFACE-RELATED MULTIPLE SUPPRESSION IN 2D MARINE SEISMIC DATA USING PREDICTIVE DECONVOLUTION AND COMBINATION OF SURFACE-RELATED MULTIPLE ELIMINATION AND PARABOLIC RADON FILTERING

Pimpawee Sittipan[1]
Assoc. Prof. Dr. Pisanu Wongpornchai[2]
[1, 2] Department of Geological Sciences, Chiang Mai University, Thailand

ABSTRACT

Some of the important petroleum reservoirs accumulate beneath the seas and oceans. Marine seismic reflection method is the most efficient method and is widely used in the petroleum industry to map and interpret the potential of petroleum reservoirs. Multiple reflections are a particular problem in marine seismic reflection investigation, as they often obscure the target reflectors in seismic profiles. Multiple reflections can be categorized by considering the shallowest interface on which the bounces take place into two types: internal multiples and surface-related multiples. Besides, the multiples can be categorized on the interfaces where the bounces take place, a difference between long-period and short-period multiples can be considered. The long-period surface-related multiples on 2D marine seismic data of the East Coast of the United States-Southern Atlantic Margin were focused on this research. The seismic profile demonstrates the effectiveness of the results from predictive deconvolution and the combination of surface-related multiple eliminations (SRME) and parabolic Radon filtering. First, predictive deconvolution applied on conventional processing is the method of multiple suppression. The other, SRME is a model-based and data-driven surface-related multiple elimination method which does not need any assumptions. And the last, parabolic Radon filtering is a moveout-based method for residual multiple reflections based on velocity discrimination between primary and multiple reflections, thus velocity model and normal-moveout correction are required for this method. The predictive deconvolution is ineffective for long-period surface-related multiple removals. However, the combination of SRME and parabolic Radon filtering can attenuate almost long-period surface-related multiple reflections and provide a high-quality seismic images of marine seismic data.

Keywords: *Long-period multiple reflections, Marine seismic reflection survey, Multiple reflections, Petroleum exploration, Surface-related multiple reflections*

INTRODUCTION

The Marine seismic reflection method is widely used in the petroleum industry to map and interpret the potential of petroleum reservoirs. The marine zones of marine seismic exploration include the shallow-water areas (water depth of less than

30 to 40 meters) and the deep-water areas associated with seas and oceans. When the energy of the seismic wave travels through the water surface and reflects back to receivers, each reflected signal in the seismic record theoretically has only one reflection point, it is called primary reflection. Many problems limit the ability of marine seismic exploration and generate noise even if they are random noise from environment activities or coherent noise such as swell noise, generated by streamer cables, and the big problem; multiple reflections, due to the strong reflector with a reflectivity close to unity. Multiple reflections are the events in the seismic record and have the reflection point more than one before traveling to the receivers. They are treated as unwanted events. Multiple reflections can be classified by considering the shallowest interface on which the bounces take place [1]. Two subdivisions of multiples are internal multiples and surface-related multiples. The internal multiples have a downward bounce at the reflector below the surface. The surface-related multiples have a downward bounce at least one at the surface. Besides, the multiples can be categorized on the interfaces where the bounces take place, a difference between long-period and short-period multiples can be made. The long-period or long-path multiples having the distinct arrival times from the primaries are the multiple events that can be differentiated from the primary events. On the other hand, short-period or short-path multiples generated by thin layer and interfering with the primaries are the multiples that cannot be separated from the primaries.

Due to the multiples being the unwanted events, subsurface imaging without removing them may be the big problems and misunderstanding for the interpreters. Several multiple removal techniques are used in seismic data processing. However, the well-known techniques, predictive deconvolution, surface-related multiple eliminations (SRME) and parabolic Radon filtering will be discussed in this research.

Predictive deconvolution can remove not only the seismic wavelets but also the repetitive events [2]. However, predictive deconvolution becomes less acceptable as the water depth increases and the complex structure. The large of the multiple reflection period and the complexity of structure yield the poor estimation of the periodic events [3], [4]. SRME [5], [6], [7], [8], [9] and Parabolic Radon filtering [8], [9], [10], [11] are the complementary methods effectively removing the surface-related multiple reflections for the complex geological setting data.

This research attempt to eliminate the surface-related multiples on marine seismic data. The two separated flows will be used for multiple removals. The first processing flow includes predictive deconvolution. The other contains SRME and parabolic Radon filtering.

METHODOLOGY

Predictive Deconvolution

The recorded seismic signal is considered as the convolutional model in the time domain. The source wavelet, $w(t)$, is sent through the subsurface and convolved with the Earth response (Earth's reflectivity), $r(t)$, to produce the seismic traces. Random noise, $n(t)$ is generated by activities in environment while

the seismic acquisition is working. The seismic records, $s(t)$, can be mathematically expressed as

$$s(t) = w(t) * r(t) + n(t) \quad (1)$$

Deconvolution is the inverse of the convolution process. The inverse filter operator, $h(t)$, estimated from seismic traces is convolved with the seismic records, $s(t)$. In principle, the deconvolution process sharpens the seismic traces by removing source wavelet and yields only the Earth's reflectivity.

$$r(t) = h(t) * s(t) \quad (2)$$

In practice, because the seismic data is not noise-free data, this condition may reduce the effectiveness of the deconvolution process and cause errors.

Predictive deconvolution is the most commonly used technique in seismic processing. This procedure not only removes the source wavelet but also suppresses the repetitive events in seismic data. Fig. 1 shows the autocorrelation functions of seismic traces containing long-period multiples. The α parameter indicates the repetition of the seismic events. In predictive deconvolution, the prediction lag α must be designed to predict and suppress the multiples [12].

In Fig. 2, the prediction lag (α) and prediction operator length (n) were designed.

The shorter prediction lags yield more compression of the source wavelet. While the prediction lag increases, the effectiveness the compression wavelet is reduced [12].

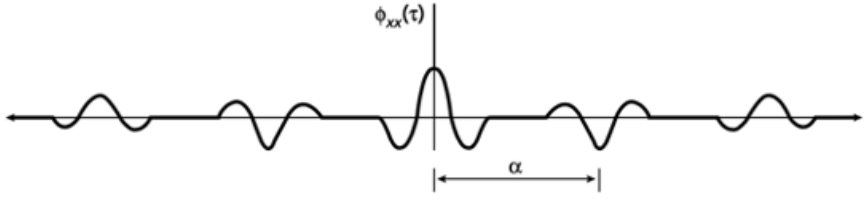

Fig. 1. *Autocorrelation functions of seismic traces containing with long-period multiples, [modified from [13]].*

The shorter length of n is the length of the first-order event and the longer length of n is the length of the second-order event. The prediction operator length (n) can be defined in order to suppress one or more orders of multiples. The autocorrelation of the output trace shows the very low energy of repetitive patterns after the deconvolution process.

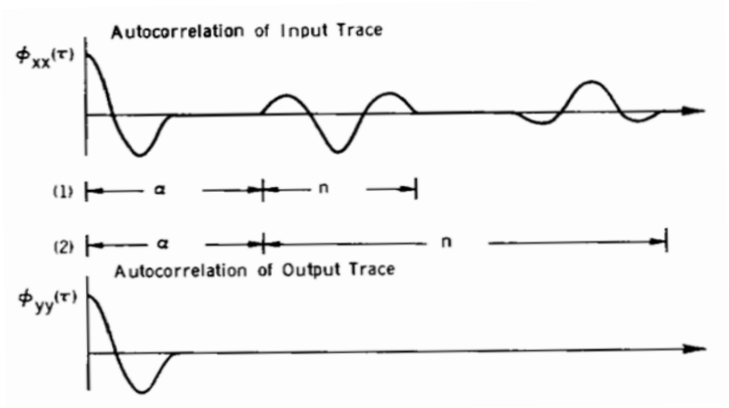

Fig. 2. *Upper diagram illustrates the autocorrelation of trace with long-period multiples. Lower diagram illustrates the autocorrelation output after applying predictive deconvolution, [modified from [2]].*

Surface-related Multiple Elimination (SRME)

The principle of SRME process is that multiples are a combination of primaries. First-order multiples are the spatial convolution of primaries and primaries, second-order multiples are the spatial convolution of primaries and the first-order multiples, and so on. These steps are referred to the prediction of the multiple reflection model.

First, the forward model of surface-related multiples for the 1D situation is explained. The impulse response of the Earth is defined by and contains all primary and multiple reflections. When these events hit the free surface, they all reflect back into the medium. Hence each event in the primary response acts as a new source wave for the complete round trip. Each event from the impulse response will be convolved with the complete impulse response to become a sequence of the first-order multiples. The construction of the first-order surface-related multiples can be expressed as [1].

$$m_1(t) = -x_0(t) * x_0(t) \tag{3}$$

where the minus sign describes the reverse phase of the signal. Next, these events arrive at the surface again, and each first-order multiple acts as a source for the second-order multiples. Thus, the second-order multiples can be written as

$$m_2(t) = -x_0(t) * m_1(t) = x_0(t) * x_0(t) * x_0(t) \tag{4}$$

The total response *x(t)* with all surface-related multiples becomes a series as

$$x(t) = x_0(t) - x_0(t) * x_0(t) + x_0(t) * x_0(t) * x_0(t) - \ldots \tag{5}$$

The surface-related multiples response from the full wavefield can be expressed by a series of auto-convolutions as

$$x_0(t) = x(t) + [(x)t * x(t)] + [x(t) * x(t) * x(t)] + [x(t) * x(t) * x(t) * x(t)] + \ldots \quad (6)$$

For the 2D situation, the integral expression of multiple prediction is given by

$$M_0(x_r, x_s, f) = -\sum_{x_k} X_0(x_r, x_k, f) P(x_k, x_s, f) \quad (7)$$

where X_0 is the primary impulse response function, P is the total recorded field, x_s is the source location, x_r is the receiver location and x_k is the lateral coordinate over which the data are summed [14]. Fig. 3 illustrates the construction of the first-order multiple for 2D seismic data.

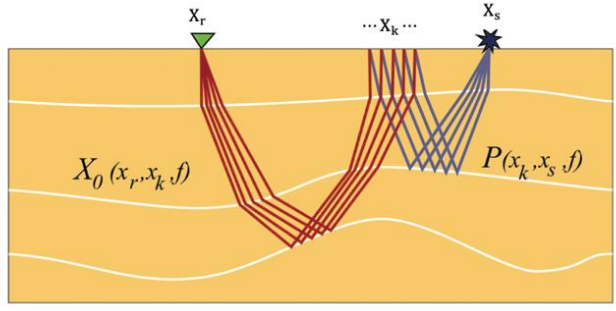

Fig. 3. *The construction of the first-order multiple [1].*

The model of multiple reflections from (7) is subtracted from the input data using a least-square method with a matching operator *A(f)* expressed as (8). The operator $A(f)$ is an inverse source property relating between data with and without multiples. The correct operator $A(f)$ obtains the minimum energy of multiples in the output [15].

$$P_0(x_r, x_s, f) = P(x_r, x_s, f) - A(f) M(x_r, x_s, f) \quad (8)$$

Parabolic Radon Filtering

The Radon transform is a mathematical technique having been widely used in the seismic data processing. This method transforms the input data from the offset-time (x-t) domain to the Radon domain, where it is modified and then transform back to the x-t domain. In this research, the parabolic Radon filtering is used for multiple removals. The forward parabolic Radon transform is expressed as

$$m(q, \tau) = \sum_{n=1}^{N} d(x_n, t = \tau + q x_n^2) \quad (9)$$

where $d(x_n, t)$ is the data in offset-time *(x-t)* domain, *N* is the number of traces and $m(q, \tau)$ is the data in parabolic Radon domain [10]. The transformed data are a

function of the curvature q and the zero offset intercept time τ. After a temporal Fourier transformation, the parabolic Radon transform is calculated for each temporal frequency component ω. The forward and inverse transform are expressed in (10) and (11), respectively [10].

$$M(q,\omega) = \sum_{n=1}^{N} D(x_n,\omega) exp(j\omega q x_n^2) \quad (10)$$

$$D(x_n,\omega) = \sum_{i=1}^{N_q} M(q_i,\omega) exp(-j\omega q_i x_n^2) \quad (11)$$

where $M(q,\omega)$ and $D(x_n,\omega)$ are the temporal Fourier transform of $m(q,\tau)$ and $d(x_n,t)$, respectively, and N_q is the number of q values.

Parabolic Radon filtering is the process based on the moveout differences between primary and multiple reflections in common depth point (CDP) gather. The schematic of parabolic Radon filtering is illustrated in Fig. 4. The normal moveout (NMO) correction with the velocities of primary reflections is applied to input CDP gather. After NMO correction, the primary reflections turn into straight lines and the multiple reflections turn into parabolas. The NMO corrected CDP gather is transformed to the $\tau - q$ domain by parabolic Radon domain transform, the primaries and multiples can be discriminated, and the multiples are muted out. The muted data is transformed back to the CDP domain, and the inverse NMO correction is applied to obtain the data without multiples.

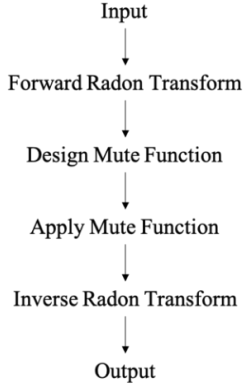

Fig. 4. *The procedure of parabolic Radon filtering.*

2D MARINE SEISMIC DATA

The 2D marine seismic data of the East Coast of the United States-Southern Atlantic Margin used for this research are the open data and available on the U.S. Geological Survey website. A number of survey lines were carried out approximately 25,000 km with multichannel seismic reflection survey between 1974 and 1978 to address hydrocarbon resource potential and stratigraphic history. The used dataset is a second quarter part of line number 31. The details of shot and receiver parameters collected from the USGS report and observer's log are shown in Table 1.

Table 1. *The information of 2D marine seismic data*

Line number	31
Distance	52250 m
Number of shots	999
Number of receivers	48
Shot interval	50 m
Group interval	50 m
Minimum offset	359 m
Maximum offset	2709 m
Trace length	12 s
Sampling rate	4 ms
Fold coverage	24

RESULT AND DISCUSSION

2D marine seismic data contain the long-period surface-related multiple reflections. Predictive deconvolution, surface-related multiple eliminations (SRMEand parabolic Radon filtering were conducted to remove surface-related multiple reflections. Predictive deconvolution was limited to suppress the long period of multiple reflections and dipping reflectors in 2D marine seismic data. The multiple reflections are remained as shown in Fig. 5 and Fig. 6 and indicated by the rectangle and the ellipse.

SRME and parabolic Radon filtering can efficiently remove surface-related multiple reflections. While SRME successfully removed near-offset multiple reflections, however far-offset multiple reflections had remained. For the reason that the construction of multiples model uses an approximate velocity from the input data. The amplitude between the estimated model of multiples and the original input data are different, especially in far offset. Thus, this situation limits the ability of SRME. However, the residual far offset multiple reflections were removed by parabolic Radon filtering.

The random noise appearing in 2D marine seismic data was very problematic. Due to this troublesome noise, the performance of multiple removal methods was limited. The stacked section at CDP numbers around 12000 to 13200 contains the noise obscuring the reflectors. SRME and parabolic Radon filtering could remove the most of multiple reflections, however they have remained. The residual multiple reflections in noisy data are shown in Fig. 7 and indicated by the rectangle. Nevertheless, Fig. 8 displays the results from the success of SRME and parabolic Radon filtering. The long period multiples reflections were almost removed, the results will not give any misunderstandings in the interpretation.

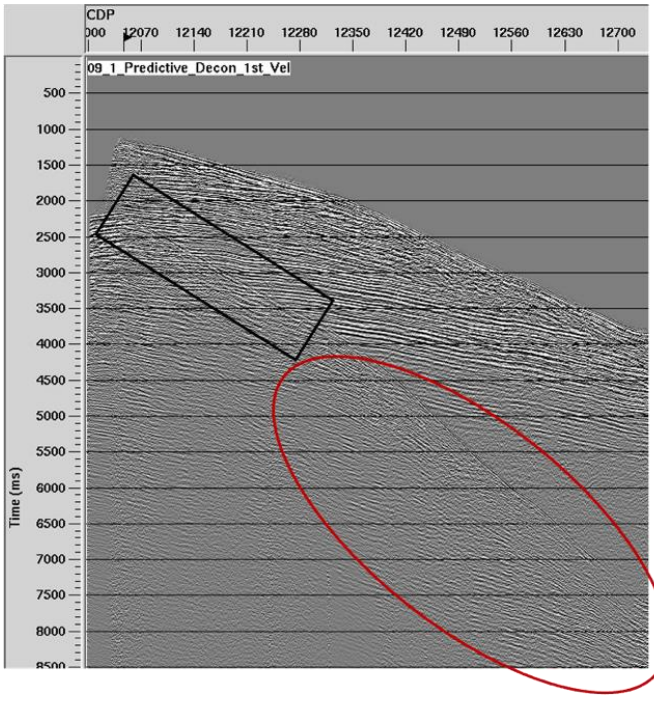

Fig. 5. *The stacked section of 2D marine seismic data at CDP numbers 12000 to 12730 from multiple removals by the predictive deconvolution.*

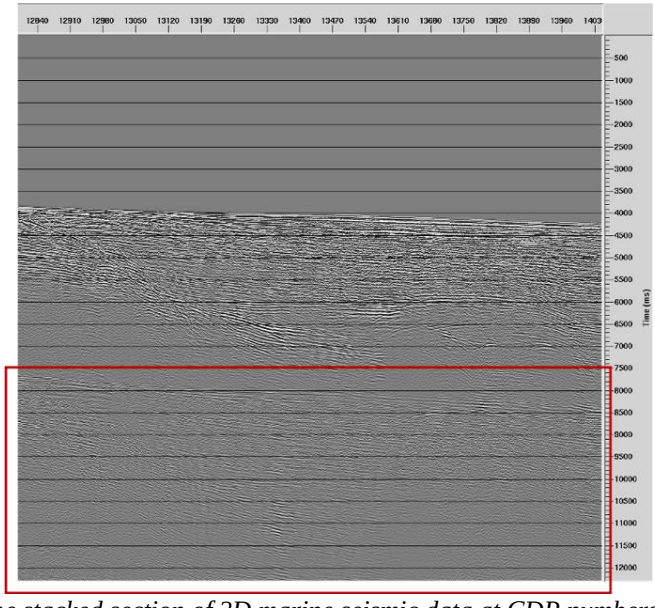

Fig. 6. *The stacked section of 2D marine seismic data at CDP numbers 12800 to 14030 from multiple removals by predictive deconvolution.*

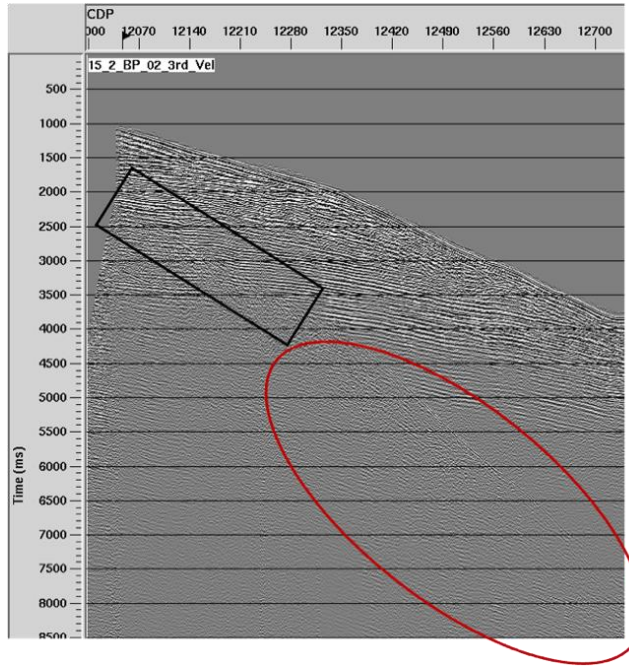

Fig. 7. *The stacked section of 2D marine seismic data at CDP numbers 12000 to 12730 from multiple removals by the combination of SRME and parabolic Radon filtering, respectively.*

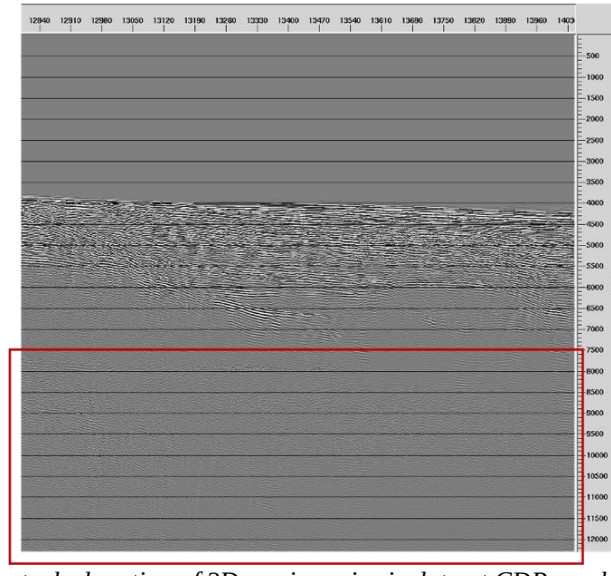

Fig. 8. *The stacked section of 2D marine seismic data at CDP numbers 12800 to 14030 from multiple removals by the combination of SRME and parabolic Radon filtering, respectively.*

CONCLUSION

This research used three multiple removal methods in order to analyze the long-period surface-related multiple reflections. The predictive deconvolution cannot attenuate the long-period multiple reflections in seismic data. The performance of the predictive deconvolution process is degraded when the multiple period changes, such as the dipping reflectors and the complexity of geological structures. SRME and parabolic Radon filtering are effective in removing long-period surface-related multiple reflections. The combination of these two methods increases signal-to-noise ratio. The near-offset multiples are effectively removed by SRME. The residual far-offset multiples are suppressed by parabolic Radon filtering. However, the performance of multiple removal methods is limited by the random noises obscuring the signals. The more noise is cleaned, the better results will be.

ACKNOWLEDGEMENTS

We would like to thank Halliburton for SeisSpace® ProMAX 2D software support and the U.S. Geological Survey for the dataset used in this research.

REFERENCES

[1] Verschuur D.J., Seismic multiple removal techniques: past, present and future. EAGE, Houten, 2013.

[2] Peacock K.L., Treitel S., Predictive deconvolution: Theory and practice, Geophysics, vol. 34, no. 2, pp 155-169, 1969.

[3] Schoenberger M., Houston L.M., Stationarity transformation of multiples to improve the performance of predictive deconvolution, Geophysics, vol. 63, no. 2, pp 723-737, 1998.

[4] Jian X., Zhu S., Predictive deconvolution for attenuation of multiple reflections in marine seismic data processing, Journal of Coastal Research, vol. 73, pp 310-314, 2015.

[5] Verschuur D.J., Berkhout A.J., Wapenaar C.P.A., Adaptive surface-related multiple elimination, Geophysics, vol. 57, no.4, pp 1166-1177, 1992.

[6] Naidu P., Santosh, Chand S., Saxena U.C., Surface related multiple elimination: A case study from east coast India, in Proc. 10th Biennial International Conference & Exposition, Kochi, 2013, p 217.

[7] Kim T., Jang S., Increasing signal-to-noise ratio of marine seismic data: A case study from offshore Korea, Journal of Applied Geophysics, vol. 134, pp 136-145, 2016.

[8] Hadidi M.T., Baumstein A.I., Kim Y.C., Surface-related multiple elimination on wide-tow marine data, The Leading Edge, vol. 21, no. 8, pp 787-790, 2002.

[9] Lester R., McIntosh K., Multiple attenuation in crustal-scale imaging: examples from the TAIGER marine reflection data set, Marine Geophysical Research, vol. 33, pp 289-305, 2012.

[10] Hampson D., Inverse velocity stacking for multiple elimination, in SEG Technical Program Expanded Abstracts, 1986, pp 422-424.

[11] Abbadi S., Jaiswal P., Attenuating ling-period multiples in short-offset 2D streamer data: Gulf of California, in SEG Houston 2013 Annual Meeting, 2013, pp 4201-4205.

[12] Dondurur D., Acquisition and processing of marine seismic data. Elsevier, Amsterdam, 2018.

[13] Kearey P., Brooks M., Hill I., An introduction to geophysical exploration. Third Edition, Blackwell Science Ltd, Oxford, 2002.

[14] Berkhout A.J., Seismic migration, imaging of acoustic energy by wave field exploration, Part A: theoretical aspects. Elsevier, Amsterdam, 1982.

[15] Berkhout A.J., Verschuur D.J., Integrated multiple elimination and source wavefield estimation, in SEG Technical Program Expanded Abstracts, 1993, pp 1095-1098.

MODIFICATION AND APPLICATION OF HIGH FREQUENCY SIGNAL RECORDER FOR ELECTRICAL EXPLORATION GEOPHYSICAL WORKS

Prof. Dr. Vadim Zhmud [1]
Dr. Vladimir Semibalamut [2]
Yury Fomin [3]
Aleksandr Rybushkin [4]
Prof. Dr. Lubomir Dimitrov [5]
[1] Novosibirsk State Technical University, Novosibirsk, Russian Federation
[2, 3, 4] Siberian Branch of the Federal State Budgetary Inst. of Science of the Federal Research Center "Unified Geophysical Service of the RAS", Novosibirsk, Russia
[5] Technical University of Sofia, Sofia, Bulgaria
[1] Institute of Laser Physics SB RAN

ABSTRACT

Electrical research in geology is used quite widely and with great efficiency. The use of ready-made signal recorders for these purposes is possible, but not effective enough, since in any case, they need to be modified to provide additional functions. Such functions include the synchronization of measurements with signals from positioning systems GPS or GLONASS. This synchronization is necessary in order for the measurement results to be linked to actual space and time coordinates as accurately as possible. The same measurements taken at different times may give different results due to changes in the orientation of the Earth relative to the Sun and Moon, as well as for other uncontrollable reasons. The need to accurately determine the coordinates of the measurement is obvious. The creative team of the commonwealth of organizations, the key of which is the Siberian Branch of the Federal State Budgetary Institution of Science of the Federal Research Center "Unified Geophysical Service of the Russian Academy of Sciences", carried out the development and initial testing of a specialized signal recorder for electrical research. The additional modification was required to eliminate the identified deficiencies. This paper reports the main technical solutions when creating this recorder, describes the modification ,and gives an example of using this recorder for field measurements.

Keywords: *electrical measurements, electrical control, geoinformatics, informatics, ADC, DAC, GPS, GLONASS*

INTRODUCTION

Fundamental research in the field of geology and geophysics requires the use of a variety of methods for obtaining information about the structure of the earth's crust and processes in it. The study of these processes is not only of great theoretical importance, since it allows us to better understand the structure of the most important natural object for mankind - the Earth, but also an important practical

application. One of the most important practical tasks is to find precursors of earthquakes and other cataclysms and use them to predict the place and strength of upcoming cataclysms. This helps to reduce the damage from these natural phenomena. Methods for studying the earth's crust can be divided into stationary and mobile. Stationary research facilities are installed in mines and operate around the clock to monitor various processes, for example, to monitor lunisolar tidal movements of the earth's crust [1], [2]. Mobile methods include electrical reconnaissance methods, which consist in measuring electrical and electromagnetic signals of various nature, including responses to various influences. In a geophysical experiment, various impact generators can be involved. Electrical recorders are an obligatory component of the instrument park for electrical prospecting. Such recorders always contain several channels of analogue-to-digital conversion and means of recording and processing the received data streams [3], [4], [5], [6], [7].

If commercial electro measuring and recording devices (further – recorders) are available for such studies and their specifications meet the requirements, then there is no need to develop prototypes of such recorders. The totality of a large number of requirements for such recorders has led to the fact that the acquisition of a ready-made recorders is impossible, and the use of a commercial meter, which is additionally modified to obtain the required characteristics, is impractical, since the most irrational way to create the required equipment is to modify other people's developments. It is more efficient to use completely your own development of the recorder. The list of requirements includes high accuracy, high sensitivity, wide bandwidth, uniform transmission characteristics and synchronization of measurements with absolute time from a global positioning system such as GPS or GLONASS. It is also necessary to determine the geographic coordinates of the measurement site using signals from the same systems. This paper analyses the technical solutions for creating such a recorder and the hardware for synchronizing with the signals of the global positioning system.

STATEMENT OF THE PROBLEM

The recorder is a multichannel ADC with functions of synchronization of measurement results with data received in real-time from global satellite systems. The device is provided with special software, developed on the basis of the demanded function of the signal processing. Critical requirements are autonomous communication with global systems and low-time error. The frequency band should ensure reception of signals up to 256 kHz with minimal distortion; also, to save memory and traffic, a dichotomous reduction of the frequency band is provided, i. e. reduction in multiples of two to an integer power to a minimum value of 16 kHz. Accuracy of registration of signals should correspond to a twenty-four-bit ADC. When changing the signal amplitude, in order to maintain the value of relative accuracy, it is necessary to proportionally match the range of the input signal with the range of admissible input signals of the ADC. This is achieved by changing the gain of the input amplifier. Accordingly, the gain changes from a value of 1 to a value of 64 on four bands, thus, each band differs in gain from the neighboring one by 4 times. Also, the accuracy of synchronization of the received samples with the

absolute time from the global satellite system is required with an error of no more than 500 ps, this value is called jitter.

METHOD FOR SOLVING THE PROBLEM

The proposed block diagram of the electric signal recorder is shown in Fig. 1. The recorder is provided with galvanic isolation, differential input, deep common mode interference suppression, switchable gain, differential filter amplifier with switchable frequency range, and other units. In particular, there is a unit with an antenna for receiving signals from global satellite systems, there is also a synchronization unit “Real Time” and a data buffering unit “Buffer”, a communication interface “MCU I/O” with a microcontroller. For synchronization purposes, an auxiliary precision clock generator is used, the frequency of which is synchronized with the precise time signals from the global positioning system using a phase-locked loop. The phase-locked loop system is controlled digitally using a DAC. The control microcontroller generates the corresponding code at the input of this DAC to control the generator in a loop with negative feedback based on the phase difference between the reference signal and the signal from the output of the tunable generator. The functions of generating the exciting current are also implemented, which is necessary for various experiments. The recorder can be controlled using the control panel on the device, i. e. manually. It is also possible to program the recorder to perform a series of sequential measurements without operator intervention. The measurement results can be stored in the recorder or transmitted for further processing further via a wired communication line. The input differential amplifier gain is ± 2 V.

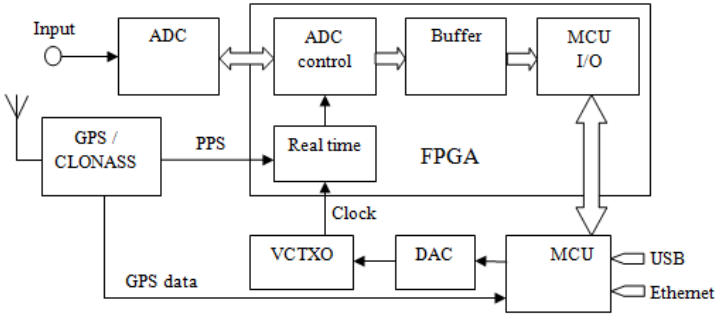

***Fig. 1**. Block diagram of the recorder*

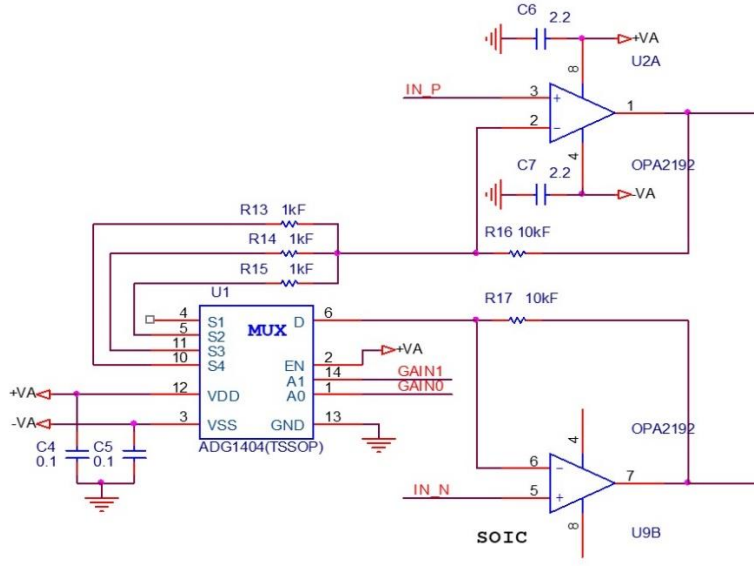

Fig. 2. *Schematic diagram of the input differential instrumentation amplifier*

Accuracy, speed and other characteristics of the recorder are determined by the input circuits, the type of ADC and the quality of synchronization. The input ADC is proposed to be implemented on the basis of the 24-bit sigma-delta-ADC ADS127L01 [8]. This microcircuit turns on normally, so there is no need to give a schematic diagram. The schematic diagram of the input amplifier is shown in Fig. 2. This amplifier, under the action of the program or controls, can change the gain in multiples of 4. The schematic diagram of the input filter is shown in Fig. 3. This filter can change the frequency band by a factor of 2. The entire electronic part, including the input amplifiers, filters, ADC, control device for ADC, stabilized reference voltage sources, oscillator, DAC and synchronization circuit is located on a 90 × 90 cm^2 board. The appearance of this board is shown in Fig. 4, and the appearance of the assembled recorder is shown in Fig. 5. Power stabilizers are based on APD3331 and REF5025 microcircuits. The recorder inputs are protected from static and induced discharges. Common-mode voltage is suppressed by a differential amplifier circuit.

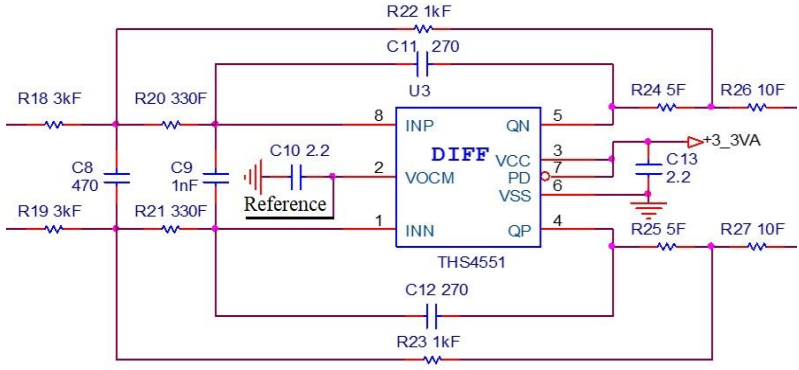

Fig. 3. *Schematic diagram of the differential filter*

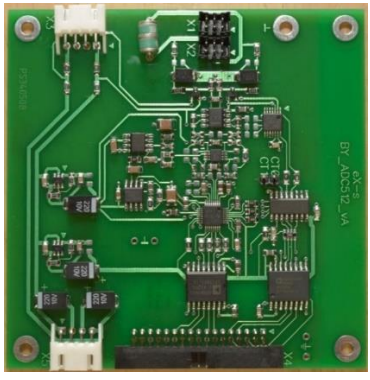

Fig. 4. *Printed circuit board of the recorder with installed electronic components*

Fig. 5. *External view of the signal recorder for electrical exploration*

PROVIDING COMMUNICATION WITH A POSITIONING SYSTEM

The block diagram for communication with global positioning systems is shown in fig. 6. The appearance of the corresponding section of the printed circuit board, on which this block is implemented, is shown in fig. 7. The recorder, which contains all the described nodes, is shown in fig. 8, where the node for communication with global positioning systems is located closer to the front panel of the recorder. The synchronization error of the clock (every second pulse) of the installed node does not exceed 20 ns. This GPS_PPS signal is fed as a clock to the "Real time" node in the FPGA (field-programmable gate array) synthesizing system time stamps. The clock frequency for the time synthesizer is generated by a voltage controlled temperature compensated precision oscillator of 16.384 MHz.

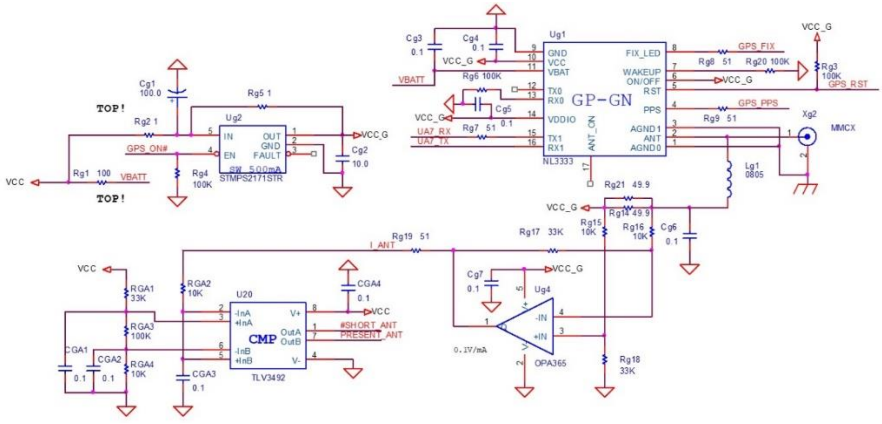

Fig. 6. *Schematic diagram of the connection for GPS-GLONASS node*

Fig. 7. *GPS-GLONASS node installed on the board*

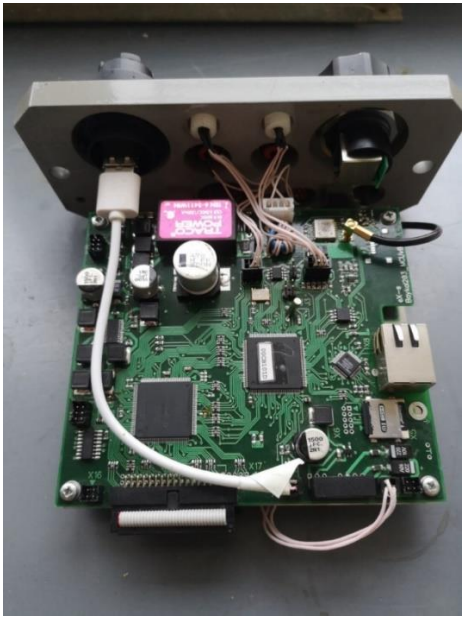

Fig. 8. *External view of the recorder without a protective casing*

RESULTS OF TESTING OF THE RECORDER

The electrical prospecting measurements were carried out by the method of sounding the formation of the field in the Uimon Hollow of the Altai Mountains. An experiment was carried out to register the process of field formation on pk119 area with two sets of measuring equipment. Figure 9 shows a field work area, designated pk119 area, which is located in the centre of the intermontane basin. Figure 10 shows the distribution of the electrical resistance of the sedimentary cover

to the depths of the basement, calculated from the transient process registration data. The measurements were carried out with equipment with a sampling frequency of 100 kHz. At this point, an experiment was carried out with the registration of the transient process of the formation of the field by equipment with a sampling frequency of 512 kHz. The parameters of the installation of radiation and registration of the signal of the field formation in the experiment were as follows: the generator loop of the GP 250 × 250 meters, the measuring loop of the IP 100 × 100 meters is passive, the measurements were carried out at two levels of the current pulse, a large one of about 18.0 ÷ 3.1A currents in the transmitter loop and at different gains in the receiving loop (K_1 = 1; K_2 = 16).

Fig. 9. *Site of work named pk119 area*

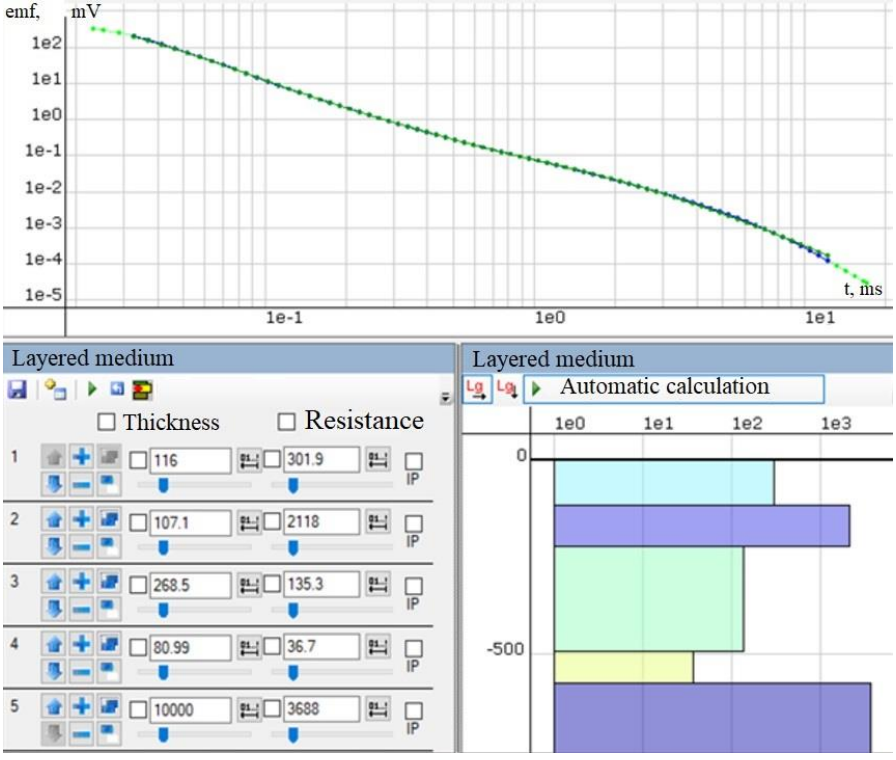

Fig. 10. *Geoelectric models based on the ZS 2019 data, Uimon Hollow, pk119 area (EMF vs time)*

The results of comparing the recorded processes of the formation of the field by two sets of measuring equipment with different values of the digitization frequencies are shown in Fig. 11.

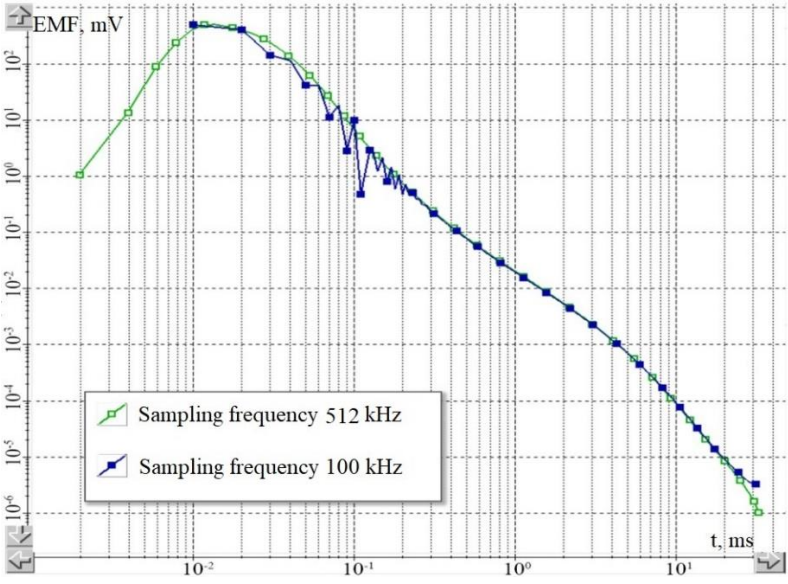

Fig. 11. *Results of experiments at different quantization frequencies in the pk119 region (EMF vs time)*

An analysis of the comparison of registration processes leads to the following conclusions:

1. The initial registration time by the equipment is 2 μs, which makes it possible to improve the detailing of the upper part of the geological section when constructing a geoelectric model.

2. In the range of recording times up to 200 μs with equipment with a sampling frequency of 100 kHz, an oscillatory process is observed, which is associated with the parameters of the ADC. There are no oscillations in the recorded process of field formation by equipment with a sampling frequency of 512 kHz.

3. In the late stage of the formation of the field at times of the order of 20–30 ms, the equipment with a sampling rate of 512 kHz more confidently reflects the deep part of the geological section.

CONCLUSION

The developed recorder has been successfully applied for field tests. Its characteristics correspond to the required values or exceed these values, for example, in terms of the accuracy of the reference of the readings to the absolute time scale from the global satellite system. The information obtained is of scientific interest for geophysical research in the Mountain Altai region.

Field test results:

1. The sampling frequency of 512 kHz made it possible to more reliably register the process of formation of the EMF of the transient process in the time interval 0.002–0.2 ms.

2. In the time interval from 0.2 ms to 30 ms, the error in registering the processes of EMF formation of the transient process lies in the interval less than 1%.

3. In the late stage of registration at a time of 30 ms, the registration level with frequent digitization of 512 kHz is $+1.0 \cdot 10^{-6}$ mV, which is much better than the registration level with a frequency of 100 kHz ($5.0 \cdot 10^{-6}$ mV). The levels of the recorded signals are given with the parameter of the installation with radiation at a current in the generator circuit of 1A.

REFERENCES

[1] A.Yu. Rybushkin, Yu.N. Fomin, V.A. Zhmud, V.A. Vasil'ev, N.A. Kusyakin, V.M. Semibalamut, and L.V. Dimitrov, “Results of Measurements of Ultra-Small Deformations of The Earth's Crust at The Talaya Observatory Near Baikal Lake”. GEOLINKS 2019 International Scientific Conference, 26-29 March, Athens, Greece, ISSN 2603-5472, ISBN 978-619-7495-02-7, GEOLOGY Section. ISBN 978-619-7495-02-7. DOI: 10.32008/GEOLINKS2019/B1/V1.

[2] V.A. Zhmud, V.M. Semibalamut, L.V. Dimitrov, Yu.N. Fomin, “Optoelectronic intellectual systems for monitoring of Earth seismic dynamics: results and developing directions”, 16th International Multidisciplinary Scientific GeoConference CGEM 2016. Conference proceedings. Book 1. Dcience and Technologies in Geology, Ecploration and Mining. Volume III. P. 567–574. ISSN 1314-2704. DOI: 10.5593/sgem2016B13. URL: www.sgem.org.

[3] J.G. Huang, B.Y. Ruan, and J.L. Wang, “A study on the anomaly of borehole-to-ground joint resistivity surveying system,” Chin. J. Geophys., vol. 52, no. 5, pp. 1348–1362, 2009.

[4] C. Rujun, L. Weibing and H. Jishan, "High Precision Multi-frequency Multi-function Receiver for Electrical Exploration," 8th International Conference on Electronic Measurement and Instruments, 2007, pp. 1-599-1-601, doi: 10.1109/ICEMI.2007.4350521. https://ieeexplore.ieee.org/document/4350521

[5] I. Shirokov, E. Redkina and E. Shirokova, "Design of Receiving Inductive System for Equipment for Electrical Exploration of Earth's Crust," 2018 International Multi-Conference on Industrial Engineering and Modern Technologies (FarEastCon), 2018, pp. 1-4, doi: 10.1109/FarEastCon.2018.8602583. https://ieeexplore.ieee.org/document/8602583

[6] A.A. Murasev and A.A. Spektor, "Estimation of signals of airborne electrical exploration of mineral products," 2012 IEEE 11th International Conference on Actual Problems of Electronics Instrument Engineering (APEIE),

2012, pp. 42-47, doi: 10.1109/APEIE.2012.6628991. https://ieeexplore.ieee.org/document/6628991

[7] G.Q. Xue, N. N. Zhou, W.Y. Chen, H.Li, and S. Yan, “Research on the application of a 3-m transmitter loop for TEM survey in mountainous areas,” J. Environ. Eng. Geophys., vol. 19, no. 1, pp. 3–12, 2013.

[8] ADS127L01 24-Bit, High-Speed, Wide-Bandwidth Analog-to-Digital Converter. https://www.alldatasheet.com/datasheet-pdf/pdf/833555/TI1/ADS127L01.html

MULTICOMPONENT DEPOSITS WITH BY-PRODUCT AS THE MAIN SOURCE OF FELDSPAR RAW MATERIALS FOR MODERN TECHNOLOGIES

Dr. Geol.-Mineral. Sci., Dr. Geogr. Sci., Dr. Eng. Sci., Prof. Georgii Rudko[1]
Assoc. Prof. Ph.D. Mariia Kurylo[2]
Ph.D. Student Maksym Ozerko[3]
[1] State Commission of Ukraine on Mineral Resources, Kyiv, Ukraine
[2, 3] National Taras Shevchenko University of Kyiv, Kyiv, Ukraine

ABSTRACT

Feldspar is raw materials with a growing volume of production every year, as well as a price for it. Feldspar consumption has been gradually increasing in ceramics, glass industry for solar panels, housing, and building construction.

Feldspar raw materials include intrusive, effusive rocks, weathering crust of crystalline rocks, sedimentary altered and altered rocks, as well as partially medium and basic aluminosilicate rocks. It was defined an industrial application for each species of feldspar. Potassium feldspars (orthoclase, microcline, sanidine) are used in electroceramic, electrode, abrasive, and ceramics industries. For these productions, the potash module is fixed in a ratio of 2: 1. For some industries, in particular the manufacture of high-voltage ceramics, the necessary feldspars are as close as possible to pure potassium (with a modulus of at least 4: 1, which corresponds to 80% of the orthoclase component). Potassium-sodium raw materials, from a potassium modulus of at least 0.9, are used for building construction. Sodium minerals with non-standardized potassium modulus are used for the glass industry, the production of enamels, and products such as vitreous porcelain. Calcium feldspars, represented by plagioclase of higher numbers, have limited practical application and their presence in feldspar concentrates is undesirable.

According to mineral associations, all types of feldspar raw materials can be divided into five types: 1) feldspar (syenites, trachitis); 2) quartz-feldspar (pegmatites, granites, sands, etc.); 3) nepheline-feldspar (nepheline syenites, alkaline pegmatites); 4) quartz-sericite-feldspar (shales, secondary quartzites); 5) quartz-kaolinite-feldspar (sands, alkaline kaolins, secondary quartzites).

It is shown on the example of Ukrainian deposits of feldspar minerals that complex deposits with by-products become the main source for production. Especially if these are new mining operation facilities. The authors have identified three main types of such complex multicomponent deposits: 1) deposits of intrusive rocks where weathering crust of crystalline rocks are mined as a byproduct; 2) complex deposits, where feldspar rocks are enclosing or overburden and can also be considered as byproducts; 3) deposits where feldspar concentrate can be produced as a product of ore components processing.

Keywords: *feldspar minerals, by-product, multicomponent deposit, Ukraine*

INTRODUCTION

Feldspar is raw materials with a growing volume of production every year, as well as a price for it. Feldspar consumption has been gradually increasing in ceramics, glass industry for solar panels, housing, and building construction.

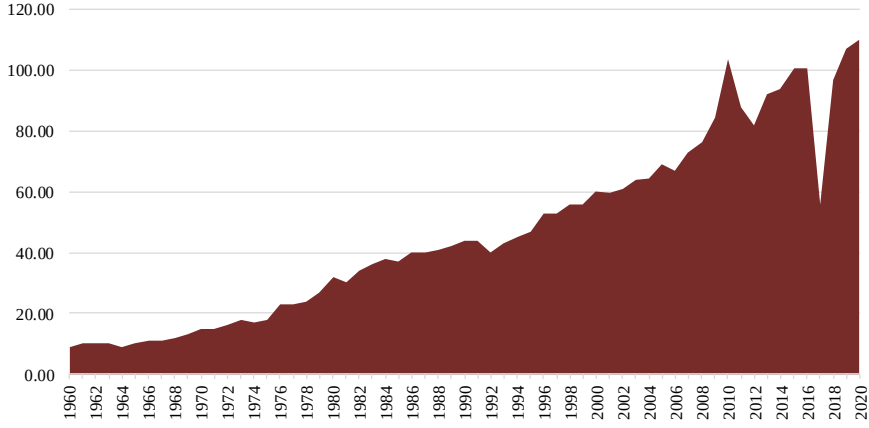

Fig. 1. *Feldspar price dynamics (according to statistical data usgs.gov [3])*

Feldspars deposits are divided into three main groups: potassium feldspars - (orthoclase, microclines) $K_2OAl_2O_3{\times}6SiO_2$, sodium feldspars - (albites) $Na_2OAl_2O_3{\times}6SiO_2$ and calcium feldspars - (anortites) $CaOAl_2O_3{\times}2SiO_2$, which are present to varying degrees in all crystalline rocks. Potassium feldspar is the primary rock-forming mineral of many igneous metamorphic and sedimentary rocks. In addition to the main groups, there are other feldspars, such as barium feldspar – $BaOAl_2O_3{\times}2SiO_2$ (celsian), but they are rarely used in ceramics. The primary parameter that characterizes feldspar concentrates is the potassium modulus (ratio K_2O:Na_2O).

According to modern concepts, feldspar raw materials include intrusive, effusive rocks, weathering crusts of crystalline rocks, sedimentary unaltered and altered rocks, as well as partially medium and basic aluminosilicate rocks.

Each type of feldspar has its field of industrial application:

- potassium feldspars (orthoclase, microcline, sanidine) are used in the electroceramic, electrode, abrasive and porcelain-earthenware industries. The potassium modulus for the porcelain-earthenware industry has been established in the ratio of 2:1. Feldspars as close as possible to pure potassium (with the modulus not less than 4:1 corresponding to 80% of the orthoclase component) are essential in several productions, particularly the production of high-voltage porcelain;
- potassium-sodium raw materials, with a potassium modulus of at least 0.9, are used in ceramic building materials;

- sodium raw materials with non-standardized potassium modulus are used in the glass industry, the production of enamels and products such as vitreous china;
- calcium feldspars represented by plagioclase of higher numbers have limited practical application, and their presence in feldspar concentrates is undesirable.

According to mineral associations, feldspar raw materials can be divided into five types:

- feldspar (syenite, trachyte);
- quartz-feldspar (pegmatites, granites, sands, etc.);
- nepheline-feldspar (nepheline syenites, alkaline pegmatites);
- quartz-sericite-feldspar (shales, secondary quartzites);
- quartz-kaolinite-feldspar (sands, alkaline kaolins, secondary quartzites).

Total balance reserves of feldspar raw materials as of 01.01.2020 amounted to 49109.07 thousand tonnes by categories A+B+C_1, cat. C_2 – 192703.8 thousand tonnes, off-balance – 192.91 thousand tonnes. The total production of feldspar raw materials in Ukraine amounted to 634.63 thousand tonnes in 2019 [1], [6], [7]. It is comparable to major global producers.

There are the following types of deposits in Ukraine:

1. Pegmatite deposits: Bilchakivske, Ustia village, Hruzlivetske, Lozuvatske, Volodymyrivske, Balka Velykoho Taboru;
2. Deposits of crystalline rocks: trachytes of the Verbova site, microgranodiorites of the Dubrynetske deposit;
3. Alkaline kaolins: Prosianivske, Pershozvanivske, Biliayivske, Katerynivske;
4. Multicomponent deposits (feldspar raw materials as a by-product): Bakhtyn (fluorite ores), Nosachivske (titanium-ilmenite ores), Perzhanske deposits of rare metals, Mazurivske (tantalum and niobium ores).

Currently, only the pegmatite deposit “Balka Velykoho Taboru” is being developed, and a special permit for the extraction of pegmatites from the “Hirne” deposit is invalid.

Feldspar raw materials were extracted from crystalline rocks - Dubrynytske deposit of microgranodiorite (Transcarpathian region), which occurs in the flysch rocks of the Carpathian Mountains in the form of a dyke-like body. The deposit was developed by OJSC “Steatyt”. Also, work was conducted to study trachytes of the Verbova site in the Telmanovo district of Donetsk region.

According to the analysis of feldspar raw material production, it is noted that the increase in feldspar raw material production is observed primarily in complex multicomponent deposits - the Piatyrichka section of the Dubrivske deposit and the Novakivska site of the Maidan-Vilske deposit, where alkaline kaolins, hard feldspar

and feldspar crystalline rocks (granites, migmatites, plagiogranites, pegmatoid granites) are developed.

The most significant object of additional study of feldspar raw materials is the Piatyrichka site of the Dubrivske deposit, which is being exploited. The Piatyrichka site of the Dubrivske alkaline kaolin deposit is located at a distance of about 400 m north of Hlynianka village (until 2016 - Piatyrichka) in the Baranivka district of Zhytomyr region.

Until 2019, the Piatyrichka site of the Dubrivske deposit was developed as a deposit of primary kaolins approved in 1991 by the protocol of the CCMR SE "Ukrbudmaterialy" in the amount of 614 thousand tonnes as raw materials for the production of refractory bricks. During 2019-2020, it was performed a geological and economic reassessment of primary kaolins as alkaline kaolins at the Piatyrichka site of the Dubrivske deposit with their reevaluation associated with a new direction of use and additional exploration of the lower part of the kaolin deposit – feldspar scree as feldspar raw materials, as well as underlying crystalline rocks (granites, migmatites, plagiogranites, pegmatoid granites) as feldspar raw materials. The quality of alkaline kaolins, feldspar scree and underlying crystalline rocks were determined by the content of SiO_2, Al_2O_3, Fe_2O_3, TiO_2, K_2O and Na_2O. In addition, the quality of crystalline rocks (granites, migmatites, plagiogranites, pegmatoid granites) as feldspar raw materials was previously studied.

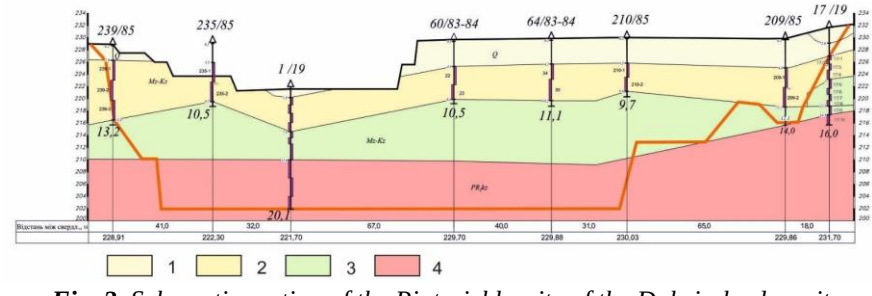

Fig. 2. *Schematic section of the Piatyrichka site of the Dubrivske deposit (according to data of the PC "Geolog")*

1 – sedimentary rocks (Q), 2 – alkaline kaolins (Mz-Kz), 3 – feldspar scree (Mz-Kz), 4 – feldspar crystalline rocks (granites, migmatites, plagiogranites, pegmatoid granites).

Table 1. *The quality of alkaline kaolins, feldspar scree, and underlying crystalline rocks of the Dubrivske deposit*

№	Component (indicator)	Content of the component (value of the indicator)		
		alkaline kaolin	feldspar scree	crystalline rock
Chemical composition (for calcined substance)				
1.	SiO_2 content, %	72,05-75,75	72,87-74,81	71,16-73,96
2.	Al_2O_3 content, %	17,55-18,63	15,33-16,17	15,12-15-64
3.	Fe_2O_3 content, %	0,64-0,68	0,61-1,16	1,10-1,15
4.	TiO_2 content, %	0,13-0,15	0,07-0,09	0,07-0,09
5.	K_2O+Na_2O content, %	6,07-6,86	7,71-7,96	8,40-8,56
Mineralogical composition				
6.	Feldspar, %	30-40	40-60	55-65
7.	Quartz, %	20-30	20-30	20-30
8.	Mica, %	2-5	2-5	2-5
9.	Kaolinite, %	30-40	5-25	0-5

It has been noted that the content of feldspars decreases from the bottom up due to the kaolinization of plagioclase, the content of alumina increases from the bottom up and accumulates in alkaline kaolins. The content of iron oxide is low. The refractory value of alkaline kaolins at the Piatyrichka site of the Dubrivske deposit was 1380-1710 C, feldspar scree – 1320-1580 C, and crystalline rocks – not determined.

Technological tests of laboratory-technological samples to check technological parameters of feldspar masses production in the industrial conditions were carried out at the ISU "Ceramic tile plant" of LLC Epicenter K in ceramic masses with the following content of raw materials.

Table 2. *Technological parameters of feldspar masses production*

№ ceramic mass	Content index			
	clay PJSC "Vesko"	alkaline kaolin site "Piatyrichka"	feldspar scree site "Piatyrichka"	pegmatite
Ceramic mass № 1	40,0	5,0	15,0	40,0
Ceramic mass № 2	40,0	10,0	10,0	40,0

Obtained ceramic masses were ground up and demagnetized from ferrous and weakly magnetic materials using a rod magnet. A mixture of masses was prepared; its technological parameters met the production and state technological requirements B B.2.7-117-2002 "Ceramic tiles for floors. Technical conditions". Currently, the ISU "Ceramic tile plant" of LLC Epicenter K uses both alkaline kaolin and feldspar raw materials for the manufacture of ceramic tiles [7], [9].

One of the complex multicomponent deposits of feldspar raw materials is the Mazurivske deposit of rare metal nepheline-feldspar ores (niobium, tantalum, zirconium) with approved reserves. It is one of the first discovered zircon deposits, where the industrial significance of the discovered ores was established in the course of exploration works in 1934-1948. The Mazurivske deposit was considered as a formation containing 2 ore types: zircon ores of the alkaline complex and

ilmenite ores of basic and ultrabasic rocks. The deposit was operated until 1967 when it was preserved with the advent of cheaper raw materials of the Vilnohirsk Mining and Metallurgical Plant. Due to the absence of an economic technological enrichment scheme, metals were not processed and were sent in the form of sludge (99% of the initial volume of ore) to dumps, where they were stored. About 2 million tonnes of ore were processed. Currently, accumulated "tailings" of the enrichment plant contain nepheline, feldspar, pyrochlore, rare metal, and rare earth minerals, and it is a technogenic deposit – a potential source of feldspar.

44 ore bodies were found at the deposit (Mazurivske ore node), including 10 within the studied area (within the project quarry). Ore bodies are traced at considerable distances, often more than 1000 m for some bodies. Their width is mostly more than 300 m, and the thickness varies from 1 to 45-80 m. Contacts of ore bodies with host rocks are clear, rapid, well-mapped visually in the core holes [4], [5], [8].

The deposit belongs to the geological-industrial type of rare metal albitite associated with nepheline syenites. The main industrial type of ore is disseminated, complex tantalum-niobium-zircon ore. The main carrier of niobium and tantalum is pyrochlore, zirconium – zircon. According to the content of conditional tantalum pentoxide, the generalizing conditional indicator that takes into account the contribution of each basic component to the cost of production, poor (common in various bodies from 16 to 33%), ordinary (28-58%), rich (15-55%) and very rich ores (0-2%) were identified within the deposit. Average contents of useful components (niobium, tantalum pentoxides and zirconium dioxide) in ores of the whole deposit were: 0.118%; 0.0057% and 0.47%, respectively; in the bodies of the detailed block - 0.116%; 0.004% and 0.49%. The distribution of niobium, tantalum and zirconium oxides in industrial bodies was uneven and extremely uneven.

During 2003-2004, state geological enterprise "Donetskgeologiya" carried out exploration works for geological and industrial assessment of technogenic enrichment wastes of the Mazurivske rare metal deposit on the area of 8.5 hectares. In 2005, the SCMR estimated the amount of feldspar raw materials in the dumps of the Eastern part of the deposit in the amount of 1133.5 thousand tonnes. Besides, the presence of associated mineral resources in the processing waste was detected in the amount of niobium pentoxide - 1053 tonnes, with the average content of Nb_2O_5 in the mineral - 0.09%, zirconium dioxide - 1313 tonnes, with the average content of ZrO_2 in the mineral - 0.11%.

During 2014-2016, LLC "Azov-Mineraltekhnika" carried out researches and developed technological regulations for feldspar raw materials. Test results showed the suitability of the material for the colored packaging glass production. Following the test results, LLC "Azov-Mineraltekhnika" developed technical conditions "Alkaline aluminosilicate flux".

Tests of feldspar concentrate with a low content of iron oxides in the ceramic tile and sanitary ware production showed that the material contains impurities, which give a darker color of the ceramic mass when firing ceramics, compared to feldspar materials of other manufacturers (with the same iron oxide content). Thus, feldspar concentrates from the enrichment waste of weathered ores of the

Mazurivske deposit with Fe_2O_3 content up to 0.5% in ceramic production are of limited use - for the production of ceramic products that are covered with opaque glaze. Calculations of technical and economic indicators characterize the economic feasibility of reserve development of the Eastern section of the weathered ore enrichment waste storage of the Mazurivske rare metal deposit [4], [5], [8].

As of 2020, balance reserves of feldspar raw materials of the Eastern section of the weathered ore enrichment waste storage amount to 826 thousand tonnes. Besides, ZrO_2 reserves in the amount of 510.8 tonnes with an average content of 0.172% and Nb_2O_5 - 283.3 tonnes, with an average content of 0.095% were calculated.

Processing stored waste allows us to free up large areas of tailings and eliminate the source of potential environmental hazard given the existing connection of tailings with the river Kalchyk basin. However, a base of feldspar raw materials can be created for the ceramic industry quite quickly and without significant investment [2]. Such production will become a testing ground for the preparation of the complex development of the Mazurivske deposit.

Due to the growing demand for rare metal raw materials, the Perzhanske ore field, within which there is the Perzhanske beryllium deposit, is of particular interest; it is represented so far by the only industrial-genetic and technological type of high-quality phenakite-genthelvin ores in alkaline (feldspar) metasomatites.

Two sites have been explored at the field: Pivnichna (5,5x1,5 km) and Krushynska (4,0x2,0 km). Ore zones occur with the extension of basic structural elements of the Sushchano-Perzhanska zone, their length reaches 5 km with a width of up to 35-100 m. Ore zones have been traced up to 400 m in depth. Each ore zone consists of a series of en echelon ore bodies with a thickness of a few meters up to 20-30 m. Ore bodies are composed of feldspar and mica-quartz-feldspar metasomatites, they form lenticular and vein-like formations of complex shape (characteristic swellings, obtuse wedging) deposits with rich genthelvite (genthelvite – $Zn_4 (BeSi_2)_3S$) mineralization (average BeO content is 0,55 %, maximum content - 8%). Ore bodies are bordered by a strip of 5-30 m of granite with blue newly formed quartz. The upper parts of ore bodies are composed primarily of albite-microcline metasomatites, the lower parts – mica-quartz-feldspar metasomatites. Phenakite mineralization, which is formed at an early stage of mineral formation, is spatially separated from the genthelvite one and localized primarily in the western part of endocontact of the Perzhanskiy granite massif forming a poor (average BeO content - 0.2%) impregnated mineralization. Cassiterite, columbite, and zircon are present as accessory minerals [10], [11].

The Perzhanske ore field is located in the central part of the Sushchano-Perzhanska tectonic-metasomatic zone of the north-eastern extension (north-western part of the Volyn megablock of the Ukrainian Shield), at its junction with the latitudinal North Ukrainian linear zone of tectonic activation [4]. This ore field together with Yastrubetske, Yurivske and Sushchanske ore-bearing fields form the Perzhanskiy ore district within the Sushchano-Perzhanska structural-metallogenic zone [10], [11].

Studies of the chemical composition of rocks in the Perzhanskiy ore node have shown that the amount of K_2O+Na_2O is 6,9-12,8 % in hydrothermal-metasomatic formations (syenites, granites, metasomatites) with a potassium modulus of 0,6-1,9, and they can serve as a material for feldspar concentrates, which will increase economic attractiveness.

One way to increase the investment attractiveness of deposits is the complex development of various ore objects in the ore field by one mining and processing plant, which would allow producing commodities for different purposes (beryllium oxide, zinc sulfide, ilmenite, apatite, disthene, zircon, rare earth, fluorite and feldspar concentrates) to ensure the development of electronic, nuclear, automotive and aviation industries and highly profitable agriculture.

It should be noted that the Mazurivske and Perzhanske deposits of rare metals are classified as priority development objects.

There are other multicomponent deposits with feldspar raw materials as a co-product - Bakhtyn (fluorite ores), Nosachivske (titanium-ilmenite ores).

Bakhtyn fluorite deposit is located in Murovanokurilovetsky district of Vinnytsia region. The deposit is confined to the Olchedaevsky and Yampolsky feldspar-quartz sandstones of the Vendian age. Deposit consists of two ore bodies (upper and lower) of a sheet-like form, consisting of disconnected lenticular bodies on an area of 700 x 1200 m, the depth of occurrence is 21.3–118.5 m. The total thickness of fluorite-containing sandstones varies from 0,4 to 4.7 m, and the fluorite content in them ranges from 5 to 48.9% (average 15%). Fluorite in sandstones is a typical epigenetic mineral replacing cement, partly quartz and feldspars. The Bakhtyn fluorite deposit is planned to be developed with an underground mine with a life of mine more than 20 years. During the operation of the deposit and flotation processing of ores, more than half of the commodity product will be feldspar concentrates.

Nosachivske apatite-ilmenite deposit is located in the Smelyansky district of the Cherkasy region of Ukraine. The deposit consists of two elongated sheet-like deposits. The length of ore bodies along the strike is up to 2000 m, the width across the strike is from 450 to 1000 m. Taking into account the mining and geological conditions of the deposit (the dip angle of deposits is 45º - 75º, the development depth is below 700 m from the earth's surface), the need to preserve the earth's surface with the existing high-grade objects and rational use of the subsoil, the most acceptable and economically feasible is the underground method of development. The output of the feldspar concentrates will be more than 2 million tons with planned productivity of 4 million tons of ore.

CONCLUSION

It is shown on the example of Ukrainian deposits of feldspar minerals that complex deposits with by-products become the main source for production. Especially if these are new mining operation facilities. The authors have identified three main types of such complex multicomponent deposits: 1) deposits of intrusive rocks where weathering crust of crystalline rocks are mined as a byproduct; 2)

complex deposits, where feldspar rocks are enclosing or overburden and can also be considered as byproducts; 3) deposits where feldspar concentrate can be produced as a product of ore components processing.

The production of feldspar concentrates as by-products with ore processing of multicomponent deposits is one of the ways of increasing their profitability. This is due to the large production volume of feldspar products and an increase in raw material prices. The price of feldspar products is not as high as that of the main components - metals, fluorite, apatite, but the huge output of these products affects the final deposit value as well as the prices of the main components.

REFERENCES

[1] Balance of mineral reserves of Ukraine. Issue 72. Feldspar raw materials. Kyiv, State Research and Production Enterprise "State Information Geological Fund of Ukraine", 2018. *(in Ukrainian)*

[2] Cherniyenko N.M. Complex use of ores of the Mazurivske deposit, Pryazovia region// http://ea.donntu.org:8080/jspui/bitstream/123456789/7226/1/215-222.pdf *(in Ukrainian)*

[3] Feldspar Statistics and Information. National Minerals Information Center. USGS// https://www.usgs.gov/centers/nmic/feldspar-statistics-and-information

[4] Haletskiy L.S., Shevchenko T.P., Cherniyenko N.M. New concepts about the geological structure and metallogeny of the territory of Ukraine // Geological Journal. № 3, pp. 74–83, 2008. *(in Ukrainian)*

[5] Haletskiy L.S., Naumenko U.Z., Cherniyenko N.M. Main types of ore-bearing structures of Ukraine // Mineral resources of Ukraine. № 4, pp. 12-19, 2016. *(in Ukrainian)*

[6] Mineral resources of Ukraine, Kyiv, State Research and Production Enterprise "State Information Geological Fund of Ukraine", 270p., 2014. *(in Ukrainian)*

[7]. Mineral resources of Ukraine, Kyiv, State Research and Production Enterprise "State Information Geological Fund of Ukraine", 270p., 2020. *(in Ukrainian)*

[8] Mostyka Yu.S., Shpylioviy K.L., Miakyshev V.M., Shpylioviy L.V. Substantiation of geological-economic, technological and ecological possibilities of industrial development of technogenic deposit of feldspar raw materials // Modern economic possibilities of development and sales of mineral resource base of Ukraine and Russia in the conditions of globalization of the mineral raw material market. IGS NAS of Ukraine. Kyiv,- pp. 219-222, 2005. *(in Russian)*

[9] Rudko H.I., Ozerko V.M., Shepel I.V. Geology and geological-economic assessment of kaolin deposits in Ukraine. Ed. by H.I. Rudko. Kyiv. 2015. *(in Ukrainian)*

[10] Voynovskiy A.S., Bochay L.V., Nechayev S.V. et al. Complex metallogenic map of Ukraine. Scale 1:500 000. Explanatory note. Kyiv, UkrDGRI,

State geological service of the Ministry of Natural Resources of Ukraine, 336 p., 2002. *(in Ukrainian)*

[11] Vysotskiy B.L., Lykov L.I., Prykhodko V.L. et al. Geological and economic assessment of the Perzhanske ore field // Collection of scientific proceedings of UkrDGRI, № 1. pp. 172–179, 2005. *(in Ukrainian)*

THREE-DIMENSIONAL SIMULATION OF FLUID FLOW THROUGH A DISCRETE FRACTURE AND MATRIX

Dr. Kunwar Mrityunjai Sharma[1]
Dr. L. K. Sharma[2]
Mr. Tariq Anwar Ansari[3]
Prof. T. N. Singh[4]
[1] Department of Earth Sciences, Uppsala University. Uppsala, Sweden
[2, 3, 4] Department of Earth Sciences, Indian Institute of Technology Mumbai, India

ABSTRACT

The study of fluid flow mechanics in fractured porous rocks is crucial in the area of oil and gas production industries, enhanced geothermal system (EGS), CO_2 sequestration, disposal of nuclear waste in deep geological repositories (DGR), etc. There are usually two types of flows in fractured rockmass setting. The dominant flow occurs through the fractures whereas there is also a slow movement of fluid through the matrix block. The fluid movement between fracture and matrix is often continuous across the fracture. The present study focuses on the development of a numerical model which can simulate the flow behavior through fracture and matrix simultaneously, which is also known as dual permeability model. To simulate this problem, a 3D model is built in COMSOL Multiphysics 4.3a where a cylindrical geometry is made, and a fracture is defined parallel to the axis of the geometry. The asperity of the fracture is defined by a variable 'a' which varies along the x-axis, in such a way that increases the value of 'a' alters the geometry of fracture and increases the roughness of fracture. Darcy flow physics is used to simulate the situation with known parameters like porosity, permeability, storage coefficient, etc. Pressure is applied as a boundary condition at two ends of the geometry which acts as driving force for fluid to flow through the block. The influence of fracture asperity on the flow behavior is examined by doing the parametric study and the study shows the decrement in the velocity magnitude with an increase in asperity. The formation of dual flow velocity regime, one along the defined fracture and the other along with the matrix, indicates the efficiency of the developed dual-porosity and permeability model.

Keywords: *Fracture flow, Dual porosity model, Darcy flow*

INTRODUCTION

Investigation of fluid flow behavior through matrix and discontinuities plays quite a major role in addressing the problems related to oil-gas exploration [1], carbon dioxide sequestration [2], enhanced geothermal system (EGS), disposal of nuclear waste in deep geological repositories [3], investigation of groundwater contamination [4], mine construction, dam designing and construction, slope stability analysis, etc. The flow structure in the karst lithology is generally comprised of multiple porosity and permeability, where the dissolution of the rock

occurs due to acid action [5]. At the pore scale, the transport mechanism associated with the fluid flow causes solid structure alterations due to chemical reactions with minerals [6]. The multiple porosity model is the combination of matrix flow, fracture flow, and flows through other conduits. In different type of aquifers, these components of the flow may dominate over each other according to the properties of the aquifer. There are dual-porosity models as well as triple porosity models depending on the presence and dominance of flow components in the different type of flow paths (porous, fracture, cracks, etc.). Different types of analysis methods are used by the research community in the past to characterise the simultaneous flow through fracture and matrix[7–9]. In recent studies, these components are studied by coupling them using numerical modelling.

In fractured porous media, there are commonly two types of flows. Preferential flows occur through fractures, macropores, and other high permeability while there is also a relatively less dominant flow through the matrix. The simultaneous flow through the matrix and other discontinuities are usually studied using dual permeability model due to its computing ability. According to this model, the rockmass comprises of matrix and discontinuous domains which are overlapping as well as interacting. One domain doesn't have specific structure and direction, also known as matrix domain while dominant flow path occurs through the discontinuities such as fracture, fissure, cracks, etc. Matrix domain has relatively low permeability as compared to that of fast flow domain, but there is a continuous exchange of fluid between the two. The dual porosity and permeability model is very helpful in simulating problems related to landslide mitigation, subsurface flow mechanism, oil and gas exploration, etc. There are many hydrological problems that cannot be explained using single permeability Richards' and Darcian flow. But most of the software packages such as FLAC and PLAXIS use single permeability model to couple flow mechanics and rock mechanics for subsurface flow modelling. Single permeability formulation is also very useful for analyses related to many commercial geotechnical models but relatively less suitable for the quantification and proper understanding of the problem.

The discontinuities present in rockmass influence the mechanical behavior of the rock in many ways. They provide a plane of weakness along which failure may occur; also they provide conduits through which fluid flow can occur. The wall roughness of the fracture influences the hydro-mechanical and transport behavior of the rockmass[10]. The fracture roughness reduces the overall conductivity of the rockmass by locating the contact points of the wall and makes the flow path tortuous [11].

In order to advance in dual/triple porosity modelling, the understanding of pore scale study is very important. In the recent past, numerous pore scale models have been developed to characterise the flow behavior using numerical as well as empirical approach [12], [13], [14]. In this study, dual porosity and permeability model is developed by coupling pore scale flow and fracture flow. The interaction between these different components of the flow have also been investigated. The flow characteristics through a single fracture enclosed in the porous matrix is examined. The roughness of the fracture is varied using a defined variable and its effect on the flow parameters is discussed. The physical properties such as porosity,

permeability, and matrix compressibility of different types of rocks are also used to study the role of rock properties on the flow behavior. To model the dual porosity and dual permeability model using numerical approach, two different dominant flows are taken in account. These are matrix flow and fracture flow, and the equations which govern this mechanism are shown and discussed in the next section.

GOVERNING EQUATIONS

Matrix flow

The fluid flow through the matrix is very common but the associated complexities make it difficult to completely understand the mechanism. The matrix flows are usually very slow and thus show laminar behavior. Equation (1) and (2) shows the time dependent formulation of Darcy's law and linearized storage model respectively.

$$\rho S \frac{\partial p}{\partial t} - \nabla . \left(\rho \frac{\kappa}{\mu} \nabla p \right) = 0 \tag{1}$$

$$S = \chi_f \varepsilon + \chi_p (1 - \varepsilon) \tag{2}$$

Where p is pore pressure, ρ and μ is the fluid density and viscosity, S is the storativity of the matrix, t is the time (s), ε and κ are the porosity and permeability of the matrix, is the dynamic viscosity of the fluid (Pa. s), χ_f and χ_p are the compressibility of the fluid and matrix (1/Pa).

$$\boldsymbol{u} = -\frac{\kappa}{\mu} \nabla p \tag{3}$$

The linear fluid flow velocity in the small pore interstices is more than Darcy's velocity, which shows that the flow velocity is distributed over pores as well as matrix.

No flow boundary condition is applied to all the faces of the cylindrical geometry as shown in equation 4.

$$\boldsymbol{n} \cdot \boldsymbol{u} = 0 \tag{4}$$

Where n is the unit vector pointing outward to the boundary, and zero dot product between **n** and **u** signifies that there is no flow across the boundary.

Fracture flow

Fractures are the most commonly occurring conduit for the fluid to flow through all kind of rockmass. The mechanism associated with the fracture flow are studied worldwide but still the proper understanding of the process is not clear to the scientific community. Experimental investigation of the flow associated with the fractures are very difficult because of the factors such as diversity, scale, and different origin of the fractures. But in the recent times after the introduction of the

numerical modelling software, the fracture flow study has become relatively convenient and fruitful.

Flow in the COMSOL is generally defined perpendicular to the boundary, not along it. However, in this study, fracture is the taken as sequence of internal boundaries along which flow takes place and velocity equation in the fracture follows modified form of equation 1 as shown in equation 5.

$$\rho S_f d_f \frac{\partial p}{\partial t} - \nabla_T . \left(\rho \frac{\kappa_f}{\mu} d_f \nabla_T p \right) = 0 \quad (5)$$

Where, S_f, κ_f and d_f are the storage coefficient, permeability and thickness of the fracture respectively.

The variable **u** provides the volumetric flow rate per unit length because of the presence of thickness variable in the equation.

$$\boldsymbol{u} = -\frac{\kappa}{\mu} d_f \nabla_T p \quad (6)$$

Where ∇_T is the gradient operator limited to tangential plane of the fracture.

MODEL SET UP

The study has been performed on a three-dimensional cylindrical block, in which a discrete fracture plane is made parallel to the axis of the cylinder and the roughness of the discrete fracture is maintained with the help of a variable 'a' which varies along the x-axis. The model geometry used for the simulation with a rough discrete fracture is shown in Figure 1a. Darcy flow physics is selected in the model component to simulate the situation with known parameters like porosity, permeability, storage coefficient, etc. Pressure is applied as a boundary condition at two ends of the geometry which acts as the driving force for fluid to flow through the block. A fracture flow-node is employed on the interior boundaries to trigger the flow and interact with the matrix flow. The pressure change along the boundary are calculated automatically by the model in the form of tangential derivatives pTx, pTy, and pTz.

The asperity (a) of the fracture surfaces is also varied in such a way that an increase in the magnitude of variable 'a' increases the asperity of the fracture wall by using inherent geometric functions of the software. The variable 'a' has been provided a numerical value corresponding to the reach of the fracture in the direction normal to the fracture length. The magnitude of the 'a' is changed periodically around eight fixed points along the fracture length to make the surface of the fracture wall undulating and rough, and the fracture roughness is quantified using this variable. The value of a is varied from 0.05 mm to 2 mm to investigate the effect of roughness on the flow system in the porous media. The values of model parameters such as porosity, permeability, and storage coefficient are taken those of different rock types like sandstone, limestone, and granite. The effect of physical

properties of the rock on the flow behavior is also studied with the help of this model.

Different types of fluids were also used as flowing media to flow through the matrix and fracture simultaneously to study the role of fluid properties in managing the fluid flow behavior in fractured porous media. In this furtherance, water, light oil, medium oil, heavy oil, and carbon dioxides are used as flowing media through a matrix of the block with a single discrete fracture. The change in flow behavior due to differences in the fluid properties such as density and fluid viscosity is also investigated.

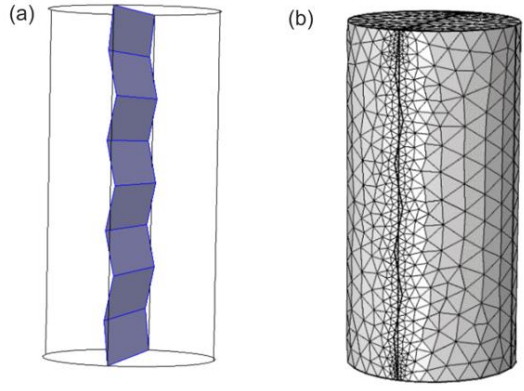

Fig. 1. *(a) Discrete fracture plane and (b) Meshing over the fractured core block*

The accuracy of the data and result obtained from the FEM model depends directly on the type of meshing used during simulation. This process of mesh refinement is a very crucial stage in validating a FEM model and gaining assurance in the model simulation results. Therefore, tetrahedral meshing is used in this model due to ease in the computation and fast processing of the model. The meshing is fine in the desired domain i.e., near the fracture plane and it is relatively coarse in the matrix domain which can be seen in Figure 1b.

RESULT AND DISCUSSION

Three-dimensional dual porosity and permeability model has been developed to simulate the flow through matrix and fracture simultaneously and investigate the mechanics associated with the flow. Generally, at a boundary, flow is defined perpendicular to the boundary, but in this study, fracture boundary is a sequence of interior boundaries that allows the flow along the boundaries. These internal boundaries are sequences using variable ‘a’ in such way that they form an undulating and rough fracture surface. The flowing media tends to favour the path along the zone of high permeability. The permeability of fracture is very high as compared to the matrix of the block. Therefore, flow is very prominent along the internal fracture boundaries but it slowly starts to move through the matrix with time. Since this is a time dependent study, the pressure drop in the cylinder is taken

as a function of time. Figure 2**Error! Reference source not found.** shows the p ressure drop contours in the block at the final output time. The magnitude of the pressure distribution is shown in the legend. The arrows in the block represents the flow velocity magnitude and direction along the fracture boundary and represent the dominance of flow along the interior fracture boundaries.

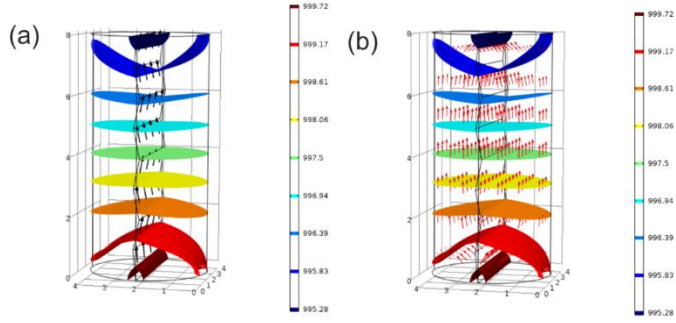

Fig. 2. *Fluid flow distribution in (a) discrete fracture, and (b) matrix block*

The flow through the fracture is dominant and the magnitude of the flow velocity along the fracture is represented by the black arrows as shown in the Figure 2a. The various colours of the isosurfaces are indicating different pressure in the geometry. The colour of the isosurfaces as shown in the legend ranges from (highest pressure) to dark blue (least pressure). The fluid is chasing the path of the fracture and the flow showing dominance along the rough path of the fracture. The shape of the pressure isosurfaces becomes curved near the extreme ends of the flow due to the enhanced flow activity at the fracture ends, later becomes relatively flatter because of regular exchange between matrix block and fracture. The curved nature of the pressure isosurfaces near the fracture inlet and outlet represents the distribution of the pressure at extreme boundaries due to excessive fluid movement in the fracture. As the fluid enters the fracture, it experiences high permeability, but due to relatively less permeable matrix block, the migration of the fluid from fracture to matrix becomes difficult. But as soon as fluid reaches the centre of the geometry, the pressure isosurfaces become flat because of even distribution of fluid pressure due to relatively easy exchange between fracture and matrix. The continuous distribution of the pressure in the block indicates the continuous exchange of flow between the blocks. However, the pressure isosurfaces bend represents the presence of different flow regime within the geometry. The arrows indicate velocities in the fracture zone and it is evident that the flow is dominant in the fractures. The distribution of the pressure isosurfaces suggests the drop in the pressure over time.

Similarly, Figure 2b represents the linear velocities of the fluid in the matrix along with the pressure isosurfaces. With no flow out of the matrix, the only fluid source is the fracture. The arrows indicate that fluid exits from the fracture at the outlet. The matrix flow is feed by the fracture at the inlet. The size of the arrow indicates the magnitude of the flow velocity, therefore is smaller than that of fracture.

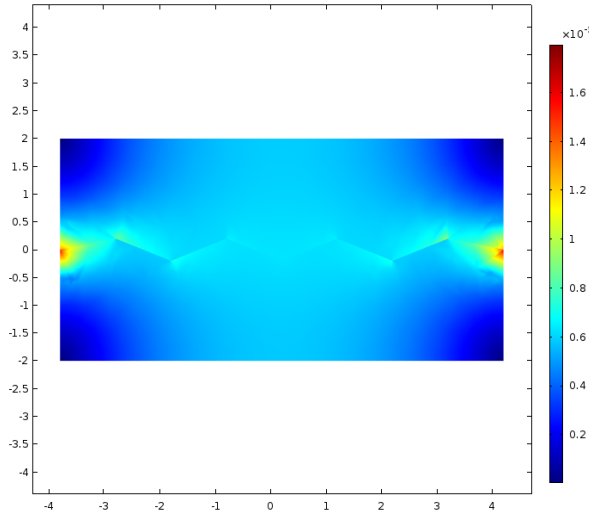

Fig. 3. *Surface plot of Darcy velocity parallel to the axis of the model geometry*

This model focuses on the qualitative investigation of flow through the matrix and fracture concurrently and shows anticipated flow behavior in the results. To study the role of fracture asperity on the flow behavior, asperity of the fracture is varied and the Darcy's velocity is plotted for each condition. The geometry of the fracture is varied using auxiliary sweep so that the asperity changes. Figure 4 shows the Darcy velocity profile for a range of asperities and surface plot of Darcy velocity parallel to the axis of the model geometry. It can be observed that with an increase in asperity, the velocity magnitude is decreasing. Also, Darcy velocity is maximum near the centre where the fracture is present, and it is lowering as fluid moves in the matrix. Asperity is varied using auxiliary sweep in the model geometry using a variable named 'a'.

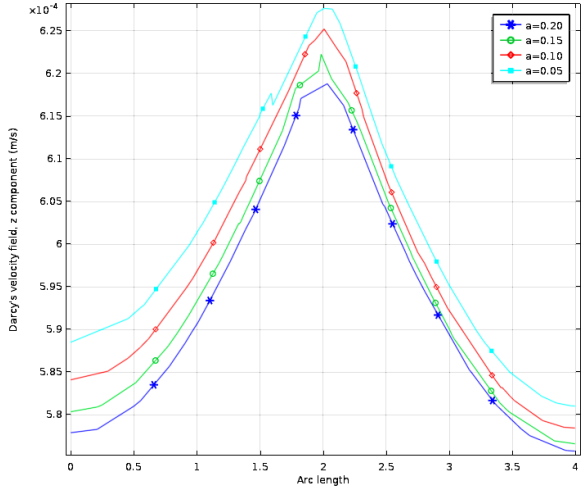

Fig. 4. *Flow velocity magnitude for different fracture asperities*

The Darcy's velocity magnitude is plotted and shown as the surface plot on the cross-sectional profile as shown in Figure 3. The colour spectrum shown in the legend represents the magnitude of the Darcy's velocity, dark blue colour indicates the least of the velocity as shown on the corner of the geometry. The flow through the matrix is relatively very slow as compared to the fracture, and thus represented by light blue colour. The flow through the fracture is dominant and also can be seen by the relatively light blue colour. The zig-zag pattern shown on the surface plot of Darcy's velocity indicates the fluid flow path along the fracture. The red colour of the spectrum represents the highest flow velocity and can be seen at the extreme ends of the fracture. As the fluid enters the fracture, the Darcy's velocity becomes maximum shown by red colour, and as it migrates and move towards the matrix the colour changes rom red to yellow, yellow to green and then green to blue, which represents the deceleration of the fluid in the matrix block.

The simultaneous flow through matrix and fracture can be simulated using the present dual-porosity and permeability model, which can provide information such as pressure drop, flow velocity magnitude and direction. The flow velocity distribution can be witnessed in fracture and matrix differently. The surface plot and cross-section profiles across and along the geometry helps in thorough understanding of the local velocity and pressure field.

CONCLUSION

The study focussed on the development of complex dual porosity and dual permeability model using a finite element approach to simulate the flow through matrix and a single rough fracture simultaneously. The results can be concluded in the following points:

1. The effectiveness of the model can be proved by analysing flow velocity and pressure plot in the study field. The velocity is maximum along the fracture and it is also distributed in the matrix due to the fluid exchange between fracture and the matrix depending on the porosity and permeability of the adjacent medium. The curved pressure isosurfaces plots indicates different flow stages can be observed in the early transition stage (Fracture to matrix) and the inter-porosity flow stage of matrix system to fracture system.

2. The role of fracture roughness on the flow mechanics is examined by defining a local variable that alter the relative roughness of the fracture geometry. It can be concluded that the affirmation by previous researches[10,15] that in a single fracture flow model, the flow velocity decrease with increase in fracture roughness holds true even in dual porosity and permeability model.

3. With necessary developments, this dual porosity and permeability modelling approach can be very useful in the geotechnical areas such as oil and gas reservoir modelling, Hydrogeological modelling, etc.

REFERENCES

[1] Daccord G, Touboul E, Lenormand R. Carbonate Acidizing: Toward a Quantitative Model of the Wormholing Phenomenon. SPE Prod Eng 1989;4:63–8. https://doi.org/10.2118/16887-PA.

[2] Menke HP, Bijeljic B, Andrew MG, Blunt MJ. Dynamic three-dimensional pore-scale imaging of reaction in a carbonate at reservoir conditions. Environ Sci Technol 2015;49:4407–14. https://doi.org/10.1021/es505789f.

[3] Glynn PD. Modeling Np and Pu transport with a surface complexation model and spatially variant sorption capacities: Implications for reactive transport modeling and performance assessments of nuclear waste disposal sites. Comput Geosci 2003;29:331–49. https://doi.org/10.1016/S0098-3004(03)00009-8.

[4] Nick HM, Raoof A, Centler F, Thullner M, Regnier P. Reactive dispersive contaminant transport in coastal aquifers: Numerical simulation of a reactive Henry problem. J Contam Hydrol 2013;145:90–104. https://doi.org/10.1016/j.jconhyd.2012.12.005.

[5] Kang Q, Lichtner PC, Viswanathan HS, Abdel-Fattah AI. Pore scale modeling of reactive transport involved in geologic CO2 sequestration. Transp Porous Media 2010;82:197–213. https://doi.org/10.1007/s11242-009-9443-9.

[6] Babaei M, Sedighi M. Impact of phase saturation on wormhole formation in rock matrix acidizing. Chem Eng Sci 2018;177:39–52. https://doi.org/10.1016/j.ces.2017.10.046.

[7] Elsworth BD, Bai M. Flow-Deformation Response of Dual-Porosity Media 1992;118:107–24.

[8] GHAFOURI HR, LEWIS RW. a Finite Element Double Porosity Model for Heterogeneous Deformable Porous Media. Int J Numer Anal Methods Geomech 1996;20:831–44. https://doi.org/10.1002/(SICI)1096-9853(199611)20:11<831::AID-NAG850>3.0.CO;2-6.

[9] Lemonnier P, Bourbiaux B. Simulation of Naturally Fractured Reservoirs. State of the Art. Oil Gas Sci Technol – Rev l'Institut Français Du Pétrole 2010;65:239–62. https://doi.org/10.2516/ogst/2009066.

[10] Sharma KM, Roy DG, Singh PK, Sharma LK, Singh TN. Parametric study of factors affecting fluid flow through a fracture. Arab J Geosci 2017;10. https://doi.org/10.1007/s12517-017-3142-6.

[11] Boutt DF, Grasselli G, Fredrich JT, Cook BK, Williams JR. Trapping zones: The effect of fracture roughness on the directional anisotropy of fluid flow and colloid transport in a single fracture. Geophys Res Lett 2006;33:0–5. https://doi.org/10.1029/2006GL027275.

[12] Porta GM, Bijeljic B, Blunt MJ, Guadagnini A. Continuum-scale Predictions of Solute Transport Derived from Pore-scale Velocity Distributions - Supporting Information. Geophys Res Lett 2015:1–9. https://doi.org/10.1002/2015GL065423.Received.

[13] Ramandi HL, Liu M, Tadbiri S, Mostaghimi P. Impact of dissolution of syngenetic and epigenetic minerals on coal permeability. Chem Geol 2018;486:31–9. https://doi.org/10.1016/j.chemgeo.2018.03.015.

[14] Tahmasebi P, Sahimi M, Andrade JE. Image-based modeling of granular porous media. Geophys Res Lett 2017;44:4738–46. https://doi.org/10.1002/2017GL073938.

[15] Wang H, Ju Y, Ranjith PG, Zhang Q, Mining S, Engineering DU. Numerical analysis of fluid flow in single rock fracture 2013:1769–76.

Section

SOIL SCIENCE

Soil biology and fertility
Soil contamination, soil formation and soil pollution
Soil chemistry and soil physics
Soil conservation
Plants and soil science

ASPECTS CONCERNING PEANUTS CROPS ON SANDY SOILS IN SOUTHERN OLTENIA

Dr. Milica Dima[1]
Dr. Aurelia Diaconu[2]
Dr. Reta Drăghici[3]
Dr. Drăghici Iulian[4]
Assoc. Prof. Dr. Matei Gheorghe[5]
[1, 2, 3, 4] Research & Development Station for Plant Culture on Sands Dabuleni, Romania,
[5] University of Craiova. Faculty of Agriculture, Romania

ABSTRACT

For the capitalization of the climate and soil conditions for the sandy soil region in Southern Oltenia by cultivating peanuts it is necessary to use varieties with large production abilities and proper technology for the crops.

In view of its cultivation on south Oltenia sandy soils, there were carried out in the period 2004-2006, at the Plants Crops Research and Development Station on Sandy Soils Dabuleni, experiments have been set regarding aspects such as: the optimal seeding period, the recommendation varieties with high yield potential and balanced composition.

The research was conducted under irrigation conditions, in a three-year rotation of wheat, peanut, maize.

Along with erect growth type varieties, known for their short vegetation period, rising and creeping growth type varieties can also be used; these varieties have a great production potential in our country`s conditions.

Establishing the proper time for seeding is espe since sandy soils are heating quickly but are also cooling quickly, the best seeding time is between the end of April- the beginning of May, depending on the date when the seeding depth has a steady temperature, minimal required for the seed to germinate.

Keywords: *genotype, sowing time, climate, productivity*

INTRODUCTION

Peanuts contribute to the superior valorisation of sandy soils in our country, due to reduced requirements for soil fertility, low fertilizer and water consumption, soil enrichment in symbiotically fixed nitrogen. [9].

Peanut seeds have a high protein and fat content [1], [6], [11] and can be used in food and in the food industry.

The limiting factor of peanut production is heat, which restricts the area of spreading culture in the temperate continental climate in certain areas, where the

temperature conditions are improved either due to the sandy soil or due to local climatic influences of the Mediterranean type. [9].

In the area of sandy soils in southern Oltenia, peanuts find favourable ecopedological conditions for growth and fructification, conditions that allow for the good cultivation of this species [7], occupying, within agricultural crops on sandy soils, the place of improving legumes.

In this paper are presented the results obtained at the Plants Crops Research and Development Station on Sandy Soils Dabuleni in experiences regarding recommendations for soils with high production potential and balanced composition, the optimal sowing age.

MATERIAL AND METHOD

The experiments were arranged in the field by randomized blocks method on sandy soil with a humus content of between 0.2-0.4%.

The research was conducted under irrigation conditions, in a three year rotation of wheat, peanut, maize.

In the time of the experience was respected the technology of growing peanuts on sandy soils.

The interpretation of research results was performed by variance analysis.

RESULTS

[8] have highlighted both the role of variety and cultivation technology in peanut production in the US, concluding that for the production of high yields it is necessary to use productive varieties under the conditions of applying an appropriate cultivation technology.

The International Board for Plant Genetic Resources classifies peanut varieties after plant habitus into three main groups: erect, decumbent, procumbent.[3],[4]. The characteristic of these three groups is the correlation between the type of growth and the length of the vegetation period that grows from erect to deciduous and procumbent [1], [2].

That is why the first varieties that have been tested under the conditions of our country belonged to the group with erect port, starting from the reason that they, having a shorter vegetation period, are best able to achieve at the northern limit of the peanut cultivation area, satisfactory yields due to the maturity of a larger number of pods. The results obtained with these varieties were not satisfactory [5], [9] which led to the necessity of the creation of native varieties, materialized by the approval of two varieties: Dăbuleni, Viorica with erect port. Considering the high adaptability of peanuts, including in areas with less favourable climatic conditions, as well as the fact that the varieties in the dwelling and the procumbent groups are more productive, those in the procumbent group, with no positive correlation between the number of mature pastures and production [10], within varieties of

varieties studied at the Plants Crops Research and Development Station on Sandy Soils Dabuleni were also included varieties belonging to these two groups (table 1).

Table 1. *The influence of the type of growth on the production of some peanut varieties*

Group	Genotype	Average production (kg/ha)	The difference (kg/ha)	Semnification	Average kg/ha
Witness	Dabuleni	2434	Mt.		2434
Erect	Viorica	3220	+786	*	3112
	Sadovo	3005	+571		
Decumbent	Shulamith	3326	+892	*	3363
	Province China I	3400	+966	**	
Procumbent	Province Turcia	4123	+1689	***	3565
	B28	3008	+574	*	

LSD 5%= 545 kg/ha
LSD 1%= 915 kg/ha
LSD 0.1%= 1005 kg/ha

The yields obtained, compared to the Dabuleni witness variety, in two varieties of each gup, show that even under the conditions of our country varieties with a type of growth and a procumbent growth show a higher production potential than those with erect growth type. The production increase was significant in the Shulamith variety and distinctly significant in the Province China I variety of the dominant group and very significant, respectively significant in the Province Turcia and B28 varieties from the procumbent group.

Analyzing the main elements of productivity (table 2) it is observed that the number of mature plants on the plant decreases to the dominant and procumbent types of the erect type, the production increase in the varieties of these groups based on the size of the pods, the weight of 1000 pods growing distinctly significantly to the witness. For varieties with a procumbent growth type, the number of grains in the pod was distinctly significantly smaller than the witness, but the much larger beans, the weight of 1000 grains growing significantly distinct from the control. For varieties in the erect group and in the procumbent group, the yield on peeling was significantly lower than the witness, in the first group due to smaller grains, to the other due to the achievement of a smaller number of grains in the pod.

Table 2. *The influence of the type of growth on the productivity elements of some peanut varieties*

Group	Number of mature pods on the plan	Weight a 1000 pods(g)	Number of grains in the pod	Weight a 1000 grains(g)	Yield on peeling (%)
Witness	26	1658	2.3	552	75
Erect	31.5***	1871	2.5	513	67 o
Decumbent	29.3*	2044**	2.3	660	70
Procumbent	28.5*	2111**	1.8 oo	761 **	65 o
LSD 5%=	2.5	251	0.38	121	6.8
LSD 1%=	3.4	352	0.5	168	11.6
LSD 0.1%=	5.2	497	0.72	241	18.2

The chemical composition of peanut beans is characterized by various authors [1], [6], [11] with a content of 20-30% protein and 45-60% fat. Among the analyzed varieties (table 3), those in the procumbent group are characterized by a high protein content (26.2%), and those in the decumbent group with a higher fat content (47.9%).

Table 3. *The influence of the type of growth on the chemical composition of the grain in some peanut varieties*

Group	Protein (%)	Fats (%)	Cellulose (%)	Ash (%)
Witness	23.6	45.1	2.8	3.5
Erect	22.5	46.0	2.71	3.32
Decumbent	22.9	47.9	2.85	3.45
Procumbent	26.2	45.9	2.75	3.3

Under our country's conditions, the optimum sowing time is determined by achieving a minimum seed germination temperature of 12^0C [9] in the soil at the sowing depth. Setting the sowing moment is important because the sandy soils heat up and cool down quickly, with the risk of going through periods when soil temperature falls below the minimum germination, affecting plant emergence and growth. The yields obtained at different epoch of sowing (table 4) highlight that sowing should be placed about 3 weeks after the soil temperature at 12^0C is recorded in the soil, production increase, in this case, being very significant. The sowing time for peanuts must be set according to the climatic conditions of each year, beginning with the date when the minimum germination temperature of seeds is stabilized in the soil at the seed depth and the growing tendency to grow it (the end of April - beginning of May).

Table 4. *The influence of sowing epoch on the production of peanuts*

The sowing epoch	Production (kg/ha)	Difference (kg/ha)	Semnification
120C	1320	Mt.	
120C + 7 days	1280	-40	
120C + 14 days	1575	+255	*
120C + 21 days	2237	+917	***
120C + days	1645	+325	**

LSD 5%= 185
LSD 1%= 273
LSD 0.1%= 405

CONCLUSIONS

Climate and soil conditions in the the area of sandy soils of southern Oltenia are favourable to peanut culture.

The peanuts varieties with a type of decumbent and a procumbent growth show also in our country a higher production potential than those with erect growth, those in the decumbent group also being noted for higher fat content, and those in the procumbent group with higher protein content.

The sowing epoch is determined by achieving a stable temperature of 12^0C in the soil at the sowing depth, with a certain growth trend (end of April - beginning of May).

REFERENCES

[1] Bârnaure, V. , Phytotechnie tropicale, U.NA.ZA., Kisangani-Yangambi, 1976.

[2] Delikostadinov, Gheorghiev, S., Studiul agrobiologiei și tehnologiei varietăților taxonomice ale speciei Arachis hypogaea L. încercate în Bulgaria central-sudică, teză de doctorat, Academia Agricolă, Sofia, Bulgaria, 1988.

[3] International Board for Plant Genetic Resources, Descriptors for Groundnut, IBPGR Secretariat, Roma, Italy, 1985.

[4] International Board for Plant Genetic Resources, Descriptors for Groundnut, IBPGR/ICRISAT, Roma, Italy, 1992.

[5] Marghitu Valeria,Chichea I., Cercetări privind obținerea de linii de arahide corespunzătoare condițiilor pedoclimatice din sudul Olteniei prin mutageneză și selecție individuală, în „Genetică teoretică și aplicată'', vol.XIV, nr.6, ICCPT Fundulea, Romania, 1982.

[6] Minchevici,I.A., Borcovschi,V.,E., Cultura plantelor oleaginoase, Editura Agrosilvică de Stat, București, Romania, 1953.

[7] Mitrea, I., Utilizarea resurselor ecologice și stabilirea principalelor verigi tehnologice pentru creștere producției de arahide pe nisipurile din sudul Olteniei, teza de doctorat, ASAS București, Romania, 1993.

[8] Mozingo, R.W., Coffelt, T.A., Wynne, J.C., Characteristics of Virginia type Peanut Varieties Released from 1944-1985, în ,,Southern Cooperative Series Bulletin", no.326, Blacksburg, Virginia, USA, 1987.

[9] Pop, L. and colab., Cultura alunelor de pământ, Editura Ceres, București, Romania, 1986.

[10] Radwal, S., Harbons, Singh, Effect of growth habit on correlations and Path coefficiens in groundnut, în ,, Indian Journal of Genetic and Plant Breeding'', vol.33,no.1, India, 1973.

[11] Rehm,S., Espig,G., Die Kulturpflanzen der Tropen und Subtropen, Verlag Eugen Elmer, Stuttgart, Germany, 1976

ASSESSMENT OF STRONTIUM, RUBIDIUM AND SCANDIUM STATUS IN SOILS AFFECTED BY SOLID WASTE DEPOSITS

Prof. Dr. Luminita Pirvulescu[1]
Assoc. Prof. Dr. Despina-Maria Bordean[2]
Lecturer Dr Loredana Copacean[3]
Lecturer Dr. Narcis Gheorghe Baghina[4]
Assoc. Prof. Dr. Carmen Petcu[5]
Dr. Diana Obistioiu[6]
[1, 2, 3, 4, 6] Banat's University of Agricultural Sciences and Veterinary Medicine "King Michael I of Romania" from Timisoara, Timisoara, Romania
[5] University of Agronomic Sciences and Veterinary Medicine of Bucharest, Bucharest, Romania

ABSTRACT

The aim of the study was to assess the level of contamination of soil with strontium, rubidium and scandium in the solid waste deposits. The study was performed on soil samples collected from Moldova Noua, southwest of Romania, an area with historical anthropogenic history. The soil analysis was performed using X-ray fluorescence (XRF). The samples were collected from five collection points using a random pattern from around the illegal waste deposit and all analyses were performed in triplicate. To assess the influence of wastes on the soils concentration levels of strontium (Sr), rubidium (Rb) and scandium (Sc), were calculated contamination factors (CF), and pollution index (PI_L) by reporting the concentration of the investigated elements of the upper earth crust concentrations and geo-accumulation index (I_{geo}) calculated by reporting the elements concentration values to a control sample, used as reference. The reference sample was collected from an area close to the waste deposit but located in a protected green area. The results show that from the investigated elements, scandium is the element of concern, the soil presenting a moderate contamination level with this element.

Keywords: *heavy metals, contamination factors, pollution index, geo-accumulation index*

INTRODUCTION

The rising number of illegal waste dumps represents a global problem and is the result of the increase of waste production correlated with the ever-growing population. Even if official waste disposal sites are available, illegal waste dumps occur everywhere around the world, most commonly on the periphery of colonized areas, forest margins, as well as at other places, contaminating the environment and degrading land [15]. The metal concentration and behavior of metals associated with various industrial, mines or municipal wastes in soil systems is much higher and affects metal mobility, being decidedly dependent on the waste type. The modifications in time of the environmental conditions, such as changes in pH, the

degradation of the organic waste matrix, or soil solution composition, may modify metal mobility [10].

The aim of the study was to assess the level of contamination of soil with strontium, rubidium and scandium on disposed solid wastes. Contaminations are less investigated in rubidium, strontium and scandium soils. Compared to the number of studies related to hazardous heavy metals, strontium occurs in nature, is estimated to approximately 320 ppm in the upper Earth's crust [12]. Rubidium is an alkali metal, almost as abundant as zinc. According to Rudnick et al, in the upper earth crust are approximately 84 ppm rubidium [12]. Rubidium is easily taken up by plants, similar to potassium and generally is concentrated in flowers and young leaves [6]. It is appreciated by a recent study as the best predictor variable for estimating the clay content and salinity of soils [14]. Scandium is a naturally occurring element in the soil and its concentrations vary across geographic regions. In the earth's crust, Sc is varying from 16 ppm [8] to 25 ppm [2]. The soils as well as the natural and/ or mineral water [7] have a specific natural content of metal cations, which depend on the background concentrations specific to the investigated area. The control area was chosen, as it is a protected area and due to its natural potential and ecological value. The Romanian territory shelters a huge variety of habitats, of national as well as European interest.

MATERIALS AND METHODS

Description of the Study Site: The investigated area is located in the southwest of Romania, close to Moldova Noua city and close to the Danube.

The study was conducted on soil samples from an area where an illegal waste deposit was identified and compared to soil samples from a vegetation area, practically a protected area, which is considered as a control area. All samples were collected using a random pattern from around the waste deposit (Figure 1).

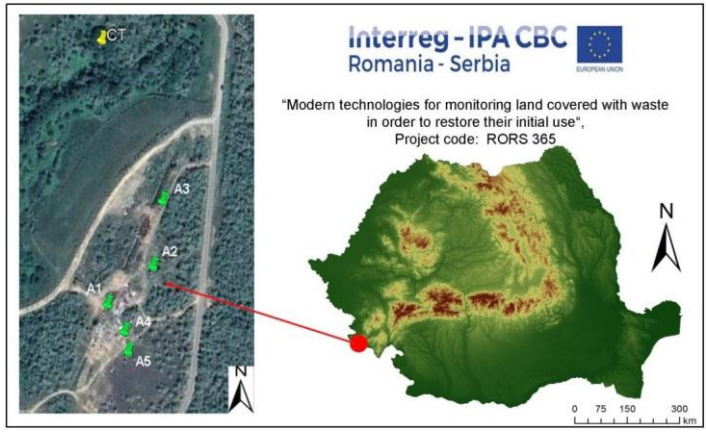

Fig. 1. *Map of the investigated experimental area [4], [5]*

Legend: A1, A2, A3, A4, A5 - Soil sampling collection points, CT – Soil sampling control point

The soil samples was collected from the topsoil (0-20 cm depth) using a standard auger. For evaluating the soil status of the experimental area (Table 1) were established five collection areas (A1, A2, A3, A4, and A5). From each collection area were sampled three replicates, which were thoroughly mixed to obtain a homogenous soil mixture.

Preparation of soil samples for analysis

For the accuracy of the analysis results, the fragments of leaves and small stones were removed and the soil samples were dried until the water content became less than 10%, and ground into a fine powder (~ 100μm). For XRF analysis, the soil sample is analyzed in a sample cup with a thin built-in polypropylene film.

Table 1. *GPS Stereo coordinates of the soil samples collection points*

Samples Area	Sample code	x	y
Illegal waste deposit	A1	362637.919	234144.254
	A2	362679.914	234201.804
	A3	362754.786	234216.725
	A4	362605.614	234163.640
	A5	362582.523	234167.162
Control sample, area with vegetation	CT	362947,015	234151,003

Legend: A1, A2, A3, A4, A5 - Soil sampling collection points, CT – Soil sampling control point

Soil analysis

The analysis of the soil samples were performed using X-MET8000 - X-Ray Fluorescence Analyzer. The apparatus is factory calibrated. All analysis were done in triplicate and result were shown as average ± SD

Contamination indices

Soil contamination with strontium, rubidium and scandium, was evaluated using pollution indices (contamination factor, pollution index of soil loadings (PI_L) and geo-accumulation index (I_{geo})) presented in Table 2. Soil Contamination Factor (CF) represents a quantification of the contamination level relative to upper earth crust composition of the investigated metals as shown in Table 2.

In this paper, we used separately, both, the concentration of elements in the Earth's crust as well as concentration of the control samples as reference values. The concentration of elements in the Earth's crust are presented in Table 3 [1], [13].

The Geo-Accumulation Index (I_{geo}) of a sample site was calculated according to the relation shown in Table 2 [9]. The classifications of contamination level based on CF, PI_L and I_{geo} are presented also, in Table 2.

Statistical Analysis

The experimental data were statistically evaluated using Excel 2007, PAST Version 2.17c and Statistica 13.5.0.17 Tibco Software Inc.

Table 2. *The classification of pollution level based on soil pollution indices*

Crt. No	Pollution index and classification of pollution level	Formula	Parameters
1	Soil Contamination Factor (CF) [3]: • CF < 1, low pollution; • 1<CF<3, moderate pollution; • 3<CF<6, high pollution; • CF>6, very high pollution [1]	$CF^i = \frac{C^i_{0-1}}{C^i_n}$	C^i_{0-1} = the mean content of investigated metals from three to five sampling sites C^i_n = the concentration level of the individual metal before depositing waste, practically the concentration of elements in the Upper Earth's crust
2	Pollution Index of Soil Loadings (PIL) [13] • PI_L< 1 no contamination with the studied metals; • PI_L= 1, baseline levels of pollutants are present • PI_L>1 metal concentrations are above the permissible level, which is producing a deterioration of the soil quality	$PI_L = (CF_1 \cdot CF_2 \cdot \ldots \cdot CF_n)^{1}$	n = the number of studied metals (three in this study) and CF is the contamination factor calculated as described $CF_1, CF_2, \ldots, CF_n$ are the contamination factors calculated as described before
3	The Geo-Accumulation Index (I_{geo}) [9] • I_{geo}≤ 0 no contamination with the studied metals; • 0 <I_{geo}≤1 mild to moderate contamination • 1<I_{geo}≤2 moderate contamination • 2<I_{geo}≤3 moderate to high contamination • 3<I_{geo}≤5 high contamination • I_{geo}≥5 exceptionally high contamination	$I_{geo} = \log_2 \frac{c^i_n}{k \cdot c^i_{ref}} = \log$	c^i_n = the measured concentration of heavy metals in the soil (mg/kg), c^i_{ref} = The background concentration of the metals, specific to the studied area Constant k = 1.5 is a correction coefficient that specifies the influence of natural fluctuations and of anthropic sources.

Table 3. *Concentration of elements in the earth's crust [12]*

Sample site	Symbol	Heavy metals concentration (ppm)		
		Sr	Rb	Sc
Upper Earth Crust	UEC	370	90	22

RESULTS AND DISCUSSIONS

The level of concentrations of the investigated soil samples are presented in Figure 2. The concentrations of Sr, Rb and Sc in the upper earth crust are appreciated in accordance with Rudnick and Gao, 2003 [12]. As we can observe Rb content is much higher in the upper earth crust and slightly higher in the control sample, which was sampled from an area with vegetation, registered as protected area. The samples with the codes A1-A5 are soil samples collected from an area where illegal wastes are deposited. Comparing the obtained heavy metals concentration values, it is visible that the highest scandium content (202 ppm) is shown by soil sample A2, while for strontium (370 ppm) and rubidium (90 ppm), the highest concentration values mentioned, are those in the upper earth crust [12]. The transfer factors for the evaluated heavy metals for all sampling areas are presented in Table 4.

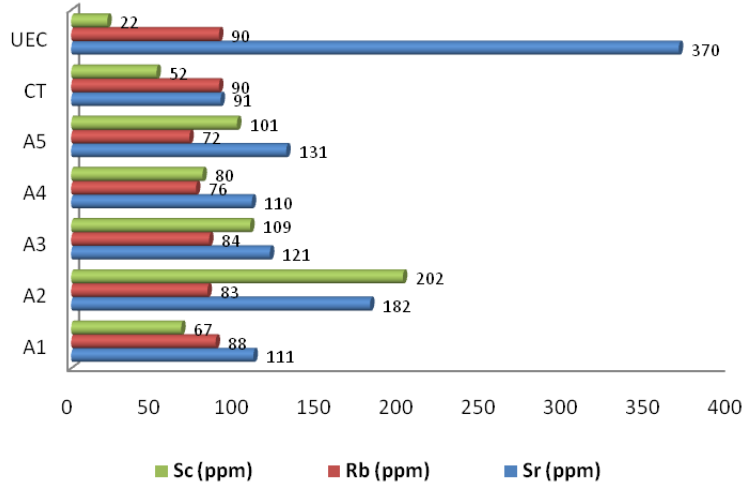

Fig. 2. *Mean values of the concentration of Sr, Rb and Sc in soil samples*

Legend: A1-A5 and CT, soil sample codes, CT – soil control sample, UEC – upper earth crust concentration values.

Table 4. *Individual Transfer Factors (CF) and Pollution Index of Soil Loadings (PI_L) for Sr, Rb and Sc in soil*

Sample code	CF_E (Sr)	CF_T (Sr)	CF_E (Rb)	CF_T (Rb)	CF_E (Sc)	CF_T (Sc)	PI_L
A1	0.35	1.22	1.05	0.98	4.79	1.29	1.209
A2	0.57	2	0.99	0.92	14.43	3.89	2.01
A3	0.38	1.33	1	0.93	7.79	2.10	1.43
A4	0.34	1.21	0.90	0.84	5.71	1.54	1.21
A5	0.41	1.44	0.86	0.8	7.21	1.94	1.36
CT	0.28	1	1.07	1	3.71	1	1.04
UEC	1	-	1	-	1	-	-

Legend: A1-A5 and CT, soil sample codes, CT – soil control sample, UEC –upper earth crust, CF_T= CF of the metal reported to the background value, CF_E = CF of metal reported to the earth crust value

The transfer factors of the individual metals were calculated both in respect to control (CF_T) as well as to the concentration of elements in the Upper Earth's crust (CF_E). In both situations, the soil samples prove to be contaminated with scandium. The contamination factors for Sr, Rb and Sc were calculated by reporting the individual concentration media for each area to two reference concentration values (CT and UEC) in order to identify the historic pollution due to mining activities of Moldova Noua area and the new pollution area created by depositing the solid wastes. The mines present in Moldova Noua area have a long history of (the Stratigraphic age of Late Cretaceous–Paleocene) Porphyry copper deposits [11].

Based on the recommendations of Ahamad et al, 2020 (Table 2), CF_E (Sc) shows high ($3<CF<6$) and very high pollution ($CF>6$), while CF_T(Sc) shows moderate ($1<CF<3$) to high pollution ($3<CF<6$). CF_E (Sr) shows low pollution ($CF < 1$) while CF_T(Sr) shows moderate pollution, which might confirm that strontium is less in the soil of Moldova Noua area compared to the concentration specific to the upper earth crust. CF_E(Rb) and CF_T(Rb) are similar. Irrespective of the concentration values used to calculate CF, the pollution level of Scandium is high.

PI_L for Sr, Rb and Sc in soil was calculated only for CFT (Figure 3), in order to evaluate the pollution level created as a result of solid waste deposits.

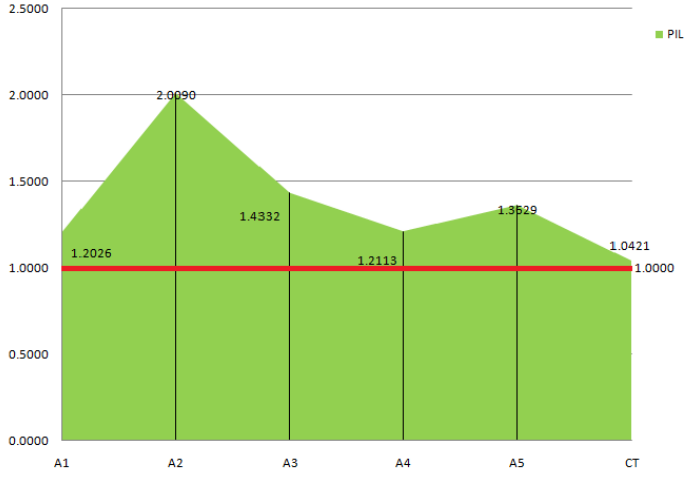

Fig. 3. *Graphical representation of Pollution Index of Soil Loadings (PI_L) for Sr, Rb and Sc*

Legend: A1-A5 and CT, soil sample codes, CT – soil control sample, PI_L - Pollution Index of Soil Loadings

PI_L shows that the entire investigated area poses a high level of pollution (PI_L > 1), even for the control area, due to the elevated level of scandium in the soil, which is causing deterioration of the soil quality.

The geo-accumulation index shows moderate contamination ($1 < I_{geo} \leq 2$) for scandium and zero contamination for strontium and rubidium (Table 5).

Table 5. *Geoaccumulation indices of Sr, Rb and Sc, for the collected soil samples*

Sample code	Igeo(Sr)	Igeo(Rb)	Igeo(Sc)
A1	-0.2983	-0.6174	-0.2193
A2	0.4150	-0.7018	1.3728
A3	-0.1739	-0.6845	0.4828
A4	-0.3114	-0.8289	0.0365
A5	-0.0593	-0.9069	0.3728
CT	-0.5850	-0.5850	-0.5850

Legend: A1-A5 and CT, soil sample codes, CT – soil control sample, Igeo – Geo-Accumulation Index of soil

CONCLUSION

The investigated soil samples, collected from the area with solid waste deposits shows a lower content of rubidium and strontium compared to the normal concentrations of these metals in the upper earth crust, but comparable with the control samples. On the other hand, scandium is present in big quantities in the soil covered by wastes, and less in the control samples. The pollution indices, CF, PI_L and Igeo demonstrate that the pollution with scandium is degrading the soil quality and is a cause for concern.

ACKNOWLEDGEMENTS

All authors are principal authors and have contributed evenly to this paper. Corresponding author: despinabordean@usab-tm.ro.

This research paper was funded by Interreg–IPA Cross–border Cooperation Romania-Serbia Programme - financed by the European Union under the Instrument for Pre-accession Assistance (IPA II) and co-financed by the partner states in the Programme, through the project "Modern technologies for monitoring land covered with waste in order to restore their initial use", 2019–2021, code e-MS: RORS 365.

REFERENCES

[1] Ahamad, M.I.; Song, J.; Sun, H.; Wang, X.; Mehmood, M.S.; Sajid, M.; Su, P.; Khan, A.J., Contamination level, ecological risk, and source identification of heavy metals in the hyporheic zone of the Weihe River, China, International journal of environmental research and public health, Switzerland, 17/3, 1070, 2020.

[2] Bordean D.M., Cojocariu A., Horablaga M., Cojocariu L., Alda S., Nica D., Alda L., Borozan A.B., Scandium, element of surprises**,** Ecology, Economics, Education and Legislation, Conference Proceedings, Bulgaria,vol. I, pp 865-872, 2013,doi:10.5593/SGEM2013/BE5.V1/S20.113, http://sgem.org/sgemlib/spip.php?article3365;

[3] Bordean, D.M.; Borozan, A.B.; Nica, D.; Alda, S.; Cojocaru, L.; Horablaga, M.; Gergen, I. Assessment of soil, copper, cobalt and chromium contamination in old mining areas from Romania, International Multidisciplinary Scientific GeoConference: SGEM, Albena, Bulgaria, 5, 101–108, 2012, June 17–23 http://toc.proceedings.com/19962webtoc.pdf.

[4] European Environment Agency (EEA): Digital Elevation Model (DEM) with spatial resolution at 25 m, Produced using Copernicus data and information funded by the European Union - EU-DEM layers; owned by the Enterprise and Industry DG (DG-ENTR) and the European Commission, Denmark, 2017,

https://www.eea.europa.eu/data-and-maps/data/copernicus-land-monitoring-service-eu-dem

[5] Geospatial database of the Real Estate Cadastre and Advertising Agency, Romania, http://geoportal.ancpi.ro/geoportal/catalog/download/download.page;

[6] Greger M., Uptake of nuclides by plants, Technical Report TR-04-14, Department of Botany, Stockholm University, Sweden, 2004, https://skb.se/upload/publications/pdf/TR-04-14.pdf.

[7] Heghedűş-Mîndru, G., Biron, R.C., Perju, D.M., Rusnac, L.M., Riviş, A., Ştef, D.S., Cation contents in natural mineral waters of Romania determined with the HPIC method, Journal of Food, Agriculture and Environment, Finland, 6, pp: 506–509, 2008, https://doi.org/10.1234/4.2008.1395.

[8] Kenneth Barbalace, Periodic Periodic Table of Elements - Scandium - Sc. EnvironmentalChemistry.com. 1995 - 2021. https://EnvironmentalChemistry.com/yogi/periodic/Sc.html

[9] Khaled, A., Abdel-Halim, A., El-Sherif, Z., Mohamed, L. A., Health risk assessment of some heavy metals in water and sediment at Marsa-Matrouh, Mediterranean Sea, Egypt, Journal of Environmental Protection, 8(01), 74, 2017

[10] McLean, J. E., Bledsoe B. E. Behavior of metals in soils (EPA/540/S-92/018). U.S. Environmental Protection Agency, Washington, D.C., USA, 1992.

[11] Porter, K. E., U.S. Bureau of Mines, Moldova Noua, Geologic information, Romania, https://mrdata.usgs.gov/mrds/show-mrds.php?dep_id=10133958.

[12] Rudnick, R.L., Gao, S., The Composition of the Continental Crust. In: Holland, H.D. and Turekian, K.K., Eds., Treatise on Geochemistry, Vol. 3, The Crust, Elsevier-Pergamon, Oxford, England, 1-64, 2003.

[13] Thomilson D.C., Wilson D.J., Harris C.R., Jeffrey D.W., Problem in heavy metals in estuaries and the formation of pollution index, Helgolander Meeresunters, Germany, 33**,** 566–575 (1980).

[14] Tóth, T., Kovács, Z. A., Rékási, M. XRF-measured rubidium concentration is the best predictor variable for estimating the soil clay content and salinity of semi-humid soils in two catenas, Geoderma, Elsevier, 342, pp. 106-108, 2019.

[15] Vaverková, M. D., Maxianová, A., Winkler, J., Adamcová, D., Podlasek, A., Environmental consequences and the role of illegal waste dumps and their impact on land degradation, Land Use Policy, Elsevier, 89(C), 2019.

COMPARISON OF SUBJECTS OF THE URAL FEDERAL DISTRICT BY THE SHARE OF VEGETABLE COVER

Dr. Sc., Prof. Peter Mazurkin
Volga State University of Technology, Yoshkar-Ola, Russia

ABSTRACT

The ecological consolidation of vegetation according to three classes of the UN soil cover (grass + shrub + trees) is considered. The ecological coefficient is calculated by dividing the share of vegetation by the share of changed land. For the rating, the forest-agricultural coefficient is convenient as the ratio of forest area to arable land. The ecological principle of the consolidation of 13 types of land is proposed, which makes it possible to carry out the ecological consolidation of the vegetation cover and altered human land. According to these proposed criteria, the ranking of the subjects of the Ural Federal District was carried out.

Keywords: *categories, lands, vegetation, ecological factors*

INTRODUCTION

According to N.F. Reimers [1], [2], the ecological balance is a continuously changing ratio. In terms of value, this dynamic ratio must be brought closer by scientific and technical measures to the golden ratio of 0.618 between the vegetation cover and the entire land area.

Ecological consolidation implies the consolidation of land belonging to the vegetation cover. Then it is necessary to identify a rational ratio of 61.8% between the vegetation cover and anthropogenic lands, that is, territories changed by man. These ratios become environmental factors. They will characterize the achieved level of ecological balance.

Land consolidation has a long history, the first work was carried out in Denmark in the middle of the 13th century; in Sweden in 1757, a land consolidation law was passed. In Russia, the process of unification of lands was carried out during the implementation of the Stolypin reform of 1906. One of the measures was the elimination of the communal form of land use, the formation of farms and cuts in order to allocate land in one place instead of numerous inter-striped areas scattered at a considerable distance from each other [3]. As a result, land plots are consolidated on a territorial basis.

Data for ecological consolidation of land are given in [4].

The purpose of the study is to distribute the shares of land from the land area [5] in the subjects of the Ural Federal District (UFO), and then to consolidate them according to the first three classes of the UN soil cover [6] and by identification method [7] to identify patterns.

According to the Land Code of the Russian Federation (No. 136-ФЗ dated 25.10.2001; 2019), agricultural land includes: 01. Arable land; 02. Deposit; 03.

Perennial plantings; 04. Hayfields; 05. Pastures. Non-agricultural lands are subdivided into types: 06. Forestlands; 07. Forest plantations not included in the forest fund; 08. Land underwater; 09. Building land; 10. Lands under the roads; 11. Swamps; 12. Disturbed lands; 13. Other lands.

MATERIALS AND METHODS

For the ecological consolidation of land, a matrix is needed, in which 13 types of land are located in columns and seven categories of the cadastre in rows. Rosstat [7] has such a matrix only as of 01.01.2013. Then the area of land underwater was subtracted from the area by categories and the land area was obtained $S_c = S - S_{08}$ (Table 1). After dividing the area of 12 land by land area (100), the proportion of land (%) was calculated. The shares of land (Table 2) are calculated as follows: $\alpha_{jk} = 100 S_{jk} / (S - S_{08})$, where j — is the number of the UFO subject, k — is the number of the type of land; S — the total area [7] of the Urals Federal District.

Table 1. *Fragment of data on UFO lands by land area [7], thousand hectares*

Cate-gory	Total area	Underwater	Land area	Land area by type					
				01	02	03	…	12	13
1	49505.1	3352.7	46152.4	7866.1	877.7	53.1	⋯	76.8	22192.2
2	2630.3	160	2470.3	308	8.9	51.3	⋯	31.5	178
3	1127.2	92.8	1034.4	15.4	0	0	⋯	67.9	97.9
4	2576.6	175.3	2401.3	0.5	0.7	0	⋯	0	619.6
5	108665.2	4847.7	103817.5	37	1.9	0.2	⋯	97.1	1082.5
6	8951.1	8681.2	269.9	0	0	0	⋯	0.1	13.4
7	8394.2	725.8	By land	103.5	73.2	0.1	⋯	9.1	2219.1
Total	181849.7	18035.5	163814.2	8370.5	962.4	104.7	⋯	282.5	26402.7

Table 2. *Shares of land species from the land area of the Ural Federal District*

Cate-gory	The share of land according to the numbers of their types of land area,%											
	01	02	03	04	05	06	07	09	10	11	12	13
1	4.802	0.536	0.032	1.354	1.750	2.172	2.252	0.028	0.084	1.567	0.047	13.547
2	0.188	0.005	0.031	0.072	0.275	0.322	0.046	0.228	0.098	0.113	0.019	0.109
3	0.009	0.000	0.000	0.018	0.006	0.211	0.008	0.113	0.136	0.030	0.041	0.060
4	0.000	0.000	0.000	0.002	0.002	0.794	0.061	0.002	0.001	0.225	0.000	0.378
5	0.023	0.001	0.000	0.219	0.130	41.276	0.001	0.016	0.166	20.823	0.059	0.661
6	0.000	0.000	0.000	0.000	0.000	0.000	0.000	0.000	0.000	0.156	0.000	0.008
7	0.063	0.045	0.000	0.279	0.150	0.442	0.701	0.001	0.007	1.632	0.006	1.355
Total	5.110	0.587	0.064	1.943	2.314	45.217	3.069	0.389	0.492	24.546	0.172	16.117

According to the UN classification [6] (soil cover classes KPP), in the first place is grass I (04 Hayfields, 05 Pastures and 11 Swamps), in the second place - bush (03 Perennial plantations and 02 Fallow, which in 4-7 years overgrown with

bushes) and on the third III - trees (06 Forest lands and 07 Forest plantations not included in the forest fund).

The vegetation cover is equal to the sum of I + II + III. Then the activity of the vegetation cover on land will be equal $\alpha_{I+II+III} = \alpha_I + \alpha_{II} + \alpha_{III}$. Negatively modified land $\alpha_N = \alpha_{01} + \alpha_{09} + \alpha_{10} + \alpha_{12}$. Then the ecological coefficient will be defined as $K_E = (\alpha_I + \alpha_{II} + \alpha_{III}) / \alpha_N$. In a simplified version, the ratio of the share of forests to the share of arable land gives the forest agricultural coefficient $K_0 = \alpha_{06} / \alpha_{01}$.

Table 3 shows that the forest agricultural coefficient K_0 is sensitive in comparison with the coefficient K_E. The share of the vegetation cover of the Ural Federal District is 75.90% and this is more than 60% according to N.F. Rey-mersu. The main share of 56.04% belongs to the forest fund of the Ural Federal District.

Table 3. *Shares (%) of soil cover classes and ecological factors*

Cate-gory	Proportion of UN soil cover classes and their sum				α_N	K_0	K_E
	α_I	α_{II}	α_{III}	$\alpha_{I+II+III}$			
1	4.672	0.568	4.423	9.664	4.960	0.45	1.9482
2	0.460	0.037	0.368	0.865	0.534	1.71	1.6213
3	0.054	0.000	0.219	0.272	0.299	22.44	0.9101
4	0.228	0.000	0.855	1.084	0.004	2602.20	295.9500
5	21.172	0.001	41.277	62.450	0.264	1827.44	236.2085
6	0.156	0.000	0.000	0.156	0.000	∞	426.5000
7	2.061	0.045	1.144	3.249	0.077	7.00	42.2429
Total	28.803	0.651	48.286	**77.740**	6.163	8.85	12.6144

The total activity of the vegetation cover of the Ural Federal District is 77.74%, which is much higher than the rational ecological balance of 61.8%.

RESULTS AND DISCUSSION

The ecological principle in land use. The main habitat is vegetation. As you know, forests with trees are the core of the planet's biosphere and thus become the main part of the vegetation cover on land [2]. The greatest anthropogenic changes in the soil cover occur in arable land. Therefore, the forest/arable land ratio becomes the first and main environmental factor.

Each person strives for the best, therefore, two vector orientations in behavior are possible [2], [5]: a) less is better (so it will be better) for anthropogenic objects; b) more is better (and this is a blessing) for natural objects.

Table 4 shows vector ecological landmarks for 12 types of land (without underwater) in relation to any territorial unit.

Table 4. *Direction of the vector is better worse by types of land*

Types of land	Less is better	Bigger is better	Types of land	Less is better	Bigger is better
1. Arable land	+	-	7. Plantations outside forests	-	+
2. Deposit	+	-	9. Building land	+	-
3. Perennial plantings	-	+	10. Land under the roads	+	-
4. Hayfields	-	+	11. Swamps	-	+
5. Pastures	-	+	12. Disturbed lands	+	-
6. Forest lands	-	+	13. Other lands	+	-

Land types 1, 9, 10 and 12 clearly belong to natural objects modified by anthropogenic interference. Many people, especially non-specialists, want the quality characteristics of the territory. This is more familiar and more convenient.

In table 5, the scales of forest cover (06 + 07) and plowing (01) are suggested. These two scales were compiled on the basis of the principle of ecological balance of the territory according to N.F. Reimers [2].

Table 5. *Scale classification of the territory of the constituent entities of Russia*

Intervals of values of the coefficient of forest agrarianity, %	Qualitative characteristics of intervals values of the ecological state of the territory	
	forest cover	plowing
More 85	Solid forest	Extremely agrarian
65 - 85	Multi-forest	Ultra-high plowing
45 - 65	Moderate forest	High plowing
25 – 45	Partial forest	Medium agricultural
10 - 25	Low-forest	Moderately agricultural
1 – 10	Non-woody	Low plowing
0 – 1	Treeless	Non-agricultural

Maintaining the ecological balance in a given territory can be carried out by specially allocated plots of land for new forests. The Ural Federal District has a share of the area under trees 48.29% (Table 3) and a share of arable land 5.11% (Table 2). According to table 5, the UFO territory is characterized as moderate forest and low agricultural.

The activity of the vegetation cover by the subjects of the Ural Federal District. Territorial units have a wide range of values in terms of area (Table 6 [4]). To be able to compare the subjects of the federation, it is necessary to switch to the relative shares of the area of categories and lands, divided by the total land area of a group of subjects (federal districts).

Table 6. *Fragment of data on the subjects of the Ural Federal District by land area, thousand hectares*

Code	Subject of the federation	General area	Under water	Square under land	Types of land		
					01	…	13
	Ural federal district	181849.7	18035.5	**163814.2**	8330.5	⋯	26402.7
45	Kurgan region	7148.8	318.6	6830.2	2402.6	⋯	54.7
66	Sverdlovsk region	19430.7	264.5	19166.2	1453.4	⋯	229.6
72	Tyumen region	16012.2	508.5	15503.7	1397.3	⋯	69.5
74	Chelyabinsk region	8852.9	275.9	8577.0	3063.4	⋯	189.4
86	Khanty-Mansiysk jsc	53480.1	3185.6	50294.5	12.9	⋯	520.5
89	Yamalo-Nenets JSC	76925.0	13482.4	63442.6	0.9	⋯	25339.0

For the subjects, the relative shares of land were calculated by dividing the area from Table 6 by the total land area of the Ural Federal District 163814.2 thousand hectares (Table 7).

Table 7. *Shares of land types of subjects of the land area of the Ural Federal District*

Code	The share of land according to the numbers of their types of land area, %											
	01	02	03	04	05	06	07	09	10	11	12	13
45	1.47	0.28	0.01	0.34	0.63	1.07	0.02	0.03	0.05	0.23	0.00	0.03
66	0.89	0.07	0.02	0.38	0.22	8.32	0.14	0.09	0.14	1.25	0.04	0.14
72	0.85	0.20	0.01	0.55	0.46	4.34	0.09	0.05	0.06	2.81	0.00	0.04
74	1.87	0.03	0.02	0.36	0.83	1.65	0.05	0.08	0.09	0.12	0.02	0.12
86	0.01	0.00	0.01	0.21	0.16	17.52	0.10	0.08	0.10	12.17	0.03	0.32
89	0.00	0.00	0.00	0.10	0.02	12.31	2.67	0.06	0.05	7.96	0.08	15.47

Table 8 shows the shares of the first three classes of soil cover according to the UN classification, the sum of the three classes as the share of vegetation cover by regions in relation to the land area of the Ural Federal District, as well as the share of human-changed lands, forest agricultural and ecological coefficients.

Table 8. *Shares (%) of soil cover classes and ecological factors*

Code	Proportion of UN soil cover classes and their sum				α_N	K_0	K_E
	α_I	α_{II}	α_{III}	$\alpha_{I+II+III}$			
45	1.20	0.29	1.10	2.59	1.55	0.732	1.669
66	1.85	0.09	8.46	10.40	1.16	9.376	8.978
72	3.82	0.21	4.43	8.46	0.96	5.090	8.784
74	1.31	0.06	1.70	3.06	2.06	0.884	1.491
86	12.54	0.01	17.61	30.16	0.22	2224.5	134.14
89	8.09	0.00	14.99	23.07	0.19	22411.1	123.48

Due to the relatively low forest cover (1.10% at the border of the treeless area according to Table 5), the Kurgan region received a forest agricultural coefficient of 0.731. However, the lowest value of 1.491 ecological coefficient is observed in

the Chelyabinsk region. The best environmental conditions are observed in the Khanty-Mansiysk Autonomous Okrug.

Rank distribution and rating of the subjects of the federation. The rank ($R = 0,1,2,3,...$) differs from the place in the rating ($I = 1,2,3,...$) by the addition of the digit 0. This allows the use of the positive semi-axis of the abscissas in modelling by the identification method [6], [7].

Table 9 shows the rating of the constituent entities of the Ural Federal District, taking into account the vectors of semantic orientation according to Table 4.

Table 9. *Ranks of lands and rating of subjects by land area of the Siberian Federal District*

Code	Ranks of lands by codes of their types from land area, %												ΣR	I
	01	02	03	04	05	06	07	09	10	11	12	13		
45	6	6	0	0	0	1	0	4	3	2	5	6	33	4
66	5	4	1	3	1	4	3	6	4	5	3	2	41	6
72	2	0	2	4	4	5	4	5	5	6	4	1	42	7
74	0	0	2	5	5	2	2	2	1	3	0	3	25	1
86	3	3	2	2	3	0	5	3	6	0	6	4	37	5
89	0	0	2	6	6	6	6	0	0	4	0	0	30	3

When ranking = RANK (T5; T$5: T$11; 1), the following designations are adopted for the Excel environment: T – is the identifier of the ranked column S01; T5, T$5 - first line; T$10 - last line; $0 \vee 1$ - ranking in descending (0) or ascending (1). The program gives places $I = 1,2,3,....$. For ranks (more convenient for modelling), the expression is used $R = I - 1$.

According to the environmental conditions from Table 4, the first place among the subjects of the Ural Federal District in 2012 was taken by the subject of the federation 74 - the Chelyabinsk region.

The ratings separately for the share of vegetation cover and separately for the ecological factors are shown in Table 10.

Table 10. *Proportion of vegetation and ecological coefficients from the influence of ranks*

Code	Vegetation		Modified land types		Forestry and agricultural coefficient		Total environmental factor	
	R_{PII}	$\alpha_{I+II+III}$	R_N	α_N	R_0	K_0	R_E	K_E
45	5	2.59	4	1.55	5	0.732	4	1.669
66	2	10.40	3	1.16	2	9.376	2	8.978
72	3	8.46	2	0.96	3	5.090	3	8.784
74	4	3.06	5	2.06	4	0.884	5	1.491
86	0	30.16	1	0.22	1	2224.5	0	134.14
89	1	23.07	0	0.19	0	22411.1	1	123.48

In terms of the share of vegetation cover, the zero rank (first place) and the general ecological coefficient is occupied by 86 - Khanty-Mansi Autonomous Okrug, and according to the least changed lands and the highest forest agricultural coefficient - 89 - Yamalo-Nenets Autonomous Okrug.

Regularities of rank distributions. By rating (Table 9), as well as by the share of vegetation cover and separately by ecological coefficients (Table 10), the models in the form of trends (due to the small number of subjects, only six) are given in Table 11.

Table 11. *Parameters of the model of rank distribution of subjects*

Indicator y	Trend equation $y = aexp(-bx^c) + dx^e\exp(-fx^g)$							Coef. correl.
	Exponential law			Biotechnical law				
	a	b	c	d	e	f	g	r
$\sum R$	23.22671	-0.084800	1	9.20654e-39	122.99813	21.99186	1	0.9994
$\alpha_{I+II+III}$	30.39541	0.094098	1	-1.36563e8	5.75246	17.02885	0.24352	1.0000
α_N	0.13270	0	0	0.27947	1.19626	0	0	0.9856
K_0	22413.7	2.52831	1	0	0	0	0	0.9999
K_E	142.77683	0.13563	1	-1.09525e9	9.11700	17.82529	0.35127	1.0000

The greatest adequacy in terms of the correlation coefficient is 1.0000 (due to the equality of the number of model parameters to the number of subjects) for the share of vegetation cover on the land of the Ural Federal District and the ecological coefficient (Fig. 1).

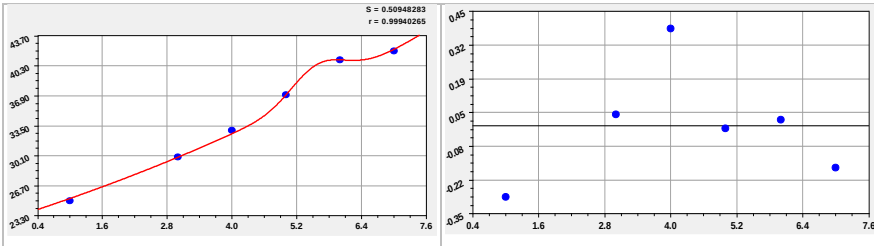

Two-term trend | Remains from the trend

Fig. 1. *Rating graphs (Table 9) the sum of ranks from place*

(S - standard deviation; r - correlation coefficient)

The first term of the trend is Laplace's law (in mathematics), Mandelbrot (in physics), Perl-Zipf (in biology) and Pareto (in econometrics).

The rest of the graphs by ranks are given in Figure 2. The share of vegetation changes according to the Mandelbrot law of exponential decline, and the biotechnical law is subtracted from it (therefore, it is a crisis law). The proportion of altered lands increases according to a power-law function.

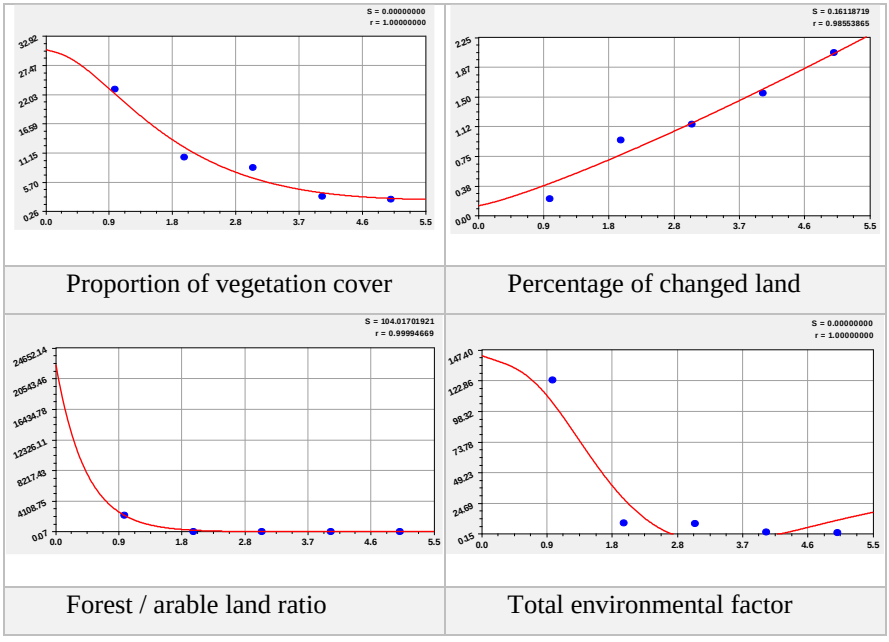

Fig. 2. *Rank distributions of subjects by vegetation parameters*

The greatest simplicity (only one component in the model) has the forest-agrarian coefficient, which decreases according to the Mandelbrot law, and the general ecological coefficient decreases with the crisis according to the biotechnical law.

CONCLUSION

The hierarchy of the constituent entities of the Ural Federal District according to the ecological possibilities of consolidation of vegetation cover according to three classes of soil cover according to the UN classification (grass + shrub + trees) is considered. On land, it is proposed to rank the shares of vegetation cover and human-modified land, as well as ecological coefficients. The total ecological coefficient is calculated by dividing the share of vegetation as a whole and by soil cover classes, the total share of anthropogenic (human-modified) lands. Particularly considered is a very accurate forest agricultural coefficient, as the ratio of forest area to arable land area.

In the future, it becomes possible, in addition to vegetation, to take into account geomorphological, climatic, socio-economic, migration and other subgroups of factors.

ACKNOWLEDGEMENTS

The reported study was funded by Russian Foundation for Basic Research, Government of Krasnoyarsk Territory, Krasnoyarsk Krai Fund of Science, to the research project: «Predictions of the ecological-economic potential for possible

“climatic” migrations in the Angara-Yenisei macroregion in a changing climate of the 21st century»

REFERENCES

[1]. Reimers N.F. Nature management: Dictionary-reference. M .: Mysl, 1990.637 p.

[2]. Mazurkin P.M., Mikhailova S.I. Territorial ecological balance: analyte. overview; Institution Ros. acad. Sciences of the State. public scientific and technical library Sib. branch of RAS, M-education and science Ros. Federation Feder. Maris. state tech. un-t. Novosibirsk: GPNTB SO RAN, 2010.430 p. (Ser. Ecology. Issue 94).

[3]. Myachina M.R., Cherkashin K.I. Consolidation of agricultural lands in Russia: history and modernity // Modern problems of science and education. 2013. No. 1. URL: http://science-education.ru/ru/article/view?id=8428 (Date of access: 14.06.2020)].

[4]. Land fund of the Russian Federation as of January 1, 2013. Moscow: Rosreestr, 2013. 694 p.. URL: doc_LandFund2012.

[5]. Mazurkin P.M. Ecological distribution of land among the subjects of Russia // Scientific and practical journal "Natural resources of the Earth and environmental protection". 2020.Vol. 1.No. 5. P. 10-19.http://dx.doi.org/10.26787/nydha-2713-203X-2020-1-5-10-19.

[6]. Global Agro-ecological Assessment for Agriculture in the 21st Century: Methodology and Results. G¨unther Fischer, Harrij van Velthuizen, Mahendra Shah, Freddy Nachtergaele. International Institute for Applied Systems Analysis, Laxenburg, Austria. Food and Agriculture Organization of the United Nations. VialedelleTerme di Caracalla. Rome, Italy, 2002. Url: http://webarchive.iiasa.ac.at/ Research/LUC/SAEZ/index.html.

[7]. Mazurkin P.M. Method of identification // 14th International multidisciplinary scientific geoconferenct & SGEM2014. GeoConferencejnnano. Bio and green – technologies for a sustainable future. Conference proceedincs. Volume 1. Section Advances in Biotechnology. 17-26 June 2014. Albena. Bulgaria. P. 427-434.

ECOLOGICAL CONSOLIDATION OF LANDS IN RUSSIA AND FEDERAL DISTRICTS

Dr. Sc., Prof. Peter Mazurkin
Volga State University of Technology, Yoshkar-Ola, Russia

ABSTRACT

It is proposed to identify the hierarchy of federal districts in terms of ecological opportunities for consolidation of vegetation cover according to three classes of soil cover according to the UN classification (grass + shrub + trees) on the land territory of Russia by ranking the shares of vegetation cover and human-modified lands, as well as ecological coefficients. The total ecological coefficient is calculated by dividing the share of vegetation by the total share of anthropogenic land. The forest-agricultural coefficient is convenient as the ratio of the forest area to the arable land area. The identification method revealed stable regularities of rank distributions in the form of trends and wave equations.

Keywords: *categories, land, vegetation, coefficients, rating, patterns*

INTRODUCTION

The article [1] analyzes the main problems of the implementation of programs for the integration of efforts of the countries of the Union of Independent States in the field of land management. New approaches and digital technologies in land management are proposed. Another article [2] shows that a decrease in the role of land management and environmental and land management expertise leads to a violation of land management and environmental legislation, soil degradation. However, the unification of soil cover classes according to the UN classification with 13 types of land adopted in Russia is still not carried out.

Changes are needed in the land classifications themselves in accordance with GOST 26640-85 (ST SEV 4472-84) and in the Land Code of the Russian Federation No. 136-FZ dated October 25, 2001 (2019 as amended) in accordance with the UN classification, as well as an understanding of ecological balance (according to NF Reimers [3]) on a specific territory. This would significantly improve the websites of Rosstat.

In the book [4], we adhered to the concept of ecological balance, developing the ideas of prof. N.F. Reimers. In this concept, the accounting time interval depends mainly on the methods and means of measuring the properties, structure and parameters of landscapes, population and the system of farms (geotriads) on the territory of these landscapes.

According to N.F. Reimers, the ecological balance is a constantly changing ratio. In terms of value, this dynamic ratio must be brought closer by scientific and technical measures to the golden ratio of 0.618 between the vegetation cover and the entire land area.

The purpose of the study is to identify stable patterns [9, 10, 11] of the distribution of land shares from the land area in federal districts (FD) according to the ecological principle, and then their consolidation according to the first three classes of the UN soil cover [12] and by the identification method [13], [14], [15] rank distributions among federal districts.

MATERIALS AND METHODS

Ecological consolidation of land. It implies the unification of land belonging to the vegetation cover. Then it is necessary to identify a rational ratio of 61.8% between the vegetation cover and anthropogenic lands, that is, territories changed by man. These ratios become environmental factors. They will characterize the achieved level of ecological balance.

Consolidation (from the Latin con - together, solido - I strengthen) - strengthening, unification, integration, the rallying of something. In computer science, it is a complex of methods and procedures aimed at extracting data from various sources [5].

Land consolidation has a long history, the first work was carried out in Denmark in the middle of the 13th century; in Sweden, in 1757 a land consolidation law was passed. In Russia, the process of land unification was carried out in the Stolypin reform of 1906. One of the measures carried out within the framework of the reform was the elimination of the communal form of land use, the formation of farms and cuts in order to allocate land in one place instead of numerous inter-striped plots scattered at a considerable distance from each other [6], [7]. As a result, land plots are consolidated according to the territorial principle.

The data for the ecological consolidation of Russian lands are given in [8].

According to GOST 26640-85 (ST SEV 4472-84), lands that are systematically used or suitable for use for specific economic purposes, and that differ in natural and historical characteristics, are called lands. Anthropocentrism flourishes in the definition. According to the Land Code of the Russian Federation (No. 136-ФЗ dated 25.10.2001), agricultural land includes: 01. Arable land; 02. Deposit; 03. Perennial plantings; 04. Hayfields; 05. Pastures. Non-agricultural land: 06. Forest land; 07. Forest plantations not included in the forest fund; 08. Land underwater; 09. Building land; 10. Land under roads; 11. Swamps; 12. Disturbed lands; 13. Other lands.

Initial data. For the ecological consolidation of land, a data matrix is needed, in which 13 types of land are located in columns, and seven categories of the land cadastre in rows (Table 1).

Table 1. *Shares of land species* α *from the land area of Russia*

Cate-gory	The share of land according to the numbers of their species from the land area, %											
	01	02	03	04	05	06	07	09	10	11	12	13
1	7.03	0.27	0.07	1.14	3.47	1.76	1.18	0.07	0.14	1.51	0.01	6.11
2	0.28	0.00	0.04	0.06	0.21	0.13	0.04	0.22	0.12	0.03	0.01	0.07
3	0.01	0.00	0.00	0.02	0.04	0.25	0.03	0.06	0.11	0.02	0.02	0.44
4	0.00	0.00	0.00	0.00	0.03	1.09	0.04	0.00	0.00	0.20	0.00	1.33
5	0.01	0.00	0.00	0.11	0.15	49.71	0.00	0.01	0.11	6.77	0.02	10.48
6	0.00	0.00	0.00	0.00	0.00	0.00	0.00	0.00	0.00	0.03	0.00	0.01
7	0.09	0.03	0.00	0.14	0.26	0.30	0.32	0.00	0.01	0.77	0.01	3.01
Total	7.42	0.30	0.11	1.47	4.15	53.24	1.61	0.35	0.49	9.33	0.06	21.44

It turned out that Rosstat [8] has such a matrix only as of 01.01.2013. Then the area of land underwater was subtracted from the area by category and the area on land was obtained $S_c = S - S_{08}$. After dividing the area of 12 lands by the land area of Russia, the share of lands was calculated (Table 1): $\alpha_{jk} = 100 S_{jk} / (S - S_{08})$, where j – is the number of federal district, k – is the number of the type of land; S – the total area [8] of the Russian Federation.

4Oscillations (wavelet signals) are written by the wave formula [3] of the form

$$y_i = A_i \cos(\pi x / p_i - a_{8i}), \qquad A_i = a_{1i} x^{a_{2i}} \exp(-a_{3i} x^{a_{4i}}),$$
$$p_i = a_{5i} + a_{6i} x^{a_{7i}}, \qquad (1)$$

where y – is the indicator

i – is the number of the component (1)

x – is the explanatory variable

$a_1 ... a_8$ – are the parameters (1)

A_i – the amplitude (half) of the wavelet

p_i – the half-period.

RESULTS AND DISCUSSION

The ecological principle in land use. The main habitat on land, including humans, is vegetation. Therefore, it is necessary to consider changes in the vegetation cover by the area of individual components (grass, bushes, trees). As is known, forests are the core of the biosphere and thus become the main part of the vegetation cover [4]. The greatest anthropogenic changes in the soil cover occur in arable land. Therefore, the forest / arable land ratio becomes the first ecological factor [9].

Each strives for the best and two vector orientations in behavior are possible [4], [11]: a) less is better for anthropogenic objects; b) more is better for natural objects (Table 2).

Table 2. *Direction of the vector is better → worse by types of land*

Types of land	Less is better	Bigger is better	Types of land	Less is better	Bigger is better
1. Arable land	+	-	7. Plantations outside forests	-	+
2. Fallow or unused arable	+	-	9. Building land	+	-
3. Perennial plantings	-	+	10. Under the roads	+	-
4. Hayfields	-	+	11. Swamps	-	+
5. Pastures	-	+	12. Disturbed lands	+	-
6. Forest lands	-	+	13. Other lands	+	-

Land types 1, 9, 10 and 12 clearly belong to natural sites modified by anthropogenic interference. Arable land has developed extensively, so nowadays, due to ineffective use, a lot of deposits are formed as a waste of arable land. Moreover, the deposits are intensively overgrown with shrubs. Other lands are classified by us as conditional anthropogenic objects due to the uncertainty of their purpose. Building land and under roads are man-made objects. Disturbed lands are objects, but require reclamation.

In Russia, even on agricultural land, there is not even a territorial consolidation of land for farms. And abroad, consolidation has long been understood for all types of land, that is, environmental consolidation is being carried out. For example, in Finland, with an average farm area of 35 hectares, a third is allocated for trees, a third for arable land, and a third includes other types of land (buildings, roads, etc.). Then in Finland the rational coefficient of forest agrarian [9], as the ratio of forest area to arable land, is equal to 1.

Many people want the quality characteristics of the territory. This is more familiar and more convenient. Table 3 suggests scales for forest cover (06 + 07) and plowed area (01).

Table 3. *Scale for the classification of the territory of the constituent entities of Russia*

Value ranges coefficient forest / arable land, %	Qualitative characteristics of intervals values of the ecological state of the territory	
	forest cover	plowing
Более 85	Solid forest	Extremely agrarian
65 - 85	Multi-forest	Superhigh-agar
45 - 65	Moderate forest	High-agar
25 – 45	Partial forest	Medium agricultural
10 - 25	Low-forest	Moderately agricultural
1 – 10	Non-woody	Low agar
0 – 1	Treeless	Non-agricultural

Russia has a share of the area under trees 53.24 + 1.61 = 54.85% and a share of arable land 7.42% (Table 1), which is much less than 40%. According to table 4, it is characterized as moderately forest and low agricultural.

Vegetation cover activity by federal districts. Territorial units have an area [8] and have a wide range of values. To be able to compare the districts, it is necessary to switch to the relative shares of the area of categories and lands, divided by the total land area (Table 4).

Table 4. *Shares of land types α in the districts from the land area of Russia*

County	The share of land according to the numbers of their species on land,%											
	01	02	03	04	05	06	07	09	10	11	12	13
CFD	1.458	0.027	0.032	0.158	0.360	1.443	0.109	0.076	0.088	0.076	0.010	0.052
NFD	0.210	0.015	0.007	0.110	0.076	5.657	0.227	0.029	0.054	1.568	0.008	1.699
SFD	1.049	0.001	0.015	0.051	0.825	0.174	0.039	0.036	0.041	0.032	0.001	0.152
NCFD	0.344	0.001	0.010	0.034	0.349	0.120	0.016	0.015	0.018	0.003	0.001	0.103
VFD	2.216	0.055	0.022	0.224	0.847	2.387	0.092	0.069	0.110	0.055	0.005	0.099
UFO	0.509	0.059	0.006	0.194	0.231	4.523	0.307	0.039	0.049	2.455	0.017	1.612
SFO	1.465	0.118	0.013	0.558	1.309	18.154	0.344	0.067	0.092	2.554	0.011	5.683
FEFD	0.167	0.027	0.004	0.137	0.153	20.779	0.474	0.024	0.035	2.588	0.011	12.040

According to the UN classification [12] (soil cover classes), in the first place is grass I (04 Hayfields, 05 Pastures and 11 Swamps), in the second place II - shrubs (03 Perennial plantations and 02 Fallows), which at first quickly overgrows grass, and after 4-7 years and shrubs) and on the third III - trees (06 Forest lands and 07 Forest plantations not included in the forest fund).

The vegetation cover is equal to the sum of I + II + III (Table 5). Then the activity of the vegetation cover on land will be equal to $\alpha_{I+II+III} = \alpha_I + \alpha_{II} + \alpha_{III}$. The negatively modified land is formed from the sum $\alpha_N = \alpha_{01} + \alpha_{09} + \alpha_{10} + \alpha_{12}$. Then the ecological coefficient will be determined from the ratio $K_E = (\alpha_I + \alpha_{II} + \alpha_{III}) / \alpha_N$. In a simplified version, the ratio of the share of forests to the share of arable land gives the forest agricultural coefficient $K_0 = \alpha_{06} / \alpha_{01}$ [9].

Table 5. *Shares (%) of soil cover classes and ecological factors*

County	Proportion of UN classes and their sums				α_N	K_0	K_E
	α_I	α_{II}	α_{III}	$\alpha_{I+II+III}$			
CFD	0.593	0.059	1.552	2.204	1.631	0.990	1.351
NFD	1.754	0.022	5.884	7.660	0.300	26.996	25.516
SFD	0.909	0.017	0.213	1.139	1.128	0.166	1.010
NCFD	0.387	0.011	0.136	0.535	0.377	0.350	1.419
VFD	1.126	0.077	2.479	3.682	2.399	1.077	1.534
UFO	2.881	0.065	4.830	7.777	0.614	8.892	12.665
SFO	4.420	0.131	18.498	23.049	1.635	12.390	14.098
FEFD	2.878	0.032	21.253	24.163	0.238	124.129	101.651

All federal districts of Russia have an environmental coefficient greater than 1.

Rank distribution and ranking of districts. The rank ($R = 0,1,2,3,\cdots$) differs from the place in the rating ($I = 1,2,3,\cdots$) by the addition of the digit 0. This allows the use of the positive semi-abscissa axis in modelling by the identification method [14, 15].

When ranking = RANK (T5; T$5: T$13; 1), the following designations are adopted for the Excel environment: T is the identifier of the ranked column; T5, T$5 - first line; T$13 - last line; $0 \vee 1$ - ranking in descending (0) or ascending (1). The program gives places $I = 1,2,3,\cdots$. For ranks (more convenient for modelling), you need to apply an expression $R = I - 1$.

In terms of environmental conditions from Table 5, the first place in 2012 was taken by the Far Eastern Federal District, the second - by the North-West and the third - by the Siberian Federal District. The ratings separately for the share of vegetation cover and separately for the environmental factors are shown in Table 6.

Table 6. *Proportion of vegetation and ecological coefficients depending on ranks*

County	Vegetation cover		Modified land		Forest agrarian coefficient		Ecological coefficient	
	R_{PII}	$\alpha_{I+II+III}$, %	R_N	α_N, %	R_0	K_0	R_E	K_E
CFD	5	2.204	5	1.631	5	0.990	6	1.351
NFD	3	7.660	1	0.300	1	26.996	1	25.516
SFD	6	1.139	4	1.128	7	0.166	7	1.010
NCFD	7	0.535	2	0.377	6	0.350	5	1.419
VFD	4	3.682	7	2.399	4	1.077	4	1.534
UFO	2	7.777	3	0.614	3	8.892	3	12.665
SFO	1	23.049	6	1.635	2	12.390	2	14.098
FEFD	0	24.163	0	0.238	0	124.129	0	101.651

According to four criteria, the Far Eastern Federal District received a zero rank.

Environmental factors for federal districts. The rank distribution of the forestry coefficient is given in Figure 1, and the ecological coefficient is shown in Figure 2.

The latter, according to the ranks of the ecological coefficient of three districts (rank 5 - North Caucasian, rank 6 - Central, and rank 7 - Southern federal districts) need agrarian ecological reforms. Here it is necessary to increase the area of forests. Such measures have been taken in the United States since 1960, and in China since 1970. The US government has allocated subsidies to farmers so that they plant one third of their territory with trees. By the end of the 20th century, yields increased and the gross harvest was higher than even before the environmental reform.

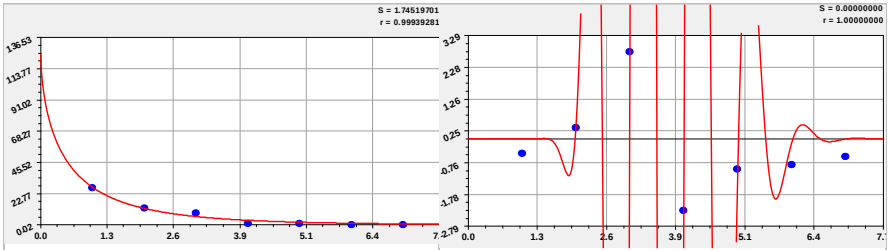

Fig. 1. *Graphs of the rank distribution of the forest agricultural (forest / arable land) coefficient*

(S *- standard deviation;* r *- correlation coefficient)*

The one-component trend is our modified Mandelbrot's law (in physics) of exponential decay. The same law is well known in mathematics (Laplace's law), in biology (Perl-Zipf's law) and in econometrics (Pareto's law). The second component is equation (1) of an asymmetric wavelet showing the oscillatory disturbance of the federal districts of Russia. Then it turns out that land use in our country occurs according to the unconscious laws of oscillatory adaptation. People try, in spite of natural adaptation, to control natural processes according to their own concepts (for example, according to the Soviet doctrine of steady growth). It is necessary to understand the ecological balance not only at the level of municipalities, but even at the level of specific land users. The main thing is the ecological consolidation of land plots at any level of land use.

According to the modified Mandelbrot's law, the trend of the rank distribution of the ecological coefficient has a similar character. Thus, the subjects of the Russian Federation receive a fractal distribution [11]. However, the calculation of the forest and agricultural coefficient (forest / arable land) is simpler due to the need to take into account only the area of the forest fund and the area of arable land. Data for these lands are available even at the structural level of landowners.

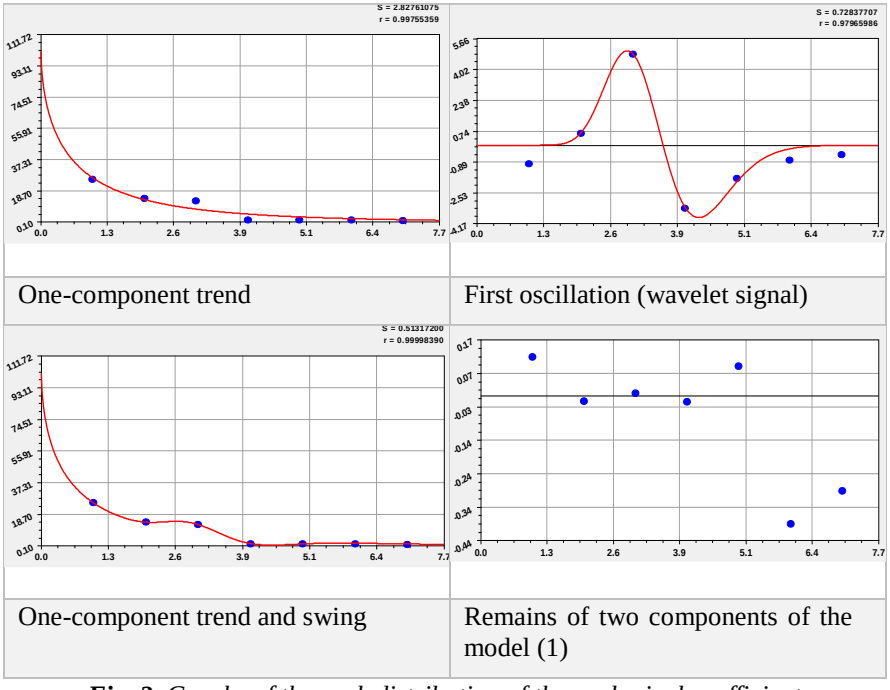

One-component trend	First oscillation (wavelet signal)
One-component trend and swing	Remains of two components of the model (1)

Fig. 2. *Graphs of the rank distribution of the ecological coefficient*

CONCLUSION

The hierarchy of the federal districts of the Russian Federation, according to the ecological possibilities of the consolidation of the vegetation cover according to the three classes of soil cover according to the UN classification (grass + shrub + trees) on the land, is proposed to be identified by the ranking of the shares of the vegetation cover and human-modified lands, as well as ecological -coefficients. The total ecological coefficient is calculated by dividing the share of vegetation in general and by soil cover class (according to the UN classification) by the total share of anthropogenic (human-modified) land. The forest and agricultural coefficient is especially considered, as the ratio of forest area to arable land area.

For the federal districts of Russia, the identification method revealed stable patterns of rank distributions of the share of vegetation, the share of anthropogenic lands, forest and agricultural coefficient, as well as the ecological coefficient.

In the future, it becomes possible to take into account geomorphological, climatic, socio-economic, and even migration subgroups of factors in addition to the land cover. However, apparently, due to the sharp difference in the values of climatic and socio-economic indicators, to expand the system of factors in the geotriad "territory + population + economy" [4], it will still be necessary to group the factors.

ACKNOWLEDGEMENTS

The reported study was funded by Russian Foundation for Basic Research, Government of Krasnoyarsk Territory, Krasnoyarsk Krai Fund of Science, to the research project: «Predictions of the ecological-economic potential for possible “climatic” migrations in the Angara-Yenisei macroregion in a changing climate of the 21st century»

REFERENCES

[1]. Volkov S.N., Shapovalov D.A., Nilishovsky V.I. International integration in the field of land management - new approaches and prospects // Land management, cadastre and monitoring of land. 2020. No. 10. P. 5-13. DOI: 10.33920/sel-4-2010-01.

[2]. Yakovlev A.S., Gordenko A.S., Sizov A.P., Ogorodnikov S.S. Modern problems of land management and environmental and land management expertise in the Russian Federation // Land management, cadastre and monitoring of lands. 2020. No. 2. P. 15-21.

[3]. Reimers N.F. Nature management: Dictionary-reference book. M .: Mysl, 1990.637 p.

[4]. Mazurkin P.M., Mikhailova S.I. Territorial ecological balance: analyte. overview; Institution Ros. acad. Sciences of the State. public scientific and technical library Sib. branch of RAS, M-education and science Ros. Federation Feder. Maris. state tech. un-t. Novosibirsk: GPNTB SO RAN, 2010.430 p. (Ser. Ecology. Issue 94).

[5]. Oreshkov V.I. Paklin N.B. Data Consolidation - Key Concepts // Chapter from the book "Business Intelligence: From Data to Knowledge". URL: https://www.cfin.ru/itm/olap/cons.shtml (Date of treatment 06/16/2020).

[6]. Myachina M.R., Cherkashin K.I. Consolidation of agricultural lands in Russia: history and modernity // Modern problems of science and education. 2013. No. 1. URL: http://science-education.ru/ru/article/view?id=8428 (Date of access: 14.06.2020)].

[7]. Ivanov N.I., Sorogin A.S. Approaches to improving the methodology of land management design in the system of the agro-industrial complex on the basis of land consolidation // Earth Sciences. 2020. No. 1. S.100-105.

[8]. Land fund of the Russian Federation as of January 1, 2013. Moscow: Rosreestr, 2013.694 p. URL: doc_LandFund2012.

[9]. Mazurkin P.M. Forest agrarian Russia and global dynamics of forest management. Yoshkar-Ola: MarSTU, 2007.334 p.

[10]. Mazurkin P.M. Factor analysis of the subjects of the Russian Federation by shares of land // Scientific and practical journal "Natural resources of the Earth and environmental protection". 2020.Vol. 1.No. 6. P. 14-23.http://dx.doi.org/10.26787/nydha-2713-203X-2020-1-6-14-23.

[11]. Mazurkin P.M. Ecological distribution of land among the subjects of Russia // Scientific and practical journal "Natural resources of the Earth and environmental protection". 2020.Vol. 1.No. 5.P. 10-19. http://dx.doi.org/10.26787/nydha-2713-203X-2020-1-5-10-19.

[12]. Global Agro-ecological Assessment for Agriculture in the 21st Century: Methodology and Results. G¨unther Fischer, Harrij van Velthuizen, Mahendra Shah, Freddy Nachtergaele. International Institute for Applied Systems Analysis, Laxenburg, Austria. Food and Agriculture Organization of the United Nations. VialedelleTerme di Caracalla. Rome, Italy, 2002. Url: http://webarchive.iiasa.ac.at/ Research/LUC/SAEZ/index.html.

[13]. Mazurkin P.M. Method of identification // 14th International multidisciplinary scientific geoconferenct & SGEM2014. GeoConferencejnnano. Bio and green – technologies for a sustainable future. Conference proceedincs. Volume 1. Section Advances in Biotechnology. 17-26 June 2014. Albena. Bulgaria. P. 427-434.

[14]. Mazurkin P.M. Wavelet Analysis Statistical Data. Advances in Sciences and Humanities. Vol. 1, No. 2, 2015, pp. 30-44. Doi 10.11648/j.ash.20150102.11.

[15]. Mazurkin P.M. Factor analysis of the parameters of samples of the steppe soil and grass of Mongolia and Inland Mongolia of China on the eastern transect of the Eurasian steppe. Journal of Geological Research. Vol. 03, Issue 01, January 2021, pp. 1-10. DOI: https://doi.org/10.30564/jgr.v3i1.2520.

PERIODIC DRAFT TILLAGE FORCES IN SOIL WORKING PROCESSES OF AGRICULTURAL EQUIPMENT

Math. Cardei Petru[1]
SR Oprescu Remus Marius[2]
Ph.D. Eng. Muraru Vergil[3]
Ph.D. Eng. Muraru Sebastian[4]
Ph.D. Eng. Muraru-Ionel Cornelia[5]
[1, 2, 3, 4, 5] The National Institute of Research – Development for Machines and Installations designed for Agriculture and Food Industry – INMA, Romania

ABSTRACT

The article presents results of the mathematical modelling of the tensile strength for equipment for opening and compartmentalizing watering furrows. This agricultural machine develops a less common traction force, with two components, one of which with oscillates behavior. The mathematical model given in the paper provides calculation formulas for the static component and for the dynamic component. Model constants are used to calibrate the model using existing experimental data for this type of machine. The paper it is specified the dynamics problems of agricultural machines in which such models are needed.

Keywords: *draft force, mathematical model, agricultural equipment*

INTRODUCTION

The tensile strength of an agricultural machine is the main component for estimating the traction power required to operate it. Knowing this is important for choosing a tractor, for estimating working speed and fuel consumption, for estimating productivity, and for improving and even optimizing the working regime.

Theoretical modelling of the tensile strength is possible through engineering intuition and assumptions that are made about a car in the design and design stage. When the machine is already made and tested, these models can be calibrated using available model constants and experimental data. Finally, theoretical-empirical formulas are obtained that can be used for the purposes listed above, for various types of soils, working regimes, and even different power sources to which the equipment can be coupled, of course taking into account the quality requirements of soil processing.

In the literature, we do not know an approach to the problem of mathematical modelling of the draft soil tillage force, for the equipment such as the one that is the subject of our research.

MATERIAL AND METHOD

The subject (material) of this research is the equipment of open and compartmentalized irrigation canals (EOCIC), [1]. The EOCIC equipment was

tested for the choice of a mathematical model of the tensile strength, and we used experimental data to calibrate the model. The main component of the tensile strength is generated by the interaction with the ground of the working member called lister or double mouldboard.

The blade that gives the final shape of the irrigation channel generates a secondary component that has values below 20% of the maximum value of the lister resistance force. In addition to the two components I wrote about above, there is also a component given by the friction with the ground of the driving wheel of the blade drive mechanism and the friction component of the ground rolling of the working depth limiting wheels.

We have neglected these forces or we will include them in the friction component of the lister resistance force, as we do not study the equilibrium of the structure in relation to the distribution of the load forces in this research. The main parameters of the model, notations, and units of measurement are listed in table 1.

Table 1. *Parameters of the interaction process between soil and the EOCIC: notations, significance, and units of measure.*

Notation	Name	Unit
m	EOCIC mass	kg
m_p	Pallet with actuating mechanism mass	kg
R_l	Draft force generated by the lister	N
R_b	Draft force generated by the blade	N
R_T	The total draft force	N
v	Working speed	m/s
b	Lister working width	m
a	Lister working depth	m
k	Coefficient that characterizes specific soil deformation resistance	MPa
ε	Coefficient which depends on the shape of the active surface of the body and the soil properties	kg/m^3
f	Coefficient analogous to friction coefficient	-
G	EOCIC weight	N
g	Gravitational acceleration	m/s^2
ρ	Soil mass density	kg/m^3
c_r	EOCIC mass distribution coefficient on the lister	-
B_d	The length of the small base of the blade	m
B_b	The length of the large base of the blade	m

Notation	Name	Unit
H_d	The height of the projection of the blade on the normal plane at the direction of travel	m
L	Average length of open channel	m
φ	Frequency of the draft soil tillage force function generated by the blade	Hz

The method of designing the model by choosing suitable models is the one described in [2]. Taking into account the specified method, a Goriacikin type formula is proposed for the tensile strength generated by the lister, [3-14]:

$$R_l(a,b,v) = f \cdot c_r \cdot m + k \cdot a \cdot b + \varepsilon \cdot a \cdot b \cdot v^2 \quad (1)$$

The resistance force generated by the blade is an approximately time-periodic component of the total resistance force. The hypothesis which we use for modelling this component considers the amplitude is given by a Goriacikin type product with coefficients similar to the force R_l, reduced accordingly taking into account that the soil that the pallet encounters in the open channel is partially disaggregated, so easier.

The area of the contact surface of the pallet with the ground is the area of the intersection surfaces between the lister open channel section and the surface of the blade projected on the normal plane at the forward direction, A_p. If the section of the channel opened by the lister is larger than the area of the projection of the blade on the plane normal to the forward direction, then function A_p is zero.

$$A_p(a,b) = \begin{cases} \frac{(B_d + B_b)H_d}{2} - ab, if \frac{(B_d + B_b)H_d}{2} - ab \geq 0 \\ 0, if \frac{(B_d + B_b)H_d}{2} - ab < 0 \end{cases} \quad (2)$$

By hypothesis, in the absence of an exact kinematic study and taking into account the random character of the soil parameters, more pronounced the harder and less humid the soil, the periodic component is modelled as a triangular signal approximated by Fourier series corresponding with the frequency given by the report between the length of the channel and working speed:

$$\varphi = \frac{v}{L} \quad (3)$$

In these conditions (hypotheses) the force generated by the action of the blade receives the expression:

$$R_b(a,b,v,t) = f \cdot g \cdot m_p + \left(k_1 + \varepsilon_1 v^2\right) A_p(a,b) \Theta(v,t). \quad (4)$$

where the function $\Theta(t)$ is a Fourier, [13, 14], series approximation for the ideal working rate of the palette:

$$\Theta(v,t) = 0.5 - \frac{1}{\pi}\sum_{j=1}^{\infty}\left\{(-1)^j \frac{\sin\left[j\cdot\frac{2\pi v}{L}\cdot\left(t+0.53\frac{L}{v}\right)\right]}{j}\right\} \quad (5)$$

For the numerical calculation, in formula (5) the amount was limited to 50 terms. It is considered a constant working speed, *v*, and then the space covered by the aggregate will be:

$$s(v,t) = v\cdot t \quad (6)$$

Function (6) is used to control the tensile strength in relation to space travelled.

RESULTS

The mathematical model (1) - (6) of the resistance forces developed in the working process by EOCIC, allows the mathematical modelling of the experimental results and, in case the model will be validated, its extension also in other environmental conditions. Next, for a deeper understanding, some graphical representations of the model behavior are given for the following values of the modelling parameters: m= 110 kg, m_p= 5 kg, g= 9.81 ms^{-2}, c_r= 0.4, ρ= 1100 kgm^{-3}, k= 70000 Pa, ε= 2000 kgm^{-3}, B_d= 0.2 m, B_b= 0.4 m, H_d= 0.1 m, L= 2.8 m, v= 0.85 ms^{-1} (3.06 km per hour).

With the numerical data above and those specified in part for each of the graphical representations in Figures 1-5, the variation in time and space of the total tensile strength and its components is still represented. The time and space (separately) dependence of the total draft tillage force of EOCIC, is represented graphically in fig. 1 and 2.

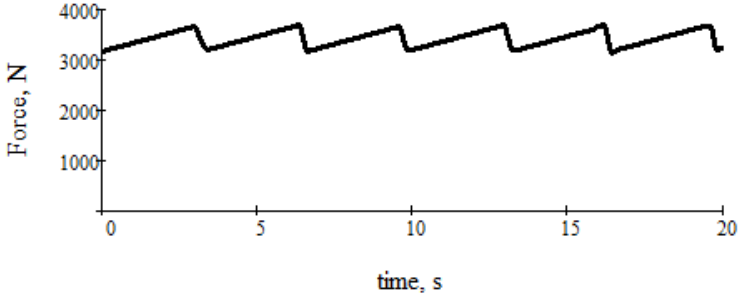

Fig. 1. *Time variation of the total tensile strength of EOCIC.*

For the working speed and the length of the channel, specified above, a frequency of the draft tillage force generated by the blade is obtained, with the value 0.304 Hz, respectively the period with the value 3.294 s. The six complete cycles in 20 s are observed (figure 1 and 4) or in approximately 17 m travelled in work.

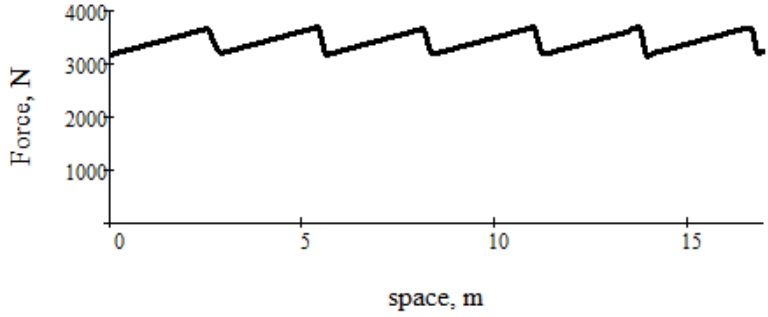

***Fig. 2**. Space dependence of the total draft tillage force generated by EOCIC in the working process.*

Figure 3 graphically represents the variation of the draft soil tillage force generated by the blade, in relation to the space travelled by the aggregate. Figure 4 compares the variation of the total tensile strength and its components, in relation to time.

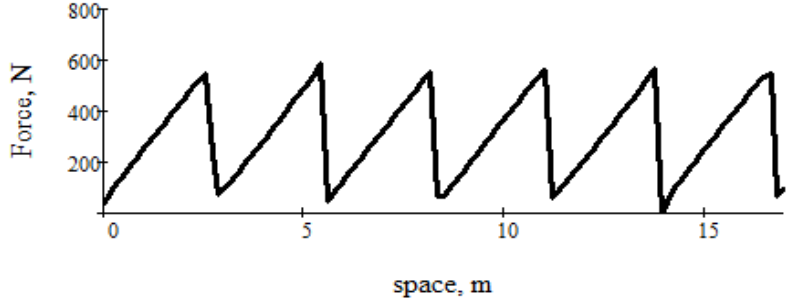

***Fig. 3.** Space dependence of the draft soil tillage force generates by the EOCIC blade, in the working process.*

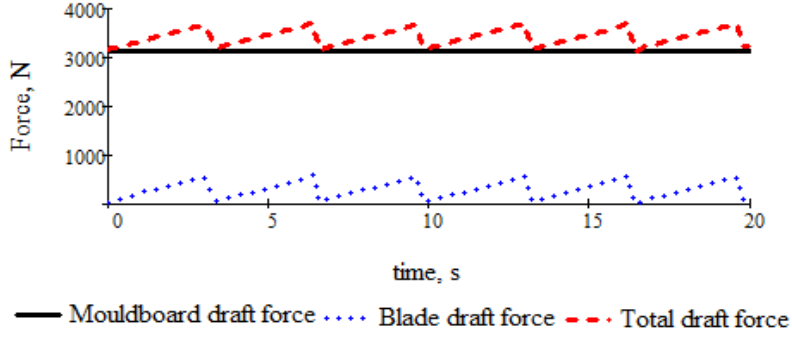

***Fig. 4.** Comparative time dependence of the total draft soil tillage force and its components.*

Figure 5 shows graphically the dependence of the total draft soil tillage force, as a function of the working depth and working speed, for four values of the working width of the lister.

The draft soil tillage formulas which are given in the model (1) - (6), give, for various choices of the working regime, values included in the experimentally determined membership intervals: 1500 - 5000 N for the total tensile strength and 0 - 800 N for the tensile strength generated by the blade, [1]. For example, under the conditions specified by the above parameters, for a = 0.1 m, b = 0.4 m and working speed 1 ms^{-1}, it is obtained at time t = 0 s, R_T = 2684 N, and at time t = 2.7 s (when a maximum of the resistance to the blade is reached), R_T = 3601 N. If the working depth is doubled, a = 0.2, R_T = 5167 N is obtained.

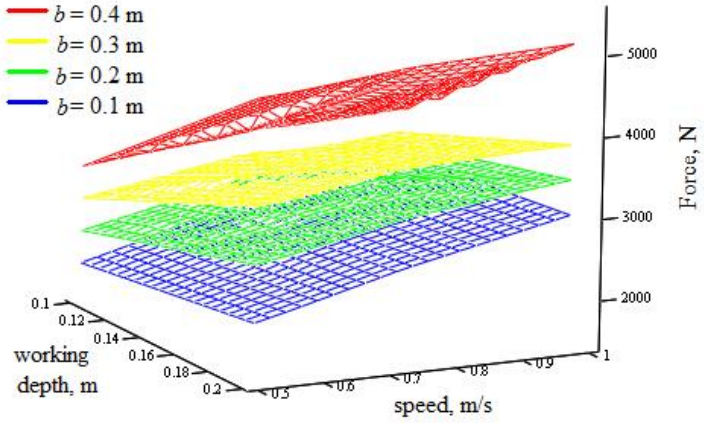

Fig. 5. *Depth and speed working dependence of the total draft soil tillage force of EOCIC, for four values of the working width of the lister.*

COMMENTS

In formula (4), normally the dependence on the length of the channel of the tensile strength force generated by the blade should be introduced. The correction can be made with a coefficient obtained by relativization at a reference length. Having no experimental data available for different values of the length of the open irrigation canal, we did not introduce this correction.

In all the formulas of the mathematical model of the tensile strength (1) - (6) we used the hypothesis that the working speed of the aggregate is constant.

The modelling of the draft soil tillage force generated by the blade made according to (4) and (5) is elementary. The reasons for this statement are: the random nature of the working process of the blade and the mode of operation with precise control of the blade. To perform a more in-depth analysis, the analysis of the blade drive mechanism must be used. The analysis of the mechanism is not simple and requires accurate information about its components. Given the random nature of soil behavior (composition, breakage, deformation, etc.) and the lack of a

minimum of the necessary information about soil behavior in the EOCIC work process, the approach to a description at this level of depth is questionable. Therefore, modelling at a higher level of depth remains for the future.

The intensity of the draft soil tillage force depends very much on the soil moisture, which appears in the model only by the soil characteristics, f, ρ, k, and ε.

CONCLUSIONS

The draft soil tillage force generated by the EOCIC equipment in operation can be modelled mathematically in many ways. In our investigation, the modelling is done with the help of relations (1) - (4). The built model has a series of constants or model parameters that allow its calibration to the experimental data known for the equipment.

The model parameters used to represent both the influence of the environmental conditions in the process and the calibration parameters specific to the model, with the role of making the model respect certain relationships between the components of the draft soil tillage force and to respect the oscillating dynamics of the process.

From a practical point of view (for the design of the load-bearing structure and the calculation of the power source), it is sufficient to estimate the maximum value of the tensile strength. In this case, it is not necessary to model the variation in time of the resistance force generated by the blade. However, if we approach problems of aggregate dynamics (variation of the draft soil tillage force, oscillating effects on the quality of the work, resonant work regimes) a model of the type offered in this paper, is necessary. However, the fineness aspects (even the oscillating characteristics) can have (depending on the qualities of the soil) effects difficult to anticipate due to the random nature of many of the soil properties. However, these problems require a large volume of experimental work and a high statistical level of data processing.

REFERENCES

[1] Oprescu M.R., Biriș S.Ș., Marin E., Sorică C., Ungureanu N., Sorică E., Dumitru I., Grigore I., Considerations on mechanically active equipment for open interrupted furrow used in technology of weeding plant cultures fruit and viticultural plantations, ISB-INMA TEH, Agricultural and Mechanical Engineering, Romania, 2017, pp 215-220;

[2] Cardei P., Condruz P., Dfiru R., Muraru C., Tests for physical laws of the draft force generated in the tillage operations, 19th International Scientific Conference Engineering for Rural Development, Latvia, 2020, pp 2-6;

[3] Letosnev M.N., Agricultural Machinery, Romania, 1959, pp 51-60;

[4] American Society of Agricultural Engineers [ASAE]. 2003a. "D497.4 Agricultural machinery management data" 373-380. In: ASAE. ASAE standards, pp 15-24, 2003;

[5] Toma D., Neagu T., Florescu I., Lepsi S., Agricultural tractors, Romania, 1978, pp 115-129;

[6] Sandru A., Popescu S., Cristea I., Neculaiasa V., Exploitation of agricultural equipment, Romania, 1983, pp 95-110;

[7] Tecusan N., Ionescu E., Tractors and automobile, Romania, 1982, pp 55-69;

[8] Scripnic V., Babiciu P., Agricultural machines, Romania, 1979, 82-95;

[9] McKyes E., Soil Cutting and Tillage, vol 7, 1st Edition, Holland, 1985, pp 41-57

[10] Sandru A., Badescu M., Sandru L., Reduction of energy consumption through the rational use of the agricultural aggregates, Romania, 1982, pp 115-132;

[11] Krasnicenko A., V., The manual of the agricultural machine manufacturer, Romania, vol. 2, pp 112-132, 1964;

[12] Fechete-Tutunaru L.V., Gaspar F., Gyorgy Z., Soil-tool interaction of a simple tillage tool in sand, EENVIRO-Sustainable Solutions for Energy and Environment, E3S Web of Conferences, Turkey vol. 85, pp 1-6, 2019.

[13] Iacob C., Craciunescu A., Cristea C., Dragos L., Gheorghita St., Trandafir R., Classical and modern mathematics, Romania, vol. II, 81-95, 1979;

[14] Serov V., Fourier Series, Fourier Transform and Their Applications to Mathematical Physiscs, USA, 2017, pp 37-44

PRELIMINARY RESULTS ON THE INFLUENCE OF THE F414 BIOLOGICAL PRODUCT ON SOME PHYSIOLOGICAL INDEXES FOR PEACHES GROWN UNDER THERMO-HYDRIC STRESS

Paraschiv Alina-Nicoleta[1]
Dima Milica[2]
Diaconu Aurelia[3]
Enache Viorel[4]
Fătu Viorel[5]
[1, 2, 3, 4] Research- Development Station for Plant Culture on Sands, Dabuleni, Romania
[5] Research-Development Institute for Plant Protection, Bucharest, Romania

ABSTRACT

On the peach species, *Springold* variety, research was conducted on the influence of the F414 biological product on some physiological indexes and processes carried out on the foliar level, the area of culture being characterized by an accentuated thermo-hydric stress during the summer. Photosynthetic gas exchange, foliar transpiration and stomatal conductance were determined with the portable LC PRO + apparatus, and the leaf water forms were determined gravimetrically, the results obtained being correlated with the meteorological data from the vegetation period. Applying the F414 to the *Springold* variety resulted in the formation of a pellicle on the surface of the leaves, which, together with the action of the thermo-hydric stress specific to the area, caused stomate closure, reduction of CO_2 supply, photosynthesis values being considerably lower compared to the control variant. As for foliar transpiration, the F414 product had a positive effect, the pellicle formed on the surface of the leaves, reducing the amount of water lost to the foliage. The application of this product has positively influenced drought resistance of the *Springold* variety, the percentages of the bound water being higher (5.1%) compared to the control variant (3.96%).

Keywords: *peach, thermo-hydric stress, physiological indexes*

INTRODUCTION

The current climatic changes, which, according to experts, will be more and more pronounced in the coming decades, obviously affect the biology of horticultural species, especially perennial wood species, such as, for example, fruit trees. The risk of desertification is a real phenomenon in Romania and is closely related to the evolution of the climate [8]. The values of the Thornthwaite aridity index define an arid area, increasing from north to south and south-west of Oltenia, from 45% to 50%. The highest values expressing pronounced aridity (about 65%) also cover the area of sandy soils in southern Oltenia [4]. This area, therefore, has a natural background favouring a significant drought impact on plants. The plants

bear a temperature rise of 5-10 ºC above the optimal temperature, and temperatures higher than 12-15 ºC show the effects of thermal stress [7]. During the vegetation period plants are exposed not only to the effects of high temperatures but also to longer or shorter drought periods. Water is a particularly important abiotic factor that influences plant metabolism. Water stress is widespread and is the most important factor limiting production in most crop plants [1]. The response of fruit trees to water stress is lower than that of annual plants, and varies with the species, organ and production phenophase [6]. The action of the thermo-hydric stress, as well as the action of different chemical and biological substances used in phytosanitary treatments in fruit trees can be appreciated by the level with which the values of the main physiological and biochemical indicators of the plants exposed to these factors change. Bioproducts are biological means made on the basis of natural compounds (plant extracts) with complex action on crop plants, bioproducts that have been shown to be stimulants for vegetative growth [9], [10]. Taking into account these considerations, the present research has proposed to know the mode of action of the F414 biological product on peach, the Springold variety, regarding the influence of this product on some physiological indexes and processes developed at the foliar level, the area of culture (the sandy soils in southern Oltenia) being characterized by an accentuated thermo-hydric stress during the summer.

MATERIALS AND METHODS

The studies were conducted during the peach vegetation period (the year 2017) at Research – Development Station for Plant Culture on Sands, Dabuleni, Romania, within the plant physiology laboratory. *Springold* peach variety was used as study material in two experimental variants. In the first variant (control) phytosanitary treatments were applied according to the peach culture technology on sandy soils, and in the second experimental variant was additionally added treatment with the F414 biological product. Photosynthetic gas exchange, foliar sweat and stomatal conductance were determined directly in the experimental field with the LC PRO + portable device, both on the sunny side of the trees and on the shaded side. The water forms in the leaves (total water, free, bound) were determined gravimetrically in the laboratory. The results obtained were correlated with the meteorological data recorded at the weather station of Dabuleni RDSPCS, during the period April-October 2017. To determine the intensity of the thermo-hydric stress on the peach trees, the experimental determinations were made in two critical moments for the area of sandy soils in southern Oltenia, the first decade of August and September.

RESULTS AND DISCUSSIONS

Experimental determinations made on peach (*Springold* variety) have highlighted a diurnal variation in photosynthesis and foliar transpiration processes, these processes being influenced by the temperature and amount of active radiation in photosynthesis, the relative air humidity at the time of the determinations, the amount of rainfall, of treatments applied in vegetation. From the climatic point of view, the April-October 2017 period is presented in Table 1.

Table 1. *Climate conditions between April and October 2017 recorded at the RDSPCS Dabuleni weather station.*

Month	IV	V	VI	VII	VIII	IX	X
Medium temperature (°C)	12	17.8	24	24.8	24.8	20.2	13.4
Maximum temperature (°C)	29.8	29	41.2	40.8	40.4	36.9	29.4
Minimum temperature (°C)	0.4	4.7	12.9	13.3	11	6.7	2.7
Precipitations (mm)	62.8	78.6	17.4	120.8	28.8	18.2	120.4
Atmospheric relative humidity (%)	72	77	67	65	63	66	80
Sum of temperature degrees (°C)	360	551.8	720	768.8	768.8	606	415.4
Multiannual medium temperature (1956-2016)	11.8	16.8	21.6	23.1	22.4	17.8	11.4
Sum of monthly multiannual precipitations (1956-2016)	47.52	62.12	69.3	53.15	37.28	41.81	41.81

From the data presented, it can be observed that during the analyzed period, the air temperature is constantly increasing, the monthly average values exceeding the multiannual average of the temperature. Very warm were the summer months, June, July, and August, with average temperatures between 24 – 24.8 °C and maximum air temperature between 40.4 – 41.2 °C. Due to the atmospheric drought, these high temperatures led to thermo-hydric stress conditions, which influenced the fruit trees metabolism, the drought period extending until September. Although the sum of the annual rainfall was higher than the multiannual sum, they were unevenly distributed, from very small amounts of about 10 mm to 100 mm in just 2-3 days. An example of this is June, when 98.8 mm precipitations were recorded in the first three days of the month, followed by very long periods (28 days) with very high temperatures and no precipitation. Globally, one of the challenges faced by fruit production is the fact that the regional climate is increasingly unpredictable from year to year. Therefore understanding the effects of drought, extreme temperatures, light, etc. on metabolic processes in plants is very important. In correlation with the studied factors, the climatic conditions of 2017 directly influenced the development of physiological processes at the *Springold* peach variety cultivated on sandy soils. In the same area of culture, it was demonstrated that as the average temperature of this area increased, the late Jerseyland and Redhaven peach-trees began to mature their fruit about 12 days earlier, and the tendency to reduce the vegetation period is significant [2]. From a physiological point of view, the application of the F414 biological product was aimed at protecting the leaf surface from intense solar radiation by means of the hydro-active pellicle, the pellicle deposited on the leaves having a high reflectance when is dry and increased absorbance when is wet. However, in the climatic conditions characteristic of the sandy soils in southern Oltenia, the application of the F414 product led to the formation of the pellicle on the surface of the leaves which, together with the action of the thermo-hydric stress specific to the area, caused stomata closure, reduction of the supply of CO_2, and obtaining leaves with a reduced assimilation surface with repercussions on the photosynthetic yield (tables 2 and 3).

Table 2. *Diurnal variation of physiological processes at Sprindold variety cultivated under thermo-hydric stress conditions (August 2, 2017).*

Hour	Experimental variant	Prunus persica, Springold variety				
		Photosynthetic active radiation µmol/m^2/s	Air temperature ^oC	Photosynthesisµmol $CO_2/m^2/s$	Foliar transpirationmmol $H_2O/m^2/s$	Stomatal conductance of H_2O mol/m^2/s
9 o'clock	Control variant	762	30.1	12.05	2.26	0.28
	Biotreatments with F414 bioproduct	667	30.1	4.02	1.98	0.18
12 o'clock	Control variant	942	30.1	11.23	1.62	0.16
	Biotreatments with F414 bioproduct	849	31.8	5.00	1.10	0.07
15 o'clock	Control variant	877	38.7	5.16	2.48	0.05
	Biotreatments with F414 bioproduct	885	38.9	1.19	1.61	0.03

From the data presented in table 2 and table 3, it results that in both analyzed phenophases the photosynthesis process was influenced both by the climatic factors in the area and by the substances used for the treatment of fruit trees. The photosynthesis values were considerably lower at the F414-treated variant in almost all times of the determinations, as compared to the control variant. The interaction between the thermo-hydric stress and the F414 product, applied on the leaves has led to a reduction in the carbon dioxide assimilation rate as a result of the drop in conductivity of the stomata. In the area of sandy soils, temperatures above 35 ^oC and relative humidity below 30% act as desiccant forces on plants, increasing foliar transpiration rate [3]. In the case of leaves treated with product F414, reducing the conductivity of stomata had a positive effect on foliar transpiration, closing of stomata, reducing the loss of plant water.

Table 3. *Diurnal variation of physiological processes at Sprindold variety cultivated under thermo-hydric stress conditions (September 7, 2017).*

Hour	Experimental variant	Prunus persica, Springold variety				
		Photosynthetic active radiation µmol/m²/s	Air temperature °C	Photosynthesisµmol $CO_2/m^2/s$	Foliar transpirationmmol $H_2O/m^2/s$	Stomatal conductance of H_2O mol/m²/s
9 o'clock	Control variant	807	25,7	6,97	2,91	0,31
	Biotreatments with F414 bioproduct	746	26,4	3,66	1,87	0,14
12 o'clock	Control variant	814	24,8	4,73	0,93	0,09
	Biotreatments with F414 bioproduct	791	26,4	3,44	1,8	0,17
15 o'clock	Control variant	689	35,1	3,56	1,95	0,05
	Biotreatments with F414 bioproduct	651	35,6	7,5	2,79	0,08

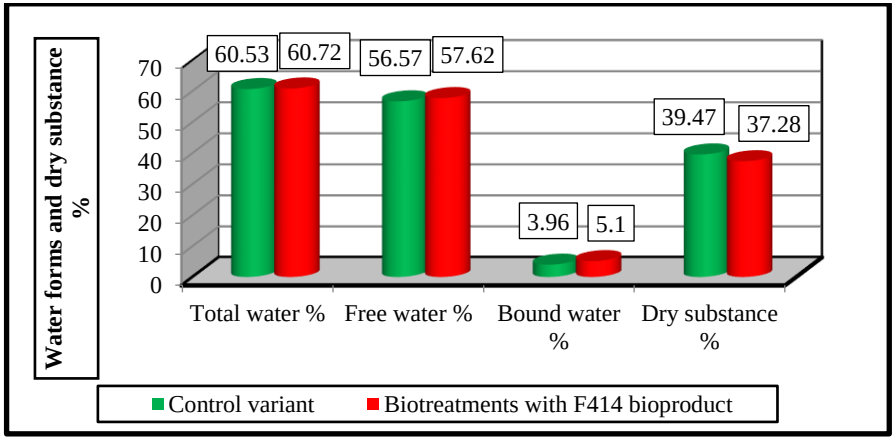

Fig. 1. *Water forms and dry substance from peach leaves grown under thermo-hydric stress*

Analyzing figure 1, it is noticeable that leaves of the *Springold* peach variety have been subjected to severe water stress. The percentage values of total water, free water and leaf-bound water were higher at the variant treated with F414. Of note is the percentage of bound water, which was 1.14% higher, indicating that application of F414 to peach has impressed increased resistance of plants to thermo-hydric stress. Similar research by Escobar-Gutierrez (1998) pointed out that the

moderate water stress caused the relative water content of the peach leaves to drop from 74% to 70% and under severe water stress, the relative water content decreased to 67% [5]. Regarding the dry substance, its highest values (39.47%) were shown by the control variant, which is explained by the higher values of photosynthesis recorded in the untreated *Springold* variety with product F414.

CONCLUSION

The intensity of the physiological processes recorded at the *Springold* peach variety was influenced both by the climatic factors specific to the southern area of Oltenia and by the phytosanitary treatments applied during the vegetation period.

Under conditions of thermo-hydric stress, with temperatures above 38 ºC and insufficient rainfall, the application of the F414 biological product led to the formation of a hydroactive pellicle on the surface of the leaves, reducing the stomatal conductance of H_2O.

Stomata closure reduced the carbon dioxide assimilation rate, and photosynthesis values were considerably lower in the variant where F414 biotratament were applied. On the other hand, the percentages of the dry substance increased directly in proportion to the photosynthesis values, being higher by 2.19% for the control variant.

As for foliar transpiration, the F414 product had a positive effect, the pellicle formed on the surface of the leaves, reducing the amount of water lost at the foliage level. The application of this product has positively influenced drought resistance of the Springold variety, the percentages of the bound water being higher (5.1%) compared to the control variant (3.96%).

ACKNOWLEDGEMENTS

This study is part of the ADER 4.1.4. Sectoral Project "Integrated technologies for the prevention and control of harmful organisms in agricultural and horticultural plants with minimal consumption of resources".

REFERENCES

[1] Boyer J.S., Plant productivity and environment, Science, U.S.A., pp 218, 443-448, 1982.

[2] Croitoru M., Enache V., Răţoi I., Evolution of the influence of climatic factors on fruit quality of peach in the conditions of sandy soils, Analele Universităţii din Craiova, Secţia Horticultură, vol. XIX, pp. 137-143, 2014.

[3] Dima M., Diaconu A., Drăghici R., Croitoru M., Paraschiv A., Fătu V., Preliminary results on the actions of some biological substances on vegetative grought on peaches cultivated on sandy soils, Romanian Journal for Plant Protection, Romania, vol. X, 2017.

[4] Dragotă C.S., Dumitrașcu M., Grigorescu I., The Climatic Water Deficit in South Oltenia Using the Thornthwaite Method. Studii şi cercetări de geografie şi protecţia mediului, Romania, vol. 10, nr.1, pp 140-148, 2011.

[5] Escobar-Gutierrez A.J., Photosynthesis, carbon partitioning and metabolite content during drought stress in peach seedling. Aust. J. Plant Physiol., Australia, pp 25, 197-205, 1998.

[6] Lakso A.N., The effects of water stress on physiological processes in fruit crops. Acta Hortic, pp 171, 275-289, 1985.

[7] Leone A., Perrotta C., Maresca B., Plant Tolerance to Heat Stress: Current Strategies and New Emergent Insight. In Abiotic Stresses in Plants. Sanita di Topi and Pavlik-Skowronska edit. Springer Science, Dordrecht, 2003.

[8] Popa, V., Borza, I., The analysis of multiannual variation on temperature and precipitation related to the desertification risk in the Banat plain. Buletin USAMVB, Romania, vol. 63, pp 231-237, 2007.

[9] Saa-Silva S., Brown Ph., Ponchet M., First World Congress on the Use of Biostimulants in Agriculture. Leuven: International Society of Horticultural Science, 2013.

[10] Sharma H.S.S., Fleming C., Selby C., Rao J.R., Martin T., Plant biostimulants: a review on the processing of macroalgae and use of extracts for crop management for reduce abiotic and biotic stresses. J. Appl. Phycol. 26, 2014.

RESEARCH ON THE BEHAVIOR OF AN ASSORTMENT OF BELL PEPPER ON THE SANDY SOILS IN SOUTH-WEST OLTENIA ACCORDING TO THE CULTIVATION METHOD USED

PhD student Alina-Nicoleta Paraschiv [1]
PhD Milica Dima [2]
PhD Aurelia Diaconu [3]
PhD Elena Ciuciuc [4]
PhD Mihaela Croitoru [5]
[1] University of Craiova, Romania
[2, 3, 4, 5] Research and Development Station for Plant Culture on Sands Dăbuleni, Romania

ABSTRACT

The pedo-climatic conditions specific to sandy soils in southwest Oltenia determine differences in performing different phenophases of growth and development of plants, both between varieties and in the physiological behavior of the same variety under different yield conditions. Therefore, at the Dăbuleni Research and Development Station for Plant Culture on Sands, research was carried out on some physiological, biochemical and production processes at five varieties of bell peppers cultivated in the open fields and solar. Determinations of photosynthesis, foliar transpiration, the biochemical composition of fruits, quantity, and quality of bell pepper production were performed. The physiological and biochemical processes studied were influenced by the environmental conditions specific to each cultivation method, but also by the studied variables. Of the 5 varieties studied, the best results on the biochemical composition of the fruits were recorded at the *Artim* variety (8.83% total dry substance, 4.60% soluble dry substance, 0.19% acidity, 3.80% carbohydrate and 36.96% vitamin C). The production was between 15,387 t / ha for open-field plants and 108,574 t / ha for plants grown in the solar, the differences between the two cultivation methods being statistically assured as distinctly significant.

Keywords: *bell pepper, photosynthesis, foliar transpiration, biochemical composition, production*

INTRODUCTION

Global climate change, customized at a regional level, requires a competent revision of the structure of vegetable crops and the implicitly used cultivars, with high adaptability to the new conditions generated by climate change. Replacing old cultivars with new, performant ones should be limited to the interest of agricultural producers to cultivate the most valuable, without the risk of their non-adaptability either to the specific climatic and soil conditions or to the technology practiced. The normal conduct of metabolic processes in plants is carried out only if environmental

conditions are provided for the requirements of each species, for each species taking into account an environmentally friendly optimum as a whole of the conditions under which the plants grow and develop normally (temperature, light, humidity, air, soil). The pedo-climatic conditions specific to the sandy soils of Southern Oltenia (sandy soils with reduced natural fertility, high temperatures and insufficient precipitation during the vegetation period, spread unevenly) determine differences in the various fenofases of growth and development, both between varieties and the behaviour of the same variety in different conditions of culture [4]. Internationally, in the field of vegetable growing research has been geared towards diversifying the assortment of species, creating high-performance cultivars, with great productivity and continuous improvement of cultivation technologies. There is a series of research on the influence of environmental factors (temperature, water, luminous intensity, mineral substances, etc.) on the conduct of physiological processes in plants, as well as on production obtained. If the level of these factors does not fall within the optimum limits, they are sources of stress, the emphasis of research being placed on physiological disorders occurring in the vegetal organisms subjected to abiotic stress. After Hall (2001) [3] heat stress is caused by the temperature whose level, duration of exposure and growth rate can cause damage to plants. Klueva et all (2001) [5] considers that the upper-temperature limits to which plants can survive are between 40-55 °C and vary according to species and duration of exposure. Exposure of peppers to temperatures higher than 38-40 °C determines, after Rabinowitch et all [7], the generation of superoxide radicals, by the action of light on chlorophyll. The lesions are characterized by the appearance of a whitish color and some small blisters, on the epicarp of the fruit. In a more advanced phase, water loss and tissue death are found. Cell death provides good conditions for the development of parasitic microorganisms, especially for Alternaria spp. Exposure of peppers at a temperature of 40 °C for 6 hours resulted in the reduction of this physiological disease [6]. Elena Ciuciuc and Marieta Ploae (2012) [1] have shown that by protecting the crops of bell pepper and eggplant, there are different conditions of microclimate with influence on the conduct of the main physiological processes in plants. Starting from the premise that the technology ensures the productive and qualitative potential of the variety, research carried out within the Research and Development Station for Plant Culture on Sands Dăbuleni on pepper culture on the sandy soils of south-west Oltenia acquires great importance in the scientific substantiation of cultivation technologies with detailed physiological and biochemical studies on the resistance or tolerance of plants to abiotic stress factors can be established.

MATERIALS AND METHODOLOGY

In order to scientifically substantiate the technologies of culture through physiological researches, both in the open field and in protected space (solar) culture in 2018, physiological, biochemical and production studies were initiated on 5 cultivars of bell pepper following to be recommended most valuable, both in terms of resistance to area-specific stressors, as well as quantitatively and qualitatively.

The experience was bifactorial, based on the subdivision parcel method, in 3 repetitions.

In each variant, were planted at the beginning of May 10 plants/row at a distance of 70 cm between the rows and 30 cm between plants per row, the surface area of one variant being 2.1 m^2.

It has been applied the cultivation technology of the bell pepper, developed by the Research and Development Station for Plant Culture on Sands Dăbuleni.

The variants of the experience were:

Factor A - Method of cultivation:
a_1 - open field culture;
a_2 - protected culture (in the solar).

Factor B – the cultivar:
b_1 – Artim;
b_2 – Barbara;
b_3 – Işalniţa 85V;
b_4 – Karola;
b_5 – Șimnic.

One month after planting, determinations of the diurnal variation of photosynthesis, foliar transpiration, stomatal conductance were performed in five moments of the day, using the portable LC Pro+ photosynthesis assay system. To determine the quality of the bell pepper, the fruit was harvested at the technological maturity, and in the laboratory the following determinations were made:

- water and total dry matter (%) - gravimetric method;
- soluble dry substance (%) - refractometric method;
- vitamin C (mg/100 g fresh substance) - iodometric method;
- titratable acidity (g malic acid at 100 g fresh substance) - titrimetric method;
- carbohydrate content (%) - Fehling-Soxlet method.

The determination of production was made in dynamics as the bell pepper fruits matured, the data obtained being calculated and interpreted statistically by analysis of the variance and by the mathematical functions.

Climate conditions were monitored using the weather station of the Research and Development Station for Plant Culture on Sands Dăbuleni.

RESULTS AND DISCUSSIONS

From a climatic point of view, 2018 was a warm year, rich in rainfall, the monthly sums being much higher compared to the multi-annual sum of precipitation. The data recorded at the meteorological station of the Research and Development Station for Plant Culture on Sands Dăbuleni are presented in *table 1*.

Generally, Capsicum annum is pretentious to light, temperature, and humidity. The climatic conditions specific to May, June and July 2018 have particularly influenced the unprotected pepper culture. A large amount of rainfall recorded, compared to the multiannual amount of rainfall recorded between 1956 and 2016, led to the intensification of the physiological processes at the foliar level, but the high number of warm and humid days also showed a number of disadvantages related to the higher frequency of disease and pests, with direct influence on the production obtained in unprotected plants. On the other hand, one month after planting, precipitations were accompanied by hail, which caused leaf damage, with major implications for the normal development of the metabolism of plants grown in the open field (*Figure 1, a, b*).

Table 1.*Climatic conditions recorded during the growing season of bell pepper (2018)*

Year	Climatic element	Month				
		May	June	July	August	September
2018	Medium temperature (°C)	20,7	22,5	23,6	25,1	21,6
	Minimum temperature (°C)	10,6	9,0	14,1	14,1	14,0
	Maximum temperature (°C)	31,8	35,7	34,9	35,7	30,7
	Precipitations (mm)	106,6	195,2	147,9	30	12,6
	Atmospheric relative humidity (%)	73	79	79,2	73,2	67,8
Multiannual medium temperature (1956-2016)		16,8	21,6	23,1	22,4	17,8
Precipitations, multiannual total (1956-2016)		62,12	69,30	53,15	37,28	47,83

Protected crop

Open field crop

Fig. 1. *Aspects in the experimental field (a. Protected crop; b. Open field crop) one month after planting*

The results on the diurnal variation of photosynthesis (*Figure 2*) showed a slightly different behavior of the five cultivars of peppers depending on the cultivation method used. The average daily CO2 accumulation was between 19.13 µmol $CO_2/m^2/s$ for plants grown in the sun and 22.73 µmol $CO_2/m^2/s$ for open-field plants.

The process of transpiration was more intense in plants grown in the open field, because during the period when the determinations were made, the leaves of the pepper were affected by the hailstones. Most varieties studied showed the maximum values of transpiration at noon, the differences between cultivars being insignificant (*figure 3*).

The average daily sweat was between 5.26 mmol $H_2O/m^2/s$ at protected plants and 6.80 mmol $H_2O/m^2/s$ at unprotected plants.

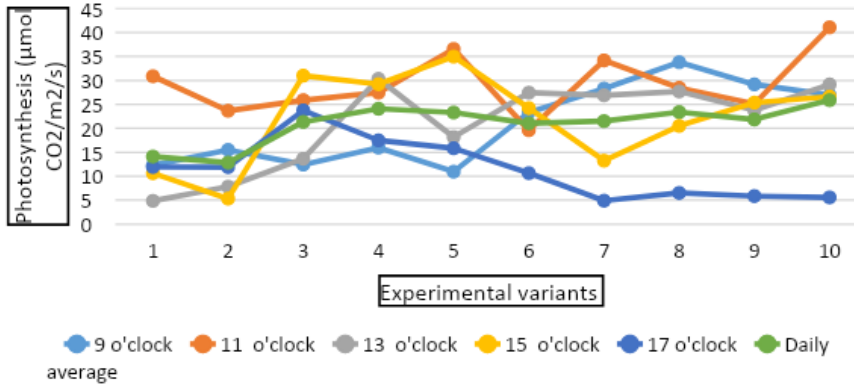

Fig. 2. *Daily variation of photosynthesis depending on variety and cultivation method*

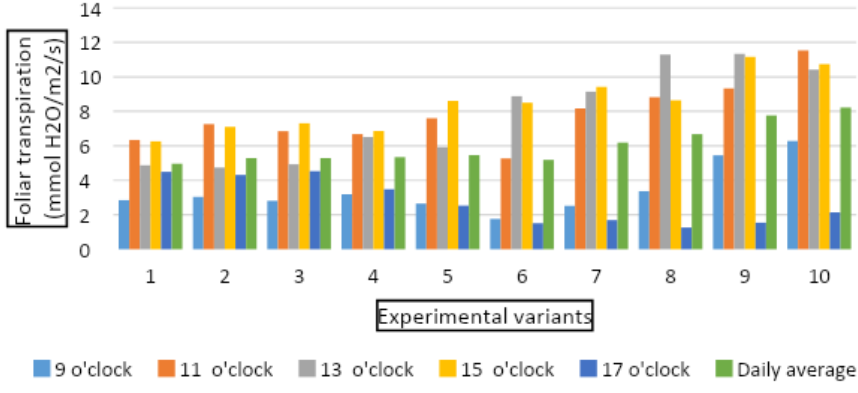

Fig.3. *Daily variation of foliar transpiration depending on variety and cultivation method*

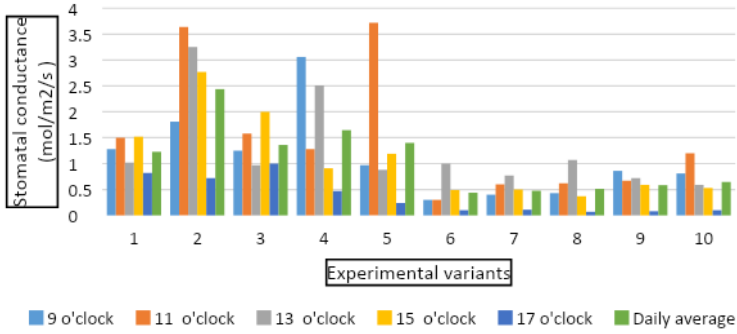

Fig. 4. *Daily variation of stomatal conductance depending on variety and cultivation method*

Figure 4 shows results on stomatal conductance values. It can be noticed that the microclimate provided by the protection of the sweet pepper culture favoured the opening of the stomata. The differences between the varieties were insignificant, but there were differentiations related to the time of the determinations and the method of cultivation used. The average stomatal conductance was between 0.52 mol/m²/s for open-field plants and 1.61 mol/m²/s for protected plants.

The results of the quality indices are presented in *table 2*. These results highlight the influence of the cultivar studied and the cultivation method. The total dry substance was between 4.75% for cultivar Barbara in the protected variant and 10.05% for Artim cultivar in the protected variant.

Table 2. *Influence of the cultivation method and cultivar on the biochemical composition of the bell pepper*

Cultivar	Cultivation method	Dry substance (%)	Water (%)	Soluble dry substance (%)	Acidity (g of malic acid/100g fresh substance)	Carbohydrates (%)	C vitamin (mg/100g fresh substance)
Artim	Solar	10,05	89,95	4,60	0,23	3,80	36,96
	Open field	7,61	92,39	4,60	0,14	3,80	36,96
Barbara	Solar	4,75	95,25	4,00	0,18	3,35	29,04
	Open field	6,92	93,08	5,00	0,17	4,17	45,36
Işalnița 85V	Solar	6 ,88	93,12	4,20	0,24	3,50	25,52
	Open field	8,02	91,98	4,20	0,16	3,50	41,36
Karola	Solar	6,26	93,74	4,00	0,22	3,30	27,28
	Open field	6,96	93,04	4,00	0,19	3,30	30,28
Șimnic	Solar	6,78	93,22	4,20	0,20	3,47	29,92
	Open field	9,22	90,78	4,20	0,19	3,46	41,36

In all cultivars studied, less Artim cultivar, higher values of total dry substance content were obtained in unprotected variant. With the accumulation of a total dry substance in peppers, the amount of water in the fruit decreases. The amount of soluble dry substance was less influenced by the protection system and ranged between 4% and 5%. The carbohydrate content of the peppers ranged from 3.30% to Karola irrespective of the protection system and 4.17% in Barbara cultivar in the unprotected system.

The titratable acidity (TA) in fruit and vegetables is used together with carbohydrates as an indicator of maturity [2].

The acidity of the pepper fruit was between 0.14 g malic acid/100 g fresh substance in Artim cultivar in unprotected variant and 0.24 g malic acid/100 g fresh substance in the cultivar Isalnița 85V in the protected variant. In unprotected variants, acidity values were lower in all cultivars than in solar. The amount of pepper vitamin C was quite low. It ranged from 27.28 mg to Karola cultivar in the solar and 45.36 mg to Barbara in the unprotected variant.

Research by Zoran S. Ilić et al., 2017 [8], found in peppers that the highest concentration of soluble dry substance (SUS) was determined in open-field pepper (8.03%). Fruit peppers obtained in plastic tunnels had a significantly lower SUS content (6.58%). Total acidity was 0.19% in open-field and 0.25% in fruit grown in plastic tunnels. The highest concentration of vitamin C was determined in the pepper cultivated in plastic tunnels (175.77 mg 100 g^{-1}). Only limited data has been found in the literature that has as subject the vitamin C content of pepper in response to growing conditions, especially variations in solar radiation and temperature. Vitamin C from pepper has been affected by cultural practices (genotype and agronomic technique) on the one hand (Topuz, Ozdemir, 2007) and abiotic factors (light and temperature) on the other hand (López-Marín et al., 2011).

Unprotected plants were affected by the climatic conditions of 2018, the abundance of rainfall in May-July with negative impacts on production obtained (*table 3*). Between the two methods of cultivation, there were distinctly significant differences, statistically ensured, detaching the Simnic cultivar, with an average production of 69 t / ha.

Table 3. *Interaction of cultivar x cultivation method influence on production*

Interaction of cultivar x cultivation method		Production (t/ha)	The difference (t / ha)	Signification
Artim	Open field	14,666	Control variant	
	Solar	94,022	+79,356	**
Barbara	Open field	12,951	Control variant	
	Solar	109,269	96,318	**
Işalniţa 85V	Open field	18,015	Control variant	
	Solar	111,377	+93,362	**
Karola	Open field	16,253	Control variant	
	Solar	104,999	+88,746	**
Șimnic	Open field	15,05	Control variant	
	Solar	123,202	+108,152	**
DL 5% = 28,582 t/ha DL 1% = 55,974 t/ha DL 0,1% = 151,373 t/ha				

CONCLUSION

Different cultivation methods determine differences in performing different phenophases of growth and development of pepper plants cultivated on sandy soils from Romania.

The physiological and biochemical processes studied were influenced by the environmental conditions specific to each cultivation method, but also by the studied cultivars.

Of the 5 varieties studied, the best results on the biochemical composition of the fruits were recorded at the *Artim* variety (8.83% total dry substance, 4.60% soluble dry substance, 0.19% acidity, 3.80% carbohydrate and 36.96% vitamin C). The production was between 15,387 t / ha for open-field plants and 108,574 t / ha for plants grown in the solar, the differences between the two cultivation methods being statistically assured as distinctly significant.

REFERENCES

[1] Ciuciuc Elena, Ploae Marieta, Studiul microclimatului creat prin protejarea culturii de ardei gras şi impactul acestuia asupra plantelor pe solurile nisipoase. Anale ICDLF Vidra, Romania, 2012.

[2] F. Gonzalez-Cebrino1 , M. Lozano1 , M. C. Ayuso2 *, M. J. Bernalte2 , M. C. Vidal-Aragon3 and D. Gonzalez-Gomez, Characterization of traditional tomato varieties grown in organic conditions, Spanish Journal of Agricultural Research 2011 9(2), 444-452.

[3] Hall A. E., Crop Responses to the Environment, CRC Press, Boca, 2001.

[4] Ifrim A., Buică V., Cercetări privind comportarea unor soiuri şi linii de pătlăgele vinete pe solurile nisipoase din sudul Olteniei, Lucrări Ştiinţifice SCCCPN Dăbuleni, vol. VIII, Romania, 1994.

[5] Klueva N.Y., Marmiroli E., Nguyen H.T., Mechanism of thermotolerance in crops. In Crop Responses and Adaptation to Temperature Stress. Basra A.S. edit. Food Products Press, Binghampton, New York, 2001.

[6] Rabinowitch H. D., Ben David B., Friedmann M., Light is essential for sunscald induction in cucumber and pepper fruits, whereas heat conditioning provides protection, Scientia Hortic. 29, 21 – 30, 1986.

[7] Rabinowitch H. D., Sklan D., Superoxide dismutase activity in ripening cucumber and pepper fruits, Physiol. Plant. 52: 380 – 384, 1981.

[8] Zoran S. Ilić, Lidija Milenković, Ljubomir Šunić, Saša barać, Jasna Mastilović, Žarko Kevrešan, Elazar Fallik, Effect of shading by coloured nets on yield and fruit quality of sweet pepper, Zemdirbyste-Agriculture, vol. 104, No. 1 (2017), p. 53–62, 2017.

RESEARCHES ON REPORTING THE ATTACK OF SOME PEANUTS DISEASES CULTIVATED ON SANDY SOILS

PhD Milica Dima [1]
PhD Aurelia Diaconu [2]
PhD Reta Drăghici [3]
PhD student Alina-Nicoleta Paraschiv [4]
PhD student Coteț Gheorghe [5]
[1, 2, 3, 4, 5] Research & Development Station for Plant Culture on Sands Dabuleni, Romania
[5] University of Craiova, Craiova, Romania

ABSTRACT

Peanuts (Arachis hypogaea L.) are widely grown as a food and oleaginous species. Cultivation of peanuts offers important economic benefits, but one of the most important challenges that growers confront is the fight against destructive diseases. Culture is susceptible to a variety of pathogens, such as bacteria, fungi, viruses, and nematodes, resulting in low yields and degradation of grain quality. Among the most devastating fungal diseases of peanuts are Cercospora arachidicola, Puccinia arachidis, Sclerotium rolfsii which cause substantial loss of production. Loss of yields due to the incidence of peanut disease may be up to 50%. Fungicides can be used to combat fungal diseases, but there are alternative disease control options, such as cultural practices, cultivation of resistant varieties, which can be useful in combating diseases by reducing the frequency of application of fungicides.

Keywords: *peanuts, disease, fungi, control*

INTRODUCTION

Peanuts are mainly grown for human consumption, they have many uses, as whole or processed seeds to make peanut butter, oil, and other products. The seeds contain 25-30% protein and 42-52% oil [3].

Cultivating peanuts offers important economic benefits, but one of the most important challenges peanuts that farmers confront is disease control. Culture is susceptible to a variety of pathogens, such as bacteria, fungi, viruses and nematodes, resulting in low yields and degradation of grain quality. Among the most devastating fungal diseases of peanuts are Cercospora arachidicola, Cercosporidium personatum, Puccinia arachidis, Sclerotium rolfsii which cause substantial losses at the production level. Loss of yields due to the incidence of peanut disease may be up to 50%. The damage caused depends on the stage of plant development when the disease occurs. The largest damage is recorded when the disease is on the leaves before the flowering of the plants. Cercospora arachidicola greatly reduces the weight of the pods, the number of ginophores and not only the number of pods, but also the average weight of the grains. In peanut cultures in

southern Oltenia, Cercospora occurs towards the end of the vegetation period, therefore the damage is small and varies according to the variety.

The integrated pest management system of resistant varieties improved soil cultivation practices and cultural practices, together with the low application of chemical fungicides, can help combat fungal diseases in peanuts.

In peanuts, erect growth varieties are less susceptible to the attack of pathogens than those with a protuberant growth whose leaves can get more into contact with soil [7]. Growing erect growth varieties reduces the incidence of disease by limiting the contact between the plant and the soil mushroom spores [7].

MATERIAL AND METHODOLOGY

The study was conducted at SCDCPN Dabuleni during 2013-2015 on some peanut varieties in the germplasm collection. Biological material with fungal attack symptoms from the peanut brew field was taken.

The biologically affected material was maintained in the humid chamber until the formation of taxonomic mycelia. From these, pure cultures were obtained on the nutritive medium, which was identified by microscope according to the morphological characteristics of the specialists.

RESULTS AND DISCUSSIONS

The environmental-specific conditions to sandy soils favour the spread and evolution of a wide spectrum of pathogenic fungi. Along with the known and ubicvistic species, the soils of Fusarium, Rhizoctonia, Sclerotinia, Macrophomina, Phoma, Roesleria and Eutypa have been reported as frequent in the area of sandy soils.

Within these genres have been identified species that produce fusarium peanuts Fusarium oxysporum f.sp. [8], Roesleria hypogea and Eutypa lata [6], the drying and decline of vines (Phoma viniferae), Cytospora vitis, Fusarium oxisporium, Fusarium equiseti, Fusarium sambucinum [2], [7] wilting and staining of green melons - Fusarium oxysporum, Fusarium equiseti [14], Drying of castor oil - Macrophomina phaseolina, Fusarium moniliforme [1], Fusarium oxysporum f.sp. niveum [9].

In the collection of peanut germ plasm, during the period 2013-2015, SCDCPN Dăbuleni observed partial or total drying of peanut plants, more frequently in August-September.

In 2014, the drying of the plants was sporadic, evidencing the associated attack of fungi Fusarium oxysporum f.sp. vasinfectum, Rhizoctonia solani and Sclerotinia minor, and 2015 there was a frequency of dried plants with a very large amplitude of between 0.1 and 62.8% (Table 1). Depending on the genotype, the frequency of dry plants ranged from 0-6.1% for the Viviana variety (germ cell culture variety) and 13.4-62.8% (33.8% for the average / 3 repetitions) to the Brazilian Begici variety. Plant drying, variable from one genotype to another, was induced

predominantly by the attack of the fungus Fusarium oxysporum f.sp. vasinfectum identified on plants in different phenological phases.

The fungus produces damage to peanuts cultivated at SCDCPN Dăbuleni [9], [10] and in all peanut cultivation countries [4].

On the nutritive medium the fungus forms white colonies with characteristic hyphae and elongated conidia. The diameter of the colony after 7 days of development measures 73 mm at 3-10 values of the pH of the nutrient medium, which means that the fungus can grow on any soil regardless of its reaction (Table 2).

Table 1. *Attack of pathogenic fungi in the field of peanuts*

Genotype Genotype	Frequency of dry plants(%)	
	Amplitude	Average/3repetitions
Dăbuleni	12,1-26,3	18,3
Brazilian Begici	13,4-62,8	33,8
Velican	6-9,2	8,1
Early of China	2,6-17,8	10,2
T55	7,5-41	23,5
Provenance China 1	3,9-35	17,3
Provenance China 2	7,1-19,2	13,3
Ning	3,8-8,9	5,0
Henan Province	2,3-6,8	3,5
Viviana	0-6,1	1,9
Provenance Turkish	0-6,2	2,3

Table 2. *Influence of the pH values of the nutrient medium on the development of some fungal fungi after 7 days of development*

Fungus	The diameter of the colony (mm) to the pH values of the nucleating medium							
	3	4	5	6	7	8	9	10
Fusarium oxysporum f.sp. vasinfectum	73	73	73	73	73	73	73	73
Phoma arachidicola	18	40	71	73	73	73	57	41
Cylindrocladium(Calonectria) crotalariae	37	48	70	73	73	73	42	26
Fusarium oxysporum f.sp. niveum	73	73	73	73	73	73	73	73

From the dried and defoliated plants of line T55, the pathogenic fungus Phoma arachidicola was isolated. It forms on the nutritive medium colonies white-yellowish, peach with brown-reddish reverse. Between hyphae there is a growing number of dark-brown, conspicuous picnids, which at maturity release a number of oval and hyalini picnosporids through osteol. The attack produced by this fungus in peanuts cultivated in the USA, Japan, China, Australia was associated with a decrease in production [5], [11].

In the Early of China variety from the dried herbs was isolated Cylindrocladium (Calonectria) crotalariae. The dried roots of these plants showed numerous

microscleroses that transferred to the nutrient medium, forming yellowish, then brown, brownish-colored colonies. The highest growth (73 mm diameter) of the colony of this fungus was recorded at the pH values of the nutrient medium ranging from 6-8 (Table 2). The attack of this fungus causes the rotting of the pods, roots and stems [13]. Since its first appearance in Georgia in 1965, the disease has spread, with significant damage being reported to peanut cultures in the USA, India and Australia [12].

The determinations made in some peanut genotypes revealed a significant reduction in the waste and production of the attacked plants. Due to the attack of the predominant fungus Fusarium oxysporum f.sp. vasinfectum, to the Provenienta China 2 genotype was determined the most significant reduction in the waist and production of the attacked plants (Table 3). The production of pods on an unattacked plant was 121.5 g compared to 26.1 g in an attacked plant.

Table 3. *Pathogenic action of fungi identified in some peanut genotypes*

Genotype Genotype	Dominant pathogenic pathogepapathogenic fungus Dominant pathogenic fungus	The height of the plant				The production of pods			
		Unattacked plants		Attacked plants		Unattacked plants		Attacked plants	
		1	2	1	2	1	2	1	2
Dăbuleni	Fusarium oxysporum f.sp. vasinfectum	41	-	26	-	37	-	0	-
Brazilian Begici	Fusarium oxysporum f.sp. vasinfectum	37	-	22	-	37,2	-	0	-
Velican	Fusarium oxysporum f.sp. vasinfectum	44	-	41	-	56	-	0	5
Early of China	Cylindrocladium(Calonectria) crotalariae	28	-	27	-	53,3	-	14,6	-
T55	Phoma arachidicola	27	-	20	25	35,5	-	0	16,2
Provenence China 1	Fusarium oxysporum f.sp. vasinfectum	26	-	20	23	40,2	-	6,0	11,2
Provenence China 2	Fusarium oxysporum f.sp. vasinfectum	32	-	31	-	121,5	-	26,1	-
Ning	Fusarium oxysporum f.sp. vasinfectum	42	-	18	33	21,2	-	0	11,8
Henan Province	Fusarium oxysporum f.sp. vasinfectum	35	-	24	-	38,2	-	6,4	-
Viviana	Fusarium oxysporum f.sp. vasinfectum	31	-	26	27	42,3	-	0	12,3
Provenence Turkish	Fusarium oxysporum f.sp. vasinfectum	41	-	40	-	55	-	0	5

*Determinations made on unleavened plants (production = 0) were completed with those from plant 2.

CONCLUSION

Under the ecological conditions of sandy soils, pathogenic fungi have been identified in peanuts: Fusarium oxysporum f.sp. vasinfectum, Phoma arachidicola, Cylindrocladium (Calonectria) crotalariae.

It has been observed that the genotypes in the peanut germ cell collection all three pathogenic species are transmissible through soil and seeds.

In order to limit the area of peanuts, marked on peanuts it is necessary to cultivate resistant varieties within an integrated protection system.

REFERENCES

[1] Ciurea Alexandra, Țîrcomnicu Marina, Fetoiu Adriana, Daniela Ion, Săndulescu Daniela, Contribuții la cunoașterea florei micologice a viței de vie cultivată pe nisipuri. Lucrări științifice SCCCPN Dăbuleni, vol. IX, Romania, 1989.

[2] Ciurea Alexandra, Maria Oprea, Doina Cojocaru, Două boli păgubitoare pentru ricin și sorg în Romania. Analele ICPP București, vol. XXIV, Romania, 1992.

[3] Jackson, C.R, and Bell, D.K. Diseases of peanut (groundnut) caused by fungi. Res. BIII/. 56: Univ. Georgia. Coil. of Agcrl. Exp. Stn., 1969.

[4] Joffes, A.Z., Fusarium species on groundnut kernels and grouuundnut soil, Plant Soil, pg.439-446, 1973.

[5] Lutrell, E. S., Smith, D. H., Peanut web bloth. Symptom and field production. Phytopatologie, nr.71, pg.892, 1981.

[6] Oprea Maria, Ciuperci implicate în declinul biologic al viței de vie. Teza de doctorat USAMV Cluj Napoca, Romania, 1997.

[7] Shew, B.B., J. C. Wynne, and M. K. Beute, Field, microplot and greenhouse evaluations of resistance to Sclerotium rolfsii in peanut. Plant Disease, vol. 71, pp. 188–191, 1987.

[8] Șearpe Cojocaru Doina, Oprea Maria, Dumitrescu Violeta, Prevenirea atacului ciupercii Fusarium oxysporum f.sp. vasinfectum la arahide. Analele ICPP București, vol. XXVII, Romania, 1996.

[9] Șearpe Doina, Principalii agenți patogeni și dăunători la pepenii verzi în zona sudică a Olteniei și unele posibilități de limitare a atacului acestora. Lucrări științifice SCCCPN Dabuleni, vol.XII, pg.127-128, Romania, 2000.

[10] Șearpe Doina, Ciolacu Floarea, Dima Milica, Comportarea unor cultivare de grâu, porumb, floarea soarelui și arahide la atacul agenților patogeni și dăunătorilor. Lucrări științifice SCCCPN Dabuleni, vol.XIII, pg. 145-146, Romania, 2001.

[11] Taber R.A., Identy of peanut web bloth fungus in Unitted States of American, Journal Peanut Research, nr.13, pg.99, 1981.

[12] Taber R.A., Cylindrocladium black Rit. Compendium of peanut diseases, ASP Press The American Phythopath. Society, pg.9-11, 1984.

[13] Tommimatsu,G.S., Griffin,G.J., Inoculum potential of Cylindrocladium crotalariae. The American Phythopath.Society, vol.72, nr.5, pg.511-517, 1982.

[14] Țârcomnicu Marina, Ion Daniela, Specii de Fusarium implicate în ofilirea și pătarea pepenilor verzi. Lucrări științifice SCCCPN Dabuleni, vol.VI, pg.235-242, Romania, 1984

SIGNIFICANT PROGRESS ACHIEVED IN COWPEA BREEDING IN ROMANIA

Dr. Reta Draghici[1]
Dr. Iulian Draghici[2]
Dr. Aurelia Diaconu[3]
Dr. Mihaela Croitoru[4]
Dr. Milica Dima[5]
[1, 2, 3, 4, 5]Research & Development Station for Plant Culture on Sands Dabuleni, Romania

ABSTRACT

Climate change has led to drought, the expansion of desertification, loss of wetlands, loss of biodiversity, declining agricultural output and productivity. In the area of sandy soils in the southwest of Romania, where, compared to the multiannual average, the average air temperature in the May-August period increased by 1.01^0C and the precipitations recorded insignificant increases (5.97 mm), being very low (227. 82 mm) and unevenly distributed in relation to plant requirements. In these conditions, it is necessary to cultivate some species of plants resistant to drought and to preserve and improve some genetic resources adapted to the arid climate. For the efficient use of the microclimate in the sandy soils areas at the Dabuleni Research & Development Station for Plant Culture on Sands, three genotypes of Aura 26, Ofelia, Doljana were developed, which were studied in a comparison comparative culture with Jiana variety. The production potential of the new varieties (2120-2706 kg / ha) was clearly superior to the control variety, the production differences being significant and very significant.

Keywords: *Vigna unguiculata L. Walp, sandy soil, biology, productivity, quality*

INTRODUCTION

In Romania, the phenomenon of drought is a specific characteristic, due to the fact that our country is located in a temperate climate zone with very high deviations from the normal values of the climatic, agroclimatic, hydrological and pedological parameters. The accentuation of this phenomenon from the last period and the specific microclimate, which is created especially in the southern part of Romania, required extensive studies at the Dabuleni Research & Development Station for Plant Culture on Sands (R & DSPCS Dabuleni), which led to the promotion of some plant species, including cowpea (Vigna unguiculata L. Walp), a plant that capitalizes with good results the ecopedological potential of sandy soils. Originally from Central Africa, the cowpea is considered to be one of the oldest legume crops for beans on the three continents of the "Old World" [5], [14], being an important vegetable for East, South, Central and Western African agriculture [6]. Through plant physiology, cowpea is a drought-resistant plant with wide ecological plasticity that can be cultivated widely in both high and low rainfall areas in South Africa.

Considering that ensuring genetic progression in agriculture starts from the evaluation of existing germplasm resources and their specificity for a particular area [1], [2], [3], many studies have been made on the improvement of cowpea plants in various parts of the world. The research conducted by the Institute for Agricultural Research, Ahmadu Bello University Zaria, Nigeria, highlights drought-resistant cowpea genotypes and resistantce to Striga gesnerioides (Willd.) [9]. The results obtained in Romania regarding the behavior of 144 genotypes of cowpea revealed the variability of the species in terms of plant biology, morphology and productivity [11]. Of the 144 studied cowpea genotypes, 38% allowed selection for the production of grain varieties for beans, 26% allowed selection of fetal genotypes for fodder, and 36% allowed the selection of genotypes for green fertilizer.

MATERIAL AND METHODS

In order to promote a sustainable agriculture system in areas with sandy soils subject to aridisation, the choice of species and variety with high adaptability to the climatic and soil conditions is a necessity in obtaining high and safe production. In this regard, 3 cowpea genotypes created at R & DSPCS Dabuleni (Aura 26, Ofelia, Doljana) were studied in a comparative competition culture, compared to the control variety, Jiana (the first Romanian variety of cowpea). The study was conducted on a low fertility psamosol, poorly supplied in nitrogen (0.039%), medium supplied in phosphorus of 30.5 parts per million ("ppm") and low in potassium (129 ppm). Experience has been placed under irrigation conditions in a 3 year crop: cowpea - rye - sorghum. The cowpea genotypes were sown in the period of May 1-10, when in the soil the average temperature was 10-12^{0}C, being fertilized with 60 kg/ha of nitrogen, 60 kg/ha of phosphorus and 60 kg/ha of potassium. During vegetation, soil moisture was maintained above the minimum 30% of the active humidity range, on a depth of 50 cm, in the phase of floral organs formation, flowering, and the formation of pods, by application of 2 - 3 watering with a norm of 150-200 m^3 water per hectare. They were carried out observations and observations of biology, morphology, productivity, and quality of the cowpea genotypes, and the results obtained were interpreted by variance analysis and mathematical functions.

RESULTS AND DISCUSSIONS

The analysis of climatic conditions recorded during the vegetation period of the cowpea (May to August) (Figure 1) shows an increased temperature in the last decade, compared to the annual average, which combined with rainfall records, they have resulted in increased droughts. Thus, compared to the multiannual average, average air temperature on rose by 1.01^{0}C and rainfall increased insignificantly (5.97 mm). The 227.82 mm rainfall, registered in the period 2008-2017, was unevenly distributed in relation to the requirements of most plants. The meteorological conditions recorded during the study period of the cowpea genotypes (2015-2017) highlight the increase of the drought phenomenon in the vegetation period, by increasing the air temperature by 1.41 ^{0}C, compared to the multiannual average. Through the plant's biological attributes, regarding increased drought resistance and reduced requirements for soil fertility, the cowpea may be a

good alternative for bean culture and for soybean culture, plants are very sensitive to stress factors in areas with excessive drought [4], [13].

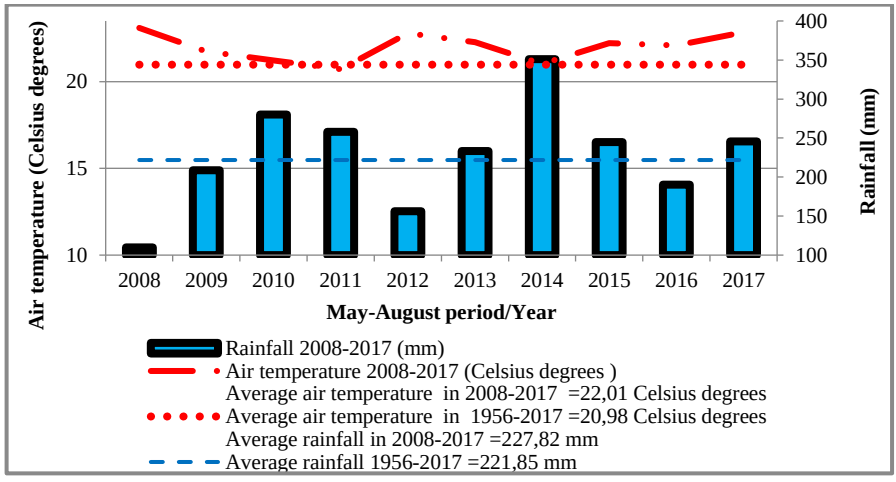

Fig. 1. *Climatic conditions recorded at the meteorological station of R&DSPCS Dabuleni during the cowpea vegetation period (Mai-August)*

Compared to beans, the cowpea has a very strong root system with a high absorption power, a waxy layer on the leaves, which gives it greater resistance to the climatic conditions that occur in the sandy soil area. Often, elevated soil temperatures (+ 60 °C), accompanied by low atmospheric humidity, lead to bean flower abortions, partially or totally compromising culture [3], [10]. From germination to the end of the vegetation period, all the vital processes of the cowpea plant were carried out under high-temperature conditions above 10^0C. Under the study conditions, the vegetation period of cowpea genotypes ranged over 91-103 days, with a thermal demand of 2096 - 2353.9 °C (Table 1). Compared to the Jiana variety, which is very late, the Aura 26 and Doljana genotypes have been highlighted through an early 11-12 days, when maturing the pods. Early plant life is an objective of creating varieties in areas subject to aridisation, in order to avoid drought periods from the moment the plants flourish. Being a leguminous plant, the fascia forms on its roots numerous nodosites in which the bacterium develops and fixes atmospheric nitrogen. Nitrogen, biologically fixed by the leguminous plants, compared to mineral nitrogen, has advantages because it does not consume fossil energy and is environmentally non-polluting. The results obtained in Nigeria, by K.O.Awonaike, on treatment the seeds of three cowpea varieties (Ife Brown, Ife BPC and AFB 1757) with Bradyrhizobium cowpea, revealed the biological fixation of about 74-116.87 kg / ha of atmospheric nitrogen [8]. The determinations carried out on the four cowpea genotypes, emphasize intense symbiotic activity in the blooming phase of the plant (111.6-129.5 nodules / root), which confirms the plant's role in fixing the biological atmospheric nitrogen (Table 1). Statistical analysis of the functional connections of the leaf area index (L.A.I.) and the vegetative growth of the plant, reveals positive correlations with the height of the plant and significantly positive with the weight of the plant biomass. Type of plant growth

allows selection and use biotypes of cowpea in the plant breeding process, according to the desired variety (grains, feed or green fertilizer).

Table 1. *Biological characteristics of some cowpea varieties studied under the conditions of sandy soils in Romania*

Genotypes	Vegetation period of the cowpea plant		The height of the plant (cm)	Plant weigh t (g)	L.A. I.	Plant growth type	No. nodules / root at flowering
	No. days	Amount degrees of temperatur e in air (^{0}C)					
Jiana	103	2353.9	111.33	173.7 5	7.26 5	erect, undetermin-ed	129.5
Aura 26	91	2096	82.33	147	5.13	erect, determined	114.8
Ofelia	95	2187.8	91.87	136.5 5	5.49 5	erect, undetermin-ed	136.2
Doljana	92	2115.4	81.4	151.6 5	6.58	erect, undetermin-ed	111.6
Correlation between L.A.I. and plant weight			$Y = 15.728x^2 – 181.04x + 659.75$; $R^2 = 0.972$; $r = 0.985$*				
Correlation between L.A.I. and plant height			$Y = 14.646x^2 – 171.95x + 584.93$; $R^2 = 0.7027$; $r = 0.838$				
Correlation between the height and weight of the plant			$Y = 0.1093x^2 – 20.288x + 1077.7$; $R^2 = 0.996$; r= 0.998**				

The plant productivity determines a number of pods in the range of 8.4-20.6 pods/plant, with a podshell length of 12.73-14.22 cm and a number of grains in the pod with values between 10.12-10.45 grains, depending on the genotype (Table 2). The genotypes Aura 26 and Ofelia were highlighted by higher percentages of grains/pods and grain weights. Similar results have been obtained in Brazil by Salvador B. Torres, which shows that the number of grains / pods per 10 cowpea genotypes ranged from 12 to 16 and the best results were obtained in the Amapá variety, which is the earliest [12],. An important role in the production of grain is represented by the percentage of grains / pods and the thousand weight grains (TWG). In this respect, all three varieties created in Dabuleni registered a percentage of grains in the pod net superior to the witness variety, Jiana. In terms of grain weights (TWG), this indicator is a varietal character and has a range of 182.2 g (Aura 26) and 130.5 g (Doljana).

Table 2. *Productivity characteristics of some cowpea genotypes studied under the conditions of sandy soils in Romania*

Genotypes	No. pods/plant	No. grains/pods	Length pods cm	% of grains in the pod	TWG g
Jiana	8.4	10.12	14.22	76.3	174.7
Aura 26	14.23	10.6	14.0	82.6	182.2
Ofelia	17.27	10.37	12.73	82	175.5
Doljana	20.6	10.45	13.77	81	130.5

Under the conditions of 2015-2017, cowpea recorded between 1522-2706 kg/ha of grain, depending on the variety (Table 3). High yields revealed the Aura 26 and Ofelia varieties, which recorded very significant production differences from the control variant (Jiana). The color of the grain is an aspect of the cowpea breeding process, depending on the requirements of the consumers, and in this respect, the researches carried out at Dabuleni aimed at obtaining the cowpea genotypes with white color of the grains. Thus, the Doljana variety, although having a lower production, due to its pleasant commercial appearance (the white color of the grain) is increasingly used in human nutrition. As a result of high protein content in both plant and bean, cowpea is considered to be the queen of psamosol areas, having multiple uses: in man's diet as pods or grains, in improving soil fertility, by cultivating the plant in crops from the sands or by incorporation into the soil as a green fertilizer [7], in animal nutrition, by participating with sorghum or rye in the formation of dried and silage feed. Analyzing the quality of grain production in fascia genotypes, is highlighted a crude protein content of 21.8-22.9%, a fat content between 2.2-2.7%, and a boiling shell content ranging from 7.23-11.36%. The three genotypes created in Dabuleni showed superior nutritional values to the control Jiana variety, both chemically and physically.

Table 3. *Level and quality of production obtained from some cowpea genotypes studied under the conditions of sandy soils in Romania*

Genotypes	Grai yield			Quality of grain			
	Kg/ha	The difference compared to the control Kg/ha	Significance	Color of the grain	Crude protein %	Fats %	Shell %
Jiana	1522	control	control	reddish brown	21.8	2.2	11.36
Aura 26	2706	1184	***	white with reddish brown hill	22.9	2.6	7.23
Ofelia	2530	1008	***	white with black hill	22.5	2.3	8.12
Doljana	2120	598	*	white	22.2	2.7	7.52

LSD 5% = 546.66
LSD 1% = 978.665
LSD 0.1% = 735.99

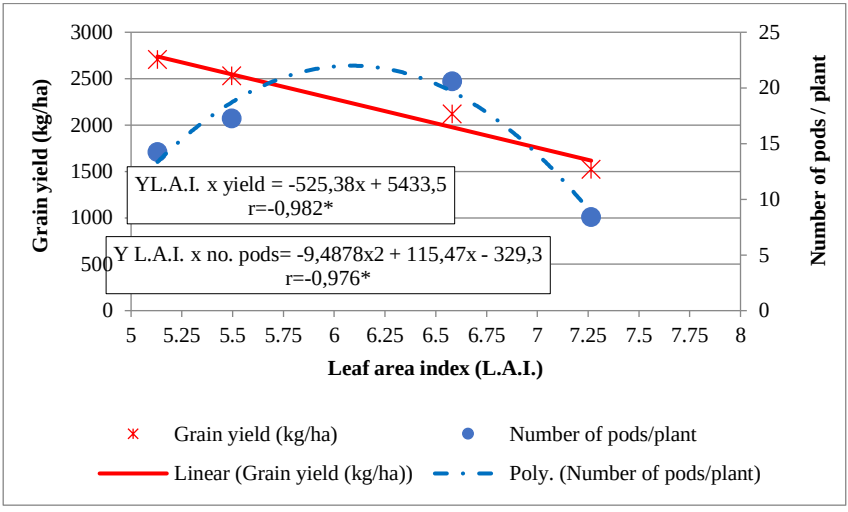

Fig. 2. *Correlations between Leaf area index and cowpea plant productivity*

The intraspecific competition between plants is carried out during the development of the foliar system and the root system, and the results show that higher increases of energy biomass are achieved as the plant is cultivated in an area more similar to that of origin [10]. The results obtained in cowpea varieties show that they developed a rich vegetative mass, with an index of foliar surface in the blooming phase ranging from 5.13-7.265, which correlates negatively with the number of pods/plant and the grains yield obtained (Figure 2). From this point of view, the genotypes of cowpea with high-value foliar surface index can be an important source of bioenergy for sandy soils.

CONCLUSIONS

Due to the plant's biological features, increased drought resistance and reduced soil fertility requirements, the cowpea may be a good alternative for bean culture and soybean culture, plants that are very sensitive to stress factors in areas with excessive drought.

The vegetation period of the cowpea genotypes experimented to R&DSPCS Dabuleni was carried out during 91-103 days with a thermal demand of 2096 - 2353.9 ° C.

The results obtained in the four genotypes of cowpea show that they developed a rich vegetative mass with a leaf aria index, in the blooming phase, between 5.13-7.265, which correlates positively with the height and weight of the plant and negative with the number of pods/plant and grain yields.

They were revealed by high yields (2530-2706 kg/ha) Aura 26 and Ofelia varieties, which have been very significant differences compared to the Jiana control production.

The cowpea genotypes created at Dabuleni (Aura 26, Ofelia and Doljana) showed superior nutritional values to the control Jiana, both chemically (crude protein = 22.2-22.9%, fats = 2.3-2.7%) as well as physically (percentage of boiling shells = 7.23-8.12%).

REFERENCES

[1] Abe S Gerrano, Patrick O Adebola, Willem S Jansen van Rensburg & Sunette M Laurie. Genetic variability in cowpea (Vigna unguiculata (L.)Walp.) genotypes. South African Journal of Plant and Soil, Volume 32, 2015 - Issue 3, DOI: 10.1080/02571862.2015.1014435, Online ISSN: 2167-034X, South Africa, 2015, pp. 165-174;

[2] B.B. Singh, D.R. Mohan Raj, K.E. Dashiell, and L.E.N. Jackai. Advances in Cowpea Research. International Institute of Tropical Agriculture, Ibadan, Nigeria and Japan International Research Center for Agricultural Sciences Tsukuba, Ibaraki. ISBN 978131 110 X, Japan, 1997, pp. 30-50;

[3] Baudoin J.P., Marechal R. Wide crosses and taxonomy of pulse crops, with special emphasis on Phaseolus and Vigna. In: Ng NP, Perrino P, Attere F, Zedan H (eds) Proceedings of an African plant genetic resources Workshop, International Institute of Tropical Agriculture, 17–20 October 1988, Nigeria,1991, pp 287–302;

[4] Boukar O, F. Massawe, S. Muranaka, J. Franco, B. Maziya-Dixon, and C. Fatokun. Evaluation of cowpea germplasm lines for minerals and protein content in grains. 5th World Cowpea Research Conference, 27 September–1 October 2010, Palm Beach Hotel, Saly, Senegal, 2010, pp.18;

[5] Draghci Reta. "Contributions to the growing technology cowpea (Vigna unguiculata (L.) Walp) on irrigated sands in southern Oltenia", PhD thesis, Unversity Craiova, Romania, 1999, pp 89-105;

[6] Emongor V. Gibberellic acid (GA3) influence on vegetative growth, nodulation and yield of cowpea (Vigna unguiculata (L.) Walp.). Journal of Agronomy Volume 6; Issue; eISSN: 1812-5417; p ISSN: 1812-5379, Botswana, 2007, pp. 509–517;

[7] Ion Petre. Dynamics of organic matter in soil and its influence on production capacity with special regard to soils with coarse texture. PhD thesis, ASAS Bucharest, Romania, 1981, pp.82-84;

[8] K.O. Awonaike, K.S.Kumarasinghe, S.K.A.Danso. Nitrogen fixation and yield of cowpea (Vigna unguiculata) as influenced by cultivar and Bradyrhizobium strain, Field Crops Research. ISSN: 0378-4290, Volume 24, Issues 3–4, October, Nigeria, 1990, pp.163-171;

[9] M.F. Ishiyaku and H. Aliyu. Field Evaluation of Cowpea Genotypes for Drought Tolerance and Striga Resistance in the Dry Savanna of the North-West Nigeria. International Journal of Plant Breeding and Genetics, Volume 7 (1): eISSN: 2152-3347 pISSN: 1819-3595, Nigeria, 2013, pp. 47-56;

[10] R.B. Dadson, F.M. Hashem, I Javaid, J. Joshi, A.L.Allen, T.E. Devine. Effect of Water Stress on the Yield of Cowpea (Vigna unguiculata L. Walp.) Genotypes in the Delmarva Region of the United States. Journal of Agronomy and Crop Science. Online ISSN:1439-037X. Volume 191, Issue 3, USA, 2005, pp. 210-217;

[11] Reta Draghici, Iulian Draghici, Aurelia Diaconu, Milica Dima. Variability of genetic resources of cowpea (Vigna unguiculata L. Walp) studied in the sandy soil conditions from Romania. Annals of the University of Craiova-Agriculture, Montanology, Cadastre Series. Vol. XLVI. ISSN: 1841-8317, Romania, 2016, pp. 147-153;

[12] Salvador B Torres, Fabrícia N de Oliveira, Regina C de Oliveira, João B Fernandes. Yield and morphology of cowpea accessions in Mossoró, Rio Grande do Norte State, Brazil. Horticultura Brasileira, Print version ISSN 0102-0536; On-line version ISSN 1806 - 9991, vol.26 no.4, Brasília, 2008, pp. 537-539;

[13] Thomas R. Sinclair, Anju Manandhar, Ouhoun Belko, Mandeep Riar, Vincent Vadez and Philip A. Roberts. Variation among Cowpea Genotypes in Sensitivity of Transpiration Rate and Symbiotic Nitrogen Fixation to Soil Drying. Crop Science Society of America, Vol. 55 No. 5, ISSN: 1435-0653 Print ISSN: 0011-183X, USA, 2015, pp. 2270-2275;

[14] Zavoi A. Contributions related to biology, improvement and agrotechnology of cowpea. Vigna sinensis (Torn) Endl – PhD thesis, University of Cluj Napoca, Romania,1967, pp 122-200.

SOILS OF SMALL ARCHAEOLOGICAL SETTLEMENTS IN THE STEPPE ZONE AS A RESULT OF BRONZE AGE ANTHROPOGENIC IMPACT

Assoc. Prof. Dr. Liudmila N. Plekhanova
Institute of Physicochemical and Biological Problems in Soil Science under Pushchino Scientific Center for Biological Research of the Russian Academy of Sciences, the Federal Research Center, Russia

ABSTRACT

The contemporary direction of natural pedogenesis/soil science is ancient anthropogenic impact and climate fluctuations changes. A large number of settlements in the river valleys are unique objects with a long history of development and modern soil cover formation. We studied the soil between the dwellings for a small settlement ***Zarya*** of the Bronze Age. The settlement was part of the economic zone of cattle breeding (horses and cows and sheep) of the large early Bronze Age fortified city Sarym-Sakla, one of the country's Proto-Iranian Cities of the Trans-Ural Plateau. The activity of ancient societies changed the terrestrial ecosystem functioning at macro and microscales. Increased heterogeneity of microrelief forms led to the diversity of soil cover. We found the unusual soil types on microelevations and microdepressions. The enrichment of the cultural layer with phosphorus compounds was revealed, and the hypothesis of the formation of a "reverse" ratio of chernozems-solonetzes of the soil cover of the low above-floodplain terrace as a consequence of several stages of ancient anthropogenic pressure and climatic aridization was confirmed in this area.

We focused on the determination of organic carbon content, magnetic susceptibility, salt composition, cation exchange capacity, and the distribution of mobile phosphates along the soil profile as possible indicators of ancient anthropogenic influence.

The degree of soil properties changes during the anthropogenic impact is commensurate with their transformation in the natural evolution of centuries and even several millennia. Past anthropogenic changes leave a mark in the history of the development of the soil cover predetermining the modern danger of the degradation phenomena.

Moreover, we draw parallels in the history of ecosystems formation and outlined tasks for further research.

Keywords: *overgrazing, unfortified settlements, paleoclimate, steppe, Bronze Age.*

INTRODUCTION

Recording and accurate dating of paleo-processes traces in modern ecosystems can act as a key for understanding the current state and interpreting the history of

landscape development, which has numerous and multifactorial confirmations of long-term economic development for the steppe zone in Russia [2], [12]. The stratigraphy of the layers of little archaeological sites provides a possibility to link paleo-solonets traces to certain periods and archaeologically date the enclosing context.

The natural horizons of soils that disappeared under the influence of an ancient anthropogenic factor were replaced by stable pedosedimentary natural-anthropogenic formations – cultural layers. The anthropogenic pressure led to destruct the natural horizons of soils, which than were replaced by stable pedosedimentary natural-anthropogenic formations – cultural layers. The cultural layer consists of artifacts and placeholder. The aggregate is usually formed from the material of the initial soil with an admixture of remnants of construction and household garbage.

For the cultural layers, the most characteristic feature is the increased content of humus and phosphorus [1], [3], [6], [8], [10], the simultaneous increase of which is their diagnostic sign.

The profile distribution of phosphorus in soils with a cultural layer reflects the enrichment of cultural layers with mobile forms of phosphates. During the mineralization of organic matter entering the soil, phosphorus is fixed in the form of hardly soluble calcium phosphates, which persist for hundreds and thousands years. Anomalous zones or layers of concentration of this element are formed. Within the area of ancient settlements, significant fluctuations in the content of phosphates in the soil have long been noted [4], which is explained by the heterogeneity of the settlement of individual parts of the settlements. The use of the phosphate method in archaeological fieldwork to establish the sites of ancient settlements [13], as well as to clarify the details of excavations [11] , can significantly reduce the amount of exploration work.

OBJECTS AND METHODS

The investigated territories are located in the steppe zone on the eastern slope of the Ural mountainous country within the Trans-Ural plateau (200-500 m above sea level) - a peneplain formed as a result of the destruction of the ancient mountain system. The geographical position makes the main feature of the climate continentality with significant daily and annual temperature ranges. In the warm season, about 70% of the annual precipitation falls in the steppe region. At the same time, there is often an influx of continental tropical air from Central Asia, accompanied by the establishment of particularly hot and dry weather. The prevalence of low-cloud anticyclonic weather during the year results in a significant duration of sunshine. The number of hours of sunshine per year in the steppes beyond the Urals reaches 2100-2300, while in the steppes, for example, in Ukraine, - 1800-1900. In terms of thermal resources, the Trans-Ural steppes are closer to the Asian ones than to the steppes of the Eurasian part of Russia. The amount of atmospheric precipitation is up to 250-300 mm in the steppe zone (the long-term average is 330 mm). The climate of the study area is sharply continental with little snow and cold winters, dry and hot summers. Average annual temperatures

fluctuate between 1.1-2.6°C, the sum of positive temperatures above 5°C is equal to 2460°C, the sum of average daily temperatures above 10°C is 1950-2300°, the frost-free period lasts about 120 days, the average duration the growing season is 170 days, 250-330 mm of precipitation falls per year, of which 45% in summer and 12% in winter, and only 130-180 mm during the growing season. The character of summer precipitation is predominantly stormy. In low-cloud weather, the soil heats up strongly (up to 65°C), and is exposed to dry winds (up to 30 m/s). The annual evaporation rate is 1.5-2 times higher than the annual precipitation. The depth of soil freezing is 80-200 cm, depending on the particle size distribution. During the spring snowmelt, water is not absorbed into the thawed soil, but flows down its surface. Dry years give way to years with excess rainfall.

In the valley of the river Zingeyka (left tributary of the Ural River, Kizilsky District, Chelyabinsk Region), the settlements Zarya XI (2.5 km south-west of the Zarya settlement, archaeologist F.N.Petrov), Lebyazhye VI (5 km to northeast of the Katsbakhsky settlement, archaeologist L.Yu. Petrova). The settlements are located on the first terrace above the floodplain. The demarcation of the two bends of the river is a hill, in the southern part of which (260 m from the village of Zarya) is the Lebyazhye menhir. In one of the river bends there is the Lebyazhye settlement, in the neighboring one - the Zarya settlement. The direct distance between the centers of the settlements is 720 m. Both settlements are located in close proximity to the fortified settlement of Sarym-Sakly - one of the most striking monuments of the "Country of Cities", and represent an unfortified settlement area.

The granulometric composition of soils was determined according to Kachinsky, the organic carbon content according to Tyurin, mobile phosphorus for saline steppe soils was determined according to Machigin, magnetic susceptibility using a KT-5 device, and other analyzes according to generally accepted methods.

RESULTS AND DISCUSSIONS

The excavation of the Zarya settlement (single-layer character) was laid in the inter-dwelling space. The ceramic complex is identified as Alakul, with pronounced early Alakul features. The state of plant communities at the sites and the adjacent territory is good, since the area of the projective cover is not less than 70% in all cases, the communities are at 1-2 stages of pasture digression, and the associations are mainly herb-grasses. Within the two settlements, 15 sections were laid. The position of the settlements in the immediate vicinity of the river, at an absolute height of 360 m above sea level, at the level of the first above-floodplain terraces with a close (2-3 m) groundwater occurrence suggests hydromorphism as a feature that determines the external appearance of the studied soils.

The soils of the Zarya XI settlement are formed on a binomial: the lower part of the section is heavy loamy-clayey, the upper one is represented by light loams. The Zarya-11-00 cross-section was laid in place of a pit with a humus filling. The humus horizon is heterogeneous, subdivided into non-boiling A1 layer and boiling part - A1* layer , the total thickness varies from 30 to 70 cm, the transition boundary to the B_{CA} is lingual. On the cultural layer containing many artifacts, A1 of low thickness was formed - in total with A_D horison reaching 10 cm.The

thickness of the underlying cultural layer reaches 20-25 cm.The B_{CA} horizon under the cultural layer is powerful - 55 cm, and decreases under the filling of the pit. The BC horizons of both sections are similar; they are characterized by the presence of numerous rusty ferruginous nodules, 2-3 mm in diameter. In the walls of the excavation site (Fig. 31), the thickness (A_D + A_1) layers also does not exceed 10 cm, the thickness of the ashpit cultural layer varies from 10 to 40 cm, the calcined cultural layer- 10-12 cm. The total thickness of natural anthropogenic layers, in including those covered by soil formation, mainly fluctuates within 30-40 cm, in some cases increasing to 70 cm.

The granulometric composition of the soils of the sites reflects their formation on a binomial - the lower part is heavier - medium-heavy loam, while in the upper part of the soil - a lightening of the granulometric composition in all cases to light loam, in the background soil to sandy loam, but this is explained by the formation of a suprasaline horizon.

While the strata of the cultural layer acted as a parent rock, the light loamy composition remains a marker of the boundaries of the distribution of cultural layers as the most conservative soil property. Accordingly, the “background” soils of the settlement are actually not such, but are located on the outskirts of the settlement, where there are no longer artifacts, but an anthropogenically transformed layer is present. Moreover, the complexity of the cover, inherent in the first terraces above the floodplain in this region, is formed regardless of the presence of the cultural layer.

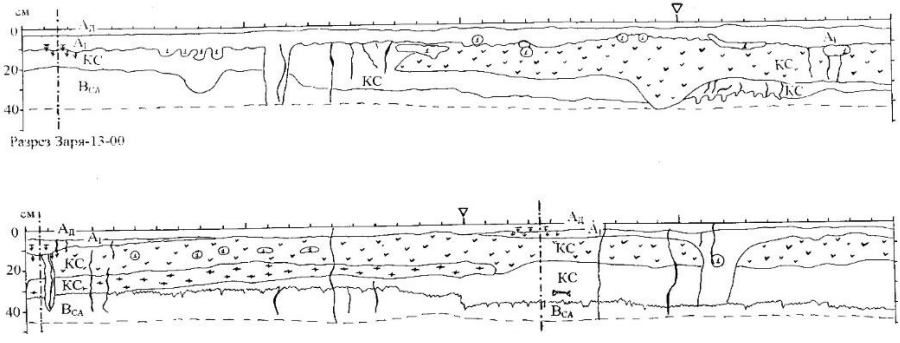

Fig. 1. *Stratigraphy of layers and soil sections of the eastern cross-section of the ancient settlement of Zarya in the South Urals. The cultural layer is designated «КС». Layer diagnostics scheme is made by the author.*

The humus content in the sod and A1 horizon of the settlement and in the background soil of the is higher than 10%, which indicates the formation of chernozem-meadow soil. In the soil of the background microdepression, the humus content reaches 5%. The large drop (decrease by 4 times) in the humus content from 10.08% in the A1 horizon to 2.56% in "A1" is explained by the presence of natural-anthropogenic sediment in the upper part of the section, enriched with organic matter. With depth, the humus content gradually decreases, in horizons B, BC it

varies from 0.49 to 0.75%. New formations of carbonates are represented by impregnating forms. Carbonate profile of background soils with one maximum. In the soil of the microdepression, it is located at a depth of 50-70 cm (16.4%), and at a depth of 30-40 cm in the soil of the microdepression (20.8%). At the settlement, an increase (by a factor of 2) is noted in the $CaCO_3$ content in the ashpit cultural layer (from 4.6% in the A1 horizon to 10.8% in the cultural layer). The increased content of carbonates in the cultural layer is probably determined not only by the enrichment of the layer with ash, but also by the introduction of carbonate-containing rocks in the process of economic or ritual activities of the population. Deeper is again a decrease in the content of CaCO3 in the first buried soil (up to 6%), again an increase (almost 3 times) in AB_{CA} to 20.6%, and a gradual decrease with depth - up to 13%; The absence of a humus peak in [A] 50-60 cm suggests a humus filling of the dwelling cavity.

The maximum gypsum content (0.31% in the background rise, horizon "B_{CA}", 0.45% in the background microdepression, horizon B_{CA}) coincides in depth with the horizons of maximum carbonate content. At the settlement, gypsum is 2 times more (0.65%). The reaction of the medium in the soil of microelevation (background 1) is neutral in the upper part (pH 7.0 - A_D, A1 layers), in the lower part it is alkaline (pH 9.2-9.1) In background 2 (microdepression) it is alkaline (from 8.0 to 9.2). In the soil of the settlement, the reaction of the solution lies in the alkaline region - from 8.0 to 9.5 in the lower part of the profile. The acidic reaction of soil solutions favours the dissolution of bases, including bones, and the transition of mineral compounds to a mobile state. The established reaction of the cultural layer is alkaline (pH 9.0), which contributes to the preservation of artifacts. The composition of the salts according to the results of the analysis of the water extract is as follows. The soil of the rise (background 1) is slightly saline (the sum of salts does not exceed 0.1%), the salinity is predominantly hydrocarbonate-magnesium, in the soil of the microdepression (background 2) the sum of salts varies from 0.2 to 0.5%, in the lower horizons the salinity is sulfate-chloride-sodium, in AB_{SL} layer sodium bicarbonate. The composition of exchangeable cations is dominated by magnesium, the sodium content in the mountains. AB_{SL}, B_{CA} is 21-22% of the catonic exchange capacity. At the settlement in the soil buried under the cultural layer, the sum of salts is 0.27-0.60%, with a maximum in [AB_{Sl}]. In the cultural layer itself, the sum of salts is 0.13%, the lowest salinity in A1 is 0.07%. the type of salinity in the lower horizons is chloride-sulphate-sodium, in the filling of the dwelling depression it is predominantly sulphate-magnesium, in the cultural layer it is chloride-hydrocarbonate-calcium, above it is hydrocarbonate-magnesium-calcium.

The amount of oxides in the backgrounds is comparable, the maxima are at a depth of 80-100 cm (0.56, 0.41 for Al_2O_3; 0.43, 0.34 for Fe_2O_3, respectively). In the sod of the settlement, the content of Al_2O_3 is increased (0.7%), in the cultural layer - 0.6%, and in [A] layer - 0.4%. The maximum of mobile forms of Fe_2O_3 in terms of values is comparable to the maximums of backgrounds, but it is located higher - at a depth of 0-20 cm, their highest content is characteristic of the cultural layer. The distribution of potassium content in background soils is biogenic with a maximum in the upper horizons (78-96 meq / 100 g of soil). The concentration of

potassium compounds is high. In the soil of the settlement, the values increase in comparison with the background by 2 times (144-200 meq / 100 g of soil - A_D and cultural layer). The general appearance of the curves is similar in the backgrounds and at the settlement - a smooth decrease with depth, but at the settlement the values are increased by 7-10 times (12-20 mEq / 100 g of soil in the lower horizons of the backgrounds and 100-140 mEq / 100 g soil in the settlement), which gives grounds to speak of the introduction of organic substances (economic or ritual activities) into the cultural layer of the settlement and the substrate that filled the dwelling cavity.

The distribution of phosphorus compounds in the backgrounds of the settlement, as well as potassium, is biogenic in nature - the maxima are in AB (background 1, 3.6 meq / 100 g of soil), A_1A_2 layer (background 2, 2.8 meq / 100 g of soil). The second maximum in both backgrounds falls on B_{CA} and is 2.0 meq / 100 g of soil. The minimum in the microelevation falls on horizons buried under sediment. The values are 0.7 mg-eq / 100 g of soil; in the microdepression, on AB_{SL}, the values are 1.4 mg-eq / 100 g of soil. In general, the values are of the same order of magnitude. At the settlement, close to the background (maximum) values only in the BC mineral horizon (90-100 cm) - 2.4 mg-eq / 100 g of soil. The greatest difference in comparison with the background is characteristic of the 40-50 cm AB_{CA} horizon - 10.7 meq / 100 g of soil - the greatest "use" of the layer, the greatest enrichment of it with organic substances. The increased values at a depth of about one meter can be explained by diagenetic intraprofile redistribution. The course of the profile distribution curve does not correspond to the background one, and rather has the opposite form, which is associated with anthropogenic impact. The maximum content of mobile phosphorus in AB_{CA} can be interpreted in accordance with natural processes. In the backgrounds, the maximum also falls on the B_{CA}.

At the Zarya settlement, the magnetic susceptibility of the underlying rocks is significantly lower (16 units) than at Lebyazhye (70-125 units - BC horizons), located nearby. The minimum values are typical for the B_{CA} horizons (or cultural layer with calcium); the maxima - for the humus-rich horizons, both for the buried and the modern ones - 170-187 units for Lebyazhy, 48-66 units for Zarya.

The study of the microbiological characteristics of ancient soils is actively developing today, both buried under embankments and cultural layers [5, 6, 7, 14, 15]. It is necessary to continue the study of ancient small settlements of cattle-breeding specialization in the direction of studying the enzymatic and microbiological activity of soils.

The characteristic features of the soils of the depressions are low thickness (up to 10 cm), low humus content (2.44%) of the upper horizon in comparison with the soils of elevations, for which the average thickness of the humus horizon is 80 cm, and the amount of humus in the upper part reaches 6% and very decreases smoothly with depth up to 1.5-0.2%. The residual-granular residual-coprolite structure of the humus horizon of the soils of micro-elevations at a depth of 50-70 cm was noted, which indicates a well-developed chernozem-meadow soil of this area in ancient times, before the beginning of anthropogenic pressure.

It is characteristic that in the immediate vicinity of the fortified cult and production centres of Sarym-Sakly and Arkaim of the Chelyabinsk region of the Russian Federation, there was no reverse complexity, while at a distance of 1 km there were small unfortified satellite settlements of ancient pastoralists, in the vicinity of which soil pits many times the reverse complexity is fixed. This made it possible to assume that the cause of the inversion complexity of the soil and vegetation cover is overgrazing in antiquity [9].

The first stage of overgrazing took place in the Late Bronze Age. It was during this period, no later than the middle of the 2nd millennium BC, that the first violations of the natural confinement of the soil and vegetation cover to the elements of the microrelief occurred. This conclusion is confirmed by the close confinement of the identified inversion soil-plant associations to the vicinity of the monuments of the Late Bronze Age and the almost complete absence of stationary settlements in this area in the subsequent period [10]. Aridization of the climate in the 1st millennium BC (the early Iron Age) allowed the prevailing inverse relationships to gain a foothold, and widespread grazing at a later time contributed to their maintenance.

CONCLUSION

In all cases, the formation of complexes of chernozem-meadow soil and solonetzes takes place, both in the vicinity of the monuments and in the settlements themselves, with the only difference that anthropogenically transformed layers act as the parent rock in the settlements. In our study sites, the formation of complexes of chernozem-meadow soil and solonetzes takes place, both in the vicinity of the monuments and in the settlements themselves. The difference is anthropogenically transformed layers act as the parent rock in the settlements In general, soil formation proceeds according to the chernozem-meadow type, which is characteristic of the soils of the corresponding above-floodplain river terraces in the vicinity. The soil formation proceeds according to the chernozem-meadow type, which is usual of the soils of the above-floodplain river terraces in the area of paleo settlements.

The soils of ancient settlements are formed under the joint influence of natural and anthropogenic factors, and are special formations, since their normal development is interrupted by anthropogenic impact and the growth of natural-anthropogenic sediments. The soils of ancient settlements are formed simultaneously of natural and anthropogenic factors. These soils are special formations, since their normal evolution is interrupted by the anthropogenic impact and the growth of natural-anthropogenic sediments.

The thickness of the soils of the ancient settlements ranges from 20 to 150 cm. The sediment includes the last stage of soil formation, which covered 10-18 cm, and the ashy cultural layer, which was unaffected by soil formation. The ash pan usually has a thickness of 20-30 cm, sometimes it is subdivided into “ash pan” and “calcined”, the latter has a slightly more brownish tint in comparison with the ash pan, but mostly the same properties.

The features of the cultural layers are light granulometric composition, low density, morphological heterogeneity. The cultural layer is characterized by an

increase in the content of humus and phosphorus, high carbonate content, alkalinity, low salinity, and low values of magnetic susceptibility.

Overgrazing and the associated degradation of the vegetation cover, including the subsequent erosion of soils, caused the development of combinations of soil-vegetation cover and microrelief, which are typical for the steppe region. The revealed examples of the development of saline soils in microdepressions and zonal soils on microelevations were found only in a kilometer zone in the vicinity of numerous large settlements of the Late Bronze Age.

It should be noted that there is a clear lack of information about the influence of ancient cattle breeding on steppe soils, and especially on the soils of steppe river valleys. Taking into account that in the steppe zone, almost all archaeological sites are confined to river valleys, the importance of studying this issue increases even more.

ACKNOWLEDGEMENTS

This work was supported by the grant under the State Assignment No AAAA-A18-118013190175-5, using the resources of the Research Equipment Sharing Center (TsKP) of the Institute of physicochemical and biological problems in soil science under Pushchino Scientific Center for Biological Research of the Russian Academy of Sciences, the Federal Research Center (Pushchino, the Russian Federation).

REFERENCES

[1] Borisov A.V., Chernysheva E.V., Korobov D.S. Buried Paleoanthrosols of the Bronze Age agricultural terraces in the Kislovodsk basin (Northern Caucasus, Russia) // Quaternary International. 2016. V. 418. P. 28–36.

[2] Chibilev A.A., Ryabukha A.G. History of economic development and anthropogenic transformation of sandy lands of the steppe zone of the Orenburg region // Arid ecosystems. 2016. No. 1 (66). P. 48-55 (in russian).

[3] Demkin V.A., Borisov A.V., Demkina T.S., Udaltsov S.N. 2012. Soil Evolution and Climate Dynamics in the Steppes of South-East Russian Plain within the Neolith and Bronze Epochs (IV–II MIL. BC). Izvestiya Rossiiskoi Akademii Nauk. Seriya Geograficheskaya. P. 46-57. doi.org/10.15356/0373-2444-2012-1-46-57 (in russian).

[4] Detyuk A.N., Taranenko N.P. Analysis of soils for the content of phosphates as a method for determining the locations of ancient settlements // Natural-scientific methods in field archeology. Issue 1. Moscow: Institute of Archeology RAS, 1997. P. 43-58 (in russian).

[5] Kashirskaya, N., Chernysheva, E., Plekhanova, L., Borisov, A. 2019. Thermophilic microorganisms as an indicator of soil microbiological contamination in antiquity and at the present time // International Multidisciplinary Scientific GeoConference Surveying Geology and Mining Ecology Management, SGEM, Bulgaria. 19 (3), pp. 569-574. DOI: 10.5593/sgem2019/3.2/S13.074

[6] Kashirskaya, N.N., Plekhanova, L.N., Chernisheva, E.V., Yeltsov M.V., Udaltsov, S.N., Borisov, A.V. 2020. Temporal and Spatial Features of Phosphatase Activity in Natural and Human-Transformed Soils// Eurasian Soil Science 53(1), P. 97-109. DOI: 10.1134/S1064229320010093.

[7] Kashirskaya, N.N., Plekhanova, L.N., Udaltsov, S.N., Chernysheva, E.V., Borisov, A.V. 2017. The Mechanisms and Time Factor of the Enzyme Structure of a Paleosoil // Biophysics (Russian Federation), 62 (6), pp. 1022-1029. DOI: 10.1134/S0006350917060094 .

[8] Lisetskii F. N., Rodionova M. E. Transformation of dry-steppe soils under long-term agrogenic impacts in the area of ancient Olbia// Eurasian Soil Science. April 2015, Volume 48, Issue 4, pp 347–358. DOI: 10.1134/S1064229315040055

[9] Plekhanova, L.N. 2019. Anthropogenic Degradation of Soils on River Terraces in the Volga–Ural Region in the Bronze Age and Its Effect on the Modern Soil–Plant Cover // Arid Ecosystems, 9 (3), pp. 187-192.

[10] Plekhanova, L.N. 2017. Searching for benchmark soils in the steppe zone of the Trans-Ural Plateau to compile the Red Book of Soils // Arid Ecosystems, 7 (3), pp. 171-177. DOI: 10.1134/S2079096117030076

[11] Rusakov A., Popov A., Makeev A., Kurbanova F., Puzanova T., Khokhlova O., Kust P., Lebedeva M., Chernov T., Golyeva A. 2019. Paleoenvironmental reconstruction based on soils buried under scythian fortification in the southern forest-steppe area of the East European plain // Quaternary International. Т. 502. № Part B. P. 197-217. DOI: 10.1016/j.quaint.2018.05.016

[12] Stobbe A., Gumnior M., Ruhl L., Schneider H. 2016. Bronze Age human-landscape interactions in the southern Transural steppe, Russia - evidence from high-resolution palaeobotanical studies // Holocene, 26 (10), pp. 1692-1710, doi 10.1177/0959683616641740

[13] Velleste L. Analysis of phosphate compounds of the soil for establishing the places of ancient settlements // Brief communications of the Institute of History of Material Culture of the USSR Academy of Sciences, vol. XLII, 1952. P. 135-140 (in russian)

[14] Zhuravleva A.I., Demkin V.A., Blagodatskaya E.V., Yakimov A.S. 2012. Mineralization of soil organic matter initiated by the application of an available substrate to the profiles of surface and buried podzolic soils // Eurasian Soil Science. Т. 45. № 4. P. 435-444. DOI: 10.1134/S1064229312040163

[15] Zhuravleva A.I., Myakshina T.N., Blagodatskaya E.V. 2011. The effect of pyrogenically modified substrates on mineralizing activity and growth strategies of microorganisms of grey forest soil // Microbiology (Mikrobiologiya). Т. 80. № 2. P. 194-204. DOI: 10.1134/S0026261711020202

Section

WATER RESOURCES

Water quality, water use and water planning
Hydrology and hydrodynamics
Saltwater, freshwater and groundwater
Purge technologies and water monitoring
River basin, ocean and coastal management

A SUSTAINABLE APPROACH FOR TREATMENT OF WASTEWATER USING CHICKEN FEATHERS

Dr. Vandana Gupta[1]
Athira Nair[2]
Saurabh Pandey[3]
[1, 2, 3] Asstant Professor, B. K. Birla College of Arts, Science and Commerce, Kalyan, India

ABSTRACT

Since the last few decades, environmental remediation through a sustainable approach is gaining importance. One such attempt has been made in the present work to remove heavy metals from industrial effluents using one of the most prominent animal wastes, the chicken feathers. Biosorption has been a promising technique to remove heavy metals from industrial effluents. In the present work, cleaned but untreated chicken feathers were used to remove Cu(II) ions from electroplating industry wastewater. The physicochemical characteristics like colour, pH, ash content, iodine number and bulk density of chicken feathers were also determined. The FT-IR spectrum of chicken feathers did not show a recognizable difference after biosorption which indicated physical adsorption. The adsorption isotherm study showed that the Freundich isotherm model was the best fit as compared to Langmuir isotherm model. The results obtained were supported statistically by using Chi-square test. In the desorption study, EDTA was found to be a most effective desorbing agent in comparison with acid, alkali and deionized water. Thus, the present work explores the efficiency of chicken feathers to act as biosrbent as remove heavy metals from industrial effluents in a simple, economic and sustainable manner.

Keywords: *biosorption, chicken feathers, physiochemical characteristics, adsorption isother, desorption*

INTRODUCTION

Industrial discharge of toxic heavy metals has been one of the major reasons of pollution to receiving water bodies. The indigenous micro-organisms find it very difficult to degrade these heavy metals *in situ*. These metals ions through the process of bioaccumulation and biomagnification pass from one organism to another especially through microorganisms, aquatic flora and fauna, which in turn, may enter into the human food chain and result in health problems.[1] The symptoms of heavy metal pollution depend upon its type and concentration and they vary from simple metabolic disruption to lethal and genetic disorders. A lot of environmental nuisance has been reported which has raised the need of the treatment of industrial effluents for removel of heavy metals before its discharge into water bodies.

Various physicochemical treatment processes for metal-contaminated waste streams include chemical precipitation, ion exchange, membrane filtration, carbon

adsorption, and co-precipitation/adsorption [2]. All these techniques have their own advantages and limitations. As compared to different techniques, the adsorption process has been found to be one of the most promising technologies in water pollution control in terms of cost, simplicity of design and operation [3]. Activated carbon is explored worldwide for the waste water treatment applications but its high capital and regeneration cost limits its large-scale applications for the removal of metals and other aquatic pollutants, which have encouraged researchers to look for low-cost alternative adsorbents utilizing agro-industrial wastes [4], [5], [6].

Biosorption is a passive adsorption process, based mainly on the affinity between biosorbent and the sorbate [7]. Earlier, the study of biosorption technique was restricted to micro-organism. But the need of developing an economical, simple and sustainable methods for biosorption process diverted the attention of researchers to explore different agricultural animal and industrial wastes. Presently different agricultural and industrial have been explored for biosorption of different heavy metals from industrial effluents. A number of investigations have been carried out for the removal of heavy metals from aqueous systems using agricultural waste and by-products[8]. But very few references are available for biosorption of heavy metals using animal wastes.

The demand for chickens for its meat and eggs has been increasing over the years. Intensive poultry production causes difficulties for handling waste and managing pests and diseases caused by poultry wastes. Some poultry waste like chicken feathers, eggshells, etc can be studied for pollution control. This can create an industrial applications of poultry waste. This will also lead to sustainable development where solid waste can be used for the removal of pollutants from liquid waste by a simple process of biosorption. A chicken has about 5% to 7% of its body weight in feathers so chicken feathers are an important by-product of the poultry industry. Chicken feather is composed of 90 % keratin. Keratin operates through active polar sites on their surface to attract metal ions via physical and chemical adsorption process [9]. Hence chicken feathers can act a good biosorbent for binding to metal ions. Considering the pollution and health hazard aspect of discarded chicken feathers, the present work was carried out to find the application of this poultry waste for copper ion biosorption from industrial effluents. Further, a mathematical model for biosorption was studied using Freundlich and Langmuir adsorption isotherm. A desorption study was also carried out with the aim to regenerate biosorbent.

MATERIALS AND METHODS

Collection and preparation of biosorbent: The chicken feathers were collected from a local slaughterhouse shop in Mumbai (MS), India. The feathers were cleaned multiple times with tap water followed by rinsing with deionized water. The washing process was done to remove blood, dirt and dung attached to chicken feathers. After complete oven drying at 60^{o}C, the feathers were cut into fine pieces using scizzors and preserved in air-tight container till further use. This sample was used as biosorbent.

Preparation of salt solution: Stock solution (1000 mg/L) of Cu(II) ions were prepared by dissolving the required amount of analytical grade $CuSO_4.5H_2O$ in deionized water. The working standard solutions were prepared by diluting the stock solution to appropriate volumes.

Characteristics of biosorbents: The physical, chemical and surface characteristics of untreated biosorbent *viz.* chicken feather were studied to determine their properties.

- **Colour:** The colour of the biosorbent was identified by visual observation.
- **Iodine number:** The iodine number was evaluated by using the method given by [10]. 0.1 g of biosorbent was placed with 25 ml of iodine solution in 250 ml conical flask and the solution were shaken for 1 minute. After that the evaluation were filtered and 10 ml of the filtrates were titrated with 0.01 N sodium thiosulfate solution until clear solution were obtained. The iodine number of the biosorbent was determined by using the given formula:

$$\text{Iodine number (mg/g)} = \frac{V * (T_i - T_f) * C_i * M_i}{T_i * g}$$

Where, V = volume of iodine solution (ml)

Ti = volume of sodium thiosulfate solution used for the titration of 10 ml filtrate

g = weight of adsorbent (0.1 g)

Mi = molar weight of iodine (126.9044 g/mol)

Ci = concentration of iodine solution (0.01 N)

- **Bulk Density:** The bulk density of the biosorbent was determined by gravimetric method. The weight of the dried measuring cylinder (10 ml capacity) and cylinder tightly packed with biosorbent were found out. The difference in their weights represented the mass of the biosorbent and it was divided by the volume occupied by the biosorbent. Bulk density was calculated by using the following formula:

$$\text{Bulk density (g/mol)} = \frac{M_2 - M_1}{V}$$

Where, M2 = mass of measuring cylinder + sample (g)

M1 = mass of empty measuring cylinder (g)

V = volume of cylinder (ml)

- **pH of the biosorbent:** The pH of the aqueous extract of biosorbent was determined by using pH meter.
- **Ash content** The determination of ash content evaluates the mineral content present in the biosorbent. 1 g of biosorbents was taken in a

pre-weighted silica crucible and was heated in muffle furnace at 500 °C for three hours. The residue was allowed to cool in a desiccator and weighed. The ash content (%) was estimated using following formula:

$$\text{Ash content (\%)} = \frac{W_2 - W_0}{W_1 - W_0} \times 100$$

Where, W_0 = weight of empty crucible (g)

W_1 = weight of empty crucible + biosorbents (g)

W_2 = weight of empty crucible + ash content (g)

- **FT –IR analysis:** Fourier Transform InfraRed (FT-IR) Spectrophotometer (Jasco FT/IR-4100 type A C208161016) was used to assess the presence of functional groups on the surface of the biosorbent. The study was carried out by using potassium bromide (KBr) disc method. The spectrum of the biosorbent was recorded within range of 400 to 4000 cm^{-1} wavenumbers.

Biosorption process: Biosorption process was conducted using batch method. 100 mL of Cu(II) ions solution (50 mg/L) was treated with 0.1 g of biosorbent in 250 mL conical flask at 30 °C and the solution was shaken at 100 rpm in an orbital shaker. After an hour, the solution was filtered using Whatman filter paper No. 1. The Cu(II) ions from the filtrate was estimated using Standard Neocuprine method. The aqueous solution of biosorbent under study was used as blank. Under optimum condition, the effluent from electroplating industry was also treated with biosrbent.

Factors affecting Biosorption process: The effect of various factors *viz.* pH, temperature, metal ion concentration, biosorbent dosage, contact time and agitation speed on biosorption process using chicken feathers were studied.

- **Effect of pH**: To study the effect of pH on biosorption process, 0.1 g of biosorbent was added to 100 mL of aqueous solutions containing 50 mg/L of Cu(II) ions in 250 mL conical flasks and the biosorption process was studied at different pH *viz.* 2, 4, 6, 8 and 10 for 60 mins at 30 °C.
- **Effect of temperature**: 0.1 g of biosorbent into aqueous solutions containing 50 mg/L Cu(II) ions at different temperatures *viz.* 20, 30 and 40 °C were shaken at 100 rpm 60 mins at pH 6.
- **Effect of metal ion concentration**: The effect of concentration of was studied by adding 100 mL of different Cu(II) ions concentration (10, 50, 100 mg/l) to 0.1 g of biosorbent in 250 mL conical flasks and the biosorption process was carried out for 60 mins at 30 °C with orbital stirrer at 100 rpm at pH 6.
- **Effect of biosorbent dosage**: The effect of biosorbent dose was studied by adding different doses (0.1, 0.5, 1g) of biosorbent to 250 mL conical flasks containing 100 mL solutions of 50 mg/L of Cu(II) ions at pH 6 and the biosorption process was carried out for 60 mins at 30 °C with orbital stirrer at 100 rpm.

- **Effect of contact time**: The effect of contact time on biosorption process was studied by adding 0.1 g of biosorbent to 100 mL of aqueous solutions containing 50 mg/L Cu(II) ions at pH 6 and the biosorption process was carried out for different time period like 30, 60, 90, 120 minutes at 30 ^{o}C.
- **Effect of agitation speed**: 0.1 g of biosorbent was added into 100 mL of aqueous solutions having different agitation speed (0, 50, 100, 150, 200 rpm) and containing 50 mg/L aqueous solution at pH 6 and biosorption process was carried out for 60 minutes at 30 ^{o}C.

Study of adsorption isotherm: Freundlich and Langmuir Adsorption isotherms were determined by taking 100 mL of metal solution of various concentrations ranging from 10 to 50 mg/L in conical flask and maintaining the optimum conditions. The residual concentration of Cu(II) ions after biosorption was analysed by Neocuprine estimation method using UV Spectroscopy at 450 nm. The graph of Freundlich and Langmuir isotherm was plotted using excel sheet.

Desorption process: Desorption was carried out by batch experimental method. In this study the adsorbents was regenerated by using 0.1 N NaOH, 0.1 N HCl, 0.1 N EDTA and distilled water. 100 mL of each desorbents sample were taken in conical flask containing 0.1 g of already used biosorbent. The flasks were shaken for 1 hour in a mechanical shaker at 50 rpm. The residual concentration of respective metal ions after adsorption was analysed by Neocuprine estimation method using UV spectroscopy at 450 nm.

Statistical analysis: Chi-square test was applied to the data collected from the experiments conducted for determining adsorption isotherm. The parameters used in this test were experimental value obtained for biosorption capacity (q_{exp}) and biosorption capacity calculated from model (q_{calc}). The Chi-square (χ^2) test can be calculated as follows:

$$\chi^2 = \frac{(q_{e\,exp} - q_{e\,cal})^2}{q_{e\,cal}}$$

where $q_{e\,exp}$ (mg/g) is the equilibrium capacity obtained experimentally

$q_{e\,cal}$ (mg/g) is the equilibrium capacity obtained by calculation from the model.

RESULTS AND DISCUSSION

The chicken feathers as a biosorbent for the biosorption of copper ions from industrial effluents was studied in the present work. The pH of biosorbent was found to be 6.0 + 0.5. The bulk density was found to be 0.27 g/ml that is less than 1.2 mg/l which shows that biosorbent is fine in nature. Iodine index was found to be 144.43 while Ash content was estimated to be 33.27 %. The above characterization shows that chicken feathers have good adsorption properties FT-IR spectroscopy was used to study functional groups present in the biosorbent. Fig 1a and fig 1b show before and after treated FT-IR spectra of the biosorbent.

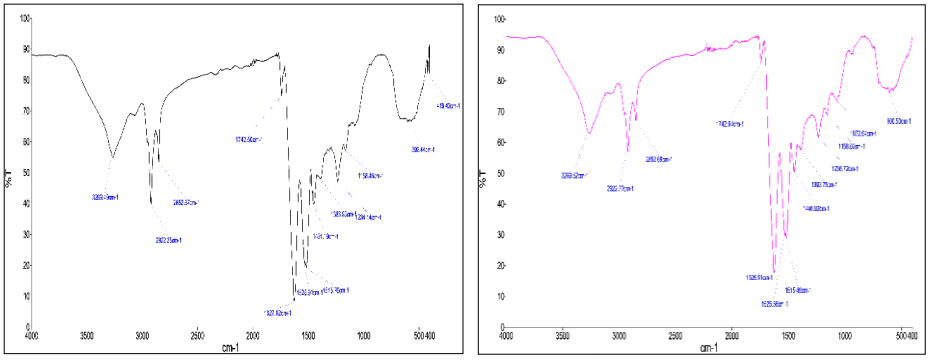

Fig 1. *FT–IR spectra of biosorbent (a) Before (b) After biosorption*

Each specific chemical bond often shows a unique energy absorption band in FTIR analysis and it has been used as a useful tool to identify the presence of certain functional groups of the biosorbent. The surface of the adsorbent contains numerous functional groups so their spectra are complex. The broad and intense peaks around 3269.52 cm−1 in the spectrum correspond to -OH stretching vibration. It indicates the free -OH group on the surface of the adsorbent and confirms the presence of alcohols and polyphenols as in cellulose and lignin. The peak observed at 2922 cm−1 corresponds to C-H stretching, the peaks around 1742 cm−1 is due to C=O group and 1627 cm−1 due to C=C stretching. The broadband around 600 cm−1 cans be assigned to the bending mode of aromatic compounds. Considerable changes in the wavenumbers were not observed in most of the cases after the biosorption process. The vibration shown were to be weak bond since there was no distinct shift in variation. Hence the biosorption can be physical in nature.

The biosorption process and factors affecting the same are presented in figures 2-6.

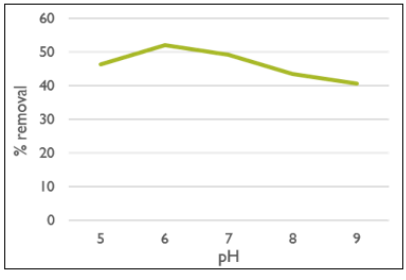

Fig. 2. *Effect of pH*

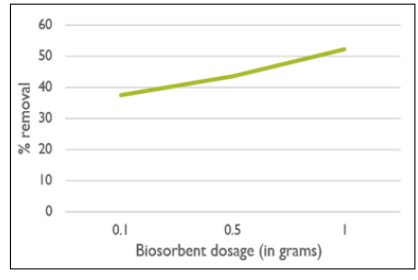

Fig. 3. *Effect of biosorbents dosage*

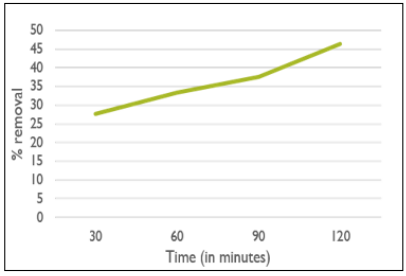

Fig. 4. *Effect of contact Time*

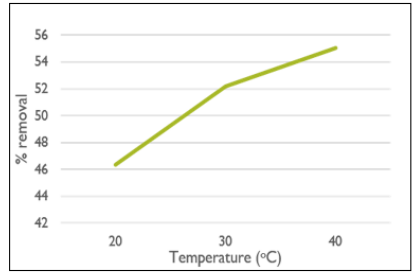

Fig. 5. *Effect of Temperature*

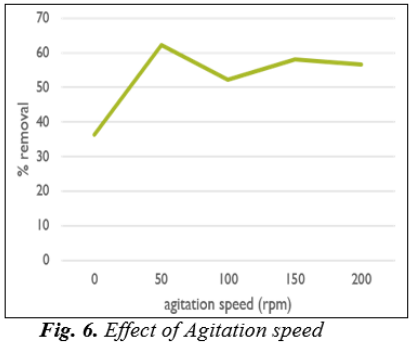

Fig. 6. *Effect of Agitation speed*

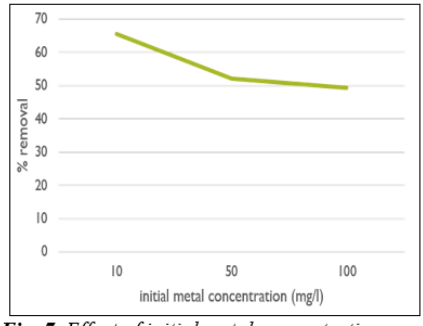

Fig. 7. *Effect of initial metal concentration*

From the above experiment, the optimum conditions for maximum biosorption were found to be pH 6 using 1 g of biosorbent for 120 minutes at 40 oC subjectd to agitation speed of 50 rpm having initial metal concentration of 10 mg/L.

The Electroplating industrial effluents had 59 mg/L of Cu(II) ios and was treated in optimum condition. The percent removal under optimum condition was found to 23%. The synthetic waste water solution under optimum condition was found to have 49.50% removal. Since effluent sample contains different components which can interfere with the biosorption process. Hence as compare to the spiked solution the removal of these heavy metals from the actual industrial was found to be less.

Basically, adsorption isotherm showed the interactions between the adsorbate (copper ions) and biosorbent (chicken feather). Adsorption isotherm considered as an important factor in designing of adsorption process. Fitted isotherm can be used to figure biosorbent capacity in adsorbing the pollutant. While on other side, it also can be used to determine the optimum of biosorbent usage. In this study, most optimum performance of biosorbent was then applied for linear equations of Langmuir and Freundlich to fit the data, results are shown in Figures 8 and 9. Table 1 shows various adsorption parameters.

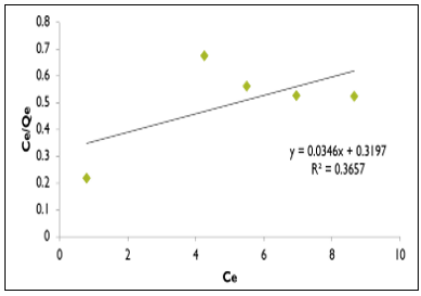

Fi.g 8. Langmuir Isotherm

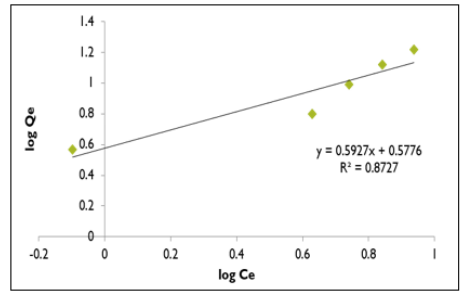

Fig. 9. Freundlich Isotherm

Table 1. *Equilibrium parameters for Freundlich and Langmuir isotherm models*

Metal ion	Freundlich isotherm model				Langmuir isotherm model			
	K_F (L/g)	1/n	N	R^2	q_m	b (L/g)	R_L	R^2
Cu(II)	3.7809	0.5927	1.69	0.8727	28.90	0.0883	0.2817	0.3657

From the above experiment, Freundlich isotherm showed better fit as compared to Langmuir isotherm.

Desorption step is very important in the adsorption process, as it can improve efficiency and economy of removal of metal ions from wastewater. The possibility of regeneration of the biosorbent and recovery of the metal ions can be explored by using desorption study. Desorption was carried out by using batch experimental method. In this study, the adsorbent was regenerated by using 0.1 N HCl, 0.1 EDTA, 0.1 N NaOH and deionized water (D/W). In figure 10, it was observed that the removal of Cu(II) ions was less by using deionized water as compared to other desorbing agents under study. The chelating agent (EDTA) showed maximum desorption of metal ion from biosorbent. Further the desorption process was found to be better by HCl as compared to NaOH. Evidently the adsorbent can be used repeatedly for metal adsorption from aqueous solution.

Fig. 10. *Desorption process*

The chi square value for different concentration of Cu(II) ions were studied for Freundlich isotherm and Langmuir isotherm. It is clear from table 2 that Freundlich model could fit the data statistically also. Hence, statistically it justify that biosorption process using chicken feathers followed Freundlich isotherm, hence is heterogenous in nature

Table 2. *Chi-square test values for different concentration of Cu(II) ions*

Cu(II) ions	**Isotherm model**	
	Freundlich	**Langmuir**
10	0.0349	1.2487
20	0.5952	7.6777
30	0.0349	25.9812
40	0.7673	42.51
50	0.9758	72.6076

CONCLUSION

Heavy metal pollution is a major problem in the present era. The present work explores the capacity of one of commonly discarded waste i.e. chicken feathers and the study is for the efficiency for the removal of copper ions from effluents. It was observed that chicken feathers were efficient in the removal of Cu(II) ions from electroplating industrial effluent. The characterization of the biosorbents indicated of the chicken feathers can be utilized as eco-friendly commercial biosorbent. Hence a present work gives a commercial to the chicken feathers in the field of environmental remediation. This might also help in reducing the pollution load of chicken feathers in a sustainable manner.

REFERENCES

[1] A.M.F. Orozco, E.M. Contreras, N.E. Zaritzky, Modelling Cr(VI) removal by a combined carbon-activated sludge system, J. Hazard. Mater. 150 (2008) 46–52.

[2] S.E. Bailey, T.J. Olin, R.M. Bricka, D.D. Adrian, A review of potentially low-cost sorbents for heavy metals, Water Res. 33 (1999) 2469–2479.

[3] S.D. Faust, O.M. Aly, Adsorption Process for Water Treatment, Butterworths Publishers, Stoneham, 1987.

[4] R.C. Bansal, M. Goyal, Activated Carbon Adsorption, CRC Press, Taylor & Francis Group, LLC, Boca Raton, 2005.

[5] S. Babel, T.A. Kurniawan, Low-cost adsorbents for heavy metals uptake from contaminated water: a review, J. Hazard. Mater. B 97 (2003) 219–243.

[6] J.M. Dias, M.C.M. Alvim-Ferraz, M.F. Almeida, J. Rivera-Utrilla, M. Sanchez-Polo, Waste materials for activated carbon preparation and its use in aqueous-phase treatment: a review, J. Environ. Manage. 85 (2007) 833–846.

[7] B. Volsky, Biosorption and me, Water. Res. 41 (2007) 4017–4029.

[8] S. Chakravarty, A. Mohanty, T.N. Sudha, A.K. Upadhyay, J. Konar, J.K. Sircar, A. Madhukar, K.K. Gupta, Removal of Pb(II) ions from aqueous solution by adsorption using bael leaves (Aegle marmelos), J. Hazard. Mater. 173 (2010) 502–509.

[9] Saha, S., Zubair, M., Khosa, M.A. et al. Keratin and Chitosan Biosorbents for Wastewater Treatment: A Review. J Polym Environ 27, 1389–1403 (2019). https://doi.org/10.1007/s10924-019-01439-6

[10] Shrestha, B., Kaur, J., Ghimire, K. (2016) Adsorptive Removal of Heavy Metals from Aqueous Solution with Environmental Friendly Material—Exhausted Tea Leaves, Advances in Chemical Engineering and Science, 6(4) http://dx.doi.org/10.4236/aces.2016.64046

ASSESSMENT OF CARCINOGENIC RISK OF DRINKING SURFACE WATER CONSUMPTION OF THE TRANSBOUNDARY BASIN OF THE SELENGA RIVER IN THE TERRITORY OF MONGOLIA

Dr. Irina Ulzetueva[1]
Prof. Bair Gomboev[2]
Dr. Daba Zhamyanov[3]
Dr. Valentin Batomunkuev[4]
Dr. Natalia Gomboeva[5]
[1, 2, 3, 4] Baikal Institute of Nature Management SB RAS, Russia
[2, 5] Banzarov Buryat State University, Russia

ABSTRACT

The assessment of the carcinogenic risk of the impact of drinking surface waters on the population health of the transboundary basin of the Selenga river in Mongolia is described in the article. We carried out expeditionary studies of the quality of drinking surface waters on the territory of four aimags, which represent different degrees of economic development and are completely included in the Selenga river basin: Khuvsgul, Arkhangai, Bulgan and Selenge. In this work, we used the methodology used by the US Environmental Protection Agency to quantify the carcinogenic risk of exposure to chemical compounds present in surface waters using the example of these aimags in Mongolia. The application of this methodology for risk assessment gives a great advantage over traditional methods of regulation. It has been established that on the territory of the Selenge aimag, the risk of developing a carcinogenic effect from the impact of priority pollutants on public health associated with the quality of drinking water is high and in the territory of Bulgan, Khuvsgul and Arkhangai aimags are medium, which requires state regulation of the risk and the development of appropriate standards.

Keywords: *transboundary basin of the Selenga river, anthropogenic factors, risk assessment, drinking water*

INTRODUCTION

The study of water quality is the most important subject of study in territories with transboundary water bodies. In connection with the intensively growing anthropogenic load on surface waters as a result of economic development, the main task in the implementation of the state policy of each country in the field of water sources protection is to ensure human health and well-being. [1].

The transboundary basin of the Selenga river is located on the territory of two states - Mongolia and Russia. The Selenga river originates from the confluence of the two rivers Ider and Delger-Muren on the territory of Mongolia, and flows into the lake Baikal on the territory of Russia. The Selenga river basin in Mongolia

includes: the Capital Region (Ulaanbaator) and territories of 11 aimags, of which four are included in the basin only in minor parts (Khentii, Zavkhan, Bayankhongor, Uvurkhangai). The rest entirely cover the territory under consideration: Khuvsgul, Arkhangai, Bulgan, Orkhon, Selenge, Darkhan-Uul, Tuv (Central). We carried out expeditionary studies of the quality of drinking surface waters on the territory of four aimags, which represent different degrees of economic development and are completely included in the Selenga river basin: Khuvsgul, Arkhangai, Bulgan and Selenge.

Analysis of literature data shows that the most promising approach to ranking influencing environmental factors of various nature is the concept of health risk assessment [2]. Health risk assessment refers to the process of establishing the likelihood of development and the severity of adverse effects on human health or the health of future generations due to the impact of environmental factors (WHO, 2000). It also includes damage to the population within statistical limits justified by environmental, technical or other considerations. The US Environmental Protection Agency (EPA US) characterizes risk as "the likelihood of injury, illness, or death under certain circumstances" [3]. The results obtained from the concept of risk are usually presented either as upper limits of additional risk (the expected incidence of disease from exposure to pollutants at a given concentration), or as upper levels of concentration of pollutants at a given level of risk. In this case, it is not a safety threshold that is set, but an acceptable threshold, i.e. limit, beyond which one cannot go.

METHODS AND METHODOLOGY

In this work, we used the methodology used by the US Environmental Protection Agency [1-3] to quantify the carcinogenic risk of exposure to chemical compounds present in surface waters using the example of these aimags in Mongolia. The application of this methodology for risk assessment gives a great advantage over traditional methods of regulation, which are based on comparing the levels of actual pollution and the standard values of these pollutans in the development of health-improving measures. The methodology also allows one to obtain quantitative characteristics of the real and potential damage to public health from the effects of pollution of surface water sources within the framework of a single decision-making process, based on which measures to reduce the risk are determined along with restrictions on resources and time. With the help of this technique, a forecast of the situation is carried out, namely, the calculations of the risk for the current situation and for the future are carried out. This is of great practical importance in the organization of sanitary protection zones of industrial enterprises, reclamation of contaminated areas, assessment of action plans, protection of water sources from pollution, especially in the context of intensively developing mining.

The calculation of the lifetime carcinogenic risk (Risk) was calculated by multiplying the average daily dose (ADD) (or average daily intake) for the entire period of life by the value of the relative carcinogenic strength of inorganic compounds SF_0 (the factor of carcinogenic potential for a carcinogen):

$$Risk = ADD \times SF_0 (1),$$

where the Risk value characterizes the upper limit of the carcinogenic risk for the average life expectancy of the population [4]. To calculate the exposure doses, the recommended standard values of human physiological constants for the oral route of exposure were used, developed by IARC (International Agency for Research on Cancer) and WHO (human weight (BW) - 70 kg, average volume of daily consumed water (DW) - 2 l/day). Thus, the Risk value is an estimate of the risk of developing a neoplasm over the average life span of a person.

In many countries of the world, the classification of individual life-long risk, recommended by WHO (World Health Organization) in 1996, 1999, 2000, is adopted, as well as approved by a number of methodological documents of a number of foreign countries [5]: high risk>10^{-3}, average risk 10^{-3} -10^{-4}, low (acceptable) risk 10^{-4} -10^{-6}, minimum (desirable) target risk <10^{-6}.

DISCUSSION

According to analytical data provided by the Mongolian hydrometeorological service, as well as data obtained during expeditionary operations in Mongolia [6], priority pollutants were identified on the content of inorganic substances in drinking surface waters of four aimags. To assess the exposure, five chemicals with proven carcinogenic properties were selected, which were found in drinking water samples (chromium, arsenic, cadmium, nickel and lead). For these substances, the carcinogenic risk to public health was calculated during their consumption. Due to the fact that multicomponent chemical pollution of drinking surface waters is present in the study area, it becomes necessary to study the total risks caused by the simultaneous complex effect of several chemicals and compounds at once during their oral intake. Consequently, within the framework of the risk assessment methodology, the combined effect of carcinogens is usually considered additive.

Data on the relative carcinogenic strength of inorganic compounds (SF_0) and their content in drinking and surface waters in a number of aimags of Mongolia that pollute water are given in the table 1.

Table 1. *Carcinogenic potential contaminants SF_0, and their content is, for drinking and surface waters Mongolia*

Compound	SF_0 (mg/(kg×day))$^{-1}$	C, mg/l×10^{-3}									
		Aimag									
		Bulgan		Selenge			Khuvsgul				Arkhangai
		C_{min}	C_{max}	$C_{med.}$	C_{min}	C_{max}	$C_{med.}$	C_{min}	C_{max}	$C_{med.}$	C_{max}
Chromium	0.42	3.6	3.7	3.65	3.6	29	10.12	3.6	3.6	3.6	3.6
Arsenic	1.5	2.1	4.3	3.03	2.1	31	10.2	2.1	3.9	2.57	3.8
Cadmium	0.38	6.2	11,2	7.86	2.7	13	7.15	0.38	11,0	6.07	11,1
Nickel	1.7	0.18	0.24	0.2	0.21	2.2	0.69	0.04	0.2	0.11	0.09
Lead	0.047	0.66	2.13	1.1	0.72	3.1	2.2	0.05	0.56	0.7	0.09

According to the table 1, the content of arsenic of the Selenga aimag and cadmium in the waters of all the considered aimags in drinking surface waters indicate an excess of their normative content in drinking water, adopted by the water quality standard in Mongolia [7].

The results of calculating the carcinogenic risk from the consumption of water containing inorganic toxicants are shown in table 2. The total risk was calculated using the usual additive scheme (tab. 2).

Table 2. *Values of carcinogenic risk (Risk) for water consumption which are containing pollutants in the aimags of Mongolia, 10^{-4}*

Compound	Risk*									
	Aimag									
	Bulgan			Selenge			Khuvsgul			Arkhangai
	$Risk_{min}$	$Risk_{max}$	$Risk_{med.}$	$Risk_{min}$	$Risk_{max}$	$Risk_{med.}$	$Risk_{min}$	$Risk_{max}$	$Risk_{med.}$	$Risk_{max}$
Chromium	0.432	0.444	0.438	0.432	3.480	1.214	0.432	0.432	0.432	0.432
Arsenic	0.900	1.843	1.299	0.900	13.286	4.371	0.900	1.671	1.101	1.629
Cadmium	0.673	1.216	0.853	0.293	1.411	0.776	0.041	1.194	0.659	1.205
Nickel	0.087	0.117	0.097	0.102	1.069	0.335	0.019	0.097	0.053	0.044
Lead	0.009	0.029	0.015	0.010	0.042	0.030	0.001	0.008	0.009	0.001
Total risk	2.101	3.626	2.702	1.737	19.287	6.727	1.393	3.402	2.255	3.300

*Note. $Risk_{min}$ - additional carcinogenic risk at the specified minimum concentration of the compound in drinking water;

$Risk_{max}$ is an additional carcinogenic risk at the specified maximum concentration of the compound in drinking water;

$Risk_{med}$ is an additional carcinogenic risk with an average content of the compound in drinking water.

Data analysis of the table 2 shows that for the considered inorganic compounds, the highest risk levels correspond to chromium ($Risk_{max}=3.48\times10^{-4}$) for the Selenge aimag, which is equivalent to 348 cases of neoplasms per 1,000,000 people; for arsenic ($Risk_{max} = 13.3\times10^{-4}$, 1.84×10^{-4}, 1.67×10^{-4}, 1.63×10^{-4}) for the Selenge, Bulgan, Khuvsgul, Arkhangai aimags, respectively; for cadmium ($Risk_{max}=1.41\times10^{-4}$, 1.22×10^{-4}, 1.2×10^{-4}, 1.19×10^{-4}) of the Selenge, Bulgan, Arkhangai, Khuvsgul, aimags, respectively, and for nickel ($Risk_{max}=1.07\times10^{-4}$) for the Selenge aimag.

With the combined action of all substances, the minimum total carcinogenic risk ($Risk_{min}=1.393\times10^{-4}$) is typical for the Khuvsgul aimag, the maximum total carcinogenic risk ($Risk_{max}$=19.297×10-4) is for the Selenge aimag. According to the WHO classification, this corresponds to an average and high level of risk.

Thus, the greatest likelihood of a carcinogenic risk of a (up to 1929 cases per 1,000,000 people) with oral water consumption arises for the Selenge aimag population.

It should be noted that arsenic has a proven carcinogenic effect and, subsequently, constant consumption of drinking water with an established arsenic content can cause chronic diseases, as well as the development of oncological diseases. Drinking water contaminated with arsenic is the cause of lung diseases, including respiratory failure, lung cancer, bronchiectasis. The action of arsenic through drinking water on the body of children at an early age or in the womb can lead to pulmonary pathology and this leads to a significant increase in mortality among young people from cancer and bronchiectasis [8].

CONCLUSION

As a result of the studies carried out, it was established that in the territory of the transboundary basin of the Selenga river in surface waters, the content of arsenic and cadmium in the territory of the Selenge aimag exceeds their hygienic standards. The calculation of the total carcinogenic risks showed that the studied surface drinking water, subject to their constant long-term use in Bulgan, Khuvsgul and Arkhangai aimags, form the medium permissible levels of carcinogenic risk for the population health, and in the Selenge aimag they are high. At the same time, the sectoral structure of the economy in the Selenge aimag is also associated with the extraction of minerals, which contributes to the flow into the surface waters of the river basin. Selenga of the specified substances with industrial wastewater. High concentrations of cadmium and arsenic in drinking waters of the transboundary basin of the Selenga river cause high risks of developing diseases, which in turn determines these waters as unsuitable for economic and drinking use by the population, accordingly, certain measures are required to reduce health risks. The data obtained indicate the need to develop a methodology for state risk regulation and the development of appropriate standards, while it is necessary to take into account the methodology for assessing the risk of the impact of drinking water quality on public health in the system of environmental and hygienic monitoring.

ACKNOWLEDGEMENTS

The work was carried out within the framework of the state assignment of the Baikal Institute of Nature Management SB RAS.

REFERENCES

[1] Crouch, EAC, Wilson, R., and Zeise, L., 1983, "The Risks of Drinking Water," Water Resources Res. 19: 1359-1375;

[2] Nowell LH (1), Resek EA. National standards and guidelines for pesticides in water, sediment, and aquatic organisms: application to water-quality assessments. Reviews of environmental contamination and toxicology. Springer-Verlag.NY: Inc. 1994. Vol. 140, p. 1-164;

[3] Moghissi AA, Narland RE, Congel FJ Eckerman KF Methodology for environmental human exposure and health risk assessmen. // Dyn. Exposure and Hazard Assessment Toxic chem. Ann Arbor., Michigan, USA, 1980, p. 471 – 489;

[4] The Integrated Risk Information System (IRIS), prepared and maintained by the US Environmental Protection Agency (US EPA). Health and Environmental Assessment, ECAD, Cincinnati, OH, 1987-1996;

[5] Duffus JH, Park MV Chemical Risk Assessment. Training Module # 3, UNEP / IPCS, 1999;

[6] Integral Assessment of Anthropogenic Pressure on Water Bodies in the Lake Baikal Basin / Ulzetueva, I.D., Gomboev, B.O., Zhamyanov, D.Ts.-D., Batomunkuev, V.S., Banzaraktsaev Z.E. // GEOLINKS 2020 International Scientific Conference, 5-7 October, Plovdiv, Bulgaria, ISSN 2603-5472, ISBN 978-619-7495-07-2, WATER RESOURCES Section / Book No. 1-pp. 273-280. DOI: 10.32008 / GEOLINKS2020 / B1 / V2 / 27;

[7] 1051-1058 MNS (Mongolian National Standard) 4568 (1998) Water Quality Standard, Mongolia;

[8] Nasolodin V.V. Interaction of microelements in the process of their metabolism in the body / V.V. Nasolodin, V.L. 1999. No. 4. P. 10–13.31.

CAPILLARY RISE CHARACTERISTICS AND SALTWATER PROPAGATION IN FINE AGGREGATE: TOWARD DEVELOPING THE ANTI-SALINITY SHALLOW FOUNDATION

Assoc. Prof. Dr. Nguyen Ngoc Truc [1]
Msc. Nguyen Van Hoang [2]
Msc. Tran Ngoc Tu [3]
[1] VNU-School of Interdisciplinary Study, Vietnam National University, Hanoi, Vietnam
[2] Vietnam institute of Geosciences and Mineral resources, Hanoi, Vietnam
[3] Graduate Institute of Applied Geology, National Central University, Taiwan

ABSTRACT

This study is carried out to determine the capillary rise over time of fine aggregate in different saline media. The obtained results showed that the capillary height in fine aggregate is inversely proportional to the salt concentration of the capillary solution. The aggregate that has a particle size over 2.0 mm shows the best ability to limit capillary rise. The capillary height of the aggregate gets the highest value when there is no salt in the solution and gets the lowest one with the solution at the highest salinity tested, i.e. 33.0 g/L. The obtained results on capillary characteristics lead to an idea of design a shallow foundation that has a function of anti-corrosion, anti-salinity proactively and effectively.

Keywords: *Capillary rise, Anti-salinity, Anti-capillary, Saline intrusion*

INTRODUCTION

Saline intrusion is taking place strongly in the coastal areas of the coastal countries including Vietnam. Saline intrusion is a type of natural hazard where soil salinity is determined by the concentration of salt in the aqueous extract of saturated soil.

For a long time, scientists studied the effects of saline intrusion on the economy, society, environment, and infrastructure, etc. Several significant studies were carried out by Terletskaya and Metonidze [1]; Oradovskaya and Pagurova [2] on many different soil types. Recently, Mihova and Truc [3,4]; Truc and Mihova [5,6]; Truc et al. [7] evaluated the variability of soil properties under salinity conditions, deformation characteristics, primary and secondary consolidation, and analyzed the load-bearing capacity of salt-affected soils. In these studies, the authors found that salt in groundwater causes much harm to the infrastructure system, especially civil construction. Salt in groundwater is brought up by the capillary rise, penetrating into the body of the building, leading to the destruction of structures, reducing the functions and lifespan of the building.

As the result of Karagiannis et al. [8], water penetrates a building material through the capillary rise of ground moisture, rain, and condensation of air humidity causing several physicals, chemical and, biological problems to buildings. Besides, Hird and Bolton [9], made an experiment to describes the rising of the capillary height of water through columns of initially dry sand. Previously, Karoglou et al. [10] also recognized that the presence of water in the capillary of the material is also one of the factors causing the deterioration of the building. Besides, the need for urban and infrastructure development in coastal cities on salt-affected soils remains a major question for planners. Civil constructions on salt-affected soil have to face salt capillaries.

Faced with the above situation, this study will contribute to finding solutions to meet the needs of infrastructure development on salt-affected soils. It is an urgent, scientific and practical issue.

MATERIALS AND METHODS

Sample preparation

To comprehend the capillary characteristics and saltwater propagation in the fine aggregate, the authors have prepared 25 kg naturally fine aggregate. In the laboratory, the materials are dried, sieved, and divided into 4 groups of particle size equivalent to gravel (5.0-2.0 mm), coarse sand (2.0 - 1.0 mm), medium sand (1.0 - 0.5 mm), and fine sand (0.5 - 0.1 mm). The number of samples prepared was 28, which were divided into 7 batches, each batch corresponding to one salt concentration.

The capillary solution is saltwater with seven salt concentrations, i.e. 0.0 g/L, 4.95 g/L, 9.9 g/L, 14.75 g/L, 19.8 g/L, 24.75 g/L, and 33.0 g/L. These are the salt concentrations corresponding to the salinity of 0, 15, 30, 45, 60, 75, and 100% of natural seawater if the average salinity of seawater is 33.0 g/L. The use of different salt concentrations in the media of different particle grades is to determine the capillary height of each particle group in order to find the optimal particle grade for the anti-salinity shallow foundation solutions of coastal civil construction works.

Determining the capillary rise of fine aggregate

The salt capillary phenomenon occurs when saltwater is in contact with the materials for enough time. Saltwater absorbs through a capillary mechanism in a space between particles with a diameter of around 20 to 40 micrometers. Saltwater intrudes through the gaps in the contact surface, and then propagates through the capillaries, which can cause permeation and salinity. The nature of the capillary phenomenon is due to the wet sticky force itself. When the wet adhesive force is greater than the surface tension, the solution is pulled up a certain distance above the liquid surface. The capillary height depends on the particle size, the uniformity of the material in the capillary medium (capillary tube cross-section), and the chemical composition of the capillary solution [11].

The rise of a liquid column inside the capillary tube is due to the surface tension. The capillary rise of a solution in the material (hk) is determined by the formula (1):

$$hk = \frac{2\delta.cos\theta}{r\gamma g} \quad (1)$$

where: δ is surface tension; θ is the wetting angle; g is the gravitational acceleration; r is the capillary tube radius; γ is the density of water.

The reference values of ultimate capillary height over time of natural loose materials corresponding to particle sizes are given in Table 1:

Table 1. *Time to reach the stable capillary rise depends on the particle size*

Material particle size (mm)	Capillary height (hk, cm)	Time (day)
5 - 2	3.5	3
2 - 1	6.5	4
1.0 - 0.5	13	6
0.5– 0.1	25	8

Determining the hydraulic conductivity by constant head method

The constant head method is mainly used in determining the permeability of fine aggregates such as sand and gravel. The permeability coefficient is calculated based on Darcy's law using the following formula:

$$K = \frac{\vartheta \cdot H}{t \cdot A \cdot \Delta h} \quad (2)$$

Where: ϑ - volume of water collected (ml); H –height of the material column between the two piezometric tubes (cm); t – time needed to collect the water (s); A - cross-section area of the permeameter (cm2), and Δh – differential pressure, Δh = h1-h2.

Firstly, the mass of soil in the permeameter was determined, and a filter disc was placed at the bottom of the permeameter. The volume of the sample was calculated, based on the height of the sample. The flow was computed using the volumetric method and the pressure difference was read using the piezometric tubes.

RESULTS

The studied fine aggregate is well-graded distribution (Fig. 1). It was divided into four particle groups of the gravel, coarse sand, medium sand, and fine sand by sieving. They were used for determination of the capillary height and hydraulic conductivity.

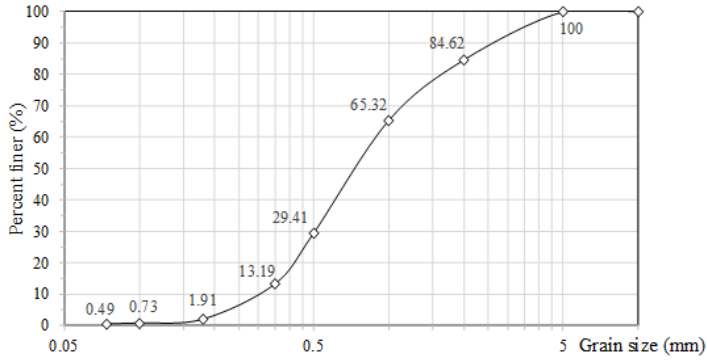

Fig. 1. *Particle size distribution curve of the studied materials*

The experiment to determine the permeability coefficient was carried out to each particle size group above. The obtained results showed that natural sand has the average permeability coefficient of 8.76x10-5 cm/s; that of gravel has the largest permeability coefficient, around 5.86x10-4 cm/s; meanwhile, that of fine sand has the smallest permeability coefficient, around 1.39x10-5 cm/s.

Parallel to determine the permeability coefficient of the materials, the authors conducted the experiments to evaluate the effect of salt on capillary heights at different particle groups and different salt concentrations. The capillary test has been conducted continuously for at least 3 days. The experiment result of the capillary height of each particle size and each salt concentration is the ultimate value measured. The obtained results are given in Table 2.

Table 3. *Capillary height of saltwater solutions in the natural fine aggregate*

Particle group	Salinity of capillary solution (g/L)						
	0.0	4.95	9.9	14.85	19.8	24.75	33.0
Fine sand	39.0	37.0	32.0	31.0	34.5	33.5	31.4
Medium sand	32.0	30.0	28.0	27.0	22.0	24.0	22.4
Coarse sand	10.8	9.0	8.5	8.0	6.8	7.2	7.4
Gravel	5.1	4.8	4.60	4.0	4.2	3.8	4.3

From the obtained results, one can see that the capillary height of each specimen

From the obtained results, one can see that the capillary height of each specimen reaches the highest value when the capillary solution is not salty, equivalent to a salt concentration of 0.0 g/L, and gets the lowest value when the solution reaches a salinity equivalent to natural seawater, i.e. 33.0 g/L.

Figure 2 shows the experimental results to determine the ultimate capillary height of fine aggregate corresponding to the salt concentrations of capillary solutions. It can realize that, generally, the capillary rise of fine aggregate decreases as salt concentration increases. However, this relationship varies among particle groups.

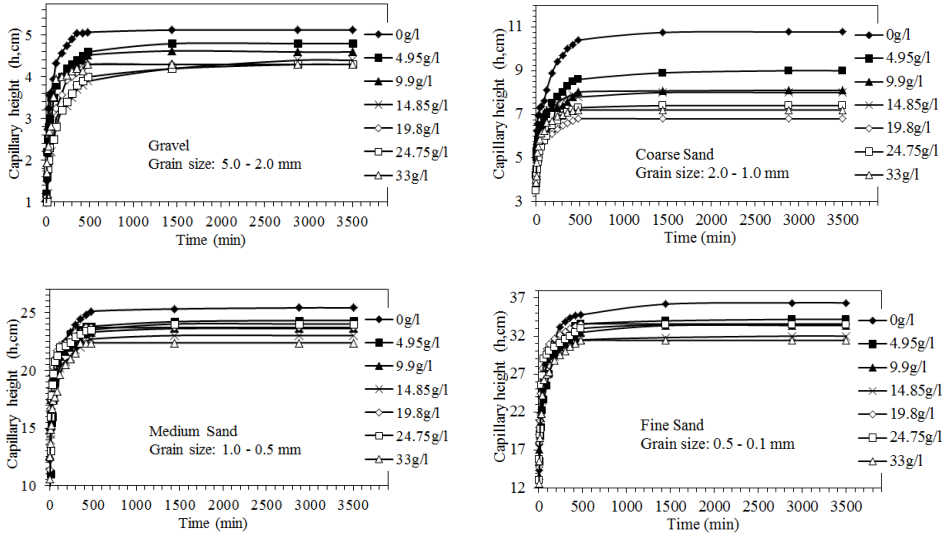

Fig. 2. *Capillary height (h) over time (t) of four particle groups of natural fine aggregate*

For four - particle size groups of fine aggregate and 7 salt concentrations of the capillary solution, one can build an equation to demonstrate their relationship. The relation curves of capillary height versus time express into two segments, the curve in the early experiment and the straight in the stable one (Fig. 2).

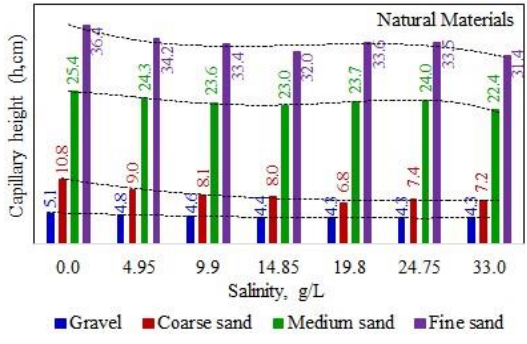

Fig. 3. *Ultimate capillary height of fine aggregate in different capillary solutions*

Figure 3 shows the ultimate capillary height of four - particle groups of fine aggregate versus different capillary solutions. For the gravel group, capillary height is stable and unchanged at h = 4.3 cm since the salinity of solution reaches 19.8 g/L to 33.0 g/L. For coarse sand, capillary height decreased from h = 10.8 cm at salinity = 0.0 g/L to h = 6.8 cm at salinity = 19.8 g/L, then the height capillary increased strongly at the salinity = 24.75 g/L. It decreases to 7.2 cm at the maximum salinity of 33.0 g/L. For the medium sand and fine sand, the relationship of capillary height versus salinity evolves over time in three phases:

The first phase, the capillary height and salt concentration of the capillary solution are inversely related. Capillary height tends to decrease gradually as the salt concentration increases, most evident when the capillary solution has a salinity of 0.0, 4.95, 9.9, and 14.85 g/L. At this stage, the capillary height value gets maximum when the specimen has not been salty, i.e. salinity = 0.0 g/L, and gets the lowest when the salinity reaches 14.85 g/L.

In the second phase, the relation of the capillary height and salt concentration of the capillary solution is proportional. When salt concentration increased from 19.8 to 24.75 g/L, the capillary height of fine sand and medium sand increased considerably.

In the third phase, the capillary height and salt concentration of the capillary solution are inversely related. This phase lasts from the salt concentration of 24.75 g/L until 33.0 g/L. The capillary height decreases and reaches the minimum value when the salt concentration of the capillary solution reaches the maximum value, i.e. 33.0 g/L. Thus, in general, the presence of salt in the solution leads to reduce capillary height in the fine aggregate, although the change is not homogeneous.

DISCUSSION

The capillary rise depends on the uniformity of the capillary medium, the shape and size of the material particles in the medium, and the concentration of the capillary solution. Therefore, a fairly clear difference can be seen between the material samples, the particle grades, and the salt concentration of the solution.

Capillary height and particle size of fine aggregate are inversely proportional. Similarly, capillary height is inversely proportional to the salt concentration in the capillary solution. The more salt concentration in the test solution, the less the capillary height. Indeed, in the studied saltwater media, the capillary height depends on three dominant factors including particle size, uniformity, and chemical composition.

In saltwater media, the capillary height of fine aggregate is higher when salt concentration equals zero, because the higher the salt concentration of the solution, the higher the density γ of the water. The increased salt concentration leads to a decrease in the surface tension δ, this leads to an increase in the wetting angle θ of the solution, then the cosine value in equation (1) decreases. At the same time, the chemical composition of the capillary solution also significantly affects the capillary height. In this case, it is sodium, an important factor makes it decrease capillary.

For the figuration of the curves of capillary height versus time, at the first phase of the experiment, the relational curve takes the form of the logarithmic function $y = a.\ln(x)+b$. This is the period when the capillary height increases rapidly in a short period of time. Initially, the material absorbs water strongly to reach saturation state, followed by capillary force bringing the water up rapidly following the capillary system between material particles. At the second phase of the experiments, the capillary height - time relationship becomes linear. The relation can be represented as the form of equations $y = ax + b$. This is the period in which the

capillary height approaches stabilization, the water column rising in the capillary system slows down and then stops.

SUGGESTION FOR DESIGNING AN ANTI-SALINITY SHALLOW FOUNDATION ON SALT-AFFECTED SOIL

Currently, technical solutions to design an anti-salinity shallow foundation are not really effective and still local, even still not considered. Therefore, the authors suggested a model of the shallow foundation that has the function of anti-corrosion, anti-salinity proactively and effectively. Based on the obtained results of capillary height value of each particle group, the foundation is suggested to design with the bottom-up structure of bearing layer in order of the fine material at the bottom, the material with the coarse particle size above and finally, the layer has a particle size equivalent to gravel. The fine aggregate should be applied below and inside the foundation. The wall of the foundation should be enveloped by geomembrane material to avoid groundwater absolutely. To maximize the anti-capillary capacity of fine aggregate, all the layers of materials should be placed above the highest groundwater level (Fig. 4).

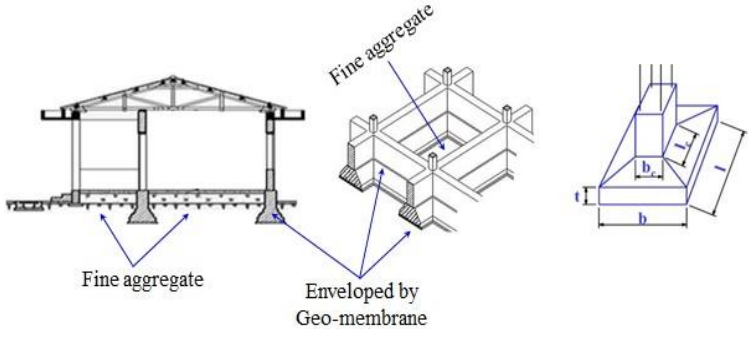

Fig. 4. *The idea of structure of the anti-salinity foundation*

The general characteristics of capillary rise in loose materials are a gradual decrease from fine grain soils to coarse grain ones. Silty soil has the highest capillary rise and it reduces in order of sand, gravel, and pebble. The local materials can be used as the bottom layer because this layer is act as a lining. Meanwhile, the upper layers are more important. They must be loose materials that particle size as bigger as possible. For geomembrane enveloping the foundation wall, it must be thick enough to avoid breaching during the construction process. This is geosynthetic material popular in the market. The design and coupling between geomembrane and fine aggregate to increase the capillary resistance to the absolute limit is a difficult technique. It will be mentioned in the next studies.

The Proposal of an anti-salinity foundation is a big problem. This paper just suggests an idea based on the studied results on the capillary rise in loose materials. This idea supplies a technique that is easy to apply, saves costs, and does not affect the environment.

CONCLUSION

The study was carried out to determine the capillary height over time of natural loose materials in different saline media. A series of experiments were conducted including sieving analysis, hydraulic conductivity, and capillary rise. The fine aggregate was divided into four groups of particle size equivalent to gravel (5.0 - 2.0 mm), coarse sand (2.0 - 1.0 mm), medium sand (1.0 - 0.5 mm), and fine sand (0.5 - 0.1 mm). Saline solutions with seven salt concentrations, i.e. 0.0 g/L, 4.95 g/L, 9.9 g/L, 14.75 g/L, 19.8 g/L, 24.75 g/L, and 33.0 g/L, equivalent to natural saline intrusion process in coastal areas were prepared.

The obtained results showed that the capillary height in fine aggregate was inversely proportional to the salt concentration of the solution. The authors have also identified the particle size group capable of interrupt the capillary flow and propagation of salt in the structure. Accordingly, the aggregate that has a particle size over 2.0 mm showing the best ability. For the capillary solution, it is recognized that the capillary height gets the highest value when there no salt in the solution and get the lowest one with a solution at the highest salinity experimental, i.e. 33.0 g/L.

From the experimental results, an idea of design a shallow foundation that has the function of anti-corrosion, anti-salinity proactively and effectively was given. The suggested foundation has a general structure be three layers, i.e. the fine material at the bottom, the material with the coarse particle size above and finally, the layer has a particle size equivalent to gravel. The foundation wall is enveloped by geomembrane. The fine aggregate and geomembrane are connected together by a special technique.

REFERENCES

[1] Terletskaya, M. N., Metonidze, N. V.: Increase of the stability of structures in gypsinate loesslike soils. Minvodkhoz SSSR, TsBNTI, Ser. 5, No. 11, (1986).

[2] Oradovskaya A. E., Pagurova, V. I.: Convective diffusion of salts in a radial flow of groundwater. Journal of Applied Mechanics and Technical Physics 7, 87–88 (1966). https://doi.org/10.1007/BF00916988

[3] Mihova, L., Truc, N. N.: Constitutive models for settlement analysis of soft salt-affected ground. 14th International Scientific Conference VSU 2014, (2014).

[4] Mihova, L., Truc, N. N.: Study of deformation of salt-affected soils by FEM, a case study of soft soil in the Red River delta, Vietnam. ECSMGE 2015, 17 (12), pp. 4013-4018. ICE Publishing, (2015). DOI:10.1680/ecsmge.60678.vol7.634

[5] Truc, N. N., Mihova, L.: Soft soil in salt – affected media, Vietnam National University Press 9/2015, (2015).

[6] Truc, N. N., Mihova, L.: Hanoi Cohesive Soil in Salt-Affected Conditions: Soil Properties and 2D Consolidation Analysis. International Journal of Civil Engineering 18, 137–150 (2020). https://doi.org/10.1007/s40999-019-00422-5

[7] Truc, N. N., Hoang, N. V., Ha, D.N., Ly, N.T.: Capillary characteristics and applicability of coal bottom ash as an anti-capillary material for coastal

constructions. VNU Journal of Science: Earth and Environmental Sciences Vol. 36, No. 4, 17-27 (2020). https://doi.org/10.25073/2588-1094/vnuees.4517

[8] Karagiannis, N., Karoglou, M., Bakolas, A., Krokida, M., Moropoulou, A.: Drying kinetics of building materials capillary moisture. Construction and Building Materials, (2017). https://doi.org/10.1016/j.conbuildmat.2017.01.094

[9] Hird, R., Bolton, M. D.: Clarification of capillary rise in dry sand. Engineering Geology 230 (2017) 77-83. https://doi.org/10.1016/j.enggeo.2017.09.023

[10] Karoglou, M., Moropoulou, A., Giakoumaki, A., Krokida, M.K.: Capillary rise kinetics of some building materials. Journal of Colloid and Interface Science 284 (2005) 260–264. https://doi.org/10.1016/j.jcis.2004.09.065

[11] ASTM C1585-20: Standard Test Method for Measurement of Rate of Absorption of Water by Hydraulic-Cement Concretes. American Society for Testing and Materials, (2020).

CHANGES IN THE VANADIUM MIGRATION FORMS ON GEOCHEMICAL BARRIERS IN THE RIVER-SEA MIXING ZONES

PhD Victoria Khoroshevskaya
Hydrochemical Institute, Russia

ABSTRACT

The article is devoted to the study of vanadium, a metal capable of stimulating the growth of phytoplankton *in situ* and has the greatest biological activity in dissolved form. The pattern of an increase in the concentration of vanadium dissolved forms in the mixing zones during the transition from river waters to seawaters is known. In this article, we examine the behavior, ratio and change in the concentrations of vanadium dissolved and suspended forms during the passage of geochemical barriers. The estuarine zone of the Razdolnaya River–Amur Bay (Sea of Japan) is considered as "river-sea" mixing zone. Modelling of physicochemical processes was carried out using the Selector-S and MINTEQA2/PRODEFA2 software systems. Ion-associative models of sea and river water were built and the modelling of the process of their mixing was carried out using the Selector-S software package. The sorption process was simulated using the MINTEQA2/PRODEFA2 software package. The results of modelling physicochemical processes occurring at geochemical barriers help to understand the reasons for changes in concentrations, both total vanadium and biologically active dissolved vanadium forms, during the passage of geochemical barriers in the "river-sea" mixing zones. The results showed that there is a change in the dissolved forms of vanadium migration, their transformation and an increase in the concentration of dissolved forms of vanadium at the geochemical barrier.

Keywords: *vanadium migration forms, vanadium dissolved forms, geochemical barrier, the Razdolnaya River*

INTRODUCTION

Estuaries and bays are mixing zones of river and sea waters, where the most of allochthonous suspended and dissolved organic matter of soil genesis is deposited. Here, at the geochemical barriers, there is a change in the migration forms of most elements. When river and sea waters mix, the processes of sorption and desorption of microelements, their transition from a dissolved to a suspended state and from a suspended to a dissolved state occur [1], [2].

Establishing the physicochemical forms of metal migration in various types of natural waters is one of the most important tasks in biogeochemistry, since the physicochemical form of their presence largely determines the degree of biometals assimilation by aquatic organisms. Concerning this, the transformation of the metal migration forms during mixing of river and sea waters, where geochemical barriers

are formed, in which not only a change in the migration forms occurs but also the removal of metals from solutions, is of considerable interest.

Most of the metals, including vanadium, enter these zones with river runoff from the catchment. Vanadium is a metal capable of stimulating phytoplankton growth *in situ* [3], and it has the greatest biological activity in a dissolved form; therefore, we aimed to study the behavior of vanadium forms on geochemical barriers in estuarine zones.

MATERIAL AND METHODS

Modelling of physicochemical processes of the behavior of vanadium forms during mixing of sea and river waters for the estuarine zone of the Razdolnaya River–Amur Bay (Sea of Japan) was carried out using the Selector-S and MINTEQA2/PRODEFA2 software packages [4]. The first software system was used to build ion-associative models of sea and river water and to model the process of their mixing; the second was used to simulate the sorption process based on the approach described in [5] and to determine the total vanadium concentration.

THEORY/CALCULATION

Vanadium form content calculation. Thus, vanadium is present in natural waters in various forms, the total vanadium concentration (V_{tot}) was calculated as the sum of the dissolved (V_{sol}) and suspended (V_{sorb}) forms. On average, about 98% of vanadium is in suspended form and only 2% migrate in dissolved form [6, 7]. Table 1 shows the vanadium various form concentrations, as well as its main chemical forms of presence in natural waters [2], [8].

Table 1. *Mean concentrations of vanadium in river and ocean waters and its main chemical forms*

Chemical element	Main chemical forms	River waters			Ocean waters	
		$\frac{V_{sorb}}{V_{sorb}+V_{sol}}$ (%)	V_{sorb}, (%)	V_{sol}, (μg/L)	V_{sorb}, (%)	V_{sol}, (μg/L)
Vanadium	$VO_2(OH)_3^{2-}$, HVO_4^{2-}, $H_2VO_4^-$, NaH_2VO^-	98	$1.3\cdot10^{-2}$	1.0	$00.3\cdot10^{-2}$	1.5

The same amount of vanadium dissolved forms is contained, on average, in the river runoff is mentioned in the literary sources [1], [9]. In the reservoir of the final runoff (ocean), the fluctuations in vanadium concentrations are small, 1-2 μg/L, and the mean concentration is close to 1.5 μg/L. Suspended matter in the oceans contains about 0.008 μg/L of vanadium or $3\cdot10^{-3}$% of vanadium of dry suspension. The surface suspension of the Indian Ocean can contain twice as much of this element – 0.016 μg/L or 6 10^{-3}% of dry suspension, and in some cases the vanadium concentration increases to 0.28 μg/L or 15 10^{-3}% of dry suspension [10].

Comparison of the mean concentrations of vanadium in the suspension of the world's rivers and in the lithosphere shows a significant amount of this element in the river suspension [6]. A distinctive geochemical feature of vanadium is the biophilic nature of behavior. River suspension is enriched with this element due to its participation in biological processes, as well as due to its ability to form strong organoelement complexes [8].

Assessment of the sorption effect on vanadium form content. River suspension is conventionally divided into three forms: 1) silicate – mineral particles; 2) biogenic – organic particles of the suspension, amorphous silica, calcium carbonate, nitrogen and phosphorus; 3) hydrogenic (readily soluble). The content of the latter is calculated as the difference between the total content of the suspension and the first two forms. These include the amount of metal adsorbed on mineral and organic particles of suspension, as well as for some elements (for example, iron) in the form of particles or films of hydroxide and precipitated with them.

Iron and manganese hydroxides covering the suspended matter particles can make up 40-50% of the total iron and manganese in the river suspended matter. In the experiment to study the ability of amorphous oxides of iron and manganese to sorption of various metals, a number of elements were investigated (according to the increasing role of sorption). The results showed that vanadium has the lowest sorption capacity [1].

The modelling of the process of the influence of sorption on the metal removal from the solution of the mixing zone was carried out under the following assumptions: the salinity is 5.33 ‰; up to 95% of suspended solids are lost at the geochemical barrier; the concentration of suspended matter in the estuary is 200 mg/L; the concentration of suspended matter in the river is 50 mg/L.

The degree of influence ($\Delta V_{tot}\%$) of sorption processes on the vanadium migration during mixing of sea and river waters was calculated by the formula

$$\Delta V_{tot}\% = 100\% \cdot (V_{tot}^{New2} - V_{tot}^{sea}) / V_{tot}^{sea}.$$

Where, V_{tot}^{New2} is the total vanadium concentration formed at the geochemical barrier, V_{tot}^{sea} is the total vanadium concentration in sea water.

RESULTS

At the first stage of the experiment on physicochemical modelling of the vanadium form behavior, the concentration of the element was determined in the form of simple and complexions, associates and ion pairs under the physicochemical conditions [11].

The overwhelming part of organic matter in river water is represented by humic and fulvic acids (more than 90%) [12], therefore, when modelling the interaction of metal ions with organic matter, only these substances were taken into account.

Concentrations of humic and fulvic acids in river water were $3.5 \cdot 10^{-7}$ mol/kg and $7.8 \cdot 10^{-7}$ mol/kg, respectively; only fulvic acids ($2.8 \cdot 10^{-7}$ mol/kg) were found in seawater [5]. The results of the experiment showed that the organic vanadium

compound amount in both types of waters is negligible. The contents of vanadium were $1.96 \cdot 10^{-8}$ mol/kg and $2.94 \cdot 10^{-8}$ mol/kg in the river and seawater, respectively [7]. The values of the total concentration of vanadium were $1.1115 \cdot 10^{-4}$ mol/kg and $4.6335 \cdot 10^{-7}$ mol/kg in the river and seawater, respectively.

Table 2 shows data on the distribution of physicochemical forms of vanadium in sea and river water, as well as in the estuary as a mixing zone.

Table 2. *Vanadium chemical form concentrations and pH in river, estuary and sea waters*

Vanadium chemical forms	River	Estuary	Sea
	pH		
	7.04	7.72	8.10
	Vanadium mass percentage (%)		
$VO_2NO_3^0$	0.2	0.02	0.0035
$HV_2O_7^{3-}$	0.21	1.153	2.04
$H_2VO_4^-$	90.5	51.32	22.75
HVO_4^{2-}	9.45	47.46	75.2

With the mixing of river and sea water, a sharp increase in pH values is observed (Fig. 1), which was regarded during the experiment as the formation of a geochemical barrier. At this barrier, there is a change in the dissolved forms of vanadium migration and their transformation (Table 2).

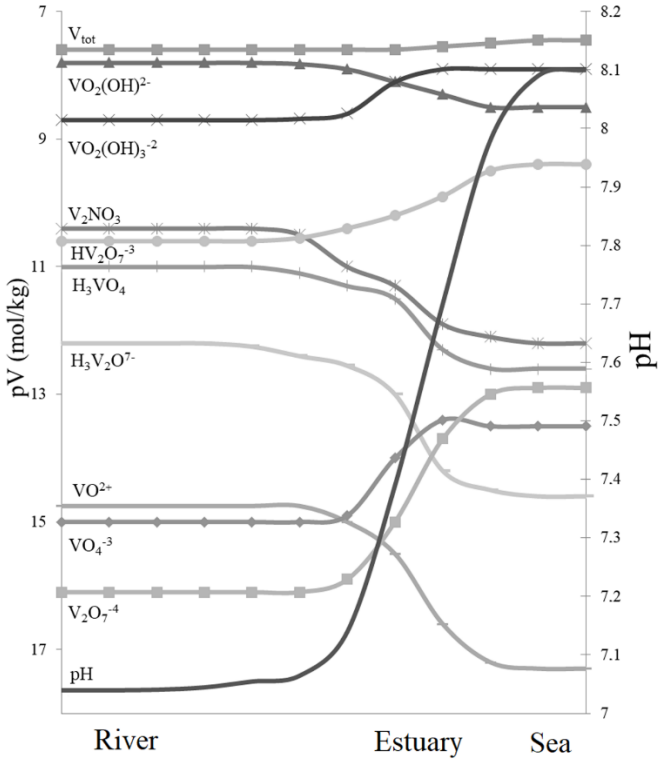

Fig. 1. *Vanadium form distribution and concentrations at the river-sea geochemical barrier*

At the next stage of the study, an attempt was made to assess the effect of physical sorption on the decrease in the total vanadium concentration during mixing at the geochemical barrier.

When sea and river waters mix, suspended matter of river water (and associated chemical elements) is deposited and new suspended matter is formed due to coagulation processes, which leads to an increase in turbidity.

Avalanche sedimentation and coagulation of colloids occurs at salinity from 2 to 5-6 ‰. In this area, up to 95% of suspended solids are lost. At a given salinity, the river suspended matter and newly formed suspended matter are removed, the concentration of the latter is calculated as the difference between the concentrations of suspended matter in the estuary and suspended matter in the river.

To simulate the sedimentation process, 95% of the microelements associated with suspended matter from the river are removed from the system. New values of the total vanadium concentration are obtained, which are used when calculating the sorption equilibrium with a concentration of newly formed suspended matter of 150 mg/L. Then, 95% of the vanadium associated with the newly formed suspended matter is removed from the system. The values of the total vanadium concentrations that should be in seawater when vanadium passes through the geochemical barrier

are obtained, provided that the change in contents is associated with physical sorption by 100%.

The results of modelling the vanadium behavior at the geochemical barier are shown in Table 3.

Table 3. *Vanadium form concentrations in river and sea waters*

Vanadium concentrations (mol/kg)			
River water		Sea water	
V_{tot}	$1.1115 \cdot 10^{-4}$	V_{tot}	$4.6335 \cdot 10^{-7}$
V_{sol}	$1.959 \cdot 10^{-8}$ (0.05%)	V_{sol}	$2.94 \cdot 10^{-8}$ (6.5%)
V_{sorb}	$1.111 \cdot 10^{-4}$ (99.95%)	V_{sorb}	$4.4405 \cdot 10^{-7}$ (93.5%)

The results showed an increase in the concentration of vanadium dissolved forms by 1.5 times when passing the geochemical barrier.

As a result of experiments on physicochemical modelling of the behavior of vanadium forms [11], the role of sorption processes in the migration of vanadium, as well as the reasons for the change in their concentrations during the transition from river to sea waters, have been established.

CONCLUSION

As a result of the study, it was found that, during the transition from river to sea waters, an increase in the concentration of vanadium dissolved forms is observed, which is associated with the desorption of the latter with river suspended matter when passing through the geochemical barrier of the mixing zones of the river and sea waters.

In the study of estuarine zones, the main attention is paid to changes in the total element concentrations at the geochemical barrier, as well as the relationship between suspended and dissolved, organic and inorganic forms. At the same time, there is practically no information about the role of physicochemical biological processes in the formation of the acid-base barrier, where an increase in the concentration of vanadium dissolved forms play an important role in stimulating and enhancing biological processes.

REFERENCES

[1] Ocean biogeochemistry, edited by Monin A.S., Lisitsyn A.P., Russia, 1983, p. 368.

[2] Oceanology. Ocean chemistry, edited by Bordovsky O.K., Ivanenkov V.N., Russia, vol. 1, 1979, p. 518.

[3] Khoroshevskaya V.O., Predeina L.M., Kozhevnikov A.V., Koreneva K.O., Experiment to determine the effect of vanadium on phytoplankton vital activity, Water: chemistry and ecology, Russia, vol. 4, pp. 79-86, 2016.

[4] Chudnenko K.V., Karpov I.K., Bychinsky V.A., Kulik D.A., Water-Rock Interaction, edited by Kharaka Y.S., Chudaev O.V., Netherlands, 1995, p. 725-727.

[5] Dzombak D.A., Morel M.M., Surface complexation model. Hydrous ferric oxide, USA, 1990, p. 393.

[6] Gordeev V.V., River runoff into the ocean and features of its geochemistry, Russia, 1983, p. 160.

[7] Gordeev V.V., Features of geochemistry of river runoff in the ocean, Lithology and useful minerals, Russia, vol. 5, pp. 29-50, 1984.

[8] Korzh V.D., Geochemistry of the elementary composition of the hydrosphere, Russia, 1991, p. 242.

[9] Vinogradov A.P., Selected Works. Isotope geochemistry and problems of biogeochemistry, Russia, 1993, p. 236.

[10] Lukashin V.N. Forms of chemical elements in sediments on meridional sections in the Indian Ocean, Proceeding of V All-Union School of Marine Geology, Russia, vol. 1, pp. 106-113, 1982.

[11] Savchenko A.V., Gramm-Osipov L.M., Mar'yash A.A., Physicochemical modeling of the behavior of microelements (As, V, Cr, Co, and Hg) under the mixing of riverine and marine waters (the Razdol'naya river-Amur bay system), Oceanology, Russia, vol. 49/issue 1, pp. 39-46, 2009.

[12] Varshal G.M., Koscheeva I.Ya., Sirotkina I.S., Study of organic matter in surface waters and their interaction with metal ions, Geochemistry, Russia, vol. 4, pp. 598-607, 1979.

FLOCCULATION OF FINE APATITE AIMED AT REDUCING ENVIRONMENTAL WATER USE PROBLEMS IN MINERAL PROCESSING PLANTS

Alexandr V. Artemev[1]
G. V. Mitrofanova[2]
[1, 2] Mining Institute of the Kola Science Centre of the Russian Academy of Sciences, Apatity, Russia

ABSTRACT

Water treatment technologies involving pre-treated industrial effluents without transporting them to the tailing dump are of interest primarily from an environmental point of view, as they reduce the environmental burden. The paper studies the possibility of purification of process waters from apatite concentrate production from suspended particles and water-soluble impurities using polyacrylamide flocculants.

By studying the processes of adsorption of H^+ and OH^- ions from aqueous solutions, the acid-base properties of the surface of the solid phase of the most polluted technological product - the drain of the apatite concentrate thickener - the mineral composition of which is 90% apatite have been studied. The influence of the reagents present in the processing technology on the quantitative ratio of acid-base centres on the apatite surface has been evaluated. It has been shown that the interaction of these reagents with the mineral creates prerequisites for a greater efficiency of the anionic flocculant.

The electro-surface properties of apatite treated with various reagents were studied using the laser Doppler electrophoresis method. The mechanism of fixation of ions present in the dispersion medium on the surface of apatite was studied by infrared spectroscopy.

In order to determine the conditions under which various flocculants are in the most ionized state, studies were conducted on the change in the viscosity of the polyelectrolyte solution at different pH values. The position of the isoionic point for samples of cationic and anionic flocculants in the presence of reagents used in the apatite flotation and dehydration of apatite concentrate was studied.

A research has been carried out on "model" and real suspensions in circulating water for a number of cationic, anionic and nonionic flocculants. The kinetic and concentration dependences of the flocculating capacity of the studied reagents were determined, which confirmed the high efficiency of the anionic type reagents.

Keywords: *water-preparation process, reagents-flocculants, flotation, phosphorus-containing ores*

INTRODUCTION

At present, water treatment technologies are of some interest in order to involve pre-treated wastewater from mineral processing plants without transporting them to the tailing pond. The study of the composition of various waters from mineral processing plants working with apatite-containing ores has shown that the main impurities affecting the technological parameters of obtaining conditioned apatite concentrate are suspended particles and calcium ions [1]. The most contaminated processing product transported to the tailing dump is a drain of the apatite concentrate thickener which is characterized by high hardness, increased concentration of polyvalent ions and a high content of suspended particles due to applying of an inorganic coagulant.

A well-known and widely practiced way to reduce the amount of suspended particles is the use of organic flocculants [2]. The flocculation process and its efficiency are influenced by many parameters and in each case the choice of the optimal flocculant should be based on the study of the surface properties of the dispersed phase, the ionic composition of the dispersion medium and the characteristics of the flocculant itself (molecular weight, ionicity, etc.).

MATERIALS AND METHODS

The substantiation and selection of the most effective flocculant for the purification of industrial waters of apatite-nepheline processing plant were carried out on the drain of the apatite concentrate thickener, the most contaminated product. According to X-ray phase analysis, the mineral composition of the thickener's drain solid phase is almost 90% represented by apatite sludge (Table 1). The efficiency of water treatment largely depends on the surface properties of this mineral; therefore apatite was used as the solid phase of the model system.

Table 1. *Results of X-ray phase analysis of solid phase of apatite concentrate thickener drain*

Mineral	***Content, %***
Fluorapatite	88.42
Nepheline	5.38
Aegirine	0.96
Aegirin-augite	0.7
Arfvedsonite	0.8
Orthoclase	1.02
Sodalite	0.29
Natrolite	0.55
Titanite	1.09
Ilmenite	0.55
Annite	0.24

The surface properties of apatite were studied by the following methods: the acid-base surface properties were researched by investigating the adsorption of H^+ and OH^- ions from aqueous solutions; the electro-surface properties were studied by laser Doppler electrophoresis on Malvern Zetasizer Nano-ZS laser analyzer (Great Britain). The zeta potential measurements were carried out in the apatite suspension

in distilled water in the presence of an indifferent electrolyte (KCl 0.01 M). The particle size distribution of apatite used in the research was determined on a laser granulometer Malvern Mastersizer 3000 (Great Britain) and shown in Figure 1.

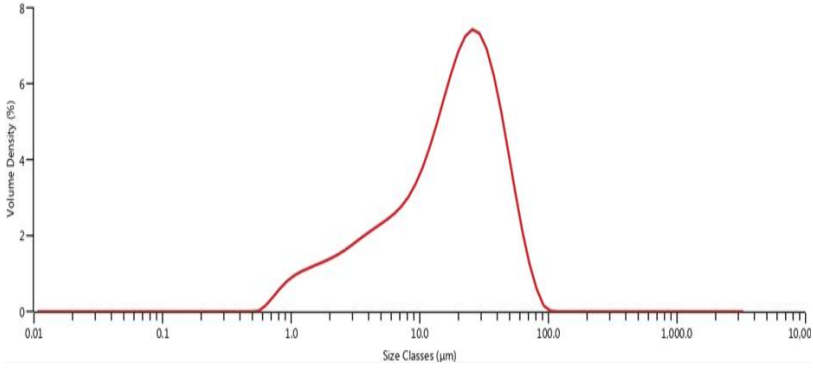

Fig. 1. *The apatite particle size distribution*

Flocculants' efficiency was evaluated on a "model" disperse system, which was a suspension of fine apatite concentrate particles with a dispersed phase content of 2% prepared in circulating water. The suspension was prepared with the apatite concentrate (particle size -0.071 mm) with a P_2O_5 content of 39.34%.

For flocculation of fine apatite particles the authors studied polyacrylamide cationic (FO series) and anionic (AN series) SNF flocculants (France) with various ionicity.

RESULTS AND DISCUSSION

The surface of apatite is heterogeneous and bifunctional and bears both acidic and basic centres of different strength. It is known [3], that H+, OH-, CO32- ions are potential-forming ions for apatite; therefore the surface properties were studied using the pH-metric method based on the study of the adsorption from aqueous solutions of H+ and OH- ions. The method is to measure the suspension effect (SE), which is the difference between the concentrations of counter-ions in the suspension (dispersed system) and the filtrate. According to the theory [4], the SE value allows estimating which centres dominate on the mineral particles surface and characterizes the exchange processes occurring between the liquid phase and the surface, depending on the characteristics of the dispersion medium.

The SE evaluation in a suspension of apatite particles prepared in distilled water (Fig. 2) showed the predominance of the basic centres on the apatite surface. This creates the prerequisites for the interaction of positively charged reagents with the apatite surface.

Zeta potential measurements results also show that the potential-forming layer on the apatite surface is formed by anions. According to the composition and apatite structure, anions are represented with phosphate and hydroxylic groups [5]. Evaluation of the zeta potential of apatite under the action of cationic and anionic flocculants (Fig. 3) has shown that both anionic and cationic flocculants are fixed

on the apatite surface in the absence of any polyvalent cations. A cationic flocculant, which has a lower ionicity, more strongly changes the zeta potential of the apatite surface, recharging it, compared with a decrease in the zeta potential in the case of anionic flocculant fixing on the surface. To put in another way, the fixation of the flocculant on the mineral surface due to the interaction of differently charged groups determines the greater amount of the adsorbed reagent.

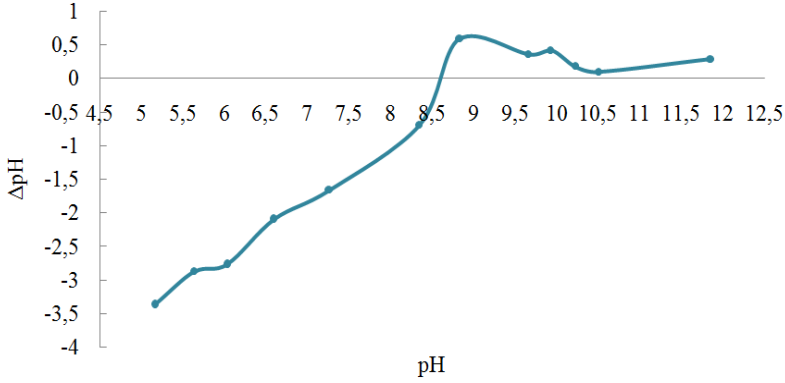

Fig. 2. *Dependence of the SE on pH in apatite suspension in distilled water*

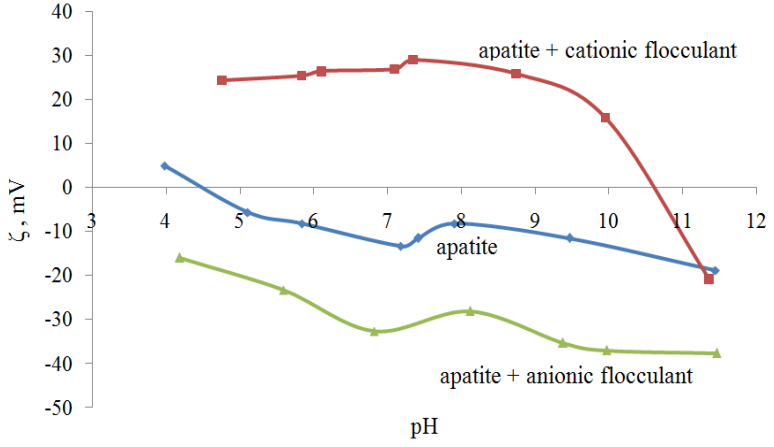

Fig. 3. *Dependence of the zeta-potential of apatite under the action of cationic and anionic flocculants at different pH values*

It is known that the circulating water of processing apatite-nepheline ores plants contains a large amount of polyvalent metal cations, which will also interact with the basic apatite surface. Evaluation of the electro-surface properties of apatite in the presence of calcium and iron salts (Fig. 4) has shown that the adsorption of calcium cations with a concentration of 40 mg/l Ca^{2+} decreases the negative value of the zeta potential and shifts the zero point of charge to a higher pH range. A further increase of calcium ions concentration can lead to a complete recharge of the surface and change the sign of the apatite surface to positive [6], [7]. Iron cations, which have a higher positive charge, neutralize negatively charged groups

on the apatite surface to a greater extent, and even at Fe^{3+} concentration of 40 mg/l the apatite surface is recharged.

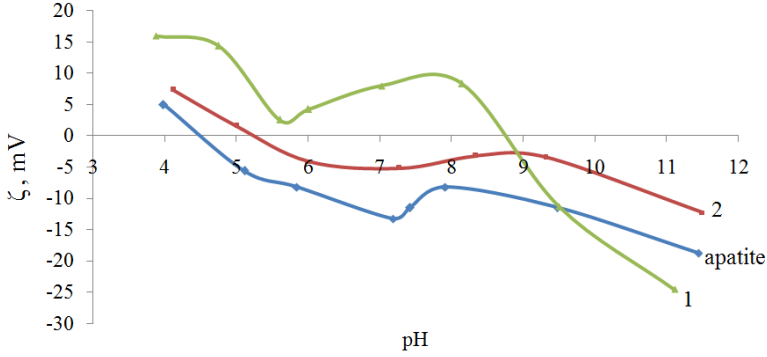

***Fig. 4**. The impact Fe^{3+} ions (1) and Ca^{2+} (2) ions on zeta potential of apatite: Ca^{2+} - 40 mg/l, Fe^{3+}- 40 mg/l*

Thus, it can be assumed that in the circulating water contaminated with salts of polyvalent metals positive ions are fixed on the apatite surface and prerequisites for more effective action of the anionic flocculant are produced.

The higher efficiency of flocculation is known to depend on the characteristics of the used organic polymer, the more charged flocculant is used. It is important to understand to which pH range corresponds this flocculant being in the most ionized state. This state determines more expanded conformation of molecules due to the mutual repulsion of equally charged parts of the polymer chain [8].

Evaluation of the solution viscosity of the cationic and anionic polyacrylamide has shown (Fig. 5) that the anionic flocculant has the maximally expanded state in the alkaline pH range. For a cationic flocculant the regularities are different: when pH value increases, the charges of the polycation will be bound. Consequently, in the alkaline region the cationic flocculant molecule is in unexpanded state, which is ineffective for bridge-type flocculation.

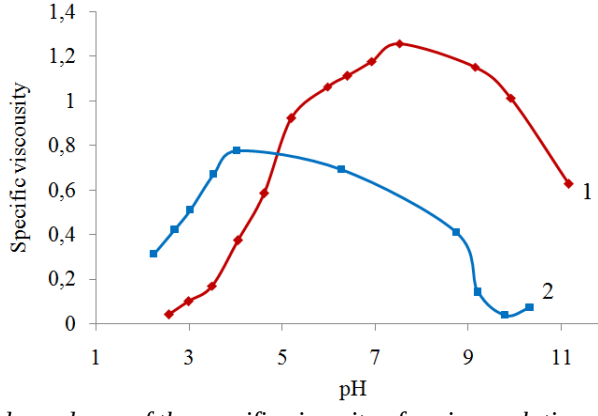

***Fig. 5**. The dependence of the specific viscosity of various solutions of flocculants depending on pH (1 - anionic flocculant, 2 - cationic flocculant)*

The obtained concentration and kinetic curves of the clarification degree of the "model" suspension (Fig. 6) confirm anionic flocculants to be more effective and much lower costs for anionic flocculants are required to achieve the similar characteristics of water clarification. The advantage of the anionic flocculant appears more in the first minutes of clarification. Among anionic flocculants, reagents with a higher ionicity (from 30%) have a higher efficiency.

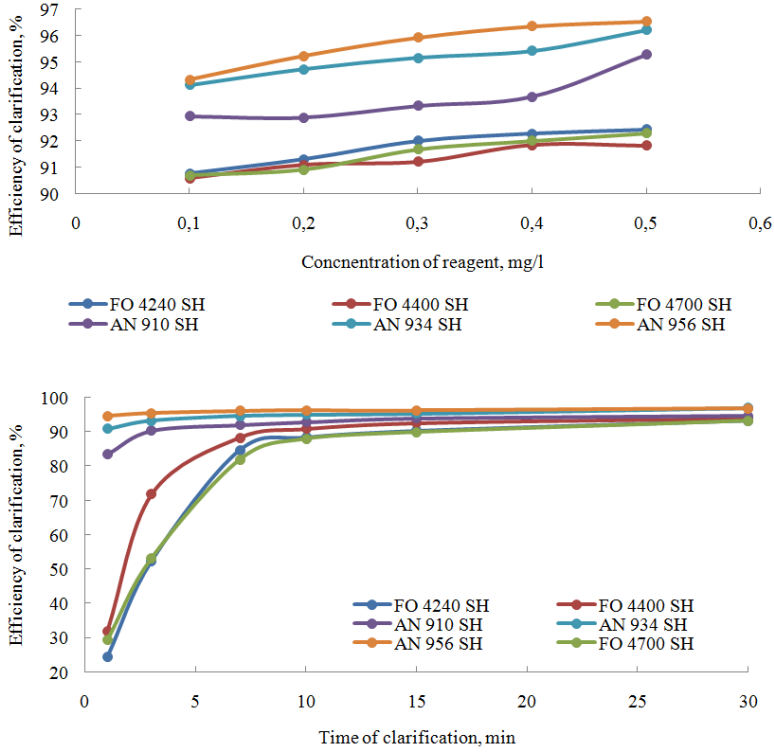

Fig. 6. *Concentration and kinetic curves of the clarification degree of a model suspension of apatite concentrate in recycled water for a number of cationic (FO series) and anionic (AN series) flocculants*

CONCLUSION

The authors have studied the effect of anionic and cationic organic flocculants during cleaning the drain of the apatite concentrate thickener as the most contaminated product obtained in the apatite-nepheline ores processing. It was found that the influence of the applied reagents and ions of the liquid phase changes the surface properties of the dispersed phase. Polyvalent metal cations are fixed on the surface of apatite providing conditions for the effective application of anionic polyacrylamide flocculant.

The authors have analyzed the results and assumed the following mechanism of action of an anionic flocculant:

- oleate ion is adsorbed on apatite particles;
- iron ions (or its hydroxocomplexes) are fixed under the action of ferrous sulfate making a positive charge to the particle surface;
- anionic flocculant due to the formation of complex compounds with iron ions is fixed on the particles of the dispersed phase;
- the calcium ions present in the solution also enhance the flocculating effect due to the formation of complex bridges of the "particle - macroion - Ca^{2+} - macroion - particle" type, thereby increasing the effective size of the flocculant molecule.

ACKNOWLEDGEMENTS

This publication has been produced with the assistance of the European Union. The contents of this publication are the sole responsibility of the following authors: A.V.Artemev, Mitrofanova G.V. and can in no way be taken to reflect the views of the European Union.

REFERENCES

[1] Golovanov V.G., Petrovsky A.A., Brylyakov Yu.E., Introduction of recycled water supply at ANOF-2 // Gornyi Zhurnal. - 1999. - № 9. - pp. 48-50.

[2] Gandurina L.V. Wastewater treatment using synthetic flocculants. M.: DAR/VODGEO, 2007. 197 p.

[3] Brylyakov Yu.E. Development of the theory and practice of complex beneficiation of apatite-nepheline ores of the Khibine deposits: Ph.D.in Eng. Thesis: 25.00.13: Kirovsk, 2004. - 358 p.

[4] Ikonnikova K.V., Ikonnikova L.F., Minakova T.S., Sarkisov Y.S. Theory and practice of pH-metric determination of acid-base properties of solid surfaces: textbook - Tomsk: Publishing house of Tomsk Polytechnic University, 2011. - 85 p.

[5] - Skwarek E., Janusz W. / The Influence of Carbonate Ions on the Structure of the Electrical Double Layer at the Interface of Hydroxyapatite/Electrolyte Solution / Materials Science, Vol. 22, No. 2. 2016, pp. 174-178, https://doi.org/10.5755/j01.ms.22.2.7817

[6] Yaoyang Ruan, Zeqiang Zhang, Huihua Luo, Chunqiao Xiao, Fang Zhou and Ru-an Chi / Effects of Metal Ions on the Flotation of Apatite, Dolomite and Quartz / *Minerals* 2018, *8*(4), 141; https://doi.org/10.3390/min8040141

[7] Fang Zhou, Qi Liu, Xu Liu, Wanchun Li, Jian Feng and Ru-an Chi / Surface Electrical Behaviors of Apatite, Dolomite, Quartz, and Phosphate Ore / Front. Mater., 18 February 2020; https://doi.org/10.3389/fmats.2020.00035

[8] Holmberg K., Jönsson B.,. Kronberg B,. Lindman B / Surfactants and polymers in liquid solutions / BINOM. Laboratory of knowledge, 2007 - 528 p.

INTEGRATING OF GEORADAR ANS SEISMIC STUDIES OF THE TAILINGS DAM

Researcher A. Dyakov[1]
Dr.(Eng), Leader Researcher A. Kalashnik[2]
[1, 2] Mining Institute Kola Science Centre RAS, Apatity, Russia

ABSTRACT

Identification of water-saturated zones in the tailings dams is an actual scientific and practical task in terms of providing, first of all, their mechanical strength and filtration stability. The prevention of accidents in tailings is complicated by the circumstance that the processes of increased filtration, appearing and developing in the dam body, are not fixed on the initial stages by visual and traditional methods. Insufficiency, from the point of view of data completeness, of networks of piezometric boreholes on tailings dams does not allow solving the tasks of necessary information hydrological support. At the same time, the use of active-sounding geophysical study methods allows obtaining sufficiently detailed information about the peculiarities of the internal structure of the tailings dam and the degree of water saturation of the composing soils. A reasoned choice of geophysical methods, as well as their combination, allows increasing the level and reliability of obtained data at subsurface studies. The paper presents the results of in-situ experiments on the study of the tailings dam of the mining enterprise by different in nature wave GPR (georadar) and seismic methods. A comparative analysis of the conducted studies has allowed clarifying the internal structure and assessing the dam's condition, paying special attention to the identification of local zones of increased water saturation and filtration. Based on the calculated correlation coefficient of electromagnetic and seismic wave velocity values, it was revealed that synchronization of geophysical surveys allows significantly increasing the reliability of in-situ determinations, as well as obtaining more reliable data. The results of the studies are the basis for predicting the most vulnerable places (zones) of a bulk ground hydraulic facility, as well as the localization of water-saturated areas in the body of the ground structures with greater reliability and performance.

Keywords: *dam, an accumulator of liquid industrial waste, GPR and seismic surveys*

INTRODUCTION

Currently, the main trends of geophysics in the study of technogenically disturbed, including partially water-saturated, rocks and soils is to increase the information content and reliability of the data obtained [1-4]. A large number of applied geophysical methods indicate the absence of a single standard geophysical method, capable of providing prompt and high-quality obtaining the required information about the mining-geological environment, due to the complexity and ambiguity of the data obtained. At the same time, the joint use of different in-nature

wave methods: electromagnetic (GPR) and seismic profiling allows receiving more reliable operative information about the internal structure and degree of water saturation of technogenically disturbed rocks and soils [1, 5, 6]. Therefore, the choice and integration of these geophysical methods can improve the performance and reliability of the data obtained in solving various problems [7], [8], [9].

In mining operations, a large number of industrial facilities are potentially hazardous and are therefore classified as hazardous and technically complex facilities that require regular inspections and monitoring. One of such industrial facilities is the tailing dumps with systems of embankment structures, a breach of which stability and functionality can lead to an abnormal (or emergency) situation in the technological mining chain.

The world practice of mining nature management has typical examples of accidents at the tailing dumps, which led to significant financial and socio-economic consequences [7], [10]. A comprehensive examination and monitoring of the internal structure and condition of the tailings with the use of operational geophysical methods create an information and technical basis for minimizing the risks of man-made accidents. The purpose of the work is to substantiate methodological approaches to the complex georadar and seismic survey of the tailings dam.

METHODS

To assess the state of water saturation and the internal structure of the technogenically disturbed rocks of the tailings dam, two cycles of integrated observations were carried out using seismic and GPR profiling methods [11], [12], [13]. The following indicators were taken for further analysis: for the seismic method - the ratio of longitudinal velocity to transverse velocity Vs/Vp; for the GPR method - electromagnetic wave velocity V.

Figure 1 shows the main results of the performed integrated research as a radarogram of the electromagnetic wave velocity V (a) and a seismic tomogram of the ratio of longitudinal to transverse velocity Vs/Vp (b). The Figure visually notes the similarity in the colour palettes reflecting the internal structural features and water saturation of the surveyed soil section. For quantitative comparison of seismic and georadar values, plots of the variability of the accepted controlled parameters of the obtained results along the profiling traces in separate sections at two pickets (Fig. 2, 3) were built.

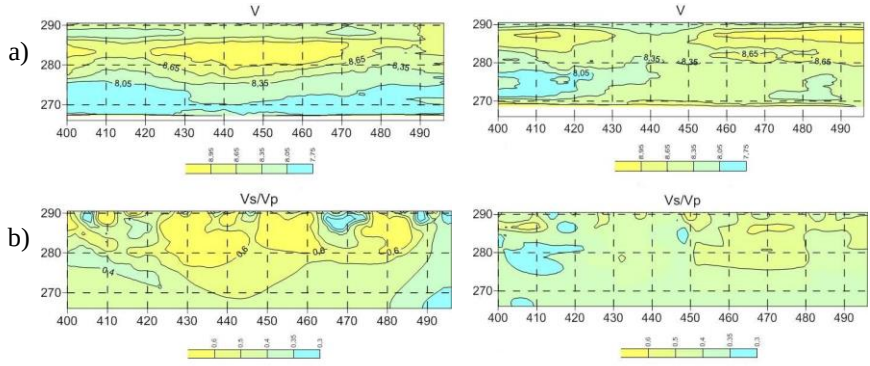

Fig. 1. *Results of integrated studies of soils with georadar (a) and seismic (b) profiling methods (left- 1st study cycle, right-2nd study cycle)*

EXAMPLES

Interpretation of the results of the first cycle of integrated seismic and GPR measurements (Fig. 1, left) suggests the following: In the central part, both the radarogram and the seismogram, the distribution of data reflecting the presence of dense soils of natural moisture has a fairly good visual convergence.

At the same time, in some areas, the colour palettes of the radarogram and seismogram reflect a visual discrepancy in the nature of the distributions of the values of the adopted indicators: *V* and *V*s/*V*p. On the radarogram we can clearly stand out the near-surface zone up to 2 m thick on two intervals of the profile (400-430 m and 470-480 m), in which the wetted soils prevail. At the same time on the seismogram the near-surface zone of moist soils is localized by small areas up to 5 m, and only at the end of the profile, at the interval of 470 m, a direct coincidence with the georadar profiling data is observed. In turn, according to seismic profiling data, water-saturated grounds are identified at the very end of the profile, in the interval 485-498 m, distributing over the whole depth of the seismogram, and according to GPR data, water-saturated grounds are identified throughout the profile, from a depth of 15 m and more (absolute marks 270-275 m).

These discrepancies can be explained, first of all, by the fact that seismic and georadar profiling were not performed simultaneously, but with a time difference of several days [14, 15]. During this period, the influence of natural (abundant precipitation such as rain) and technogenic (discharge of industrial water from an operating enterprise) factors, which also cannot be excluded, could have had an effect.

Interpretation of the analysed results of the 2nd cycle (Fig. 1, right), with synchronous seismic and GPR measurements, suggests the following. On the radarogram, the near-surface zone (to a depth of 1-1.5 m) of the profile up to 289 m, exposed to surface sediment penetration, is characterized by initial low-velocity *V* = 8.1-8.22 cm/nc, with its further sharp increase to *V* = 8.36-8.71 cm/nc at 8-10 m depth from surface (marks 282.5-280 m). Most likely, this is caused by density growth and decrease of ground humidity.

In the interval of heights 280-270 m there is a zone of sharp fall of velocity values to the values V = 7.35-7.71 cm/nc. Similar changes of Vs/Vp index are noted on the seismogram at the same marks, the values of which are 0.30-0.35, which allows us to conclude that soils here are subjected to considerable water saturation.

To compare the values of seismic and georadar results, we plotted the correlation between the values of the monitored parameters in the same sections at two pickets (Fig. 2, 3), for the first and second cycles of measurements, respectively.

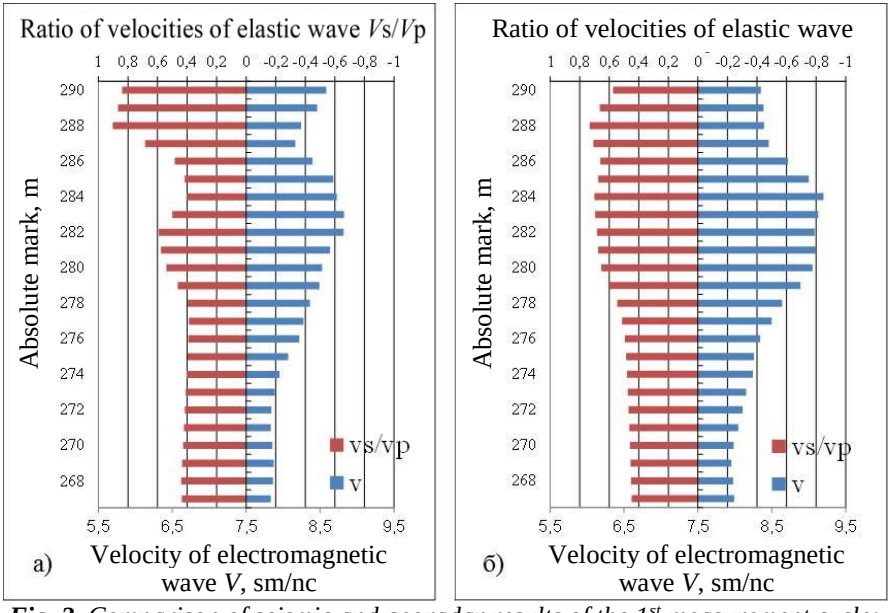

Fig. 2. *Comparison of seismic and georadar results of the 1st measurement cycle:*

a) PK4+10m, b) PK4+60 m

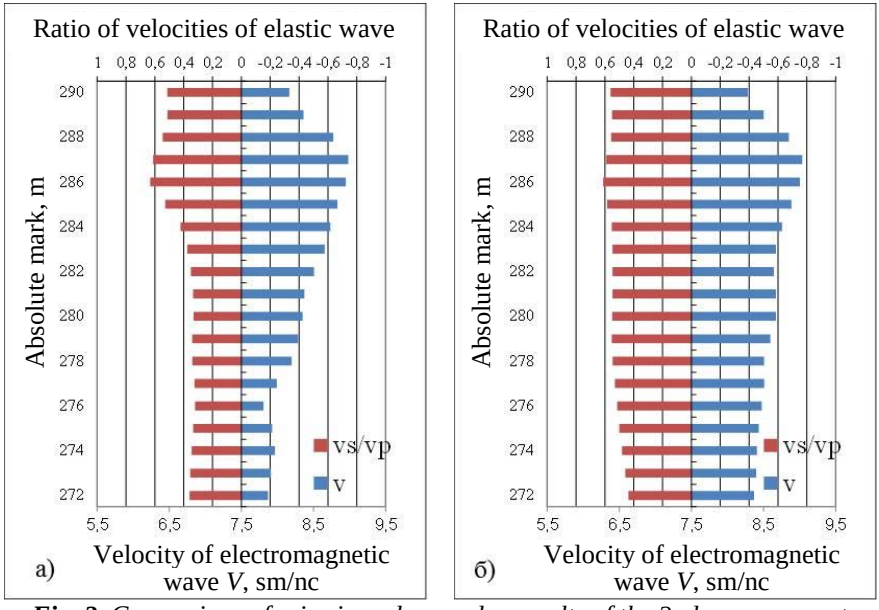

Fig. 3. *Comparison of seismic and georadar results of the 2nd measurement cycle:*

a) PK4+10m, b) PK4+76 m

Comparison of georadar and seismic profiling data, both on the first cycle and on the second, as well as in the aggregate on two cycles of measurements, showed the presence of confident correlation (convergence) of the obtained results. At the same time, GPR and seismic data of the second cycle of measurements have a closer correlation (Fig. 3), which is caused by the synchronization of measurements by two methods, in spatial-temporal coordination. In general, the correlation ratio calculated for the two measurement cycles has a range of values from 0.17 to 0.83 (except for individual values), with a predominant number of values from 0.4 to 0.6 or more (Fig. 4).

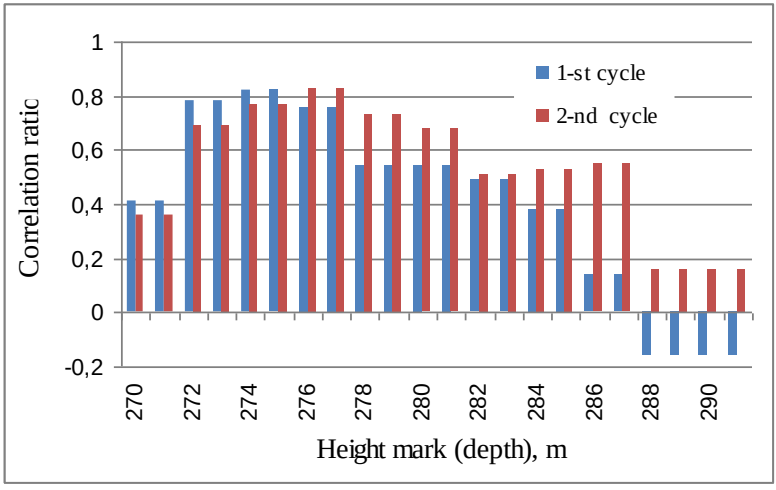

Fig.4. *Correlation ratio of studied indices of georadar and seismic profiling*

CONCLUSIONS

To study the internal structure and state of technogenically disturbed soils of the tailings dam we carried out their research with a combination of GPR and seismic profiling, in two cycles: with a difference of several days and synchronously. Results of executed integrated surveys have allowed getting more reliable information about internal heterogeneity of technogenically disturbed soils due to unevenness of their water saturation. Zonal filtration heterogeneity of soils was revealed and their structure was clarified in the investigated area.

A comparative analysis of the values of the adopted indicators was performed: for the seismic method - the ratio of longitudinal velocity to transverse velocity *V*s/*V*p; for georadar method - electromagnetic wave velocity *V*. Good convergence of analysed indices for both cycles was revealed. At that, on the basis of the calculated correlation ratio of the analysed values, it was discovered that the synchronization of GPR and seismic surveys allow significantly increasing the reliability of in-situ studies, as well as to obtain more reliable data. The obtained results and new knowledge serve as an information-technical basis for integrating of georadar and seismic profiling of technogenically disturbed soils and substantiation of methodical approaches to comparative analysis of their results.

REFERENCES

[1] Starovoitov A.V., Ground penetrating radar data interpretation, Moscow: MMU Publ., Russia, 2008, 192 p.

[2] Maruddani B., Sandi E., The Development of Ground Penetrating Radar (GPR) Data Processing, Intern. J. Machine Learning and Computing, Singapore, Vol. 9, No. 6, December, pp. 768–773, 2019.

[3] Kumlu D., Erer I., Clutter reduction in GPR images using non-negative matrix factorization, J. Electromagn. Waves and App., United Kingdom, Vol. 32, No. 16, pp. 2055–2066, 2018.

[4] Melnikov N.N., Kalashnik A.I., Zaporozhets D.V., Dyakov A.Yu., Maksimov D.A., Experience of applying GPR subsurface studies in the western part of the Russian Arctic sector, Problems of the Arctic and Antarctic, Russia, No. 1, pp .39-49, 2016.

[5] Kalashnik A.I., Zaporozhets D.V., Georadiolocation studies at mining enterprises of Kola region, Conference Proceedings, Engineering and Mining Geophysics 2020, EAGE, vol. 2020, 51089, 2020.

[6] Demetrius Cunha Gonçalves da Rocha, Marco Antonio da Silva Braga, Camilla Tavares Rodrigues, Geophysical methods for BR tailings dam research and monitoringin the mineral complex of tapira – minas gerais, Revista Brasileira de Geofísica, Brazil, vol. 37, No. 3, pp. 275-289, 2019.

[7] Melnikov N.N., Kalashnik A.I., Kalashnik N.A., Zaporozhets D.V., Application of modern methods for complex research of the state of hydraulic structures of the Barents Sea region, Proceedings of the Murmansk State Technical University, Russia, vol. 20, No. 1, pp. 13-20, 2017.

[8] Del Sole L., Calafato A., Antonellini M., Combining Ground-Penetrating Radar profiles with geomechanical and petrophysical in situ measurements to characterize sub-seismic resolution structural and diagenetic heterogeneities in porous sandstones (Northern Apennines, Italy), Marine and Petroleum Geology, Netherlands, 2020.

[9] Comisi F., De Giorgi L., Leucci G., Integrated use of GPR and TDR for wood permittivity evaluation, IMEKO TC-4 International Conference on Metrology for Archaeology and Cultural HeritageTrento, Italy, October 22-24, pp.1-4, 2020.

[10] Jorge Luís Porsani, Felipe Augusto Nascimento de Jesus, Marcelo Cesar Stangari, GPR Survey on an Iron Mining Area after the Collapse of the Tailings Dam I at the Córrego do Feijão Mine in Brumadinho-MG, Remote Sensing, Brazil, No. 11(7), 860, 2019.

[11] Abramov N.N., Dyakov A.Y., Kalashnik A.I., Identification of Water-Saturated Zones in a Protective Hydraulic Earthen Structure by Synchronous Electromagnetic and Seismic Sounding, Power Technology and Engineering, Russia, No. 53 (2), pp. 167-171, 2019.

[12] Danilkin A.A., Kalashnik A.I., Zaporozhets D.V., Maksimov D.A., Monitoring the condition of the protective dam in the mining zone of the secondary deposit of Kovdorsky GOK, Mining informational and analytical bulletin (scientific and technical journal), Russia, No. 7, pp 344-351, 2014.

[13] Kalashnik A.I., Zaporozhets D.V., Kalashnik N.A., Identification of filtration and deformation processes in the tailings dam, Herald of the Kola Science Centre RAS, Russia, No 2, pp. 13-17, 2013.

[14] Kalashnik A.I., Dyakov A.Y., Information technologies in problems of monitoring of hydraulic facilities of mining enterprises through subsurface GPR sounding, Mining informational and analytical bulletin (scientific and technical journal), Russia, No 23, pp. 283-291, 2017.

[15] Chromcak J., Grinc M., Panisova J., Vajda P., Kubova A., Validation of sensitivity and reliability of GPR and microgravity detection of underground cavities in complex urban settings: Test case of a cellar, Contributions to Geophysics and Geodesy, Slovakia, Vol. 46/1, pp. 13-32, 2016.

MARINE FORECAST FOR THE EASTERNMOST PART OF THE BLACK SEA

DSc. Demuri Demetrashvili[1]
MSc.Vepkhia Kukhalashvili[2]
Dr. Diana Kvaratskhelia[3]
DSc. Aleksandre Surmava[4]
[1, 2, 3, 4] M. Nodia Institute of Geophysics of Ivane Javakhishvili Tbilisi State University, Georgia
[1, 4] Institute of Hydrometeorology of Georgian Technical University, Georgia
[3] Sokhumi State University, Georgia

ABSTRACT

Modelling and forecasting of dynamic processes and distribution of various substances of anthropogenic and natural origin in coastal and shelf zones of the seas and oceans are of great interest due to the high anthropogenic load of these zones. The aim of this paper is to present some examples of modelling and short-term forecasting of dynamic fields – the current, temperature and salinity in the easternmost Black Sea covering Georgian sector of the Black Sea and adjacent water area using a high-resolution regional model of the Black Sea dynamics. The z-level regional model is based on a full system of ocean hydro-thermodynamics equations and is nested in the basin-scale model of the Black Sea dynamics of Marine Hydrophysical Institute (Sevastopol). To solve the model equation system, a numerical algorithm based on the splitting method is used. Calculations show that circulation processes in the easternmost water area of the Black Sea are characterized by a permanent alternation of different circulation modes with the formation of mesoscale and submesoscale eddies throughout the year, which significantly affect the formation of thermohaline fields; atmospheric wind forcing substantially determines not only the peculiarities of the sea surface horizontal circulation, also the vertical structure of the current field.

Keywords: *numerical modelling, hydro-thermodynamic processes, thermohaline fields, system of equations, boundary conditions*

INTRODUCTION

Modelling and forecasting hydro and thermodynamic processes in the upper layer of the Black Sea is one of the main issues of the Black Sea oceanography and is of great theoretical and practical importance. One of the main factors determining the importance of studying dynamic processes, occurring in the upper layer of the sea, is a significant contribution of the Black Sea to the formation of the regional weather and climate. The Black Sea and the atmosphere are the main objects of the unified hydrodynamic system, between which the processes of energy and substance exchange take place continuously. The features of these exchange processes are significantly influenced by the dynamic processes occurring in the upper layer of the sea, and vice versa, the formation of the spatial-temporal

distribution of hydrophysical fields in the upper layer is significantly determined by the interaction between the sea and the atmosphere.

There are especially important studying and forecasting circulation processes in the coastal areas that are subject to the greatest anthropogenic impact. The importance of studying coastal circulation processes is due to their significant role in the spatial and temporal distribution of thermohaline fields and various substances of natural and anthropogenic origin strongly affecting the marine ecosystem. Sea currents are the main mean of transporting pollutants in the coastal zone and make a significant contribution to the formation of features of temperature and salinity fields having feedback on the circulation through the density field. From this point of view, the easternmost water area covering Georgian sector of the Black Sea and surrounding water area is of considerable interest, which is a dynamically very active region with formation and evolution of various mesoscale and submesoscale eddies.

Over the last two decades researches on the Black Sea dynamics have been widely developed. The attraction of new observation technologies, including satellite measurement methods, creation of highly resolving mathematical models allowing to reproduce basin-scale and coastal dynamic processes by sufficiently high adequacy, raised the Black Sea oceanography to a higher level (e. g., [1-5]). The development of effective data-computing systems has led to the creation of the Black Sea nowcasting/forecasting system [4], [6]. [7], [8]. Such an achievement of the Black Sea operative oceanography became possible as a result of close cooperation of oceanologists from the Black Sea countries in the framework of the EU projects ARENA, ASCABOS, ECOOP. One of the components of this system is a high-resolution regional forecasting system for the easternmost part of the Black Sea based on the regional model of the Black Sea dynamics of M. Nodia Institute of Geophysics of I. Javakhishvili Tbilisi State University (RM-IG) [9], [10], [11].

In the present paper, some results of 3-days forecast of main hydrophysical fields – the current, temperature and salinity using the RM-IG are analyzed illustrating variability of regional hydrophysical processes in the easternmost part of the Black Sea limited from the open part of the basin by the liquid boundary passing along the meridian 39.08^0E.

MATERIALS AND METHODS

The high-resolution RM-IG is obtained by adaptation of the basin-scale model [12] to the easternmost regional area with increasing of spatial resolution to 1 km. The RM-IG is a z-level hydrostatic model based on a solution of a full system of ocean hydro and thermodynamics equations, which is nested in the basin-scale model of Black Sea dynamics with 5 km spatial resolution of Marine Hydrophysical Institute (MHI, Sevastopol) using one-way nesting technology. All input data used for the initial and boundary conditions of the model equation system are available from MHI via ftp site. The RM-IG provides a 3-days forecast of 3D flow, temperature, salinity and density fields in the easternmost water area of the Black Sea. To solve the equation system with corresponding initial and boundary conditions splitting method is used [13]. The 3D solution domain is covered with a

grid consisting of 30 horizons with non-uniform vertical steps – minimal equal to 2 m near the sea surface and maximal equal to 100 m from depth 206 m to the bottom. The number of grid points on each horizon is 215x347 with a spatial horizontal resolution 1 km. The time step is 0.5 h. The simulated and predicted sea surface temperature (SST) and currents were compared with available observational data – satellite SST derived from NOAA satellites and Geostrophyc currents reconstructed on the basis of satellite altimeter data. The comparison showed sufficient reliability of the model results [9], [10], [11].

RESULTS AND DISCUSSION

The computations of the marine forecast, carried out by us regularly last decade, have shown that the hydrophysical processes in the easternmost water area of the Black Sea are characterized by a significant variety and specific features of the spatial-temporal distribution of dynamic fields, accompanied by the permanent generation and evolution of mesoscale and submesoscale eddies with cyclonic and anticyclonic rotation. The nonstationary atmospheric processes over the sea basin, having a direct effect on the formation of the Black Sea hydrological structure under Earth's rotation, play an important role in the seasonal and interannual variability of sea dynamic processes, but the specificity of this variability is largely determined by the sea bottom relief and the configuration of the coastline, baroclinicity, turbulent diffusion.

One of the general patterns characteristic for the processes taking place in the easternmost water area is that the hydrological modes are significantly different for the warm (April-October) and cold periods (November-March). In winter, the regional circulation as a hole is often cyclonic, against the background of which cyclonic and anticyclonic eddies with a diameter of about 20-40 km are often formed.

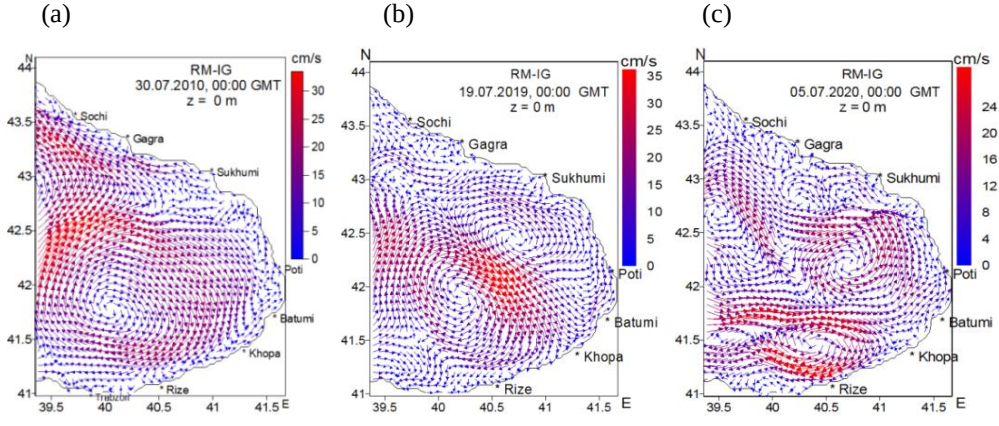

Fig.1. *Predicted surface current fields at 00:00 GMT for the following days and years: (a) - 30 July 2010 (start of forecast 27.07.2010, 00:00 GMT); (b) – 19 July 2019 (start of forecast 17.07.2019, 00:00 GMT); (c) - 5 July 2020,(start of forecast 3.07.2020, 00:00 GMT).*

In summer and early autumn, anticyclonic movement predominates in the easternmost waters, although the formation of cyclonic structures can also be observed against this background. In many cases, the formation of an intense anticyclonic vortex, known as the Batumi eddy, is observed in the warm periods. The Batumi eddy, which vertically covers a layer of about 300-400 m, is found with different intensities in different years.

Fig.1 illustrates prognostic sea surface circulation patterns corresponding to July 2010, 2019, and 2020, which clearly show that in the same seasons of different years the sea surface circulation modes can differ significantly from each other.

Fig.1a and the analysis of other calculations carried out by us shows that the regional circulation in the summer and September 2010 in the easternmost water area was characterized by the formation of an intense Batumi eddy, which was characterized by great stability.

The circulation in July 2019 was characterized by the formation of dipole structure "cyclone-anticyclone" (Fig.1b). The Batumi eddy together with cyclonic eddy created the dipole structure, which underwent minor changes during summer of 2019. Fig.1c shows the typical circulation for July 2020, where the Batumi eddy is not clearly dominated and the surface circulation is characterized by the formation of mesoscale and submesoscale eddies with cyclonic and anticyclonic rotations.

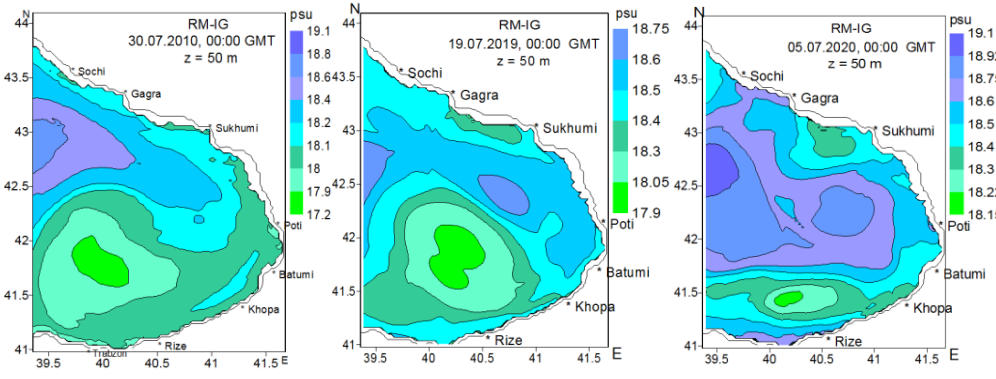

Fig. 2. *Predicted salinity fields on depths of 50 m at the same time moments as in Fig.1.*

The structure of the circulation is largely reflected in the distribution of salinity field, which is clearly illustrated in Fig. 2. The salinity fields are shown at the horizon z= 50 m on the same days and years as in Fig.1. From a comparison of Figs.1 and 2 it is clearly seen that the areas of relatively low salinity waters coincide with an allocation of the centres of anticyclonic eddies, and the areas of relatively high salinity coincide with the cyclonic movement. The anticyclonic vortex structure forms a downward flow that transfers waters with relatively low salinity from the upper layers downwards, while the upward flows formed at the centres of the cyclonic vortices raise salt water from the lower to the upper layers. Marine

living organisms are highly sensitive to water salinity and thus the sea circulation regime can have a significant impact on the marine ecosystem.

Fig. 3 shows the sea surface temperature (SST) on the same moments of time as in the previous Figures. Peculiarities of SST fields are significantly influenced by heat fluxes on the sea surface. Summer of 2010 was characterized by abnormally high air temperatures, which were also reflected in the distribution of SST fields. That is why the maximum SST 29^0C on July 30, 2010 (Fig.3a) was higher than it was on July 19, 2019 (Fig.3b) and July 5 2020 (Fig.3c).

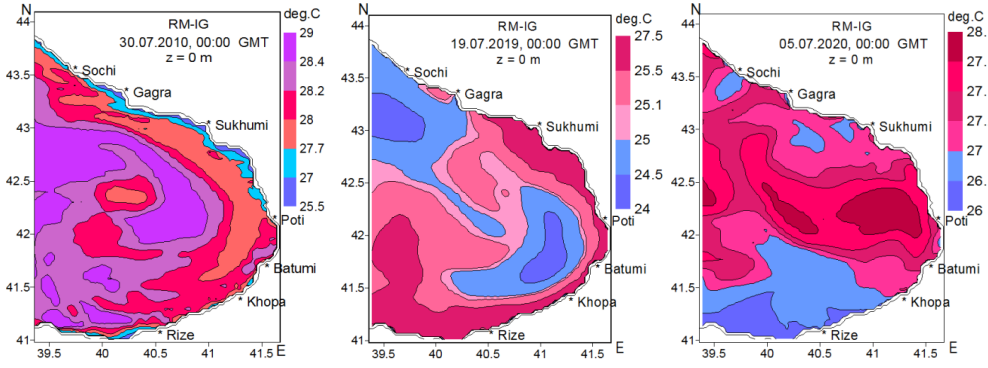

Fig. 3. *Predicted SST at the same time moments as in previous Figures.*

Considerable interest is the question of the vertical structure of the flow field under different atmospheric wind forcing. Our calculations show that the atmospheric wind field above the sea surface substantially determines not only the peculiarities of the sea surface circulation horizontally, but also the vertical structure of the current field.

For the purpose of illustration, Fig. 4 shows the circulation field on the sea surface and at a depth of 20 meters under two atmospheric forcing: in cases of strong (Fig. 4a and b) and relatively weak wind stresses (Fig. 4c and d). From Fig.4a is visible, that the intense atmospheric circulation operated above the easternmost Black Sea on December 25, 2018, caused high speed of drift currents on the sea surface with a maximum speed of 70 cm/s and provided practically vortex-free flow. Strong wind stress on the sea surface acts as an external smoothing factor and prevents the formation of vortex structures.

On June 9, 2020, relatively weak winds developed over the sea, which contributed to the formation of vortex structures on the sea surface (Fig.4c). A large difference in the vertical variability of the flow field in cases of strong and weak atmospheric wind forcing is clearly visible from a comparison of Figs.4b and 4d.

Under strong atmospheric conditions, the circulation pattern undergoes sharp qualitative and quantitative changes with depth, while in the absence of strong winds, the circulation pattern changes slightly. In the first case, the maximum speed decreased from 70 cm/s on the sea surface to 30 cm/s at a depth of 20 m, but in the second one - from 28 cm/s to 24 cm/s. By the depth, the effect of the wind stress

weakens and the role of such internal factors as the configuration of the seashores, baroclinicity, etc. becomes the main one.

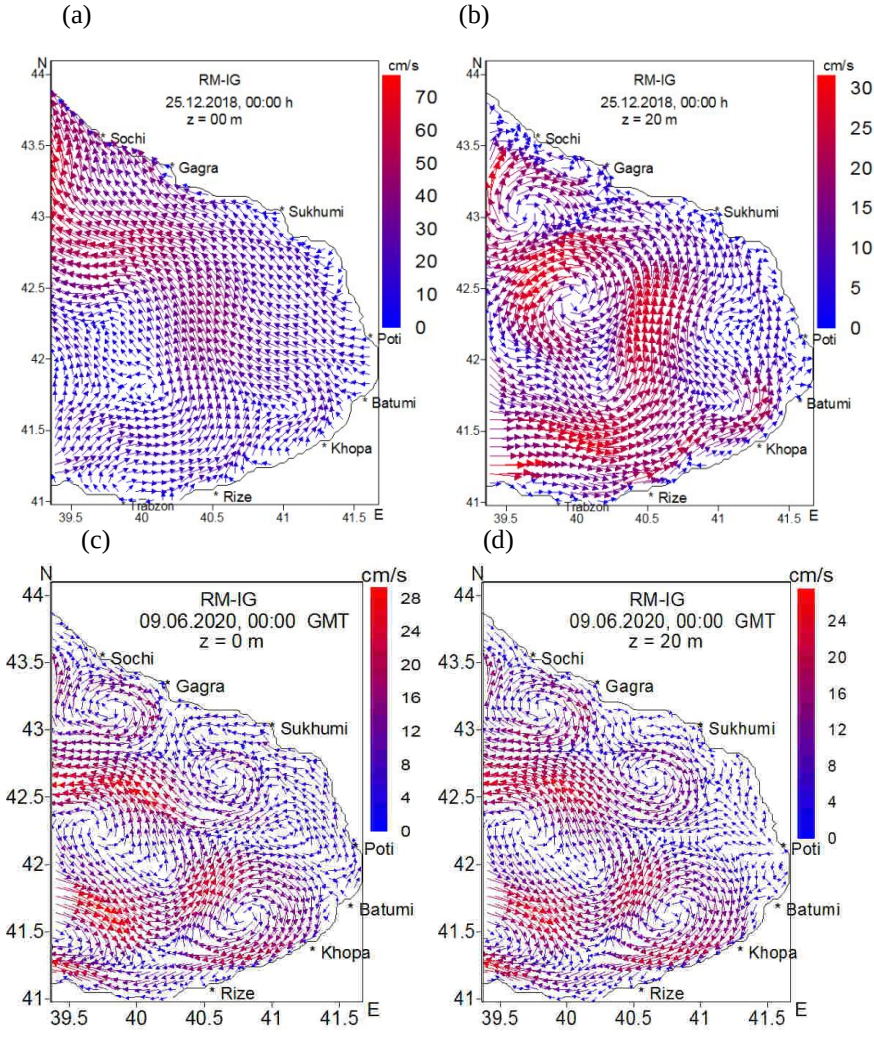

Fig. 4. *Forecasted sea current fields on horizons of 0 m and 20 m: (a), (b) - in conditions of strong atmospheric forcing, corresponding to December, 25 2018; (c), (d) – in conditions of weak atmospheric forcing, corresponding to June 9, 2020.*

CONCLUSION

Marine forecasting for the easternmost part of the Black Sea is based on a z-level, hydrostatic RM-IG with 1 km resolution, which is nested in the basin-scale model of MHI with 5 km resolution using one-way nesting technology. The RM-IG is based on a full system of ocean hydrothermodynamics equations and provides

a 3-days forecast of main 3D dynamic fields – flow, temperature, salinity and density with 1 km spacing.

Numerous calculations show that the Georgian sector of the Black Sea and adjacent area are characterized by the diversity of the hydrological regime, where the continuous development and evolution of various vortex structures takes place throughout the year.

Analysis of the prognostic fields shows a significant difference in the vertical hydrological structure of the upper layer of the Black Sea under different atmospheric forcing. Strong winds cause "abrasion" of vortex formations on the sea surface. With depth, due to the weakening role of the wind stress and the increasing role of internal factors, the system of sea currents in the upper layer undergoes sharp changes with eddy formations.

The Batumi eddy, which very often is the main element of the regional circulation in the easternmost water area of the Black Sea during the warm season, is characterized by different intensities and stability in different years. The circulation regime has a strong influence on the distribution of the salinity field, which is a very important factor for marine living organisms.

REFERENCES

[1] Korotaev G., Oguz T., Nikiforov A., Koblinsky C. Seasonal, interannual, and mesoscale variability of the Black Sea upper layer circulation derived from altimeter data. J. Geophys. Res., 2003, v.108, No. C4, 3122, pp. 19-15.

[2] Stanev E. Understanding Black Sea dynamics: Overview of recent numerical modeling. Oceanography, 2005, v.18. № 2, pp. 52-71.

[3] Zatsepin A. G., Baranov V. I., Kondrashov A. A., Korzh A. O., Kremenetskiy V. V., Ostrovskii A. G., Soloviev D. M. Submesoscale eddies at the Caucasus Black Sea shelf and the mechanisms of their generation. Oceanology, 2011, vol.51, № 4, pp. 554-567.

[4] Marchuk G. I., Paton B. E., Korotaev G. K., Zalesny V. B. Data-computing technologies: a new stage in the development of operational oceanography. Izvestiya, Atmospheric and Oceanic Physics, 2013, vol.49, № 6, pp. 629-642 (in Russian).

[5] Zalesny V. B., Gusev A. V., Moshonkin S. N. Numerical model of the hydrodynamics of the Black Sea and the sea of Azov with variational initialization of temperature and salinity. Izvestiya, Atmospheric and Oceanic Physics, 2013, vol.49, № 6, pp.699-716 (in Russian).

[6] Besiktepe S. Development of the regional forecasting system for the Black Sea. Proceed. of the "Second International Conference on Oceanography of Eastern Mediterranean and Black Sea: Similarities and Differences of Two Interconnected Basin, 14-18 October, Ankara. Turkey. 2003, pp.297-306.

[7] Korotaev G.K.,Oguz T., Dorofeyev V. L., Demyshev S. G., Kubryakov A. I., Ratner Yu. B. Development of the Black Sea nowcasting and forecasting system. Ocean Science. 2011, 7, pp.629-649.

[8] Kubryakov A. I., Korotaev G. K., Dorofeev V. I., Ratner Y. B., Palazov A., Valchev N., Malciu V., Matescu R., Oguz T. Black Sea coastal forecasting system. Ocean Science, 2012, 8, pp. 183-196.

[9] Kordzadze A. A., Demetrashvili D. I. Operational Forecast of hydrophysical fields in the Georgian Black Sea coastal zone with the ECOOP. Ocean Science, 2011, 7, doi: 10.5194/os-7-793-2011, pp.973-803.

[10] Kordzadze A. A., Demetrashvili D. I. Operational forecasting for the eastern Black Sea. Proceed. of the 13th International MEDCOAST Congress on Coastal and Marine Sciences, Engineering, Management and Conservation MEDCOAST 2017, 30 October – 4 November, 2017, Melieha, Malta, t.2, pp.1215-1224.

[11] Demetrashvili D., Kukhalashvili V. High-resolving modeling and forecast of regional dynamic and transport processes in the easternmost Black Sea basin. Proceed. of the International Conference on Geosciences (GEOLINKS 2019), 26-29 March 2019, Athens, Greece, Book 3, vol.1, pp.99-107.

[12] Kordzadze A. A., Demetrashvili D. I., Surmava A. A.Numerical modeling of hydrophysical fields of the Black Sea under the conditions of atmospheric processes. Izvestiya RAS, Atmospheric and Oceanic Physics, 2008, 44, 16, pp.213-224.

[13] Marchuk G. I. Numerical solution of problems of atmospheric and oceanic dynamics. Leningrad, Gidrometeoizdat, 1974, 303 p (in Russian).

REDUCTION OF THE VOLUME OF PUMPING OF LIQUID WASTE FROM THE PRODUCTION OF APATITE CONCENTRATE DUE TO THE TECHNOLOGY OF PARTIALLY CLOSED WATER CIRCULATION

Alexandr V. Artemev[1]
Valentin V. Biryukov[2]
[1, 2] Mining Institute of the Kola Science Centre of the Russian Academy of Sciences, Apatity, Russia

ABSTRACT

The use of recycled water supply technology in mineral dressing plants solves current environmental and economic problems for the mining and processing industry. Usually, water treatment takes a long time and requires constructing large-volume tailing dumps.

The paper proposes a technology of a partially closed water circulation with the purification of watered production waste from suspended particles and water-soluble impurities that negatively affect the flotation process, based on the regularities describing the interaction of flocculants with the phases of a heterogeneous system of process waters.

The authors have determined the most effective reagents providing optimal indicators of recycled water. The proposed technology is implemented in hardware in a radial thickener and eliminates the discharge of process water into an external tailings dumps facility, which will reduce the area occupied by production waste.

Based on the particle size distribution data for various preliminary treatment options, differential and integral particle size distribution curves have been obtained. Analytical expressions of the obtained curves have been used to create discrete functions of volume fractions of particles with different sizes when constructing a model of the initial feed.

The hydrodynamic processes of highly diluted suspension flows in the thickener's body were studied using computational experiments on a model developed in the ANSYS Fluent software package, which is based on the real 3D geometry of a radial thickener. To build the geometry, the authors used a standard module GAMBIT. A computational experiment on cleaning the apatite concentrate discharge was performed on a virtual stand. The distributions of the concentrations of volume fractions of particles and the velocities of their movement in the thickener's volume were obtained.

The results of laboratory studies and computer simulation data allow the authors to tell about the prospect implementation of the technology of intra-plant water circulation, which will reduce by 10% the amount of wastewater discharged into the tailing dump. The use of the most efficient reagents will provide optimal

water parameters for the content of suspended particles and hardness cations and, ultimately, will increase the technological and environmental performance of the Khibiny apatite-nepheline ores processing.

Keywords: *water-preparation process, reagents-flocculants, flotation, apatite-nepheline ores, computer simulation*

INTRODUCTION

Along with the indisputable advantages, the introduction of recycled water supply at the mineral dressing plants has a number of problems affecting on the technological process. The ionic composition of water plays a specific role in using recycled waters for apatite-nepheline ores flotation. It has been found that the main components of recycled water are Ca^{2+}, Mg^{2+}, Fe^{2+}, K^{+}, Na^{+} cations and Cl^{-}, SO_4^{2-}, CO_3^{2-}, HCO_3^{-}, SiO_3^{2-} anions, as well as sludge and organic components [1].

The experience of the mineral dressing plants has revealed that the greatest influence on the change in the surface properties of minerals composing apatite-nepheline ores is exerted by suspended solids and Ca2 + cations. The particle size of suspended solids is usually in the range of 0.1-300 microns, i.e., from course to colloidal particles. The negative effect of sludge on the flotation process is the sorption of the collector on itself, a change in the ionic composition of the pulp and contamination of the apatite concentrate due to the mechanical removal of sludge into the froth. The study of the influence of Ca^{2+} cations on the apatite flotation has shown their interaction with soaps of fatty acids with the formation of sparingly soluble salts as colloidal dispersed formations and reducing the CMC (critical micelle concentration) of collectors. During flotation, cations activate the minerals' surface, violate selectivity, and deteriorate the concentrate quality [2,3]. Earlier works have proved that the ultimate value of calcium cations content in flotation water should not exceed 20 mg/l [4]. According to the experience of the dressing plants processing apatite-nepheline ores, the optimum amount of suspended particles is up to 900 mg/l.

Mining and processing enterprises use tailings ponds to treat process water for its further application. The water is clarified there under the action of gravitational forces. However, it takes considerable time and volumes of the tailings pond to achieve equilibrium of the processes occurring in the tailings dump. At present, the mining enterprises are interested in increasing the technological efficiency and environmental safety of ore processing by involving pre-treated process water of the processing plant without discharging it into the tailings pond.

The most promising source of water, which can be used in in-plant water circulation, is a discharge of the apatite concentrate thickener. The study of the characteristics of this product (Table 1) has shown the excess of the maximum permissible values by several times, which excludes its potential involvement in the technological process without additional purification.

Table 1. *Characteristics of the apatite concentrate thickener discharge*

Content of Ca^{2+}, mg/l	Content of suspended particles, g/l
52.2	27.363

The authors have proposed a technology of intensification of suspended particle separation by means of polyacrylamide flocculants, hardware implemented in the radial thickener [5].

Due to the complexity of industrial tests, the most perspective method to research the influence of technological parameters of the suspension on processes of thickening of the apatite concentrate discharge is a computational model experiment.

MATERIALS AND METHODS

At the first study stage the authors have assessed the efficiency of various organic flocculants differing by molecular weight, origin and quantity of ionogenic groups, in particular, the SNF company reagents, representing polyacrylamides of high molecular mass with various ionicities (Table 2).

Table 2. *Characteristic of reagents-flocculants*

Reagent class	Name	Ionicity	Molecular mass
Anionic flocculants	AN 956 SH	High, 50%	$(13.4\text{-}16.1)*10^6$
	AN 934 SH	High, 30 %	$(13.8\text{-}16.75)*10^6$
	AN 923 SH	Average, 20%	$(12.2\text{-}14.1)*10^6$
	AN 910 SH	Very low, 10%	$(11.6\text{-}13.75)*10^6$
Cationic flocculants	FO 4700 SH	High,70%	$(4.9\text{-}7.25)*10^6$
	FO 4400 SH	Average,30%	$(5.0\text{-}7.55)*10^6$
	FO 4240 SH	Low,16%	$(6.2\text{-}8.25)*10^6$

The flocculation activity of the studied polymeric reagents was determined on model and real disperse systems. As a model system the authors used a suspension of fine dispersed apatite concentrate particles (particle size -0.071 mm, P_2O_5 content - 39.34%) with the content of dispersed phase 2%, prepared on distilled and recycled water.

The hydrodynamic processes of highly diluted suspension flows were studied by means of computational experiments over a model developed in the ANSYSFluent software package. The main research task was to study the influence of technological parameters of the suspension on thickening processes and on the kinetics of the thickening process using polyacrylamide flocculants.

Proceeding from the fact, that the water treatment technology is proposed to be realized by a radial thickener in ANSYSFluent software package (license of Mining Institute KSC RAS), the mathematical model of working space of a 30-meter thickener was developed. The model is based on the real 3D geometry of a radial thickener with a central drive. The standard GAMBIT module was used to build the geometry of the radial thickener. The model is constructed of two main parts: a stationary volume (the thickener's body) and a dynamic volume (a prismatic element - thickener rake). The raking mechanism of the thickener is designed to

move the deposited disperse particles to a discharge port and consists of a central axis and four radial rakes with blades. It was modeled using "SlidingMesh" technology. This technology allows the interaction of any rotationally and progressively moving components with multiphase fluid medium and vice versa. In this case, the rotating blades of the thickener's raking mechanism at a controlled speed transmit effort to the medium consisting of dispergating and several dispersed phases of the suspension.

The computational grid of 3D geometry of the virtual stand, as close as possible to the real Outotec thickener with a diameter of 30 meters has 670,000 tetrahedral elements. Feeding of the initial suspension and discharge into the model is performed through the upper and lower nipples of the cylindroconical body. It is possible to control the flow rates of supply and discharge of the suspension. The clarified water is drained through the upper section of the model. The flow of a highly diluted suspension was simulated in the working space of the thickener by multiphase Euler equations for one dispergating and several dispersed phases.

RESULTS AND DISCUSSION

The influence of ionicity on flocculation of fine disperse apatite concentrate particles was studied through concentration and kinetic dependences of the degree of clarification of the model apatite concentrate suspension in recycled water for a number of cationic and anionic flocculants (Fig. 1).

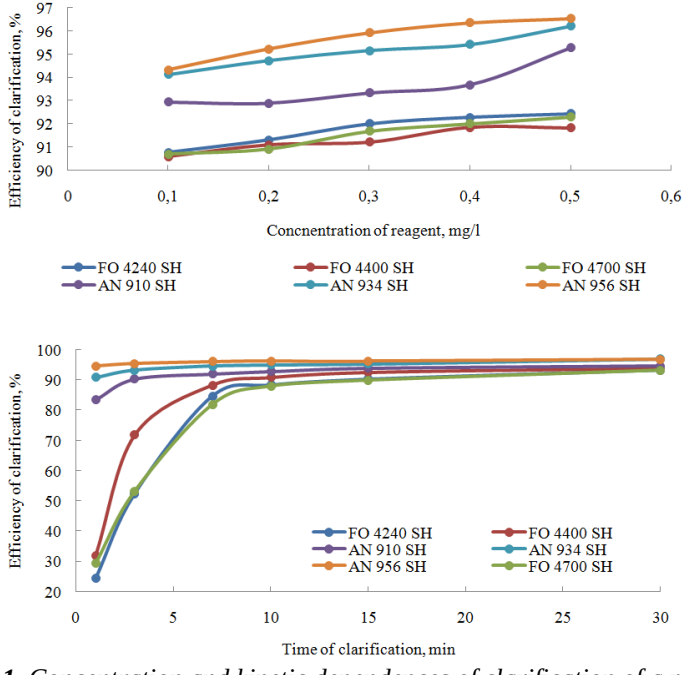

Fig. 1. *Concentration and kinetic dependences of clarification of a model apatite concentrate suspension in recycled water for a number of cationic (FO series) and anionic (AN series) flocculants*

The data show that anionic flocculants are more effective in their action. The advantage of an anionic flocculant is mainly seen in the first minutes of clarification. The anionic reagents-flocculants with a higher degree of ionicity (from 30 %) have a higher efficiency.

Further studies were aimed at creating models of initial feed for different preparation regimes. The real discharge of apatite concentrate's thickener was taken as a basis. As the majority of disperse systems, it contains particles of different sizes, and their content is not equal. Determination of particle sizes of the disperse phase and construction of the curves of particle size distribution is the essence of the sedimentation analysis.

Its use is limited by conditions of the Stokes equation application. To meet these conditions, the industrial thickener discharge with suspended particle content of 109.3 g/l was diluted with distilled water. The concentration of dispersed phase obtained is 1%. The sedimentation analysis was carried out according to known methods [6].

The studies were carried out in two modes:

- sedimentation of the apatite concentrate thickener's discharge without the use of chemical reagents;
- sedimentation of the apatite concentrate thickene's discharge using the developed technology: input of 0.2 mg/l of anionic flocculant AN 934 SH into the initial feed at pH-11.

The relative mass (share) of the sediment of the dispersed phase of the low-concentration suspension of the apatite concentrate thickener's discharge, accumulated during the sedimentation time τ is described by the following empirical functions:

- for a test without chemical reagents:
$$F(\tau) = 100(1 - e^{-0.25\tau}) - \tau(25e^{-0.25\tau})$$
- for a test with flocculant AN 934 SH at pH-11:
$$Z(\tau) = 100(1 - e^{-0.68\tau}) - \tau(68e^{-0.68\tau})$$

To characterize the fractional composition of the settling suspensions, the authors have plotted the integral and differential curves of particle size distribution, which show the mass share of each fraction (Fig. 2). The distribution curves were plotted by an analytical method [7].

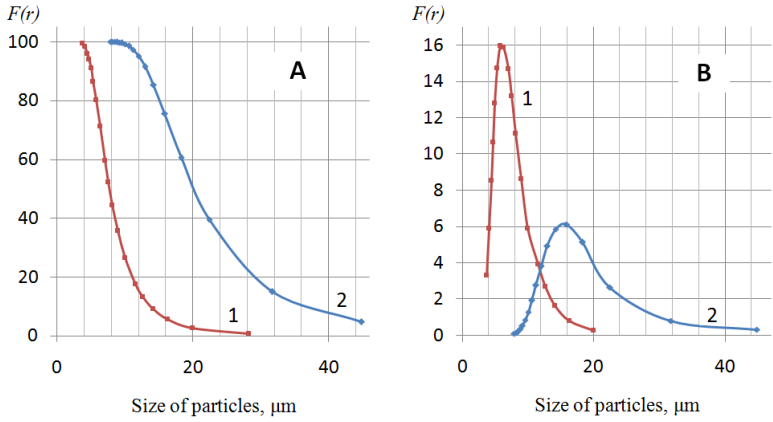

Fig. 2. *The integral (A) and differential (B) curves of particle size distribution form the apatite concentrate's discharge: 1 – without a flocculant, 2 - 0.2 mg/l AN 934 SH at pH-11*

The analytical expressions of the differential curves of particle mass distribution of the suspension by equivalent radius were obtained by differentiating the analytical expression of the integral distribution curves by the variable r. For a test without chemical reagents: $F(r) = -(16.129\tanh(0.323r - 2.226)^2 - 16.129$; for a test with flocculant AN 934 SH at pH-11: $F(r) = -(14{,}706\tanh(0.294r - 2.206)^2 - 14{,}706$

The obtained expressions were used to create discrete functions of volume fractions of particles with different particle sizes when constructing models of initial feed of each water preparation mode.

The computational experiments on the research of sedimentation of the apatite concentrate thickener's discharge under conditions of using a flocculant effectively binding apatite particles (anionic flocculant AN 934 SH with a degree of ionicity 30%) and without reagents (particles sedimentation by gravity) were set on the virtual bench.

The authors have obtained the distributions of concentrations of volume fractions of particles (Table 3, Fig. 3,4) and velocities of their movement in the volume of the thickener (Fig. 5).

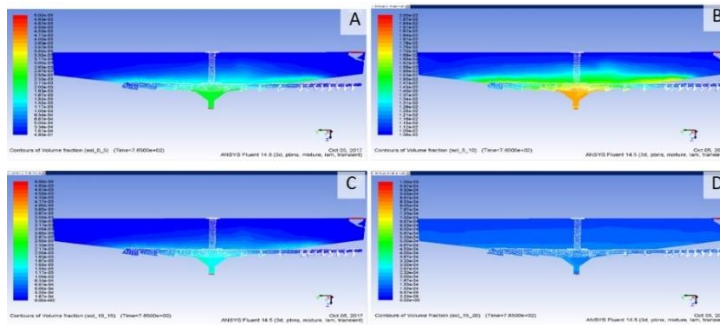

Fig. 3. *Fields of volume concentrations of solid phases of different coarseness of the suspension on the vertical section of the thickener's model (at sedimentation without reagents-flocculants);*

A - coarseness $0 – 5 \cdot 10^{-6}$ m; B – $5 \cdot 10^{-6} – 1 \cdot 10^{-5}$m; C – $1 \cdot 10^{-5}$ - $1.5 \cdot 10^{-5}$m; D - $1.5 \cdot 10^{-5} – 3 \cdot 10^{-5}$m

Table 3. *Distribution of volume fractions of particles*

Fract-ion of initial sus-pension, μm	Concentration of volume fractions, kg/s			Fract-ion of initial suspen-sion, μm	Concentration of volume fractions, kg/s		
	Test without chemical reagents				Test with AN 934 SH at pH-11		
	Initial feed	Sands of thick-ener	Dis-charge of thick-ener		Initial feed	Sands of thicken-er	Dischar-ge of thicken-er
water	60,43	3,91	79,99	water	77,78	3,16	76,80
0-5	0.232	$5.88 \cdot 10^{-5}$	$4.36 \cdot 10^{-10}$	0-20	0.12	0.00168	0.02278
5-10	3.121	0.0039	0.0286	20-70	1.55	0.034	0.208
10-15	0.1032	$2.66 \cdot 10^{-5}$	$1.86 \cdot 10^{-10}$	70-85	0.65	0.034	0.041
15-30	0.000258	$3.48 \cdot 10^{-7}$	$1.93 \cdot 10^{-6}$	85-120	0.82	0.0776	0.0248
				120-170	0.499	0.0965	0.0064
				170-250	0.2699	9.4745	0.2327
				250-500	0.19	7.4389	0.34105
				500-850	0.0699	5.8578	0.1355

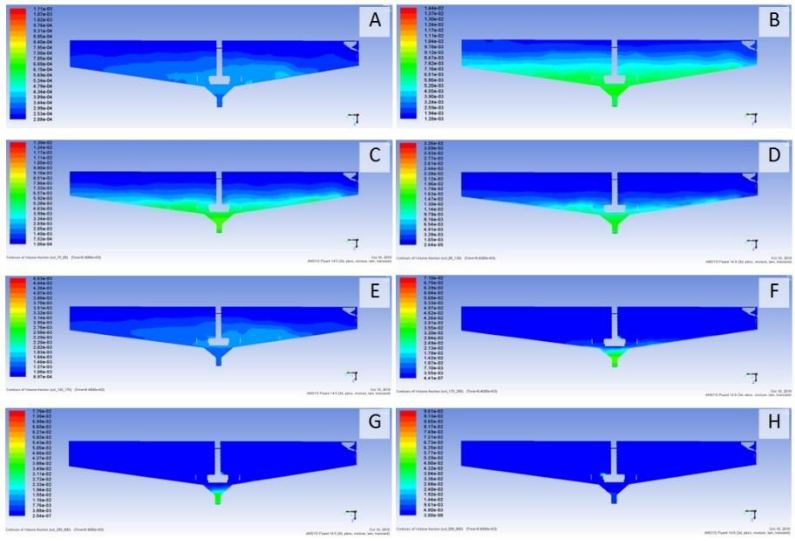

Fig. 4. *Fields of volume concentrations of solid phases of different coarseness of the suspension on the vertical section of the thickener's model (at sedimentation with flocculant AN 934 SH):*

A – coarseness 0 – $2 \cdot 10^{-5}$m; B - $2 \cdot 10^{-5}$ – $7 \cdot 10^{-5}$m; C - $7 \cdot 10^{-5}$ – $8.5 \cdot 10^{-5}$m; D – $8.5 \cdot 10^{-5}$ – $1.2 \cdot 10^{-4}$m; E – coarseness $1.2 \cdot 10^{-4}$ – $1.7 \cdot 10^{-4}$m; F – $1.7 \cdot 10^{-4}$ – $2.5 \cdot 10^{-4}$m; G – $2.5 \cdot 10^{-4}$ – $5 \cdot 10^{-4}$m; H - $5 \cdot 10^{-4}$ – $8.5 \cdot 10^{-4}$m

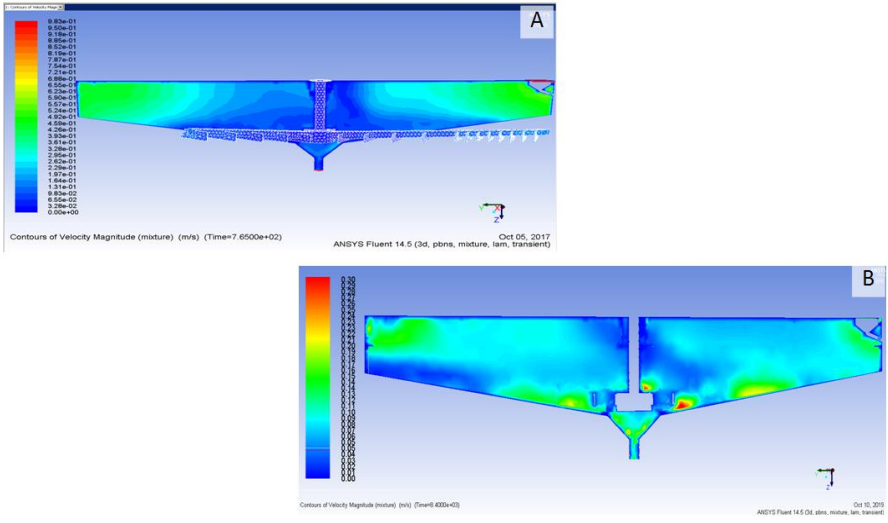

Fig. 5. *The velocity field of the suspension on the vertical section of the thickener's model*

A – at sedimentation without flocculants, B - at sedimentation with flocculant AN 934 SH

CONCLUSION

The authors have analysed the data obtained at this study stage and according to their conclusion, if the reagents-flocculants are not used, the main mass of volume fractions of the initial suspension accumulates on the inclined plane of the thickener's bottom and only a small part comes out through the discharge hole due to transportation with the rakes, but the sands of the thickener are heavily watered.

Thus, water preparation in a radial thickener cannot be carried out without flocculants due to the difficulty of achieving acceptable specific loads on solids. In case of using flocculants, according to the computational experiment results, there is an increase in particle settling velocities, due to enlargement of finely dispersed apatite particles and the density of the resulting thickener's sands. Rotating rotor rakes facilitate the movement of the sedimented suspension to the discharge hole of the thickener, and form the necessary operating mode which can provide mixing and amount of particle collisions necessary for floc formation.

The results of laboratory studies and computer simulation data allow to tell about the prospect implementation of the technology of intra-plant water circulation, which will reduce by 10% the amount of wastewater discharged into the tailing dump.

ACKNOWLEDGEMENTS

This publication has been produced with the assistance of the European Union. The contents of this publication are the sole responsibility of the following authors: A.V.Artemev, V.V. Biryukov and can in no way be taken to reflect the views of the European Union.

Kolarctic CBC
EU FINLAND NORWAY RUSSIA SWEDEN

REFERENCES

[1] Malinskaya I.S., Bacheva E.D. Research of features of selective apatite flotation under recycled water supply conditions. - Processing of oxidized ores. - M: Nauka, 1985. - pp. 205-211

[2] Golovanov G.A. Flotation of the Kola apatite ores. - M: Chemistry, 1976. - 216 p.

[3] Golovanov V.G., Petrovsky A.A., Brylyakov Yu.E., Introduction of recycled water supply at ANOF-2. - Gornyi Zhurnal. - 1999. - № 9. - pp. 48-50.

[4] Gershenkop A.Sh., Mukhina T.N., Artemev A.V. Features of the mineralogical composition of apatite-nepheline ore from the Oleniy Ruchey deposit and their impact on the processing performance. - Ore beneficiation, No. 3, 2014, pp. 33-36.

[5] Mitrofanova, G.V. Ivanova, V.A. Artemev A.V. Use of reagents-flocculants in water-preparation processes during phosphorous-containing ore

processing. - 17th International Multidisciplinary Scientific GeoConference SGEM 2017, SGEM2017 Conference Proceedings , June 29 - July 5, 2017, Issue 11, Vol. 17, 1143-1150 pp.

[6] Practicum on colloidal chemistry, edited by I.S. Lavrov. - M: Higher School, 1983. - 206 p.

[7] Zimon, A.D., Leshchenko N.F. / Colloidal Chemistry. - M: Agar, 2001. - 318 p.

SEA LEVEL PREDICTION IN THE NORTH-WESTERN BLACK SEA USING AUTOREGRESSIVE INTEGRATED MOVING AVERAGE AND MACHINE LEARNING MODELS

Dr. Maria Emanuela Mihailov[1]
Dr. Alecsandru Vladimir Chirosca[2]
Dr. Gianina Chirosca[3]
[1] National Institute for Marine Research and Development "Grigore Antipa" Constanta, Romania
[1] Maritime Hydrographic Directorate, Constanta, Romania
[2, 3] Faculty of Physics, University of Bucharest, Magurele, Ilfov, Romania

ABSTRACT

Data prediction models are essential for estimating extreme environmental changes and predicting anomalies by learning when the actual data is outside previously accepted values. This paper focuses on predicting two years of sea level in the North-Western Black Sea region. Data from the UNESCO/ IOC tsunami observation and Permanent Service for Mean Sea Level archives were analysed using Auto Regression - and Seasonal-Regression Integrated Moving Average models. This work proposes one such model obtained by using modern Machine Learning algorithms, and the results are compared with standard models such as ARIMA obtained for the same data. Using Machine Learning can produce software models ready to run with hardware using much lower specifications than those used for model training which is not the case for standard statistical models. The merged dataset in the analysed period (2006-2016) from the tide gauges along the Romanian Black Sea Coast is consistent and satisfactorily used to develop and validate a Seasonal Regression Integrated Moving Average and Machine Learning model for sea-level forecasts. The data show that the sea level evolution in cyclical changes of the other parameters that influence it. Furthermore, slight demarcation of the two models was observed between the comparison of observed and predicted values.

Keywords: *sea level, ARIMA, SARIMA, Machine Learning, Black Sea*

INTRODUCTION

The socio-economic developments and infrastructures around the world have been concentrated in the coastal area. As a nodal point for naval transport (commercial, recreational, research, or military purposes) or the richness of marine resources, this area offers many future perspectives at the interface between land and sea. The most predominant concern worldwide is the sea level rise that can negatively affect/endangering the coastal area's infrastructure and inhabitants. That implies a change in the mean sea level due to the climate change perspective, but locally, it can induce wind and storm / extreme events frequencies that contribute to coastal zone vulnerability. [1] estimate a rise in all scenarios within a range of 0.6 - 0.7m in 2100 regarding the "global mean sea level" rise. Various statistical sea level forecasting strategies using ANN (Artificial neural network), ARMA (Mixed Autoregressive-Moving Average process), ARIMA (Autoregressive Integrated

Moving Average process), ARFIMA (Autoregressive Fractionally Integrated Moving Average process) are used in the scientific community to find the best-fit model for the time series data for the sea level measurements [2], [3], [4].

In the Black Sea, few studies evaluated, estimated or modelled the sea level based on in-situ measurements or satellite altimetry for the entire Black Sea basin [5, 6] or for coastal areas: the Turkish and Georgian coast [7], the Russian coast [8], and for Romanian [9]. For the entire Black Sea basin, the estimated rate of the mean sea level rate calculated from satellite data is 7.6 ± 0.3 mm/year [6]. On the other hand, the average annual amplitude of sea-level variations is about 0.35 mm from the altimetry or 0.56 mm from the tide gauges [5], [7]. Furthermore, from available in-situ data, for the entire Black Sea coast, the sea level shows different ascendent rates/patterns (sea level rise): about 1.37 mm/year at Constanta (Romania), at Varna (Bulgaria) 1.22 mm/year, Bourgas (Bulgaria) a rate of 1.91 mm/year, Batumi (Georgia) by 1.96 mm/year, 6.68mm/year at Poti (Georgia), Sevastopol (Ukraine) 1.26 mm/year and at Tuapse (Russia) with 2.46 mm/year [9].

In the present study, the long-term time series on the regional scale (Western Black Sea coast) is used to detect a historical data pattern and then extrapolated for future forecasts. The analysis and models are performed using a Python environment. This paper is focused on the time decomposition of sea level in the Western Black Sea and the formulation of short-term forecasts using ARIMA modelling. Using data prediction models is suitable for identifying the seasonal and non-seasonal parameters that determine current and future hydrological conditions based on historical data analysis. One of the most popular time-series analyses is ARIMA. Still, the main challenge remains to set up models that accurately describe temporal hydrodynamic conditions and enable accurate forecasts. Furthermore, further observation of time series usually reveals significant, non-random relationships.

MATERIALS AND METHODS

Study area and data source. The Black Sea, a semi-enclosed basin located in Eastern Europe, connects with the Marmara Sea through the Bosporus Strait and northeast with the Sea of Azov through the Kerch Strait.

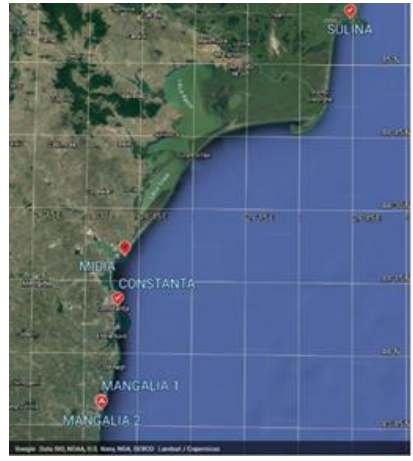

Fig. 3. *Coastal sea level tide gauges on the Romanian Black Sea shelf [10]*

In this paper, for developing sea level short-term ARIMA forecasts on the Western Black Sea coast, Constanta stations mean sea level, and "csta" and "csta2" are used for the 2006 – 2018 periods. Also, for other coastal stations as Sulina – station no. 93 (2016 - 2018), available data, are used for correlation with other sea-level coastal stations and similar for Mangalia -station no. 91(2016 – 2018) from Joint Research Centre Sea level database. All monitoring stations along the Romanian Black Sea coast are illustrated in Fig. **3**. On the Romanian Black sea coast, three organisations record and analyse the sea level for different purposes. National Institute for Marine Research and Development "Grigore Antipa" (NIMRD), "csta" station, use a systematic recording of sea level realised at Constanta (44.17N, 28.67E) through a mechanical level recorder [9] For station "csta2", since 2015, the National Institute for Earth Physics (NIEP) installed a radar tide gauge sensor OTT model RLS used to record sea level at Constanta (44.15N, 28.67E) as a component of a network for marine seismicity purposes (Fig. **3**). Furthermore, we specify that annually high precision GPS measurements at the landmarks of all tides and their zeros will be unified with the ultimate goal of updating the zeros "sea-level" of the Black Sea. These measurements are carried out by the Institute of Geodesy, Photogrammetry, Cartography and Cadastral Bucharest Romania (for NIMRD and NIEP tide gauges).

Model setup. We build prediction models using the recorded data, starting with a conservative approach using the standard seasonal ARIMA model with exogenous regressor - SARIMAX. It is appropriate for our data pattern [11], [12]. We further increase the prediction accuracy by using machine learning methods first through Long-Term Short-Term memory layers [13], followed by an encoder-decoder pattern [A4 14] that provides better accuracy than the previous two. Seasonal ARIMA (Seasonal Auto-Regressive Integrated Moving Average with eXogeneus Regressors Model) prediction model uses a set of parameters (p, d, q) presented in eq. 1 where L is the lag function. Our model was fitted against the sea level data using Akaike Information Criteria (AIC) [15] minimisation. AIC, eq. 2, evaluates

the model deviation against the actual data for the distribution probability f with the measured data g.

$$(p,d,q)\ x\ (P,D,Q)_S, \phi p(L) < \phi >_P (L^s)\Delta^d \Delta\ {}_s^D D_s y_t = A(t) + < \theta_q > (L) < \theta_Q > (L^s)\zeta t \quad (1)$$

$$I(g:f) = E\ log\ g(x) - Elog\ f(x) \quad (2)$$

Recurrent network design was implemented using the Keras framework with TensorFlow backend. Our model consists of 3 layers. The first two LSTM types with 36 fully connected neurons use rectified linear unit activation function and one layer with a single neuron for output (**Error! Reference source not found.**). The o ptimiser is nadam with an error estimation of type mean squared error.

Table 4. *Machine Learning model for sea-level prediction using LSTM layers*

Layer (type)	Output Shape	Parameters #
1stm_23 (LSTM)	(None, 60, 36)	5472
1stm_24 (LSTM)	(None, 36)	10512
Dense_15 (Dense)	(None, 1)	37
Total params: 16,021 Trainable params: 16,021 Non-trainable params: 0		

No overfitting was identified for our model using a window of 60 records for 200 epochs. However, introducing dropout layers increases the model uncertainty.

RESULTS AND DISCUSSIONS

Data sets. Recorded data is always susceptible to missing data points due to device malfunction or other external factors. Our dataset has only a few missing data points (11 missing data points from the total dataset of 385 records). To achieve data evaluation and build prediction models (data has to be continuous) and for the missing points, a linear approximation was performed, taking into account two value points before and after the missing data point. For such cases, a polynomial regression model was performed for the 4 data points, and thus we obtained the analytical function used to interpolate missing data. *Fig.* ***4*** shows how an interpolation model for one missing data point was built.

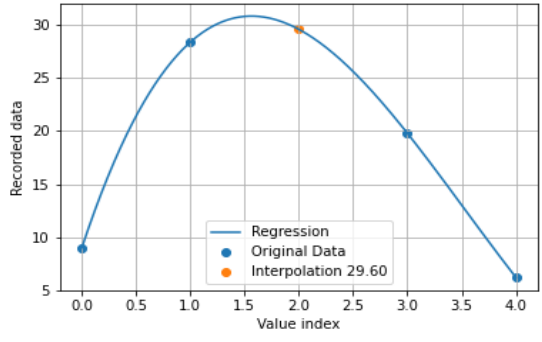

Fig. 4. *Data interpolation using a 3rd order polynomial regression. For this case, the obtained polynomial is* $1.2x^3$-$12.7x^2$+$30.9x$+9.

From the 85 years of the monthly dataset, 83 years are used for model calibration (1933 - 2016), while the last two years (2017 - 2018) validate the statistical model. All databases described (PSML, IOC) were integrated into one, and the duplicates were excluded. Box and whisker plots were realised: the median, minimum and maximum values, and the lower (25%) and upper (75%) quartiles. The quartiles delimit each box, and the whiskers represent the extreme values. The dataset contains 982 instances of approximately 40 years from 1933 to 2018 with six attributes, as shown in *Table 5*.

Table 5. *Merged sea-level data description and dataset attributes*

Variable Name	Description
YEAR	Year
MONTH	Month
STATION	Station name
LEVEL	Numerical Sea-Level
SLP	Sea level pressure
FLOW	Danube Discharge

The sea level data: the Romanian Black Sea. We consider that: if time series show gradual shifts to relatively higher or lower values over a more extended period, then it can be stated that a pattern exists in the datasets. However, limited understanding of the dynamic processes that influence the sea level rise determines low confidence in quantitative projections. Relevant processes on the western Black Sea coast are river discharge (Danube river), river and sea ice melting (during intense winters), and climate change.

The linear function y=Bx+A was used (*Fig. **5***) to determine the quantitative relationship between the river discharge and the sea- level**Error! Reference source not found.**. Danube river discharge and the sea level have an excellent correlation coefficient in the range of 0.64. Therefore, the slope (coefficient B) could show the river discharge influence on the mean sea level. Meanwhile, coefficient B has negative values. Considering the Constanta Port data as basic in analysing the other tide gauges - Sulina and Mangalia - the correlation was made between the Romanian coastal sea-level stations. The coefficient of correlation is very good ($r_a = 0.78$; $r_b = 0.79$, and $r_c = 0.85$), and the slope of the regression is close to unity. The following correlations are determined following the linear function ($y=Bx+A$), as *Fig. **5***:

a) $Z_{Mangalia} = 0.94\ Z_{Constanta} + 124.8$ (r = 0.79)

b) $Z_{Sulina} = 1.01\ Z_{Constanta} + 20.3$ (r = 0.78)

c) $Z_{Sulina} = 0.91\ Z_{Mangalia} - 89.0$ (r = 0.85)

were, the differences between the free terms correspond to the different zeros of the tides.

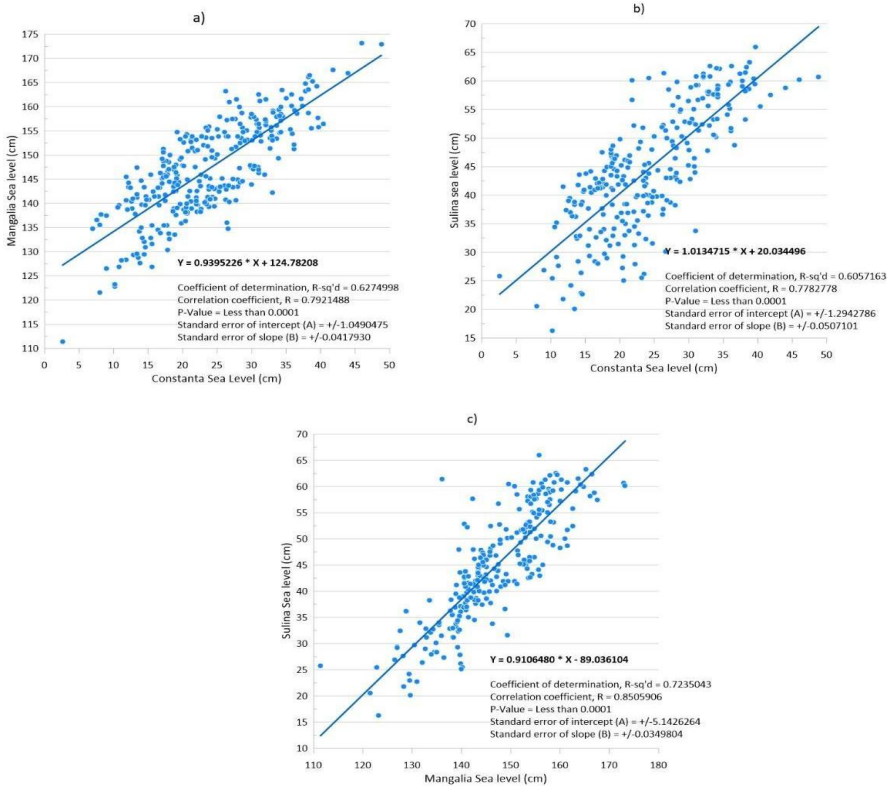

Fig. 5. *The correlation between sea level (cm) recorded at the tide gauges, 2016 - 2018 period: a) Constanta and Mangalia; b) Constanta - Sulina, and c) Mangalia and Sulina.*

Pre-processing, Model setup and analysis. We evaluated the correlation and partial correlation for our data (*Fig.* ***6***). The autocorrelation clearly shows the need for seasonal models.

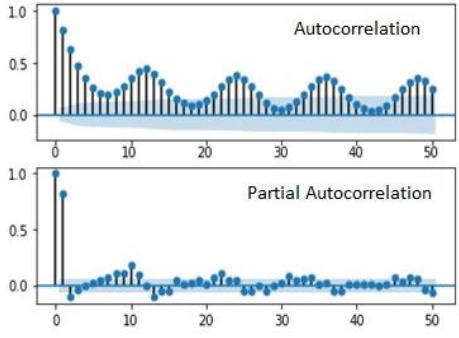

Fig. 6. *Autocorrelation and partial autocorrelation for sea level data at Constanta (1933 - 2018)*

For SARIMAX model development, we used a 12 months window. We evaluated the AIC for a large set of model parameters obtaining the minimal AIC value for the parameters collection (2,1,2) x (2,1,2,12), getting an AIC value of 6583.19. The predicted values for our model are presented in *Fig. **7***.

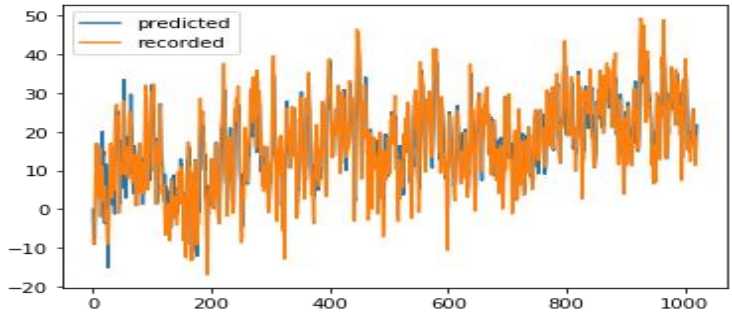

***Fig. 7.** SARIMAX predicted versus measured sea-level data at Constanta (2006 - 2018)*

A time-series pattern can be identified by evaluating the monthly movements in historical data, as shown in *Fig. **8***. However, SARIMAX predictions have significant errors (RMEs) for the inflexion data points, providing a mean RME of 18, showing that more parameters (water flow, the temperature a.s.o) need to be evaluated for better accuracy. To maintain univariate data (1D input data), we employ a Machine Learning (ML) method for the same dataset using a Recurrent Neural network using the sea level monthly means (2006 – 2018). The ML model trained for 10 hours using the provided dataset (monthly averages for 2006-2015) and delivered the results presented in *Fig. **8***.

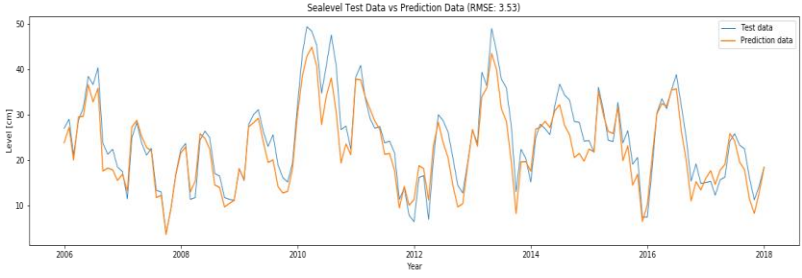

***Fig. 8.** Machine Learning using LSTM layers predicted versus measured sea level data at Constanta site (2006 - 2018)*

The ML model provided a better RMS than the SARIMA model (3.53) for the provided dataset. The accuracy plot presented in **Error! Reference source not found.** shows that univariate data suggests intrinsic variations that lead to higher errors. Our model was improved using an encoder-decoder pattern for seq2seq time series prediction to assess such parameters properly.

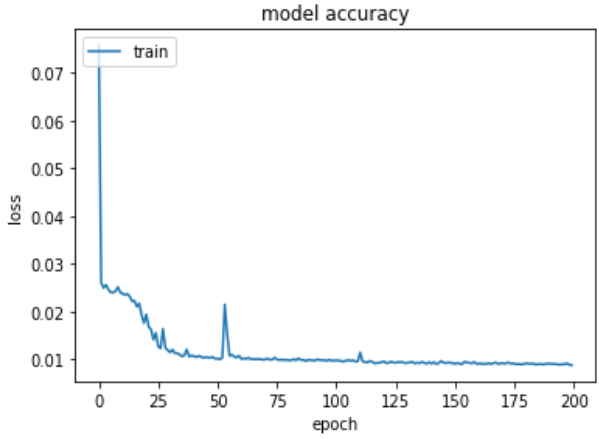

Fig. 9. *Machine Learning using LSTM accuracy plot for each epoch (each time the model sees the data).*

From the last two figures (*Fig.* ***8***, **Error! Reference source not found.**), the accuracy cannot be improved by increasing the epoch counts, and new models have to be used to increase the model accuracy.

CONCLUSION

Sea-level simulation shows the potential capability of machine learning algorithms to forecast based on historical time-series data. In general, satisfactory predictions with the values of correlation coefficients equal to 0.7–0.9, root mean square errors of about 10% of the tidal range and scatter indexes equal to 0.1–0.2 were produced. The validated neural methodology can be successfully applied to other coastal regions provided site-specific training and appropriately carried out validations. The neural technique was successfully implemented to predict hourly sea levels in the first set of simulations, with lead times from 1 to 24 hours, and afterwards to correct the initial simulations results. An ancillary correcting neural network improved the quality of the initial hourly simulations when assimilating the outcomes of more complex nets. Simultaneously, its application led to overfitting when the input data were coming from the network with the same number of inputs–processing–output units. ANNs were implemented to forecast sea levels in the second set of simulations, averaged over 12-h, 24-h, 5-day and 10-day periods, three-time steps ahead. This produced high-quality predictions over the first two time steps rather than over the third time interval. The latter's lack of accuracy was attributed to the reduced number of input-output training pairs and weak interrelations.

ACKNOWLEDGEMENTS

We thank Permanent Service for Mean Sea Level, UNESCO / IOC tsunami observation / alerting network and European Commission Joint Research Centre - ISPRA - Space, Security and Migration Directorate (JRC) for maintaining the

servers and the long-term data availability. MEM study has been carried out with financial support from the Monitoring Study Contract – Romanian Ministry of Water and Forests no.55/2018. Furthermore, MEM continued the work, performed under the Sectorial Research-Development Plan of the Romanian Ministry of National Defence 2020 and 2021.

REFERENCES

[1] Church JA, et al., Sea level change. Climate Change 2013: The Physical Science Basis, Contribution of Working Group I to the Fifth Assessment Report of the Intergovernmental Panel on Climate Change, Cambridge Univ Press, Cambridge, UK, pp 1137–1215, 2013 (https://www.eea.europa.eu/data-and-maps/indicators/sea-level-rise-5/nicholls-et-al-2010-sea, accessed 1.25.21).

[2] Ercan A., Kavvas M.L., Abbasov R.K., Long-Range Dependence and Sea Level Forecasting, SpringerBriefs in Statistics. Springer International Publishing, pp 51, 2013.

[3] Fernandez Q.F.R., Montero N.B., Po III R. B., Addawe R. C., Diza H. M. R., Forecasting Manila South Harbor mean sea level using Seasonal Arima models, Journal of Technology Management and Business, vol. 5/issue 1, 2018.

[4] Srivastava P.K., Islam T., Singh S.K., Petropoulos G.P., Gupta M., Dai Q., Forecasting Arabian Sea level rise using exponential smoothing state space models and ARIMA from TOPEX and Jason satellite radar altimeter data: Forecasting Sea level rise using altimeter data, Meteorological Applications, vol. 23, pp 633–639, 2016.

[5] Avsar N.B., Jin S., Kutoglu H., Gurbuz G., Sea level change along the Black Sea coast from satellite altimetry, tide gauge and GPS observations, Geodesy and Geodynamics, vol. 7, pp 50–55, 2016.

[6] Kubryakov A.A., Stanichnyi S.V., The Black Sea level trends from tide gauges and satellite altimetry, Russian Meteorology and Hydrology, vol. 38, pp. 329–333, 2013.

[7] Avsar N.B., Jin S., Kutoglu S.H., Recent sea level changes in the Black Sea from satellite gravity and altimeter measurements. The International Archives of the Photogrammetry, Remote Sensing and Spatial Information Sciences, vol. XLII-3/W4, pp 83–85, 2018.

[8] Goriacikin I.N., Ivanov V.A., Black Sea Level: Past, Present, Future, EKOCI-Gidrofizica, Sevastopol, pp 210, 2006. (in Russian)

[9] Mihailov M.-E., Buga L., Spînu A.-D., Dumitrache L., Constantinoiu L.-F., Tomescu-Chivu M.-I., Interconnection between Winds and Sea Level in the Western Black Sea Based on 10 Years Data Analysis from the Climate Change Perspective, Cercetări Marine - Recherches Marines, vol .48 / issue 1, pp 171–178, 2018.

[10] https://earth.google.com/web/

[11] Vagropoulos S.I., Chouliaras G., Kardakos E.G., Simoglou C.K., Bakirtzis A., Comparison of SARIMAX, SARIMA, modified SARIMA and ANN-based models for short-term PV generation forecasting, 2016 IEEE International Energy Conference (ENERGYCON), Leuven, 2016, pp 1-6.

[12] Durbin J, Koopman S.J., Time Series Analysis by State Space Methods: Second Edition. Oxford University Press, 2012.

[13] Hochreiter S., Schmidhuber J., Long Short-Term Memory, Neural Computation, vol. 9/ issue 8, pp 1735-1780, 1997.

[14] Cho K., van Merrienboer B., Gulcehre C., Bahdanau D., Bougares F., Schwenk H., Bengio Y., Learning Phrase Representations using RNN Encoder-Decoder for Statistical Machine Translation, Proceedings of the 2014 Conference on Empirical Methods in Natural Language Processing (EMNLP), Doha, Qatar, 2014, pp 1724–1734.

[15] Akaike H., Akaike's Information Criterion, International Encyclopedia of Statistical Science, Lovric M. (eds) Springer Berlin Heidelberg, pp 25, 2011.

THE POSSIBILITY OF USING THE ENERGY POTENTIAL OF WASTE POOL WATER

Ing. Anna Predajnianska[1]
Prof. Ing. Ján Takács, PhD.[2]
[1, 2] Slovak Univerzity of Technology in Bratislava, Slovakia

ABSTRACT

Thermal baths in Slovakia are producers of wastewater, which hides considerable energy potential. The wastewater from the thermal pools has often exceeds the maximum permissible value of the temperature of the wastewater discharged into the water recipient. As a result, there is undesirable damage to the environment, which results in sanctions for the operators of these facilities. Our aim is to present the concept of a single- and double-step heat recuperation system of waste pool water using applications of various types of heat exchangers or heat pumps. The aim of this application is to ensure a suitable temperature to the discharged waste pool water, efficient use of the energy potential of the waste water and saving of primary energy in the form of geothermal water, thus extending the life of the entire system.

Keywords: *waste pool water, geothermal, energy*

INTRODUCTION

Slovakia´s energy intensity is one of the highest in the Member States of the European Union. High energy prices also force recreational facility operators to look for suitable and environmentally friendly ways to save operating costs. The most appropriate way is to prioritize renewable energy sources. Combinations of renewable energy sources with other technical equipment belong to the highly efficient and operationally reliable way of saving energy, environment and operating costs. The advantage is their ability to respond to individual requirements in the environment in which they are located [3]. Pursuant to Article 9 of the Regulation of the European Parliament and the Council of the EU 2018/1999 on the Management of the Energy Union and Climate Action of 11 December 2018, the Ministry of Economy of the Slovak Republic prepared the Integrated National Energy and Climate Plan for 2021-2030 [1], [2]. This plan updates the current energy policy. Energy policy priorities include, but are not limited to developing energy infrastructure, reducing energy intensity, and promoting the use of renewable energy sources [1]. There are 32 perspective areas in Slovakia with geothermal potential of 215 MW of heat output, provided that the geothermal water is not returned to the geological subsoil. In these areas we can find up to 176 registered geothermal wells, with geothermal water temperature ranging from 30 °C to 130 °C [4, 5]. Geothermal energy in Slovakia is used up to 60 % in recreational facilities. It has also been used in centralized heat supply systems, heat transfer stations, but also in agriculture for heating greenhouses and foilhouses [6]. Fields of geothermal energy utilization and installed heat output is summarized in Table

1. Until 1990, there was not much interest in heat pumps in Slovakia due to low energy prices. However, the situation has changed and they are being applied more and more. The task of these devices is to transform or pump the low-temperature energy of the environment to a higher temperature level by supplying additional energy of higher quality, which is represented by electrical, mechanical or high-temperature thermal energy [7], [8]. The dimensioning of the heat pump depends on economic investments, but also on the condition of the surrounding environment in which it will operate [3].

Table 1. *Fields of geothermal energy utilization [6].*

Field	Installed heat output (MW)
Recreational facilities	128,3
Systems of centralized heat supply	35,9
Greenhouse and foilhouse heating	34,8
Heat pumps	10,4
Fish farming	5,6
Sum	215,0

SWIMMING POOL TYPES

In Slovakia two basic pool systems are used in thermal baths:

- flow pool system,
- circulation pool system.

Flow pool systems operate on the principle of direct inflow of geothermal water into pools. This system can be used if the geothermal water has a temperature below 50 °C and has a suitable mineralisation. If geothermal well provides a geothermal water with higher temperature than 50 °C, this water cannot be discharged directly into the pool and must be diluted with cold water in the mixing chamber. From this system waste pool water is discharged into recipient without further usage. The disadvantage of flow systems is their high energy consumption and the fact that they require a large yield of the source of geothermal and cold water. Flow based pool system filled with only geothermal water can be seen on Figure 1 on the left side. Flow based pool system filled with mixed geothermal and cold water can be seen on Figure 1 on the right side [6].

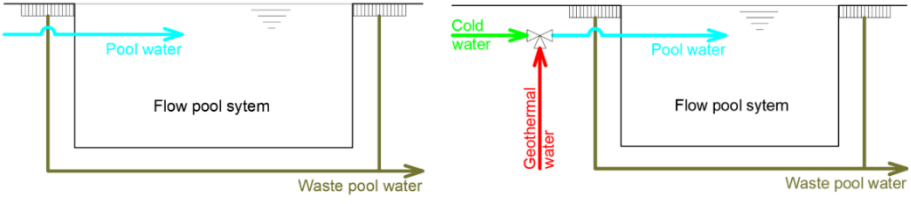

Fig. 1. *Scheme of the flow pool system filled with only geothermal water (left) and scheme of the flow pool system filled with mixed geothermal and cold water (right) [Author]*

More technically demanding, but still more used are the circulation systems of swimming pools, which include a buffer tank. Geothermal water is mixed with cold water in a buffer tank to reach the required pool water temperature. The mixed water is drained from a buffer tank into a sand filter from where it flows directly into the pool. Pool water flows again into the buffer tank. Only after overfill the buffer tank does the waste pool water flow out of the system, which is discharged into the recipient. Circulation pool system can be seen on Figure 2 [6].

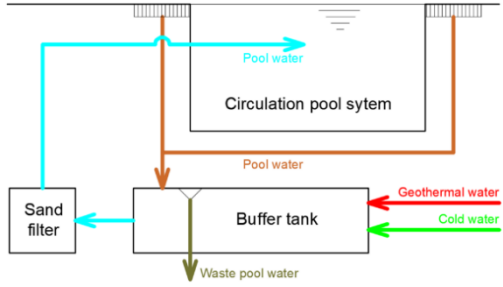

Fig. 2. *Scheme of circulation pool system filled with mixed geothermal and cold water [Author].*

CURRENT SITUATION IN RECREATIONAL FACILITIES IN SLOVAKIA

Recreational facilities use thermal water to fill their pools. In many cases, the degree of utilization of geothermal energy in thermal baths is less than 50%. Another problem in many recreational facilities is that they discharge waste pool water at too high a temperature. The maximum temperature of the waste pool water 26 °C, which can be discharged into the water recipient, is prescribed by Law no. 364/2004 on water and on the amendment of the Law of the Slovak National Council no. 372/1990 Coll. on offenses as amended (Water Law) and Regulation of the Government of the Slovak Republic laying down a requirement for achieving good water status no. 269/2010. Exceeding the prescribed temperature may result in a sanction for environmental pollution up to a maximum of 160 000 € [9]. Therefore, it would be appropriate to propose energy-saving measures in recreational facilities, thanks to which we could achieve important aspect. These aspect are reducing the temperature of the waste pool water to the prescribed temperature, increasing the degree of utilization of geothermal energy, extending the lifetime of the geothermal energy system and reducing or eliminating sanctions for environmental pollution [6].

UTILIZATION OF WASTE POOL WATER ENERGY

The proposal of energy-saving measures consists in the reuse of waste energy potential, which has waste pool water leaving the swimming pools. Thanks to these measures, it would be possible to achieve cooling of the waste pool water. In the article, we want to show up the possibility of one-step and two-step energy-saving

measures by including heat recovery exchanger in the first step and by including a heat pump as a second step of waste pool water cooling.

This proposal consists in the inclusion of a recuperative heat exchanger in the circuit of waste pool water. The task of the heat exchanger will be to preheat the cold water using heat from the waste pool water. Waste pool water with higher temperature transfers its heat to cold water. The preheated cold water is transported to a mixing chamber, where it is mixed with geothermal water. Since we have heated the cold water due to the waste heat, a lower flow of geothermal water and a higher flow of cold water in the mixing chamber will be needed to reach the same desired pool water temperature. In addition, the rate of geothermal energy use will increase and the lifetime of the geothermal well will be extended [8]. A one-step energy-saving measure can be seen in Figure 3.

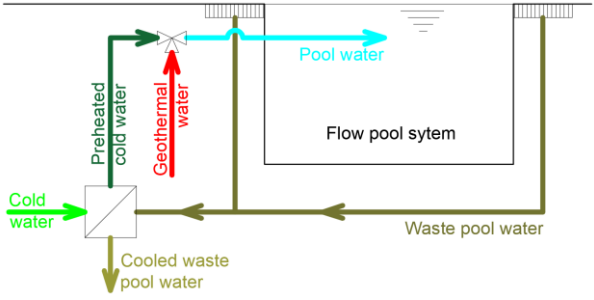

Fig. 3. *Scheme of one-step energy-saving measure by including heat exchanger into the waste pool water circuit [Author].*

The second stage of cooling waste pool water is the inclusion of a heat pump after the first cooling circuit. After cooling waste pool water in the heat exchanger, it is led to the evaporator of the heat pump, where it is cooled to such a value to meet the requirements for the protection of environment. Heat pumps can cool the waste pool water to lower values, it is only necessary to select a suitable heat pump [8]. Two-step energy-saving measure can be seen on Figure 4.

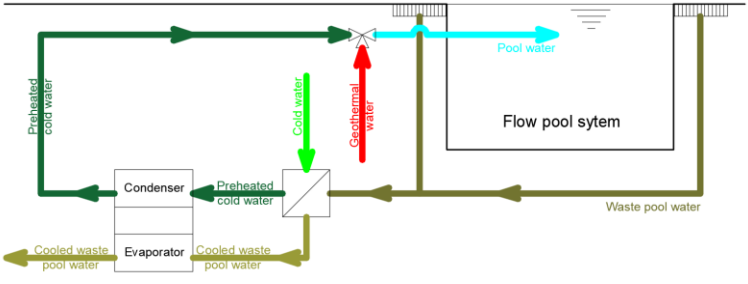

Fig. 4. *Scheme of two-step energy-saving measure by including heat exchanger and heat pump into the waste pool water circuit [Author].*

MATHERIALS AND METHODS

Before heat recovery system will be propose, we need to know energy balance of the pools in recreational facility. It is necessary to made energy balance calculation of solved pools which produce waste pool water. In this calculation we need to know key input values:

- water area or floor area of the pool,
- volume of the pool,
- water depth,
- geothermal water temperature,
- cold water temperature,
- required pool water temperature,
- days during which the pool will be in operation (annual, summer or winter operation),
- days for maintenance and cleaning of the pool [6].

Using the energy balance calculation, we find important output values – energy potential provided by a source of geothermal water, usefully used geothermal water energy, waste pool water energy and rate of geothermal water energy usage. In many cases, the degree of utilization of geothermal energy in thermal baths is less than 50%. The remaining 50% of energy is considered as waste. This is why we need to energy-saving proposal by including heat recovery exchanger into the circuit of waste pool water.

We need to know required waste pool water temperature to secure right recovery exchanger proposal. The more water cooling we required, the more exchanger power is needed. In this step we can use calorimetric equation:

$$\dot{Q} = \dot{m} \cdot c \cdot \Delta T \cdot \rho \quad (1)$$

Explanation: $\dot{Q}$ – Heat exchanger power (kW),
$\dot{m}$ – Water flow (l/s),
c – Specific heat capacity ($kJ \cdot kg^{1} \cdot K^{-1}$),
ΔT – Temperature change (°C),
ρ – water density ($kg.m^{-3}$) [10].

CONCLUSION

In this paper, we want to show the possibility of one-step and double-step heat recovery from waste pool water, thanks to which important aspects could be achieved:

Reduce the temperature of the waste pool water to a maximum temperature of 26 °C by means of the one-step heat recovery system by including heat exchanger into the circuit of waste pool water. The cold water can be preheated from 15 °C to 27 °C to reduce the geothermal water demand. This system is suitable for those geothermal water sources where the yield of geothermal water is high.

Reduce the temperature of the waste pool water to a temperature of 15 °C by application of one- and double-step heat recovery system by including heat

exchanger and heat pump into the circuit of waste pool water. The cold water can be preheated from 15 °C to 32 °C to reduce the geothermal water demand. This system is suitable for those geothermal water sources where the yield of geothermal water is low. In the winter months when pools operation are limited, the outputs from the heat pump (condenser side) can be used for active thermal protection systems of recreational facility buildings, possibly deicing of roads or sidewalks.

Increase the energy use of geothermal water and thus ensure the extension of the lifetime of an open geothermal system.

Reduce or eliminate the sanctions for environmental pollution that must be paid by operators of recreational facilities.

To contribute to the fulfilment of the commitments made by Slovakia in connection with Directive 31/2010 on Energy Efficiency, which enshrines an increase in the share of the use of renewable energy sources and a reduction in the production of greenhouse gases.

ACKNOWLEDGEMENTS

This article was supported by the Ministry of Education, Science, Research and Sports of Slovak Republic through a grant VEGA 1/0303/21, VEGA 1/0304/2021 and KEGA no. 005STU-4/2021.

REFERENCES

[1] Integrated National Energy and Climate Plan for 2021-2030. Prepared according to the Regulation of the EP and the Council (EU) no. 2018/1999 on governance of the Energy Union and climate action. Ministry of Economy of the Slovak Republic. Bratislava. October 2019. Available on the Internet: https://www.mhsr.sk/uploads/files/zsrwR58V.pdf

[2] Regulation 2019/1999 of the European Parliament and of the Council of 11 December 2018 on energy governance and climate action. Available online: https://eur-lex.europa.eu/legal-content/SK/TXT/?uri=CELEX:32018R1999

[3] Jandačka J, Holubčík M, Patsch M, Vantúch M 2016 Modern heat sources for heating. Žilina: EDIS – publishing center ŽU, 264 p. ISBN 978-80-554-1230-6.

[4] Franko O 1995 Atlas of Geothermal Energy of Slovakia, Dionýz Štúr State Geological Institute in Bratislava, p 233

[5] Franko O 1995 Atlas of Geothermal Energy of Slovakia, Dionýz Štúr State Geological Institute in Bratislava, p 233

[6] Predajnianska A Takács J 2020 Recuperation of waste heat produced by public pools and low-enthalpy energy utilization, In proceedings of conference E-nova 2020, Internationale Konferenz. Technologie- und Klimawandel. Energie-Gebäude-Umwelt, 26 – 27 November 2020, 501 - 507 p., ISBN 978-3-7011-0460-4.

[7] Mudrá M 2019 Streamlining the operation of the TP5 heat source for the West housing estate in Brezno [diploma thesis], Bratislava, Slovak University of Technology in Bratislava, Faculty of Civil Engineering, Department of Building Services, 106 p.

[8] Petráš D, Lulkovičová O, Takács J, Furi B 2009 Renewable energy sources for low temperature systems, Bratislava, Jaga Group, s. r. o., 223 p, ISBN 978-80-8076-075-5.

[9] Government decree No. 120/1966 on the imposition of fines for breach of obligations established to protect waters against pollution, Available on the internet: https://www.slov-lex.sk/pravne-predpisy/SK/ZZ/1966/120/vyhlasene_znenie.html

[10] Pavelek M 2011 Thermomechanics Academic Publishers CERM, 192 p., ISBN 9788021443006